CHAPTER 2

Materials and Methods

2. Materials and Methods

2.1. Chapter 3

2.1.1. Materials

DSPC and CHOL were obtained from Avanti Polar Lipids, Inc. (Alabaster, Alabama, US). [^{3}H]Cholesteryl hexadecylether ([^{3}H]CHE) was purchased from PerkinElmer, Inc. (Waltham, Massachusetts, US). [^{14}C]5-Fluorouracil ([^{14}C]5-FU) was purchased from Moravek Biochemicals, Inc. (Brea, California, US). A23187 was purchased from Sigma-Aldrich Co. (Oakville, Ontario, CA). Saline, 5% dextrose (D5W), irinotecan hydrochloride trihydrate (Camptosar®, Sandoz), and 5-FU (Alfa Aesar) were obtained from the BC Cancer Agency Pharmacy (Vancouver, British Columbia, CA). The alamarBlue® reagent, fetal bovine serum (FBS), L-glutamine, and sodium bicarbonate were purchased from Invitrogen Canada, Inc. (Burlington, Ontario, CA). Eagle's minimum essential medium (MEM) with Earle's balanced salt solution (BSS), McCoy's 5A medium, Hank's balanced salt solution (HBSS), non-essential amino acids, sodium pyruvate, and penicillin/streptomycin were purchased from StemCell Technologies, Inc. (Vancouver, British Columbia, CA). All other chemicals were of analytical grade.

2.1.2. Cell Culture

The human colorectal cell lines LS174T and HT-29 were obtained from ATCC (Manassas, Virginia, US). The LS174T cells were cultured in Eagle's MEM with Earle's BSS supplemented with 2 mM L-glutamine, 1 mM sodium

pyruvate, 0.1 mM non-essential amino acids, 1.5 g/L sodium bicarbonate, 1% (v/v) penicillin/streptomycin, and 10% (v/v) FBS, at 37°C in a 5% CO_2 environment. The HT-29 cells were cultured in modified McCoy's 5A medium supplemented with 1.5 mM L-glutamine, 2.2 g/L sodium bicarbonate, 1% (v/v) penicillin/streptomycin, and 10% (v/v) FBS, at 37°C in a 5% CO_2 environment.

2.1.3. Preparation of Irinophore C™

Irinophore C™ was prepared as described by Ramsay *et al.* (1). Briefly, DSPC:CHOL (55:45 molar ratio) liposomes were prepared as previously outlined (2, 3), using trace amounts of a non-metabolizable, non-exchangeable lipid tracer, [^{3}H]CHE (4). The thin lipid film was hydrated with 300 mM $CuSO_4$ solution at 65°C, the resulting lipid vesicles were subjected to 5 cycles of freeze-and-thaw, and then the liposomes were extruded to a diameter of ~100 nm. Unencapsulated $CuSO_4$ was removed via column chromatography with buffer (300 mM sucrose, 20 mM HEPES, 15 mM ethylenediaminetetraacetic acid (EDTA); pH 7.5). Liposomes were incubated with A23187 at 0.5 μg A23187/mg total lipid for 30 min at 60°C. CPT-11 was added to the liposomes at a molar drug-to-lipid ratio of 0.2:1, and the mixture was incubated at 50°C for 1 h. Unencapsulated drug was removed via column chromatography, and drug loading efficiency was determined after measuring CPT-11 absorbance at 370 nm. When required, Irinophore C™ was concentrated at 3,000 x *g* using centrifugal filter tubes (molecular weight cutoff 100 kDa).

2.1.4. In Vitro Cytotoxicity Assays

The viability of human CRC cell lines following exposure to different concentrations of Irinophore C™ or CPT-11 and/or 5-FU *in vitro* was determined using the alamarBlue® assay (5, 6). The cells (LS174T, 10,000 cells/well; HT-29, 5,000 cells/well) were seeded in flat-bottomed 96-well plates and were incubated overnight to permit cell adherence. Increasing concentrations of drug were added to the cells for a 1-72 h incubation period, with drug washout as required. In the ratio dependency experiments, the LS174T and HT-29 cells were exposed to 10:1, 1:1, or 1:10 molar ratios of 5-FU:CPT-11 for 72 h. In the combination exposure time dependency experiment, the HT-29 cells were exposed to a 1:1 molar ratio of 5-FU:CPT-11 for 1-48 h, with drug washout as required. For all experiments, cell viability was assessed at 72 h after the start of drug incubation. The alamarBlue® reagent was added to each well at a 1:10 dilution, and the cells were incubated for an additional 4-8 h before fluorescence was measured (excitation, 544 nm; emission, 590 nm). The fluorescence of cell-free wells containing only medium and alamarBlue® reagent (blank) was subtracted from the fluorescence of all control and treatment wells. Following this adjustment, readings were normalized to the fluorescence of control (untreated) wells. Viability data are presented as fraction affected relative to control. Each point represents the mean +/- standard deviation (n = 3-9) from 2-3 experiments. Cytotoxicity data were fitted with a sigmodial dose-response – fixed slope equation using GraphPad Prism 5.00 for Windows software (GraphPad Software, Inc.; La Jolla, California, US). Data points were omitted from Fig. 3.1 for visual clarity.

For the ratio dependency and combination exposure time dependency studies, combination index (CI) values were calculated to assess the nature of the interaction between CPT-11 and 5-FU *in vitro*. A CI value of 1 represents additive cytotoxicity, less than 1 represents synergistic cytotoxicity, and greater than 1 represents antagonistic cytotoxicity. Drug interaction data are presented as the calculated combination index values across all effect levels, as determined from concentration-effect cytotoxicity data points (n = 3-24) compiled from 2-4 experiments.

For the ratio dependency study, cytotoxicity curves were generated for the drugs as single agents, and in combination at 10:1, 1:1, and 1:10 molar ratios. The concentration-effect data from the five cytotoxicity curves were used to calculate CI values, at all effect levels, for each of the drug combinations. The calculation of the CI values for each of the three ratios was based on the Median-Effect Principle (7), and was completed using CompuSyn software (ComboSyn, Inc.; Paramus, New Jersey, US) (8).

Similarly, for the combination exposure time study, cytotoxicity curves were generated for 5-FU and CPT-11 as single agents following 1, 8, or 48 h of exposure, as well as for the drug combination at a 1:1 molar ratio following 1, 8, or 48 h of exposure. The exposure time-specific concentration-effect data were utilized to calculate CI values, across a range of effect levels, for the drug combination at the three different exposure times. The calculation of the CI values for each of the exposure times was based on the Median-Effect Principle (7), and was completed using CompuSyn software (8).

2.1.5. In Vitro Irinophore C™ Drug Retention Study

Irinophore C™ was prepared as described above, and then diluted in PBS (pH 7.4), 50% serum (v/v; in PBS; pH 7.4), or supplemented culture medium. Initial aliquots were taken to determine lipid and CPT-11 concentrations via the liquid scintillation counting (LSC) or HPLC analyses, respectively, as described above. Drug retention studies were conducted using 96-well plates. To each well containing 100 μL of diluent, 100 μL of Irinophore C™ was added to achieve a final concentration of 10 or 60 μM CPT-11. Plates were maintained at 37°C in a humidified, 5% CO_2 incubator for up to 72 h. Immediately upon addition of Irinophore C™ to the wells, and at various time points throughout the incubation, aliquots were taken and added to Sephadex™ G-50 spin columns equilibrated with PBS (pH 7.4). Columns were centrifuged for 3 min at 623 x *g* and the eluate was immediately stored at -70°C until HPLC and LSC analyses were performed. Drug-to-lipid ratios were calculated, relative to the initial sample.

2.1.6. Animals

All *in vivo* experiments were conducted using Rag2-M mice obtained from the British Columbia Cancer Research Centre's Animal Resource Centre (Vancouver, British Columbia, CA). All animal experiments were conducted in accordance with the Canadian Council on Animal Care Guidelines and all protocols were approved by the University of British Columbia Animal Care Committee. Mice were housed under standard conditions, with access to food and

water *ad libitum*, in the Animal Resource Centre at the British Columbia Cancer Agency's Research Centre.

2.1.7. Animal Models

2.1.7.1. Orthotopic CRC Model

Male Rag2-M mice (9-12 weeks old) were anaesthetized and the abdomen was prepared for surgery. Small incisions through the skin and abdominal wall were made to expose the spleen. Next, 5 x 10^6 LS174T cells, in 30 μL of HBSS, were injected under the capsule in the lower half of the spleen, and then the incisions were closed with sutures. To provide pain control, buprenorphine (0.1 mg/kg) was injected prior to surgery and every 6-12 h after surgery, as required. Following intra-splenic inoculation, cells migrated from the spleen to the liver, where they became lodged and developed into cancerous lesions, mimicking the hepatic metastases that are often associated with advanced CRC. Surgeries were completed by the Advanced Therapeutics Animal Research Technicians.

2.1.7.2. Subcutaneous CRC Model

The central lower back of male Rag2-M mice (6-9 weeks old) was shaved prior to cell inoculation. Mice were inoculated subcutaneously in the central dorsal posterior with 5 x 10^6 HT-29 cells, in 50 μL of unsupplemented medium. Rapidly growing solid tumors developed at the site of inoculation. Cell inoculations were performed by the Advanced Therapeutics Animal Research Technicians.

2.1.8. Pharmacokinetics/Biodistribution (PK/BD)

Naïve, male Rag2-M mice (8-10 weeks old; 4/time point/formulation) were injected intravenously via the lateral tail vein (i.v), with [^{3}H]CHE-labelled Irinophore C™ (40 mg CPT-11/kg), [^{14}C]5-FU (40 mg/kg), or a combination of the two agents at the same doses. At various time points post-injection, mice were euthanized via CO_2 asphyxiation. Blood was immediately collected via cardiac puncture, and centrifuged to separate the plasma. Organs were harvested and divided into 2 pieces; half of the plasma/organ was prepared for LSC of the associated radioactivity (lipid and 5-FU), while the other half of the plasma/organ was processed for high performance liquid chromatography (HPLC) analysis of the associated irinotecan and SN-38. To limit conversion between the lactone and carboxylate conformations, plasma samples and organs were kept on ice and stored at -70°C. Injections were performed by the Advanced Therapeutics Animal Research Technicians, who also provided assistance with organ harvesting.

In preparation for LSC, organs were solubilized and all samples were bleached. Scintillation cocktail was added to samples, and, following dark-equilibration, the radioactivity ([^{3}H]CHE and [^{14}C]5-FU) associated with the plasma and organs was quantitated via LSC. In preparation for HPLC analysis, the second half of each organ was homogenized in ice-cold water. Drug and metabolites were extracted from the homogenate using ice-cold acetonitrile/methanol (1:1 v/v) solution and centrifugation at 14,000 x *g* for 15 min to precipitate proteins. The supernatant was collected and the concentrations

of CPT-11 (lactone and carboxylate) and SN-38 (lactone and carboxylate) in the organ supernatant and plasma samples were determined via HPLC. HPLC analysis was completed as outlined by Ramsay *et al.* (9). Data are presented as μg of drug or μmol of lipid per gram of organ or per mL of plasma. Each point represents the mean +/- standard deviation (n = 4) from one experiment. HPLC analysis was completed by Ms. Malathi Anantha.

2.1.9. Therapeutic Effect

The dose-effect relationship of Irinophore C™ treatment was investigated in a subcutaneous xenograft model of CRC, described above. Dosing was initiated when tumor volumes reached ~100 mm^3 (day 15 post-inoculation). At 15, 22, and 29 days post-inoculation, mice (6/group) were injected intravenously via the lateral tail vein (i.v.) with saline, free CPT-11 (40 mg/kg), or Irinophore C™ (2.5, 5, 10, or 40 mg CPT-11/kg). Mice were weighed 2-3 times per week, and were monitored daily for signs of poor health indicating drug toxicity and/or disease progression. Data are presented as percent of initial body weight. Each point represents the group median (n = 6), calculated until fewer than 3 mice remained, from one experiment. Intersecting tumor dimensions were measured 2-3 times per week; tumor volume was calculated using $(ab^2)/2$ (a, larger dimension; b, smaller dimension). Mice were euthanized if body weight loss exceeded 20%, tumor volume exceeded 1000 mm^3, or if tumor ulceration or significant deteriorations in health were observed. Data are presented as tumor volume (mm^3) from one experiment. Each point represents the group median tumor

volume (n = 6), calculated until fewer than 3 mice remained. Survival data are presented as median group survival (days), as calculated by GraphPad Prism 5.00 software. Injections were performed by the Advanced Therapeutics Research Technicians.

The therapeutic activity of Irinophore C™ plus 5-FU was investigated in an orthotopic model of CRC, described above. At 7, 14, and 21 days after intra-splenic implantation of LS174T cells, mice (7/treatment group; 8 in control group) were injected i.v. with saline, free CPT-11 (40 mg/kg), 5-FU (40 mg/kg), Irinophore C™ (40 mg CPT-11/kg), free CPT-11 + 5-FU (40 mg/kg + 40 mg/kg), or Irinophore C™ + 5-FU (40 mg CPT-11/kg + 40 mg/kg). The mice were weighed 2-3 times per week, and were monitored daily for signs of poor health indicating drug toxicity and/or disease progression. Mice were euthanized if body weight loss exceeded 20% or if significant deteriorations in health were observed. Data are presented as group percent survival from one experiment. Median group (n = 7-8) survival time (days) was compared between treatments as a measure of therapeutic effect. Injections were performed by the Advanced Therapeutics Research Technicians.

The therapeutic potential of Irinophore C™ plus 5-FU was investigated in a subcutaneous xenograft model of CRC, described above. Dosing was initiated when tumor volumes reached 100-150 mm^3 (day 14 post-inoculation). Treatments were administered to mice (6/group) as follows: saline + D5W, 5-FU (16 mg/kg), free CPT-11 (60 mg/kg), Irinophore C™ (40 or 60 mg CPT-11/kg), free CPT-11 + 5-FU (60 mg/kg + 16 mg/kg), or Irinophore C™ + 5-FU (40 or 60

mg CPT-11/kg + 16 mg/kg). D5W and 5-FU were administered qdx5 (x 3 weeks) via intraperitoneal (i.p.) injection; all other treatments were administered i.v. q7dx3. When mice received both 5-FU and irinotecan/Irinophore C™ in one day, 5-FU was administered at least 2 h prior to the irinotecan/Irinophore C™. Mice were weighed 2-3 times per week, and were monitored daily for signs of poor health indicating drug toxicity and/or disease progression. Data are presented as percent of initial body weight from one experiment. Each point represents the group median body weight (n = 6), calculated until fewer than 3 mice remained. Intersecting tumor dimensions were measured 3 times per week; tumor volume was calculated using $(ab^2)/2$ (a, larger dimension; b, smaller dimension). Mice were euthanized if body weight loss exceeded 20%, if tumor volume exceeded 1000 mm^3, or if tumor ulceration or significant deteriorations in health were observed. Data are presented as fold tumor volume increase. Each point represents the group mean +/- standard deviation (n = 6) from one experiment. This study was completed by scientists from the Centre for Drug Research and Development (Vancouver, British Columbia, CA).

2.1.10. Statistical Analysis

Statistical significance for the PK/BD study was calculated via two-way analysis of variance (ANOVA) with Bonferroni post-test using GraphPad Prism 5.00 software. Survival curves for the dose-effect study and the orthotopic model therapeutic study were analyzed for significance via the log-rank test with

Bonferroni correction for multiple comparisons using GraphPad Prism 5.00 software.

2.2. Chapter 4

2.2.1. Materials

Cell culture media, FBS, penicillin/streptomycin/L-glutamine (P/S/G; 10,000 U/mL, 10,000 μg/mL, 29.2 mg/mL, respectively), and supplements were obtained from Gibco Laboratories Life Technologies, Inc. (Grand Island, New York, US). HSPC and DXR were kind gifts from Alza Pharmaceuticals, Inc. (Mountain View, California, US). All other lipids were purchased from Avanti Polar Lipids, Inc. Polycarbonate membranes for extrusion were purchased from Northern Lipids, Inc. (Burnaby, British Columbia, CA). VCR was produced by Tocris Cookson, Inc. (Ellisville, Missouri, US). [^{3}H]CHE, [^{125}I]sodium iodide, and Solvable™ were purchased from PerkinElmer, Inc. [^{3}H]Vincristine ([^{3}H]VCR) was obtained from Moravek Biochemicals, Inc. The CBQCA (ATTO-TAG™ CBQCA derivatization reagent) Protein Quantitation Kit was purchased from Molecular Probes, Inc. (Eugene, Oregon, US). IODO-Beads® were purchased from Pierce Biotechnology, Inc. (Rockford, Illinois, US). All other reagents were of analytical grade.

2.2.2. Antibodies and Peptides

The humanized αHER2 monoclonal antibody trastuzumab (Genentech, Inc.; South San Francisco, California, US) was purchased from the University of Alberta Hospital Pharmacy (Edmonton, Alberta, CA). Angiogenic vasculature-

specific peptide motifs NGR and cRGD were used as liposomal targeting ligands. The NGR peptide (NH2-GNGRGGVRSSSRTPSDKYC) was a custom synthesis by the American Peptide Company, Inc. (Sunnyvale, California, US). The mismatched control peptide (ARA; NH2-GARAGGVRSSSRTPSDKYC) was a custom synthesis by Sigma Genosys, Inc. (Oakville, Ontario, CA). The cyclic RGD (cRGD) peptide (c(RGDf(ε-S-acetylthioacetyl)K)) and the control cRAD peptide (c(RADf(ε-S-acetylthioacetyl)K)) were kind gifts from Prof. Dr. Gert Storm (Universiteit Utrecht, Heidelberglaan, Utrecht, NL). All peptides were coupled to liposomes via the formation of a covalent thioether bond between a free sulfhydryl group on the peptide (C-terminal cysteine of NGR and ARA peptides, and thioacetyl group on serine residue of cRGD and cRAD peptides) and the maleimide derivatization on the termini of the PEG groups anchored in the phospholipid bilayer.

2.2.3. Iodination of αHER2 Monoclonal Antibodies

The iodination of αHER2 monoclonal antibodies (mAb) was completed following the technique described by Lopes de Menezes *et al.* (10). Briefly, 1 mg of mAb in 300 μL of HBS (pH 7.4) was incubated with 185 MBq of [^{125}I]sodium iodide in the presence of IODO-Beads® at room temperature for 1 h. Iodinated antibodies were separated from unreacted [^{125}I]sodium iodide by size exclusion chromatography on a Sephadex™ G-25 column, equilibrated with HBS (pH 7.4). Iodination reaction was completed by Ms. Elaine Moase.

2.2.4. Cell Culture

The KS1767 Kaposi's sarcoma cell line was a kind gift from Dr. Renata Pasqualini (MD Anderson Cancer Center, Houston, Texas, US). The cells were cultured in MEM, supplemented with 10% (v/v) FBS, 1% (v/v) P/S/G, 1% (v/v) MEM vitamins, and 1% (v/v) non-essential amino acids. HUVEC were purchased from ATCC. The cells were cultured in Ham's Kaighn's Modification F12, supplemented with 10% (v/v) FBS, 1% (v/v) P/S/G, 0.1 mg/mL heparin, and 0.04 mg/mL endothelial cell growth supplement. The $4T1.2^{ErbB\text{-}2}$ murine mammary carcinoma cell line (retrovirally transduced to over-express human HER2) was a kind gift from Dr. Phillip K. Darcy (Peter MacCallum Cancer Institute, East Melbourne, Victoria, AU). The human embryonic kidney (HEK) 293 cell line was a kind gift from Dr. Susan Dunn (University of Alberta, Edmonton, Alberta, CA). The $4T1.2^{ErbB\text{-}2}$ and the HEK 293 cells were cultured in Dulbecco's modified Eagle's medium (DMEM), supplemented with 10% (v/v) FBS and 1% (v/v) P/S/G. All cell lines were sub-cultured one to three times per week for up to 20 generations. Cells were maintained in exponential growth, at 37°C in a humidified, 5% CO_2 incubator.

2.2.5. Preparation of Liposomal Drug

Stealth® (PEGylated) liposomes (SL) and Stealth® (PEGylated) immunoliposomes (SIL) were composed of HSPC:CHOL: mPEG-DSPE (with or without 1 mol% maleimide-derivatized PEG-DSPE as a coupling lipid) at a molar ratio of 2:1:0.1. [^{3}H]CHE or [^{14}C]cholesteryl oleate was included as lipid tracer.

The lipids were dissolved in chloroform, mixed at the appropriate ratio, dried by rotary evaporation, and then kept under vacuum to remove any residual solvent. The thin lipid film was hydrated in 250 mM $(NH_4)_2SO_4$, and was heated at 65°C and vortexed until homogeneous. The resulting liposomes were extruded through polycarbonate membranes with pore sizes of 0.4, 0.2, 0.1, or 0.08 μm to produce liposomes of approximately 100-120 nm in diameter. Unencapsulated $(NH_4)_2SO_4$ was removed by size exclusion chromatography on a Sephadex™ G-50 column, equilibrated with sodium acetate buffer (100 mM sodium acetate trihydrate, 70 mM NaCl; pH 5.5), or with 10% (w/v) sucrose solution.

When required, DXR and VCR were loaded using the ammonium sulfate gradient method (11). Doxorubicin or vincristine was added to the liposomes at the appropriate drug-to-lipid ratio (0.2 μmol doxorubicin/μmol phospholipid or 0.5 μg vincristine/μg total lipid), and the mixture was incubated at 65°C for 30 min or 60 min, respectively. [^{3}H]VCR was used as a tracer when required. Following drug loading, unencapsulated drug was removed by size exclusion chromatography on a Sephadex™ G-50 column, equilibrated with HEPES-buffered saline (HBS; pH 7.4). Vincristine encapsulation efficiency was determined by measuring the amount of loaded radio-labelled tracer; doxorubicin encapsulation efficiency was determined by measuring the absorbance at 480 nm. After preparation (or coupling, see below, when required), liposomes were stored at 4°C, and were passed through a 0.22 μm filter prior to use.

To prepare empty liposomes, the lipid film was formulated as above, hydration was completed in HBS (pH 7.4), and extrusion was performed as outlined above.

2.2.6. Preparation of Ligand-modified Liposomes

Immediately prior to coupling, NGR and ARA peptides were hydrated in de-gassed HBS (pH 7.4) at a concentration of 10 μg/μL. NGR- and ARA-modified PEGylated liposomes (NGR-SL and ARA-SL, respectively) were prepared by an overnight incubation of liposomes, containing the coupling lipid maleimide-PEG-DSPE, with the hydrated peptides (1:1 w/w), with continuous stirring at 4°C in an oxygen-free environment. Uncoupled peptides were removed by size exclusion chromatography on a Sepharose® CL-4B column, equilibrated with HBS (pH 7.4). When lower liposomal surface densities of NGR peptides were required, the coupling ratio was reduced as necessary. Coupling efficiency was determined using the CBQCA Protein Quantitation Kit.

In preparation for coupling, cRGD and cRAD peptides were activated by deacetylation of the acetyl-protected thioacetyl group at the lysine residue via incubation in deacetylation buffer (0.05 M HEPES, 0.05 M hydroxylamine hydrochloride, 0.03 mM EDTA; pH 7.0) at a concentration of 1 μg/μL for 30 min at room temperature. cRGD- and cRAD-modified PEGylated liposomes (cRGD-SL and cRAD-SL, respectively) were prepared by an overnight incubation of liposomes, containing the coupling lipid maleimide-PEG-DSPE, with freshly deacetylated peptides (5 nmol peptide/μmol total lipid), with continuous stirring at

4°C in an oxygen-free environment. Uncoupled peptides were removed by size exclusion chromatography on a Sepharose® CL-4B or Sephadex™ G-50 column, equilibrated with HBS (pH 7.4). Successful coupling of cRGD peptides to liposomes was determined by comparing the cellular association of the cRGD-SL and SL with the HUVEC or KS1767 cells *in vitro*.

Immediately before coupling, αHER2 monoclonal antibodies (in HBS; pH 8.0) were thiolated via a 1 h incubation with a 10-fold molar excess of 2-iminothiolane at room temperature. [^{125}I]-labelled αHER2 antibodies were included in trace amounts. Following thiolation, unreacted 2-iminothiolane was removed by size exclusion chromatography on a Sephadex™ G-50 column, equilibrated with de-gassed HBS (pH 8.0). To prepare αHER2-modified PEGylated immunoliposomes (αHER2-SIL), thiolated antibodies were immediately mixed with liposomes, containing the coupling lipid maleimide-PEG-DSPE, at a concentration of 100 μg antibody/μmol phospholipid; the mixture was incubated overnight with continuous stirring at 37°C in an oxygen-free environment. Uncoupled antibodies were removed by size exclusion chromatography on a Sepharose® CL-4B column, equilibrated with HBS (pH 7.4). Coupling efficiency was determined by quantitating the amount of coupled radio-labelled tracer.

2.2.7. In Vitro Cellular Association Studies

The cellular association studies were completed using radio-labelled liposomes following the radioactivity method described by Lopes de Menezes *et*

al. (12). Briefly, the assays were conducted using liposomes prepared with [^{3}H]CHE, a non-metabolizable, non-exchangeable lipid marker (4), at 2 μCi/μmol phospholipid, or [^{14}C]cholesteryl oleate at 0.5 μCi/μmol phospholipid. Drug-free liposomes were used in the cellular association assays, except where noted. In triplicate, 1 x 10^{6} 4T1.2^{ErbB-2} cells, KS1767 cells, HUVEC, or HEK 293 cells were incubated for 1 h at 4°C or 37°C with untargeted or ligand-modified liposomes at increasing phospholipid (PL) concentrations, to achieve a final PL concentration between 0.1 and 1.8 μmol PL/mL. The cells and liposomes were diluted in unsupplemented culture medium. After incubation, the cells were washed twice with ice-cold phosphate-buffered saline (PBS; pH 7.4) to remove unassociated liposomes, and the remaining cell-associated radioactivity was quantitated via LSC (Beckman LS-6500 or LS-6800 scintillation counter). Cellular association data are presented as nmol PL/10^{6} cells. Each point or bar represents the mean +/- standard deviation (n = 3) from one representative experiment.

2.2.7.1. Comparison of Radioactivity Method and Fluorescence Method

In order to determine whether the radioactivity method accurately quantitates liposomal cellular association, the radioactivity method and the fluorescence method were compared by using them in parallel to assess the cellular association of radio-labelled SL or NGR-SL, loaded with the fluorescent drug DXR.

In sextuplicate, 1 x 10^{6} KS1767 cells were incubated for with increasing PL concentrations of radio-labelled SL[DXR] or NGR-SL[DXR] for 1 h at 37°C.

Additional tubes containing 1 x 10^6 KS1767 cells were incubated with medium to be used when preparing the DXR standard curve, described below. After the 1 h incubation period, the cells were washed twice with ice-cold PBS (pH 7.4) to remove unassociated liposomes. Half of the samples underwent LSC to quantitate the remaining cell-associated radioactive lipid label. The other half of the samples, as well as those to be used in the preparation of the DXR standard curve, underwent a DXR extraction assay and were subsequently analyzed for DXR fluorescence via fluorometry.

The DXR extraction assay procedure was based on the method of Mayer *et al.* (13), with slight modification, as described by Laginha *et al.* (14). To extract the DXR, each sample tube received 1.5 mL of 0.075 N acidified isopropanol (90% isopropanol, 10% 0.75 N HCl; v/v), 100 μL of 10% (w/w) Triton X-100, 200 μL of distilled, de-ionized H_20, and 200 μL of PBS (pH 7.4), and was then stored at -20°C overnight. The samples were warmed to room temperature and vortexed for 5 min before being centrifuged at 15,000 x *g* for 20 min. The supernatant was decanted and fluorometrically analyzed for DXR fluorescence (excitation, 470 nm; emission, 590 nm). To account for non-specific background fluorescence, samples were analyzed against a DXR standard curve that was prepared by adding known amounts of free DXR (diluted in PBS, pH 7.4) to the cell blanks, described above. Cellular association data were converted from ng DXR to nmol PL based on the drug-to-lipid ratio of each liposome preparation (0.194, SL[DXR]; 0.209, NGR-SL[DXR]). Data are presented as nmol PL/10^6 cells. Each point represents the mean +/- standard deviation (n = 3) from one

representative experiment. Correlation between the cellular association data generated with the radioactivity method and the fluorescence method was determined via linear regression analysis, using GraphPad Prism 5.00 software.

2.2.7.2. Procedural Modifications to Radioactivity Method

Some experiments required alteration of the standard radioactivity method for assessing liposomal cellular association. Specific procedural modifications are detailed as follows. To gain further insight into the receptor-mediated endocytosis of the αHER2-SIL, receptor "stripping" experiments were completed (15, 16) using the 4T1.2^{ErbB-2} cells; following incubation and washing, the samples were subjected to two 10 min incubations with 50 mM glycine solution (pH 2.8) to remove surface proteins, or two 10 min incubations with PBS (pH 7.4) as a control. To determine how the cellular association of the αHER2-SIL was affected by the presence of excess free targeting ligand, the 4T1.2^{ErbB-2} cells were pre-incubated at 37°C for 15 min with 50-fold excess free αHER2 monoclonal antibody (diluted in HBS; pH 7.4) prior to liposome addition. To assess the time-course of cellular association with the 4T1.2^{ErbB-2} cells, the incubation period for the cells and liposomes was varied between 5 and 60 min. To assess the effect of diluent composition on cellular association, the KS1767 cells and liposomes were diluted in different combinations of PBS (pH 7.4) or MEM, alone or supplemented with 10% (v/v) FBS and/or 1% (v/v) P/S/G. To determine how the cellular association of the vasculature-targeted liposomes was affected by the presence of excess free targeting ligand, the HUVEC were pre-incubated at 37°C

for 15 min with 50-fold excess free cRGD or cRAD peptide (diluted in HBS; pH 7.4) prior to liposome addition.

2.2.8. In Vitro Cytotoxicity Assays

The 3-(4,5-dimethylthiazol-2-yl)-2,5-diphenyltetrazolium bromide (MTT) assay (17) was utilized to assess cell viability (mitochondrial activity) following *in vitro* exposure to several formulations of DXR and VCR. The cells (KS1767, 5,000 cells/well; 4T1.2^{ErbB-2}, 1,000 cells/well) were seeded in 96-well, flat-bottomed plates in complete medium. The plates were incubated overnight to allow for cell adherence. In triplicate, graded concentrations of free drug and untargeted and targeted liposomal drug were added to the cells, and incubated for 1 h at 37°C. After 1 h, the drug was washed out and replaced with fresh medium, and the plates were returned to the incubator for an additional 47 h (KS1767 cells) or 95 h (4T1.2^{ErbB-2} cells). At the end of the incubation period, MTT reagent (25 μg in unsupplemented medium) was added to the wells as previously described (17). The plates were incubated for a final 2-4 h before the fluorescence was measured at dual wavelengths of 570 and 650 nm with a microplate reader. Background fluorescence was subtracted from each well, and the fluorescence of treated cells was determined relative to the fluorescence of control cells. Cell viability data are presented as percent of control viability. Each point represents the mean +/- standard deviation (n = 3) from one representative experiment. Cytotoxicity data were fitted using a sigmoidal dose response – fixed slope equation (GraphPad Prism 5.00 software), which also calculated the IC_{50} values.

2.2.9. Statistical Analysis

Statistical comparison of liposomal cellular association was completed at the highest PL concentration tested, via one-way ANOVA with Tukey's Multiple Comparison Test, two-way ANOVA with Bonferroni post-test, or Student's t-test (two-tailed), using GraphPad Prism 5.00 software.

2.3. Chapter 5

2.3.1. Materials

MEM, DMEM, FBS, and P/S/G (10,000 U/mL, 10,000 μg/mL, 29.2 mg/mL, respectively) were obtained from Gibco Laboratories Life Technologies, Inc. HSPC and DXR were kind gifts from Alza Pharmaceuticals, Inc. All other lipids were purchased from Avanti Polar Lipids, Inc. Polycarbonate membranes for extrusion were purchased from Northern Lipids, Inc. VCR powder was produced by Tocris Cookson, Inc. [^{3}H]CHE, [^{125}I]sodium iodide, Solvable™, and Ultima Gold™ were purchased from PerkinElmer, Inc. [^{14}C]Doxorubicin ([^{14}C]DXR), [^{14}C]cholesteryl oleate, Sephadex™ G-50, and Sephadex™ G-25 were purchased from Amersham Biosciences Corp. (Piscataway, New Jersey, US). [^{3}H]VCR was obtained from Moravek Biochemicals. The CBQCA Protein Quantitation Kit was purchased from Molecular Probes, Inc. Immobilized pepsin was purchased from Pierce Biotechnology, Inc. Dithiothreitol (DTT) was purchased from Fisher Scientific Company (Ottawa, Ontario, CA). 2-iminothiolane and Sepharose® CL-4B were obtained from Sigma-Aldrich Co. All other reagents were of analytical grade.

2.3.2. Antibodies and Peptides

The αHER2 antibody trastuzumab was purchased from the University of Alberta Hospital Pharmacy. The NGR peptide (NH2-GNGRGGVRSSSRTPSDKYC) was a custom synthesis by the American Peptide Company, Inc. The ARA peptide (NH2-GARAGGVRSSSRTPSDKYC) was a custom synthesis by Sigma Genosys, Inc. The cyclic RGD (cRGD) peptide (c(RGDf(ε-S-acetylthioacetyl)K)) and the control cRAD peptide (c(RADf(ε-S-acetylthioacetyl)K)) were kind gifts from Prof. Dr. Gert Storm.

2.3.3. Generation of αHER2 F(ab′)$_2$ Fragments

The αHER2 monoclonal antibodies were hydrated in digestion buffer (20 mM sodium acetate trihydrate; pH 4.5) and were combined with immobilized pepsin, according to product specifications. A 14 h incubation at 37°C, with constant agitation, was required for optimal degradation of the Fc region to yield F(ab′)$_2$ fragments. The digestion was quenched by the addition of 1 M tris base (pH 10.0). The F(ab′)$_2$ fragments were exchanged into HBS (pH 8.0) for coupling.

2.3.4. Iodination of αHER2 Monoclonal Antibodies and αHER2 F(ab')$_2$ Fragments

The iodination reactions were completed following the technique described by Lopes de Menezes et al. (10). Briefly, 1 mg of mAb or F(ab')$_2$ fragments, in 300 μL of HBS (pH 7.4), was incubated with 185 MBq of [^{125}I]sodium iodide in the presence of IODO-Beads® at room temperature for 1 h. Iodinated antibodies

or Fab′ fragments were separated from unreacted [^{125}I]sodium iodide by size exclusion chromatography on a Sephadex™ G-25 column, equilibrated with HBS (pH 7.4). Iodination reactions were completed by Ms. Elaine Moase.

2.3.5. Preparation of Liposomal Drug

The phospholipid bilayers of Stealth® (PEGylated) liposomes and Stealth® (PEGylated) immunoliposomes were composed of HSPC:CHOL:mPEG-DSPE, with or without 1 mol% maleimide-derivatized PEG-DSPE as a coupling lipid, at a molar ratio of 2:1:0.1. [^{3}H]CHE was included in trace amounts or at 2 μCi/μmol phospholipid; alternatively, [^{14}C]cholesteryl oleate was included in trace amounts or at 0.5 μCi/μmol phospholipid. The lipids were dissolved in chloroform, mixed at the appropriate ratio, dried by rotary evaporation and then kept under vacuum to remove any residual solvent. The thin lipid film was hydrated in 250 mM $(NH_4)_2SO_4$, and was heated at 65°C and vortexed until hydrated. The resulting liposomes were extruded through polycarbonate membranes with pore sizes of 0.4, 0.2, 0.1 or 0.08 μm to produce liposomes of approximately 100-120 nm in diameter.

Unencapsulated $(NH_4)_2SO_4$ was removed by size exclusion chromatography on a Sephadex™ G-50 column, equilibrated with sodium acetate buffer (100 mM sodium acetate trihydrate, 70 mM NaCl; pH 5.5), or with 10% (w/v) sucrose solution. DXR or VCR was added to the liposomes at the appropriate drug-to-lipid ratio (0.2 μmol DXR/μmol phospholipid or 0.5 μg VCR/μg total lipid), and the mixture was incubated at 65°C for 30 min or 60 min, respectively. [^{14}C]DXR

or [^{3}H]VCR were used as tracers when required. Following drug loading, unencapsulated drug was removed by size exclusion chromatography on a Sephadex™ G-50 column, equilibrated with HBS (pH 7.4). VCR encapsulation efficiency was determined by measuring the amount of loaded radio-labelled tracer; DXR encapsulation efficiency was determined by measuring the absorbance at 480 nm. Liposomes were stored at 4°C, and were passed through a 0.22 μm filter prior to use.

To prepare empty liposomes, the lipid film was formulated as above, hydration was completed in HBS (pH 7.4), and extrusion was performed as outlined above. Sterile-filtration and storage were as described.

2.3.6. Preparation of Ligand-modified Liposomes

Immediately prior to coupling the NGR and ARA peptides to liposomes via their free C-terminal cysteine residues, the peptides were hydrated in de-gassed HBS (pH 7.4) at a concentration of 10 μg/μL. NGR- and ARA-modified PEGylated liposomes (NGR-SL and ARA-SL, respectively) were prepared by an overnight incubation of liposomes, containing the coupling lipid maleimide-PEG-DSPE, with the hydrated peptides (1:1 w/w), with continuous stirring at 4°C in an oxygen-free environment. Uncoupled peptides were removed by size exclusion chromatography on a Sepharose® CL-4B column, equilibrated with HBS (pH 7.4). Coupling efficiency was determined using the CBQCA Protein Quantitation Kit.

In preparation for coupling, cRGD and cRAD peptides were activated by deacetylating the acetyl-protected thioacetyl group at the lysine residue.

Activation was accomplished by incubating the peptides in deacetylation buffer (0.05 M HEPES, 0.05 M hydroxylamine hydrochloride, 0.03 mM EDTA; pH 7.0) at a concentration of 1 μg/μL for 30 min at room temperature. cRGD- and cRAD-modified PEGylated liposomes (cRGD-SL and cRAD-SL, respectively) were prepared by an overnight incubation of liposomes, containing the coupling lipid maleimide-PEG-DSPE, with freshly deacetylated peptides (5 nmol peptide/μmol total lipid), with continuous stirring at 4°C in an oxygen-free environment. Uncoupled peptides were removed by size exclusion chromatography on a Sepharose® CL-4B or Sephadex™ G-50 column, equilibrated with HBS (pH 7.4). An *in vitro* cellular association assay (see 2.3.11) was used to determine the successful coupling of cRGD peptides to the liposomes; verification of coupling was taken as a significantly greater degree of cellular association of the cRGD-modified liposomes, than of the untargeted or cRAD-modified liposomes, with the KS1767 cells.

Immediately before coupling, αHER2 monoclonal antibodies (in HBS, pH 8.0) were thiolated via a 1 h incubation with a 10-fold molar excess of 2-iminothiolane at room temperature. [^{125}I]-labelled αHER2 antibodies were included in trace amounts. Following thiolation, unreacted 2-iminothiolane was removed by size exclusion chromatography on a Sephadex™ G-50 column, equilibrated with de-gassed HBS (pH 8.0). To prepare αHER2-modified PEGylated immunoliposomes (αHER2-SIL), thiolated antibodies were immediately mixed with liposomes, containing the coupling lipid maleimide-PEG-DSPE, at a concentration of 100 μg antibody/μmol phospholipid, and the

mixture was incubated overnight with continuous stirring at 4°C in an oxygen-free environment. Uncoupled antibodies were removed by size exclusion chromatography on a Sepharose® CL-4B column, equilibrated with HBS (pH 7.4). Coupling efficiency was determined by quantitating the amount of coupled radio-labelled tracer.

For the coupling of αHER2 Fab′ fragments to liposomes, just prior to coupling, the disulfide bonds in the hinge region of the αHER2 $F(ab')_2$ fragments were reduced using a 5 mM DTT solution for 15-20 min at room temperature. [^{125}I]-labelled αHER2 $F(ab')_2$ fragments were included in trace amounts. The resulting αHER2 Fab′ fragments, possessing a free terminal thiol group, were separated from unreacted DTT via size exclusion chromatography on a Sephadex™ G-25 column, equilibrated with de-gassed HBS (pH 8.0). αHER2 Fab′-modified PEGylated immunoliposomes (αHER2 Fab′-SIL) were prepared by an overnight incubation liposomes, containing the coupling lipid maleimide-PEG-DSPE, with Fab′ fragments (60 μg Fab′/μmol phospholipid), with continuous stirring at 4°C in an oxygen-free environment. Uncoupled Fab′ fragments were removed by size exclusion chromatography on a Sepharose® CL-4B column, equilibrated with HBS (pH 7.4). Coupling efficiency was determined by measuring the amount of coupled radio-labelled tracer.

2.3.7. Cell Culture

The 4T1 murine mammary carcinoma cells were purchased from the ATCC. The 4T1.2^{ErbB-2} cells (a mouse mammary carcinoma clone, retrovirally transduced

to over-express human HER2) were generously provided by Dr. Phillip K. Darcy. Cells were cultured in MEM (4T1) or DMEM (4T1.2^{ErbB-2}), supplemented with 10% (v/v) FBS, and 1% (v/v) P/S/G, and were maintained in a humidified 37°C and 5% CO_2 environment.

2.3.8. Animals

Female BALB/c SCID (CBySmn.CB17-*Prkdc*^{scid}/J) or ICR SCID (ICRSC-M-F; IcrTac:ICR-*Prkdc*^{scid}) mice (4-6 or 6-8 weeks old) were purchased from The Jackson Laboratory (Bar Harbor, Maine, US) or Taconic Farms, Inc. (Hudson, New York, US), respectively, and were kept in virus antigen-free conditions in the Health Sciences Laboratory Animal Services housing facility. As a prophylactic measure, Novo-Trimel® was added to the drinking water of all SCID mice. Inbred 6-8 week old, female BALB/c Cr/Alt BM mice were obtained from Health Sciences Laboratory Animal Services at the University of Alberta and were kept in standard housing. All experiments were approved by the Health Sciences Animal Policy and Welfare Committee of the University of Alberta.

2.3.9. Animal Models

2.3.9.1. Orthotopic Breast Cancer Model

A mouse model of orthotopic breast cancer was utilized for *in vivo* investigation of the dual-targeted approach. Methoxyflurane was used to induce and maintain surgical plane anaesthesia in the mice. At the start of surgery, the abdomen was shaved and sterilized (with Betadine®), and a small skin incision was made near the mammary fatpad. The fatpad was exposed, and 1 x 10^4 4T1 or

4T1.2^{ErbB-2} cells, in 10 μL of unsupplemented medium, were slowly injected into the fatpad. The incision was closed with tissue adhesive or a wound clip, which was removed 7 days post-surgery. Tumors became palpable between 7 and 10 days post-implantation, and typically reached 1000 mm^3 between 20 and 25 days post-implantation. Technical assistance during surgery was provided by Ms. Elaine Moase.

2.3.9.2. Subcutaneous Breast Cancer Model

To compare the PK/BD of two different lipid doses of the SL and NGR-SL, a subcutaneous model of breast cancer was established using female BALB/c or BALB/c SCID mice (6-8 weeks old). Following the induction of a brief period of anaesthesia using methoxyflurane, mice were prepared for cell inoculation by shaving the right rear flank and swabbing the area with ethanol. Subsequently, 5 x 10^5 4T1 or 4T1.2^{ErbB-2} cells, in 0.1 mL of unsupplemented medium, were slowly injected subcutaneously into the prepared flank. Tumors became palpable between 8 and 11 days post-inoculation. Technical assistance during inoculation was provided by Ms. Elaine Moase.

2.3.10. Pharmacokinetics/Biodistribution

In order to determine the *in vivo* fate of the encapsulated drug and the liposomes, PK/BD experiments were conducted in 6-8 week old, female, 4T1 tumor-bearing BALB/c mice, or female BALB/c SCID or ICR SCID mice bearing 4T1.2^{ErbB-2} tumors, using dual radio-labelled liposomes ([^{3}H]CHE and [^{14}C]DXR or [^{14}C]cholesteryl oleate and [^{3}H]VCR). The liposomes were injected at 10-18

days post-cell implantation. Mice (3/time point) were injected i.v. with untargeted, NGR-, ARA-, cRGD-, cRAD-, αHER2-, or αHER2 Fab′-modified drug-loaded liposomes at a dose of 3 mg DXR/kg or 1.5 mg VCR/kg. For the study comparing the PK/BD of two different lipid doses of SL and NGR-SL, radio-labelled, drug-free liposomes were injected at 0.5 or 2.5 μmol PL/mouse. At different time points post-injection, mice were euthanized via halothane or isoflurane overdose and cervical dislocation. The blood and major organs were harvested, solubilized with Solvable™, bleached with 30% hydrogen peroxide, and mixed with Ultima Gold™ before the radio-labelled lipid and drug were quantitated via liquid scintillation counting. Data are presented as percent of injected dose of lipid +/- standard deviation (n = 3). The drug-to-lipid ratio for untargeted liposomes was calculated as the ratio of percent of injected drug dose to percent of injected lipid dose at each time point, and was normalized to the drug-to-lipid ratio at the time of injection. Injections were performed by Ms. Elaine Moase, who also provided assistance with organ harvesting in the first PK/BD study.

2.3.11. In Vitro Cellular Association Studies

The *in vitro* cellular association assays were conducted with liposomes prepared with [^{3}H]CHE, a non-metabolizable, non-exchangeable lipid marker (4). Increasing phospholipid concentrations of SL, αHER2-SL, or αHER2 Fab′-SIL were incubated with 1 x 10^6 4T1.2^{ErbB-2} cells for 1 h at 37°C, suspended in unsupplemented medium. After incubation, cells were washed twice with ice-

cold PBS (pH 7.4) and the remaining cell-associated radioactivity was quantitated by LSC. Data are presented as nmol PL/10^6 cells +/- standard deviation (n = 3). Results from one representative experiment are presented.

When required, verification of coupling of the cRGD peptides to liposomes prepared for *in vivo* analysis was completed by conducting a cellular association assay, as described above, with the cRGD-SL[VCR] and the KS1767 cells. The assay was completed in parallel with the NGR-SL and ARA-SL as positive and negative controls, respectively. Successful coupling was taken as the demonstration of greater cellular association of the cRGD-SL, relative to the SL or cRAD-SL, with the KS1767 cells.

2.3.12. In Vitro Cytotoxicity Assays

The sensitivity of 4T1.2^{ErbB-2} cells to VCR was tested *in vitro* using the MTT assay (17). The cells were seeded at 8,000 cells/well in 96-well, flat-bottomed plates in complete medium. The plates were incubated overnight to allow for cell adherence. In triplicate, graded concentrations of free VCR were added to the cells, and incubated for 1 h at 37°C. After 1 h, the drug was washed out and replaced with fresh medium, and the plates were returned to the incubator for an additional 47 h. At the end of the incubation period, MTT reagent (25 μg in unsupplemented medium) was added to the wells as previously described (17). The plates were incubated for a final 2-4 h before the fluorescence was measured at dual wavelengths of 570 and 650 nm. Background fluorescence was subtracted from each well, and the fluorescence of treated cells was determined relative to

the fluorescence of control cells. Cell viability data are presented as percent of control viability. Each point represents the mean +/- standard deviation (n = 3) from one representative experiment. Cytotoxicity data were fitted using a sigmoidal dose response – fixed slope equation (GraphPad Prism 5.00 software), which also calculated the IC_{50} values.

2.3.13. Therapeutic Effect

The *in vivo* effectiveness of the dual-targeted combination approach was investigated using a mouse model of orthotopic HER2-positive breast cancer, outlined above. On various days post-implantation, 4-6 week old, female ICR SCID mice (6-8/group) received i.v. injections of saline, tumor-targeted, and/or vasculature-targeted liposomes. VCR-loaded liposomes were dosed at 0.75 or 1.5 mg VCR/kg; DXR-loaded liposomes were dosed at 1.5 or 3 mg DXR/kg. In one study, DXR-loaded liposomes were administered at a reduced dose of 2.5 mg DXR/kg following the observation of drug toxicity in the form of body weight loss. The health of the mice was monitored daily and intersecting tumor dimensions were measured twice per week as an assessment of therapeutic effect. Tumor volume was calculated using the formula $0.4ab^2$, where 'a' is the smaller dimension and 'b' is the larger dimension. Mice were euthanized if significant deteriorations in health (including significant weight loss) were observed, if tumor volume exceeded 1000 mm^3, or if the tumor ulcerated through the skin. Data are presented as median tumor volume (mm^3). Injections were completed by Ms. Elaine Moase.

2.3.14. Temporal Timing and Tumor Accumulation of Liposomes

The HER2-positive breast cancer model, described above, was utilized to investigate whether treatment of tumors with vasculature-targeted liposomes during the initial phase of vasculogenesis affected the tumor accumulation of a second dose of injected liposomes. At the start of vascular development, which is day 7 post-implantation in the orthotopic model, described above, mice (3-5/time point/treatment) received an i.v. injection of one of the following three treatments: vasculature-targeted therapy (NGR-SL[VCR]) at 1.5 mg VCR/kg, control liposomes (empty NGR-SL) at an equivalent lipid dose, or tumor-targeted therapy (αHER2 Fab′-targeted liposomal DXR; αHER2 Fab′-SIL[DXR]) at 3 mg DXR/kg. All mice also received an i.v. injection of 3 mg DXR/kg of dual radio-labelled αHER2 Fab′-SIL[DXR] liposomes, either simultaneously with, or at 4, 7, or 11 days after, the pre-treatment. At 48 h post-injection of the second dose of liposomes, the biodistribution of the radio-labelled carrier ([^{3}H]CHE) and drug ([^{14}C]DXR) were determined as outlined for the PK/BD experiment. Data are presented as percent of injected dose per gram of tumor +/- standard deviation (n = 3). Injections were completed by Ms. Elaine Moase.

2.3.15. Statistical Analysis

Statistical analysis was performed using GraphPad Prism 5.00 software. Statistical significance for the cellular association assays was calculated using one-way ANOVA with Tukey's Multiple Comparison Test. Statistical significance for the PK/BD studies was calculated using the two-tailed Student's

t-test, one-way ANOVA with Tukey's Multiple Comparison Test, or two-way ANOVA with Bonferroni post-test. Statistical significance for the temporal sequencing study was calculated using two-way ANOVA with Bonferroni post-test.

2.4. References – Chapter 2

1. Ramsay E, Alnajim J, Anantha M, Zastre J, Yan H, Webb M, Waterhouse D, Bally M. A novel liposomal irinotecan formulation with significant anti-tumour activity: use of the divalent cation ionophore A23187 and copper-containing liposomes to improve drug retention. *Eur. J. Pharm. Biopharm.* 2008; 68: 607-617.

2. Hope MJ, Bally MB, Mayer LD, Janoff AS, Cullis PR. Generation of multilamellar and unilamellar phospholipid vesicles. *Chem. Phys. Lipids* 1986; 40: 89-96.

3. Hope MJ, Bally MB, Webb G, Cullis PR. Production of large unilamellar vesicles by a rapid extrusion procedure. Characterization of size distribution, trapped volume and ability to maintain a membrane potential. *Biochim. Biophys. Acta* 1985; 812: 55-65.

4. Pool GL, French ME, Edwards RA, Huang L, Lumb RH. Use of radiolabelled hexadecyl cholesterol ether as a liposome marker. *Lipids* 1982; 17: 445-452.

5. Fields RD, Lancaster MV. Dual-attribute continuous monitoring of cell proliferation/cytotoxicity. *Am. Biotechnol. Lab.* 1993; 11: 48-50.

6. Page B, Page M, Noel C. A new fluorometric assay for cytotoxicity measurements in vitro. *Int. J. Oncol.* 1993; 3: 473-476.

7. Chou TC, Talalay P. Quantitative analysis of dose-effect relationships: the combined effects of multiple drugs or enzyme inhibitors. *Adv. Enzyme Regul.* 1984; 22: 27-55.

8. Chou TC. Theoretical basis, experimental design, and computerized simulation of synergism and antagonism in drug combination studies. *Pharmacol. Rev.* 2006; 58: 621-681.

9. Ramsay EC, Anantha M, Zastre J, Meijs M, Zonderhuis J, Strutt D, Webb MS, Waterhouse D, Bally MB. Irinophore C: a liposome formulation of irinotecan with substantially improved therapeutic efficacy against a panel of human xenograft tumors. *Clin. Cancer Res.* 2008; 14: 1208-1217.

10. Lopes de Menezes DE, Pilarski LM, Allen TM. In vitro and in vivo targeting of immunoliposomal doxorubicin to human B-cell lymphoma. *Cancer Res.* 1998; 58: 3320-3330.

11. Bolotin EM, Cohen R, Bar LK, Emanuel SN, Lasic DD, Barenholz Y. Ammonium sulphate gradients for efficient and stable remote loading of amphipathic weak bases into liposomes and ligandosomes. *J. Liposome Res.* 1994; 4: 455-479.

12. Lopes de Menezes DE, Pilarski LM, Belch AR, Allen TM. Selective targeting of immunoliposomal doxorubicin against human multiple myeloma *in vitro* and *ex vivo*. *Biochim. Biophys. Acta* 2000; 1466: 205-220.

13. Mayer LD, Dougherty G, Harasym TO, Bally MB. The role of tumor-associated macorphages in the delivery of liposomal doxourbicin to solid murine fibrosarcoma tumors. *J. Pharmacol. Exp. Ther.* 1997; 280: 1406-1414.

14. Laginha KM, Verwoert S, Charrois GJ, Allen TM. Determination of doxorubicin levels in whole tumor and tumor nuclei in murine breast cancer tumors. *Clin. Cancer Res.* 2005; 11: 6944-6949.

15. Tagliabue E, Centis F, Campiglio M, Mastroianni A, Martignone S, Pellegrini R, Casalini P, Lanzi C, Menard S, Colnaghi MI. Selection of monoclonal antibodies which induce internalization and phosphorylation of p185HER2 and growth inhibition of cells with HER2/NEU gene amplification. *Int. J. Cancer* 1991; 47: 933-937.

16. Yarden Y, Gabbay M, Schlessinger J. Primary amines do not prevent the endocytosis of epidermal growth factor into 3T3 fibroblasts. *Biochim. Biophys. Acta* 1981; 674: 188-203.

17. Mosmann T. Rapid colorimetric assay for cellular growth and survival: application to proliferation and cytotoxicity assays. *J. Immunol. Methods* 1983; 65: 55-63.

CHAPTER 3

Treatment of Colorectal Cancer Using a Combination of Liposomal Irinotecan (Irinophore C™) and 5-Fluorouracil

(Prepared for submission to the Journal of Controlled Release)

3. Treatment of Colorectal Cancer Using a Combination of Liposomal Irinotecan (Irinophore C™) and 5-Fluorouracil

3.1. Introduction

CRC is the fourth-leading cause of cancer death worldwide (1). One current first-line CRC treatment regimen is FOLFIRI (leucovorin, 5-FU, and CPT-11), with or without bevacizumab (2-6). Declines in CRC patient mortality rates of 1.3% per year for males and 1.7% per year for females have recently been reported, and have been attributed to improvements in chemotherapy and other treatment modalities (7). However, these improvements in survival are modest, highlighting the need for additional research to develop new treatment strategies that significantly improve the current standard-of-care options. It is well-established that chemotherapy drugs are most effective when given in combination, and it is now being recognized that combination chemotherapy is readily applicable to liposomal nanomedicines. This chapter outlines *in vitro* and pre-clinical *in vivo* work investigating the novel combination of 5-FU and Irinophore C™ as a treatment for CRC.

Irinotecan is a water-soluble drug that can be hydrolyzed to its 100- to 1,000-fold more potent hydrophobic metabolite, SN-38 (8, 9), via the action of non-specific plasma, liver, gastrointestinal, and tumor carboxylesterases (10, 11, and references therein, 12). Irinotecan and SN-38 are S-phase-specific agents that inhibit topoisomerase I, an enzyme that causes DNA unwinding during replication. The principal clinical problem limiting the utility of irinotecan

therapy is that nearly 90% of patients experience potentially life-threatening delayed-onset diarrhea (13), due to excessive secretion of water and electrolytes into the intestinal lumen as a result of abnormal ion transport in the damaged intestinal mucosa (14). The combination of gastric sloughing with concomitant neutropenia can lead to sepsis, which is the ultimate cause of death in this population. It is postulated that the intestinal damage is caused by high local concentrations of SN-38 generated by gut carboxylesterases (15, 16). A secondary limitation to use of irinotecan is that both the parent drug and SN-38 undergo a pH-dependent hydrolytic conversion from an active lactone configuration at acidic pH, to an inactive carboxylate configuration at physiological pH, limiting the dose of active drug that reaches the target (17-20).

The toxicities and the instability of irinotecan can be ameliorated through the use of drug delivery systems, such as lipidic nanoparticles or liposomes. A novel lipid-based formulation of irinotecan (Irinophore C™) was recently developed in the Bally laboratory (21). Irinophore C™ is a formulation of 100 nm diameter, unilamellar, DSPC:CHOL (55:45 molar ratio) liposomes with an acidic aqueous interior (unbuffered $CuSO_4$) in which irinotecan is encapsulated with the use of the calcium ionophore A32187 (22). The ionophore-based loading method and the purported drug-metal precipitate formed via Cu^{2+} ion-irinotecan interaction in the liposome core are thought to be critical to the excellent drug retention properties exhibited by the liposomes *in vivo* (22-24).

Irinophore C™ has demonstrated significantly improved therapeutic activity and reduced side effects, relative to free irinotecan, when administered to mice

bearing human tumor xenografts. Compared to free irinotecan, the PK/BD profile of the liposomal drug is significantly altered, with a 1,000-fold increase in plasma AUC for free and encapsulated CPT-11 lactone, and increased CPT-11 and SN-38 concentrations in the tumor (21). Prolonged exposure to the active drug species contributes to the significantly greater tumor growth inhibition that is observed following administration of Irinophore C™, relative to free CPT-11 (21). Furthermore, in plasma carboxylesterase-deficient mice, Irinophore C™ has been administered at doses of up to 350 mg CPT-11/kg without obvious side effects (21); this represents a vast improvement in irinotecan's safety profile relative to its administration as a free drug, which has a maximum tolerated dose of 80 mg/kg in the same strain of mice (21). This observation has now been extended to Sprague-Dawley rats, in which free drug is tolerated to a maximum of 170 mg/kg before gross morbidity, in the form of diarrhea, dehydration, weight loss and lethargy, is observed; in contrast, Irinophore C™ can be administered at 800 mg CPT-11/kg with little overt toxicity (D. Waterhouse, unpublished data).

As discussed above, free irinotecan and 5-FU plus leucovorin are part of current standard-of-care therapy for CRC (5, 25, 26). It was hypothesized that the therapeutic effect of the combination of irinotecan plus 5-FU could be improved by increasing tumor cell exposure to the lactone conformation of CPT-11 through the use of a liposomal carrier, and that the combination of Irinophore C™ plus 5-FU could be a well-tolerated, effective CRC treatment. This chapter describes the first investigation of the use of Irinophore C™, or any liposomal formulation of irinotecan, in combination with 5-FU for the treatment of CRC.

3.2. Results

3.2.1. Cytotoxicity of Irinophore C™ In Vitro

Cell viability assays were conducted *in vitro* to compare the ability of free and liposomal irinotecan to mediate cytotoxicity against the LS174T and HT-29 human CRC cell lines. After an exposure period of 72 h, Irinophore C™ and free CPT-11 produced equal cytotoxicity against both cell lines, with half maximal inhibitory concentration (IC_{50}) values of 1.5 μM (LS174T) and 60 μM (HT-29). After showing that free and liposomal CPT-11 caused equal cytotoxicity against the two CRC cell lines after 72 h of exposure, exposure times between 1-72 h were investigated to determine whether differences in cytotoxicity were apparent after shorter periods of drug exposure. Free and liposomal CPT-11 produced equivalent cytotoxicity, which was dependent on exposure time, against the LS174T cells (Fig. 3.1A) and the HT-29 cells (Fig. 3.1B) *in vitro*. When tested against the HT-29 cells, the IC_{50} value for both free CPT-11 and Irinophore C™ decreased with increased exposure time (Fig. 3.1B), however, differences in the maximum cytotoxicity of free and liposomal CPT-11 were apparent at the early time points (1, 4, and 8 h). As was observed in the exposure time dependency experiments (discussed below) with free CPT-11 and the HT-29 cells, the maximal cytotoxic effect was not achieved with the free drug following an exposure period of 1, 4, or 8 h. In contrast, the liposomal formulation of CPT-11 was more effective than the free drug after 4 and 8 h of drug exposure. After 4 and 8 h of exposure, the highest concentrations of Irinophore C™ were able to achieve close to 100% of the maximal cytotoxicity.

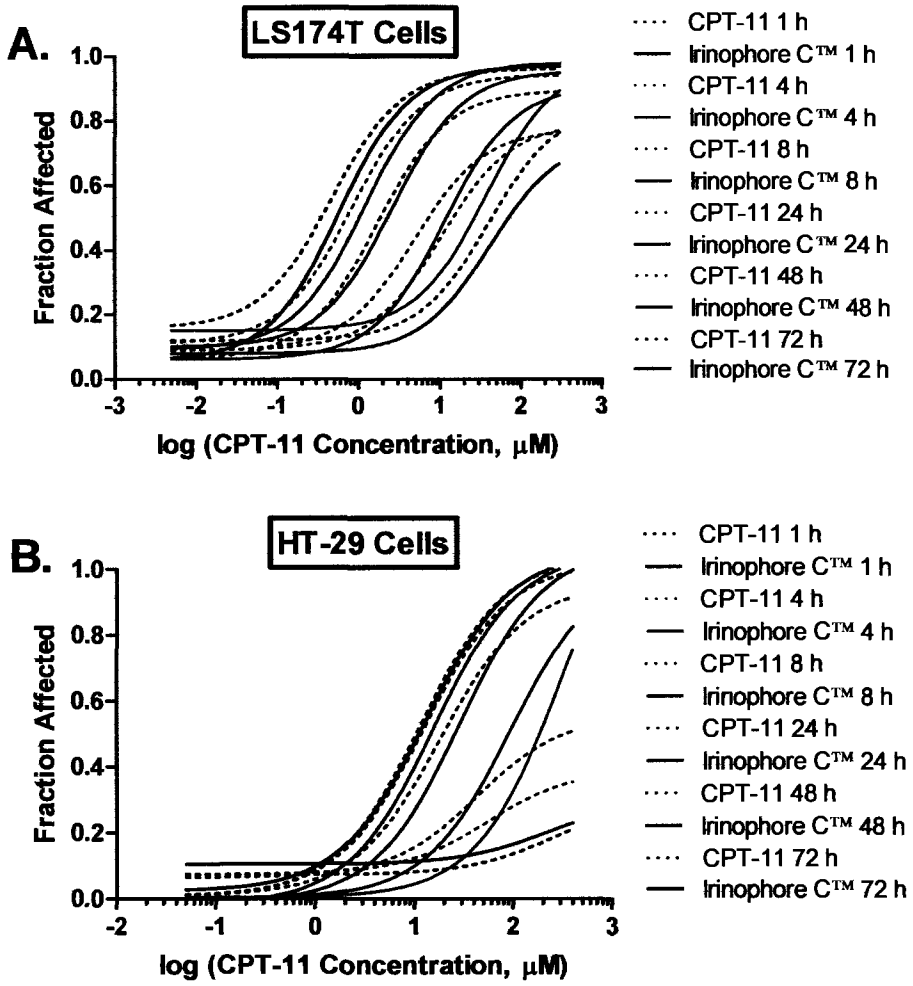

Figure 3.1. Exposure time dependency of Irinophore C™ cytotoxicity *in vitro*.

The LS174T (A) and HT-29 (B) cells were exposed to a range of concentrations of Irinophore C™ or free CPT-11 for 1, 4, 8, 24, 48, or 72 h. At 72 h after the start of drug incubation, cell viability was determined using the alamarBlue® assay, and was expressed as fraction affected (vs. control). Curves were drawn based on mean fraction affected +/- standard deviation (n = 3-9), collected over a range of concentrations, compiled from 2-3 experiments.

3.2.2. Irinophore C™ Drug Retention

The drug retention properties of Irinophore C™ were examined to determine whether the unexpectedly effective cytotoxicity achieved by liposomal CPT-11 at the early time points could be attributed to rapid drug release. Although Irinophore C™ is known to be stable in PBS, it was necessary to investigate whether a factor present in the medium or serum led to rapid and substantial drug leakage. The results of the Irinophore C™ drug retention studies are presented in Fig. 3.2. When Irinophore C™ was diluted to 10 μM CPT-11 in supplemented medium or 50% serum, the drug was well-retained for ~2 h before leakage was observed ($t_{1/2}$ = ~4 h). When Irinophore C™ was diluted to 60 μM in supplemented medium, slow leakage of ~50% of the CPT-11 was observed over the first 8 h, but no further drug leakage was observed beyond 8 h. Over the course of 72 h, very limited drug release was observed when Irinophore C™ was diluted in PBS, even when testing low drug concentrations (i.e., 10 μM).

3.2.3. Exposure Time Dependency

In order to investigate how the interaction between CPT-11 and 5-FU was affected by exposure time, it was first necessary to examine how the cytotoxicity of each drug as a single agent was affected by exposure time. The data presented in Fig. 3.3A reveal that both 5-FU and CPT-11 elicit cytotoxicity against the LS174T cells (Fig. 3.3A,B) and the HT-29 cells (Fig. 3.3C,D) in an exposure time-dependent manner, demonstrating lower IC_{50} values with prolonged drug

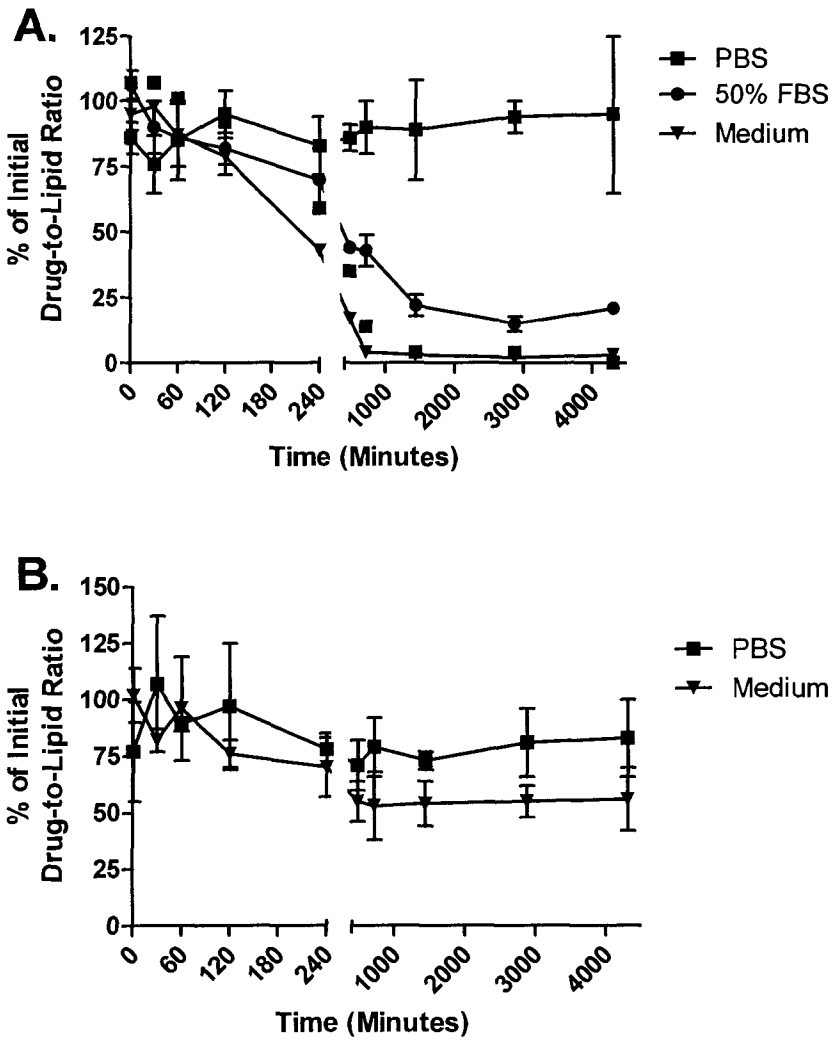

Figure 3.2. Effect of diluent and concentration on leakage of CPT-11from Irinophore C™ *in vitro*.

Irinophore C™ was diluted to a final concentration of 10 μM (A) or 60 μM CPT-11 in PBS (pH 7.4), 50% FBS, or supplemented medium, and was incubated for 72 h at 37°C. At various time points, the drug-to-lipid ratio was determined via HPLC analysis (drug) and LSC (lipid). Data are presented as percent of initial drug-to-lipid ratio. Each point represents the mean +/- standard deviation (n = 2-3) from one representative experiment.

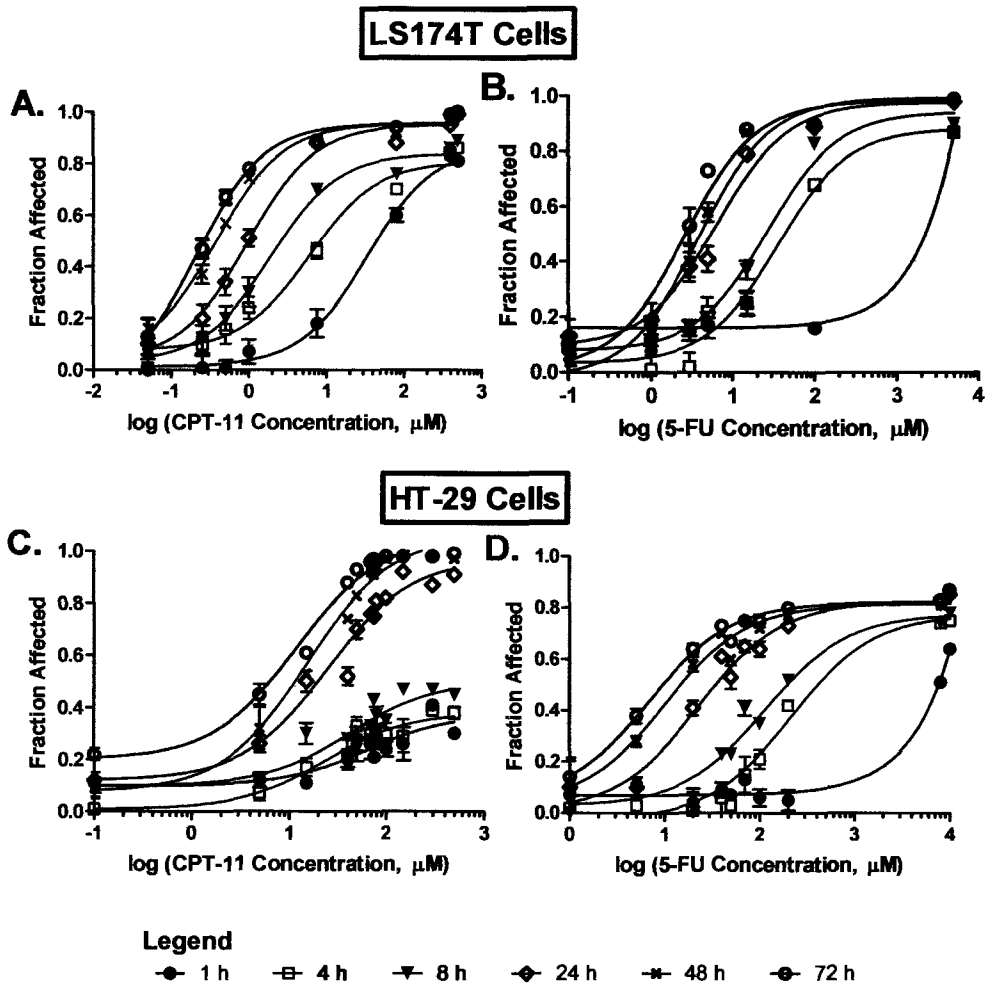

Figure 3.3. Exposure time dependency of CPT-11 and 5-FU cytotoxicity *in vitro*.

The LS174T (A and B) and HT-29 (C and D) cells were exposed to a range of concentrations of CPT-11 (A and C) or 5-FU (B and D) for 1, 4, 8, 24, 48, or 72 h. At 72 h after the start of drug incubation, cell viability was determined using the alamarBlue® assay, and was expressed as fraction affected, normalized to control. Each point represents the mean +/- standard deviation (n = 3-9) from 2-3 experiments.

exposure. For the LS174T cell line, the IC_{50} values for both drugs were over 100-fold lower after 72 h of drug exposure (5-FU, 3.0 μM; CPT-11, 0.3 μM) than after 1 h of drug exposure (5-FU, 330 μM; CPT-11, 44 μM). For the HT-29 cells, the 5-FU IC_{50} value after 72 h of drug exposure (9 μM) was over 400-fold lower than after 1 h of drug exposure (4000 μM). Even at the highest concentrations tested, CPT-11 did not elicit maximal cytotoxicity against the HT-29 cells after 1, 4, or 8 h of drug exposure. However, when the drug exposure time was 24 h or longer, complete cytotoxicity was achieved at the highest drug concentrations.

3.2.4. Ratio Dependency and Combination Exposure Time Dependency

In vitro cytotoxicity assays were conducted with the combination of 5-FU and CPT-11 to determine whether the molar ratio of the drugs affected the interaction between them, as measured by the combination index value. Information regarding the synergistic and antagonistic ratios of 5-FU:CPT-11 may be useful to consider when selecting dosing levels and target plasma drug concentrations for clinical trials. Data revealed that the molar ratio of 5-FU:CPT-11 influenced the interaction of the drug combination against the LS174T and HT-29 cells (Fig. 3.4Ai and 3.4Aii, respectively). For the LS174T cells, all three molar ratios of 5-FU:CPT-11, 10:1, 1:1, and 1:10, provided synergistic cytotoxicity at low fraction affected (FA) values up to ~0.50; at high FA values above ~0.50, the 10:1 and 1:10 ratios were antagonistic. Only the 1:1 ratio provided a synergistic profile at all FA values. Some differences were observed when the HT-29 cells were tested (Fig. 3.4Aii). The 1:1 molar ratio was

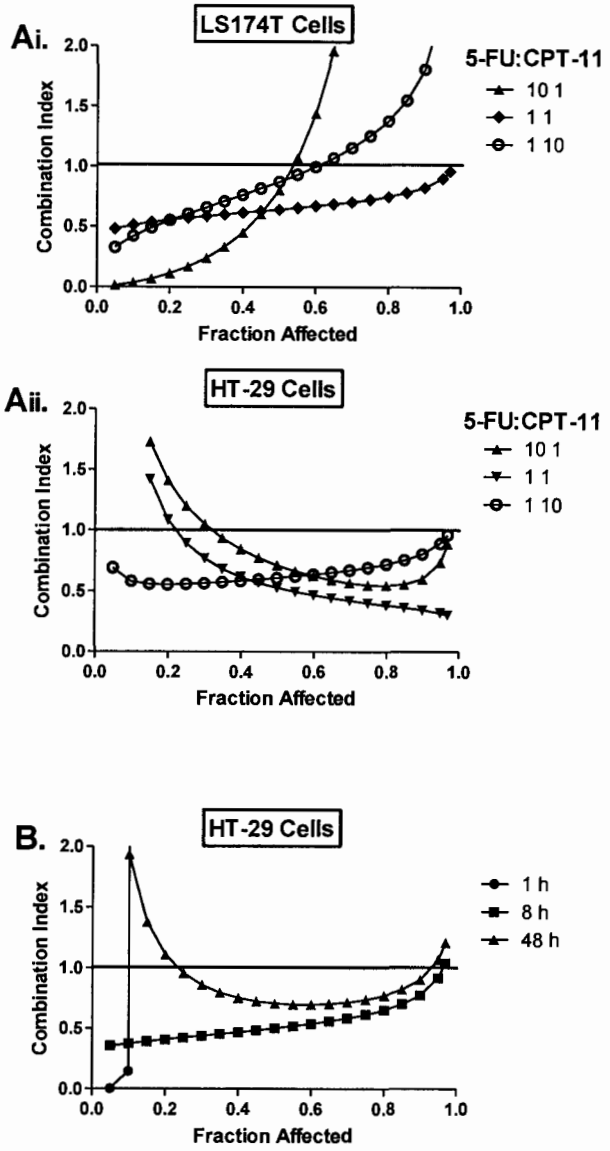

Figure 3.4. Ratio dependency and combination exposure time dependency of CPT-11 and 5-FU cytotoxicity *in vitro*.

The LS174T (Ai) and HT-29 (Aii) cells were exposed to a range of concentrations of 5-FU:CPT-11 at molar ratios of 10:1, 1:1, or 1:10 for 72 h. Separately, HT-29 cells (B) were also exposed to a range of concentrations of 5-FU:CPT-11 at a 1:1 molar ratio for 1, 8, or 48 h. At 72 h after the start of drug incubation, cell viability was determined using the alamarBlue® assay. Drug interaction data are presented as calculated combination index values, as determined from concentration-effect cytotoxicity data points (n = 3-24) compiled from 2-4 experiments. CI = 1 (black line), additive; CI < 1, synergistic; CI > 1, antagonistic.

antagonistic at low FA values below ~0.20, but then provided the greatest synergy of the three ratios beyond a FA value of ~0.50. The 1:10 ratio produced synergism and avoided antagonism across all FA values, although the interaction profile neared additivity at high FA values. The 10:1 ratio was antagonistic at low FA values and then became synergistic above ~0.35.

Experiments were completed in order to determine whether increasing the exposure time to the drug combination would achieve greater synergy. This information will be important to consider when deciding how to administer 5-FU in combination with Irinophore C™ in clinical trials. The HT-29 cells were exposed to graded concentrations of 5-FU:CPT-11 at a 1:1 molar ratio for 1, 8, or 48 h. To see how exposure time influenced the drug interaction, the combination index value at various fraction affected levels was calculated using the Median-Effect Principle, in order to compare the cytotoxicity produced by the combination to that of the single agents at each exposure time (Fig. 3.4B). An exposure time of 1 h was strongly antagonistic at FA values above ~0.10. The results indicated a high level of synergy between CPT-11 and 5-FU across the majority of FA values when the exposure time was prolonged to 8 or 48 h. With 8 h of exposure, the CI value gradually approached 1, or additivity, as the FA value increased. When the cells were exposed to the drugs for 48 h, there was an antagonistic interaction at FA values below ~0.20, and an additive or synergistic interaction at FA values above ~0.20. The greatest synergy was achieved when the HT-29 cells were exposed to both drugs *in vitro* for 8 h. Further prolongation of drug exposure to a period of 48 h produced a slightly lower level of synergy,

but the most effective anti-cancer effect of the tested combination exposure times, as suggested by the fact that the 48 h combination demonstrated the lowest IC_{50} value in the cytotoxicity assays that were used to calculate the combination index values.

3.2.5. Pharmacokinetics/Biodistribution

A PK/BD study was conducted to determine whether co-administration of Irinophore C™ and 5-FU altered the *in vivo* fate of either therapy relative to when administered as single agents. The concentration-time data for 5-FU, total lipid, CPT-11 lactone and carboxylate, and SN-38 lactone are presented in Fig. 3.5A-E. SN-38 carboxylate was not detected in any plasma or tissue samples when tested via HPLC with a limit of detection of 10 ng/mL. HPLC analysis of CPT-11 and metabolites in the liver could not be performed due to spectral interference from unknown molecules that were co-extracted with CPT-11 and SN-38 from the liver homogenate.

The plasma concentrations and tissue accumulation of 5-FU and Irinophore C™, and its metabolites, were primarily unchanged following co-administration, versus when administered alone. This is particularly evident in Fig. 3.5A and 3.5B, which show the PK/BD of 5-FU and the Irinophore C™ liposomes, represented by total lipid, respectively. One notable exception is the plasma concentration of 5-FU (Fig. 3.5Av), which was significantly higher when 5-FU was co-administered with Irinophore C™ ($P < 0.001$-0.05), even though it was rapidly cleared from circulation (half-life ($t_{1/2}$) = ~5 min). However, the

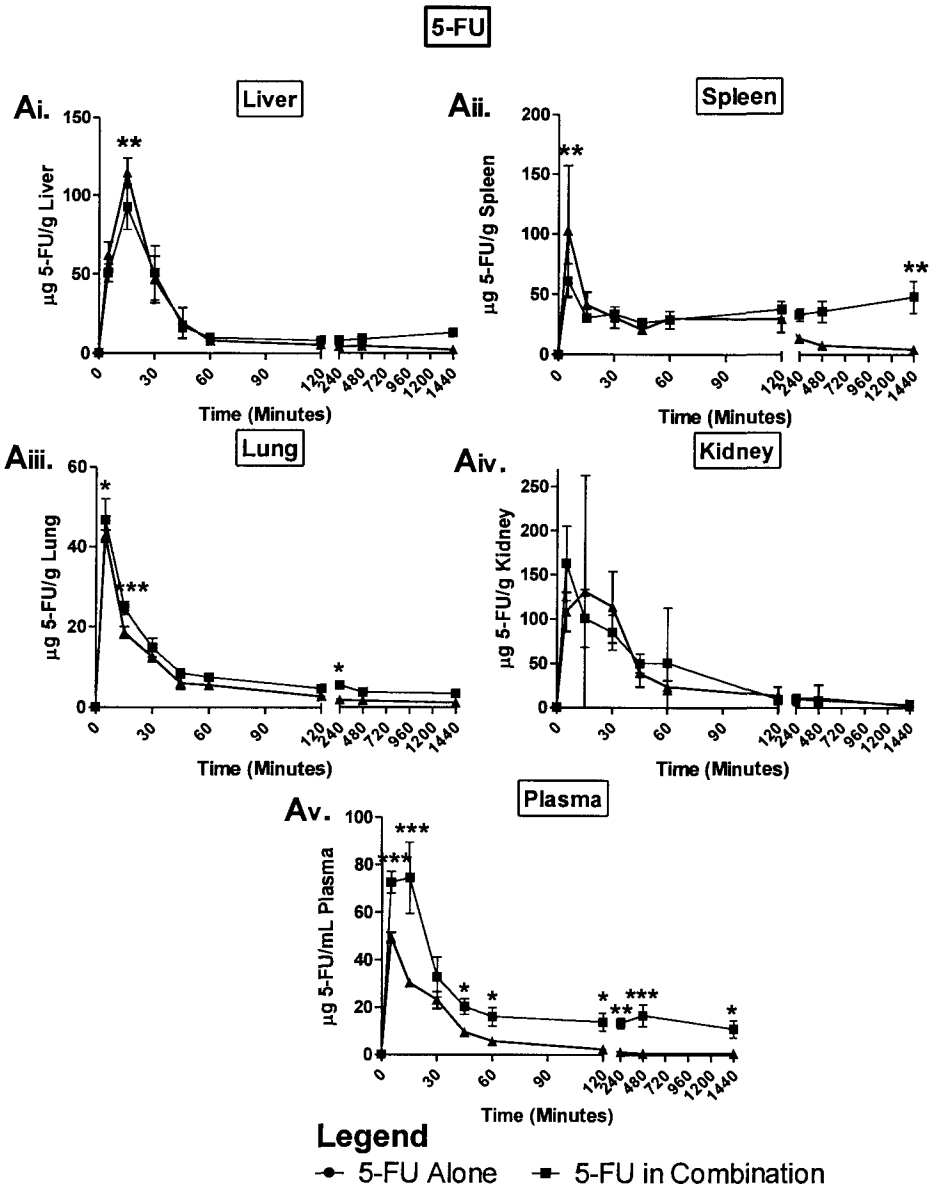

Figure 3.5. Mean organ and plasma concentrations of lipid and drug following administration of 5-FU and Irinophore C™ alone and simultaneously.

Rag2-M mice were administered [^{14}C]5-FU (40 mg/kg) or [^{3}H]CHE-labelled Irinophore C™ (40 mg CPT-11/kg), alone or in combination. At various time points post-injection, mice were euthanized, blood and organs were harvested, and the concentrations 5-FU, CPT-11, SN-38, and/or total lipid were determined.

A) Concentration of 5-FU in liver (i), spleen (ii), lung (iii), kidney (iv), and plasma (v). Data are presented as µg 5-FU per gram of organ (i-iv) or mL of plasma (v). Each point represents the mean +/- standard deviation (n = 4) from one experiment.

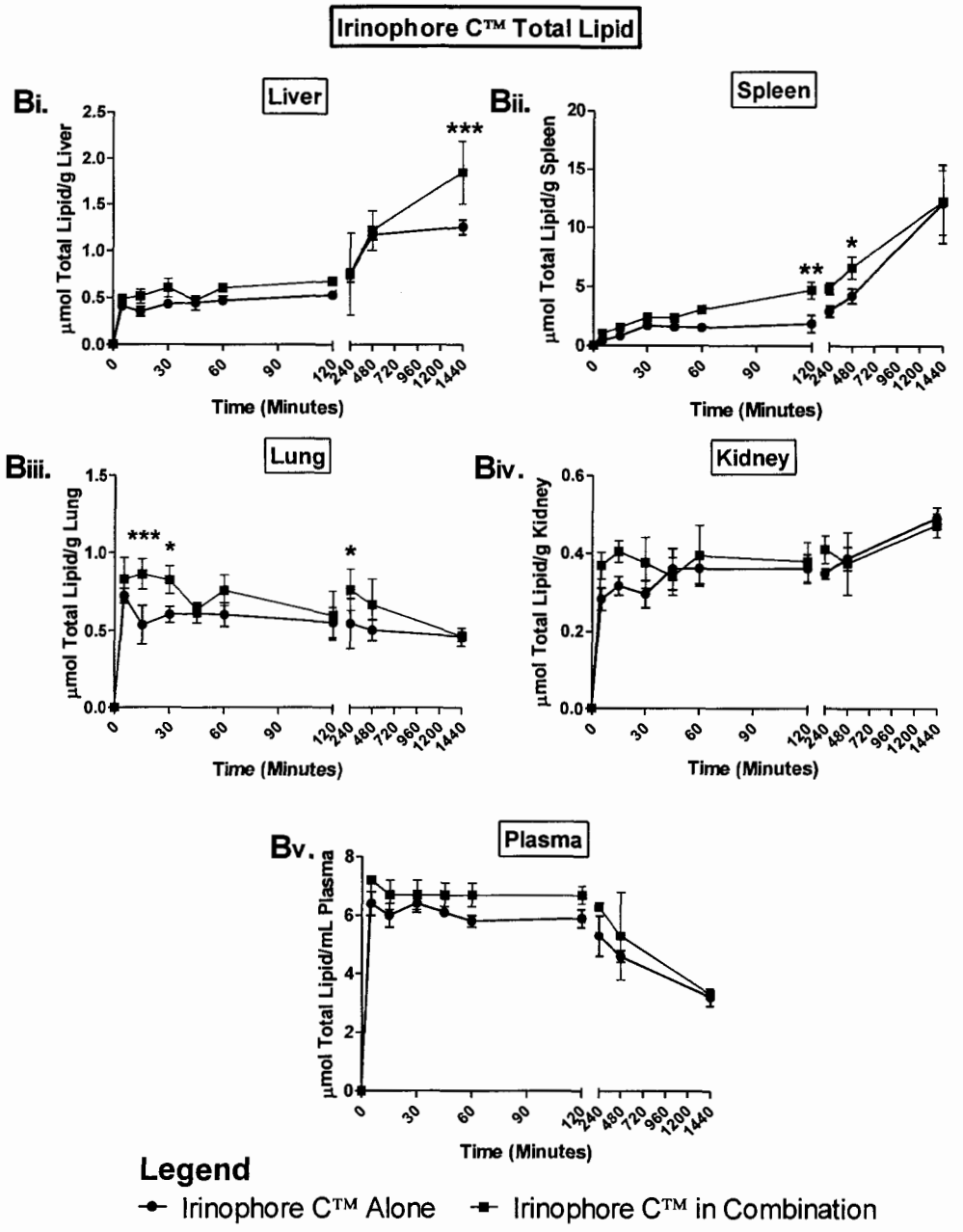

Figure 3.5 continued. Mean organ and plasma concentrations of lipid and drug following administration of 5-FU and Irinophore C™ alone and simultaneously.

B) Concentration of total lipid in liver (i), spleen (ii), lung (iii), kidney (iv), and plasma (v). Data are presented as µmol total lipid per gram of organ (i-iv) or mL of plasma (v). Each point represents the mean +/- standard deviation (n = 4) from one experiment.

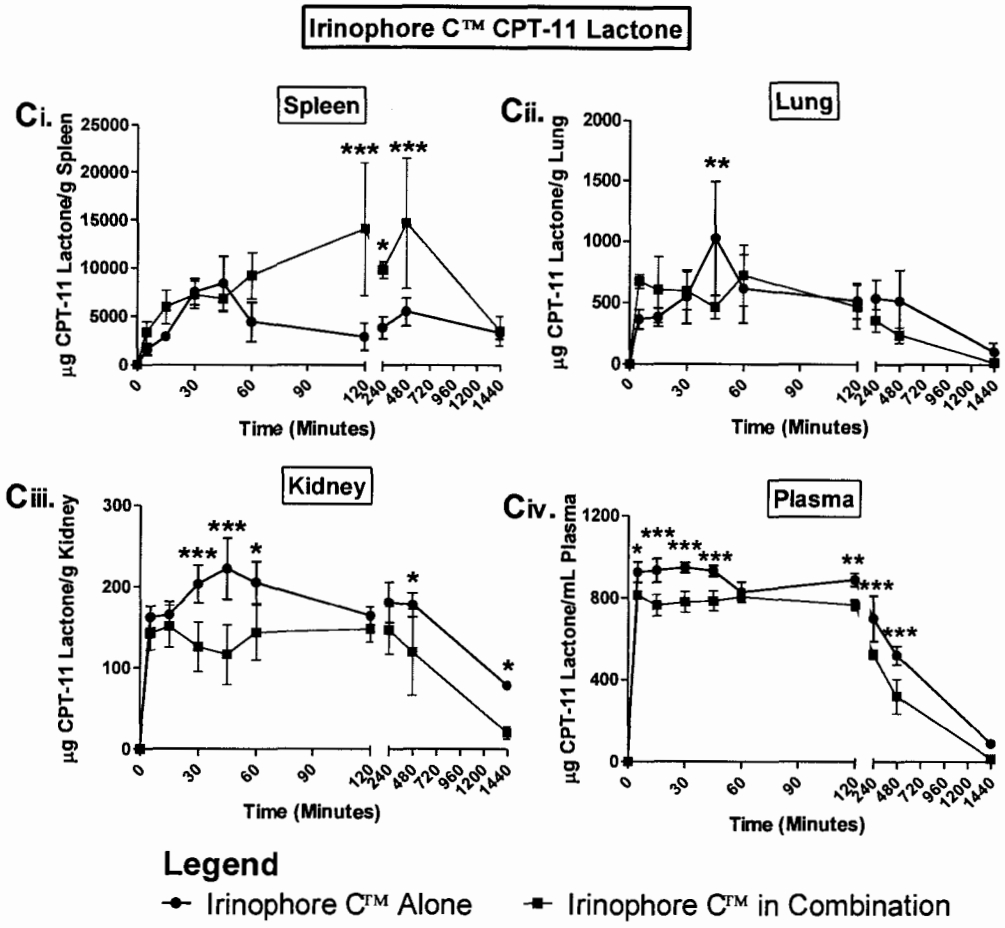

Figure 3.5 continued. Mean organ and plasma concentrations of lipid and drug following administration of 5-FU and Irinophore C™ alone and simultaneously.

C) Concentration of CPT-11 lactone in spleen (i), lung (ii), kidney (iii), and plasma (iv). Data are presented as µg CPT-11 lactone per gram of organ (i-iii) or mL of plasma (iv). Each point represents the mean +/- standard deviation (n = 4) from one experiment.

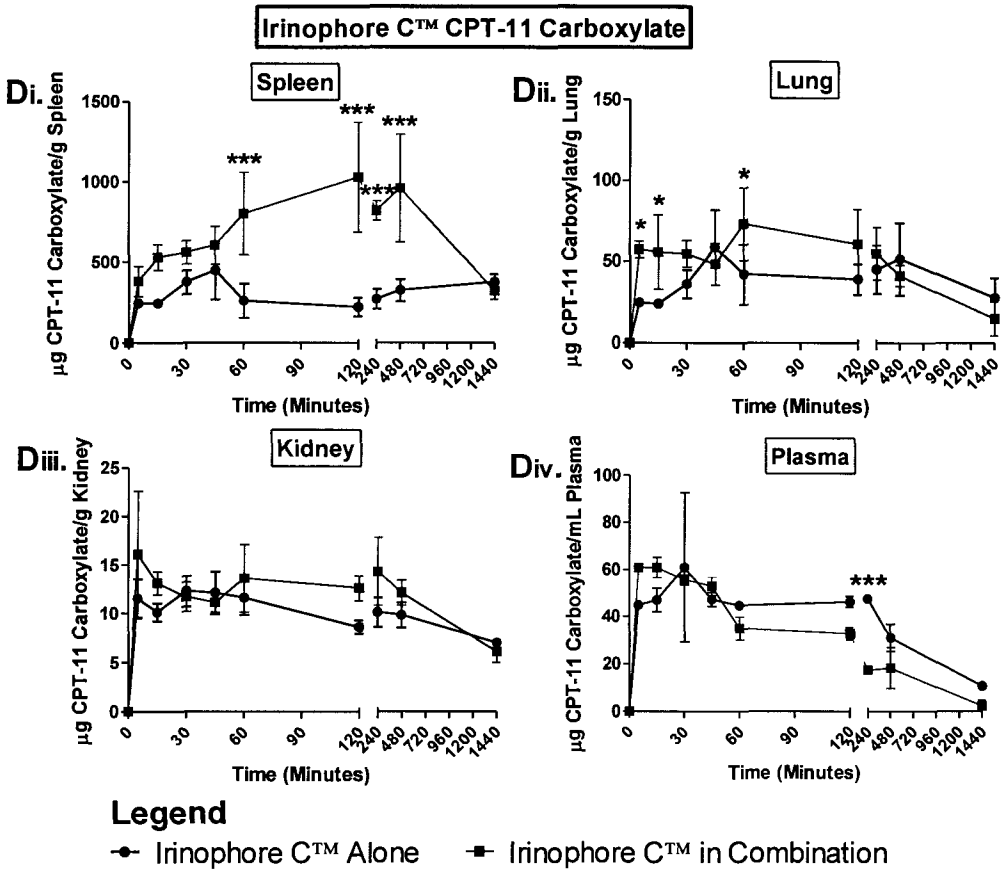

Figure 3.5 continued. Mean organ and plasma concentrations of lipid and drug following administration of 5-FU and Irinophore C™ alone and simultaneously.

D) Concentration of CPT-11 carboxylate in spleen (i), lung (ii), kidney (iii), and plasma (iv). Data are presented as µg CPT-11 carboxylate per gram of organ (i-iii) or mL of plasma (iv). Each point represents the mean +/- standard deviation (n = 4) from one experiment.

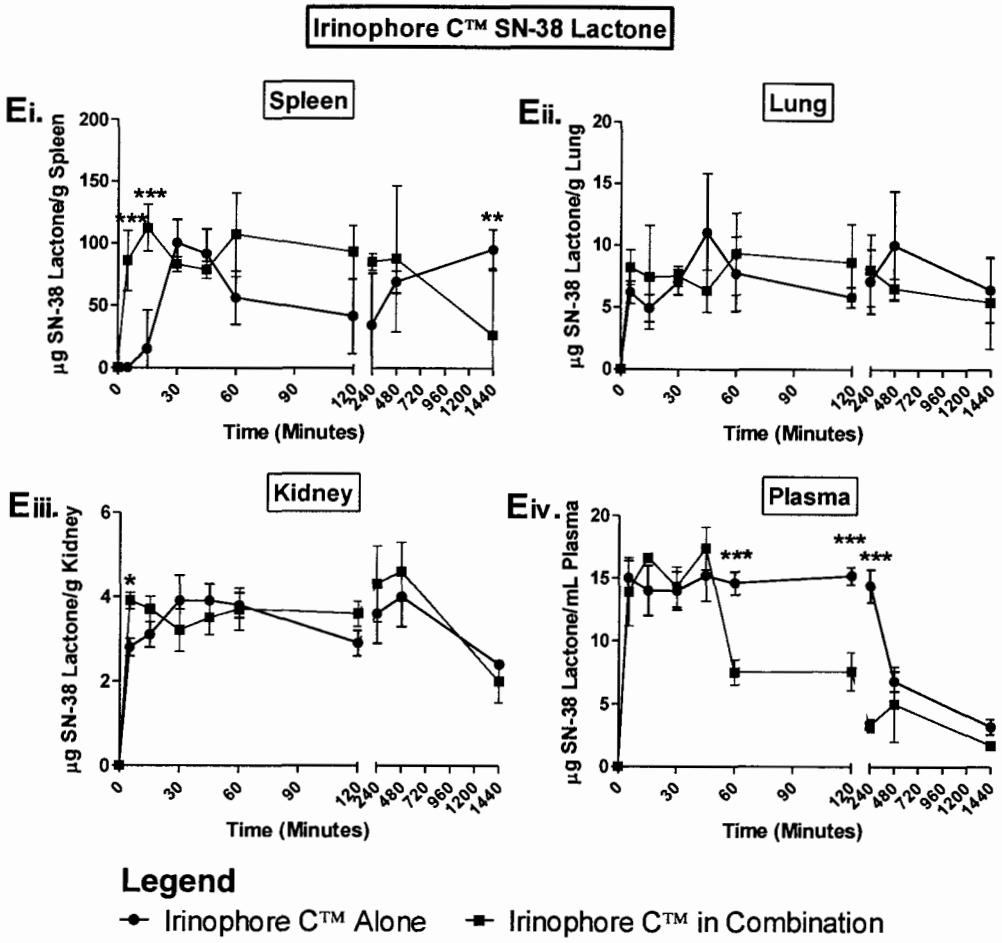

Figure 3.5 continued. Mean organ and plasma concentrations of lipid and drug following administration of 5-FU and Irinophore C™ alone and simultaneously.

E) Concentration of SN-38 lactone in spleen (i), lung (ii), kidney (iii), and plasma (iv). Data are presented as µg SN-38 lactone per gram of organ (i-iii) or mL of plasma (iv). Each point represents the mean +/- standard deviation (n = 4) from one experiment.

disparity in plasma concentration lacks therapeutic importance when considering that the plasma concentration of 5-FU was below ~3% of the injected dose within 15-30 min of injection as a single agent or in combination.

Although co-administration of Irinophore C™ and 5-FU did not generally have a significant impact on the *in vivo* fate of the therapies, some differences in biodistribution were observed, relative to when administered as single agents. The most significant difference was the increased splenic concentrations of CPT-11 lactone ($P < 0.001$-0.05; Fig. 3.5Ci) and CPT-11 carboxylate ($P < 0.001$; Fig. 3.5Di) that were observed at several time points between 1 and 8 h post-injection. A reduction in the CPT-11 lactone concentration in the plasma ($P < 0.001$-0.05; Fig. 3.5Civ), and to some extent in the kidney ($P < 0.001$-0.05; Fig. 3.5Ciii), was shown at a number of time points following the administration of Irinophore C™ in combination, possibly reflecting the enhanced levels of splenic accumulation of CPT-11 lactone that were also observed. Following the injection of Irinophore C™, CPT-11 lactone was the predominant drug species in the plasma and organs, and was present at 10-fold higher concentrations in the plasma than was CPT-11 carboxylate.

At 5 and 15 min post-injection, statistically significant increases in the splenic uptake of SN-38 lactone ($P < 0.001$; Fig. 3.5Ei) were seen following the administration of Irinophore C™ in combination with 5-FU, versus alone. Between 1 and 4 h post-injection, the SN-38 lactone concentration in plasma was significantly lower ($P < 0.001$; Fig. 3.5Eiv) following co-administration of the therapies.

3.2.6. Therapeutic Effect

After observing that doses of Irinophore C™ between 20 and 40 mg CPT-11/kg produced similar therapeutic effects in several cancer models (21), a study was completed to investigate the dose-effect relationship of low doses of Irinophore C™ in the treatment of CRC. Figure 3.6 presents data showing the therapeutic activity and toxicity of different doses of Irinophore C™ in a subcutaneous model of human CRC. Body weight loss was used as a measure of toxicity, and the study revealed that q7dx3 dosing of 40 mg/kg free CPT-11 or Irinophore C™ dosing between 2.5 and 40 mg CPT-11/kg was well-tolerated (Fig. 3.6A). Minimal body weight loss was observed: less than 8% following three injections of 40 mg/kg free CPT-11 and less than 6% following three injections of up to 40 mg CPT-11/kg Irinophore C™.

As presented in Fig. 3.6B, treatment with free irinotecan or any of the tested doses of Irinophore C™ was more effective than saline treatment, and the administration of Irinophore C™ doses as low as 5 mg CPT-11/kg also produced an increase in median group survival compared to saline treatment ($P < 0.05$-0.001; Table 2.1). The therapeutic activity of 2.5 mg CPT-11/kg Irinophore C™ was approximately equal to that of 40 mg/kg free CPT-11, which is a 16-fold dose reduction. Although 5 mg CPT-11/kg Irinophore C™ treatment provided a superior tumor growth delay relative to free CPT-11, there was not a statistically significant difference in survival between the two therapies. The administration of either 10 or 40 mg CPT-11/kg Irinophore C™ was substantially more effective than the administration of free CPT-11. Compared to treatment with free CPT-11,

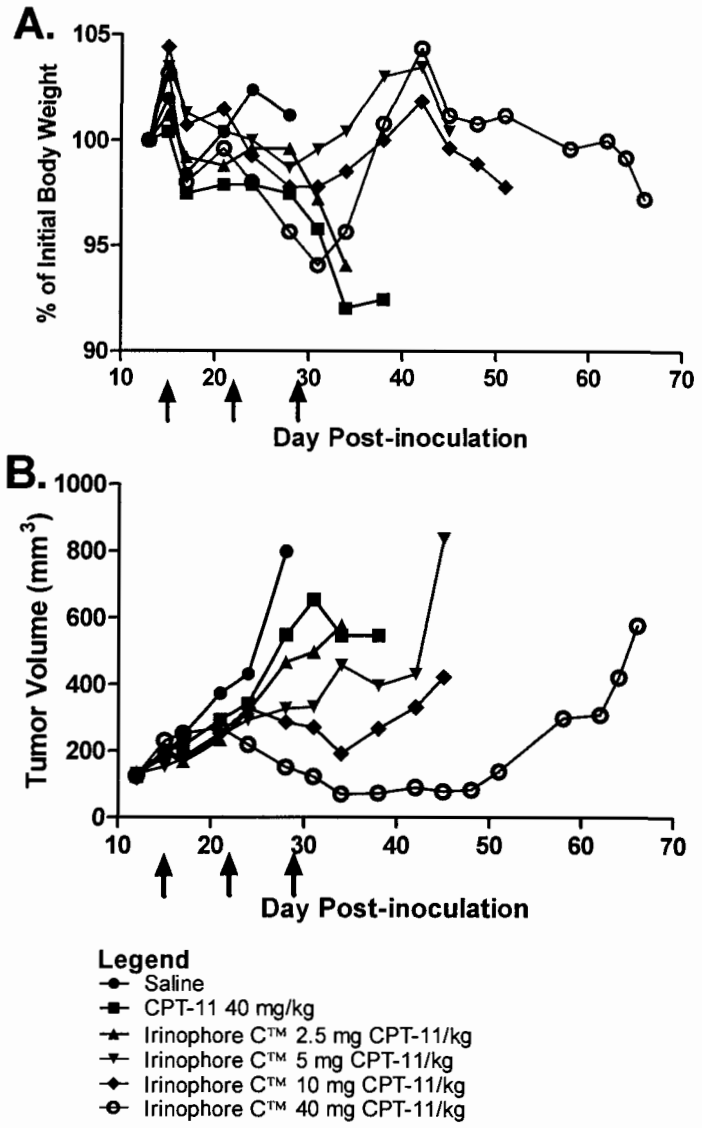

Figure 3.6. Therapeutic activity and toxicity of different doses of Irinophore C™ treatment in a subcutaneous model of CRC.

Rag2-M mice bearing subcutaneous HT-29 tumors were injected i.v. at days 15, 22, and 29 with saline, irinotecan (40 mg/kg), or Irinophore C™ (2.5, 5, 10, or 40 mg CPT-11/kg). Body weight (A) and tumor volume (B) were measured 2-3 times per week. Mice were euthanized when tumor volume exceeded 1000 mm^3, body weight loss exceeded 20%, or if tumor ulceration or severe deteriorations in health were observed. Data are presented as percent of initial body weight (A) or tumor volume (mm^3) (B). Each point represents the group median, calculated until fewer than 3 mice remained (n = 3-6) from one experiment. Arrows represent treatments.

Table 3.1. Effect of Irinophore C™ dose on median group survival.

Treatment	CPT-11 Dose (mg/kg)	Median Survival (Days)
Saline	0	28
CPT-11	40	26
Irinophore C™	2.5	34
Irinophore C™	5	41.5*
Irinophore C™	10	51**, $$, #, ^
Irinophore C™	40	65**, $$, #, ^, &&

***, P < 0.05 vs. Saline; **, P < 0.01 vs. Saline; $$, P < 0.01 vs. CPT-11; #, P < 0.05 vs. 2.5 mg CPT-11/kg Irinophore C™; ^, P < 0.05 vs. 5 mg CPT-11/kg Irinophore C™; &&, P < 0.01 vs. 10 mg CPT-11/kg Irinophore C™**

median group survival following the administration of Irinophore C™ at 10 and 40 mg CPT-11/kg was prolonged by ~1.5- and ~2-fold, respectively ($P < 0.001$). There was a trend towards tumor regression following the third treatment with 10 mg CPT-11/kg Irinophore C™, with tumor re-growth observed at 7 days after treatment cessation. Substantial tumor regression was obvious after the second treatment with 40 mg CPT-11/kg Irinophore C™, and mice treated with three injections of 40 mg CPT-11/kg Irinophore C™ did not display tumor re-growth until ~20 days after the final treatment.

A preliminary therapeutic study was completed using an orthotopic model of human CRC to compare the effectiveness of free and liposomal CPT-11 alone, and in combination with 5-FU in the treatment of hepatic metastases (Fig. 3.7). All therapies, including 5-FU alone (median survival 37 d), provided a statistically significant improvement in survival, relative to saline treatment (median survival 28.5 d; $P < 0.01$). The results clearly demonstrate the substantial therapeutic effect of Irinophore C™, and the superior activity of Irinophore C™ plus 5-FU, relative to free CPT-11 plus 5-FU, in the treatment of CRC. Treatment with Irinophore C™ was vastly superior to treatment with an equivalent dose of free CPT-11 (median survival 70 vs. 44 d, respectively; $P < 0.01$). Administration of the combination of Irinophore C™ and 5-FU was significantly more effective than treatment with free CPT-11 plus 5-FU (median survival 71 vs. 46 d, respectively; $P < 0.01$), but Irinophore C™ plus 5-FU was not more effective than Irinophore C™ alone. Median group survival was not significantly prolonged by

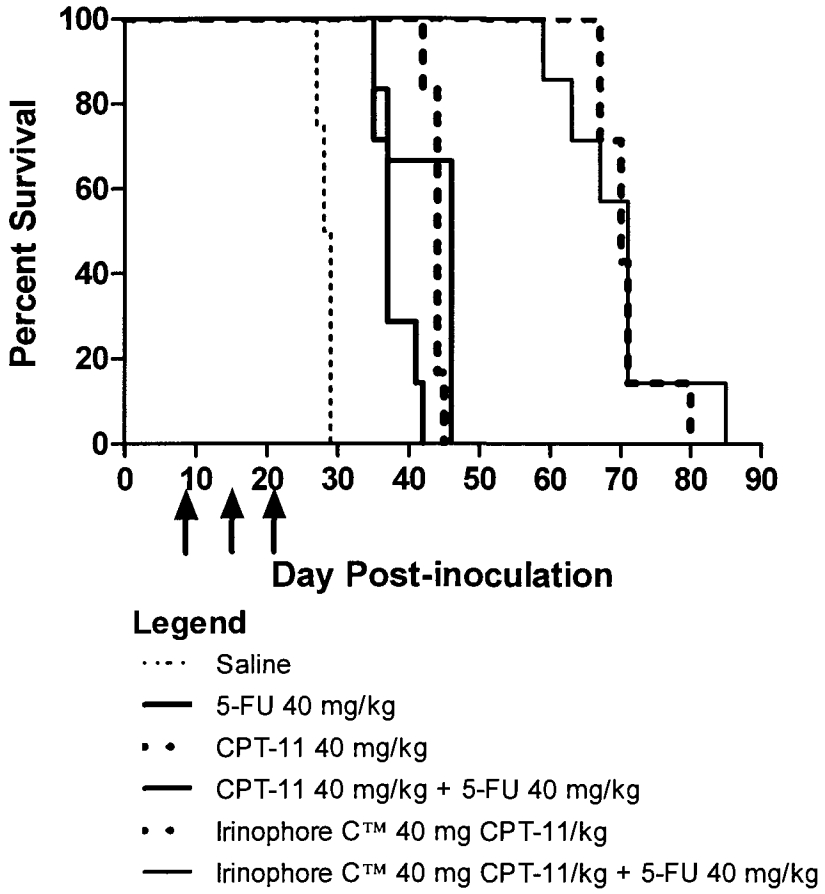

Figure 3.7. Effect of 5-FU plus free or liposomal irinotecan treatment in an orthotopic model of CRC.

Rag2-M mice inoculated intra-splenically with LS174T cells were injected i.v. at days 7, 14, and 21 with saline, 5-FU (40 mg/kg), CPT-11 (40 mg/kg), 5-FU + CPT-11 (40 mg/kg + 40 mg/kg), Irinophore C™ (40 mg CPT-11/kg), or Irinophore C™ + 5-FU (40 mg CPT-11/kg + 40 mg/kg). Mice were euthanized if body weight loss exceeded 20% or if severe deteriorations in health were observed. Data are presented as group percent survival (n = 7-8) from one experiment. Arrows represent treatments.

the addition of 5-FU to CPT-11 alone treatment (46 vs. 44 d, respectively; $P > 0.05$) or to Irinophore C™ alone treatment (71 vs. 70 d, respectively; $P > 0.05$).

Figure 3.8 presents the results of a therapeutic experiment completed to determine whether prolonged simultaneous exposure to 5-FU and CPT-11, achieved via qd5 i.p. dosing of 5-FU and the administration of Irinophore C™, would lead to an improvement in anti-cancer effect relative to Irinophore C™ monotherapy or a shorter simultaneous exposure in the form of free CPT-11 plus 5-FU. The study was completed in a subcutaneous model of CRC, and also assessed body weight loss as a measure of treatment toxicity. Figure 3.8A reveals that the mice treated with a combination of 60 mg CPT-11/kg Irinophore C™ and 16 mg/kg 5-FU showed dramatic weight loss of greater than 20% over the first week of dosing. These mice were euthanized at the start of the second cycle and the group was excluded from therapeutic analysis. Individually, the two therapies were well-tolerated, with body weight loss of ~6% after treatment with 60 mg CPT-11/kg Irinophore C™ alone, and minimal loss after treatment with 5-FU alone. Similarly, nearly 20% body weight loss was also observed after the first treatment with 60 mg/kg CPT-11 plus 16 mg/kg 5-FU. Although these mice regained some weight after the second treatment, their body weight loss reached ~20% following the third treatment, either as a result of adverse drug toxicity or disease progression.

The results presented in Fig. 3.8B demonstrate that the administration of single agent Irinophore C™ at 60 mg CPT-11/kg was significantly more effective than treatment with 60 mg/kg free CPT-11 plus 16 mg/kg 5-FU, and was equally

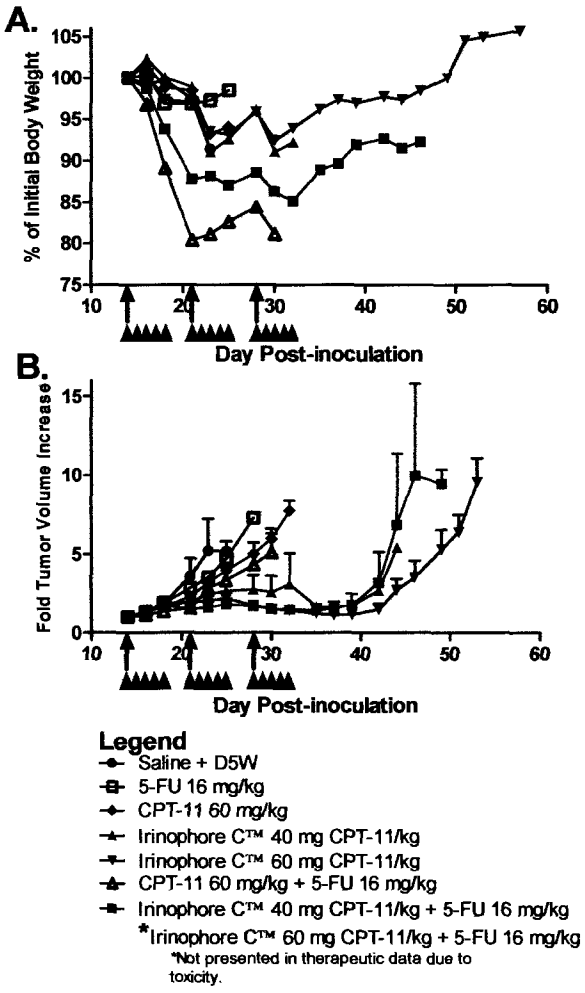

Figure 3.8. Effect of 5-FU plus free or liposomal irinotecan treatment in a subcutaneous model of CRC.

Rag2-M mice bearing subcutaneous HT-29 tumors were treated with saline + D5W, 5-FU (16 mg/kg), irinotecan (60 mg/kg), Irinophore C™ (40 or 60 mg CPT-11/kg), irinotecan + 5-FU (60 mg/kg + 16 mg/kg), or Irinophore C™ + 5-FU (40 mg CPT-11/kg + 16 mg/kg). Beginning on day 14, D5W and 5-FU were administered qdx5 for 3 weeks (arrowheads) via i.p. injection; all other treatments were administered q7dx3 via i.v. injection (solid arrows). Body weight and tumor dimensions were measured 2-3 times per week. Mice were euthanized if tumor volume exceeded 1000 mm^3, body weight loss exceeded 20%, or if tumor ulceration or severe deteriorations in health were observed. A) Body weight. Data are presented as percent of initial body weight. Each point represents the group median (n = 6), calculated until fewer than 3 mice remained, from one experiment. B) Tumor growth. Data are presented as fold tumor volume increase. Each point represents the group mean +/- standard deviation (n = 6) from one experiment.

as effective as the combination of 40 mg CPT-11/kg Irinophore C™ and 16 mg/kg 5-FU. The administration of single agent 5-FU or free irinotecan provided very modest therapeutic benefit compared to saline plus D5W treatment (26 vs. 28 vs. 23 d to reach 5-fold tumor volume increase, respectively). Following treatment with 40 mg CPT-11/kg Irinophore C™, the time to reach a 5-fold increase in tumor volume was 44 days, approximately double the time as for control mice (23 d), and significantly longer than for mice treated with free irinotecan at 60 mg/kg (28 d). Mice administered 16 mg/kg 5-FU plus 60 mg/kg irinotecan and those administered 16 mg/kg 5-FU plus Irinophore C™ at 40 mg CPT-11/kg showed similar body weight losses of ~15-18% (Fig. 3.8A). At these equitoxic doses, treatment with 5-FU plus Irinophore C™ was significantly more effective than with 5-FU plus free irinotecan (43 vs. 30 d to reach 5-fold tumor volume increase), even though a lower total dose of CPT-11 was administered using the liposomal formulation. The greatest disease control was achieved with 60 mg CPT-11/kg Irinophore C™ as a single agent (49 d to reach 5-fold volume increase), and was accompanied by low overall toxicity.

3.3. Discussion

A variety of anti-cancer agents have been encapsulated in liposomes to overcome undesirable drug properties, including severe off-target toxicity, poor stability *in vivo*, and/or unfavourable PK/BD parameters. Ramsay *et al.* have demonstrated that a novel liposomal formulation of irinotecan (Irinophore C™) has less off-target toxicity, a more favourable PK/BD profile with increased tumor

concentrations of the active drug species, and significantly more effective anti-cancer activity, relative to free irinotecan (21, 22). In the clinic, the combination of 5-FU and CPT-11 has proven to be more effective than either agent alone, and they are utilized together in front-line CRC treatment protocols. In two different murine models of CRC, it was demonstrated that the administration of single agent Irinophore C™ can achieve equivalent therapeutic activity as the combination of Irinophore C™ and 5-FU, with lower overall toxicity. Furthermore, in these CRC models, 5-FU failed to add to the therapeutic activity seen with either free irinotecan or Irinophore C™.

Unexpected results were observed in preliminary *in vitro* cytotoxicity studies investigating single agent Irinophore C™ against human CRC cell lines. The liposomal formulation of irinotecan was equally as cytotoxic as the free formulation against the LS174T and HT-29 cells, after a 72 h exposure period. The same surprising trend was also observed when cytotoxicity experiments with Irinophore C™ were completed *in vitro* using lung cancer cells (A. Thomas, unpublished data), indicating that it is not a cell type-specific anomaly. With both the CRC and lung cancer cells, it was anticipated that the liposomal formulation would be significantly less cytotoxic than the free drug, as has been previously observed with PEGylated liposomal doxorubicin versus free doxorubicin against several cell lines *in vitro* (Chapter 4 and 27, 28).

Unlike liposomal drugs, free drugs are immediately and entirely bioavailable upon incubation with the cells. In contrast, the encapsulated anti-cancer drug is not bioavailable until it is released from the liposome, which can

occur over minutes to hours to days, depending on the nature of the drug, composition of the liposomes, loading method employed, and other factors. Thus, especially following short exposure periods, when the liposomal drug will primarily remain encapsulated within the carrier, it was expected that the free drug would produce greater cytotoxicity than the liposomal drug. It is plausible that the disparity between the *in vitro* cytotoxicity of Irinophore C™ and PEGylated liposomal DXR, in relation to free CPT-11 and free DXR, respectively, may be due to the more rapid drug release properties of the liposomal irinotecan formulation ($t_{1/2}$ = 44 h) (22), relative to PEGylated liposomal DXR ($t_{1/2}$ = 90 h) (29). Alternatively, the internal Cu^{2+} ions may play a heretofore unidentified role in the substantial cytotoxic activity of Irinophore C™, although the details of this theory remain to be investigated by the Bally laboratory.

A time-course study comparing the cytotoxicity of Irinophore C™ and free irinotecan following short and long exposure periods also yielded unexpected results. Even after the shortest drug exposure period (1 h), the liposomal formulation was equally as cytotoxic as the free drug against the LS174T cells. One possible explanation for these results would be if Irinophore C™ released all of the encapsulated irinotecan immediately upon addition to the cells, making its entire payload bioavailable and active, just like the free drug.

Irinophore C™ drug retention studies were completed *in vitro* in medium, 50% serum, and PBS (pH 7.4), with Irinophore C™ present at concentrations utilized for *in vitro* cytotoxicity assays. However, the immediate release of

substantial quantities of drug was not observed under any of the conditions tested. The data revealed that the rate of liposomal drug release was increased at lower concentrations of liposomal drug (i.e., 10 μM vs. 60 μM), and was increased in medium or 50% serum, relative to in PBS (pH 7.4), but could not explain the liposomal formulation's unexpectedly effective cytotoxicity against the LS174T cells at the early time points.

These experiments were completed under cell-free conditions, and thus, did not consider that a cellular factor could have been causing drug release. To examine this possibility, a drug retention study was conducted with Irinophore C™ diluted in conditioned medium, which was obtained from a flask of cells at ~80% confluence following 72 h of culture. The data demonstrated that Irinophore C™'s drug retention properties were the same whether the formulation was diluted in conditioned or fresh medium, thereby eliminating the possibility that a soluble factor released from the cells was causing rapid drug release. As well, the pH values for the PBS (pH 7.4), 50% FBS, medium, and conditioned medium, with and without liposomes, were determined at various time points throughout the experiments. In all cases, the pH remained constant at ~7.4 over the course of the experiment, and thus was not responsible for variation in drug leakage rate.

Interestingly, after 4 and 8 h of exposure, Irinophore C™ was more cytotoxic than free irinotecan against HT-29 cells *in vitro*, while Irinophore C™ was equally as cytotoxic as the free drug following exposure periods of 1, 24, 48, and 72 h. It was postulated that the increased cytotoxicity of Irinophore C™ may

be due to the continual release of the active lactone moiety of irinotecan into the cytoplasm, while the free drug had reached a pH-dependent equilibrium between the active and inactive configurations. Burke and Mi have demonstrated that the CPT-11 lactone/carboxylate hydrolysis equilibrium half-life is ~30 min in PBS (pH 7.4), and that nearly 90% of the CPT-11 exists in the carboxylate configuration at equilibrium at pH 7.4 (20). Kobayashi *et al.* have shown that cellular uptake of CPT-11 lactone and SN-38 lactone is significantly more rapid than uptake of the carboxylate configurations, and also that the rate of drug uptake correlates with cytotoxicity in HT-29 cells *in vitro* (30). Thus, over the course of a 4 or 8 h drug exposure period, the CPT-11 lactone that was continually released from Irinophore C™ was likely taken up more quickly than the free drug at pH 7.4 equilibrium, which would have been predominantly hydrolyzed to the carboxylate form. This could lead to greater intracellular accumulation of the active drug species following exposure to Irinophore C™, compared to free drug, and a corresponding increase in cytotoxicity. Based on the results above, prolonged exposure periods to Irinophore C™ appear to overcome the unfavourable equilibrium at physiological pH and reduced rate of carboxylate uptake. It is plausible that some of the substantial cytotoxicity of Irinophore C™ *in vivo* could be attributed to this process.

The experiments presented in this chapter focused on the combination of Irinophore C™ and 5-FU, with the belief that the data will help to guide the design of future Phase II clinical trials for Irinophore C™. It has recently been shown that the interaction between two drugs may, in part, be dictated by the

drug-to-drug ratio (31-33), and that merely administering two drugs at their maximum tolerated doses may not lead to the greatest anti-cancer effect (31, 32). A study by Mayer *et al.* used three drug combinations and revealed that certain ratios caused synergistic interactions, while other ratios caused antagonistic cytotoxicity, and that the synergistic ratios varied with cell line (31). Similar to what the above data showed for 5-FU:irinotecan against the HT-29 cells, Mayer *et al.* demonstrated synergy at 1:1 and 10:1 molar ratios with floxuridine:irinotecan, and antagonism at the 1:10 ratio (31). The above results with the LS174T cells correlate well with those of Mayer *et al.* in the parental LS180 cell line, showing antagonism at high molar ratios of floxuridine:irinotecan, such as 10:1, and synergism at the 1:1 ratio (31). Researchers have co-encapsulated drugs at defined ratios in liposomes in order to achieve tumor delivery, and maintenance of, synergistic drug ratios. Liposomal formulations of fixed-ratio/co-encapsulated irinotecan and floxuridine (34), irinotecan and cisplatin (35), and cytarabine and daunorubicin (36) have been developed, and have shown strong therapeutic potential in animal studies. However, this approach is not universally applicable, as some small molecule chemotherapeutic agents (e.g., 5-FU) have low encapsulation efficiencies and are not well-retained in liposomes (37, 38), and are thus not suitable for co-encapsulation. Further, if toxicity is noted clinically, the physician is not able to titrate down the dose of one drug relative to the other with a fixed-dose combination product, therefore making the development of single liposomal agents an alternative strategy for combination treatment.

Investigation of single agent Irinophore C™ in the above dose-effect study and subcutaneous combination therapeutic study can add to results published by Ramsay *et al.* (21). Previous work with Irinophore C™ for the treatment of CRC has focused on its effectiveness as a single agent at doses of 20-60 mg CPT-11/kg (21, 22, 39, 40), and has shown that administration of Irinophore C™ at 20, 30, and 40 mg CPT-11/kg produced approximately equal anti-cancer effect in two different CRC models (21). It is now possible to state that Irinophore C™ demonstrates dose-dependent activity at concentrations up to 10 mg CPT-11/kg, and anti-cancer effectiveness that is primarily unaffected by dose between 20 and 60 mg CPT-11/kg. Even when treating with 60 mg CPT-11/kg Irinophore C™, the tumor volume did not regress below 100-200 mm^3 in the HT-29 subcutaneous xenograft model, although a slightly prolonged delay of tumor re-growth after treatment cessation was observed following the administration of Irinophore C™ at 60 mg CPT-11/kg, relative to at 40 mg CPT-11/kg.

In the above dose-effect study, administration of free irinotecan at 40 mg/kg provided approximately equal activity to that of Irinophore C™ at 2.5 mg CPT-11/kg, which is a 16-fold reduction in dose without compromising the therapeutic effect or causing noticeable off-target toxicity. Irinophore C™ has a much broader therapeutic index than does free CPT-11, and thus can be administered at concentrations well above the MTD of the free drug (~50-70 mg/kg). For example, only ~6% body weight loss was observed following three treatments of Irinophore C™ at 60 mg CPT-11/kg. Therefore, it is possible to further increase the concentrations of Irinophore C™ beyond what has been described in

published experiments and presented here. Data from Ramsay *et al.* (21) and the above results show clear evidence of tumor regression following administration of Irinophore C™ at 20 mg CPT-11/kg or higher, but do not show complete eradication of the tumor, as mentioned above. It remains to be seen what effect further increases in dose will have on the anti-cancer activity of Irinophore C™, and if it is possible to achieve complete CRC tumor regression with a sufficiently high dose, or whether the residual tumor cells are indicative of a resistant sub-population of cells. Regardless, it is necessary to explore how to kill the residual cells that remain following treatment, as it is clear that they lead to significant tumor re-growth and disease progression.

Several combination therapy options could be explored as possible treatments to kill the residual cells that survive following administration of single agent Irinophore C™. Administration of cetuximab, an antibody directed against EGFR, has been shown to have a chemosensitizing effect in CRC patients, even eliciting therapeutic responses to previously refractory treatment protocols, including irinotecan-based regimens (41). Administration of a combination of cetuximab and Irinophore C™ may lead to an improved therapeutic outcome, and is currently under investigation by the Bally group.

Co-administration of Irinophore C™ with a vasculature-targeted liposomal drug (a modification of the combined dual-targeted approach investigated in Chapters 4 and 5) or an anti-vascular agent, may improve the treatment outcome; however, careful consideration of treatment timing would be required. Although Irinophore C™ itself has been reported to alter tumor vasculature function (40,

42), it is not yet clear how significant this mechanism of action is to Irinophore C™'s substantial overall anti-cancer activity. Destruction of the tumor vasculature is a viable addition to treatment, based on proof-of-concept experiments completed in Chapter 5, and published evidence showing that vascular destruction can kill multidrug resistant tumor cells (43).

Irinotecan has been demonstrated to be a substrate for the P-glycoprotein drug efflux pump, while SN-38 has been shown to be a substrate for another drug efflux pump belonging to the superfamily of adenosine triphosphate-binding cassette transporters (44). If the less sensitive sub-population of cells is multidrug resistant, greater anti-cancer activity may be achieved by co- or subsequent administration of a ligand-modified liposomal anti-cancer agent (45), which could circumvent the actions of the efflux pumps by delivering the entire payload intracellularly following internalization of the liposome, or by combining Irinophore C™ with a drug that is not a substrate for the P-glycoprotein efflux pump, such as 5-FU (46, 47). Furthermore, Irinophore C™ treatment has been shown to increase the tumor accumulation of subsequently administered 5-FU (40), and as discussed above, the combination of 5-FU plus leucovorin and free irinotecan is a current standard-of-care regimen for CRC treatment. This knowledge provides further impetus behind the experiments presented in this chapter examining the combination of Irinophore C™ and 5-FU.

Nakajima *et al.* proved, in an HT-29 model of CRC, that administration of a micellar formulation of SN-38 plus 5-FU was more effective than CPT-11 plus 5-FU; a 100% complete response rate was observed with the former, relative to a

0% complete response rate with the latter (48). *In vivo*, the investigators demonstrated that the micellar formulation of SN-38 led to a more prolonged and more pronounced build-up of tumor cells in S-phase than did free CPT-11, postulated to be due to the sustained release properties of the micellar formulation, leading to prolonged cell exposure to SN-38 (48). Based on these results, it is likely that *in vivo* administration of liposomal CPT-11 (Irinophore C™) may produce a similar accumulation of cells in S-phase, and improvement in therapeutic effect over free irinotecan. Scientists have shown that the irinotecan-induced build-up of cells in S-phase contributes to the synergistic toxicity observed in some tumor models when 5-FU and CPT-11 are administered sequentially, with irinotecan injected 24 h prior to 5-FU (49), where the S-phase blockade increases the number of cells that are susceptible to the actions of 5-FU. When discussing the conflicting evidence, and the rationale behind the ideal sequencing for CPT-11 and 5-FU administration, Rothenberg states that clinically, it may be "more important to integrate both drugs into a coordinated therapeutic plan than to administer the drugs simultaneously on any particular sequence" (50, and references therein).

In the experiments presented above, no therapeutic advantage was observed when 5-FU was added to Irinophore C™ therapy, relative to Irinophore C™ alone. The *in vitro* data suggest that more effective cytotoxicity can be produced by increasing the 5-FU exposure time, and greater synergy and cytotoxicity can be achieved by prolonging the simultaneous exposure to 5-FU and CPT-11. In the clinic, 5-FU is administered as a continuous infusion because of the drug's

extremely short plasma half-life (8-20 min) (51). The prolonged exposure time achieved by infusional versus i.v. bolus dosing of 5-FU has translated to a higher response rate and a modest increase in survival time in CRC patients (52). Based on these results, as well as the above *in vitro* combination exposure time data, the 5-FU dosing schedule was altered (daily i.p. injections instead of weekly bolus i.v. injections) to increase the 5-FU exposure time in the therapeutic experiment in the subcutaneous xenograft model. However, even with the increased 5-FU exposure time, there was no increase in effectiveness with Irinophore C™ plus 5-FU, relative to Irinophore C™ alone, presumably because 5-FU was still not administered via its most active dosing schedule: i.v. infusion. In fact, single agent Irinophore C™ at 60 mg CPT-11/kg was the most effective treatment, demonstrating therapeutic superiority over the combination of 40 mg CPT-11/kg Irinophore C™ and 5-FU, while also resulting in lower overall toxicity in murine models of CRC.

Even though 5-FU did not make a significant therapeutic contribution in the experiments above, its utility in cancer treatment has been proven in patients for decades. This suggests that the above mouse models do not accurately reflect patient sensitivity to 5-FU, despite the fact that human CRC xenografts were used. Furthermore, it is important to note that it is probable that the full anti-cancer potential of the combination of Irinophore C™ and 5-FU may not be realized until investigated in a clinical setting. Clinically, 5-FU is easily administered as a 30 day infusion, as indicated in numerous CRC treatment protocols, to overcome its poor PK/BD profile and improve its therapeutic effect; prolonged continuous

exposure to 5-FU may then produce synergistic or additive activity with a simultaneous, prolonged exposure to CPT-11, which can be achieved via sustained release preparations, such as Irinophore C™. Finally, 5-FU is typically administered with leucovorin to improve 5-FU's therapeutic activity (53). As such, the addition of leucovorin to Irinophore C™ and 5-FU treatment may provide greater enhancement of disease control. The data presented here from two different models of CRC clearly demonstrate the superior therapeutic activity of Irinophore C™ over free irinotecan, although additional fine-tuning may be required to reach the full therapeutic potential of the combination of Irinophore C™ and 5-FU in pre-clinical studies. Further investigations into the use of Irinophore C™ in a combination chemotherapy setting are currently ongoing.

3.4. Conclusion

Most newly developed liposomal therapies will not be administered as monotherapies in the clinic. As such, it is important that pre-clinical studies include the testing of liposomal drugs in combination with other free and/or liposomal drugs. The data presented in this chapter investigated the use of liposomal irinotecan in combination with free 5-FU, and demonstrate the potential for improved clinical results when using a combination of Irinophore C™ and 5-FU for the treatment of CRC. It was hypothesized that the increased CPT-11 exposure time achieved through the use of a liposomal drug delivery system, relative to free irinotecan, would increase the therapeutic effect when administered with 5-FU. Irinophore C™ revealed an unexpected degree of

cytotoxicity *in vitro*, especially following exposure periods of 4 and 8 h. The cytotoxicity of the liposomal drug was equal to or greater than that of the free drug, and was not due to immediate drug release upon incubation with cells. The importance of achieving synergistic drug-to-drug ratios and prolonged exposure time to 5-FU and CPT-11, both when alone and in combination, was demonstrated through a series of *in vitro* cytotoxicity experiments. *In vivo* studies revealed that 5-FU and Irinophore C™ could be co-administered without significantly altering the PK/BD profile of either therapy, relative to when administered as single agents. Investigation of single agent Irinophore C™ *in vivo* showed dose-dependent therapeutic activity following administration of low doses of Irinophore C™, although a sub-population of tumor cells remained even after treatment with high doses of Irinophore C™. Therapeutic studies in mouse models of human CRC demonstrated that single agent Irinophore C™ was more effective than the combination of Irinophore C™ and 5-FU, and was significantly more active than the combination of free irinotecan and 5-FU. These results suggest that it may be possible to achieve improved disease control in the treatment of CRC by replacing free irinotecan with Irinophore C™, and that it will be important to continue pre-clinical evaluations of Irinophore C™ in a combination setting. Preparations are currently underway for a phase I clinical trial with Irinophore C™.

3.5. References – Chapter 3

1. Global Cancer Facts & Figures 2007 (Revision 2). Atlanta: American Cancer Society; 2007.

2. Goldberg RM. Advances in the treatment of metastatic colorectal cancer. *Oncologist* 2005; 10 Suppl. 3: 40-48.

3. Kelly H, Goldberg RM. Systemic therapy for metastatic colorectal cancer: current options, current evidence. *J. Clin. Oncol.* 2005; 23: 4553-4560.

4. Grothey A, Sugrue MM, Purdie DM, Dong W, Sargent D, Hedrick E, Kozloff M. Bevacizumab beyond first progression is associated with prolonged overall survival in metastatic colorectal cancer: results from a large observational cohort study (BRiTE). *J. Clin. Oncol.* 2008; 26: 5326-5334.

5. Grothey E, Chu E. The clinical efficacy of FOLFIRI and bevacizumab in combination as first-line therapy of metastatic colorectal cancer. *Clin. Colorectal Cancer* 2007; 6: 621-624.

6. Gill S, Blackstock AW, Goldberg RM. Colorectal cancer. *Mayo Clin. Proc.* 2007; 82: 114-129.

7. Canadian Cancer Statistics. Toronto: Canadian Cancer Society; 2009.

8. Kawato Y, Aonuma M, Hirota Y, Kuga H, Sato K. Intracellular roles of SN-38, a metabolite of the camptothecin derivative CPT-11, in the antitumor effect of CPT-11. *Cancer Res.* 1991; 51: 4187-4191.

9. Lavelle F, Bissery MC, Andre S, Roquet F, Riou JF. Preclinical evaluation of CPT-11 and its active metabolite SN-38. *Semin. Oncol.* 1996; 23: 11-20.

10. Senter PD, Beam KS, Mixan B, Wahl AF. Identification and activities of human carboxylesterases for the activation of CPT-11, a clinically approved anticancer drug. *Bioconjug. Chem.* 2001; 12: 1074-1080.

11. Xu G, Zhang W, Ma MK, McLeod HL. Human carboxylesterase 2 is commonly expressed in tumor tissue and is correlated with activation of irinotecan. *Clin. Cancer Res.* 2002; 8: 2605-2611.

12. Humerickhouse R, Lohrbach K, Li L, Bosron WF, Dolan ME. Characterization of CPT-11 hydrolysis by human liver carboxylesterase isoforms hCE-1 and hCE-2. *Cancer Res.* 2000; 60: 1189-1192.

13. Irinotecan. Vancouver: BC Cancer Agency; 2001; Limited revision June 2010.

14. Saliba F, Hagipantelli R, Misset JL, Bastian G, Vassal G, Bonnay M, Herait P, Cote C, Mahjoubi M, Mignard D, Cvitkovic E. Pathophysiology and therapy of irinotecan-induced delayed-onset diarrhea in patients with advanced colorectal cancer: a prospective assessment. *J. Clin. Oncol.* 1998; 16: 2745-2751.

15. Khanna R, Morton CL, Danks MK, Potter PM. Proficient metabolism of irinotecan by a human intestinal carboxylesterase. *Cancer Res.* 2000; 60: 4725-4728.

16. Guichard S, Terret C, Hennebelle I, Lochon I, Chevreau P, Fretigny E, Selves J, Chatelut E, Bugat R, Canal P. CPT-11 converting carboxylesterase and topoisomerase activities in tumour and normal colon and liver tissues. *Br. J. Cancer* 1999; 80: 364-370.

17. Mathijssen RH, van Alphen RJ, Verweij J, Loos WJ, Nooter K, Stoter G, Sparreboom A. Clinical pharmacokinetics and metabolism of irinotecan (CPT-11). *Clin. Cancer Res.* 2001; 7: 2182-2194.

18. Fassberg J, Stella VJ. A kinetic and mechanistic study of the hydrolysis of camptothecin and some analogues. *J. Pharm. Sci.* 1992; 81: 676-684.

19. Rivory LP, Chatelut E, Canal P, Mathieu-Boue A, Robert J. Kinetics of the in vivo interconversion of the carboxylate and lactone forms of irinotecan (CPT-11) and of its metabolite SN-38 in patients. *Cancer Res.* 1994; 54: 6330-6333.

20. Burke TG, Mi Z. The structural basis of camptothecin interactions with human serum albumin: impact on drug stability. *J. Med. Chem.* 1994; 37: 40-46.

21. Ramsay EC, Anantha M, Zastre J, Meijs M, Zonderhuis J, Strutt D, Webb MS, Waterhouse D, Bally MB. Irinophore C: a liposome formulation of irinotecan with substantially improved therapeutic efficacy against a panel of human xenograft tumors. *Clin. Cancer Res.* 2008; 14: 1208-1217.

22. Ramsay E, Alnajim J, Anantha M, Zastre J, Yan H, Webb M, Waterhouse D, Bally M. A novel liposomal irinotecan formulation with significant anti-tumour activity: use of the divalent cation ionophore A23187 and copper-containing liposomes to improve drug retention. *Eur. J. Pharm. Biopharm.* 2008; 68: 607-617.

23. Ramsay E, Alnajim J, Anantha M, Taggar A, Thomas A, Edwards K, Karlsson G, Webb M, Bally M. Transition metal-mediated liposomal encapsulation of irinotecan (CPT-11) stabilizes the drug in the therapeutically active lactone conformation. *Pharm. Res.* 2006; 23: 2799-2808.

24. Patankar N, Anantha M, Ramsay E, Waterhouse D, Bally M. The role of the transition metal copper and the ionophore A23187 in the development of Irinophore C. *Pharm. Res.* 2011; 28: 848-857.

25. Saltz LB, Douillard JY, Pirotta N, Alakl M, Gruia G, Awad L, Elfring GL, Locker PK, Miller LL. Irinotecan plus fluorouracil/leucovorin for metastatic colorectal cancer: a new survival standard. *Oncologist* 2001; 6: 81-91.

26. Saltz LB, Cox JV, Blanke C, Rosen LS, Fehrenbacher L, Moore MJ, Maroun JA, Ackland SP, Locker PK, Pirotta N, Elfring GL, Miller LL. Irinotecan plus fluorouracil and leucovorin for metastatic colorectal cancer. Irinotecan Study Group. *N. Engl. J. Med.* 2000; 343: 905-914.

27. Cheng WW, Das D, Suresh M, Allen TM. Expression and purification of two anti-CD19 single chain Fv fragments for targeting of liposomes to CD19-expressing cells. *Biochim. Biophys. Acta* 2007; 1768: 21-29.

28. Cheng WW, Allen TM. Targeted delivery of anti-CD19 liposomal doxorubicin in B-cell lymphoma: a comparison of whole monoclonal antibody, Fab' fragments and single chain Fv. *J. Control. Release* 2008; 126: 50-58.

29. Charrois GJR, Allen TM. Drug release rate influences the pharmacokinetics, biodistribution, therapeutic activity, and toxicity of pegylated liposomal doxorubicin formulations in murine breast cancer. *Biochim. Biophys. Acta* 2004; 1663: 167-177.

30. Kobayashi K, Bouscarel B, Matsuzaki Y, Ceryak S, Kudoh S, Fromm H. pH-dependent uptake of irinotecan and its active metabolite, SN-38, by intestinal cells. *Int. J. Cancer* 1999; 83: 491-496.

31. Mayer LD, Harasym TO, Tardi PG, Harasym NL, Shew CR, Johnstone SA, Ramsay EC, Bally MB, Janoff AS. Ratiometric dosing of anticancer drug combinations: controlling drug ratios after systemic administration regulates therapeutic activity in tumor-bearing mice. *Mol. Cancer Ther.* 2006; 5: 1854-1863.

32. Mayer LD, Janoff AS. Optimizing combination chemotherapy by controlling drug ratios. *Mol. Interv.* 2007; 7: 216-223.

33. Pavillard V, Kherfellah D, Richard S, Robert J, Montaudon D. Effects of the combination of camptothecin and doxorubicin or etoposide on rat glioma cells and camptothecin-resistant variants. *Br. J. Cancer* 2001; 85: 1077-1083.

34. Harasym TO, Tardi PG, Harasym NL, Harvie P, Johnstone SA, Mayer LD. Increased preclinical efficacy of irinotecan and floxuridine coencapsulated inside liposomes is associated with tumor delivery of synergistic drug ratios. *Oncol. Res.* 2007; 16: 361-374.

35. Tardi PG, Dos Santos N, Harasym TO, Johnstone SA, Zisman N, Tsang AW, Bermudes DG, Mayer LD. Drug ratio-dependent antitumor activity of irinotecan and cisplatin combinations in vitro and in vivo. *Mol. Cancer Ther.* 2009; 8: 2266-2275.

36. Tardi P, Johnstone S, Harasym N, Xie S, Harasym T, Zisman N, Harvie P, Bermudes D, Mayer L. In vivo maintenance of synergistic cytarabine:daunorubicin ratios greatly enhances therapeutic efficacy. *Leuk. Res.* 2009; 33: 129-139.

37. Fanciullino R, Giacometti S, Mercier C, Aubert C, Blanquicett C, Piccerelle P, Ciccolini J. In vitro and in vivo reversal of resistance to 5-fluorouracil in colorectal cancer cells with a novel stealth double-liposomal formulation. *Br. J. Cancer* 2007; 97: 919-926.

38. Fresta M, Villari A, Puglisi G, Cavallaro G. 5-Fluorouracil: various kinds of loaded liposomes: encapsulation efficiency, storage stability and fusogenic properties. *Intl. J. Pharm.* 1993; 99: 145-156.

39. Messerer CL, Ramsay EC, Waterhouse D, Ng R, Simms EM, Harasym N, Tardi P, Mayer LD, Bally MB. Liposomal irinotecan: formulation development and therapeutic assessment in murine xenograft models of colorectal cancer. *Clin. Cancer Res.* 2004; 10: 6638-6649.

40. Baker JH, Lam J, Kyle AH, Sy J, Oliver T, Co SJ, Dragowska WH, Ramsay E, Anantha M, Ruth TJ, Adam MJ, Yung A, Kozlowski P, Minchinton AI, Ng SS, Bally MB, Yapp DT. Irinophore C, a novel nanoformulation of irinotecan, alters tumor vascular function and enhances the distribution of 5-fluorouracil and doxorubicin. *Clin. Cancer Res.* 2008; 14: 7260-7271.

41. Vokes EE, Chu E. Anti-EGFR therapies: clinical experience in colorectal, lung, and head and neck cancers. *Oncology (Williston Park)* 2006; 20: 15-25.

42. Verreault M, Strutt D, Masin D, Anantha M, Yung A, Kozlowski P, Waterhouse D, Bally MB, Yapp DT. Vascular normalization in orthotopic glioblastoma following intravenous treatment with lipid-based nanoparticulate formulations of irinotecan (Irinophore C), doxorubicin (Caelyx(R)) or vincristine. *BMC Cancer* 2011; 11: 124-141.

43. Busby JE, Kim SJ, Yazici S, Nakamura T, Kim JS, He J, Maya M, Wang X, Do KA, Fan D, Fidler IJ. Therapy of multidrug resistant human prostate tumors in the prostate of nude mice by simultaneous targeting of the epidermal growth factor receptor and vascular endothelial growth factor receptor on tumor-associated endothelial cells. *Prostate* 2006; 66: 1788-1798.

44. Nobili S, Landini I, Giglioni B, Mini E. Pharmacological strategies for overcoming multidrug resistance. *Curr. Drug Targets* 2006; 7: 861-879.

45. Kobayashi T, Ishida T, Okada Y, Ise S, Harashima H, Kiwada H. Effect of transferrin receptor-targeted liposomal doxorubicin in P-glycoprotein-mediated drug resistant tumor cells. *Int. J. Pharm.* 2007; 329: 94-102.

46. Durand RE. Distribution and activity of antineoplastic drugs in a tumor model. *J. Natl. Cancer Inst.* 1989; 81: 146-152.

47. Tunggal JK, Melo T, Ballinger JR, Tannock IF. The influence of expression of P-glycoprotein on the penetration of anticancer drugs through multicellular layers. *Int. J. Cancer* 2000; 86: 101-107.

48. Nakajima TE, Yasunaga M, Kano Y, Koizumi F, Kato K, Hamaguchi T, Yamada Y, Shirao K, Shimada Y, Matsumura Y. Synergistic antitumor activity of the novel SN-38-incorporating polymeric micelles, NK012, combined with 5-fluorouracil in a mouse model of colorectal cancer, as compared with that of irinotecan plus 5-fluorouracil. *Int. J. Cancer* 2008; 122: 2148-2153.

49. Azrak RG, Cao S, Slocum HK, Toth K, Durrani FA, Yin MB, Pendyala L, Zhang W, McLeod HL, Rustum YM. Therapeutic synergy between irinotecan and 5-fluorouracil against human tumor xenografts. *Clin. Cancer Res.* 2004; 10: 1121-1129.

50. Rothenberg ML. Irinotecan (CPT-11): recent developments and future directions--colorectal cancer and beyond. *Oncologist* 2001; 6: 66-80.

51. Diasio RB, Harris BE. Clinical pharmacology of 5-fluorouracil. *Clin. Pharmacokinet.* 1989; 16: 215-237.

52. Meta-analysis Group In Cancer. Efficacy of intravenous continuous infusion of fluorouracil compared with bolus administration in advanced colorectal cancer. *J. Clin. Oncol.* 1998; 16: 301-308.

53. Arbuck SG. Overview of clinical trials using 5-fluorouracil and leucovorin for the treatment of colorectal cancer. *Cancer* 1989; 63: 1036-1044.

CHAPTER 4

In Vitro Properties of Vasculature-targeted and Tumor-targeted Liposomes

4. *In Vitro* Properties of Vasculature-targeted and Tumor-targeted Liposomes

4.1. Introduction

Liposomes, or lipidic nanoparticles, were first described by Dr. Alec Bangham nearly 50 years ago (1). Liposomes have been successfully utilized as drug delivery systems for a variety of small molecule chemotherapeutic drugs; optimized liposomal formulations of several different anti-cancer agents have demonstrated altered side effect profiles and PK/BD parameters, such as increased tumor accumulation and smaller volume of distribution, leading to greater therapeutic activity and a broader therapeutic index, relative to the free drug (2-6).

The presence of uniquely expressed and/or over-expressed proteins on cancer cells and cancer-associated cells provides an opportunity to selectively target liposomal anti-cancer agents to specific cell populations, by coupling receptor-specific ligands to the liposome surface (7-9). A number of different covalent and non-covalent coupling techniques have been investigated (10, 11), and have made it possible to utilize a variety of types of targeting moieties, including: peptides, proteins, aptamers, antibodies, and antibody fragments (12). Recognition of the versatility of ligand-modified liposomal chemotherapeutics, their applicability to the treatment of numerous types of cancer, and of the significant therapeutic potential of the approach, has led to widespread investigation around the world (12-15).

Combination chemotherapy is beginning to be explored in the context of nanomedicines, including approaches that combine different targeted liposomal

drug formulations, and provide unique opportunities for selective drug delivery. The dual-targeted combination approach that is investigated in Chapters 4 and 5 of this thesis exploits the selectivity of ligand-mediated targeting to deliver different liposomal anti-cancer agents to two distinct cell populations – the tumor cells themselves and the tumor vascular endothelial cells. In the ~15-30% of breast cancers that over-express HER2, antibodies against HER2 can be used as targeting ligands. In many different types of cancer, two common proteins that can be used as targets on tumor vasculature are APN/CD13 and the $\alpha_v\beta_3$ integrin.

APN/CD13 is a metalloprotease that cleaves the amino terminus of biologically active peptides, including angiotensins, enkephalins, and cytokines (16). It has been shown to have roles in antigen presentation and immune response, degradation of the extracellular matrix, cell migration, angiogenesis, and tumor invasion (16, 17, and references therein). CD13 is expressed by a number of different cell types in the body: angiogenic endothelial cells, a variety of types of epithelial cells, fibroblasts, smooth muscle cells, mast cells, cells in the bile duct, and cells of myeloid origin, such as macrophages, monocytes, and their hematopoetic precursors (18, and references therein). It has been demonstrated that a specific isoform of CD13 is uniquely expressed by angiogenic vascular endothelial cells; this isoform, but not the other isoforms of CD13, is selectively targeted by the NGR sequence (18, 19). The KS1767 human Kaposi's sarcoma cell line and HUVEC have been shown to express the isoform of APN that is selectively targeted by the NGR motif, and both cell lines are useful as *in vitro* models of vascular endothelium (20). The NGR sequence homes to CD13

regardless of species or tumor type (21). Drug-loaded NGR-SL have been investigated previously (22-25), notably by Pastorino *et al.* as part of a dual-targeted approach to the treatment of neuroblastoma (22).

Integrins have roles in cell adhesion to extracellular matrix proteins and cell migration, and also mediate interactions with other cells. Numerous different integrin isoforms exist, with the $\alpha_v\beta_3$ isoform being of particular relevance to this thesis. The $\alpha_v\beta_3$ integrin mediates cell adhesion, via an RGD recognition sequence (26), to a variety of components of the extracellular matrix and soluble proteins, including vitronectin, fibronectin, fibrinogen, thrombospondin, and osteopontin (27, 28). The $\alpha_v\beta_3$ integrin is expressed at low levels on a few cell types, such as intestinal, vascular, and uterine smooth muscle cells, osteoclasts, and activated leukocytes and macrophages (29), and is over-expressed on tumor vascular endothelial cells (30). The HUVEC and KS1767 cells express the $\alpha_v\beta_3$ integrin (31). The RGD motif has been identified for its ability to bind to the $\alpha_v\beta_3$ integrin (21, 28); a cyclised version of the RGD sequence has been shown to be highly selective for the $\alpha_v\beta_3$ integrin (32, 33). Peptides containing the RAD or cRAD motif function as mismatched controls for RGD and cRGD (28). As discussed by Temming *et al.*, RGD- and cRGD-modified liposomes/polymers, proteins, drugs, and radiotracers have been successfully employed as a means to deliver therapies to tumor vasculature for cancer diagnosis and treatment (33).

HER2 is a transmembrane receptor tyrosine kinase that is a member of the EGFR family, with a significant role in the regulation of cell proliferation, differentiation, and survival. The receptor has no known ligand and is

constitutively active (34), due to its constitutively exposed dimerization arm (35). HER2 is the preferred dimerization partner for other members of the EGFR family, and greatly enhances their signalling capacity (36, 37). Over-expression of HER2 provides cells with a growth advantage and is a negative prognostic indicator (38). As a result of gene amplification (39, 40), HER2 is over-expressed in a number of cancers, including ovarian, gastric, colon, lung, and 15-30% of breast cancers (41, 42, 43, and references therein). The HER2 receptor can be targeted (44) with the humanized anti-HER2 monoclonal antibody trastuzumab (45). Trastuzumab can be utilized to treat HER2-positive breast cancer (46-48), and exerts its therapeutic activity by binding to the HER2 receptor and inhibiting its downstream signalling, activating apoptosis, and initiating complement-dependent cytotoxicity and antibody-dependent cellular cytotoxicity (49). Drug-loaded PEGylated liposomes targeted to HER2-positive breast cancer cells were first investigated fifteen years ago (50, 51). Since that time, an optimized formulation of αHER2 scFv-targeted (F5-targeted) liposomal DXR has been developed, and will be entering clinical trials in the near future (52, 53).

It is well-recognized that two of the major goals of cancer therapy are to increase drug delivery to the target cells and to improve cell selectivity in order to minimize adverse effects on off-target cell populations; ligand-modified liposomes have the ability to achieve both of these goals. Upon ligand binding to an internalizing receptor, the entire receptor-ligand-liposome complex can be endocytosed into the cell (54, 55). The drug is released from the liposome in lysoendosomal compartments, and is trafficked to its intracellular site of action

(14, 56, 57). Internalization of the entire liposome leads to intracellular delivery of the entire drug content of the liposome, or tens of thousands of drug molecules when utilizing stable, slow release constructs. In contrast, untargeted liposomes slowly release encapsulated drug into the tumor interstitium, and then individual drug molecules passively diffuse into nearby cancer cells or out of the tumor (58, 59). In cancer models with significant over-expression of an internalizing receptor (52, 60), increased intracellular drug delivery and alterations in intracellular trafficking through use of ligand-modified liposomal drugs have led to improvements in therapeutic effect, over untargeted liposomal drugs (12, 14, and references therein). It has been demonstrated in a HER2-positive breast cancer model that the administration of a tumor-targeted formulation of liposomal DXR resulted in a greater nuclear drug concentration in tumors, compared to use of untargeted liposomal DXR, and the increase in tumor drug bioavailability correlated with an increase in therapeutic effect (61).

It is postulated that the combined use of two different formulations of ligand-modified liposomes could lead to selective and increased cytotoxicity against two distinct cell populations within the tumor, and thereby, superior tumor growth delay relative to either agent alone. This dual-targeted combination approach to breast cancer treatment relies on the specificity and selectivity of ligand-modified liposomes. As discussed in Chapter 1, ligand and target selection can significantly impact the therapeutic potential of a ligand-modified liposomal drug formulation. Thus, before investigating the dual-targeted approach in the complex *in vivo* environment, it was necessary to investigate the cellular

association properties of the NGR-SL and cRGD-SL (vasculature-targeted liposomes) and the αHER2-SIL (tumor-targeted liposomes) *in vitro*. This chapter presents experiments utilizing cellular models of HER2-positive breast cancer and angiogenic vascular endothelium to assess the cellular association of ligand-modified liposomes relative to control liposomes, the effect of excess free targeting ligand on cellular association, ligand-induced receptor internalization, the time-course of cellular association, the effect of ligand density and diluent composition on liposome cellular association, as well as the cytotoxicity of drug-loaded liposomes.

4.2. Results

4.2.1. Comparison of Radioactivity and Fluorescence Methods

In order to ensure that the liposomal cellular association data generated via the radioactivity method correlated well with data generated using a second method, cellular association was compared using two assay techniques in parallel. Incubating KS1767 cells with DXR-loaded, radio-labelled liposomes enabled quantitation of liposome association via both scintillation counting of the cell-associated radioactive lipid label (Fig. 4.1A) and fluorometric analysis of the cell-associated fluorescent liposomal drug (Fig. 4.1B).

Data from each method demonstrated a significant increase in the degree of the cellular association of the NGR-SL[DXR], relative to the SL[DXR], at 1.6 μmol PL/mL. The radioactivity method showed over a 9-fold difference in cellular association between the formulations ($P < 0.001$; Fig. 4.1A); the fluorescence method showed a lower (~5-fold) increase ($P < 0.001$; Fig. 4.1B),

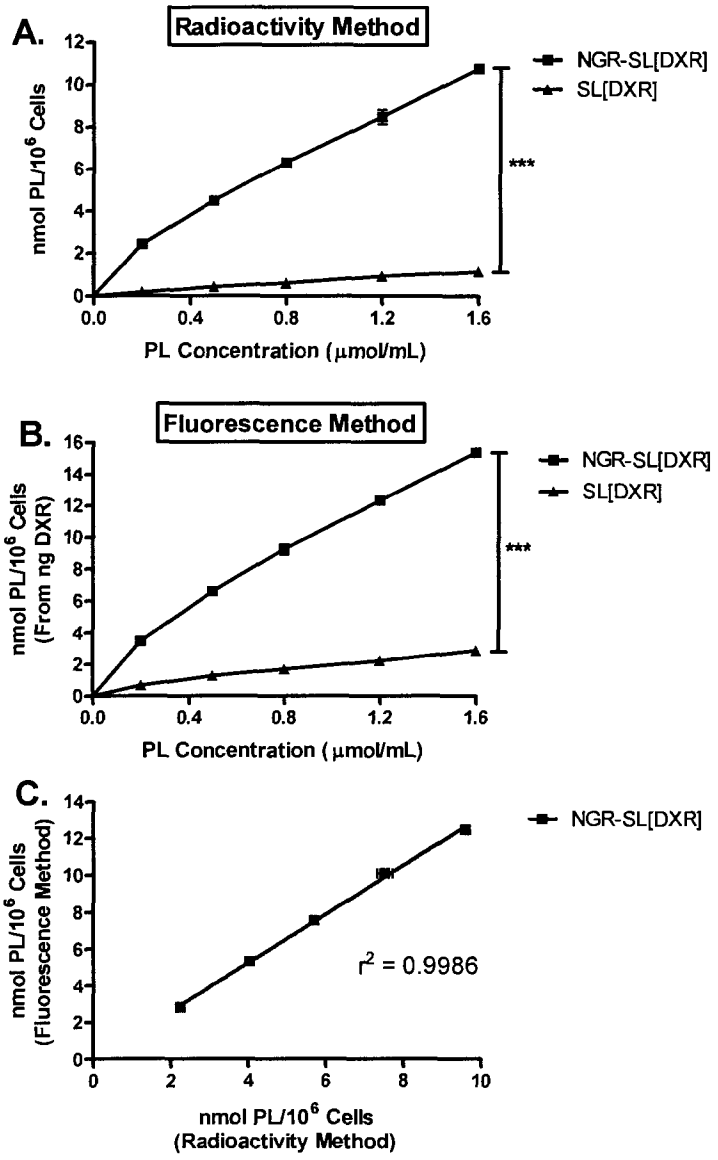

Figure 4.1. Comparison of the radioactivity method and the fluorescence method for assessing liposomal cellular association.

The KS1767 cells were incubated with increasing concentrations of radio-labelled SL[DXR] or NGR-SL[DXR] for 1 h at 37°C. Cells were washed twice with ice-cold PBS (pH 7.4). Samples then underwent LSC to quantitate the remaining cell-associated radioactivity (A) or fluorometric analysis of cell-associated DXR following DXR extraction (B). Fluorescence data were converted from ng DXR to nmol PL equivalents using the drug-to-lipid ratio of the formulation. C) Comparison of the NGR-SL[DXR] cellular association data generated via each method. Data are presented as nmol PL/10^6 cells. Each point represents the mean +/- standard deviation (n = 3) from one representative experiment. ***, $P < 0.001$.

possibly due to incomplete extraction of DXR from the cells that had internalized the NGR-SL[DXR], which would not be an issue with the non-internalizing SL. Figure 4.1C shows the correlation between the radioactivity method and the fluorescence method for quantitating the cellular association of the NGR-SL[DXR]. Under the experimental conditions described above, the relationship between the two methods was determined to be linear (goodness of fit (r^2) = 0.9986), with a slope of 1.32 +/- 0.03 (nmol PL from fluorescence method/nmol PL from radioactivity method). Although the correlation should be confirmed using different cell lines and formulations, this study suggests that the radioactivity method is suitable for assessing liposomal cellular association, as it generates data comparable with those generated via the fluorescence method.

4.2.2. Tumor-targeted Liposomes

4.2.2.1. Cellular Association and Internalization

Target-specific cellular association and internalization of ligand-modified liposomal formulations is important for achieving selective drug delivery. Studies were completed to determine whether coupling αHER2 monoclonal antibodies to the surface of liposomes increased the degree of cellular association with HER2-positive tumor cells, relative to untargeted liposomes. Figure 4.2 presents the cellular association of the SL and αHER2-SIL with the $4T1.2^{ErbB-2}$ cells *in vitro*. At 1.6 μmol PL/mL, the αHER2-SIL showed 2- to 3-fold greater cellular association than did the SL at both 4°C ($P < 0.001$) and 37°C ($P < 0.05$).

To explore whether receptor-mediated internalization and receptor recycling were observed following binding of the targeted liposomes, it was

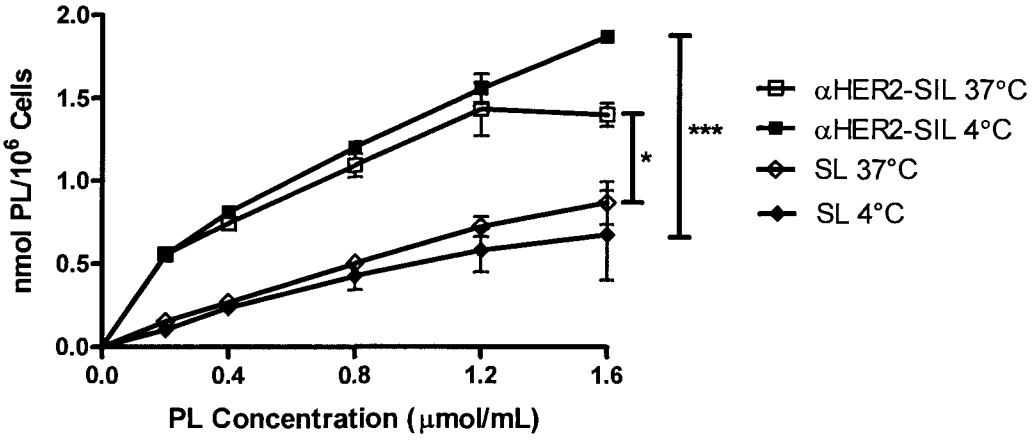

Figure 4.2. Cellular association of αHER2-SIL and SL with 4T1.2^{ErbB-2} cells *in vitro*.

The 4T1.2^{ErbB-2} cells were incubated with increasing concentrations of radio-labelled SL or αHER2-SIL for 1 h at 4 or 37°C. Liposomal cellular association was quantitated by scintillation counting of cell-associated radioactivity. Data are presented as nmol PL/10^6 cells. Each point represents the mean +/- standard deviation (n = 3) from one representative experiment. *, $P < 0.05$; ***, $P < 0.001$.

necessary to compare the cellular association of the liposomes at a permissive and a non-permissive temperature for internalization. The degree of the cellular association of the SL did not differ between 4 and 37°C, suggesting that the liposomes were not internalized. Unexpectedly, there was also not a statistically significant difference between the cellular association of the αHER2-SIL at 4 and 37°C, however, a trend towards greater cellular association of the αHER2-SIL at 4°C was apparent (Fig. 4.2).

4.2.2.2. Cellular Association Following Surface Protein Removal

The internalization of the αHER2-SIL into the $4T1.2^{ErbB-2}$ cells was further investigated by comparing liposomal cellular association before and after cell surface proteins were cleaved using an acidic glycine solution (Fig. 4.3). The cellular association of the SL was the same at 4 and 37°C, and was unchanged by surface stripping. In contrast, protein stripping significantly reduced the cellular association of the αHER2-SIL at both 4°C ($P < 0.001$) and 37°C ($P < 0.001$). Following the removal of surface proteins, the αHER2-SIL demonstrated a reduction in cellular association of 15-30% at 4°C ($P < 0.001$) and 35-50% at 37°C ($P < 0.001$), relative to control conditions. The cellular association of the αHER2-SIL was significantly greater at 4°C than at 37°C, both after surface stripping ($P < 0.001$) and without surface stripping ($P < 0.01$).

4.2.2.3. Cellular Association in the Presence of Excess Free Targeting Ligand

To gain greater insight into the specificity of the cellular association of the αHER2-SIL, an experiment was completed to compare the *in vitro* cellular

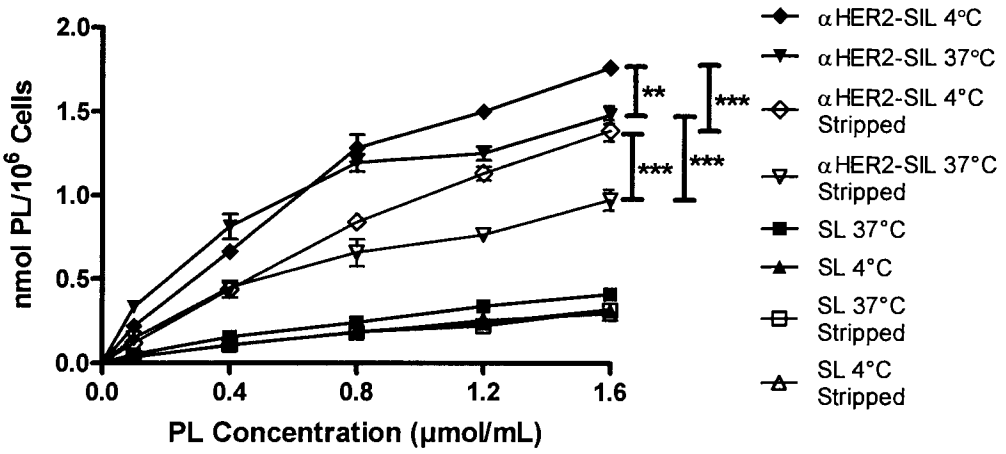

Figure 4.3. *In vitro* cellular association of αHER2-SIL with 4T1.2^{ErbB-2} cells before and after removal of surface proteins.

The 4T1.2^{ErbB-2} cells were incubated with increasing concentrations of radio-labelled SL or αHER2-SIL for 1 h at 4 or 37°C. Cells were washed twice with ice-cold PBS (pH 7.4), then underwent two 10 min stripping incubations with 50 mM glycine solution (pH 2.8; stripped) or two 10 min control incubations with PBS (pH 7.4). Liposomal cellular association was quantitated by scintillation counting of cell-associated radioactivity. Data are presented as nmol PL/10^6 cells. Each point represents the mean +/- standard deviation (n = 3) from one representative experiment. **, $P < 0.01$; ***, $P < 0.001$.

association of the αHER2-SIL with the 4T1.2^{ErbB-2} cells in the presence and absence of 50-fold excess free targeting antibody (Fig. 4.4). In the absence of excess αHER2 monoclonal antibody, the αHER2-SIL displayed 3- to 5-fold greater cellular association at 1.6 μmol PL/mL than did the SL ($P < 0.001$), at 4°C (Fig. 4.4A) and 37°C (Fig. 4.4B). As observed above, the cellular association of the αHER2-SIL with the 4T1.2^{ErbB-2} cells was greater at 4°C than at 37°C. When the cells were pre-saturated with 50-fold excess antibody, the cellular association of the αHER2-SIL was significantly reduced, and was equivalent to the cellular association of the SL, which associate with cells in a non-specific manner.

4.2.2.4. Time-course of Cellular Association

The time dependency of the cellular association of the SL and the αHER2-SIL with the 4T1.2^{ErbB-2} cells was investigated *in vitro*, and the results are presented in Fig. 4.5. The cellular association of the SL reached its maximum after 5 min of incubation with the 4T1.2^{ErbB-2} cells at 4 or 37°C. No further increases in the cellular association of the SL were observed when the incubation period was prolonged to 18, 30, or 60 min, and this was consistent for both 0.4 μmol PL/mL (Fig. 4.5A) and 1.2 μmol PL/mL (Fig. 4.5B). A similar trend was demonstrated with the tumor-targeted liposomes at 1.2 μmol PL/mL, when incubated at 4 or 37°C. Under these conditions, ~90% or more of the cellular association of the αHER2-SIL occurred within 5 min of the start of the incubation with the 4T1.2^{ErbB-2} cells. Lengthening the incubation period from 5 min to 30 or 60 min only allowed for very slight, although statistically significant ($P < 0.05$ or

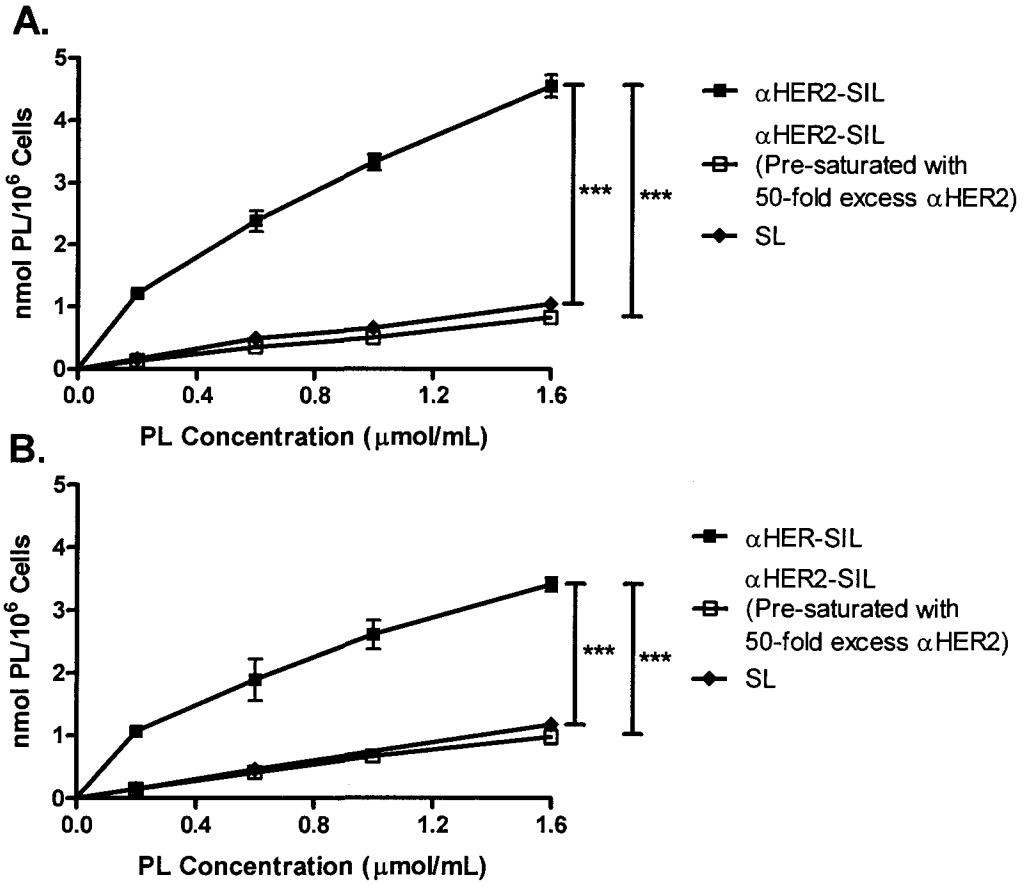

Figure 4.4. Cellular association of αHER2-SIL with 4T1.2^{ErbB-2} cells *in vitro*.

The 4T1.2^{ErbB-2} cells were incubated with increasing concentrations of radio-labelled SL or αHER2-SIL for 1 h at 4°C (A) or 37°C (B). As required, cells were pre-saturated with 50-fold excess αHER2 mAb for 15 min prior to addition of αHER2-SIL. Liposomal cellular association was quantitated by scintillation counting of cell-associated radioactivity. Data are presented as nmol PL/10^6 cells. Each point represents the mean +/- standard deviation (n = 3) from one representative experiment. ***, $P < 0.001$.

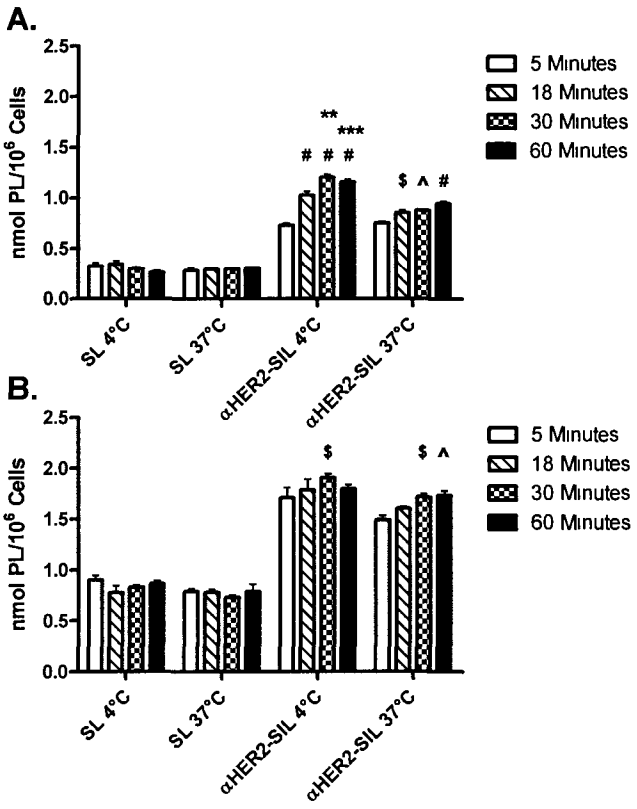

Figure 4.5. Time-course of αHER2-SIL cellular association with 4T1.2^{ErbB-2} cells *in vitro*.

The 4T1.2^{ErbB-2} cells were incubated with radio-labelled SL or αHER2-SIL at a final concentration of 0.4 μmol PL/mL (A) or 1.2 μmol PL/mL (B) for 5, 18, 30, or 60 min at 4°C or 37°C. Liposomal cellular association was quantitated by scintillation counting of cell-associated radioactivity. Data are presented as nmol PL/10^6 cells. Each bar represents the mean +/- standard deviation (n = 3) from one representative experiment. $^{\$}$, $P < 0.05$ vs. 5 min; ^, $P < 0.01$ vs. 5 min; $^{\#}$, $P < 0.001$ vs. 5 min; **, $P < 0.01$ vs. 18 min; ***, $P < 0.001$ vs. 18 min.

0.01, respectively, vs. 5 min), additional increases in the cellular association of the αHER2-SIL at 1.2 μmol PL/mL.

At 0.4 μmol PL/mL (Fig. 4.5A), the magnitude of the cellular association of the αHER2-SIL increased with incubation time ($P < 0.05$-0.001 vs. 5 min; $P <$ 0.01-0.001 vs. 18 min). This trend was observed to a greater extent at 4°C than at 37°C. Nevertheless, well over 50% of the liposomal cellular association occurred within 5 min following the start of the incubation. This *in vitro* study with the $4T1.2^{ErbB-2}$ cells demonstrated that, especially at 37°C, a substantial portion of the cellular association of the SL and the αHER2-SIL occurs within 5 min of the start of the incubation with cells.

4.2.2.5. Cytotoxicity of Tumor-targeted Liposomal DXR

Cell viability assays were completed to compare the *in vitro* cytotoxicity of tumor-targeted and untargeted liposomal DXR formulations against the $4T1.2^{ErbB-2}$ cells (Fig. 4.6A). The free DXR control was the most cytotoxic, with an IC_{50} value of 1.5 μg/mL (95% confidence interval = 1.3 to 1.8 μg/mL). As expected, the two liposomal formulations of DXR were significantly less cytotoxic than free DXR, as the entrapped drug only becomes bioavailable slowly. The DXR-loaded αHER2-SIL (αHER2-SIL[DXR]) were approximately 2-fold more cytotoxic than the SL[DXR], with IC_{50} values of 150 μg DXR/mL (95% confidence interval = 136 to 165 μg DXR/mL) and 317 μg DXR/mL (95% confidence interval = 277 to 363 μg DXR/mL), respectively. The free targeting ligand, αHER2 antibody, alone was not cytotoxic at any concentration tested (Fig. 4.6B).

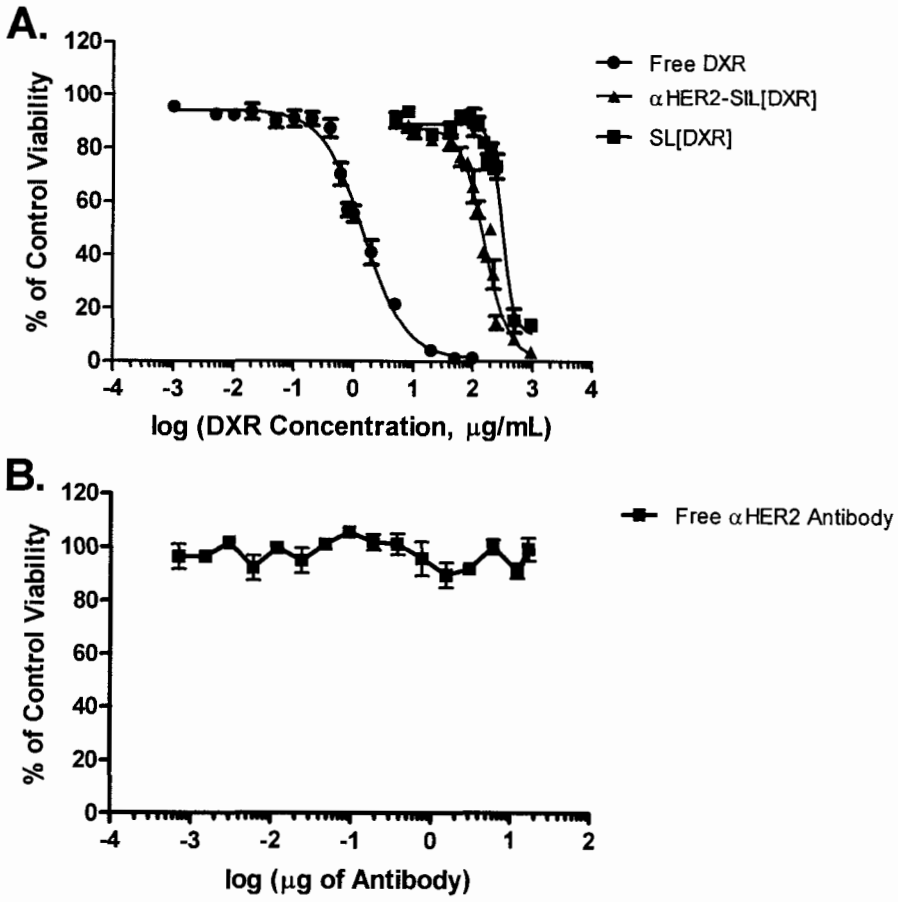

Figure 4.6. Cytotoxicity of free and liposomal DXR and free αHER2 antibody against 4T1.2^{ErbB-2} cells *in vitro*.

The 4T1.2^{ErbB-2} cells were exposed to increasing concentrations of (A) SL[DXR], αHER2-SIL[DXR], or free DXR, or (B) free αHER2 antibody for 1 h at 37°C. Drug was washed out and the cells were incubated for an additional 95 h before cell viability was assessed via an MTT assay. Data are presented as percent of control viability. Each point represents the mean +/- standard deviation (n = 3) from one representative experiment.

4.2.3. Vasculature-targeted Liposomes

4.3.3.1. Effect of Targeting Peptide Density on Cellular Association

Figure 4.7 presents data from an *in vitro* study with the NGR-SL investigating how targeting ligand density affects liposomal cellular association with the KS1767 cells. Different peptide-to-lipid coupling ratios were employed to prepare liposome formulations presenting different numbers of targeting ligands, as determined using the CBQCA assay. The data reveal that a threshold number of NGR peptides per liposome is required to achieve a statistically significant increase in cellular association, relative to the SL, in this model of angiogenic endothelium. The cellular association of the liposomes presenting 147 copies of the NGR peptide was equal to the cellular association of the untargeted liposomes, which associate non-specifically. The liposomes presenting 260 or 412 surface copies of NGR demonstrated ~1.5-fold ($P < 0.001$) or ~3-fold ($P < 0.001$) greater cellular association than did the untargeted liposomes. This study was completed with assistance from Ms. Kim Laginha. Future experiments with NGR-modified liposomes were conducted using liposomes presenting at least 300 copies of NGR peptide.

4.2.3.2. Cellular Association of Control Peptide-modified Liposomes

It was necessary to determine whether or not the increased cellular association of the NGR-SL, relative to the SL, observed above, could be attributed to the presence of peptide (regardless of sequence) on the liposome surface. A study was completed *in vitro* with the KS1767 cells to compare the cellular association of the vasculature-targeted NGR-SL with the control peptide-modified

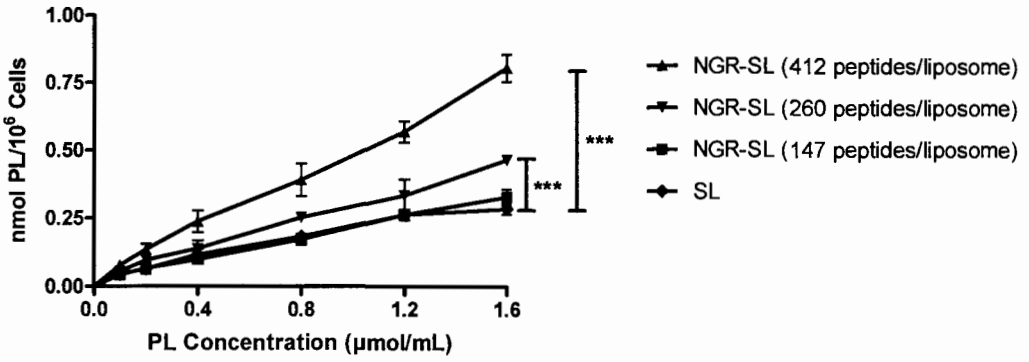

Figure 4.7. Effect of peptide density on cellular association of NGR-SL with KS1767 cells *in vitro*.

The KS1767 cells were incubated with increasing concentrations of radio-labelled SL or NGR-SL, presenting differing numbers of NGR peptides, for 1 h at 37°C. Liposomal cellular association was quantitated by scintillation counting of cell-associated radioactivity. Data are presented as nmol PL/10^6 cells. Each point represents the mean +/- standard deviation (n = 3) from one representative experiment. ***, $P < 0.001$.

ARA-SL. The data presented in Fig. 4.8 reveal that the NGR-SL showed substantially greater cellular association with the KS1767 cells than did the ARA-SL ($P < 0.001$). Despite the presence of peptide coupled to the liposome surface, the ARA-SL did not demonstrate greater cellular association than the SL, which are known to associate with cells in a non-specific manner.

4.2.3.3. Cellular Association with CD13-negative Cell Line

The NGR-SL demonstrated a greater degree of cellular association than did the SL with the KS1767 cells, which are CD13-positive. To explore whether this could be attributed to the presence of the CD13 receptor, a cellular association assay was completed with a CD13-negative cell line – the HEK 293 cell line. The results presented in Fig. 4.9 reveal that the degree of cellular association of the NGR-SL with the CD13-negative cell line is very low. Although there was a statistically significant difference between the cellular association of the two formulations at 1.6 μmol PL/mL ($P < 0.001$), it is a negligible difference when considered in concert with other experiments showing 3- to 5-fold differences in cellular association between the targeted and untargeted liposomes and cellular association of greater than 1.5 nmol PL/10^6 cells for targeted liposomes in many experiments.

4.2.3.4. Effect of Diluent Composition on Cellular Association

A study was completed to explore the effect of serum, culture media, and media supplements on liposomal cellular association *in vitro* (Fig. 4.10) in order to gain greater understanding of how cellular association of the formulations may

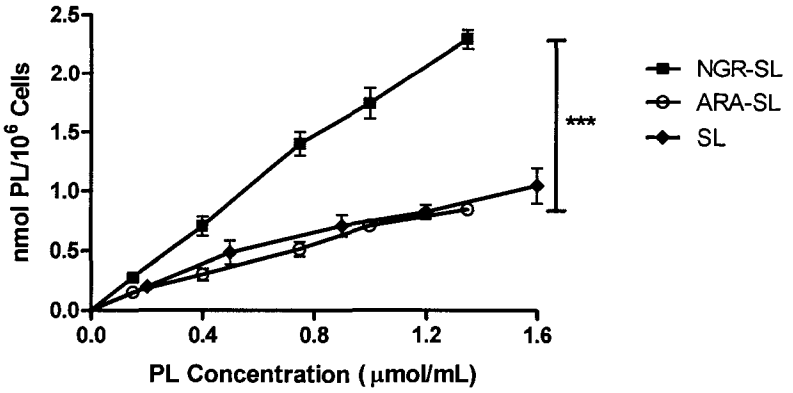

Figure 4.8. Cellular association of vasculature-targeted and control peptide-modified liposomes with KS1767 cells *in vitro*.

The KS1767 cells were incubated with increasing concentrations of radio-labelled SL, NGR-SL, or ARA-SL for 1 h at 37°C. Liposomal cellular association was quantitated by scintillation counting of cell-associated radioactivity. Data are presented as nmol PL/10^6 cells. Each point represents the mean +/- standard deviation (n = 3) from one representative experiment. ***, $P < 0.001$.

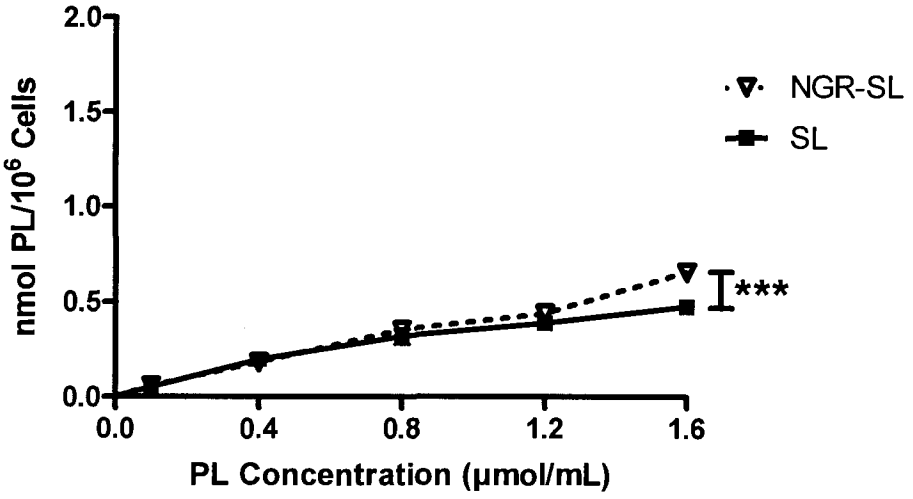

Figure 4.9. Cellular association of NGR-SL and SL with HEK 293 cells *in vitro*.

The HEK 293 cells were incubated with increasing concentrations of radio-labelled SL or NGR-SL for 1 h at 37°C. Liposomal cellular association was quantitated by scintillation counting of cell-associated radioactivity. Data are presented as nmol PL/10^6 cells. Each point represents the mean +/- standard deviation (n = 3) from one representative experiment. ***, $P < 0.001$.

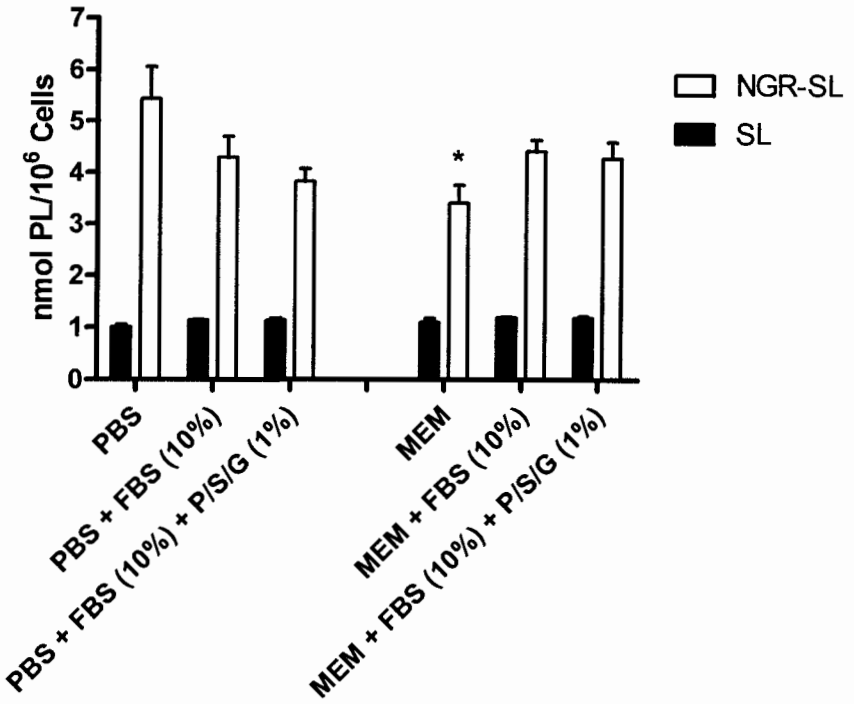

Figure 4.10. Comparison of *in vitro* NGR-SL cellular association with KS1767 cells in PBS, culture media, serum, and/or P/S/G.

The KS1767 cells were incubated with radio-labelled SL or NGR-SL at a final concentration of 1.6 μmol PL/mL for 1 h at 37°C. Liposomal cellular association was quantitated by scintillation counting of cell-associated radioactivity. Data are presented as nmol PL/10^6 cells. Each bar represents the mean +/- standard deviation (n = 3) from one representative experiment. *, $P < 0.05$ vs. PBS.

be affected following *in vivo* administration. The degree of the cellular association of the SL with the KS1767 cells *in vitro* was not affected by the composition of the cell and liposome diluent. When the NGR-SL and the KS1767 cells were incubated in unsupplemented MEM (culture media), the cellular association of the NGR-SL was slightly lower than that observed in PBS (pH 7.4; $P < 0.05$). Furthermore, the cellular association of the NGR-SL was the same when the cells and liposomes were incubated in fully or partially supplemented MEM, or PBS (pH 7.4) plus 1% (v/v) P/S/G and/or 10% (v/v) FBS.

4.2.3.5. Cellular Association and Internalization – NGR-SL

The specific cellular association and internalization of liposomal drugs is often critical to achieving an enhanced therapeutic effect. The data presented in Fig. 4.11 show a comparison of the cellular association of the NGR-SL and the SL with the KS1767 cells *in vitro*, both at 4 and 37°C. The NGR-SL demonstrated significantly greater cellular association at 37°C, which is permissive for receptor internalization, compared to at 4°C, which is non-permissive for receptor internalization ($P < 0.001$). There was a statistically significant increase in the non-specific cellular association of the SL at 37°C, relative to at 4°C ($P < 0.05$). At 1.8 μmol PL/mL, the cellular association of the NGR-SL with the KS1767 cells was ~4-fold higher than was that of the SL ($P < 0.001$ at 4°C and 37°C).

4.2.3.6. Cellular Association and Internalization – cRGD-SL

In addition to the NGR peptide motif, the cRGD peptide motif was also

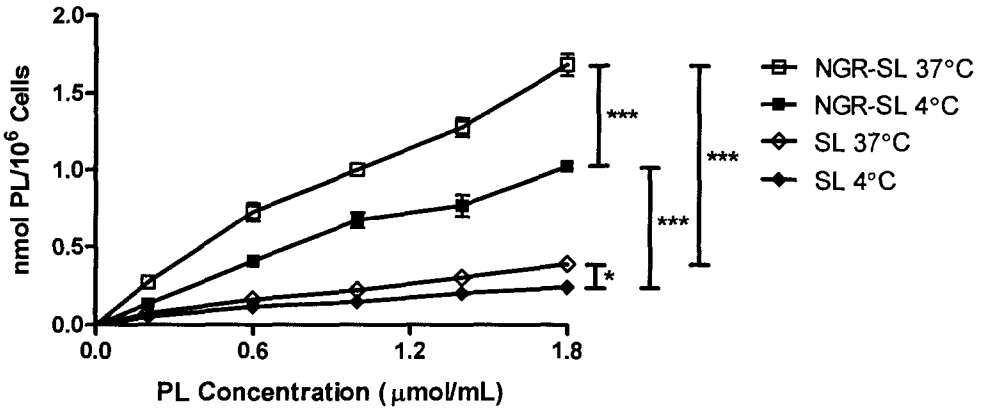

Figure 4.11. Cellular association of NGR-SL with KS1767 cells *in vitro*.

The KS1767 cells were incubated with increasing concentrations of radio-labelled SL or NGR-SL for 1 h at 4 or 37°C. Liposomal cellular association was quantitated by scintillation counting of cell-associated radioactivity. Data are presented as nmol PL/10^6 cells. Each point represents the mean +/- standard deviation (n = 3) from one representative experiment. *, $P < 0.05$; ***, $P < 0.001$.

investigated as a tumor vasculature-specific targeting ligand for the liposomes. The results of the *in vitro* investigation into the cellular association and internalization of the cRGD-SL and SL with the HUVEC are presented in Fig. 4.12. At 37°C, the cellular association of the cRGD-SL was significantly greater than that of the SL ($P < 0.01$); however, this same trend was not observed at 4°C. The cRGD-SL demonstrated significantly greater cellular association with the HUVEC when incubated at 37°C compared to at 4°C ($P < 0.05$), suggesting that the increased cellular association may be the result of receptor-mediated internalization and recycling, which is observed at 37°C (permissive for internalization) but not at 4°C (non-permissive for internalization). In contrast, there was no difference in the cellular association of the SL between 4 and 37°C.

4.2.3.7. Cellular Association in the Presence of Excess Free Targeting Ligand

The cellular association of the cRGD-SL and cRAD-SL with the HUVEC was explored *in vitro* in the presence and absence of excess free targeting ligand in order to gain greater insight into the specificity of the ligand-receptor interaction. The results are presented in Fig. 4.13, and the trends discussed below were observed at both 0.8 μmol PL/mL (Fig. 4.13A) and 1.6 μmol PL/mL (Fig. 4.13B). It was demonstrated that pre-saturation of the HUVEC with 50-fold excess free cRGD peptide prior to incubation with the cRGD-SL resulted in a statistically significant decrease in the magnitude of the cellular association of the cRGD-SL, versus no pre-saturation ($P < 0.001$). Following pre-saturation with cRGD, the cellular association of the cRGD-SL was equal to that of the SL.

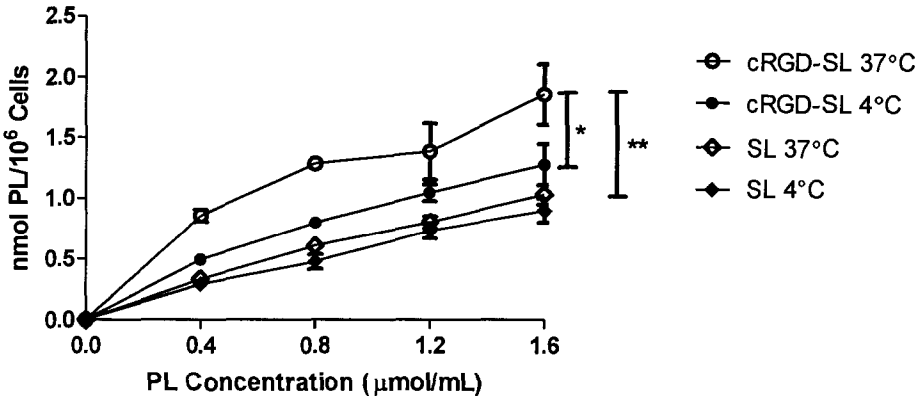

Figure 4.12. Cellular association of cRGD-SL with HUVEC *in vitro*.

The HUVEC were incubated with increasing concentrations of radio-labelled SL or cRGD-SL for 1 h at 4 or 37°C. Liposomal cellular association was quantitated by scintillation counting of cell-associated radioactivity. Data are presented as nmol PL/10^6 cells. Each point represents the mean +/- standard deviation (n = 3) from one representative experiment. *, $P < 0.05$; **, $P < 0.01$.

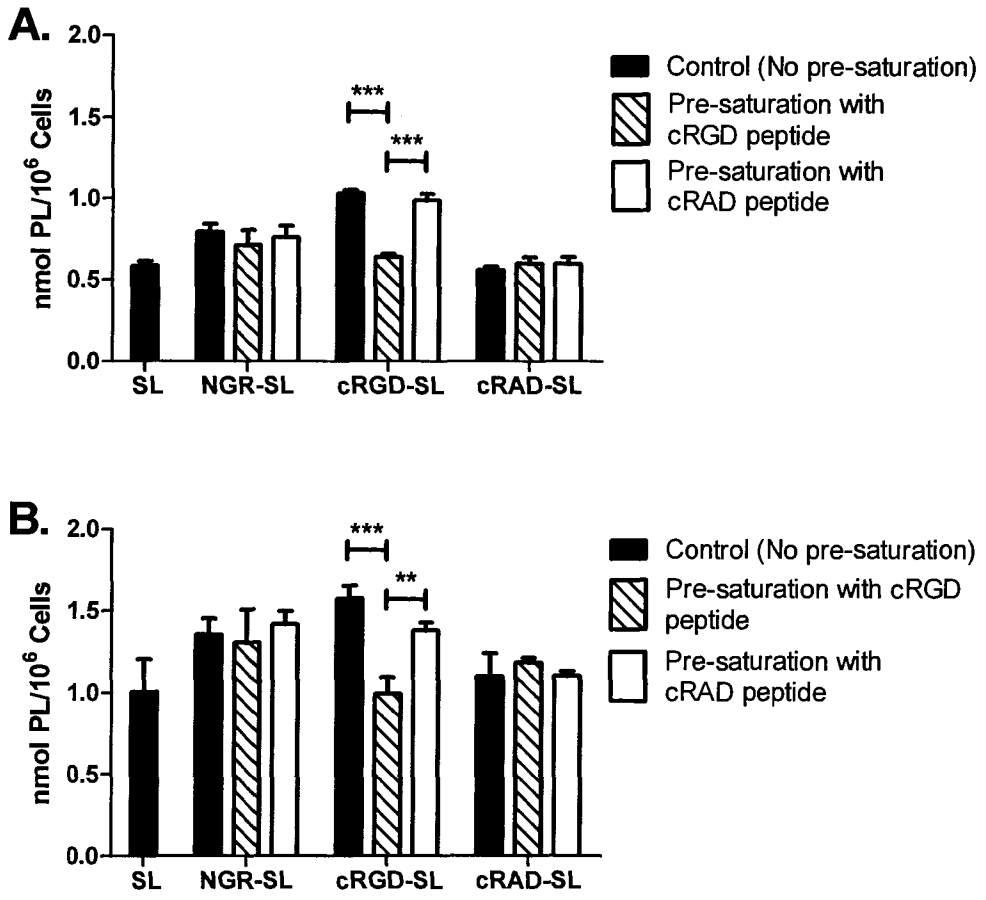

Figure 4.13. ***In vitro*** **cellular association of vasculature-targeted liposomes with HUVEC in the presence of excess targeting peptide.**

The HUVEC were incubated with radio-labelled SL, NGR-SL, cRGD-SL, or cRAD-SL at a final concentration of 0.8 μmol PL/mL (A) or 1.6 μmol PL/mL (B) for 1 h at 37°C. As required, cells were pre-saturated with 50-fold excess cRGD or cRAD peptide for 15 min prior to addition of targeted liposomes. Liposomal cellular association was quantitated by scintillation counting of cell-associated radioactivity. Data are presented as nmol PL/10^6 cells. Each bar represents the mean +/- standard deviation (n = 3) from one representative experiment. **, $P < 0.01$; ***, $P < 0.001$.

Importantly, pre-saturation of the HUVEC with 50-fold excess mismatched control (cRAD) peptide did not lead to a reduction in the cellular association of the cRGD-SL, versus no pre-saturation. Without pre-saturation, the cellular association of the cRAD-SL was equal to that of the SL, and no change in the cellular association of the cRAD-SL was observed following pre-saturation of the HUVEC with 50-fold excess free cRGD or cRAD peptide.

Figure 4.13 also shows the cellular association of the NGR-SL with the HUVEC, which are known to express CD13. The cellular association of the NGR-SL was the same under all three conditions tested: no pre-saturation, pre-saturation with excess cRGD peptide, and pre-saturation with excess cRAD peptide. This means that, as expected, the presence of excess free cRGD or cRAD peptide did not affect the cellular association of the NGR-SL. Although the cellular association of the NGR-SL was lower than that of the cRGD-SL, the NGR-modified liposomes demonstrated greater cellular association with the HUVEC than did the two control formulations: untargeted and mismatched control peptide-modified liposomes.

4.2.3.8. Cytotoxicity of Vasculature-targeted Liposomal VCR

The cytotoxicity of targeted and untargeted liposomal VCR against the KS1767 cells *in vitro* was compared using an MTT assay (Fig. 4.14A). The data revealed that the VCR-loaded SL and NGR-SL (SL[VCR] and NGR-SL[VCR], respectively) were equally cytotoxic against the KS1767 cells *in vitro*, with IC_{50} values of 40 μg VCR/mL (95% confidence interval = 31 to 53 μg VCR/mL) and 42 μg VCR/mL (95% confidence interval = 33 to 52 μg VCR/mL), respectively.

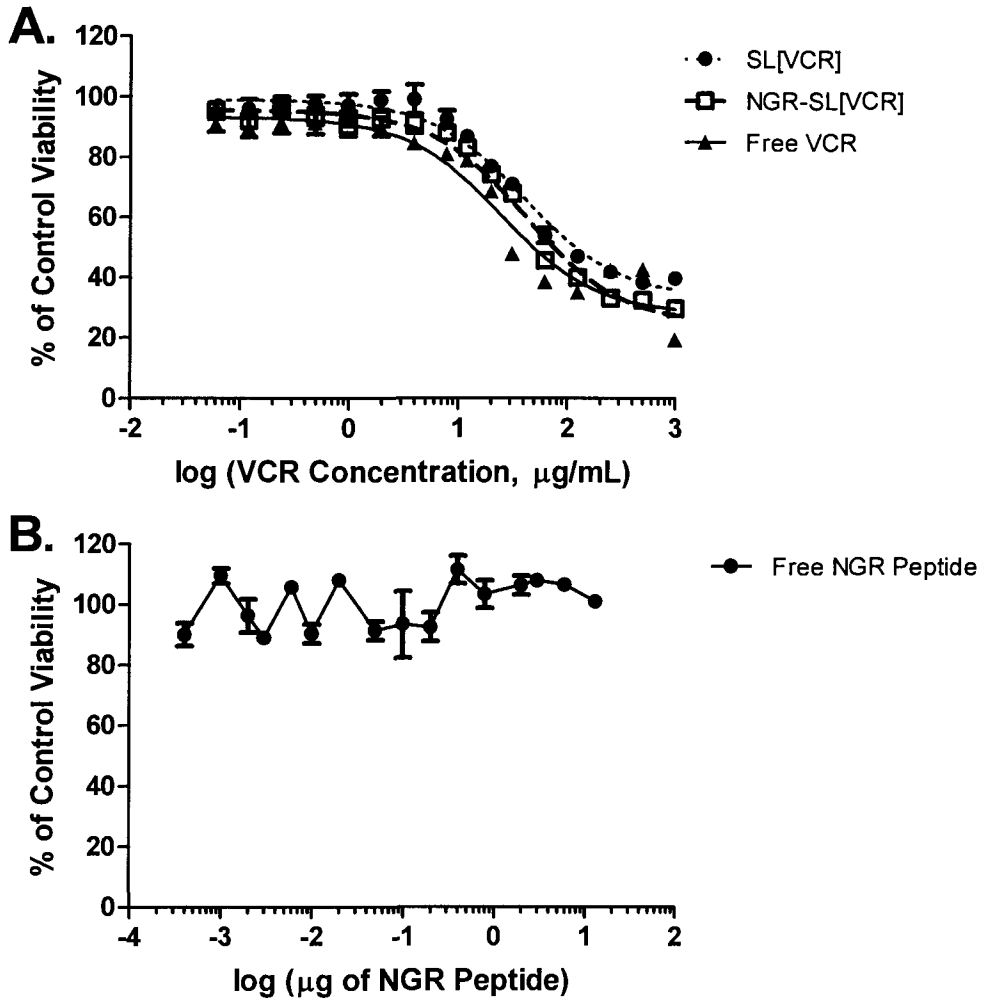

Figure 4.14. Cytotoxicity of free and liposomal VCR and free NGR peptide against KS1767 cells *in vitro*.

The KS1767 cells were exposed to increasing concentrations of (A) SL[VCR], NGR-SL[VCR], or free VCR, or (B) free NGR peptide for 1 h at 37°C. Drug was washed out and the cells were incubated for an additional 47 h before cell viability was assessed via an MTT assay. Data are presented as percent of control viability. Each point represents the mean +/- standard deviation (n = 3) from one representative experiment.

The free VCR control was more cytotoxic than were the liposomal formulations, with an IC_{50} value of 25 μg VCR/mL (95% confidence interval = 17 to 36 μg/mL). The free targeting ligand, NGR peptide, was not cytotoxic at any concentration tested (Fig. 4.14B).

4.3. Discussion

When designing targeted therapies, numerous factors must be considered while selecting the target receptor/protein and targeting ligand. Many of these considerations are discussed in Chapter 1. Amongst other criteria, it is important to consider ligand stability, immunogenicity, affinity, ease of productivity, specificity, and ability to trigger internalization, as well as antigen expression levels/density and homogeneity, distribution, accessibility, shedding, and ability to undergo internalization (12, 14). For example, only certain antibodies that target the HER2 receptor are able to induce internalization (62), while some of the early antibodies utilized to target liposomes elicited a strong HAMA response (63), and some receptors have widespread distribution throughout the body. Selection of an unsuitable target or ligand may not only limit the therapeutic benefit achieved with use of the formulation, but may even lead to a *reduction* in the therapeutic effect and/or an increase in adverse effects compared to other/untargeted formulations. This is especially true if the targeting ligand leads to a more rapid removal of the initial dose or of subsequent doses from plasma, decreased circulation half-life, reduced delivery to the target site, and/or increased accumulation in off-target tissues.

This chapter explored some of the *in vitro* properties of ligand selection that should be considered when developing a targeted therapeutic agent. Results are presented from experiments investigating the cellular association and cytotoxicity of liposomal formulations targeted selectively to tumor cells and angiogenic vascular endothelial cells. The tumor-targeted and vasculature-targeted formulations demonstrated significantly greater cellular association with the target cell lines than did the untargeted and mismatched control peptide-modified liposomes. The selectivity of the enhanced cellular association of the NGR-SL, relative to the SL, was further demonstrated by the observation of very low degree of cellular association with the HEK 293 cells, which are CD13-negative. These data suggest that the CD13 receptor is important for the NGR-SL to demonstrate greater cellular association than the SL, further supporting the notion that there is a specific and selective interaction between the NGR-SL and the CD13 receptors.

Since the potential benefits of employing targeted therapeutics are heavily dependent upon a selective interaction with the target protein, some of the cellular association experiments were completed in the presence of excess free targeting ligand. It is postulated that the free ligands and the ligands coupled to the surface of the liposomes will bind to the target receptor in a competitive fashion. The cellular association of the αHER2-SIL and cRGD-SL was significantly reduced following pre-saturation of the target cells with free αHER2 antibody or cRGD ligand, respectively. These data suggest that the free ligand and the ligand-modified liposomes may be binding to the target receptor in a competitive fashion. To demonstrate competitive binding, it would be necessary to show that

the total number of available binding sites (B_{max}) for the targeted liposomes did not change in the presence of the free ligand, and that the addition of sufficiently high concentrations of the targeted liposomes displaced all bound free ligand. Similar to the results presented above, Schiffelers *et al.* have also demonstrated a reduction in the cellular association of the cRGD-SL in the presence of excess free cRGD peptide (64), while Cai and Chen have demonstrated that RGD peptides and RGD-modified quantum dots can displace an $\alpha_V\beta_3$-specific radioligand bound to cells *in vitro* (65).

Experiments were completed to investigate the cellular association of NGR peptides and NGR-SL in the presence of excess free NGR peptide. When the KS1767 cells were pre-saturated with excess unlabelled NGR peptide, the cellular association of free NGR peptide was decreased by over 50%, however, a decrease in the cellular association of the NGR-SL with the KS1767 cells could not be demonstrated. Even when the cells were pre-incubated with 500- or 1000-fold excess free NGR peptide, there was no decrease in the cellular association of the NGR-SL relative to no pre-saturation.

These results were unexpected because the data presented above suggest that the NGR-SL may associate with the KS1767 cells in a specific manner, compared to both the untargeted and mismatched control peptide-modified liposomes. Furthermore, the data show an increase in the cellular association of the NGR-SL at 37°C over 4°C, which is consistent with a selective ligand-receptor interaction leading to receptor internalization and recycling (discussed below).

Data published by Garde *et al.* and Wang *et al.* suggest that NGR-modified liposomes and NGR-modified polymeric micelles, respectively, may associate with CD13-positive cells in a competitive manner (25, 66). The discrepancy between the results reported by Garde *et al.* and the above results with the NGR-SL and the KS1767 cells could possibly be attributed to the fact that Garde *et al.* utilized a different cell line, assay method, and temperature, and may have used liposomes presenting a different number of NGR peptides, as the ligand density was not stated in the article (25).

Other researchers have published *in vivo* results that further support a specific interaction between NGR and CD13. For example, it has been demonstrated that the co-injection of soluble NGR peptide and NGR-modified liposomal DXR completely blocks tumor-specific DXR uptake (67). Similarly, the co-administration of NGR-modified tumor necrosis factor (NGR-TNF) and excess free targeting peptide significantly decreased the *in vivo* therapeutic activity of the NGR-TNF, such that it was no more effective than untargeted tumor necrosis factor (TNF) (68). A reduction in the therapeutic effect of NGR-TNF was also observed when it was co-administered with a monoclonal antibody against CD13 (68). These data suggest that the targeting ability of NGR moiety plays a role in achieving the improved therapeutic effect, and that the free NGR peptide and the antibody against CD13 interact with the same target as the NGR-modified therapies, but again these studies do not confirm that it is a competitive interaction.

One advantage of the liposome platform when utilized for targeted therapeutics is that it allows multivalent ligand presentation, which can increase the ligand's affinity/avidity for the target (69). In preliminary studies, the presence of excess free NGR peptide reduced the cellular association of the free NGR peptide, but not the NGR-SL; this suggests that there may be a difference in affinity/avidity between monovalent and multivalent presentation of NGR. Although it cannot be confirmed without determining the dissociation constants for the free peptide and the targeted liposomes, it is plausible that the NGR-SL investigated in this thesis show an increase in avidity for CD13, compared to free NGR peptide, as has been observed with other multivalent ligand platforms (69). Support for this notion comes from evidence in the literature showing that multivalent presentation of NGR peptides on liposomes can achieve an approximately 10-fold increase in the peptide's affinity/avidity for CD13-positive HT-1080 cells, relative to linear NGR (70). Thus, it is possible that the multivalent NGR-SL, which are postulated to have an increased avidity for CD13, were able to displace the free linear NGR peptides with which the cells had been pre-saturated. This could explain why pre-saturation of the cells with peptide did not lead to a reduction in the cellular association of the NGR-SL. To further explore this theory, the cells could be pre-saturated with cyclic NGR peptide, which shows 2- to 3.5-fold higher affinity for the CD13 isoform of interest than does linear NGR peptide (70, 71), or with unlabelled NGR-SL, which would possess equal avidity as the radio-labelled NGR-SL.

The propensity for multivalent and cyclic ligands to demonstrate greater affinity for their targets has also been demonstrated with RGD. For example, some cyclic RGD peptide sequences have demonstrated 100- to 200-fold increases in affinity for the $\alpha_V\beta_3$ integrin compared to linear RGD sequences (32, 72). As well, a peptide-like scaffold that presents four cRGD molecules was shown to have ~10-fold greater affinity for the target receptor than did monovalent cRGD (73), while a multivalent cRGD construct with a protein backbone demonstrated a 250-fold increase in affinity for HUVEC relative to a single cRGD peptide (74).

Some evidence suggests that the NGR motif may also show affinity for the $\alpha_V\beta_3$ integrin as a linear peptide (75), although the affinity may be three orders of magnitude less than that of the RGD peptides (28), or following asparagine deamidation to form an isoaspartate-glycine-asparagine (isoDGR) sequence (17). The isoDGR sequence binds competitively to the RGD site of the $\alpha_V\beta_3$ integrin (17, 76). In either situation, it is possible that some of the NGR-SL were homing to the $\alpha_V\beta_3$ integrin on endothelial cells, rather than to the angiogenic vasculature-specific isoform of CD13. However, new data in the literature has revealed that deamidation of NGR to isoDGR is primarily observed with cyclic NGR sequences, and that linear NGR sequences only generate small amounts of isoDGR (77). The theory was investigated, but experimental data revealed that pre-saturation of the HUVEC with excess cRGD peptide did not reduce the cellular association of the NGR-SL relative to no pre-saturation (Fig. 4.13).

As discussed above, the targeting ligands utilized in this thesis were selected for their ability to selectively bind proteins uniquely expressed or over-expressed on tumor and tumor vasculature cells. Importantly, it has been recognized that selective binding typically must be accompanied by receptor internalization in order to achieve an improved therapeutic outcome. For example, this notion is highlighted by studies demonstrating that the administration of liposomes targeted to internalizing antigens, such as CD19, produced a superior anti-cancer effect compared to the administration of liposomes targeted to non-internalizing antigens, such as CD20 (78). Furthermore, published research highlights the need for the internalization of targeted liposomes in order to achieve superior anti-cancer effect *in vitro* (50, 79) and *in vivo* (50).

The cellular targets of relevance to this thesis – the HER2 (80), the CD13 isoform specific to angiogenic vascular endothelium (21, 81), and the $\alpha_V\beta_3$ integrin (82-84) – have been shown to be internalizing proteins. To gain greater insight into ligand-induced receptor internalization and receptor recycling with the NGR-SL, cRGD-SL, and αHER2-SIL, the cellular association of the formulations was assessed at both 4°C, which is non-permissive for receptor internalization, and at 37°C, which is permissive for receptor internalization. Typically, when utilizing formulations targeted to internalizing proteins, greater cellular association would be expected at 37°C as a result of receptor recycling following ligand-induced receptor-mediated endocytosis.

Both the cRGD-SL and NGR-SL showed significantly greater cellular association at 37°C than at 4°C, consistent with rapid receptor internalization and

recycling to the cell surface. These data support published reports of the ability of the NGR-modified (25) and RGD-modified (85, 86) liposomes to induce internalization upon binding to their target receptors at 37°C. Evidence suggests that multivalent, but not monovalent, RGD constructs are co-internalized with the $\alpha_V\beta_3$ integrin (82, 87), via clathrin-dependent endocytosis (73, 84).

Garde *et al.* provided clear evidence that NGR-modified liposomes were trafficked through the endolysosomal pathway following internalization (25), which has been shown to occur in a caveolin-dependent manner (88). As well, qualitative and quantitative assays have shown that NGR-modified polymeric micelles were internalized into two CD13-positive cell lines (66). One recent report demonstrated that NGR-modified liposomes were not internalized into CD13-positive cells unless a cell-penetrating peptide was also presented on the surface of the liposome (89), although this observation is not supported by the results presented above or by other researchers (25, 66). Furthermore, receptor-mediated endocytosis of the NGR-SL and cRGD-SL was demonstrated to be the result of a specific interaction. Data presented above reveal that the liposomes targeted with either control peptide sequence (ARA or cRAD) did not show evidence of internalization, as the cellular association of the ARA-SL and cRAD-SL with the target cells at 37°C was only equal to that of the non-internalizing untargeted liposomes.

The untargeted liposomes do not possess the targeting ligands that are required for specific interaction with cell surface receptors; therefore, the untargeted liposomes associate with cells in a non-specific manner.

Consequently, the SL do not undergo receptor-mediated internalization, and are not expected to show substantial increases in cellular association at 37°C, relative to at 4°C. Supporting this idea, the majority of the results presented above show equal cellular association of the SL at 4°C and 37°C. One experiment demonstrated a statistically significant increase in the cellular association of the SL at 37°C, but this may be the result of increased Brownian motion at increased temperatures.

In contrast to the two vasculature-targeted liposomal formulations, the αHER2 monoclonal antibody-modified liposomes showed reduced cellular association with the 4T1.2^{ErbB-2} cells at 37°C than at 4°C, in all studies presented in this thesis. Interestingly, this same trend was observed when cellular association studies were completed with liposomes targeted with the αHER2 Fab′ fragment (Chapter 5). Based on data showing that the cellular association of the αHER2-SIL was reduced in the presence of excess free targeting ligand, and the fact that researchers have previously demonstrated receptor-mediated internalization of αHER2 scFv- and αHER2 Fab′-modified liposomes into endosomes or late endosomes at 37°C (53, 79, 90), it is unclear why greater cellular association was observed at a temperature that was non-permissive for receptor internalization than at a permissive temperature. Different splice variants of human HER2 have been identified, some of which have been shown to interfere with receptor endocytosis (91). The expression of such a HER2 splice variant by the 4T1.2^{ErbB-2} cells could explain why there was not greater cellular

association observed at 37°C, compared to at 4°C, although this was not investigated.

The αHER2-SIL cellular association results presented above are inconsistent with data from Yang *et al.*, which showed increased uptake of αHER2-modified liposomes at 37°C, relative to at 4°C (92). It is possible that the discrepancy is due to the prolonged incubation period (2 h vs. 1 h) utilized by Yang *et al.*, which might have allowed for sufficient receptor internalization and recycling to occur to overshadow the phenomenon observed above at 4°C, or the difference in cell line tested (human BT-474 and SK-BR-3 vs. mouse $4T1.2^{ErbB-2}$). Alternatively, it is possible that cellular stress, such as incubation at 4°C, may have resulted in a compensatory increase in HER2 expression, which would lead to an increase in liposomal cellular association, although this may not be physiologically relevant. This explanation is supported by the time-course binding data. The data show significant time-dependent increases in the cellular association of the αHER2-SIL at a low phospholipid concentration at 4°C, which cannot be explained by receptor internalization as 4°C is non-permissive. In contrast, with most of the other formulations/temperatures, nearly 90% of the cellular association occurred within the first five minutes of the start of the incubation.

Another potential explanation for the reduced cellular association of the αHER2-SIL at 37°C versus 4°C is due to one of trastuzumab's purported mechanisms of action – its ability to cause receptor down-regulation by directing HER2 to a Cbl-dependent endocytosis and degradation pathway (43, 93), instead of causing the receptor to be recycled back to the plasma membrane. A similar

down-regulation of EGFR following exposure to a nanobody-liposome construct has recently been reported (94). Furthermore, research has shown that multivalent αHER2 antibodies are internalized more rapidly than single antibodies, but still follow the same endocytic pathway into acidic endosomes (95). As well, ligand-mediated cross-linking/clustering of receptors, which could be achieved with a multivalent antibody construct such as αHER2-modified liposomes, has been shown to increase the rate and/or efficiency of internalization (96, 97). If binding of the αHER2-SIL, which present numerous copies of trastuzumab, can cause HER2 cross-linking, rapid internalization, and endocytic degradation in lieu of being recycled to the cell surface, this could lead to down-regulation of the HER2 on the $4T1.2^{ErbB-2}$ cells at 37°C. This same receptor down-regulation would not be observed with the $4T1.2^{ErbB-2}$ cells at 4°C (non-permissive for internalization), thereby possibly creating a situation where approximately equal, or perhaps even slightly greater, cellular association of the targeted liposomes may be observed at 4°C, relative to at 37°C.

Further investigation into the unexpected cellular association results at 4°C versus 37°C was undertaken with a receptor stripping experiment that utilized a low pH glycine solution to remove cell surface receptors (62, 98). Cleavage of cell surface proteins should remove liposomes bound to cell surface proteins or receptors, leaving only internalized liposomes. As predicted, receptor stripping had no effect on the cellular association of the SL, which bind non-specifically, and thus, are not internalized. Following surface stripping, the cellular association of the αHER2-SIL was reduced by 35-50% at 37°C, suggesting that a

portion of the liposomes had been internalized and thus were unaffected by surface stripping. This is consistent with results published by Lee and Low, who, after showing evidence of folate-modified liposome internalization, demonstrated a 50% reduction in the cellular association of folate-modified liposomes with KB cells at 37°C following an acid wash (55).

At 4°C, surface stripping reduced the cellular association of the αHER2-SIL by 15-30%, but this did not reach the level of the cellular association of the SL. The reduction in the cellular association of the αHER2-SIL following surface stripping was smaller at 4°C than at 37°C, which is the opposite of what would be expected if the liposomes were internalized at 37°C, but not at 4°C. If the bound αHER2-SIL were exclusively located on the outside of the cells, as would be expected at a non-permissive temperature for internalization, such as 4°C, surface stripping should cause a large decrease in liposomal cellular association. It is unclear why a greater reduction in binding following stripping was not observed at 4°C. However, it is important to note that reports indicate that the low pH glycine solution can cause incomplete dissociation of receptor-bound ligands (99, 100), complicating the interpretation of the results.

Significantly greater cellular association of the αHER2-SIL, relative to the SL, was clearly demonstrated in all experiments presented above. However, as discussed, the unexpected observation of greater cellular association of the αHER2-SIL at 4°C than at 37°C made it difficult to determine whether the interaction between the αHER2-SIL and the HER2 receptor on the $4T1.2^{ErbB-2}$ cells led to internalization of the entire ligand-liposome-receptor package. It is

known that the αHER2 monoclonal antibody trastuzumab and its antibody fragments are able to induce receptor-mediated endocytosis upon binding to cell surface HER2 (101). With liposomes, published results have revealed that *in vitro* internalization is dependent on ligand density (102, 103) and target receptor density (92, 103, 104). However, the antibody density on the αHER2-SIL was close to the optimal number for tumor cell uptake (30 whole antibody molecules/liposome), as determined by Maruyama *et al.* (105).

Although published results reveal a strong likelihood that the αHER2-SIL utilized in this thesis would be internalized, if the HER2 receptor density on the cells was below the threshold required to induce significant internalization, it is possible that the αHER2-SIL may not have been internalized in the above experiments. Down-regulation of HER2 surface expression could reduce the receptor density below the threshold level. To achieve greater clarity regarding the cellular association and internalization of the αHER2-SIL, future investigations could include analysis of receptor density at 4°C and 37°C, and/or several different studies that have been utilized to demonstrate internalization of αHER2-modified liposomes, including confocal microscopy, a "chelated ligand internalization assay" (106), imaging of quantum dot-conjugated targeted liposomes (107), or electron microscopy of gold-loaded liposomes (79).

In vitro cell viability assays were completed to compare the cytotoxicity of free drug, and untargeted and targeted liposomal drug. Free DXR was expected to be the most cytotoxic formulation *in vitro* because it is immediately 100% bioavailable, unlike liposomal DXR, which must first be released from the carrier

in order to be therapeutically active. *In vivo* PK/BD experiments revealed no drug leakage from SL[DXR] after 48 h, thus, very little drug leakage was expected to occur during the 1 h incubation period during the cytotoxicity assay. Therefore, it was predicted that the αHER2-modified formulation, which can achieve intracellular delivery of the drug following receptor-mediated internalization into endolysosomes, would show greater cytotoxicity than the untargeted formulation, which is not internalized (103, 108).

The importance of liposome internalization to therapeutic effect has been demonstrated in published data showing that internalizing αHER2 Fab′- and αHER2 scFV-modified liposomal DXR were significantly more cytotoxic than non-internalizing untargeted liposomal DXR against breast cancer cells *in vitro* (103, 108). The above results demonstrated a similar trend to that observed in published experiments, although the magnitude of the increase in the cytotoxicity of the αHER2-SIL[DXR] over SL[DXR] was less than has been observed in literature. In an effort to ensure the adherent cells were not dislodged during drug aspiration and washout, these steps were completed as "gently" as possible. Unfortunately, this may have led to residual, non-specifically bound SL remaining associated with cells following drug washout; these liposomes would continue to release drug into the well over the course of the 95 h incubation, leading to greater than anticipated cellular cytotoxicity. Alternatively, even low levels of drug that were released from the SL during the 1 h exposure period would have had a significant length of time (95 h) to mediate cytotoxic effects against multiple cells via the bystander effect. Finally, small amounts of unencapsulated DXR may

have been present in the liposomal drug preparations, and could be responsible for much of the observed cytotoxicity due to the potency of free DXR against the $4T1.2^{ErbB-2}$ cells.

The data from cellular association experiments with the NGR-SL showed evidence of internalization and greater cellular association than the SL, however, the NGR-SL[VCR] failed to demonstrate greater cytotoxicity than the untargeted liposomal VCR. As discussed above, there is considerable evidence in the literature, showing greater cytotoxicity following incubation with a wide variety of targeted liposomal drugs, compared to untargeted liposomal drugs. Previously published work with NGR-modified liposomal DXR has not included *in vitro* cytotoxicity assays. However, DXR-loaded NGR-SL have been proven to be superior to DXR-loaded ARA-SL *in vivo* (23), likely due to liposome internalization and intracellular drug delivery following administration of NGR-targeted liposomal DXR, but not ARA-targeted liposomal DXR. Thus, the unexpected cytotoxicity results presented in the experiments above are likely not representative of the true therapeutic potential of NGR-modified liposomal drug formulations, which bind selectively and undergo receptor-mediated internalization.

The *in vivo* drug retention half-life of the liposomal VCR formulation investigated in this thesis was ~20 h (see Chapter 5), which is significantly shorter than that of liposomal DXR. Although little drug leakage was expected during the 1 h exposure period, the free VCR was only 2-fold more cytotoxic than the liposomal formulations. These results suggest that some free VCR may have been

present in the liposomal preparations, and may have been responsible for a considerable portion of the observed cytotoxicity.

Finally, therapies that are targeted to vascular cells may exert a less significant 'bystander effect', relative to therapies that accumulate in the tumor interstitium, because any drug released from liposomes outside of the cells will have a greater likelihood of being rapidly carried away by the bloodstream rather than being well-retained in the interstitium and diffusing through the tumor. This situation is not accurately mimicked *in vitro*, where all the drug that is released from the liposomes will remain in the well and will not be cleared, thereby providing continuous drug exposure for the duration of the incubation. Additionally, any free drug present in the liposomal formulations would be rapidly and non-specifically distributed throughout the body *in vivo*, but in an *in vitro* assay, the free drug would remain in the well for the 1 h exposure period, artificially increasing the cytotoxicity of the liposomal formulations. *In vivo*, there are clear advantages to using internalizing formulations of vasculature-targeted therapies, such as the NGR-SL, and these therapies are postulated to lead to greater therapeutic effect than untargeted formulations, even if they do not provide greater cytotoxicity *in vitro*.

4.4. Conclusion

The experiments presented in this chapter characterized the *in vitro* cellular association and cytotoxicity properties of the tumor-targeted αHER2-SIL and vasculature-targeted NGR-SL and cRGD-SL. All three formulations demonstrated significantly greater cellular association than did the untargeted

liposomes. The NGR-SL and cRGD-SL also showed increased cellular association relative to the mismatched control ARA-SL and cRAD-SL, and evidence of receptor-mediated internalization at 37°C. An unexplained trend towards greater cellular association of the αHER2-SIL at 4°C, versus 37°C, was observed in all experiments. Pre-saturation of the $4T1.2^{ErbB-2}$ cells with free αHER2 monoclonal antibody, and pre-saturation of HUVEC with free cRGD peptide, significantly reduced the cellular association of the αHER2-SIL and cRGD-SL, respectively, suggesting that the ligand-receptor interaction was specific in nature. The αHER2-SIL[DXR] were twice as cytotoxic as the SL[DXR], while, unexpectedly, the NGR-SL[VCR] were equally as cytotoxic *in vitro* as were the SL[VCR]. Finally, an improved understanding of the formulations' *in vitro* properties was achieved by determining the effect of time, peptide density, and diluent composition on selective cellular association. Based on the *in vitro* data acquired in this chapter, the formulations are suitable for further investigation as a combined vasculature-targeted and tumor-targeted approach to the treatment of metastatic breast cancer. The pharmacokinetic/biodistribution properties and therapeutic activity of the tumor-targeted and vasculature-targeted liposomes are examined in Chapter 5.

4.5. References – Chapter 4

1. Bangham AD, Standish MM, Watkins JC. Diffusion of univalent ions across the lamellae of swollen phospholipids. *J. Mol. Biol.* 1965; 13: 238-252.

2. Maurer N, Fenske DB, Cullis PR. Developments in liposomal drug delivery systems. *Expert Opin. Biol. Ther.* 2001; 1: 923-947.

3. Allen TM, Cullis PR. Drug delivery systems: entering the mainstream. *Science* 2004; 303: 1818-1822.

4. Allen TM, Cheng WW, Hare JI, Laginha KM. Pharmacokinetics and pharmacodynamics of lipidic nano-particles in cancer. *Anticancer Agents Med. Chem.* 2006; 6: 513-523.

5. Drummond DC, Meyer O, Hong KL, Kirpotin DB, Papahadjopoulos D. Optimizing liposomes for delivery of chemotherapeutic agents to solid tumors. *Pharmacol. Rev.* 1999; 51: 691-743.

6. Torchilin VP. Recent advances with liposomes as pharmaceutical carriers. *Nat. Rev. Drug Discov.* 2005; 4: 145-160.

7. Leserman LD, Barbet J, Kourilsky F, Weinstein JN. Targeting to cells of fluorescent liposomes covalently coupled with monoclonal antibody or protein A. *Nature* 1980; 288: 602-604.

8. Heath TD, Fraley RT, Papahdjopoulos D. Antibody targeting of liposomes: cell specificity obtained by conjugation of $F(ab')_2$ to vesicle surface. *Science* 1980; 210: 539-541.

9. Sapra P, Tyagi P, Allen TM. Ligand-targeted liposomes for cancer treatment. *Curr. Drug Deliv.* 2005; 2: 369-381.

10. Nobs L, Buchegger F, Gurny R, Allemann E. Current methods for attaching targeting ligands to liposomes and nanoparticles. *J. Pharm. Sci.* 2004; 93: 1980-1992.

11. Hansen CB, Kao GY, Moase EH, Zalipsky S, Allen TM. Attachment of antibodies to sterically stabilized liposomes: evaluation, comparison and optimization of coupling procedures. *Biochim. Biophys. Acta* 1995; 1239: 133-144.

12. Allen TM. Ligand-targeted therapeutics in anticancer therapy. *Nat. Rev. Cancer* 2002; 2: 750-763.

13. Allen TM, Sapra P, Moase E, Moreira JN, Iden DL. Adventures in targeting. *J. Liposome Res.* 2002; 121: 5-12.

14. Noble CO, Kirpotin DB, Hayes ME, Mamot C, Hong K, Park JW, Benz CC, Marks JD, Drummond DC. Development of ligand-targeted liposomes for cancer therapy. *Expert Opin. Ther. Targets* 2004; 8: 335-353.

15. Park JW, Benz CC, Martin FJ. Future directions of liposome- and immunoliposome-based cancer therapeutics. *Semin. Oncol.* 2004; 31: 196-205.

16. Luan Y, Xu W. The structure and main functions of aminopeptidase N. *Curr. Med. Chem.* 2007; 14: 639-647.

17. Curnis F, Longhi R, Crippa L, Cattaneo A, Dondossola E, Bachi A, Corti A. Spontaneous formation of L-isoaspartate and gain of function in fibronectin. *J. Biol. Chem.* 2006; 281: 36466-36476.

18. Curnis F, Arrigoni G, Sacchi A, Fischetti L, Arap W, Pasqualini R, Corti A. Differential binding of drugs containing the NGR motif to CD13 isoforms in tumor vessels, epithelia, and myeloid cells. *Cancer Res.* 2002; 62: 867-874.

19. Pasqualini R, Koivunen E, Kain R, Lahdenranta J, Sakamoto M, Stryhn A, Ashmun RA, Shapiro LH, Arap W, Ruoslahti E. Aminopeptidase N is a receptor for tumor-homing peptides and a target for inhibiting angiogenesis. *Cancer Res.* 2000; 60: 722-727.

20. Bhagwat SV, Lahdenranta J, Giordano R, Arap W, Pasqualini R, Shapiro LH. CD13/APN is activated by angiogenic signals and is essential for capillary tube formation. *Blood* 2001; 97: 652-659.

21. Arap W, Pasqualini R, Ruoslahti E. Cancer treatment by targeted drug delivery to tumor vasculature in a mouse model. *Science* 1998; 279: 377-380.

22. Pastorino F, Brignole C, Di Paolo D, Nico B, Pezzolo A, Marimpietri D, Pagnan G, Piccardi F, Cilli M, Longhi R, Ribatti D, Corti A, Allen TM, Ponzoni M. Targeting liposomal chemotherapy via both tumor cell-specific and tumor vasculature-specific ligands potentiates therapeutic efficacy. *Cancer Res.* 2006; 66: 10073-10082.

23. Pastorino F, Brignole C, Marimpietri D, Cilli M, Gambini C, Ribatti D, Longhi R, Allen TM, Corti A, Ponzoni M. Vascular damage and anti-angiogenic effects of tumor vessel-targeted liposomal chemotherapy. *Cancer Res.* 2003; 63: 7400-7409.

24. Pastorino F, Di Paolo D, Piccardi F, Nico B, Ribatti D, Daga A, Baio G, Neumaier CE, Brignole C, Loi M, Marimpietri D, Pagnan G, Cilli M, Lepekhin EA, Garde SV, Longhi R, Corti A, Allen TM, Wu JJ, Ponzoni M. Enhanced antitumor efficacy of clinical-grade vasculature-targeted liposomal doxorubicin. *Clin Cancer Res* 2008; 14: 7320-7329.

25. Garde SV, Forte AJ, Ge M, Lepekhin EA, Panchal CJ, Rabbani SA, Wu JJ. Binding and internalization of NGR-peptide-targeted liposomal doxorubicin (TVT-DOX) in CD13-expressing cells and its antitumor effects. *Anticancer Drugs* 2007; 18: 1189-1200.

26. Pierschbacher MD, Ruoslahti E. Cell attachment activity of fibronectin can be duplicated by small synthetic fragments of the molecule. *Nature* 1984; 309: 30-33.

27. Faull RJ, Ginsberg MH. Inside-out signaling through integrins. *J. Am. Soc. Nephrol.* 1996; 7: 1091-1097.

28. Ruoslahti E. RGD and other recognition sequences for integrins. *Annu. Rev. Cell Dev. Biol.* 1996; 12: 697-715.

29. Eliceiri BP, Cheresh DA. Role of alpha v integrins during angiogenesis. *Cancer J.* 2000; 6: S245-S249.

30. Max R, Gerritsen RR, Nooijen PT, Goodman SL, Sutter A, Keilholz U, Ruiter DJ, De Waal RM. Immunohistochemical analysis of integrin alpha vbeta3 expression on tumor-associated vessels of human carcinomas. *Int. J. Cancer* 1997; 71: 320-324.

31. Wang W, Ke S, Wu Q, Charnsangavej C, Gurfinkel M, Gelovani JG, Abbruzzese JL, Sevick-Muraca EM, Li C. Near-infrared optical imaging of integrin alphavbeta3 in human tumor xenografts. *Mol. Imaging* 2004; 3: 343-351.

32. Gurrath M, Muller G, Kessler H, Aumailley M, Timpl R. Conformation/activity studies of rationally designed potent anti-adhesive RGD peptides. *Eur. J. Biochem.* 1992; 210: 911-921.

33. Temming K, Schiffelers RM, Molema G, Kok RJ. RGD-based strategies for selective delivery of therapeutics and imaging agents to the tumour vasculature. *Drug Resist. Updat.* 2005; 8: 381-402.

34. Yarden Y. Agonistic antibodies stimulate the kinase encoded by the neu protooncogene in living cells but the oncogenic mutant is constitutively active. *Proc. Natl. Acad. Sci. U.S.A.* 1990; 87: 2569-2573.

35. Burgess AW, Cho HS, Eigenbrot C, Ferguson KM, Garrett TP, Leahy DJ, Lemmon MA, Sliwkowski MX, Ward CW, Yokoyama S. An open-and-shut case? Recent insights into the activation of EGF/ErbB receptors. *Mol. Cell.* 2003; 12: 541-552.

36. Tzahar E, Waterman H, Chen X, Levkowitz G, Karunagaran D, Lavi S, Ratzkin BJ, Yarden Y. A hierarchical network of interreceptor interactions determines signal transduction by Neu differentiation factor/neuregulin and epidermal growth factor. *Mol. Cell. Biol.* 1996; 16: 5276-5287.

37. Karunagaran D, Tzahar E, Beerli RR, Chen X, Graus-Porta D, Ratzkin BJ, Seger R, Hynes NE, Yarden Y. ErbB-2 is a common auxiliary subunit of NDF and EGF receptors: implications for breast cancer. *Embo. J.* 1996; 15: 254-264.

38. Slamon DJ, Clark GM, Wong SG, Levin WJ, Ullrich A, McGuire WL. Human breast cancer: correlation of relapse and survival with amplification of the HER-2/neu oncogene. *Science* 1987; 235: 177-182.

39. Hynes NE, Stern DF. The biology of erbB-2/neu/HER-2 and its role in cancer. *Biochim. Biophys. Acta* 1994; 1198: 165-184.

40. Pauletti G, Godolphin W, Press MF, Slamon DJ. Detection and quantitation of HER-2/neu gene amplification in human breast cancer archival material using fluorescence in situ hybridization. *Oncogene* 1996; 13: 63-72.

41. Revillion F, Bonneterre J, Peyrat JP. ERBB2 oncogene in human breast cancer and its clinical significance. *Eur. J. Cancer* 1998; 34: 791-808.

42. Slamon DJ, Godolphin W, Jones LA, Holt JA, Wong SG, Keith DE, Levin WJ, Stuart SG, Udove J, Ullrich A, *et al.* Studies of the HER-2/neu proto-oncogene in human breast and ovarian cancer. *Science* 1989; 244: 707-712.

43. Yarden Y. Biology of HER2 and its importance in breast cancer. *Oncology* 2001; 61 Suppl 2: 1-13.

44. Drebin JA, Stern DF, Link VC, Weinberg RA, Greene MI. Monoclonal antibodies identify a cell-surface antigen associated with an activated cellular oncogene. *Nature* 1984; 312: 545-548.

45. Carter P, Presta L, Gorman CM, Ridgway JB, Henner D, Wong WL, Rowland AM, Kotts C, Carver ME, Shepard HM. Humanization of an anti-p185HER2 antibody for human cancer therapy. *Proc. Natl. Acad. Sci. U. S. A.* 1992; 89: 4285-4289.

46. Cobleigh MA, Vogel CL, Tripathy D, Robert NJ, Scholl S, Fehrenbacher L, Wolter JM, Paton V, Shak S, Lieberman G, Slamon DJ. Multinational study of the efficacy and safety of humanized anti-HER2 monoclonal antibody in women who have HER2-overexpressing metastatic breast cancer that has progressed after chemotherapy for metastatic disease. *J Clin Oncol* 1999; 17: 2639-2648.

47. Baselga J, Tripathy D, Mendelsohn J, Baughman S, Benz CC, Dantis L, Sklarin NT, Seidman AD, Hudis CA, Moore J, Rosen PP, Twaddell T, Henderson IC, Norton L. Phase II study of weekly intravenous recombinant humanized anti-p185HER2 monoclonal antibody in patients with HER2/neu-overexpressing metastatic breast cancer. *J. Clin. Oncol.* 1996; 14: 737-744.

48. Baselga J. Herceptin alone or in combination with chemotherapy in the treatment of HER2-positive metastatic breast cancer: pivotal trials. *Oncology* 2001; 61: 14-21.

49. Disis ML, Cheever MA. HER-2/neu protein: a target for antigen-specific immunotherapy of human cancer. *Adv. Cancer Res.* 1997; 71: 343-371.

50. Goren D, Horowitz AT, Zalipsky S, Woodle MC, Yarden Y, Gabizon A. Targeting of Stealth liposomes to erB-2 (Her/2) receptor: in vitro and in vivo studies. *Br. J. Cancer* 1996; 74: 1749-1756.

51. Kirpotin D, Park JW, Hong K, Keller G, Benz C, Paphadjopoulos D. Binding and endocytosis of sterically stabilized anti-HER2 immunoliposomes by human breast cancer cells. *Proc. Am. Assoc. Cancer Res.* 1996; 37: 3186.

52. Park JW, Hong K, Kirpotin DB, Colbern G, Shalaby R, Baselga J, Shao Y, Nielsen UB, Marks JD, Moore D, Papahadjopoulos D, Benz CC. Anti-HER2 immunoliposomes: Enhanced efficacy attributable to targeted delivery. *Clin. Cancer Res.* 2002; 8: 1172-1181.

53. Kirpotin D, Park JW, Hong K, Zalipsky S, Li W-L, Carter P, Benz CC, Papahadjopoulos D. Sterically stabilized anti-HER2 immunoliposomes: design and targeting to human breast cancer cells *in vitro*. *Biochemistry* 1997; 36: 66-75.

54. Foldvari M, Mezei C, Mezei M. Intracellular delivery of drugs by liposomes containing P0 glycoprotein from peripheral nerve myelin into human M21 melanoma cells. *J. Pharm. Sci.* 1991; 80: 1020-1028.

55. Lee RJ, Low PS. Delivery of liposomes into cultured KB cells via folate receptor-mediated endocytosis. *J. Biol. Chem.* 1994; 269: 3198-3204.

56. Lopes de Menezes DE, Kirchmeier MJ, Gagne J-F, Pilarski LM, Allen TM. Cellular trafficking and cytotoxicity of anti-CD19-targeted liposomal doxorubicin in B lymphoma cells. *J. Liposome Res.* 1999; 9: 199-228.

57. Sapra P, Allen TM. Ligand-targeted liposomal anticancer drugs. *Prog. Lipid Res.* 2003; 42: 439-462.

58. Huang SK, Mayhew E, Gilani S, Lasic D, Martin FJ, D. P. Pharmacokinetics and therapeutics of sterically stabilized liposomes in mice bearing C-26 colon carcinoma. *Cancer Res.* 1992; 52: 6774-6781.

59. Yuan F, Leunig M, Huang SK, Berk DA, Papahadjopoulos D, Jain RK. Microvascular permeability and interstitial penetration of sterically stabilized (Stealth) liposomes in a human tumor xenograft. *Cancer Res.* 1994; 54: 3352-3356.

60. Lopes de Menezes DE, Pilarski LM, Allen TM. In vitro and in vivo targeting of immunoliposomal doxorubicin to human B-cell lymphoma. *Cancer Res.* 1998; 58: 3320-3330.

61. Laginha KM, Moase EH, Yu N, Huang A, Allen TM. Bioavailability and therapeutic efficacy of HER2 scFv-targeted liposomal doxorubicin in a murine model of HER2-overexpressing breast cancer. *J. Drug Target.* 2008; 16: 605-610.

62. Tagliabue E, Centis F, Campiglio M, Mastroianni A, Martignone S, Pellegrini R, Casalini P, Lanzi C, Menard S, Colnaghi MI. Selection of monoclonal antibodies which induce internalization and phosphorylation of p185HER2 and growth inhibition of cells with HER2/NEU gene amplification. *Int. J. Cancer* 1991; 47: 933-937.

63. Harding JA, Engbers CM, Newman MS, Goldstein NI, Zalipsky S. Immunogenicity and pharmacokinetic attributes of poly(ethyleneglycol)-grafted immunoliposomes. *Biochim. Biophys. Acta* 1997; 1327: 181-192.

64. Schiffelers RM, Koning GA, ten Hagen TL, Fens MH, Schraa AJ, Janssen AP, Kok RJ, Molema G, Storm G. Anti-tumor efficacy of tumor vasculature-targeted liposomal doxorubicin. *J. Control. Release* 2003; 91: 115-122.

65. Cai W, Chen X. Preparation of peptide-conjugated quantum dots for tumor vasculature-targeted imaging. *Nat. Protoc.* 2008; 3: 89-96.

66. Wang X, Wang Y, Chen X, Wang J, Zhang X, Zhang Q. NGR-modified micelles enhance their interaction with CD13-overexpressing tumor and endothelial cells. *J. Control. Release* 2009; 139: 56-62.

67. Di Paolo D, Pastorino F, Brignole C, Marimpietri D, Loi M, Ponzoni M, Pagnan G. Drug delivery systems: application of liposomal anti-tumor agents to neuroectodermal cancer treatment. *Tumori* 2008; 94: 246-253.

68. Curnis F, Sacchi A, Borgna L, Magni F, Gasparri A, Corti A. Enhancement of tumor necrosis factor alpha antitumor immunotherapeutic properties by targeted delivery to aminopeptidase N (CD13). *Nat. Biotechnol.* 2000; 18: 1185-1190.

69. Mammen M, Choi S-K, Whitesides GM. Polyvalent interactions in biological systems: Implications for design and use of multivalent ligands and inhibitors. *Angew. Chem., Int. Ed. Engl.* 1998; 37: 2755-2794.

70. Negussie AH, Miller JL, Reddy G, Drake SK, Wood BJ, Dreher MR. Synthesis and in vitro evaluation of cyclic NGR peptide targeted thermally sensitive liposome. *J. Control. Release* 2010; 143: 265-273.

71. Colombo G, Curnis F, De Mori GM, Gasparri A, Longoni C, Sacchi A, Longhi R, Corti A. Structure-activity relationships of linear and cyclic peptides containing the NGR tumor-homing motif. *J. Biol. Chem.* 2002; 277: 47891-47897.

72. Koivunen E, Wang B, Ruoslahti E. Phage libraries displaying cyclic peptides with different ring sizes: ligand specificities of the RGD-directed integrins. *Biotechnology (N. Y.)* 1995; 13: 265-370.

73. Sancey L, Garanger E, Foillard S, Schoehn G, Hurbin A, Albiges-Rizo C, Boturyn D, Souchier C, Grichine A, Dumy P, Coll JL. Clustering and

internalization of integrin alphavbeta3 with a tetrameric RGD-synthetic peptide. *Mol. Ther.* 2009; 17: 837-843.

74. Kok RJ, Schraa AJ, Bos EJ, Moorlag HE, Asgeirsdottir SA, Everts M, Meijer DK, Molema G. Preparation and functional evaluation of RGD-modified proteins as alpha(v)beta(3) integrin directed therapeutics. *Bioconjug. Chem.* 2002; 13: 128-135.

75. Majhen D, Gabrilovac J, Eloit M, Richardson J, Ambriovic-Ristov A. Disulfide bond formation in NGR fiber-modified adenovirus is essential for retargeting to aminopeptidase N. *Biochem. Biophys. Res. Commun.* 2006; 348: 278-287.

76. Spitaleri A, Mari S, Curnis F, Traversari C, Longhi R, Bordignon C, Corti A, Rizzardi GP, Musco G. Structural basis for the interaction of isoDGR with the RGD-binding site of alphavbeta3 integrin. *J. Biol. Chem.* 2008; 283: 19757-19768.

77. Curnis F, Cattaneo A, Longhi R, Sacchi A, Gasparri AM, Pastorino F, Di Matteo P, Traversari C, Bachi A, Ponzoni M, Rizzardi GP, Corti A. Critical role of flanking residues in NGR-to-isoDGR transition and CD13/integrin receptor switching. *J. Biol. Chem.* 2010; 285: 9114-9123.

78. Sapra P, Allen TM. Internalizing antibodies are necessary for improved therapeutic efficacy of antibody-targeted liposomal drugs. *Cancer Res.* 2002; 62: 7190-7194.

79. Park JW, Hong K, Carter P, Asgari H, Guo LY, Keller GA, Wirth C, Shalaby R, Kotts C, Wood WI, Papahadjopoulos D, Benz CC. Development of anti-p185^{HER2} immunoliposomes for cancer therapy. *Proc. Natl. Acad. Sci. U.S.A.* 1995; 92: 1327-1331.

80. Sarup JC, Johnson RM, King KL, Fendly BM, Lipari MT, Napier MA, Ullrich A, Shepard HM. Characterization of an anti-p185HER2 monoclonal antibody that stimulates receptor function and inhibits tumor cell growth. *Growth Regul.* 1991; 1: 72-82.

81. Ellerby HM, Arap W, Ellerby LM, Kain R, Andrusiak R, Rio GD, Krajewski S, Lombardo CR, Rao R, Ruoslahti E, Bredesen DE, Pasqualini R. Anti-cancer activity of targeted pro-apoptotic peptides. *Nat. Med.* 1999; 5: 1032-1038.

82. Schraa AJ, Kok RJ, Berendsen AD, Moorlag HE, Bos EJ, Meijer DK, de Leij LF, Molema G. Endothelial cells internalize and degrade RGD-

modified proteins developed for tumor vasculature targeting. *J. Control. Release* 2002; 83: 241-251.

83. Hart SL, Knight AM, Harbottle RP, Mistry A, Hunger HD, Cutler DF, Williamson R, Coutelle C. Cell binding and internalization by filamentous phage displaying a cyclic Arg-Gly-Asp-containing peptide. *J. Biol. Chem.* 1994; 269: 12468-12474.

84. De Deyne PG, O'Neill A, Resneck WG, Dmytrenko GM, Pumplin DW, Bloch RJ. The vitronectin receptor associates with clathrin-coated membrane domains via the cytoplasmic domain of its beta5 subunit. *J. Cell Sci.* 1998; 111 (Pt 18): 2729-2740.

85. Xiong XB, Huang Y, Lu WL, Zhang X, Zhang H, Nagai T, Zhang Q. Intracellular delivery of doxorubicin with RGD-modified sterically stabilized liposomes for an improved antitumor efficacy: in vitro and in vivo. *J. Pharm. Sci.* 2005; 94: 1782-1793.

86. Holig P, Bach M, Volkel T, Nahde T, Hoffmann S, Muller R, Kontermann RE. Novel RGD lipopeptides for the targeting of liposomes to integrin-expressing endothelial and melanoma cells. *Protein Eng. Des. Sel.* 2004; 17: 433-441.

87. Castel S, Pagan R, Mitjans F, Piulats J, Goodman S, Jonczyk A, Huber F, Vilaro S, Reina M. RGD peptides and monoclonal antibodies, antagonists of alpha(v)-integrin, enter the cells by independent endocytic pathways. *Lab. Invest.* 2001; 81: 1615-1626.

88. Nomura R, Kiyota A, Suzaki E, Kataoka K, Ohe Y, Miyamoto K, Senda T, Fujimoto T. Human coronavirus 229E binds to CD13 in rafts and enters the cell through caveolae. *J. Virol.* 2004; 78: 8701-8708.

89. Takara K, Hatakeyama H, Ohga N, Hida K, Harashima H. Design of a dual-ligand system using a specific ligand and cell penetrating peptide, resulting in a synergistic effect on selectivity and cellular uptake. *Int. J. Pharm.* 2010; 396: 143-148.

90. Nielsen UB, Kirpotin DB, Pickering EM, Hong K, Park JW, Refaat Shalaby M, Shao Y, Benz CC, Marks JD. Therapeutic efficacy of anti-ErbB2 immunoliposomes targeted by a phage antibody selected for cellular endocytosis. *Biochim. Biophys. Acta* 2002; 1591: 109-118.

91. Scott GK, Robles R, Park JW, Montgomery PA, Daniel J, Holmes WE, Lee J, Keller GA, Li WL, Fendly BM, et al. A truncated intracellular

HER2/neu receptor produced by alternative RNA processing affects growth of human carcinoma cells. *Mol. Cell. Biol.* 1993; 13: 2247-2257.

92. Yang T, Choi MK, Cui FD, Kim JS, Chung SJ, Shim CK, Kim DD. Preparation and evaluation of paclitaxel-loaded PEGylated immunoliposome. *J. Control. Release* 2007; 120: 169-177.

93. Klapper LN, Waterman H, Sela M, Yarden Y. Tumor-inhibitory antibodies to HER-2/ErbB-2 may act by recruiting c-Cbl and enhancing ubiquitination of HER-2. *Cancer Res.* 2000; 60: 3384-3388.

94. Oliveira S, Schiffelers RM, van der Veeken J, van der Meel R, Vongpromek R, van Bergen En Henegouwen PM, Storm G, Roovers RC. Downregulation of EGFR by a novel multivalent nanobody-liposome platform. *J Control Release* 2010; 145: 165-175.

95. Miller K, Meng G, Liu J, Hurst A, Hsei V, Wong WL, Ekert R, Lawrence D, Sherwood S, DeForge L, Gaudreault J, Keller G, Sliwkowski M, Ashkenazi A, Presta L. Design, construction, and in vitro analyses of multivalent antibodies. *J. Immunol.* 2003; 170: 4854-4861.

96. Hommelgaard AM, Lerdrup M, van Deurs B. Association with membrane protrusions makes ErbB2 an internalization-resistant receptor. *Mol. Biol. Cell* 2004; 15: 1557-1567.

97. Friedman LM, Rinon A, Schechter B, Lyass L, Lavi S, Bacus SS, Sela M, Yarden Y. Synergistic down-regulation of receptor tyrosine kinases by combinations of mAbs: implications for cancer immunotherapy. *Proc. Natl. Acad. Sci. U. S. A.* 2005; 102: 1915-1920.

98. Yarden Y, Gabbay M, Schlessinger J. Primary amines do not prevent the endocytosis of epidermal growth factor into 3T3 fibroblasts. *Biochim. Biophys. Acta* 1981; 674: 188-203.

99. Matzku S, Moldenhauer G, Kalthoff H, Canevari S, Colnaghi M, Schuhmacher J, Bihl H. Antibody transport and internalization into tumours. *Br. J. Cancer Suppl.* 1990; 10: 1-5.

100. Tsaltas G, Ford CH. Cell membrane antigen-antibody complex dissociation by the widely used glycine-HCL method: an unreliable procedure for studying antibody internalization. *Immunol. Invest.* 1993; 22: 1-12.

101. Neve RM, Nielsen UB, Kirpotin DB, Poul MA, Marks JD, Benz CC. Biological effects of anti-ErbB2 single chain antibodies selected for

internalizing function. *Biochem. Biophys. Res. Commun.* 2001; 280: 274-279.

102. Saul JM, Annapragada A, Natarajan JV, Bellamkonda RV. Controlled targeting of liposomal doxorubicin via the folate receptor in vitro. *J. Control. Release* 2003; 92: 49-67.

103. Park JW, Hong K, Kirpotin DB, Meyer O, Papahadjopoulos D, Benz CC. Anti-HER2 immunoliposomes for targeted therapy of human tumors. *Cancer Lett.* 1997; 118: 153-160.

104. Park JW, Kirpotin DB, Hong K, Shalaby R, Shao Y, Nielsen UB, Marks JD, Papahadjopoulos D, Benz CC. Tumor targeting using anti-HER2 immunoliposomes. *J. Control. Release* 2001; 74: 95-113.

105. Maruyama K, Takizawa T, Yuda T, Kennel SJ, Huang L, Iwatsuru M. Targetability of novel immunoliposomes modified with amphipathic poly(ethylene glycol)s conjugated at their distal terminals to monoclonal antibodies. *Biochim. Biophys. Acta* 1995; 1234: 74-80.

106. Nielsen UB, Kirpotin DB, Pickering EM, Drummond DC, Marks JD. A novel assay for monitoring internalization of nanocarrier coupled antibodies. *BMC Immunol.* 2006; 7: 24-39.

107. Weng KC, Noble CO, Papahadjopoulos-Sternberg B, Chen FF, Drummond DC, Kirpotin DB, Wang D, Hom YK, Hann B, Park JW. Targeted tumor cell internalization and imaging of multifunctional quantum dot-conjugated immunoliposomes in vitro and in vivo. *Nano Lett.* 2008; 8: 2851-2857.

108. Kirpotin DB, Drummond DC, Shao Y, Shalaby MR, Hong K, Nielsen UB, Marks JD, Benz CC, Park JW. Antibody targeting of long-circulating lipidic nanoparticles does not increase tumor localization but does increase internalization in animal models. *Cancer Res.* 2006; 66: 6732-6740.

CHAPTER 5

Combined Vasculature-targeted and Tumor-targeted Approach to HER2-positive Breast Cancer Treatment

(Prepared for submission to the Journal of Controlled Release)

5. Combined Vasculature-targeted and Tumor-targeted Approach to HER2-positive Breast Cancer Treatment

5.1. Introduction

Worldwide, breast cancer is the second-leading cause of cancer death in women (1). Many of the current chemotherapy regimens for metastatic breast cancer treatment involve administering combinations of drugs at or near their maximum tolerated doses (2, 3). Although this approach provides disease control for some patients, thousands of deaths each year result from the failure of current cancer therapies and from severe morbidities due to non-specific side effects (2, 3). There is a significant unmet need for the development of new treatment approaches and novel strategies to improve the therapeutic effect of established agents. This chapter presents research using targeted nanomedicines in a combination setting to explore an innovative and promising new approach – combined vasculature-targeted and tumor-targeted therapy – for the treatment of metastatic breast cancer.

Anti-vascular and anti-angiogenic therapies have been extensively researched in recent years (4, and references therein). Once solid tumors reach 1-2 mm in diameter, the oxygen and nutrients supplied by the normal host vasculature become insufficient, forcing the tumor cells to send out signals to recruit the growth of new blood vessels from existing host vasculature (a process known as angiogenesis) (5). Dr. Judah Folkman first suggested that the inhibition of angiogenesis in dormant cancerous lesions, in order to prevent the formation of

new tumor vasculature, may be an effective way to control tumor growth and metastasis (6, 7). However, it is not always possible to begin treatment before tumors have initiated angiogenesis. Anti-vascular therapies can be targeted towards existing angiogenic endothelial cells in the tumor (8). Destruction of a tumor's vascular supply network can starve the tumor, leading to apoptosis and necrosis in the core of the tumor, and possibly a reduction in tumor size (9-11).

Despite the promise of the anti-vascular approach, there has been limited success translating it to the clinical setting (12). It has been demonstrated that a cuff of cells at the periphery of the tumor remain viable following anti-vascular therapy, because they are supplied by the normal host vasculature (13, 14). Following cessation of treatment, these residual malignant cells can lead to significant tumor re-growth and disease progression. It was hypothesized that this problem could be overcome by combining a vasculature-targeted therapy with a second therapy targeted to the residual tumor cells themselves. Targeted liposomal therapeutics provide a unique opportunity to achieve selective delivery of different drugs to both the tumor vascular endothelium and the residual malignant cells, and the results of an investigation of dual-targeted combination therapy are presented in this chapter. The validity of this approach is supported by the observation that the vasculature-targeted therapy bevacizumab improves therapeutic outcome in the clinic, when added to conventional chemotherapy regimens (15-17), but typically does not improve overall survival when employed as a single agent (16, 17).

Approximately 15-30% of breast cancers over-express HER2 (18). In 1998, the humanized anti-HER2 monoclonal antibody trastuzumab (also known as Herceptin®) was introduced as a promising new treatment for the more aggressive HER2-positive disease (19-21). However, it has recently become apparent that within a year of treatment initiation, many patients develop trastuzumab resistance, ultimately leading to disease progression (21, 22). Unfortunately, this significantly limits the effectiveness and long-term utility of trastuzumab therapy. For part of the novel treatment approach, instead of relying on trastuzumab as a therapeutic agent, the antibody's inherent specificity was exploited to target a liposomal anti-cancer drug to HER2-positive breast cancer cells.

The innovative combined vasculature-targeted and tumor-targeted approach to the treatment of HER2-positive breast cancer uses a rational combination of two different liposomal drug formulations targeted to two different cell populations. Cancer chemotherapy protocols typically employ a combination of several drugs in order to achieve improved disease control and avoid the development of resistance. Whether combination therapy employs only free drugs, or whether it employs combinations of liposomal drugs, or both, when combining chemotherapeutic agents, it is important to consider their side effect profiles, mechanisms of action, and potential for synergism or antagonism. The combination of anti-cancer agents utilized in the investigation of the dual-targeted approach, VCR and DXR, have non-overlapping side effect profiles, and exert their cytotoxic effects via different mechanisms.

VCR has been shown to be highly selective for proliferating endothelial cells: achieving the same level of cytotoxicity against proliferating and non-proliferating human microvascular endothelial cells required a 91-fold lower concentration of VCR under proliferative conditions than under non-proliferative conditions (23). Additionally, VCR has been proven to have anti-vascular and anti-angiogenic properties when administered at less than traditional cytotoxic doses or when administered using a metronomic dosing schedule (24-26). Furthermore, VCR is an S-phase-specific agent and can be encapsulated in 'classical' (27, 28) and PEGylated liposomes (29-31). Using a liposomal formulation of VCR will increase the length of time the cells are exposed to the drug, which is known to enhance the cytotoxicity of cell cycle-specific drugs. Based on this information, liposomal VCR was a logical formulation choice for the vasculature-targeted therapy. In addition, DXR was selected as the drug for the tumor-targeted therapy in the dual-targeted combination approach. PEGylated liposomal DXR (Doxil® or Caelyx®) is approved for the treatment of Kaposi's sarcoma, relapsed ovarian cancer, and for multiple melanoma in combination with bortezomib. Doxil® is also used as a non-first line therapy for breast cancer treatment for patients at a high risk of cardiac events. DXR is a cell cycle-non-specific drug due to its multiple mechanisms of action, and its activity against $4T1.2^{ErbB\text{-}2}$ cells has been demonstrated *in vitro* (see Chapter 4).

Two angiogenic endothelium-selective peptide motifs, cRGD and NGR, were investigated as potential targeting ligands for the vasculature-targeted therapy. The NGR sequence, but not its mismatched control peptide sequence,

ARA, specifically binds to the isoform of CD13/APN that is exclusively expressed on angiogenic endothelial cells (32). The cRGD peptide is selective for the $\alpha_V\beta_3$ integrin, which is expressed on angiogenic vascular endothelium; cRAD was utilized as the non-specific control peptide sequence (33).

A VCR-loaded, vasculature-targeted therapy, designed to destroy the tumor blood vessels and thereby ultimately kill the cells in the core of the tumor, was utilized in combination with a DXR-loaded, tumor-targeted therapy designed to kill the residual malignant cells, including those at the periphery of the tumor. It is hypothesized that increased disease control might be achieved by this dual-targeted combination treatment strategy. This chapter describes the selection of the targeting ligands for the tumor-targeted and vasculature-targeted liposomal drugs using pharmacokinetics and biodistribution studies, and the assessment of the therapeutic effect of a nanomedicine-based dual-targeted approach in an orthotopic model of HER2-positive breast cancer in mice.

5.2. Results

5.2.1. PK/BD of Untargeted vs. Tumor-targeted Liposomes

In order to determine whether the αHER2 mAb was well-suited as a liposomal targeting ligand for *in vivo* applications, it was necessary to compare the PK/BD properties and tumor accumulation of the αHER2-modified and untargeted liposomes. A small pilot study examining the PK/BD of dual radio-labelled ([^{3}H]CHE and [^{14}C]DXR) αHER2-SIL[DXR] and SL[DXR] was performed in the orthotopic breast cancer model. The HER2-negative 4T1 cell

line was utilized so that the tumor cells would not differentially affect the distribution of the formulations. The targeted and untargeted liposomes had different *in vivo* PK (Fig. 5.1A). The αHER2-SIL were eliminated from blood more rapidly than were the SL, with less than 25% of the injected dose of the targeted liposomes present in circulation after 2 h, versus more than 75% of the untargeted liposomes ($P < 0.001$). At 24 h, less than 2% of the αHER2-SIL remained in the blood, versus 28% of the SL ($P < 0.001$). The lower tumor accumulation of the αHER2-SIL at 24 h, relative to the SL ($P < 0.01$; Fig. 5.1C), likely reflects the shorter circulation half-life of the targeted liposomes, due to Fc-mediated uptake into the liver and spleen (34).

At both 2 and 24 h post-injection, hepatic and splenic uptake of the αHER2-modified liposomes was substantially higher than uptake of the untargeted liposomes (Fig. 5.1B, C), with nearly 40% of the αHER2-SIL accumulating in the liver by 24 h ($P < 0.05$; Fig. 5.1C). Negligible uptake (< 2% of injected dose) by lungs, heart, and kidneys was observed for each of the formulations (Fig. 5.1B, C). Similar PK/BD trends were observed when the radio-labelled DXR was quantitiated, as the formulations exhibit excellent drug retention properties (shown in Fig. 5.2A).

A PK/BD study was completed to determine whether employing antibody Fab′ fragments, which lack the Fc portion of the antibody molecule, as targeting ligands would prevent the rapid clearance of the targeted liposomes. The drug-to-lipid ratio of the SL[DXR] remained constant in blood over the course of the 48 h experiment (Fig. 5.2A), indicating that the drug was well-retained by the

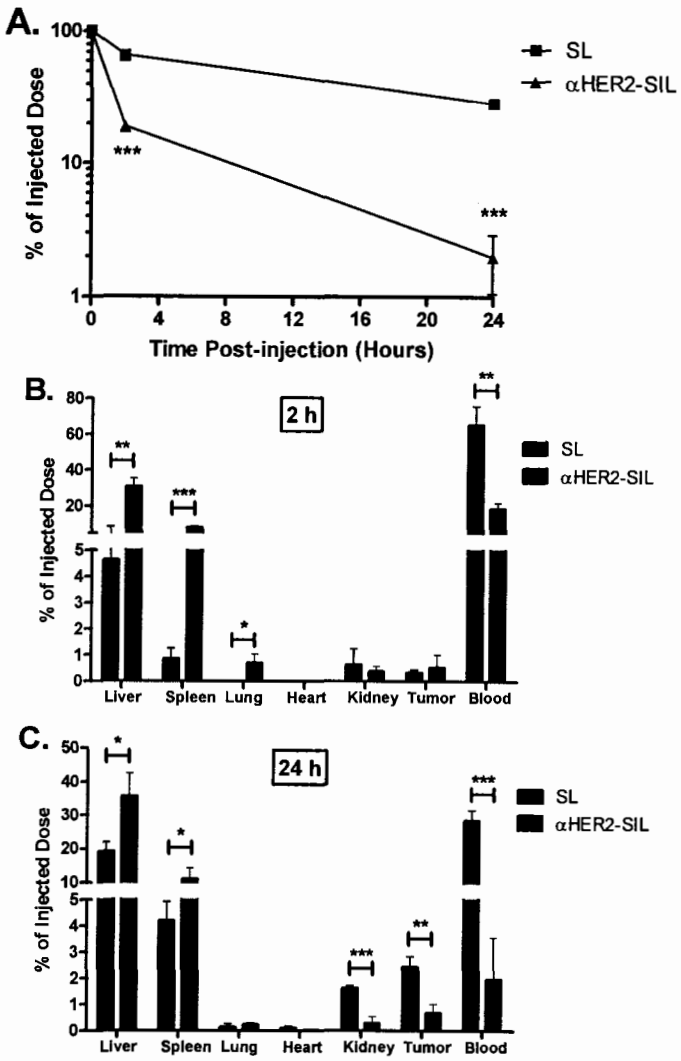

Figure 5.1. PK/BD of doxorubicin-loaded SL and αHER2-SIL.

BALB/c mice bearing orthotopic HER2-negative tumors were injected with dual radio-labelled (lipid and drug) SL[DXR] or αHER2-SIL[DXR] at 3 mg DXR/kg. At different time points post-injection, the radioactivity in blood and organs was quantitated. A) Elimination of liposomes from blood. B) Biodistribution of liposomes after 2 h. C) Biodistribution of liposomes after 24 h. Data are presented as percent of injected dose of lipid. Each point or bar represents the group mean +/- standard deviation (n = 3) from one experiment. *, $P < 0.05$; **, $P < 0.01$; ***, $P < 0.001$.

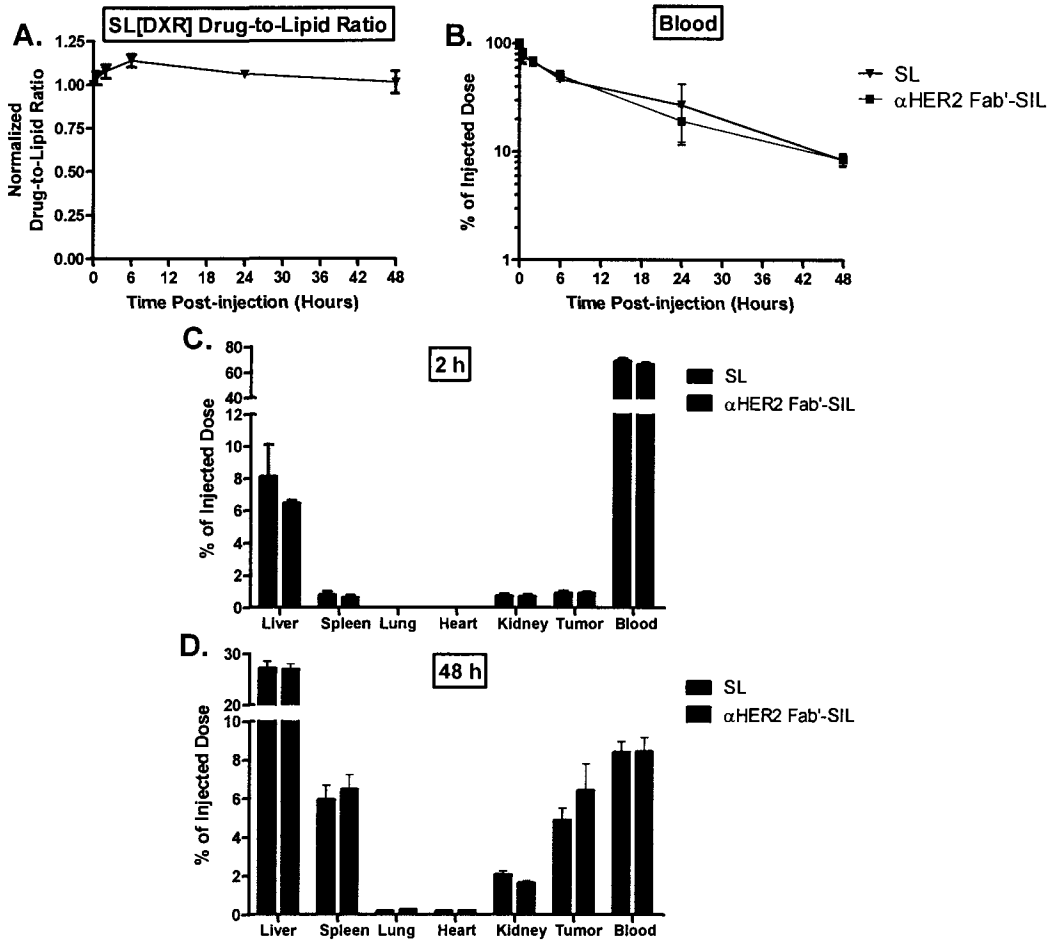

Figure 5.2. PK/BD of doxorubicin-loaded SL and αHER2 Fab'-SIL.

BALB/c SCID mice bearing orthotopic HER2-positive tumors were injected with dual radio-labelled (lipid and drug) SL[DXR] or αHER2 Fab'-SIL[DXR] at 3 mg DXR/kg. At different time points post-injection, the radioactivity in blood and organs was quantitated. A) Drug-to-lipid ratio of SL[DXR] in blood. B) Elimination of liposomes from blood. C) BD of liposomes at 2 h post-injection. D) BD of liposomes at 48 h post-injection. Data are expressed as normalized drug-to-lipid ratio (A) or percent of injected dose of lipid (B-D). Each point or bar represents the group mean +/- standard deviation (n = 3) from one experiment.

liposomes. Consequently, the PK/BD trends observed when the radio-labelled DXR was quantitiated were very similar to the results reported below for the quantitation of the radio-labelled lipid.

Similar log-linear blood pharmacokinetics were observed for both the SL and αHER2 Fab′-SIL in 4T1.2^{ErbB-2} tumor-bearing BALB/c SCID mice (Fig. 5.2B). Approximately 50% of the lipid dose of each formulation was present in the blood at 6 h post-injection. Tumor accumulation of each liposomal formulation was ~5 to 6% of the injected dose after 48 h (Fig. 5.2D). Hepatic and splenic clearance of the αHER2 Fab′-SIL was no greater than clearance of SL (Fig. 5.2C, D). Kidney, heart, and lung uptake were negligible (< 2% of injected dose; Fig. 5.2C, D).

5.2.2. Cellular Association of Tumor-targeted Liposomes

Although the αHER2 Fab′-SIL demonstrated prolonged circulation and greater tumor accumulation *in vivo* than did the αHER2-SIL, it was necessary to ensure that the ligand digestion, reduction, and coupling steps required to generate the αHER2 Fab′-SIL did not prevent them from achieving selective interaction with HER2 and internalization into the target cells. The *in vitro* cellular association of the αHER2-SIL and αHER2 Fab′-SIL were compared via a cellular association assay using the radioactivity method (Fig. 5.3). Both formulations showed enhanced cellular association with the 4T1.2^{ErbB-2} cells, relative to untargeted liposomes. At equivalent surface binding site densities, the degree of cellular association of the αHER2-SIL and αHER2 Fab′-SIL was the same.

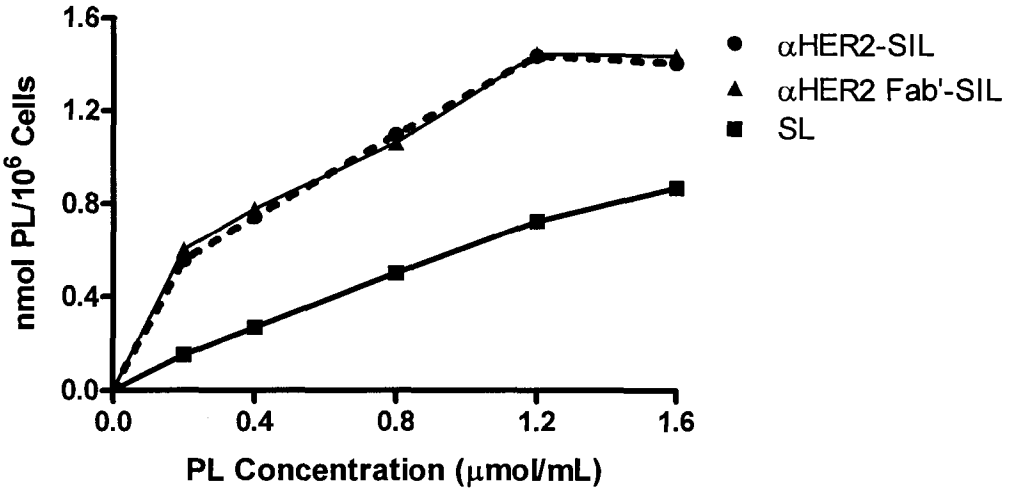

Figure 5.3. Cellular association of SL, αHER2-SIL, and αHER2 Fab'-SIL with $4T1.2^{ErbB-2}$ cells *in vitro*.

Increasing concentrations of radio-labelled SL, αHER2-SIL, or αHER2 Fab'-SIL were incubated with $4T1.2^{ErbB-2}$ cells for 1 h at 37°C. Unbound liposomes were removed and cell-associated radioactivity was quantitated. Data are presented as nmol PL/10^6 cells. Each point represents the mean +/- standard deviation (n = 3) from one representative experiment.

5.2.3. Verification of Coupling of cRGD Peptides

Before examining the PK/BD properties of the cRGD-SL and cRAD-SL *in vivo*, it was necessary to confirm that successful coupling of the peptides to the liposomes had been achieved. The cRGD and cRAD peptides are 5 amino acids long, and due to their small size, could not be detected using the CBQCA Protein Assay. Therefore, an *in vitro* cellular association assay with a model of angiogenic vascular endothelium was completed to verify coupling of the cRGD peptides.

As seen in Fig. 5.4, the cRGD-SL demonstrated significantly greater cellular association with the KS1767 cells than did the SL ($P < 0.001$) and control cRAD-SL ($P < 0.001$). Nearly 5-fold greater cellular association of the cRGD-SL was observed relative to the SL, indicating that successful coupling of the peptide was achieved. Similar results were demonstrated with the NGR-SL, which were used as a positive control following confirmation of successful coupling of the NGR peptides using the CBQCA Assay; the NGR-SL demonstrated significantly greater cellular association with the KS1767 cells than did the SL ($P < 0.001$) and control ARA-SL ($P < 0.001$).

5.2.4. PK/BD of Untargeted vs. Vasculature-targeted Liposomes

The PK/BD properties of the vasculature-targeted NGR-SL and cRGD-SL were compared in tumor-bearing mice to determine which vasculature-specific peptide would be more suitable as a liposomal targeting ligand for *in vivo* applications. Female ICR SCID mice bearing 4T1.2^{ErbB-2} tumors were injected

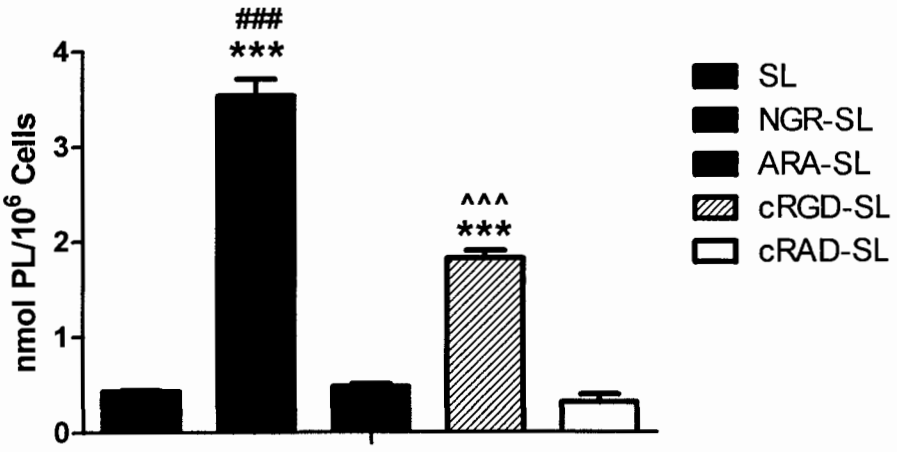

Figure 5.4. Confirmation of cRGD coupling via *in vitro* cellular association assay.

The KS1767 cells were incubated with radio-labelled SL, NGR-SL, ARA-SL, cRGD-SL, or cRAD-SL at 0.6 μmol PL/mL (final concentration) for 1 h at 37°C. Liposomal cellular association was quantitated by scintillation counting of cell-associated radioactivity. Data are presented as nmol PL/10^6 cells. Each bar represents the mean +/- standard deviation (n = 3) from one experiment. ***, $P < 0.001$ vs. SL; $^{###}$, $P < 0.001$ vs. ARA-SL; ^^^, $P < 0.001$ vs. cRAD-SL.

i.v. with dual radio-labelled ([^{14}C]cholesteryl oleate and [^{3}H]VCR) liposomes, either untargeted, or targeted via NGR, cRGD, or their respective mismatched control peptides ARA, or cRAD. The normalized drug-to-lipid ratio of the SL[VCR] in blood decreased with time (Fig. 5.5A), and the half-life of VCR release from the untargeted liposomes was determined to be ~20 h.

Figure 5.5B shows the elimination of liposomes from blood for each of the formulations. At 2 h post-injection, the percent of the injected lipid dose of the cRGD-SL that remained in circulation was less than half of that of the other formulations ($P < 0.001$ vs. SL). Only ~5% of the injected dose of the cRGD-SL was present at 6 h after injection ($P < 0.001$ vs. SL), and less than 1% remained by 24 h post-injection ($P < 0.01$ vs. SL). The circulation half-life of the cRGD-SL was on the order of 1 h, compared to 10 h for the other formulations, which did not differ significantly from each other. This resulted in the tumor levels of the cRGD-SL being 4- to 6-fold lower than those of the SL ($P < 0.01$), the NGR-SL ($P < 0.01$), and the cRAD-SL ($P < 0.05$) at 48 h post-injection (Fig. 5.5D).

The short blood half-life and low tumor accumulation of the cRGD-SL were likely the result of the rapid hepatic and splenic uptake of the cRGD-SL. At 2 h post-injection, the hepatic accumulation of the cRGD-SL was over 2-fold greater than that of the NGR-SL ($P < 0.001$), and 6- to 10-fold greater than that of the cRAD-SL ($P < 0.001$) and SL ($P < 0.001$), respectively (Fig. 5.5C). Similarly, nearly 10-fold greater splenic uptake of the cRGD-SL was observed, relative to all other formulations at 2 h ($P < 0.001$; Fig. 5.5C).

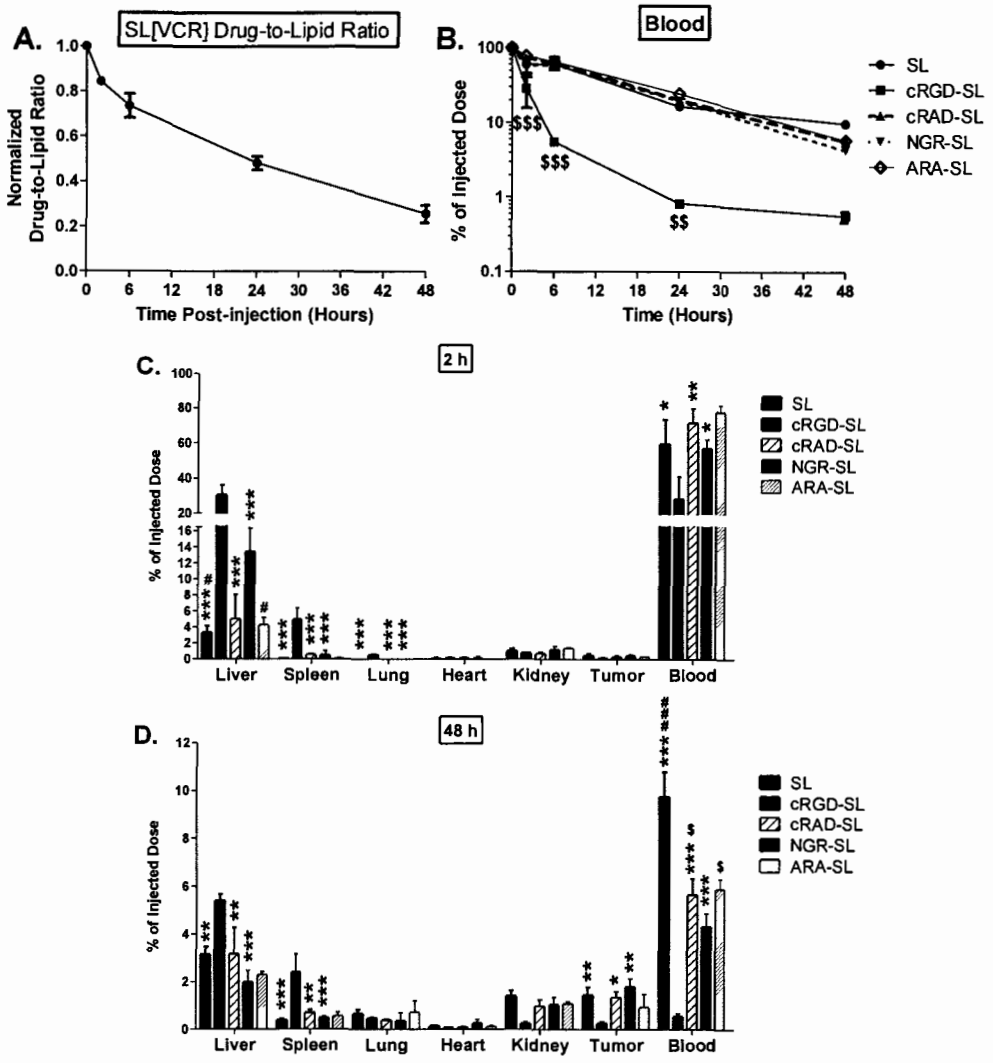

Figure 5.5. Pharmacokinetics and biodistribution of untargeted vs. vasculature-targeted liposomal vincristine.

Mice bearing orthotopic HER2-positive tumors were injected with dual radio-labelled (lipid and drug) SL[VCR], cRGD-SL[VCR], NGR-SL[VCR], cRAD-SL[VCR], or ARA-SL[VCR] at 1.5 mg VCR/kg. At different time points post-injection, the radioactivity in blood and organs was quantitated. A) Drug-to-lipid ratio of SL[VCR] in blood. B) Blood elimination of liposomes. C) BD of liposomes at 2 h post-injection. D) BD of liposomes at 48 h post-injection. Data are presented as normalized drug-to-lipid ratio (A) or percent of injected dose of lipid (B-D). Each point or bar represents the group mean +/- standard deviation (n = 3) from one experiment. *, $P < 0.05$ vs. cRGD-SL; **, $P < 0.01$ vs. cRGD-SL; ***, $P < 0.001$ vs. cRGD-SL; $^{\#}$, $P < 0.05$ vs. NGR-SL; $^{\#\#\#}$, $P < 0.001$ vs. NGR-SL; $^{\$}$, $P < 0.05$ vs. SL; $^{\$\$}$, $P < 0.01$ vs. SL; $^{\$\$\$}$, $P < 0.001$ vs. SL.

Importantly, the PK/BD properties of the NGR-SL were similar to those of the SL (Fig. 5.5B-D). However, at 2 h post-injection, there was significantly greater liver accumulation of the NGR-SL, relative to that of the SL ($P < 0.05$) and ARA-SL ($P < 0.05$; Fig. 5.5C). A minor (< 5% of the injected dose), but statistically significant, decrease in the percent of the injected dose in blood was observed between the NGR-SL and the SL ($P < 0.001$) at 48 h post-injection, although there was no difference between the NGR-SL and the ARA-SL at the same time point (Fig. 5.5D).

As expected, the blood pharmacokinetics and tissue distributions of the mismatched control peptide-modified formulations were similar to those of the untargeted liposomes (Fig. 5.5B-D). Although there was a statistically significant difference between the percent of the injected dose of the SL and the two mismatched control peptide-modified formulations ($P < 0.05$) remaining at 48 h post-injection, it was a negligible difference of only ~3% of the injected dose. Following the administration of all formulations, negligible quantities (< 2% of injected dose) of radio-labelled lipid were found in the lungs, heart, and kidneys after 2 h (Fig. 5.5C) or 48 h (Fig. 5.5D).

5.2.5. Effect of Lipid Dose on PK/BD of SL and NGR-SL

The PK/BD properties of two different lipid doses of SL and NGR-SL were compared in subcutaneous 4T1 and $4T1.2^{ErbB-2}$ breast cancer models. This experiment was completed to determine whether the high doses of liposomes (2.5-5 μmol PL/mouse) required for magnetic resonance imaging of liposome binding

demonstrate the same PK/BD properties as liposomes administered at the normal lipid dose (0.5 μmol PL/mouse). Figure 5.6 shows primarily dose-independent PK/BD for the SL and NGR-SL in both the subcutaneous HER2-negative (Fig. 5.6A, B) and HER2-positive (Fig. 5.6C, D) breast cancer models, although some statistically significant differences in blood and organ lipid levels were observed. Relative to the normal dose of the SL, slight increases in liver accumulation of the high doses of the SL and NGR-SL at 24 h post-injection were shown. However, importantly, this disparity was typically less than 5% of the injected dose, and would not be expected to affect the imaging of liposomal tumor binding as tumor accumulation levels were unchanged. Statistically significant decreases in splenic accumulation of the high doses of the SL and NGR-SL were observed at 24 h post-injection in the 4T1 model; however, these decreases were less than 1% of the injected dose (Fig. 5.6B).

5.2.6. Cytotoxicity of VCR Against 4T1.2^{ErbB-2} Cells In Vitro

The cytotoxicity of VCR against the 4T1.2^{ErbB-2} cells was tested to determine whether VCR released from vasculature-targeted liposomes could mediate direct cytotoxicity against surrounding tumor cells. The data presented in Fig. 5.7 show that the 4T1.2^{ErbB-2} cells are sensitive to VCR, with an IC_{50} value of 12.3 μg/mL (95% confidence interval = 9 to 18 μg/mL), which is approximately half the IC_{50} value of free VCR against the KS1767 cells *in vitro* (25 μg/mL; Fig. 4.14).

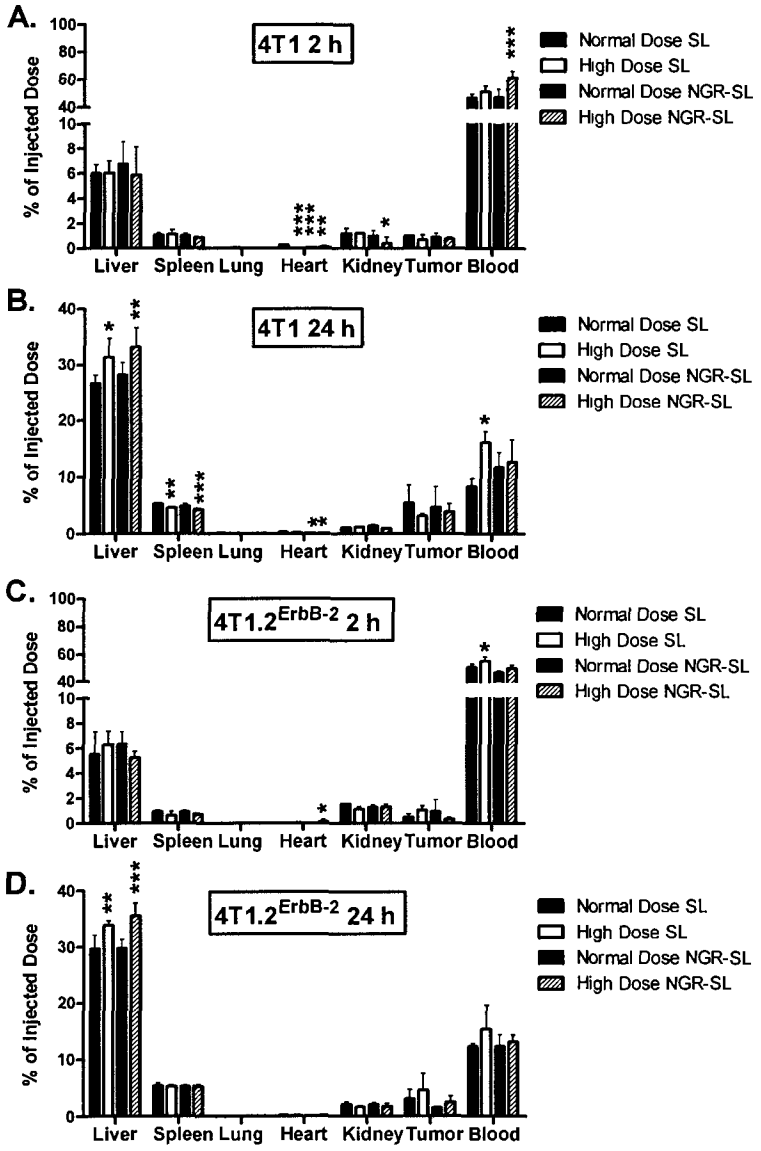

Figure 5.6. Comparison of PK/BD properties of high and normal lipid doses of SL and NGR-SL.

BALB/c mice bearing subcutaneous 4T1 tumors (A and B) or BALB/c SCID mice bearing 4T1.2^{ErbB-2} tumors (C and D) were injected with drug-free radio-labelled SL or NGR-SL at 0.5 μmol PL/mouse (normal dose) or 2.5 μmol PL/mouse (high dose). At 2 h (A and C) or 24 h (B and D) post-injection, the radioactivity in blood and organs was quantitated. Data are expressed as percent of injected dose of lipid. Each bar represents the group mean +/- standard deviation (n = 3) from one experiment. *, $P < 0.05$ vs. Normal Dose SL; **, $P < 0.01$ vs. Normal Dose SL; ***, $P < 0.001$ vs. Normal Dose SL.

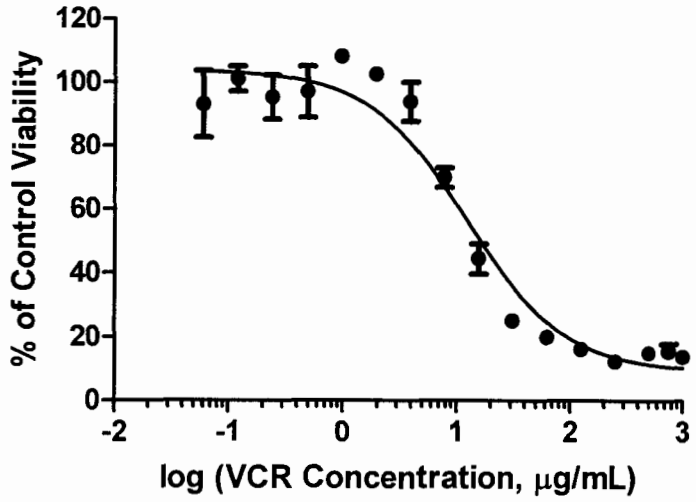

Figure 5.7. Cytotoxicity of free VCR against 4T1.2^{ErbB-2} cells *in vitro*.

The 4T1.2^{ErbB-2} cells were exposed to increasing concentrations of free VCR for 1 h at 37°C. Drug was washed out and the cells were incubated for an additional 47 h before cell viability was assessed via an MTT assay. Data are presented as percent of control viability. Each point represents the mean +/- standard deviation (n = 3) from one representative experiment.

5.2.7. Combination Therapy vs. Monotherapy

As an initial investigation into the therapeutic potential of the dual-targeted approach, the anti-cancer effect of the tumor-targeted and vasculature-targeted therapies were compared as monotherapies and in combination, using an orthotopic HER2-positive breast cancer model, described above. The resulting tumor growth curves are presented in Fig. 5.8. Following a single injection of the vasculature-targeted NGR-SL[VCR] or tumor-targeted αHER2 Fab′-SIL[DXR], a reduction in tumor growth rate was observed, relative to saline-treated mice. When the therapies were injected simultaneously on day 7, the combination was superior to the single injections alone, and produced an approximately additive therapeutic effect. Similar reductions in tumor volumes were achieved regardless of the order in which the dual-targeted therapy was administered: therapies administered simultaneously at day 7, vasculature-targeted therapy at day 7 and tumor-targeted therapy at day 14, or vice versa. On day 28 of the study, the average tumor size of the mice treated with combination treatments, administered in any order, was half the average tumor size for mice treated with either single treatment.

5.2.8. Tumor Accumulation

In the clinic, chemotherapy is typically administered as multiple cycles of treatment; when employing cytotoxic therapies that are known to have effects on the tumor vasculature, it becomes important to determine whether the tumor accumulation of subsequent therapies is affected by treatment-induced vascular

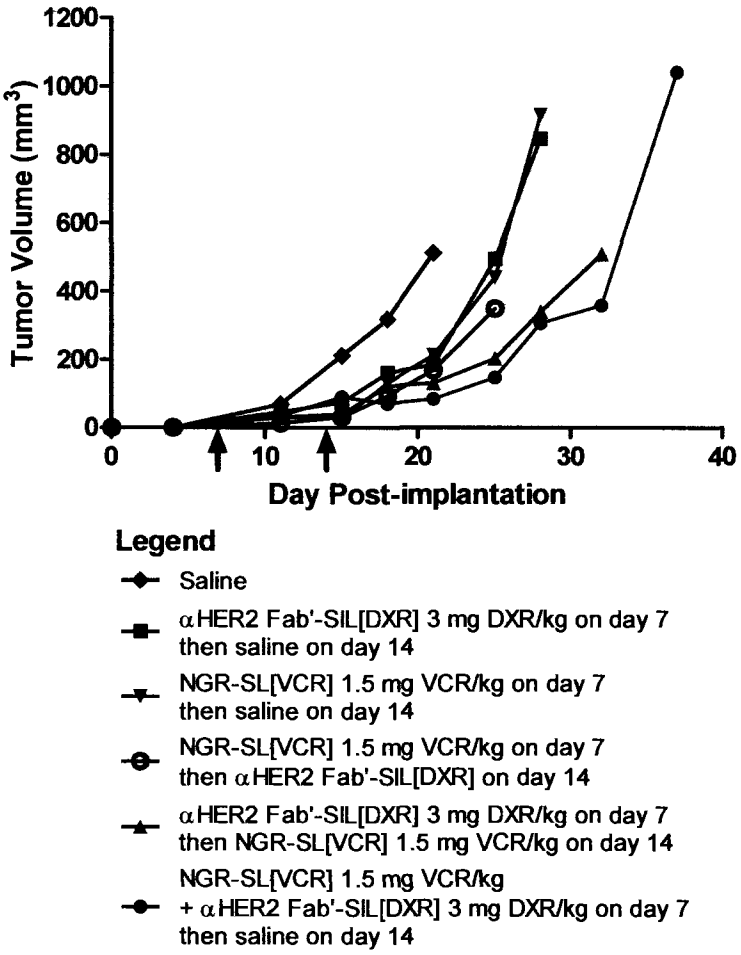

Figure 5.8. Therapeutic effect of monotherapies and combination therapies.

BALB/c SCID mice bearing orthotopic HER2-positive tumors were injected i.v. at days 7 and 14 with saline, NGR-SL[VCR] (1.5 mg VCR/kg), and/or αHER2 Fab'-SIL[DXR] (3 mg DXR/kg). Data are presented as tumor volume (mm^3). Each point represents the group median tumor volume (n = 7), calculated until fewer than 3 mice remained. Arrows represent treatment.

alterations. Because liposomal DXR and liposomal VCR can mediate effects against angiogenic vasculature, it was necessary to determine how the administration of an initial dose of liposomal drug affected the tumor accumulation of a second dose of liposomes administered at various times following pre-treatment. Figure 5.9 shows a comparison of the tumor accumulation of a second dose of liposomes administered simultaneously with, or at 4, 7, or 11 days after, pre-treatment with drug-free liposomes, NGR-SL[VCR], or αHER2 Fab′-SIL[DXR].

When the pre-treatment was given at day 7 post-implantation, the highest accumulation of the second dose of liposomes per gram of tumor was observed when the second dose was injected at 4 days after pre-treatment with either tumor-targeted or vasculature-targeted liposomal drug. Following pre-treatment with VCR- or DXR-loaded formulations, a substantial decline in uptake of liposomes per gram of tumor was observed when the second dose was administered at 7 days after pre-treatment, versus 4 days after pre-treatment. A further decrease in accumulation of the second dose was observed when it was injected at 11 days after pre-treatment. After pre-treatment with drug-free control liposomes, there was a steady decrease in the accumulation of the second dose of liposomes per gram of tumor over the course of the experiment. In order to avoid DXR toxicity and receptor-based competition between the two doses of liposomes, the biodistribution of simultaneously administered first and second liposome doses was not tested in mice that received DXR-loaded liposomes as their first treatment.

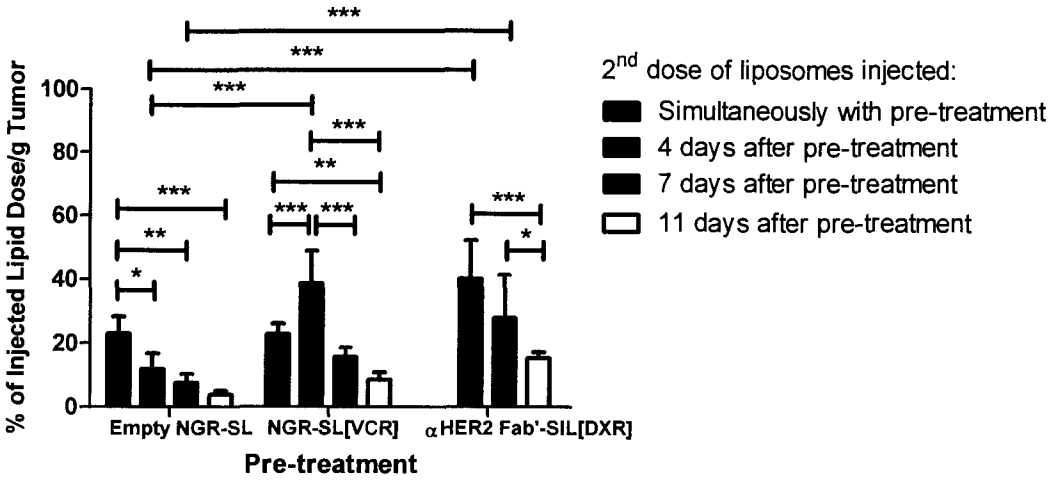

Figure 5.9. Tumor accumulation of second dose of liposomes following pre-treatment with vasculature-targeted liposomes.

ICR SCID mice bearing orthotopic HER2-positive tumors were pre-treated with empty NGR-SL, NGR-SL[VCR] at 1.5 mg VCR/kg, or αHER2 Fab′-SIL[DXR] at 3 mg DXR/kg. A second dose of liposomes (dual radio-labelled αHER2 Fab′-SIL[DXR]) was injected simultaneously with pre-treatment, or at 4, 7, or 11 days after pre-treatment. At 48 h after injection of the second dose of liposomes, the radioactivity in tumors was quantitated. Data are presented as percent of injected dose of lipid per gram of tumor. Each bar represents the group mean +/- standard deviation (n = 3-5) from one experiment. *, $P < 0.05$; **, $P < 0.01$; ***, $P < 0.001$.

5.2.9. Effect of Dosing Schedule on Therapeutic Activity

Two different dosing schedules were investigated to determine whether the increased accumulation of the second liposome dose at 4 days after pre-treatment could be exploited to improve therapeutic effect (Fig. 5.10). All mice received their first treatment on day 7 post-implantation. Mice that received the second injection at 4 days later demonstrated slower disease progression than the mice that received the second injection at 7 days later. This trend was observed for all three treatment regimens: simultaneously administered NGR-SL[VCR] and αHER2 Fab′-SIL[DXR], NGR-SL[VCR] followed by αHER2 Fab′-SIL[DXR] at 4 or 7 days later, and αHER2 Fab′-SIL[DXR] monotherapy. Exploiting the window of increased accumulation by administering the second treatment at 4 days after the initial treatment led to the greatest improvement in the therapeutic outcome of the simultaneously administered combination therapy.

All treatments, regardless of schedule, were superior to saline treatment (Fig. 5.10). However, overall, there was not a statistically significant difference between the therapeutic outcomes of the three different treatment regimens when the second dose was given at 4 days after the first dose. In contrast, when the second treatment was given at 7 days after the first dose, mice treated with both NGR-modified and αHER2 Fab′-modified liposomes simultaneously had poorer tumor control than the other two groups.

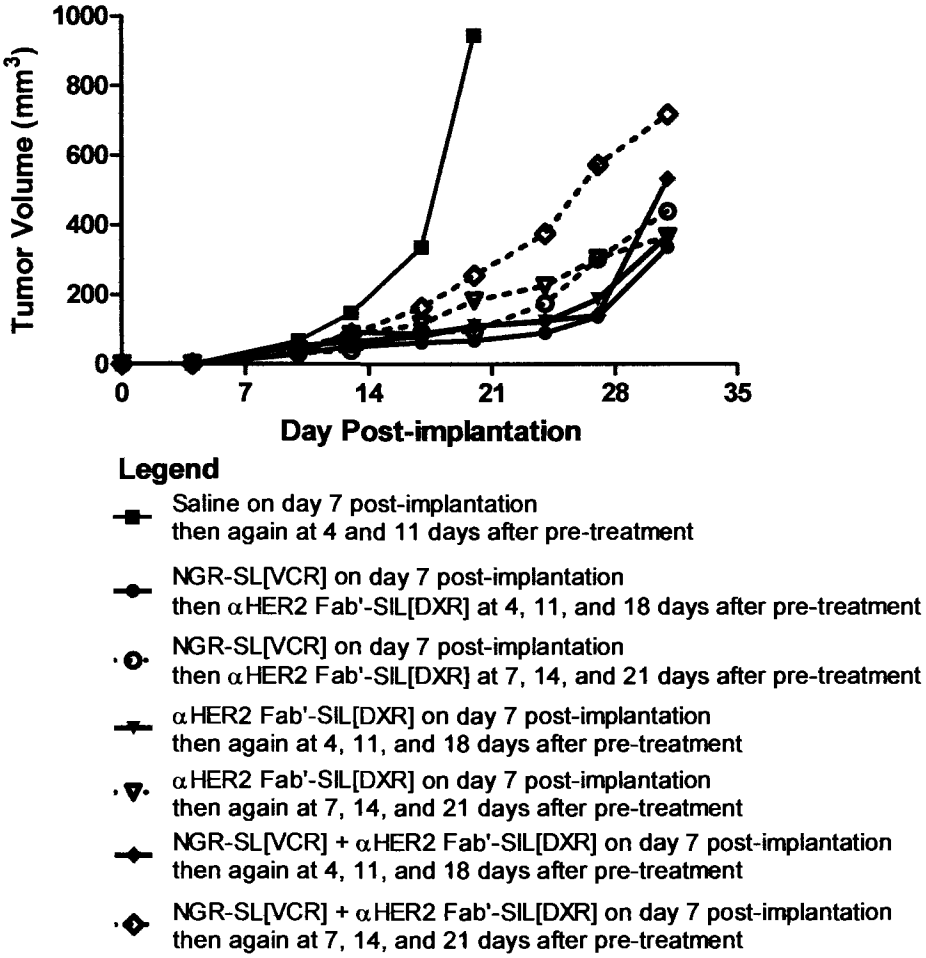

Figure 5.10. Effect of dosing schedule on therapeutic activity.

ICR SCID mice bearing orthotopic HER2-positive tumors were injected i.v. at day 7 with saline, NGR-SL[VCR] (1.5 mg VCR/kg), αHER2 Fab′-SIL[DXR] (3 mg DXR/kg), or NGR-SL[VCR] + αHER2 Fab′-SIL[DXR] (0.75 mg VCR/kg + 1.5 mg DXR/kg). At either 4 or 7 days after pre-treatment, mice received a second i.v. injection of saline, NGR-SL[VCR] + αHER2 Fab′-SIL[DXR], or αHER2 Fab′-SIL[DXR]. On a q7d schedule, mice then received two further injections of the same treatment at the same dose (NGR-SL[VCR] + αHER2 Fab′-SIL[DXR]) or a reduced dose (2.5 mg DXR/kg; αHER2 Fab′-SIL[DXR]). Data are presented as tumor volume (mm^3). Each point represents the group median tumor volume (n = 8), calculated until fewer than 3 mice remained.

5.3. Discussion

The results presented in this chapter describe the therapeutic potential of a nanomedicine-based combined vasculature-targeted and tumor-targeted approach to the treatment of HER2-positive breast cancer. Proof-of-concept studies illustrated that, by exploiting the ability of targeted liposomes to selectively deliver two different drugs to two different cell populations, the combination of the vasculature-targeted and tumor-targeted therapies could be administered at half the dose of tumor-targeted monotherapy, with less overall toxicity and no loss of anti-cancer activity. Based on the data presented above, and the knowledge that the dual-targeted approach is easily adaptable, and thus applicable to the treatment of a wide range of solid tumors, the strategy warrants further investigation and optimization. The research outlined in this thesis as well as future studies, should contribute valuable knowledge to the field regarding the unique interaction and interdependence between tumor cells and tumor vasculature, and how this interdependence can be exploited to improve treatment options, either in the context of combinations of liposomal nanomedicines or combinations of cell population-specific free drugs.

The literature reveals that a variety of "dual-targeting"/combination chemotherapy approaches have previously been investigated for cancer treatment. The majority of these approaches consist of combinations of free agents, such as classical chemotherapeutic drugs, biological agents, and small molecule inhibitors, which are co-administered in an attempt to simultaneously interfere with multiple proteins/pathways/processes that are fundamental to cancer biology.

For example, administration of a combination of bevacizumab and paclitaxel for metastatic breast cancer treatment is designed to interfere with both angiogenic vascular development and tumor growth. Bevacizumab prevents the formation of new blood vasculature and reduces tumor vessel density while paclitaxel mediates a direct cytotoxic action against the proliferating tumor cells. The rationale behind the combination of bevacizumab and paclitaxel is similar to that of the combined dual-targeted approach investigated in this chapter. In both instances, the treatments were selected to be complementary when used in combination as they are designed to kill different cell populations. Although administration of bevacizumab in combination with paclitaxel has demonstrated therapeutic activity in patients (35), there are still concerns regarding the relatively non-specific distribution and off-target side effects associated with the use of classical chemotherapeutic agents like paclitaxel (36). As discussed previously, the use of drug carriers can help to surmount these challenges by increasing tumor drug delivery and reducing accumulation in non-target tissues.

Interest in nanomedicines has soared over the last decade, and in recent years, lipid and polymer delivery systems have been incorporated into dual-targeting approaches to enable selective delivery of chemotherapeutic drugs, RNAi and gene therapy, and diagnostic agents to specific cell populations within the body. The improvements in targeting that can be achieved with nanomedicines bring new meaning to the concept of a dual-targeted approach. Scientists have applied this concept in a variety of ways in an attempt to overcome obstacles associated with cancer treatment.

The numerous nanomedicine-based dual-targeting approaches published in the literature can be differentiated by: 1) the number of drugs/therapies being delivered, 2) the number of formulations being administered, 3) the number of ligands per formulation, and 4) the number of specific cell populations being targeted. The majority of the previously published dual-targeting work has focused on the administration of one drug/therapy, in a single nanomedicine formulation presenting: two different ligands targeted to one cell population, such as tumor cells (37, 38) or tumor vascular cells (39, 40), two different ligands targeted to two different cell populations, such as tumor cells and tumor vascular cells (41), two different ligands with different purposes (42, 43), such as cell penetration and targeting of tumor cells/tumor vascular cells (44), or one ligand containing recognition sequences for two different targets on the same cell population (45). Instead of administering one therapy in a single targeted formulation, other dual-targeting strategies have focused on co-administration of two formulations of the same drug, each targeted via a different ligand; the different ligands have been targeted to different antigens on the same cell population (37, 46) or to different antigens on different cell populations (47). Using the liposome platform, it would be possible to combine a number of these strategies. For instance, one possible variation of the dual-targeted approach investigated in this thesis would be: liposomal VCR presenting both pericyte-specific ligands and endothelial-specific ligands and liposomal DXR presenting both tumor cell-specific ligands and cell-penetrating sequences. However,

increasing the complexity of the therapeutic approach makes it significantly more complicated to translate to the clinic.

Some additional "dual-targeting" strategies have been explored, but they are more accurately described as combination chemotherapy that employs nanomedicines, rather than dual-targeted chemotherapy, as they fail to achieve the same degree of rationally designed selectivity and specificity that is uniquely possible utilizing the approaches outlined above. Examples include: the administration of one formulation that non-specifically mediates cytotoxicity against two cell populations, such as a coated cationic liposomal formulation of oxaliplatin (48), and the administration of a two different drugs encapsulated within a single formulation targeted by a ligand that shows affinity for two cell types and delivers the drugs to both populations, such as a RGD-modified liposomal formulation of DXR and combretastatin A-4 (49).

The dual-targeted combination approach that was the foundation of this chapter expands upon the above strategies, particularly that of Pastorino *et al.* (47), by using two different formulations of two different anti-cancer drugs, each targeted to a different cell population via a selective ligand. There are several advantages to utilizing two different targeted formulations, which may be at least partially responsible for the therapeutic success of the combined, dual-targeted approach observed in the proof-of-concept studies presented above. By using two formulations, two different drugs can be selectively delivered to two different cell populations, while maintaining the ability to individually alter the dose of one drug to reduce toxicity or increase/decrease the magnitude of its effect as

required, and the effect of administering the therapies following different temporal sequences can be explored.

Pastorino *et al.* have previously demonstrated the success of a combined vasculature-targeted and tumor-targeted combination approach in a neuroblastoma model using DXR in both liposomal formulations (47, 50). In this chapter, the approach of Pastorino *et al.* (47) has been modified and refined by utilizing two different drugs to exploit the benefits of dual-targeted combination chemotherapy for the treatment of HER2-positive breast cancer. By targeting liposomal VCR to the tumor vasculature, and liposomal DXR to the tumor cells themselves, the combination is expected to have activity on two cell population, leading to an improvement in therapeutic effect. This is believed to be the first study that has investigated a combined anti-vasculature and anti-tumor (dual-targeted) approach using a combination of two different liposomal drug formulations targeted to two different cell populations.

The dual-targeted approach provided a superior tumor growth delay, and an improvement in overall survival that was at least additive, relative to either therapy administered alone. The dose of each drug in the simultaneously administered combination was reduced by 50% without compromising disease control, relative to the individual monotherapies and the vasculature-targeted therapy followed by the tumor-targeted therapy. These studies provide additional evidence that the combination chemotherapy strategy that is commonly used in conventional chemotherapy can be successfully extended into the nanomedicine field to exploit the additional benefits of targeted drug delivery.

The data collected in PK/BD experiments were utilized to differentiate between the possible targeting ligands for the tumor-targeted therapy and the vasculature-targeted therapy to be used in efficacy studies. The whole antibody-modified liposomes appeared to be cleared from the plasma of tumor-bearing mice with biphasic pharmacokinetics, although additional early time points would need to be tested to confirm this. As has been suggested for other whole antibody-modified liposomes, the initial phase of rapid clearance is likely mediated by Fc receptors (51-53). It is plausible that decreasing the surface density of the targeting antibody on the liposomes may reduce their hepatic uptake or clearance, which has been demonstrated by Koning *et al.* (54, 55) and others (56), and allow for a corresponding increase in circulation half-life and tumor accumulation, although this was not investigated in this thesis.

As liposomes require 24 to 48 h to achieve maximal localization in solid tumors, liposomal formulations with short circulation half-lives have been shown to exert a reduced therapeutic effect (57-60). As predicted, the liposomes targeted via αHER2 Fab′ fragments, which lack the Fc region of the antibody, displayed similar PK/BD properties as did the untargeted liposomes. These data support the results of Maruyama *et al.*, who demonstrated that liposomes targeted to pulmonary endothelial cells via monoclonal antibody Fab′ fragments displayed lower hepatic uptake and longer circulation half-lives than liposomes targeted via whole antibodies, even when the surface ligand density of the Fab′ fragment-modified liposomes was 10-fold higher than that of the whole antibody-modified liposomes (61).

Importantly, the αHER2 Fab′-SIL demonstrated equivalent *in vitro* cellular association with the $4T1.2^{ErbB-2}$ cells compared to the liposomes targeted with whole antibodies. In other words, any loss of binding affinity when the antibodies were converted to Fab′ fragments was restored when the fragments were presented in a multivalent array on a liposomal particle. The above results support published reports from other researchers (62-64), including scientists from the Allen laboratory working with liposomes targeted via αCD19 whole antibodies and αCD19 Fab′ fragments (30, 65).

In $4T1.2^{ErbB-2}$ tumor-bearing mice, a very rapid initial clearance and substantial splenic uptake of cRGD-modified liposomes was observed; this was not observed for the liposomes targeted with either NGR peptides or αHER2 Fab′ fragments. This led to a corresponding decrease in tumor accumulation of cRGD-SL, relative to the NGR-SL and other formulations. However, it is important to consider that it may be possible to decrease the density of the cRGD peptides on the liposomes such that their ability to be internalized into target cells is retained, but the splenic uptake of the liposomes is reduced. This would not compromise the liposomes' ability to deliver the encapsulated drug intracellularly, while increasing their circulation half-life and tumor accumulation, and presumably therapeutic effect, although this was not investigated.

The difference in circulation half-life between NGR-modified liposomes and RGD-modified liposomes has been noted in the literature (66). Schiffelers *et al.* attribute the disparity in half-life to the selective expression of APN on angiogenic endothelial cells versus the more widespread distribution of the α_V

integrin on both angiogenic endothelial cells and macrophages (66). Furthermore, significantly elevated splenic uptake of RGD mimetic-modified liposomes has been reported in the literature (67). This coincides with reports that cRGD-modified protein conjugates localize to cells in the red pulp in the spleen, indicative of association with macrophages (68). The same group also found increased accumulation in liver and kidneys, relative to cRAD-modified antibodies, but no decrease in tumor accumulation for the cRGD-modified protein conjugates (68).

As mentioned, in the PK/BD data presented above, there was no difference in splenic uptake of NGR-modified liposomes and untargeted liposomes. In contrast, Pastorino *et al.* have published data from an orthotopic neuroblastoma model showing ~10- to 20-fold greater splenic uptake of NGR-SL[DXR], relative to SL[DXR], as early as 2 h post-injection (50). The reason for the discrepancy may be attributable to the targeting ligand density, as NGR-SL have been administered at five times the normal lipid dose in HER2-negative and HER2-positive subcutaneous breast cancer models and did not show greater uptake by the spleen than did the SL, at 2 or 24 h post-injection. Liposomes with increased clearance have the potential to limit the therapeutic effectiveness of a dual-targeted approach; NGR-SL reached significantly higher tumor levels than cRGD-SL, hence the selection of NGR-modified liposomes over cRGD-modified liposomes for further examination in therapeutic experiments.

In the orthotopic tumor model, the tumors become palpable around day 7 to10 post-implantation, with vascular development beginning around the same

time (J. Hare, unpublished data). Initiating the first treatment at 7 days after cell implantation was hypothesized to take advantage of the possibility of increased endothelial cell susceptibility during a period of rapid division and cell immaturity, the potential for increased vascular permeability of immature vasculature, and increased tumor concentrations of liposomes via the EPR effect.

It was initially postulated that vasculature-targeted therapy followed by tumor-targeted therapy would provide the greatest disease control. Interestingly, the order in which the combination therapies were administered did not impact anti-cancer activity in a murine model of orthotopic HER2-positive breast cancer. Furthermore, dose reductions of the liposomal drugs failed to distinguish between the different orders of administration; simultaneous administration, administration of vasculature-targeted then tumor-targeted therapy at 7 days later, or vice versa, provided equivalent disease control. It is possible that there were not significant differences between the treatment orders because of eventual cross-activity between the formulations. Arap *et al.* have shown that phage displaying the NGR peptide spread outside of the tumor vasculature and into the tumor cells at 24 h after phage injection (69), and speculate that it may be the result of the EPR effect or phage uptake by tumor vascular endothelial cells and subsequent transfer to tumor tissue (69, 70). It follows that a similar penetration of NGR-presenting liposomes out of the tumor vasculature and into the surrounding tumor is likely to occur. In fact, in an adrenal tumor model, Pastorino *et al.* have demonstrated a strong presence of drug in the tumor vasculature at 16 h post-injection of NGR-SL[DXR], with subsequent leakage of NGR-SL[DXR] into the tumor tissue at 24

h post-injection (50). Therefore, following administration of NGR-SL[VCR], the cytotoxic activity would initially take place in the angiogenic blood vessels, but would later also occur in the tumor cells themselves, which have been shown to be sensitive to VCR *in vitro* (Fig. 5.7). It is plausible that a similar bystander effect may be observed with the tumor-targeted formulation – following apoptosis of tumor cells, drug molecules would be released into the tumor interstitium and may be able to exert cytotoxic effects against vascular endothelial cells in close proximity. Because the anti-cancer actions of the vasculature-targeted therapy have been shown to extend beyond the vasculature, and the reverse action with the tumor-targeted formulation is also foreseeable, administration of either therapy alone may ultimately have an effect on both the tumor cell population and the tumor vasculature. In some ways, this parallels simultaneous administration of a vasculature-targeted and a tumor-targeted formulation.

The cytotoxic actions of vascular-active therapies fall along a spectrum, from the rapid and severe vascular collapse produced by vascular disrupting agents, to the prevention of new blood vessel growth and normalization of tumor blood vessels that can be achieved by inhibiting VEGF or employing metronomic chemotherapy. Some anti-vascular therapies have been reported to increase tumor vessel permeability and cause changes in interstitial fluid pressure (IFP) (71, 72, and references therein, 73). Increases and decreases in IFP have been observed following anti-vascular treatment, and are dependent on the severity and stage of vascular shutdown (72, and references therein). Potent anti-vascular agents, such as combretastatin, can cause complete collapse of the angiogenic vasculature,

substantially limiting the tumor delivery of subsequently administered therapeutics (74-76). It has been demonstrated that reductions in IFP (77, 78) and increases in capillary permeability (79) can increase tumor accumulation of large molecules; however, researchers have yet to determine how the administration of vasculature-targeted liposomal drugs will impact the delivery of subsequently administered macromolecules. Thus, it was necessary to understand the implications of the vascular effects produced by the NGR-SL[VCR].

When investigating how pre-treatment with vasculature-targeted liposome formulations affected the tumor accumulation of subsequently administered liposomes, a steady decrease in liposome accumulation per gram of tumor was observed with increased time after pre-treatment with empty NGR-SL. In contrast, it was determined that a window of increased tumor liposome accumulation existed after pre-treatment with NGR-SL[VCR]; the percent of the injected dose of lipid per gram of tumor reached a maximum when the second liposome dose was administered at 4 days after pre-treatment, but decreased substantially when the second dose was administered at later time points. It is possible that the drug-loaded formulations decreased tumor cell density, either via direct cytotoxicity agains the tumor cells of via indirect cytotoxicity resulting from vascular damage, and the reduced tumor cell density allowed greater tumor delivery of the second dose of liposomes, similar to reports by Abu Lila *et al.* (48). Because of the sustained release properties of the liposomal drug formulations, it is plausible that continued drug exposure from the pre-treatment may have lead to "over-pruning" of the vascular network (80), and reduced

liposome delivery to tumors as the time between pre-treatment and the administration of the second dose increased.

The sustained release properties of liposomal drug formulations mimic metronomic dosing regimens, which are known to exert anti-proliferative and cytotoxic effects against activated vascular endothelial cells (81). Furthermore, as noted above, therapies that cause endothelial cell cytotoxicity can increase capillary permeability and induce changes in IFP. Taken together, this could explain why, versus pre-treatment with empty NGR-SL, αHER2 Fab′-SIL[DXR] pre-treatment led to increased tumor liposome delivery when the second dose was administered at 4 or 7 days after pre-treatment.

A number of samples were collected for examination of the effect of the vasculature-targeted therapy via histological analysis and immunohistochemistry. However, the utility of microvessel density (MVD) as a measure of the effectiveness of vascular-directed therapies has been severely criticized (82). Alterations in MVD are often accompanied by significant changes in function, including blood flow patterns and rates, vascular permeability, interstitial fluid pressure, etc.. Importantly, it is the changes in vascular function that are most relevant when considering how the tumor delivery of subsequently administered therapies might be affected. This is particularly true since blood vessel distribution throughout solid tumors is extremely heterogeneous and changes in MVD would vary throughout the tumor due to the differences in therapy penetration, oxygenation status, blood flow and necrosis. In light of these

considerations, it was decided that more relevant and useful information could be obtained through studies such as biodistribution studies, reported above.

Based on the tumor accumulation data, a study was completed to investigate whether or not the short window, in which increased tumor accumulation of a second dose of liposomes was observed, could be exploited to increase the therapeutic effect. Particularly for the simultaneously administered combination therapy, giving the second treatment at 4 days after the first treatment was more effective. This suggests that it is possible to improve the therapeutic effect by exploiting the short window of increased accumulation. Several features of the vasculature-targeted therapy could be investigated in further studies for their effects on cellular toxicity, the accumulation of subsequently administered therapies, and the overall anti-cancer potential of the dual-targeted approach. These include: the choice of encapsulated drug, or even investigation of bevacizumab or CA4P, the lipid composition of the formulation and the drug release rate, and the dose and number of cycles.

It is necessary to recognize that there is an increase in dose intensity when the treatments are administered on a shorter time scale with the second dose at day 4 after first treatment versus day 7, and that this may have contributed to the observed improvements in activity, rather than exploitation of the window of increased liposome accumulation. However, if this hypothesis is correct, different results would have been expected from the first therapeutic study (Fig. 5.8), where the most dose-intense schedule – the simultaneously administered therapies – did not yield the greatest therapeutic effect. One of the major problems with

providing dose-intense treatments is the development of severe adverse effects. Mice receiving αHER2 Fab′-SIL[DXR]experienced severe weight loss of close to 20% when the second injection was given only 4 days after the first. This necessitated a reduction in DXR dose to 2.5 mg DXR/kg for the remaining two injections. In contrast, no toxicity-related reductions in dose were required for the simultaneous combination therapy; drugs were dosed at half the dose of the other regimens with an equivalent therapeutic outcome. Thus, two of the advantages of utilizing two different drugs in a dual-targeted combination therapy approach are: the ability to utilize a dose-intense treatment schedule without causing severe toxicity and the ability to administer the two therapies at half doses without compromising therapeutic activity.

It was postulated that the use of the dual-targeted approach would achieve more significant therapeutic gains than were observed above. This may reflect some of the limitations of using liposomal DDS for the treatment of solid tumors, including focalized and non-uniform drug delivery, which are observed with both liposomal monotherapies and liposomal combination therapies. Alternatively, the lack of significant improvement in therapeutic effect with the dual-targeted approach, relative to multiple cycles of tumor-targeted monotherapy, may be because the anti-cancer actions of some single agent liposomal drugs, including liposomal DXR, may be partially elicited via anti-vascular effects, as demonstrated by Verreault *et al.* (23).

Although tumor regression was not demonstrated with simultaneously administered vasculature-targeted and tumor-targeted therapies, the treatment

achieved effective disease control: throughout the four treatment cycles, no increases in tumor volumes were observed. Importantly, the dual-targeted approach may be useful for prolonged disease management, due to the ability to administer significantly lower doses of drug without compromising the therapeutic effect; however, this would need to be confirmed over substantially prolonged treatment periods.

The studies presented in this thesis were designed as preliminary investigations to determine whether the dual-targeted approach examined by Pastorino *et al.* was applicable to the treatment of HER2-postive breast cancer, and whether expanding upon the approach to exploit the benefits of combination chemotherapy by delivering a second drug would provide additional therapeutic benefit. As such, it is recognized that the dual-targeted approach explored in this thesis has not been optimized, and that a superior therapeutic effect may be able to be achieved with further fine-tuning. In order to complete additional optimization, it would be beneficial to conduct a cellular level investigation of the specific tumor localization and effects of each individual therapy via an assessment of liposome distribution, cell proliferation, apoptosis, necrosis, vascular damage, and vascular permeability, but this was beyond the objectives of the initial proof-of-concept studies completed in Chapter 4.

Finally, as this dual-targeted therapy research builds off of and expands upon work published by Pastorino *et al.* (47), a number of controls were omitted from the therapeutic studies outlined above. These studies were only designed to be a preliminary investigation of the therapeutic potential of the modified

approach; as a result, only the most important treatments were included in the experiments presented in this chapter, in order to keep costs reasonable and ensure that the experiments did not become unmanageable in size. It is recognized that many additional control groups, such as drug-free targeted liposomes, free targeting ligands, untargeted liposomal drugs, and free VCR and free DXR, must be included in future investigations, particularly if the approach is being developed for clinical translation.

5.4. Conclusion

This chapter examined nanomedicine-based combination chemotherapy employing two different targeted liposomal drug formulations, and described proof-of-concept studies exploring the therapeutic potential of a combined tumor-targeted and vasculature-targeted approach to the treatment of HER2-positive breast cancer. Results showed that the choice of the particular vasculature- and tumor-targeting ligands can influence the circulation half-lives and levels of tumor accumulation of the liposomal formulations. In the above experimental model, the order of therapy administration for the dual-targeted combination approach did not impact treatment activity. Also, it was observed that treatment with either the αHER2 Fab′-SIL[DXR] or NGR-SL[VCR] influenced the tumor accumulation of a second dose of liposomes, and that a small window of increased liposome delivery existed at 4 days following pre-treatment, which could be exploited to improve the therapeutic outcome. This chapter demonstrated the proof-of-concept therapeutic results for the dual-targeted

combination chemotherapy strategy, but considerable fine-tuning of the approach will be necessary before it may become ready for translation to the clinic.

5.5. References – Chapter 5

1. Global Cancer Facts & Figures 2007 (Revision 2). Atlanta: American Cancer Society; 2007.

2. Fossati R, Confalonieri C, Torri V, Ghislandi E, Penna A, Pistotti V, Tinazzi A, Liberati A. Cytotoxic and hormonal treatment for metastatic breast cancer: a systematic review of published randomized trials involving 31,510 women. *J. Clin. Oncol.* 1998; 16: 3439-3460.

3. Carrick S, Parker S, Wilcken N, Ghersi D, Marzo M, Simes J. Single agent versus combination chemotherapy for metastatic breast cancer. *Cochrane Database Syst. Rev.* 2005: CD003372.

4. Eichhorn ME, Strieth S, Dellian M. Anti-vascular tumor therapy: recent advances, pitfalls and clinical perspectives. *Drug Resist. Updat.* 2004; 7: 125-138.

5. Folkman J, Merler E, Abernathy C, Williams G. Isolation of a tumor factor responsible for angiogenesis. *J. Exp. Med.* 1971; 133: 275-288.

6. Folkman J. Tumor angiogenesis: therapeutic implications. *N. Engl. J. Med.* 1971; 285: 1182-1186.

7. Folkman J. Anti-angiogenesis: new concept for therapy of solid tumors. *Ann. Surg.* 1972; 175: 409-416.

8. Denekamp J. Endothelial cell proliferation as a novel approach to targeting tumour therapy. *Br. J. Cancer* 1982; 45: 136-139.

9. Denekamp J. The tumour microcirculation as a target in cancer therapy: a clearer perspective. *Eur. J. Clin. Invest.* 1999; 29: 733-736.

10. Thorpe PE. Vascular targeting agents as cancer therapeutics. *Clin. Cancer Res.* 2004; 10: 415-427.

11. Denekamp J. Vascular endothelium as the vulnerable element in tumours. *Acta Radiol. Oncol.* 1984; 23: 217-225.

12. Eichhorn ME, Kleespies A, Angele MK, Jauch KW, Bruns CJ. Angiogenesis in cancer: molecular mechanisms, clinical impact. *Langenbecks Arch. Surg.* 2007; 392: 371-379.

13. Chaplin DJ, Pettit GR, Hill SA. Anti-vascular approaches to solid tumour therapy: evaluation of combretastatin A4 phosphate. *Anticancer Res.* 1999; 19: 189-195.

14. Chaplin DJ, Hill SA. The development of combretastatin A4 phosphate as a vascular targeting agent. *Int. J. Radiat. Oncol. Biol. Phys.* 2002; 54: 1491-1496.

15. Hurwitz H, Fehrenbacher L, Novotny W, Cartwright T, Hainsworth J, Heim W, Berlin J, Baron A, Griffing S, Holmgren E, Ferrara N, Fyfe G, Rogers B, Ross R, Kabbinavar F. Bevacizumab plus irinotecan, fluorouracil, and leucovorin for metastatic colorectal cancer. *N. Engl. J. Med.* 2004; 350: 2335-2342.

16. Grothey A, Ellis LM. Targeting angiogenesis driven by vascular endothelial growth factors using antibody-based therapies. *Cancer J.* 2008; 14: 170-177.

17. Mayer RJ. Two steps forward in the treatment of colorectal cancer. *N. Engl. J. Med.* 2004; 350: 2406-2408.

18. Slamon DJ, Clark GM, Wong SG, Levin WJ, Ullrich A, McGuire WL. Human breast cancer: correlation of relapse and survival with amplification of the HER-2/neu oncogene. *Science* 1987; 235: 177-182.

19. Vogel CL, Cobleigh MA, Tripathy D, Gutheil JC, Harris LN, Fehrenbacher L, Slamon DJ, Murphy M, Novotny WF, Burchmore M, Shak S, Stewart SJ. First-line Herceptin monotherapy in metastatic breast cancer. *Oncology* 2001; 61 Suppl 2: 37-42.

20. Robert N, Leyland-Jones B, Asmar L, Belt R, Ilegbodu D, Loesch D, Raju R, Valentine E, Sayre R, Cobleigh M, Albain K, McCullough C, Fuchs L, Slamon D. Randomized phase III study of trastuzumab, paclitaxel, and carboplatin compared with trastuzumab and paclitaxel in women with HER-2-overexpressing metastatic breast cancer. *J. Clin. Oncol.* 2006; 24: 2786-2792.

21. Slamon DJ, Leyland-Jones B, Shak S, Fuchs H, Paton V, Bajamonde A, Fleming T, Eiermann W, Wolter J, Pegram M, Baselga J, Norton L. Use of chemotherapy plus a monoclonal antibody against HER2 for metastatic breast cancer that overexpresses HER2. *N. Engl. J. Med.* 2001; 344: 783-792.

22. Esteva FJ, Valero V, Booser D, Guerra LT, Murray JL, Pusztai L, Cristofanilli M, Arun B, Esmaeli B, Fritsche HA, Sneige N, Smith TL,

Hortobagyi GN. Phase II study of weekly docetaxel and trastuzumab for patients with HER-2-overexpressing metastatic breast cancer. *J. Clin. Oncol.* 2002; 20: 1800-1808.

23. Verreault M, Strutt D, Masin D, Anantha M, Yung A, Kozlowski P, Waterhouse D, Bally MB, Yapp DT. Vascular normalization in orthotopic glioblastoma following intravenous treatment with lipid-based nanoparticulate formulations of irinotecan (Irinophore C), doxorubicin (Caelyx(R)) or vincristine. *BMC Cancer* 2011; 11: 124-141.

24. Mabeta P, Pepper MS. A comparative study on the anti-angiogenic effects of DNA-damaging and cytoskeletal-disrupting agents. *Angiogenesis* 2009; 12: 81-90.

25. Hayot C, Farinelle S, De Decker R, Decaestecker C, Darro F, Kiss R, Van Damme M. In vitro pharmacological characterizations of the anti-angiogenic and anti-tumor cell migration properties mediated by microtubule-affecting drugs, with special emphasis on the organization of the actin cytoskeleton. *Int. J. Oncol.* 2002; 21: 417-425.

26. Pasquier E, Andre N, Braguer D. Targeting microtubules to inhibit angiogenesis and disrupt tumour vasculature: implications for cancer treatment. *Curr. Cancer Drug Targets* 2007; 7: 566-581.

27. Mayer LD, Bally MB, Loughrey H, Masin D, Cullis PR. Liposomal vincristine preparations which exhibit decreased drug toxicity and increased activity against murine L1210 and P388 tumors. *Cancer Res.* 1990; 50: 575-579.

28. Boman NL, Mayer LD, Cullis PR. Optimization of the retention properties of vincristine in liposomal systems. *Biochim. Biophys. Acta* 1993; 1152: 253-258.

29. Zhu G, Oto E, Vaage J, Quinn Y, Newman M, Engbers C, Uster P. The effect of vincristine-polyanion complexes in STEALTH liposomes on pharmacokinetics, toxicity and anti tumor activity. *Cancer Chemother. Pharmacol.* 1996; 39: 138-142.

30. Sapra P, Moase EH, Ma J, Allen TM. Improved therapeutic responses in a xenograft model of human B-lymphoma (Namalwa) for liposomal vincristine versus liposomal doxorubicin targeted via anti-CD19 IgG2a or Fab' fragments. *Clin. Cancer Res.* 2004; 10: 1100-1111.

31. Allen TM, Newman MS, Woodle MC, Mayhew E, Uster PS. Pharmacokinetics and anti-tumor activity of vincristine encapsulated in sterically stabilized liposomes. *Int. J. Cancer* 1995; 62: 199-204.

32. Pasqualini R, Koivunen E, Kain R, Lahdenranta J, Sakamoto M, Stryhn A, Ashmun RA, Shapiro LH, Arap W, Ruoslahti E. Aminopeptidase N is a receptor for tumor-homing peptides and a target for inhibiting angiogenesis. *Cancer Res.* 2000; 60: 722-727.

33. Ruoslahti E. RGD and other recognition sequences for integrins. *Annu. Rev. Cell Dev. Biol.* 1996; 12: 697-715.

34. Aragnol D, Leserman L. Immune clearance of liposomes inhibited by an anti-Fc receptor antibody in vivo. *Proc. Natl. Acad. Sci. U. S. A.* 1986; 83: 2699-2703.

35. Miller K, Wang M, Gralow J, Dickler M, Cobleigh M, Perez EA, Shenkier T, Cella D, Davidson NE. Paclitaxel plus bevacizumab versus paclitaxel alone for metastatic breast cancer. *N. Engl. J. Med.* 2007; 357: 2666-2676.

36. Rowinsky EK, Eisenhauer EA, Chaudhry V, Arbuck SG, Donehower RC. Clinical toxicities encountered with paclitaxel (Taxol). *Semin. Oncol.* 1993; 20: 1-15.

37. Laginha K, Mumbengegwi D, Allen T. Liposomes targeted via two different antibodies: assay, B-cell binding and cytotoxicity. *Biochim. Biophys. Acta* 2005; 1711: 25-32.

38. Saul JM, Annapragada AV, Bellamkonda RV. A dual-ligand approach for enhancing targeting selectivity of therapeutic nanocarriers. *J. Control. Release* 2006; 114: 277-287.

39. Murase Y, Asai T, Katanasaka Y, Sugiyama T, Shimizu K, Maeda N, Oku N. A novel DDS strategy, "dual-targeting", and its application for antineovascular therapy. *Cancer Lett.* 2010; 287: 165-171.

40. Li D, Tang GP, Li JZ, Kong Y, Huang HL, Min LJ, Zhou J, Shen FP, Wang QQ, Yu H. Dual-targeting non-viral vector based on polyethylenimine improves gene transfer efficiency. *J. Biomater. Sci. Polym. Ed.* 2007; 18: 545-560.

41. Quan CY, Chang C, Wei H, Chen CS, Xu XD, Cheng SX, Zhang XZ, Zhuo RX. Dual targeting of a thermosensitive nanogel conjugated with transferrin and RGD-containing peptide for effective cell uptake and drug release. *Nanotechnology* 2009; 20: 335101-335111.

42. Du J, Lu WL, Ying X, Liu Y, Du P, Tian W, Men Y, Guo J, Zhang Y, Li RJ, Zhou J, Lou JN, Wang JC, Zhang X, Zhang Q. Dual-targeting topotecan liposomes modified with tamoxifen and wheat germ agglutinin significantly improve drug transport across the blood-brain barrier and survival of brain tumor-bearing animals. *Mol. Pharm.* 2009; 6: 905-917.

43. Ying X, Wen H, Lu WL, Du J, Guo J, Tian W, Men Y, Zhang Y, Li RJ, Yang TY, Shang DW, Lou JN, Zhang LR, Zhang Q. Dual-targeting daunorubicin liposomes improve the therapeutic efficacy of brain glioma in animals. *J. Control. Release* 2010; 141: 183-192.

44. Takara K, Hatakeyama H, Ohga N, Hida K, Harashima H. Design of a dual-ligand system using a specific ligand and cell penetrating peptide, resulting in a synergistic effect on selectivity and cellular uptake. *Int. J. Pharm.* 2010; 396: 143-148.

45. Meng S, Su B, Li W, Ding Y, Tang L, Zhou W, Song Y, Li H, Zhou C. Enhanced antitumor effect of novel dual-targeted paclitaxel liposomes. *Nanotechnology* 2010; 21: 415103-415109.

46. Sapra P, Allen TM. Improved outcome when B-cell lymphoma is treated with combinations of immunoliposomal anticancer drugs targeted to both the CD19 and CD20 epitopes. *Clin. Cancer Res.* 2004; 10: 2530-2537.

47. Pastorino F, Brignole C, Di Paolo D, Nico B, Pezzolo A, Marimpietri D, Pagnan G, Piccardi F, Cilli M, Longhi R, Ribatti D, Corti A, Allen TM, Ponzoni M. Targeting liposomal chemotherapy via both tumor cell-specific and tumor vasculature-specific ligands potentiates therapeutic efficacy. *Cancer Res.* 2006; 66: 10073-10082.

48. Abu Lila AS, Doi Y, Nakamura K, Ishida T, Kiwada H. Sequential administration with oxaliplatin-containing PEG-coated cationic liposomes promotes a significant delivery of subsequent dose into murine solid tumor. *J. Control. Release* 2010; 142: 167-173.

49. Zhang YF, Wang JC, Bian DY, Zhang X, Zhang Q. Targeted delivery of RGD-modified liposomes encapsulating both combretastatin A-4 and doxorubicin for tumor therapy: in vitro and in vivo studies. *Eur. J. Pharm. Biopharm.* 2010; 74: 467-473.

50. Pastorino F, Brignole C, Marimpietri D, Cilli M, Gambini C, Ribatti D, Longhi R, Allen TM, Corti A, Ponzoni M. Vascular damage and anti-angiogenic effects of tumor vessel-targeted liposomal chemotherapy. *Cancer Res.* 2003; 63: 7400-7409.

51. Koning GA, Kamps JA, Scherphof GL. Interference of macrophages with immunotargeting of liposomes. *J. Liposome Res.* 2002; 12: 107-119.

52. Allen TM, Sapra P, Moase E, Moreira JN, Iden DL. Adventures in targeting. *J. Liposome Res.* 2002; 121: 5-12.

53. Derksen JTP, Morselt HWM, Scherphof GL. Uptake and processing of immunoglobulin-coated liposomes by subpopulations of rat liver macrophages. *Biochim. Biophys. Acta* 1988; 917: 127-136.

54. Koning GA, Morselt HW, Gorter A, Allen TM, Zalipsky S, Scherphof GL, Kamps JA. Interaction of differently designed immunoliposomes with colon cancer cells and Kupffer cells. An in vitro comparison. *Pharm. Res.* 2003; 20: 1249-1257.

55. Koning G, G.A., Morselt HWM, Gorter A, Allen TM, Zalipsky S, Kamps JAAM, Scherphof GL. Pharmacokinetics of differently designed immunoliposome formulations in rats with or without hepatic colon cancer metastases. *Phamaceut. Res.* 2001; 18: 1291-1298.

56. Harding JA, Engbers CM, Newman MS, Goldstein NI, Zalipsky S. Immunogenicity and pharmacokinetic attributes of poly(ethyleneglycol)-grafted immunoliposomes. *Biochim. Biophys. Acta* 1997; 1327: 181-192.

57. Charrois GJR, Allen TM. Rate of biodistribution of STEALTH® liposomes to tumor and skin: influence of liposome diameter and implications for toxicity and therapeutic activity. *Biochim. Biophys. Acta* 2003; 1609: 102-108.

58. Gabizon A, Goren D, Horowitz AT, Tzemach D, Lossos A, Siegal T. Long-circulating liposomes for drug delivery in cancer therapy: a review of biodistribution studies in tumor-bearing animals. *Adv. Drug Del. Rev.* 1997; 24: 337-344.

59. Papahadjopoulos D, Allen TM, Gabizon A, Mayhew E, Matthay K, Huang SK, Lee KD, Woodle MC, Lasic DD, Redemann C, Martin FJ. Sterically stabilized liposomes: improvements in pharmacokinetics and antitumor therapeutic efficacy. *Proc. Natl. Acad. Sci. U.S.A.* 1991; 88: 11460-11464.

60. Gabizon A, Catane R, Uziely B, Kaufman B, Safra T, Cohen R, Martin F, Huang A, Barenholz Y. Prolonged circulation time and enhanced accumulation in malignant exudates of doxorubicin encapsulated in polyethylene-glycol coated liposomes. *Cancer Res.* 1994; 54: 987-992.

61. Maruyama K, Takahashi N, Tagawa T, Nagaike K, Iwatsuru M. Immunoliposomes bearing polyethyleneglycol-coupled Fab' fragment show prolonged circulation time and high extravasation into targeted solid tumors *in vivo*. *FEBS Lett.* 1997; 413: 177-180.

62. Goding JW. Monoclonal Antibodies: Principles and Practice (3rd Edition). 3rd ed. San Diego, California: Academic Press Inc.; 1996.

63. Brignole C, Marimpietri D, Gambini C, Allen TM, Ponzoni M, Pastorino F. Development of Fab' fragments of anti-GD(2) immunoliposomes entrapping doxorubicin for experimental therapy of human neuroblastoma. *Cancer Lett.* 2003; 197: 199-204.

64. Park JW, Hong K, Carter P, Asgari H, Guo LY, Keller GA, Wirth C, Shalaby R, Kotts C, Wood WI, Papahadjopoulos D, Benz CC. Development of anti-p185^{HER2} immunoliposomes for cancer therapy. *Proc. Natl. Acad. Sci. U.S.A.* 1995; 92: 1327-1331.

65. Cheng WW, Allen TM. Targeted delivery of anti-CD19 liposomal doxorubicin in B-cell lymphoma: a comparison of whole monoclonal antibody, Fab' fragments and single chain Fv. *J. Control. Release* 2008; 126: 50-58.

66. Schiffelers RM, Fens MH, Janssen AP, Molema G, Storm G. Liposomal targeting of angiogenic vasculature. *Curr. Drug Deliv.* 2005; 2: 363-368.

67. Xiong XB, Huang Y, Lu WL, Zhang X, Zhang H, Nagai T, Zhang Q. Enhanced intracellular delivery and improved antitumor efficacy of doxorubicin by sterically stabilized liposomes modified with a synthetic RGD mimetic. *J. Control. Release* 2005; 107: 262-275.

68. Schraa AJ, Kok RJ, Moorlag HE, Bos EJ, Proost JH, Meijer DK, de Leij LF, Molema G. Targeting of RGD-modified proteins to tumor vasculature: a pharmacokinetic and cellular distribution study. *Int. J. Cancer* 2002; 102: 469-475.

69. Arap W, Pasqualini R, Ruoslahti E. Cancer treatment by targeted drug delivery to tumor vasculature in a mouse model. *Science* 1998; 279: 377-380.

70. Hart SL, Knight AM, Harbottle RP, Mistry A, Hunger HD, Cutler DF, Williamson R, Coutelle C. Cell binding and internalization by filamentous phage displaying a cyclic Arg-Gly-Asp-containing peptide. *J. Biol. Chem.* 1994; 269: 12468-12474.

71. Eikesdal HP, Landuyt W, Dahl O. The influence of combretastatin A-4 and vinblastine on interstitial fluid pressure in BT4An rat gliomas. *Cancer Lett.* 2002; 178: 209-217.

72. Skliarenko JV, Lunt SJ, Gordon ML, Vitkin A, Milosevic M, Hill RP. Effects of the vascular disrupting agent ZD6126 on interstitial fluid pressure and cell survival in tumors. *Cancer Res.* 2006; 66: 2074-2080.

73. Strieth S, Eichhorn ME, Werner A, Sauer B, Teifel M, Michaelis U, Berghaus A, Dellian M. Paclitaxel encapsulated in cationic liposomes increases tumor microvessel leakiness and improves therapeutic efficacy in combination with Cisplatin. *Clin. Cancer Res.* 2008; 14: 4603-4611.

74. Sengupta S, Eavarone D, Capila I, Zhao G, Watson N, Kiziltepe T, Sasisekharan R. Temporal targeting of tumour cells and neovasculature with a nanoscale delivery system. *Nature* 2005; 436: 568-572.

75. Ley CD, Horsman MR, Kristjansen PE. Early effects of combretastatin-A4 disodium phosphate on tumor perfusion and interstitial fluid pressure. *Neoplasia* 2007; 9: 108-112.

76. Ma J, Pulfer S, Li S, Chu J, Reed K, Gallo JM. Pharmacodynamic-mediated reduction of temozolomide tumor concentrations by the angiogenesis inhibitor TNP-470. *Cancer Res.* 2001; 61: 5491-5498.

77. Tong RT, Boucher Y, Kozin SV, Winkler F, Hicklin DJ, Jain RK. Vascular normalization by vascular endothelial growth factor receptor 2 blockade induces a pressure gradient across the vasculature and improves drug penetration in tumors. *Cancer Res.* 2004; 64: 3731-3736.

78. Netti PA, Hamberg LM, Babich JW, Kierstead D, Graham W, Hunter GJ, Wolf GL, Fischman A, Boucher Y, Jain RK. Enhancement of fluid filtration across tumor vessels: implication for delivery of macromolecules. *Proc. Natl. Acad. Sci. U. S. A.* 1999; 96: 3137-3142.

79. Reilly RM, Sandhu J, Alvarez-Diez TM, Gallinger S, Kirsh J, Stern H. Problems of delivery of monoclonal antibodies. Pharmaceutical and pharmacokinetic solutions. *Clin. Pharmacokinet.* 1995; 28: 126-142.

80. Jain RK. Normalization of tumor vasculature: an emerging concept in antiangiogenic therapy. *Science* 2005; 307: 58-62.

81. Bocci G, Nicolaou KC, Kerbel RS. Protracted low-dose effects on human endothelial cell proliferation and survival in vitro reveal a selective

antiangiogenic window for various chemotherapeutic drugs. *Cancer Res.* 2002; 62: 6938-6943.

82. Hlatky L, Hahnfeldt P, Folkman J. Clinical application of antiangiogenic therapy: microvessel density, what it does and doesn't tell us. *J. Natl. Cancer Inst.* 2002; 94: 883-893.

CHAPTER 6

Discussion

6. Discussion

6.1. Cancer and Drug Delivery Systems

Cancer is a major worldwide health problem, and is expected to cause over 11 million deaths by the year 2030 (1), highlighting the significant need to improve current cancer treatment protocols. Cancer chemotherapy has traditionally consisted of the administration of small molecule anti-cancer agents that mediate cytotoxicity against rapidly proliferating cells. Unfortunately, the effectiveness of many of these drugs is limited by their non-specific distribution throughout the body, which often manifests as severe toxicities against normal tissues and limited drug concentrations in the target tissue. It is well known that one of the major goals for improving cancer chemotherapy is to increase treatment selectivity in order to reduce adverse side effects and enhance therapeutic effect. As a greater understanding of cancer processes is achieved, there will be new opportunities to develop highly selective, effective, and safe chemotherapeutic agents. However, until these opportunities have been realized, small molecule anti-cancer drugs will likely remain a mainstay for many cancer treatment protocols.

In recent years, the application of nanotechnology to medicine (i.e., nanomedicine) has been intensely explored across the world. The limitations of conventional chemotherapeutic agents have been acknowledged, and a wide variety of nanometre-sized drug delivery platforms have been developed and successfully utilized to ameliorate some of the undesirable properties associated with some small molecule anti-cancer agents. To this end, the unique capabilities

of niosomes, dendrimers, nanotubes/nanorods, quantum dots, metallic nanoparticles, liposomes, solid lipidic particles, colloids, polymers, and numerous other nanotechnology platforms are being investigated by multidisciplinary teams for cancer therapy and imaging (2, 3).

Liposomes are the archetypal drug delivery system, first suggested as drug carriers nearly 40 years ago (4, 5), and were the first nanomedicine utilized to deliver anti-cancer drugs (6). Additional target cell selectivity and increased drug delivery (in certain circumstances) can be achieved using actively targeted liposomes (as reviewed in 7). The therapeutic effectiveness of liposomal anti-cancer agents has been established both *in vitro* and *in vivo*. A host of nanomedicines are currently in various stages of pre-clinical and clinical development (3), and there are now more than 20 drug delivery system-based therapies that have received FDA approval, with approximately half of these constructs being liposomal drugs (for review please see 2). As a result of the recent surge in research into the application of nanotechnology to medicine, the FDA Nanotechnology Task Force was created in 2006 to determine the critical scientific and regulatory concerns for nanomedicines (8).

6.2. Combination Chemotherapy and Drug Delivery Systems

As new liposomal anti-cancer agents receive FDA approval, particularly as replacements for free formulations of the drug, they are poised to be become substantially more prevalent in cancer treatment. Based on the longstanding clinical precedent and success of combination chemotherapy over monotherapies,

it is likely that liposomal anti-cancer drugs will be administered in combination with other free and/or liposomal drugs and/or molecularly targeted therapies. Therefore, it is advantageous to explore plausible treatment combinations in pre-clinical studies to gain a greater understanding of any adverse toxicities associated with the combinations, as well as their therapeutic potential and the effects of different temporal dosing sequences on disease control. The knowledge and information gained from these studies could be used to rationally design clinical trials to provide the greatest likelihood of a successful outcome.

Although the development of molecularly targeted therapies is not a new concept (9-11), at the present time, it is one of the most intensely investigated fields in cancer research (12, 13). With the desire to progress towards providing "personalized" cancer therapy, there is a substantial research focus on molecularly targeted therapies, as they are designed to provide a greater degree of target selectivity over traditional anti-cancer drugs. Disappointing clinical results with some molecularly targeted agents (14-16) have led to a greater understanding of the critical importance of careful selection of patient subpopulations for treatment (17, and references therein, 18), as discussed in further detail below. It has been well-established that the manipulation, blockade, or interruption of dysregulated pathways that contribute to cancer pathophysiology and progression can lead to increases in cellular drug sensitivity, and it is likely that molecularly targeted therapies will enter the clinic as part of combination chemotherapy regimens. Furthermore, the administration of molecularly targeted therapies in combination

treatment regimens will help to prevent or slow the resistance that can develop when inactivating an essential protein (19).

Selectively targeted therapies are being explored increasingly in nanomedicine research, as well. As the use of ligand-modified nanomedicines provides unique opportunities for selectivity, a variety of targeted constructs are being investigated, although there has been limited exploration of targeted nanomedicines in the context of combination chemotherapy. At present, the translation of targeted nanomedicines, particularly combinations of targeted nanomedicines, to the clinic has not proceeded rapidly. However, going forward, the future of nanomedicines, including lipid-based technologies, holds many exciting opportunities for the eventual realization of multifunctional applications using combinations of liposomal imaging agents, targeting agents, and therapeutics.

Stemming from the recent advancements in proteomics/genomics and nanotechnology, the future of nanomedicines lies in the development of multifunctional detection, diagnosis, individualized and targeted treatment, and monitoring platforms. Wang *et al.* raised the possibility of "quaternary nanoparticles with four functions...[having] the abilities of tumor-targeting, dual-drug therapy and imaging" (20). The versatility of the liposome platform means that liposomes are exquisitely situated to realize the goal of customizable, multifunctional, personalized cancer management. However, a host of other considerations arise as nanomedicines become more sophisticated and complex,

through the combination of multiple drugs or therapeutic payloads, multiple targeting moieties, and/or multiple functions.

6.2.1. Utilization of Liposomes in Combination Cancer Chemotherapy

This thesis explored the utilization of liposomes in combination cancer chemotherapy. The aim of the research described in this thesis was to determine the therapeutic potential of liposomal chemotherapy in combination with a second conventional drug, or liposomal drug, for cancer treatment. Two different strategies were investigated: the combination of a liposomal irinotecan and free 5-FU for colorectal cancer treatment, and the combination of actively targeted liposomal DXR and liposomal VCR for HER2-over-expressing breast cancer treatment.

Both of the strategies investigated in this thesis examined combination chemotherapy in the context of nanomedicines. However, it must be recognized that the two approaches are at very different stages of development, and may not be equally well-suited for translation to the clinic, at the present time. The Irinophore C™ research outlined in this thesis may be applicable to the design of clinical trials in the near future. In contrast, the research in Chapters 4 and 5 investigating a dual-targeted approach to HER2-positive breast cancer treatment should be considered, at present, to be more of an academic exploration, intended to contribute knowledge to the field regarding the role of actively targeted liposomal drugs in combination chemotherapy, and the therapeutic potential of

selectively targeting two different cell populations within a tumor using nanomedicines.

6.2.1.1. Irinophore C™ Plus 5-FU

The research presented in Chapter 3 investigated the therapeutic potential of the combination of Irinophore C™ plus 5-FU, relative to free irinotecan plus 5-FU, in the treatment of CRC. It was hypothesized that the cytotoxicity of co-administered irinotecan and 5-FU would be enhanced by increasing the duration of CPT-11 exposure through the use of a novel liposomal formulation of irinotecan (Irinophore C™) in the treatment of CRC. *In vitro* and *in vivo* experiments were completed with the aim of characterizing the therapeutic interaction between Irinophore C™ and 5-FU to help guide the rational design of clinical trials for Irinophore C™. Exposure time- and ratio-dependent cytotoxicity were demonstrated *in vitro* for 5-FU and CPT-11 as single agents and in combination. The substantial therapeutic potential and excellent safety profile of Irinophore C™ was shown *in vivo* in two different xenograft models of CRC. Data revealed that treatment with single agent Irinophore C™ was vastly superior to treatment with free irinotecan, as well as free irinotecan plus 5-FU, and was equally as effective as the combination of Irinophore C™ and 5-FU, with less overall toxicity. This was the first investigation into the therapeutic effect of a liposomal formulation of irinotecan in combination with free 5-FU for the treatment of CRC. The results suggest that Irinophore C™ may be able to replace free irinotecan in combination with free 5-FU and leucovorin as an effective and

less toxic treatment option for CRC. The safety and effectiveness of Irinophore C™ will be investigated in clinical trials in the near future.

6.2.1.2. Dual-targeting with Liposomal VCR and Liposomal DXR

The experiments discussed in Chapter 4 characterized the cellular association and cytotoxicity properties of liposomes actively targeted via vasculature- or tumor cell-specific ligands in a controlled *in vitro* environment. The cellular association of actively targeted liposomes was shown to be selective for the target receptor, and to lead to receptor internalization and recycling following binding of the NGR-SL and cRGD-SL at 37°C. A greater understanding of the *in vitro* properties of the formulations was achieved by assessing the effect of time, peptide density, and diluent composition on liposomal cellular association. Finally, the drug-loaded formulation of the αHER2-SIL was more cytotoxic than the SL, but less cytotoxic than the free drug. The *in vitro* cellular association and cytotoxicity properties of the liposome formulations were deemed suitable to begin an *in vivo* exploration of a combined, dual-targeted approach to breast cancer treatment.

Chapter 5 outlined *in vivo* experiments exploring a dual-targeted combination approach to HER2-over-expressing breast cancer treatment using actively targeted liposomal drug formulations. It was hypothesized that combinatorial administration of two different liposomal anti-cancer drugs selectively targeted to two distinct cell populations within the tumor would produce a greater therapeutic effect than when administered as monotherapies. Based on PK/BD data, NGR peptides and αHER2 Fab′ fragments were selected as

the vasculature- and tumor-targeting ligands, respectively. Therapeutic experiments with the NGR-SL[VCR] and αHER2 Fab′-SIL[DXR] demonstrated that combined vasculature-targeted and tumor-targeted therapy, administered in any order, was superior to monotherapy in an orthotopic HER2-positive breast cancer model. It was determined that exploiting the window of increased tumor accumulation of a second dose of liposomes permitted the dose of the simultaneously administered dual-targeted therapy to be halved without compromising therapeutic effect, relative to tumor-targeted monotheapy. The proof-of-concept experiments described in Chapter 5 revealed, for the first time, the promising therapeutic potential of employing two different liposomal cytotoxic drugs, selectively targeted to two distinct tumor cell populations, for the treatment of HER2-positive breast cancer. However, it is necessary to recognize that there are a number of issues that must be addressed before it would be possible to consider attempting to translate this approach to a clinical setting.

6.3. Challenges and Improvements for DDS Delivery

6.3.1. General Challenges

The abnormal structure and function of tumor vasculature is the basis for the passive, yet selective, accumulation of liposomes and other macromolecular DDS within solid tumors. However, the abnormal and heterogeneous nature of tumor vascular networks also poses a number of challenges to the efficient delivery of liposomal therapies, both alone and when used in combination. One of the major challenges limiting the therapeutic success of liposomal anti-cancer drugs in the

treatment of solid tumors is focalized, non-uniform drug delivery, which may lead to some tumor cells being exposed to sub-therapeutic drug concentrations. A discussion of some of the general obstacles facing nanomedicine delivery is important so that the limitations of the therapies investigated in this thesis can be understood in a wider context.

The distribution of angiogenic vasculature within solid tumors is not uniform, and changes with growth and treatment (21, 22); this results in heterogeneous blood flow patterns and variable delivery of liposomes throughout the tumors. The disorganized, abnormally functioning tumor vasculature leaves large areas of the tumors without adequate perfusion (22). An insufficient vascular blood supply reduces total therapy delivery to these areas and also leads to the development of hypoxia. Hypoxia has been correlated with chemoresistance (23, and references therein), further compromising the cytotoxic actions of the low concentrations of drug that may diffuse into the poorly perfused areas.

Continual changes in the structure and function of angiogenic vasculature that occur with tumor growth and in response to therapies can increase the variability in liposome delivery within each tumor, between cycles of treatment, and between patients. Importantly, even within well-vascularized regions of the tumors, liposome delivery may not be uniform. This is because blood flow patterns are often inconsistent due to the disorganized, tortuous nature of angiogenic tumor vasculature (24), and the degree of vessel (hyper)permeability is not constant (25, 26) and can be altered by therapy (21, 27), including liposomal

anti-cancer drugs (28). Finally, the permeability of tumor blood vessels decreases with increasing particle size; the microvascular permeability of 100 nm liposomes is only 16% of the permeability of bovine serum albumin (25).

As a result of impaired lymphatic drainage, coupled with the excessive permeability of tumor vasculature, the interstitial fluid pressure within solid tumors is elevated, which can limit liposome extravasation into the tumor interstitium (29-31). Following extravasation, liposomes remain in perivascular clusters, ~30 μm from blood vessels (25). Subsequent liposome penetration into tumors is minimal because of intratumoral pressure gradients (32, 33), and the dense collagen-containing extracellular matrix of some tumors, which greatly interferes with the diffusion of macromolecules (34-36) larger than ~60 nm (37). As a result of these challenges, tumor distribution and penetration of liposomes is quite variable, and may limit the therapeutic effectiveness of liposomal anti-cancer agents in the treatment of solid tumors.

Initially, liposome distribution is highly focalized, concentrated near leaky vasculature. When this limited distribution is exacerbated by the lack of subsequent liposome diffusion through the interstitium, large numbers of tumor cells may not accessible to the liposomes (22, 25). The drug molecules that are released from the liposomes are able to diffuse through the interstitium more easily because of their small size, and may mediate cytotoxicity against cells which are located in the vicinity of the released drug as a result of a 'bystander effect' (38); however, the resultant tumor drug distribution is often still not uniform, with many cells being exposed to sub-therapeutic concentrations of drug

(22). These issues contribute to the development of therapeutic resistance and tumor re-growth following treatment cessation.

6.3.2. Strategies to Increase Liposome Delivery to Solid Tumors

There is a significant need and opportunity to improve the delivery of liposomes to solid tumors, as the literature reveals that, typically, only between 5 and 10% of the injected dose reaches the tumor. Gaining a more complete understanding of the barriers to successful liposome delivery, and investigating how these barriers change with treatment and tumor growth, will be important as the field progresses forward. Exploring new approaches to overcome the challenges of delivering liposomes to solid tumors may allow for more uniform distribution and greater drug penetration into tumors, and correlated improvements in therapeutic activity.

Interesting strategies have been investigated to augment the EPR effect and increase liposome delivery to tumors, achieve higher drug concentrations in tumors, and improve liposome penetration through the extracellular matrix. Previous research that has investigated different ways to enhance liposome penetration and accumulation, including by increasing tumor blood flow and pressure, is highlighted below. The strategy of increasing tumor blood flow could be utilized in concert with the liposomal combination chemotherapy approaches investigated in this thesis, which themselves may be able to circumvent the problem of non-uniform drug delivery by their ability to increase liposome penetration and accumulation.

Techniques for augmenting the EPR effect, including increasing blood pressure/flow, have been investigated in an attempt to improve liposome delivery to solid tumors. Although increasing blood pressure may not be a suitable approach for all patients, and should be employed with the utmost caution, researchers have shown that raising blood pressure, via the use of angiotensin-II, increased the tumor delivery of macromolecules in rats (39) and several different types of human cancers (40). In humans, the moderate 20-25% increase in systemic blood pressure was brief, and was only maintained for the time period required to infuse the macromolecular treatment (~20 minutes), and blood pressure returned to normal within 5 minutes of cessation of the angiotensin-II infusion (40). Nagamitsu *et al.* suggest that angiotensin-II treatment only elevates the blood flow volume in tumors, not the blood flow volume in normal tissues, in which the accelerated blood flow is countered by a reduction in vascular diameter to maintain blood flow volume homeostasis (40, and references therein). Similarly, macromolecular delivery to tumors and therapeutic effect were also increased by topical application of nitroglycerin (41), which, in hypoxic tumor tissue, can be indirectly converted to nitric oxide (a potent vasodilator) (42). As suggested by Dr. Hiroshi Maeda, augmenting the EPR effect may be particularly helpful for macromolecular delivery to poorly vascularised tumor and smaller lesions after they have acquired vasculature (43).

The combination of hyperthermia and thermo-sensitive liposomes has the potential to increase drug delivery both by augmenting the EPR effect and via triggered release. Hyperthermia is known to increase blood flow and liposome

extravasation (44), and can trigger drug release from thermo-sensitive liposomes, leading to higher tumor drug concentrations (45, 46). As discussed in Chapter 1, other site-specific activation strategies have also been investigated to increase drug concentrations in tumors (47, and references therein).

Tumor blood flow can also be increased via the use of anti-angiogenic therapy, which has been shown to selectively prune away the most immature tumor blood vessels, leaving behind a more mature, more functional, or "normalized", tumor vasculature (48), but there have been questions about whether or not the EPR effect will still be functional in "normalized" vasculature. Vascular normalization was first discussed by Dr. Rakesh Jain, based on research showing improved tumor vessel function, more regular blood flow patterns, and increased tumor cell perfusion following reductions in IFP and microvessel density after treatment (48). His work has led to the concept of a 'normalization window' that has been successfully exploited to increase the delivery of small molecule therapeutic agents (49), although further in-depth investigation is required to fully understand how nanomedicine delivery is affected.

Some alterations in tumor vasculature may be able to augment the EPR effect, although, at the present time, there is insufficient evidence to draw concrete conclusions regarding how liposome delivery and overall therapeutic effect are affected by vascular normalization. More specifically, normal vasculature is not permeable to particles, only to small molecules, and it will be important to determine how the reduction in liposome delivery to the tumor that could result from the selective pruning of the most penetrable tumor vasculature is

countered by the improved liposome delivery that may result from increased tumor perfusion and reduced interstitial pressure during vascular normalization. This is a complex issue, which is further complicated by the temporal nature of therapy-induced vascular alterations and by the continually changing angiogenic network.

There are several different ways in which the alteration of the tumor vasculature can increase the penetration of extravasated liposomes, which is another approach that may lead to more uniform drug delivery and greater therapeutic success. Liposome penetration may be increased by reductions in tumor cell density following vascular destruction and by vascular normalization, but, as shown in Chapter 5, this increase may be very transient. Discussion of these strategies is relevant to the broader context of the use of liposomes in combination chemotherapy, as it is being recognized that many liposomal anti-cancer therapies can cause alterations in tumor vasculature (28), and these changes will impact the delivery of subsequently administered liposomes and small molecules.

Following repeated injections of a coated-cationic liposomal formulation of oxaliplatin, Abu Lila *et al.* reported that destruction of the tumor vasculature can cause a decrease in tumor cell density and thereby enable greater tumor penetration and accumulation of a third dose of liposomes (50). It is likely that similar effects are observed following treatment with the dual-targeted combination therapy examined in Chapter 5 of this thesis. However, vascular destruction may create a more hypoxic tumor microenvironment, which could

reduce the therapeutic effect of subsequently administered treatments. The research by Abu Lila *et al.* is of particular relevance to this thesis, as it highlights the importance of the interconnection between the tumor vasculature and the tumor cells, and how it can change with treatment, affecting liposome delivery and penetration as well as anti-cancer effects (50). Although not specific to tumor vasculature, degradation of the dense extracellular matrix with collagenase has been demonstrated to improve diffusion and penetration of antibodies through stroma in animal models (36), and it is possible that similar effects may be observed if the strategy is used in concert with liposomal therapies; however, this is not practical for use in humans.

In recent years, researchers have recognized the importance of understanding the vascular effects that are caused by a variety of therapies, particularly with respect to the impact that vascular changes may have on the overall therapeutic effect. Interestingly, many scientists are beginning to approach the challenge of non-uniform drug distribution in solid tumors by circumventing or minimizing the requirement for liposome extravasation, and are instead focusing on achieving tumor cell kill through cytotoxic actions against tumor vasculature, as either a primary (see Chapters 4 and 5) or secondary (see Chapter 3) mechanism of action for liposomal anti-cancer agents. Anti-vascular effects have been demonstrated following treatment with untargeted liposomal anti-cancer agents, including Irinophore C™ (28, 51), liposomal VCR (28), and PEGylated liposomal DXR (28). Verreault *et al.* postulated that selective cytotoxicity against proliferating endothelial cells may be responsible for the

vascular changes and "normalization" caused by the three liposomal anti-cancer drug formulations (28). However, as discussed above, it will be critical to determine how these "normalizing" effects impact the delivery of subsequently administered liposomal or macromolecular therapies. The research outlined in this thesis may contribute to the body of knowledge on this topic.

Many liposomal formulations may exert effects on tumor blood vessels, via their ability to mimic metronomic dosing systems, to deliver drug molecules selectively to tumor vasculature, and/or to exhibit selective cytotoxicity against proliferating endothelial cells following release of the encapsulated drug. Hence, it is important to determine how changes in the angiogenic vasculature may affect subsequent cycles of therapy. A study presented in Chapter 5 of this thesis provided some initial data that address how treatment with liposomal drug targeted via tumor vasculature-specific ligands affects the tumor accumulation of a second dose of liposomes. It is important to consider the positive and negative impact that different temporal sequences can have on therapeutic effect when designing clinical trials. Consequently, careful pre-clinical investigation of different temporal sequences may be warranted, and may be of particular benefit when administering drug combinations, liposomal drugs, and/or vasculature-targeted therapies.

Some of the disadvantages of liposomal therapy, such as reduced effect against cells in the hypoxic core of the tumor, limited effectiveness against drug resistant cells, and limited activity against cells not expressing/over-expressing the target receptor, may be overcome by use in combination with a therapy that

causes widespread, indirect cytotoxicity against tumor cells as a result of focused, direct cytotoxicity against tumor vascular endothelial cells and destruction of the vascular supply network (52, 53). The dual-targeted approach may, counter-intuitively, be well-suited (compared to other liposome-based strategies) to the treatment of poorly vascularised tumors. If untargeted or tumor-targeted liposomes are administered to patients with poorly vascularized tumors, liposome accumulation in the tumors, and likewise therapeutic outcome, will be compromised. However, the combination of tumor-targeted liposomes with a liposomal or free drug treatment that can indirectly mediate cytotoxicity against a large number of tumor cells, such as vasculature-targeted therapy, may improve overall therapeutic effect.

6.3.3. Challenges with Targeted Liposomes

Despite the theoretical advantages of targeted formulations over untargeted formulations, in practice, there is no easy answer as to whether targeted formulations will be superior to untargeted liposomes in a clinical setting. Receptor expression on both tumor cells and tumor vasculature cells is known to be heterogeneous. This would reduce the number of target cells with which the targeted liposomes could achieve specific binding, which would, in turn, reduce the amount of drug uptake when targeting internalizing antigens. In the future, as new targeted liposomal therapies enter into clinical trials, it will be important to determine whether a sufficient population of the target cells express, or over-express, the target receptor in order to predict whether targeted therapeutics would

have an advantage over untargeted therapeutics. Chapter 5 discussed some of the nanomedicine-based "dual-targeting" strategies, such as targeting multiple receptors on the same cell population, which have previously been investigated to increase specificity and targeting affinity, but may also be applicable to circumventing the drawbacks of heterogeneous target expression.

Although some optimized targeted liposomal formulations have demonstrated significant advantages over untargeted formulations in applicable animal models (54, 55), the clinical activity of targeted formulations remains to be elucidated. With targeted formulations, it will be critical to define the sub-populations of patients who are most likely to respond and, perhaps more importantly, most likely not to show any benefit if treated with a targeted formulation.

The importance of clearly understanding and identifying suitable patient sub-populations has been shown in relation to trastuzumab therapy. Initial retrospective analysis of trastuzumab clinical trials revealed that the level of HER2 protein over-expression (e.g., high (3+) versus moderate to weak (2+) or lower (+1 or 0) immunohistochemistry (IHC) rating) was sufficient to differentiate between those likely to respond and those unlikely to respond to treatment (56). However, as discussed by Perez and Baweja, for 2+ patients, it has now become clear that there is a better correlation between outcome and HER2 gene amplification than IHC status (57). Furthermore, interestingly, it has also been demonstrated that patients with the highest levels of HER2 over-expression (~13% of the HER2-positive population) do not benefit from the

addition of trastuzumab to chemotherapy regimens (58). In contrast to trastuzumab, the benefit of most targeted liposomal drug formulations is not derived from an actual inhibition of the protein or the subsequent downstream effects on signalling pathways; thus, it is expected that gene amplification status will be less important in predicting response to targeted liposomal therapy than will the degree of antigen expression, which has been demonstrated in animal models (54). Thus, as personalized cancer medicine evolves, it is important that clinicians and researchers have a clear understanding of which criteria to utilize to differentiate between those patients likely to receive benefit and no benefit from particular treatments.

The choice of targeted versus untargeted liposomes will, in the end, need to be based on the individual applications and the specific characteristics of the tumor. For instance, multidrug resistant (MDR) tumor models contain drug resistance transporters, such as P-glycoprotein, multidrug resistance-related protein, etc., in the plasma membrane that can pump drugs back out of the cell. MDR cells have been shown to be more susceptible to targeted liposomes, which deliver high concentrations of drug intracellularly and thereby avoid the pumps, than to untargeted liposomes, which release drug into the tumor interstitium where it passively diffuses into, or is transported into, cells through the plasma membrane where the MDR pumps are located (59).

Despite the utility of orthotopic tumor xenograft models as predictors of PK properties and toxicity, these models can be unsatisfactory predictors of human therapeutic response. Valuable information will be acquired as a greater diversity

and number of "animal-optimized" nanomedicines begin to enter clinical trials; it may be possible to use the empirical evidence to develop improved animal models and draw conclusions as to which types of tumors are most responsive to which types of therapies in human. The clinical trials completed over the next decade will have significant implications for the future development of liposomal anti-cancer drug formulations.

6.3.3.1. Challenges in the Clinical Translation of Nanomedicines

At the present time, there is a substantial focus on personalized medicine and the development of targeted therapies for cancer treatment. It is likely that there will be an important role for targeted nanomedicines in achieving this aim as the field progresses. To this end, the dual-targeted approach that was investigated above is easily adaptable and potentially applicable to the treatment of a wide range of solid tumors. However, the ease of adaptation is partially overshadowed by the fact that each new formulation or drug combination would still require extensive testing to receive FDA approval. Despite the future promise and potential of targeted nanomedicines, it must be recognized that translation of the technology to the clinic and to the market is a long term goal, and that receiving FDA approval will become more difficult to realize with each "layer" of complexity that is incorporated into the therapies.

Importantly, with added complexity comes added cost, both in terms of testing and manufacturing. From the onset of the design and discovery process, it will be important to evaluate the cost-to-benefit ratio, in order to ensure that the product provides a therapeutic gain that is sufficient to justify the cost of the

treatment. Although this issue delves into ethical considerations, the monetary realities of the pharmaceutical and biotechnology industry must also be understood.

Each layer of complexity adds to the total cost of the individual components and clinical quality starting materials (costs will increase exponentially when gene therapy/RNAi are delivered), cost of optimizing each component and optimizing the complex scale-up procedures, cost of the production techniques, cost of (potential) reductions in stability and shelf-life, cost of completing intensive toxicology studies for any component that has not already received regulatory approval, cost of examining the long-term toxicity of novel nanomedicines, cost and time of the experiments required to receive regulatory approval (especially if the formulation is considered a drug, medical device, and a biological agent), potential loss of profit if patents cannot be awarded, cost of therapy for the patient, and the cost of the instrumentation required to benefit from the multifunctional nature of the platform (e.g., molecular resonance imaging of patients, etc.).

The use of even the simplest drug carriers can lead to increases in the cost of treatment over free drug. Adding a ligand, such as an expensive monoclonal antibody (60) to liposomal drugs can increase their cost further and may reduce the shelf-life of the liposomal formulations. The benefits clearly outweigh the costs when costly therapeutics lead to significant improvements in treatment outcomes and/or prolonged survival. The difficulty arises when costly therapies only provide a few weeks of survival benefit, on average. This is a complicated

situation, with many moral and ethical considerations, thus, it is important to keep the cost of complexity in mind when designing new therapies.

There are currently no targeted nanomedicines that have received FDA approval, and as such, it will likely be many years before combinations of targeted nanomedicines will be approved for treatment. In addition to the time and expense involved in developing and manufacturing nanomedicines, there are a number of factors that may make it difficult for the dual-targeted approach discussed in this thesis to reach the market in the near future.

As with many treatments that act on the vasculature, traditional measures of therapeutic effect, such as tumor volume, may not be optimal for assessing patient responses to treatment, as tumor volume is not well correlated with anti-vasculature effects. It will likely be necessary to identify biomarkers that correlate with disease status and/or patient response, that preferably can be detected in plasma, to enable cost-effective, non-invasive methods for monitoring changes in tumor vasculature. To date, this has proven to be difficult in practice (61, 62), but complex imaging techniques, such as dynamic contrast-enhanced molecular resonance imaging, could be employed to monitor and exploit changes in tumor vasculature that may lead to increased accumulation of subsequently administered doses of therapies (63-65). Furthermore, as tumor vascularization can vary between patients and between tumor types, the dose, dose schedule, and/or the temporal sequence may have to be individualized to the patient, further complicating clinical trials.

As discussed above, with the current interest in targeted therapeutics and personalized medicine, methods for selecting patients who will respond to the individualized treatment are critical. Tumors that contain genetic abnormalities that cause the tumors to be "addicted" to constitutive activation of specific signalling pathways will be the most sensitive to molecularly targeted therapies that inhibit those pathways (66). The importance of careful patient selection has been demonstrated for the use of trastuzumab in the treatment of HER2-positive patients (56-58), gefitinib in the treatment of non-small cell lung cancer (67), and cetuximab in the treatment of CRC (68-71), but has been challenging when predicting benefit from the anti-angiogenic and anti-vascular actions of bevacizumab (62). Similarly, the principle of a threshold level of receptor expression applies to targeted nanomedicines, as shown by Park *et al.* (54).

The use of biomarkers to guide patient selection and predict response to therapy can be extended to combinations of targeted therapies. For example, for the dual-targeted approach investigated in this thesis, it will be important to identify tumor-specific and vasculature-specific biomarkers that can be used to select the patients that are most likely to respond to combined vasculature-targeted and tumor-targeted therapies. However, it must be recognized that the "eligible" patient population will decrease with each additional criterion/biomarker that is deemed necessary for patient selection. Although this may impact the likelihood of the combination receiving FDA approval, at least with the current guidelines and approval process, it is in line with the long term focus of being able to provide personalized cancer medicine.

Finally, recent results with agents that act on the vasculature suggest that, following treatment cessation, there is often a rapid rebound of vascular and tumor cell growth, and even acceleration of invasion or metastatic disease growth (72, and references therein), which may have an adverse effect on long term patient survival. These are notable findings in light of the intense focus on anti-angiogenic and anti-vascular research at the present time. In an attempt to reduce the growth rebound following treatment cessation, researchers have explored the continuation of vasculature-targeted therapy beyond evidence of tumor progression, and have shown some improvements in overall survival (73, 74, and references therein). Even though researchers' abilities to study the long term effects of vasculature-targeted therapies using animal models may be limited by the growth properties of the tumors and the ethical requirements that necessitate euthanization of the animals when the tumors become too large, it remains important to continue to gain a greater understanding of how treatment-induced vascular changes affect long term disease progression.

6.3.3.1.1. Improving the Suitability of the Dual-targeted Approach for Clinical Translation

The dual-targeted combination approach described in this thesis could be modified in several ways to make it more suitable for translation to the clinic. A post-insertion technique for preparing targeted liposomes may simplify the scale-up procedures that are required for pre-clinical animal testing and clinical trials, while maintaining excellent control over ligand density (75). There are currently a number of untargeted liposomal drug formulations in the clinic, in clinical trials

or nearing entry into clinical trials, including a liposomal VCR formulation (76) and Irinophore C™ (77) that could be candidates for the post-insertion approach. As a larger number of untargeted liposomal drug formulations reach the market, it may be possible to accelerate the FDA approval process for new targeted liposomal agents by generating targeted formulations of previously approved liposomal drugs, so they can come on to the market after the patent on the untargeted version has expired. Similarly, using approved monoclonal antibodies, or fragments of approved antibodies, as targeting ligands may also be able to accelerate the approval process, assuming that suitable patenting and licensing agreements can be reached with the originator of the targeting ligand.

Rather than combining the tumor-targeted therapy with a vasculature-targeted liposomal drug, it may be possible to achieve similar therapeutic efficacy by combining the tumor-targeted therapy with a free drug that is selective for proliferating endothelial cells or is known to be an effective anti-vascular agent. Especially if the vascular-active drug has already received FDA approval, this may simplify the approval process for a combined vasculature-targeted and tumor-targeted strategy.

With evidence suggesting that the therapeutic activity of some untargeted liposomal anti-cancer drugs may be partially due to cytotoxicity against tumor vasculature (28), the actions of liposomal monotherapies or combinations of untargeted liposomal drugs may be similar to "dual-targeted" effects. In light of these data, and the complexities and costs of translating combinations of targeted nanomedicines to the clinical setting, a more realistic, cost-effective, and viable

strategy for the development of a dual-targeted treatment approach may be the use of carefully selected combinations of untargeted liposomal drugs. Indeed, untargeted liposomal drug combinations are already performing well in advanced clinical trials (78).

6.4. Summarizing Conclusion

Cancer is a significant worldwide health problem, and there is a significant unmet need for effective, specific, and well-tolerated chemotherapeutic agents. Liposomal drug delivery systems have been successfully utilized to overcome some of the undesirable properties of traditional anti-cancer drugs, and have been shown to result increased therapeutic indices, relative to the free drug. Untargeted liposomal drug combinations have already entered the clinic (78), and in the future, combinations of untargeted and targeted liposomal drugs are also feasible. Therefore it is important that pre-clinical testing of novel therapies be conducted in the context of combination treatment.

This thesis investigated the therapeutic potential of two different approaches to combination liposomal chemotherapy: the combination of a 'classical' liposomal drug formulation with a free drug, and the combination of two different liposomal drug formulations targeted selectively to distinct cell populations. The results discussed in this thesis reveal that liposomal nanomedicines are well-suited for use in the combination chemotherapy setting.

The results presented in Chapter 3 reveal that Irinophore C™ is therapeutically superior to free irinotecan in the treatment of CRC, has low overall

toxicity as a single agent, and may be able to achieve an additive or synergistic therapeutic effect with free 5-FU when explored in a clinical setting. The knowledge gained through the experiments outlined in Chapter 3 of this thesis will help to guide the design of future clinical trials, which could ultimately lead to Irinophore C™ replacing free CPT-11 in first-line CRC treatment protocols. Furthermore, Irinophore C™ is known to be active against several different types of cancer; thus, future investigations may lead to new treatment options for other cancers.

The research presented in Chapters 4 and 5 provided evidence that combination chemotherapy strategies can be successfully applied to targeted nanomedicines. Proof-of-concept studies showed that a liposome-based, combination dual-targeted (vasculature-targeted plus tumor-targeted) approach to the treatment of HER2-positive breast cancer warrants additional investigation, particularly as the approach could be easily adapted for the treatment of a wide range of other types of solid tumors. However, it is recognized that translating this treatment to the clinic is not a realistic goal in the near future: at present, the cost and manufacturing complexities of using combinations of targeted nanomedicines outweighs the therapeutic benefit they can provide. This may change with further optimization, as additional untargeted liposomal drugs and antibodies receive FDA approval in the future, and as greater understanding is developed of how to monitor and assess the effects of vasculature-targeted therapies. Until this time, the nanomedicine-based dual-targeted approach is better suited for use as a tool to explore the complex, ever-changing

interconnections between tumor cells and tumor vasculature, which have been recognized to be of critical importance in cancer treatment.

6.5. References – Chapter 6

1. Cancer Fact Sheet No. 297. Lyon: World Health Organization; 2011.

2. Zhang L, Gu FX, Chan JM, Wang AZ, Langer RS, Farokhzad OC. Nanoparticles in medicine: therapeutic applications and developments. *Clin. Pharmacol. Ther.* 2008; 83: 761-769.

3. Kim KY. Nanotechnology platforms and physiological challenges for cancer therapeutics. *Nanomedicine* 2007; 3: 103-110.

4. Gregoriadis G, Ryman BE. Liposomes as carriers of enzymes or drugs: a new approach to the treatment of storage diseases. *Biochem. J.* 1971; 124: 58P.

5. Gregoriadis G. Drug entrapment in liposomes. *FEBS Lett.* 1973; 36: 292.

6. Gregoriadis G, Wills EJ, Swain CP, Tavill AS. Drug-carrier potential of liposomes in cancer chemotherapy. *Lancet* 1974; 1: 1313-1316.

7. Allen TM. Ligand-targeted therapeutics in anticancer therapy. *Nat. Rev. Cancer* 2002; 2: 750-763.

8. FDA Forms Internal Nanotechnology Task Force. FDA News Release. Silver Springs, Maryland: Released online; 2006.

9. Workman P. Pharmacogenomics in cancer drug discovery and development: inhibitors of the Hsp90 molecular chaperone. *Cancer Detect. Prev.* 2002; 26: 405-410.

10. Workman P. The opportunities and challenges of personalized genome-based molecular therapies for cancer: targets, technologies, and molecular chaperones. *Cancer Chemother. Pharmacol.* 2003; 52: S45-S56.

11. Imyanitov EN, Moiseyenko VM. Molecular-based choice of cancer therapy: realities and expectations. *Clin. Chim. Acta* 2007; 379: 1-13.

12. Witte MH. Translational/personalized medicine, pharmaco/surgico/radiogenomics, lymphatic spread of cancer, and medical ignoromes. *J. Surg. Oncol.* 2011; 103: 501-507.

13. Wistuba, II, Gelovani JG, Jacoby JJ, Davis SE, Herbst RS. Methodological and practical challenges for personalized cancer therapies. *Nat. Rev. Clin. Oncol.* 2011; 8: 135-141.

14. Herbst RS, Giaccone G, Schiller JH, Natale RB, Miller V, Manegold C, Scagliotti G, Rosell R, Oliff I, Reeves JA, Wolf MK, Krebs AD, Averbuch SD, Ochs JS, Grous J, Fandi A, Johnson DH. Gefitinib in combination with paclitaxel and carboplatin in advanced non-small-cell lung cancer: a phase III trial--INTACT 2. *J. Clin. Oncol.* 2004; 22: 785-794.

15. Herbst RS, Prager D, Hermann R, Fehrenbacher L, Johnson BE, Sandler A, Kris MG, Tran HT, Klein P, Li X, Ramies D, Johnson DH, Miller VA. TRIBUTE: a phase III trial of erlotinib hydrochloride (OSI-774) combined with carboplatin and paclitaxel chemotherapy in advanced non-small-cell lung cancer. *J. Clin. Oncol.* 2005; 23: 5892-5899.

16. Becker J. Signal transduction inhibitors--a work in progress. *Nat. Biotechnol.* 2004; 22: 15-18.

17. Harris T. Does large scale DNA sequencing of patient and tumor DNA yet provide clinically actionable information? *Discov. Med.* 2010; 10: 144-150.

18. Swanton C, Caldas C. From genomic landscapes to personalized cancer management-is there a roadmap? *Ann. N. Y. Acad. Sci.* 2010; 1210: 34-44.

19. Tortora G, Bianco R, Daniele G, Ciardiello F, McCubrey JA, Ricciardi MR, Ciuffreda L, Cognetti F, Tafuri A, Milella M. Overcoming resistance to molecularly targeted anticancer therapies: Rational drug combinations based on EGFR and MAPK inhibition for solid tumours and haematologic malignancies. *Drug Resist. Updat.* 2007; 10: 81-100.

20. Wang MD, Shin DM, Simons JW, Nie S. Nanotechnology for targeted cancer therapy. *Expert Rev. Anticancer Ther.* 2007; 7: 833-837.

21. Yuan F, Chen Y, Dellian M, Safabakhsh N, Ferrara N, Jain RK. Time-dependent vascular regression and permeability changes in established human tumor xenografts induced by an anti-vascular endothelial growth factor/vascular permeability factor antibody. *Proc. Natl. Acad. Sci. U. S. A.* 1996; 93: 14765-14770.

22. Jain RK. Physiological barriers to delivery of monoclonal antibodies and other macromolecules in tumors. *Cancer Res.* 1990; 50: 814s-819s.

23. Shannon AM, Bouchier-Hayes DJ, Condron CM, Toomey D. Tumour hypoxia, chemotherapeutic resistance and hypoxia-related therapies. *Cancer Treat. Rev.* 2003; 29: 297-307.

24. Skinner SA, Tutton PJ, O'Brien PE. Microvascular architecture of experimental colon tumors in the rat. *Cancer Res.* 1990; 50: 2411-2417.

25. Yuan F, Leunig M, Huang SK, Berk DA, Papahadjopoulos D, Jain RK. Microvascular permeability and interstitial penetration of sterically stabilized (Stealth) liposomes in a human tumor xenograft. *Cancer Res.* 1994; 54: 3352-3356.

26. Dvorak HF, Nagy JA, Dvorak JT, Dvorak AM. Identification and characterization of the blood vessels of solid tumors that are leaky to circulating macromolecules. *Am. J. Pathol.* 1988; 133: 95-109.

27. Gerber HP, Ferrara N. Pharmacology and pharmacodynamics of bevacizumab as monotherapy or in combination with cytotoxic therapy in preclinical studies. *Cancer Res.* 2005; 65: 671-680.

28. Verreault M, Strutt D, Masin D, Anantha M, Yung A, Kozlowski P, Waterhouse D, Bally MB, Yapp DT. Vascular normalization in orthotopic glioblastoma following intravenous treatment with lipid-based nanoparticulate formulations of irinotecan (Irinophore C), doxorubicin (Caelyx(R)) or vincristine. *BMC Cancer* 2011; 11: 124-141.

29. Boucher Y, Leunig M, Jain RK. Tumor angiogenesis and interstitial hypertension. *Cancer Res.* 1996; 56: 4264-4266.

30. Padera TP, Stoll BR, Tooredman JB, Capen D, di Tomaso E, Jain RK. Pathology: cancer cells compress intratumour vessels. *Nature* 2004; 427: 695.

31. Jain RK. Barriers to drug delivery in solid tumors. *Sci. Am.* 1994; 271: 58-65.

32. Baxter LT, Jain RK. Transport of fluid and macromolecules in tumors. I. Role of interstitial pressure and convection. *Microvasc. Res.* 1989; 37: 77-104.

33. Boucher Y, Baxter LT, Jain RK. Interstitial pressure gradients in tissue-isolated and subcutaneous tumors: implications for therapy. *Cancer Res.* 1990; 50: 4478-4484.

34. McKee TD, Grandi P, Mok W, Alexandrakis G, Insin N, Zimmer JP, Bawendi MG, Boucher Y, Breakefield XO, Jain RK. Degradation of fibrillar collagen in a human melanoma xenograft improves the efficacy of an oncolytic herpes simplex virus vector. *Cancer Res.* 2006; 66: 2509-2513.

35. Pluen A, Boucher Y, Ramanujan S, McKee TD, Gohongi T, di Tomaso E, Brown EB, Izumi Y, Campbell RB, Berk DA, Jain RK. Role of tumor-host interactions in interstitial diffusion of macromolecules: cranial vs. subcutaneous tumors. *Proc. Natl. Acad. Sci. U.S.A.* 2001; 98: 4628-4633.

36. Netti PA, Berk DA, Swartz MA, Grodzinsky AJ, Jain RK. Role of extracellular matrix assembly in interstitial transport in solid tumors. *Cancer Res.* 2000; 60: 2497-2503.

37. Jain RK, Stylianopoulos T. Delivering nanomedicine to solid tumors. *Nat. Rev. Clin. Oncol.* 2010; 7: 653-664.

38. Allen T, M. Liposome Targeting in Animal Models: Problems and Opportunities. *J. Liposome Res.* 1997; 7: 315-329.

39. Li CJ, Miyamoto Y, Kojima Y, Maeda H. Augmentation of tumour delivery of macromolecular drugs with reduced bone marrow delivery by elevating blood pressure. *Br. J. Cancer* 1993; 67: 975-980.

40. Nagamitsu A, Greish K, Maeda H. Elevating blood pressure as a strategy to increase tumor-targeted delivery of macromolecular drug SMANCS: cases of advanced solid tumors. *Jpn. J. Clin. Oncol.* 2009; 39: 756-766.

41. Seki T, Fang J, Maeda H. Enhanced delivery of macromolecular antitumor drugs to tumors by nitroglycerin application. *Cancer Sci.* 2009; 100: 2426-2430.

42. Feelisch M, Noack EA. Correlation between nitric oxide formation during degradation of organic nitrates and activation of guanylate cyclase. *Eur. J. Pharmacol.* 1987; 139: 19-30.

43. Maeda H. Tumor-selective delivery of macromolecular drugs via the EPR effect: background and future prospects. *Bioconjug. Chem.* 2010; 21: 797-802.

44. Kong G, Braun RD, Dewhirst MW. Characterization of the effect of hyperthermia on nanoparticle extravasation from tumor vasculature. *Cancer Res* 2001; 61: 3027-3032.

45. Kong G, Anyarambhatla G, Petros WP, Braun RD, Colvin OM, Needham D, Dewhirst MW. Efficacy of liposomes and hyperthermia in a human tumor xenograft model: importance of triggered drug release. *Cancer Res.* 2000; 60: 6950-6957.

46. Yatvin MB, Weinstein JN, Dennis WH, Blumenthal R. Design of liposomes for enhanced local release of drugs by hyperthermia. *Science* 1978; 202: 1290-1293.

47. Andresen TL, Jensen SS, Jorgensen K. Advanced strategies in liposomal cancer therapy: problems and prospects of active and tumor specific drug release. *Prog. Lipid Res.* 2005; 44: 68-97.

48. Jain RK. Normalizing tumor vasculature with anti-angiogenic therapy: a new paradigm for combination therapy. *Nat. Med.* 2001; 7: 987-989.

49. Tong RT, Boucher Y, Kozin SV, Winkler F, Hicklin DJ, Jain RK. Vascular normalization by vascular endothelial growth factor receptor 2 blockade induces a pressure gradient across the vasculature and improves drug penetration in tumors. *Cancer Res.* 2004; 64: 3731-3736.

50. Abu Lila AS, Doi Y, Nakamura K, Ishida T, Kiwada H. Sequential administration with oxaliplatin-containing PEG-coated cationic liposomes promotes a significant delivery of subsequent dose into murine solid tumor. *J. Control. Release* 2010; 142: 167-173.

51. Baker JH, Lam J, Kyle AH, Sy J, Oliver T, Co SJ, Dragowska WH, Ramsay E, Anantha M, Ruth TJ, Adam MJ, Yung A, Kozlowski P, Minchinton AI, Ng SS, Bally MB, Yapp DT. Irinophore C, a novel nanoformulation of irinotecan, alters tumor vascular function and enhances the distribution of 5-fluorouracil and doxorubicin. *Clin. Cancer Res.* 2008; 14: 7260-7271.

52. Pastorino F, Brignole C, Marimpietri D, Cilli M, Gambini C, Ribatti D, Longhi R, Allen TM, Corti A, Ponzoni M. Vascular damage and anti-angiogenic effects of tumor vessel-targeted liposomal chemotherapy. *Cancer Res.* 2003; 63: 7400-7409.

53. Pastorino F, Brignole C, Di Paolo D, Nico B, Pezzolo A, Marimpietri D, Pagnan G, Piccardi F, Cilli M, Longhi R, Ribatti D, Corti A, Allen TM, Ponzoni M. Targeting liposomal chemotherapy via both tumor cell-specific and tumor vasculature-specific ligands potentiates therapeutic efficacy. *Cancer Res.* 2006; 66: 10073-10082.

54. Park JW, Hong K, Kirpotin DB, Colbern G, Shalaby R, Baselga J, Shao Y, Nielsen UB, Marks JD, Moore D, Papahadjopoulos D, Benz CC. Anti-HER2 immunoliposomes: Enhanced efficacy attributable to targeted delivery. *Clin. Cancer Res.* 2002; 8: 1172-1181.

55. Pan XQ, Wang H, Lee RJ. Antitumor activity of folate receptor-targeted liposomal doxorubicin in a KB oral carcinoma murine xenograft model. *Pharm. Res.* 2003; 20: 417-422.

56. Vogel CL, Cobleigh MA, Tripathy D, Gutheil JC, Harris LN, Fehrenbacher L, Slamon DJ, Murphy M, Novotny WF, Burchmore M, Shak S, Stewart SJ, Press M. Efficacy and safety of trastuzumab as a single agent in first-line treatment of HER2-overexpressing metastatic breast cancer. *J. Clin. Oncol.* 2002; 20: 719-726.

57. Perez EA, Baweja M. HER2-positive breast cancer: current treatment strategies. *Cancer Invest.* 2008; 26: 545-552.

58. Joensuu H, Sperinde J, Leinonen M, Huang W, Weidler J, Bono P, Isola J, Kellokumpu-Lehtinen P, Bates M. *Breast Cancer Patients with Very High Tumor HER2 Expression Levels Might Not Benefit from Treatment with Trastzumab Plus Chemotherapy: A Retrospective Exploratory Analysis of the FinHer Trial* as found in Abstracts: Thirty-Second Annual CTRC-AACR San Antonio Breast Cancer Symposium-- Dec 10-13, 2009; San Antonio, TX. *Cancer Res.* 2009; 69: Abstract no 5083.

59. Kobayashi T, Ishida T, Okada Y, Ise S, Harashima H, Kiwada H. Effect of transferrin receptor-targeted liposomal doxorubicin in P-glycoprotein-mediated drug resistant tumor cells. *Int. J. Pharm.* 2007; 329: 94-102.

60. Tappenden P, Jones R, Paisley S, Carroll C. Systematic review and economic evaluation of bevacizumab and cetuximab for the treatment of metastatic colorectal cancer. *Health Technol. Assess.* 2007; 11: 1-128, iii-iv.

61. Gerger A, LaBonte M, Lenz HJ. Molecular predictors of response to antiangiogenesis therapies. *Cancer J.* 2011; 17: 134-141.

62. Jubb AM, Harris AL. Biomarkers to predict the clinical efficacy of bevacizumab in cancer. *Lancet Oncol.* 2010; 11: 1172-1183.

63. Jiang F, Albert DH, Luo Y, Tapang P, Zhang K, Davidsen SK, Fox GB, Lesniewski R, McKeegan EM. ABT-869, a Multitargeted Receptor Tyrosine Kinase Inhibitor, Reduces Tumor Microvascularity and Improves Vascular Wall Integrity in Preclinical Tumor Models. *J. Pharmacol. Exp. Ther.* 2011; 338: 134-142.

64. Rosen MA, Schnall MD. Dynamic contrast-enhanced magnetic resonance imaging for assessing tumor vascularity and vascular effects of targeted therapies in renal cell carcinoma. *Clin. Cancer Res.* 2007; 13: 770s-776s.

65. Knopp MV, Giesel FL, Marcos H, von Tengg-Kobligk H, Choyke P. Dynamic contrast-enhanced magnetic resonance imaging in oncology. *Top. Magn. Reson. Imaging* 2001; 12: 301-308.

66. Broxterman HJ, Georgopapadakou NH. Anticancer therapeutics: "Addictive" targets, multi-targeted drugs, new drug combinations. *Drug Resist. Updat.* 2005; 8: 183-197.

67. Lynch TJ, Bell DW, Sordella R, Gurubhagavatula S, Okimoto RA, Brannigan BW, Harris PL, Haserlat SM, Supko JG, Haluska FG, Louis DN, Christiani DC, Settleman J, Haber DA. Activating mutations in the epidermal growth factor receptor underlying responsiveness of non-small-cell lung cancer to gefitinib. *N. Engl. J. Med.* 2004; 350: 2129-2139.

68. Siena S, Sartore-Bianchi A, Di Nicolantonio F, Balfour J, Bardelli A. Biomarkers predicting clinical outcome of epidermal growth factor receptor-targeted therapy in metastatic colorectal cancer. *J. Natl. Cancer Inst.* 2009; 101: 1308-1324.

69. Laurent-Puig P, Cayre A, Manceau G, Buc E, Bachet JB, Lecomte T, Rougier P, Lievre A, Landi B, Boige V, Ducreux M, Ychou M, Bibeau F, Bouche O, Reid J, Stone S, Penault-Llorca F. Analysis of PTEN, BRAF, and EGFR status in determining benefit from cetuximab therapy in wild-type KRAS metastatic colon cancer. *J. Clin. Oncol.* 2009; 27: 5924-5930.

70. Sartore-Bianchi A, Martini M, Molinari F, Veronese S, Nichelatti M, Artale S, Di Nicolantonio F, Saletti P, De Dosso S, Mazzucchelli L, Frattini M, Siena S, Bardelli A. PIK3CA mutations in colorectal cancer are associated with clinical resistance to EGFR-targeted monoclonal antibodies. *Cancer Res.* 2009; 69: 1851-1857.

71. Avet-Loiseau H, Leleu X, Roussel M, Moreau P, Guerin-Charbonnel C, Caillot D, Marit G, Benboubker L, Voillat L, Mathiot C, Kolb B, Macro M, Campion L, Wetterwald M, Stoppa AM, Hulin C, Facon T, Attal M, Minvielle S, Harousseau JL. Bortezomib plus dexamethasone induction improves outcome of patients with t(4;14) myeloma but not outcome of patients with del(17p). *J. Clin. Oncol.* 2010; 28: 4630-4634.

72. Kerbel RS. Issues regarding improving the impact of antiangiogenic drugs for the treatment of breast cancer. *Breast* 2009; 18 Suppl 3: S41-47.

73. Grothey A, Sugrue MM, Purdie DM, Dong W, Sargent D, Hedrick E, Kozloff M. Bevacizumab beyond first progression is associated with prolonged overall survival in metastatic colorectal cancer: results from a

large observational cohort study (BRiTE). *J. Clin. Oncol.* 2008; 26: 5326-5334.

74. Ellis LM, Haller DG. Bevacizumab beyond progression: does this make sense? *J. Clin. Oncol.* 2008; 26: 5313-5315.

75. Iden DL, Allen TM. In vitro and in vivo comparison of immunoliposomes made by conventional coupling techniques with those made by a new post-insertion technique. *Biochim. Biophys. Acta* 2001; 1513: 207-216.

76. Rodriguez MA, Pytlik R, Kozak T, Chhanabhai M, Gascoyne R, Lu B, Deitcher SR, Winter JN. Vincristine sulfate liposomes injection (Marqibo) in heavily pretreated patients with refractory aggressive non-Hodgkin lymphoma: report of the pivotal phase 2 study. *Cancer* 2009; 115: 3475-3482.

77. Ramsay EC, Anantha M, Zastre J, Meijs M, Zonderhuis J, Strutt D, Webb MS, Waterhouse D, Bally MB. Irinophore C: a liposome formulation of irinotecan with substantially improved therapeutic efficacy against a panel of human xenograft tumors. *Clin. Cancer Res.* 2008; 14: 1208-1217.

78. Lancet JE, Cortes JE, Kovacsovics T, Hogge D, Kolitz JE, Tallman MS, Chiarella M, Louie AC, Feldman EJ. CPX-351 versus cytarabine (CYT) and daunorubicin (DNR) therapy in newly diagnosed AML patients age 60-75: Safety and efficacy in secondary AML (sAML). *J. Clin. Oncol.* 2011; 29: 6519.

CANCER RESEARCH

Clinical Trials

Abstract CT146: Plasma pharmacokinetics of liposomal irinotecan (nal-IRI) in pediatric oncology patients with recurrent or refractory solid tumors: South Plains Oncology Consortium Study 2012-001

Paul D. Harker-Murray, William H. Meyer, Patrick Leavey, Min H. Kang, Hwangeui Cho, Bambang S. Adiwijaya, Jonathan B. Fitzgerald, J Marc Pipas, Daryl C. Drummond, and C. Patrick Reynolds

DOI: 10.1158/1538-7445.AM2017-CT146 Published July 2017 Check for updates

Proceedings: AACR Annual Meeting 2017; April 1-5, 2017; Washington, DC

Abstract

Background/Objectives: Children with relapsed or refractory solid tumors have a poor prognosis. Irinotecan is active in some pediatric solid tumors and synergizes with alkylating agents. nal-IRI encapsulates irinotecan into long-circulating, liposome-based nanoparticles. In adults, nal-IRI demonstrated extended plasma exposure compared with non-liposomal irinotecan. In pediatric solid tumor models, nal-IRI had robust preclinical activity and synergized with cyclophosphamide, and therefore merits testing in children with relapsed and refractory solid tumors. Herein we describe a phase 1 dose-escalation study of nal-IRI in combination with cyclophosphamide (NCT02013336) and preliminary pharmacokinetic and safety results.

Methods: Cyclophosphamide was administered on days 1-5 of each cycle (250 mg/m^2/d intravenously [IV]) with a single 90-min IV infusion of nal-IRI on day 3 of a Q3-week schedule, escalating from 60 mg/m^2 to 210 mg/m^2 (expressed as irinotecan HCL trihydrate salt), in a standard 3+3 dose-escalation design to determine the maximum tolerated dose. To date, the nal-IRI dose has been escalated from 60 mg/m^2 to 150 mg/m^2. Samples for pharmacokinetic analysis were collected during the first cycle of chemotherapy before infusion and at 4h, 24h, 48h, 120h, and 168h post-infusion. Plasma pharmacokinetics of total irinotecan and SN-38 were quantified using mixed

effect modeling, and were compared with adult values from a population pharmacokinetic analysis of 6 clinical studies of nal-IRI.[1]

Results: To date, 10 males and 6 females with a median age of 12.8 years (range: 5-19) have been enrolled: 10 with Ewing sarcoma, 2 with neuroblastoma, 3 with osteosarcoma, and 1 with rhabdomyosarcoma. The estimated total irinotecan volume of distribution (V_d) was 1.9 L, clearance (CL) was 10.3 L/week, and half-life ($t_{1/2}$) was 21.2 h, which were 42% (V_d and CL) of adult values and comparable to adult values ($t_{1/2}$). The corresponding C_{max} was 72% higher than that observed in adults. SN-38 clearance was 11.4 L/week (comparable to adults), $t_{1/2}$ was 19.3 h (48% of adult values), and C_{max} was 68% of adult values. Thrombocytopenia leading to treatment delay was a dose-limiting toxicity at 150 mg/m^2 (n=1); other systemic toxicity attributed to chemotherapy within the 1st cycle was nausea/vomiting (n=1).

Conclusions: Preliminary safety and pharmacokinetic data support continued investigation of nal-IRI in pediatric oncology. Clinical outcomes including safety of patients treated in this study will be reported once a maximum tolerated dose is achieved.

1. Adiwijaya B et al. *Clin Pharmacol Ther*. 2017. In press.

Citation Format: Paul D. Harker-Murray, William H. Meyer, Patrick Leavey, Min H. Kang, Hwangeui Cho, Bambang S. Adiwijaya, Jonathan B. Fitzgerald, J Marc Pipas, Daryl C. Drummond, C. Patrick Reynolds. Plasma pharmacokinetics of liposomal irinotecan (nal-IRI) in pediatric oncology patients with recurrent or refractory solid tumors: South Plains Oncology Consortium Study 2012-001 [abstract]. In: Proceedings of the American Association for Cancer Research Annual Meeting 2017; 2017 Apr 1-5; Washington, DC. Philadelphia (PA): AACR; Cancer Res 2017;77(13 Suppl):Abstract nr CT146. doi:10.1158/1538-7445.AM2017-CT146

Previous

Back to top

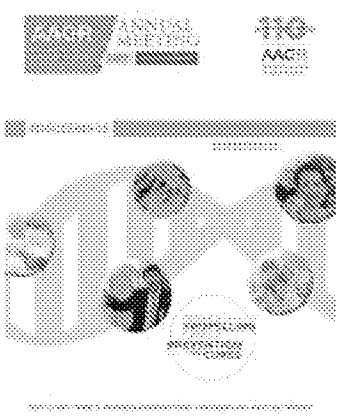

July 2017
Volume 77, Issue 13 Supplement
Table of Contents

Cancer Research Online ISSN: 1538-7445
Cancer Research Print ISSN: 0008-5472
Journal of Cancer Research ISSN: 0096-7013
American Journal of Cancer ISSN: 0096-7374

Depletion of alveolar macrophages decreases neutrophil chemotaxis to *Pseudomonas* airspace infections

SATORU HASHIMOTO, JEAN-FRANÇOIS PITTET, KEELUNG HONG, HANS FOLKESSON, GREGORY BAGBY, LESTER KOBZIK, CHARLES FREVERT, KAZUYOSHI WATANABE, SUSUMU TSURUFUJI, AND JEANINE WIENER-KRONISH
Departments of Anesthesia and Medicine and the Cardiovascular Research Institute and Cancer Research Institute, University of California, San Francisco, California 94143; Kyoto Prefectural University of Medicine, Department of Anesthesiology, Kyoto 602, Japan; Department of Physiology, Louisiana State University Medical Center, New Orleans, Louisiana 70112; Physiology Program, Harvard School of Public Health, Boston, Massachusetts 02115–6195; Institute of Cytosignal Research, Tokyo 140, Japan

Hashimoto, Satoru, Jean-François Pittet, Keelung Hong, Hans Folkesson, Gregory Bagby, Lester Kobzik, Charles Frevert, Kazuyoshi Watanabe, Susumu Tsurufuji, and Jeanine Wiener-Kronish. Depletion of alveolar macrophages decreases neutrophil chemotaxis to *Pseudomonas* airspace infections. *Am. J. Physiol.* 270 (*Lung Cell. Mol. Physiol.* 14): L819–L828, 1996.—The mechanism for neutrophil (PMN) influx into infected airspaces of the lung is not known. To determine whether alveolar macrophage products are important in the initiation of chemotaxis, we depleted rats of alveolar macrophages by aerosolizing negatively charged oligolamellar liposomes complexed to clodronate disodium. Ninety-five percent of the alveolar macrophages were depleted, and lung injury and inflammation were minimized with this depletion technique. Rats depleted of alveolar macrophages were then anesthetized, and either 5×10^6 colony-forming units (CFU) or 5×10^7 CFU of *Pseudomonas aeruginosa* were instilled into the airspaces of these animals. When recombinant macrophage inflammatory protein MIP-2 was intratracheally instilled into rats depleted of alveolar macrophages, PMN were recruited to their airspaces. Nonetheless, PMN numbers were decreased in the lavage fluids when moderate or large inoculums of bacteria were instilled into depleted rats, although the PMN response appeared dose dependent. Levels of bioactive tumor necrosis factor-α and immunoreactive proteins CINC/gro (cytokine-induced PMN chemoattractant) in the lavage fluids obtained from infected rats depleted of alveolar macrophages were significantly decreased compared with the levels in the lavage fluids obtained from normal infected rats. MIP-2 mRNA expression, as detected by Northern analysis, was also decreased in the infected lungs of depleted rats, and the lavage fluid from these rats had significantly decreased chemotactic activity. Therefore these results suggest that alveolar macrophage products play a direct role in the initial recruitment of PMN into infected lungs.

macrophage inflammatory protein; immunoreactive proteins; cytokines; chemokines

NEUTROPHIL INFLUX is necessary (18, 20, 23, 24, 28) for clearance of infectious agents in the airspaces of the lungs. However, the mechanism for the neutrophilia found in infected airspaces is not clear. Potential chemoattractants include complement fragments, bacterial products (*N*-formylmethionyl-leucyl-phenylalanine), eicosanoids, and chemokines (4, 5, 17). Recent studies have highlighted the role of the lung macrophage-derived chemoattractant cytokines, the chemokines, or platelet factor 4 (PF-4) cytokine superfamily, as critical mediators of neutrophil (PMN) influx into injured lungs (7, 9, 10, 13). While interleukin (IL)-8 is the major C-X-C chemokine in humans, the proteins CINC/gro (cytokine-induced PMN chemoattractant) and macrophage inflammatory protein MIP-2 are the major functional C-X-C chemokines in rodents (9, 10, 13, 14, 30).

Indeed, some studies have suggested that the alveolar macrophage plays a major role in PMN chemotaxis into infected airspaces (11, 20, 21, 24). To determine the importance of alveolar macrophages in initiation of PMN chemotaxis into infected airspaces, animals deficient only in this cell would be required. However, such animals do not exist, and previous methods used to deplete alveolar macrophages often affect other cells in the airspaces. Modifying published techniques for alveolar macrophage depletion (2, 3, 27, 29), we aerosolized negatively charged large oligolamellar liposomes complexed with clodronate disodium and were able to deplete, at a minimum, 95% of the alveolar macrophages in rats. This technique, in contrast to methods used previously (3, 27, 29), minimized lung inflammation and did not cause airspace neutrophilia.

We then applied this technique to formally test the role of the alveolar macrophage in mediating PMN influx to lungs infected with bacteria.

In addition to monitoring PMN influx by bronchoalveolar lavage fluids (BAL) and by histopathology, we measured chemotactic activity in BAL fluid (BALF) samples and assayed some of the relevant chemokines, CINC/gro protein concentrations, and MIP-2 mRNA levels together with tumor necrosis factor-α (TNF-α). The results provide strong, direct proof of a critical role for the alveolar macrophage in the initial recruitment of PMN into infected lungs.

METHODS

Animals and Materials

One hundred and eight pathogen-free Sprague-Dawley male rats (300–375 g; Simonsen, Gilroy, CA) were used for the entire study. All animal experiments were done at the University of California at San Francisco in compliance with the Animal Care Committee of the University of California at San Francisco.

Bacteria. A nonmucoid strain of *Pseudomonas aeruginosa* (PA103; generously provided by Dr. D. Frank) was used, as we

have found it to cause acute lung injury at inoculums found in patients (16). The strain was stored as bacterial stock at −70°C in a 10% sterile skim milk solution. After the inoculation of the bacteria on a VBMM (Vogel Bonner minimal medium) plate for 24 h at 37°C, the bacteria were cultured in trypticase soy broth supplemented with 10 mM nitriloitriacetic acid (Sigma Chemical, St. Louis, MO), 1% glycerol, and 100 mM monosodium glutamate and grown for 13 h at 32°C in a shaking incubator (19). The concentration of bacteria was measured spectrophotometrically, and quantitative cultures were done to verify the quantity of the bacterial inoculum. Cultures were serially diluted with Ringer lactate to 10^7 colony-forming units (CFU)/ml. Quantitative cultures of the homogenized lungs were also done.

Liposome Preparation

Bovine brain phosphatidylserine (PS) and egg phosphatidylcholine (PC) were purchased from Avanti polar lipids (Alabaster, AL). Cholesterol was obtained from Sigma Chemical. All lipids were stored in a chloroform solution. The liposomes were composed of PS, PC, and cholesterol at a molar ratio of 1:6:4. The lipids were first mixed in chloroform, and each batch consisted of 13.3 mg PS, 75 mg of PC, and 25.4 mg of cholesterol in 5 ml of chloroform. A stock solution of 250 mM disodium clodronate (also known as dichloromethylene diphosphonate or dichloromethylene bisphosphonate; the drug was a kind gift from Boehringer Mannheim, Mannheim, Germany) was made from 0.25 g of disodium clodronate, 1 ml of phosphate-buffered saline without calcium [PBS(−)], and 2.4 ml of distilled water. The osmolarity of this stock solution was ~600 mosM.

Both drug-containing and drug-free liposomes were prepared, using the modified reverse evaporation technique (25). The solvent in the lipid mixture was removed by reduced pressure, and the dry lipid mixture was dissolved in 4 ml of diethyl ether. Then 2 ml of the stock solution of the clodronate or PBS(−) was added. The biphasic mixture was placed in argon and then emulsified utilizing sonication for 3 min. The ether was then removed slowly by placing the solution on a rotary evaporator under reduced pressure at 30°C. Any gel phase formed was broken by vortexing the sample repeatedly to facilitate the removal of ether. The liposome suspension was then extruded sequentially through cellulose acetate syringe-type filters (Corning Glass Works, Corning, NY) with a 0.2-μm filter. Extrusion was repeated to improve the size distribution. The unencapsulated drug was separated from drug-containing liposomes by high-speed centrifugation (100,00 *g* for 60 min). The liposome pellet was resuspended in PBS(−) for aerosolization. Disodium clodronate (51 μmol) was incorporated into the liposomes during this procedure, as determined by phosphate assay (1).

Experimental Protocols

Aerosolization of liposomes. To uniformly deliver the liposomes to the airspaces, rats were placed in a nose-only aerosol chamber (Intox Products, Albuquerque, NM). The rats received aerosolized liposome-encapsulated clodronate or the same liposomes without the drug or the vehicle alone, PBS(−). Aerosols were generated by an Aerotech II nebulizer (CIS-US, Bedford, MA), driven by compressed air at a flow rate of 10 l/min. The particle size of the aerosol was measured by a cascade impactor (Intox Products, NM). Under these conditions, the mass median aerodynamic diameter was 1.6 μm, and the geometric SD was 2.5. Based on experiments where fluorescent liposomes were aerosolized to rats in the chamber, bronchoalveolar lavage was performed, and measurement of the lavage fluid for fluorescence was done, we estimated that between 0.1 and 0.5% of the aerosolized solution was delivered into the lungs of each rat or that 0.05–0.25 μmol of disodium clodronate was delivered into the airspaces of each rat. This volume is much smaller than that previously utilized in studies where 1.34 μmol of liposome-encapsulated clodronate, or 26 times more drug was delivered to the lungs of rats via intratracheal instillation (3).

The effectiveness of the liposome-encapsulated clodronate in depleting alveolar macrophages was assessed by performing BAL 6 h, 24 h, 48 h, 14 days, and 21 days after the aerosolization and counting the alveolar macrophages and leukocytes present in the lavage fluid. Cell counts were done on lavage fluids obtained from rats exposed to liposome-encapsulated clodronate, exposed to empty liposomes or exposed to the vehicle, PBS(−). The lavage was done by instilling 10 ml of 0.9% NaCl for 3 min, using 12 cm of hydrostatic pressure. The procedure was repeated three times, and ~30 ml were collected. The lavage fluid was centrifuged, the supernatant was removed, and the cell pellet was resuspended in PBS(−). The total cell number was determined with the use of a hemacytometer. The percentage of different cell types was determined on cytocentrifuge preparations (Cytospin 2; Shandon Southern Instruments, Sewickley, PA) after staining the cells with a nonspecific esterase stain (Sigma). Macrophage viability was assessed using trypan blue exclusion on macrophages obtained from BALF.

Bacterial instillation. Three days after receiving liposomes or PBS(−), rats were anesthetized with pentobarbital (60 mg/kg ip) and maintained with half of this dose of pentobarbital every 2 h. Pancuronium bromide (0.3 $mg \cdot kg^{-1} \cdot h^{-1}$) was given for neuromuscular blockade. An endotracheal tube was inserted through a tracheostomy. The animals were supine and were ventilated with a constant-volume respirator (Harvard Apparatus, South Natick, MA) with an inspired O_2 fraction of 1.0 and positive end-expiratory pressures of 3 cmH_2O. The respiratory rate was adjusted to maintain arterial P_{CO_2} between 35 and 45 mmHg. A right carotid arterial line was inserted to monitor systemic blood pressure continuously and to obtain serial blood samples.

P. aeruginosa (10^7 CFU/ml) were diluted in 1 ml of 5% rat albumin in Ringer lactate; the final bacterial concentration in this solution that was instilled was 5×10^6 CFU/ml (18). In six rats, a 10-fold larger inoculum was instilled; 5×10^7 CFU/ml was instilled in these rats. Evans blue dye (0.5 mg) was also added to the solution to locate the instillate at the end of each study. The protein solution remains in the airspaces for longer intervals than a solution containing crystalloid alone (22).

For administration of this bacterial instillate, rats were placed in the right lateral decubitus position to facilitate the deposition of this liquid into their right lungs. Over 20 min, 3 ml/kg of the protein-containing solution was instilled into the right lung with the use of a 1-ml syringe and a polypropylene tube (0.5-mm ID).

Blood samples were obtained for blood gas determinations every hour. After 4 h, the animals were killed to excise the lungs. Then BAL was done for cell counts or for the measurement of TNF-α, CINC/gro, and chemotactic factors.

Experiments in six other rats were carried out to investigate whether rats depleted of alveolar macrophages would respond normally to an airspace instillation of a chemotactic factor. All six rats were depleted of alveolar macrophages, using the techniques stated above. Three of the rats were lavaged, as described above, to ensure the depletion of alveolar macrophage depletion. The other three rats were then anes-

thetized and had 50 μg of recombinant MIP-2 instilled into their tracheas. At 4 h after the instillation, BAL was done for quantification of the cells in the airspaces.

Assessment of permeability of the alveolar epithelium and lung endothelium. Two different methods were used to measure the bidirectional flux of albumin across the lung epithelial barrier, as we have done before (16, 22). The first method requires measurement of residual ^{125}I-albumin (the airspace protein tracer) in the lung as well as the accumulation of ^{125}I-albumin in the plasma. The second method requires the measurement of ^{131}I-albumin (the vascular protein tracer) in the lungs and in the airspaces of the lung.

The total quantity of ^{125}I-albumin (the airspace protein tracer) instilled into the lung was determined by measuring duplicate samples of the instilled solution for total counts [counts per minute (cpm)/g] and then multiplying this data by the total volume instilled into the lung. To calculate the residual ^{125}I-albumin in the lung after 4 h, the average radioactivity counts of two 0.5-g samples obtained from the lung homogenate were multiplied by the total volume of lung homogenate. The calculated amount of ^{125}I-albumin in the lung homogenate was added to the recovered counts in the final aspirate of alveolar fluid to determine the total amount of instilled ^{125}I-albumin that remained in the lung after 4 h. The ^{125}I-albumin in the circulating plasma was measured from a sample of plasma obtained at the end of the experiment. The plasma fraction was accounted for by multiplying the counts per gram by the plasma volume (body wt × 0.07 [1 − Hct]).

The second method required averaging the ^{131}I-albumin counts in the plasma for the 4-h interval of the experiments. The ^{131}I-albumin counts in the final airspace samples were expressed as a ratio to the averaged plasma counts. This ratio provides a good index of equilibration of the vascular protein tracer into the airspace compartment, as we and others have shown in other experimental studies of lung epithelial permeability (16, 22).

Morphology. Three rats (of 12 examined) are presented as representative of light-microscopic findings. One rat was exposed to the clodronate-containing liposomes and was processed 3 days after the aerosolization. The two other rats received bacterial instillations after the aerosolization of clodronate-containing liposomes or the vehicle PBS(−). After a 4-h exposure to bacteria, these rats were also processed for light microscopy. All three rats were processed by utilizing deep anesthesia before the placement of a tracheal tube. The abdominal aorta was then transected, and then the lungs were filled with 10% neutral buffered Formalin. The lungs and heart were then removed en bloc and processed for light microscopy.

Analytical Procedures

Measurement of TNF-α. Nine rats that had received aerosolized liposomes containing clodronate, liposomes without the drug, or PBS(−) alone were then exposed to airspace bacteria, as described above. The lavage fluid from these rats was assayed for levels of TNF-α bioactivity by using the WEHI-164 subclone 13 cytotoxicity assay (6). Briefly, 5×10^4 cells in RPMI 1640 containing 10% fetal calf serum (FCS), 1 mM L-glutamine, and 0.5 mg/ml actinomycin D were added to serially diluted samples in microtiter plates and incubated for 20 h at 37°C and in 5% CO_2. Cytotoxicity was assessed by measuring 3,(4,5-dimethylthiazol-2-yl)-2,5-diphenyltetrazolium bromide (MTT)-tetrazolium conversion to formazan at 550 nm (12). To assess whether clodronate could influence the TNF-α concentrations measured in this assay, a log dose-response curve was made, using concentrations of 1 nmol to 1 nmol clodronate in a fluid with a known TNF-α concentration. The clodronate, at all concentrations tested, did not affect the TNF-α concentration measured by the assay. TNF-α concentrations (pg/ml) were calculated using standard recombinant muTNF-α (Genentech, South San Francisco, CA). Goat anti-muTNF-α immunoglobulin (Ig)G reduces BAL TNF-α activity to undetectable levels.

Measurement of CINC/gro. The BAL samples were assayed for CINC/gro, using a sandwich enzyme-linked immunosorbent assay (ELISA) purchased from Immuno-Biological Laboratories (no. 17132; Fujioka, Japan). The assay is sensitive to CINC/gro and does not detect human IL-8 or human gro. The standard curve was obtained using chemically synthesized CINC/gro (50 ng/ml which was serially diluted to 12.2 pg/ml). A linear response was obtained to the dilutions of the standard within this range. After incubation with 100 ml of sample, wells were washed and incubated with horseradish peroxidase-conjugated anti-CINC/gro rabbit IgG and then were incubated with 0.05% *o*-phenylenediamine. The reaction was stopped by the addition of 50 ml of 6 N H_2SO_4; the absorbance of the processed sample at 492 nm was recorded (14).

Northern blotting and hybridization of MIP-2. Northern blot analysis for MIP-2 mRNA was carried out on homogenized rat lungs from six animals; mRNA analysis was done on two samples from each of the experimental conditions. Rat lungs were obtained after the 4-h bacterial instillation and then rapidly homogenized in the presence of 10 ml of GTC solution [4 M guanidine thiocyanate, 25 mM sodium citrate (pH 7.0), 0.5% *N*-lauroyl sarcosine, 0.1 M 2-mercaptoethanol], using a Brinkmann polytron. The homogenized lungs were rapidly frozen by placement in a dry ice-methanol bath and then stored at −70°C until they were processed. Total RNA from the lungs of rats (10 μg/lane) was then denatured, resolved in 0.8% agarose-formaldehyde gels, and transferred to a Nytran filter (Schleicher & Schuell, Keene, NH), and UV cross-linked to the membrane. The quantity of RNA loaded in each lane was comparable, as evaluated by ethidium bromide staining of ribosomal RNA or by hybridization with a 1.2-kb glyceraldehyde-3-phosphate dehydrogenase (GAPDH) cDNA as an internal standard (ATCC, Rockville, MD). We previously described the MIP-2 cDNA utilized in this study and the predicted mRNA transcript size (26). Chemokine and GAPDH DNA was labeled by random priming (GIBCO-BRL, Bethesda, MD) and [^{32}P]dATP. Prehybridization and hybridization were carried out in 0.5 M $NaPO_4$ (pH 7.2), 1 mM EDTA, 7% sodium dodecyl sulfate (SDS), 150 μg tRNA/10 ml hybridization solution at 65°C (13). Blots were washed in 0.1× saline sodium citrate (SSC)-1% SDS at 37°C and in 2× at 52°C for 15 min each before autoradiography. In each experiment, mRNA levels were quantitated by scanning densitometry. Ethidium bromide staining of ribosomal RNA and hybridization with GAPDH cDNA were used to evaluate total RNA quantities analyzed per lane.

Quantitative densitometric scanning was performed with a Macintosh Quadra 650, Hewlett Packard Scan Jet IIcx DeskScan II (version 2.0) for scanning the autoradiograph, and NIH Image (version 1.52) to quantitate the darkness of the bands in question. All bands on an autoradiograph were evaluated as one image, and the message in each lane was normalized to the GAPDH signal to ensure that interpretation of the level of mRNA expression was not altered by uneven loading of the lanes or by the scanning process. Densitometric scanning results are expressed as a percentage of the GAPDH signal.

Characterization of PMN chemotactic factors in BALF. The ability of BAL to promote PMN chemotaxis was measured with a Neuroprobe 96-well microchemotaxis chamber, as

previously described (9, 10). Briefly, PMN were obtained from a peritoneal exudate induced by glycogen (Sigma Chemical) and purified (>94% PMN) utilizing a discontinuous two-step Nycodenz (Nycomed AS, Diagnostics Division, Oslo, Norway) gradient (8). After their purification, PMN were stained with 2',7'-bis(carboxyethyl)-5(6)-carboxyfluorescein acetoxymethyl ester (BCECF-AM) (Molecular Probes, Eugene, OR), and 44 ml of the BCECF-AM-labeled PMN (5×10^6 cells/ml) were added to the top wells of the chemotaxis chamber. A 10-mm thick, 3-mm porosity black (reduced florescence) polycarbonate filter (Neuroprobe, Cabin John, MD) separated the top wells from the bottom wells which contained 15 ml of lavage fluid (1:5, 1:10, 1:20, and 1:40 dilutions), zymosan-activated serum (ZAS; positive control), or RPMI 1640 media (negative control). The chemotaxis chamber was incubated for 30 min at 37°C in humidified air with 5% CO_2. After incubation, nonmigrating cells were removed from the side of the filter facing the top wells by gently washing it three times with PBS (pyrogen-free PBS, Sigma Chemical). The filter was then air-dried in the dark. Migration of cells into the filter was quantified in a Cytoflur 2300 96-well plate reader (Millipore, Bedford, MA) with an excitation filter of 485/20 nm, emission filter of 530/30 nm, and sensitivity of 3. Samples were analyzed in and results normalized to maximal chemotaxis toward the positive control (ZAS, 1×10^{-1} dilution) after the negative control had been subtracted.

Statistical Analysis

The data were expressed as means and SE. One-way analysis of variance followed by Bonferroni multiple comparisons test was used to compare all experimental groups. Values were considered significant when $P < 0.05$ (15).

RESULTS

Alveolar Macrophage and Leukocyte Counts

The changes in the cells populating the airspaces of rats that received aerosolized liposome-containing clodronate are shown in Fig. 1. The number of alveolar macrophages decreased within 6 h of aerosolization of liposomes containing clodronate; there was no change in the number of alveolar macrophages or PMN in the rats that received aerosolized liposomes not containing the drug or in rats that received aerosolized PBS(−) (Table 1). Alveolar macrophages recovered in the BAL were reduced to less than or equal to 5% of the normal number within 48 h of aerosolization of the clodronate-containing liposomes, and the number of alveolar macrophages remained decreased for 7 days (Fig. 1). Using this technique, we were able to deplete 95% of the alveolar macrophages, the most complete depletion yet reported (3). All macrophages that were recovered were viable based on the trypan blue exclusion. The normal number of alveolar macrophages was restored ~3 wk after the aerosolization of the clodronate-containing liposomes.

Clodronate is not known to have an effect on PMN, and aerosolization of free clondronate did not decrease the number of PMN in lavage fluid (Table 1). However, peripheral leukocyte counts were done on animals in each experimental condition ($n = 6$) to investigate whether the aerosolization of the clodronate-containing liposomes had an effect on peripheral PMN counts. Rats that had received aerosolized PBS(−) and then were anesthetized 3 days later had initial peripheral PMN counts of 607 ± 85 cells/μl (mean ± SE) that increased to 3,353 ± 821 cells/μl after the 4 h of airspace bacteria. Rats that had received aerosolized clodronate-containing liposomes 3 days before anesthesia had initial peripheral PMN counts of 600 ± 59 cells/μl that increased to 4,540 ± 707 cells/μl 4 h after the instillation of airspace bacteria. Rats that had not received any aerosolization and did not have bacterial instillations had initial peripheral PMN counts of 690 ± 176 cells/μl that increased to 2,737 ± 300 cells/μl after 4 h of anesthesia. Finally, rats that had received aerosolized clodronate-containing liposomes 3 days before a 4-h anesthesia, but did not receive airspace bacterial instillations, had initial peripheral PMN counts of 627 ± 35 cells/μl and final PMN counts of 3,853 ± 821 cell/μl. There is no statistical difference among these groups, suggesting that there is no effect by the clodronate-containing liposomes on the peripheral PMN count.

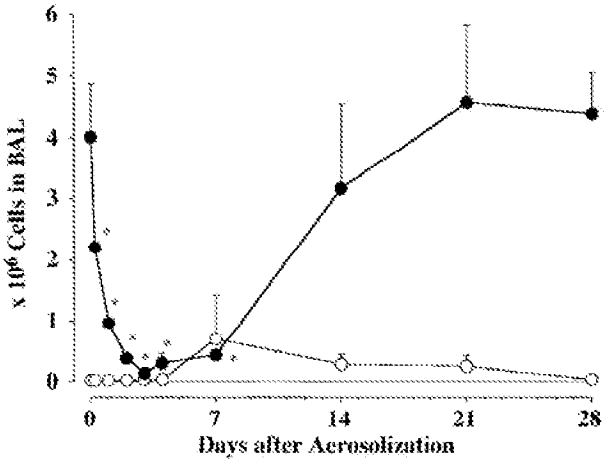

Fig. 1. No. of neutrophils (○; PMN) and macrophages (●) in bronchoalveolar lavage fluid (BALF) obtained from rats treated with aerosolized clodronate-containing liposomes. Rats were exposed to aerosolized clodronate-containing liposomes and then lavaged 6 h, 24 h, 48 h, 14 days, and 21 days after aerosolization. The nadir in alveolar macrophage counts was achieved 3 days after aerosolization. Macrophage counts remained decreased for 7 days and then normalized by 21 days. PMN counts remained nearly zero, except in rats lavaged 7 days after aerosolization; however, even these rats had very low counts except for 1 animal. Each point represents data from 4 animals; there was a significant reduction in no. of macrophages at 6 h, 1 day, 2 days, 3 days, 4 days, and at 7 days compared with controls treated with phosphate-buffered saline without calcium [PBS(−)] (means ± SE). * Significant at $P < 0.05$.

Table 1. *No. of cells in bronchoalveolar lavage 3 days after aerosolization*

Treatment	n	Total Macrophages in Lavage ($\times 10^6$)	Total PMN in Lavage ($\times 10^6$)
No pretreatment	4	4.02 ± 1.71	0.02 ± 0.01
Vehicle liposome aerosol	3	3.73 ± 0.42	0.02 ± 0.02
Clodronate liposome aerosol	4	0.14 ± 0.06*	0.04 ± 0.03
Free clodronate aerosol	3	1.23 ± 0.20*	0.02 ± 0.02

Values are means ± SE. PMN, polymorphonuclear leukocytes; n, no. of experiments. *Significant at 95% CL. Liposomes buffered saline (PBS) aerosol.

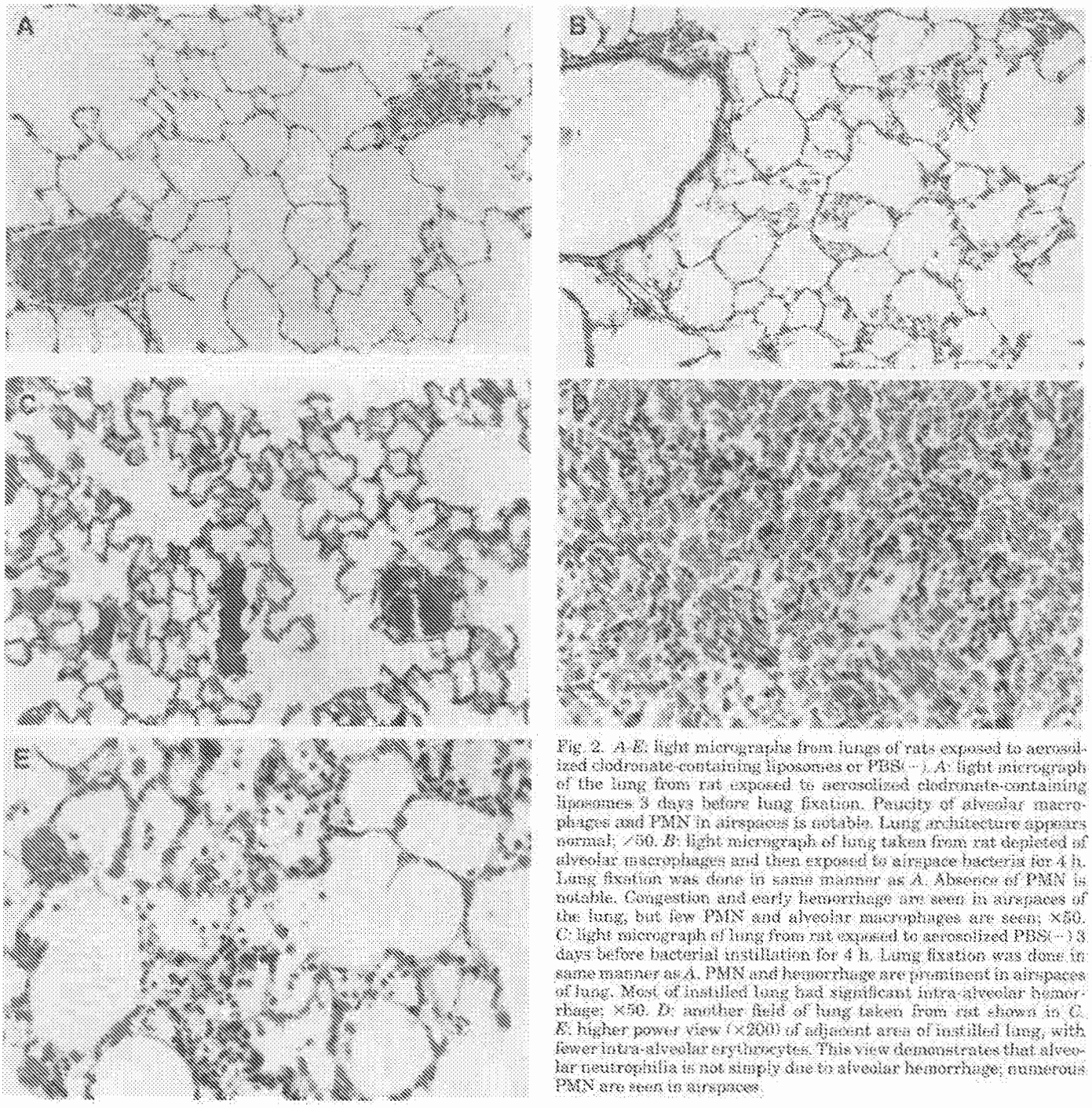

Fig. 2. *A–E*: light micrographs from lungs of rats exposed to aerosolized clodronate-containing liposomes or PBS(−). *A*: light micrograph of the lung from rat exposed to aerosolized clodronate-containing liposomes 3 days before lung fixation. Paucity of alveolar macrophages and PMN in airspaces is notable. Lung architecture appears normal; ×50. *B*: light micrograph of lung taken from rat depleted of alveolar macrophages and then exposed to airspace bacteria for 4 h. Lung fixation was done in same manner as *A*. Absence of PMN is notable. Congestion and early hemorrhage are seen in airspaces of the lung, but few PMN and alveolar macrophages are seen; ×50. *C*: light micrograph of lung from rat exposed to aerosolized PBS(−) 3 days before bacterial instillation for 4 h. Lung fixation was done in same manner as *A*. PMN and hemorrhage are prominent in airspaces of lung. Most of instilled lung had significant intra-alveolar hemorrhage; ×50. *D*: another field of lung taken from rat shown in *C*. *E*: higher power view (×200) of adjacent area of instilled lung, with fewer intra-alveolar erythrocytes. This view demonstrates that alveolar neutrophilia is not simply due to alveolar hemorrhage; numerous PMN are seen in airspaces.

In contrast to previous studies where clodronate-containing liposomes were delivered as a bolus into the tracheas of animals (3), the aerosolization of clodronate-containing liposomes did not cause an increase in the number of PMN in the airspaces of our treated animals (Table 1). The amount of lipid and clodronate that is delivered to the airspaces of the lung by aerosolization is ~100-fold smaller than that delivered by tracheal instillation (see METHODS). Furthermore, we did histologic sections on a rat in which we instilled clodronate-containing liposomes intratracheally in a similar dose to that which had been given in previous studies (3). The instillation of these liposomes in a bolus caused airspace neutrophilia (data not shown), as had been noted previously.

The liposomes containing clodronate were clearly superior to clodronate alone; four rats received aerosolized clodronate (not in liposomes) and the number of alveolar macrophages in their lavage fluid exceeded the number found in rats that had received aerosolization of liposome-encapsulated clodronate (Table 1). Light microscopy confirmed that the rats depleted of alveolar macrophages did not have PMN infiltration into the airspaces of the lungs (Fig. 2). Cytologic analysis mea-

sured lactate dehydrogenase (LDH) levels in the bronchoalveolar lavage (BAL) fluids obtained from rats that had received aerosolized clodronate-containing liposomes. The LDH levels in this fluid were the same as the LDH levels in BALF obtained from non-treated rats (3 ± 1 vs. 5 ± 1.7 IU, respectively). Therefore, the procedure and liposomes utilized did not cause neutrophilia, changes in lung morphology, or increased LDH levels in the airspaces of the lung.

The permeability of the alveolar epithelium to protein tracers was determined. Permeability changes occur when the alveolar epithelium has been injured, as occurs when live bacteria are instilled into the airspaces (16). With the use of radioactive protein tracers in the airspaces and in the vascular compartment, as we have done before (22), the alveolar epithelial permeability to these protein tracers was determined after the aersolization of the clodronate-containing liposome, or the liposomes not containing the drug, or the PBS(−) vehicle. All the permeabilities were found to be the same as in the control animals (Table 2). Therefore these results indicate that neither the aerosolizations of the liposomes nor the aerosolizations of the liposomes containing clodronate increased alveolar epithelial permeability and confirm that the technique and materials used did not cause lung injury or inflammation.

The rats that had received clodronate-containing liposomes and then were exposed to airspace bacteria for 4 h continued to have very low alveolar macrophage counts in their BAL (Fig. 3). Surprisingly, the PMN counts in these lavage fluids were nearly zero (Fig. 3). In contrast, the PMN counts in the BAL from rats that had received empty liposomes or PBS(−) were 1–1.5 × 10^6 (Fig. 3). Also, the histologic sections taken from the rats treated with PBS(−) and then received airspace bacteria for 4 h showed significant alveolar hemorrhage and neutrophilia (Fig. 2, *C* and *D*) that was not present in the depleted rats (Fig. 2*B*). Lung homogenates were cultured terminally, and there were no differences between the bacterial counts of these homogenates despite the three different pretreatments (data not shown).

To determine whether alveolar macrophage depletion affected the airspace migration of PMN in more severe lung infections, we used a 10-fold higher inoculum in eight other rats. In four rats pretreated with aerosols of PBS(−) and then 3 days later instilled with 5 × 10^7 CFU of the bacteria for 4 h, an average of 10.6 ± 5.4 ×10^6 PMN/μl were obtained in the BALF. These rats had 1.2 ± 0.4 × 10^6 macrophages/μl. In four other rats pretreated with aerosolized clodronate-containing liposomes and then instilled 3 days later with 5 × 10^7 CFU of bacteria for 4 h, the BALF contained an average of 2.7 ± 0.5 × 10^6 PMN/μl. These rats were depleted of alveolar macrophages; their BAL contained an average of 0.1 ± 0.06 ×10^6 macrophages/μl. The differences between the PMN counts in the animals pretreated with PBS(−) and the animals pretreated with clodronate were significantly different (*P* value is 0.01), as was the difference between the macrophage counts (*P* value of 0.01).

Table 2. *Bi-directional movement of tracer proteins over 4 h*

Experimental Condition	*n*	% ^{125}I in Lung	% ^{125}I in Blood	% Ratio of ^{125}I Alveolar/Plasma
PBS(−)	6	96.3 ± 3.6	0.7 ± 0.5	6.8 ± 2.2
Vehicle liposome	3	98.2 ± 1.3	0.3 ± 0.1	5.8 ± 0.9
Clodronate liposome	6	98.8 ± 1.3	0.6 ± 0.4	6.2 ± 3.3

Values are means ± SE. PBS(−), PBS without calcium; *n*, no. of experiments.

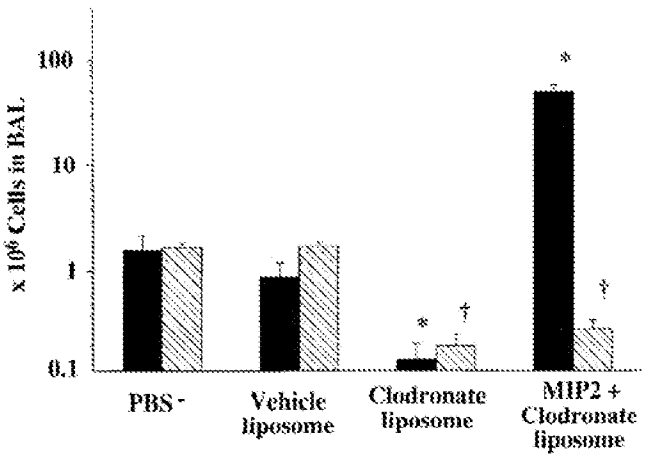

Fig. 3. No. of PMN (solid bars) and alveolar macrophages (hatched bars) in BALF obtained from pretreated rats exposed to airspace bacteria for 4 h. Each experiment was performed on 3 rats per group. Infected rats pretreated 3 days previously with aerosolized PBS(−) had ~1.5 × 10^6 PMN and alveolar macrophages in their BAL. Infected rats pretreated 3 days previously with aerosolized empty (vehicle) liposomes had similar findings, ~1 × 10^6 PMN and 1.6 × 10^6 alveolar macrophages in their BAL. There was no statistical difference between cell counts in these 2 experimental groups. Statistically significant decreases in both PMN and macrophage cell counts (as compared with both PBS(−)- and vehicle liposome-pretreated rats) were measured in BALF obtained from infected depleted rats that had been pretreated 3 days previously with aerosolized clodronate-containing liposomes [$P < 0.01$ for comparison to PBS(−) and $P < 0.05$ for comparison to vehicle liposome]. Rats were pretreated with aerosolized clodronate-containing liposomes, and 3 days later recombinant macrophage inflammatory protein-2 (MIP-2) was instilled. Note the statistically significant increase of PMN in BAL ($P < 0.001$ for comparisons to all other groups), while macrophage no. remained statistically significantly decreased ($P < 0.05$) compared with PBS(−)- or vehicle liposome-pretreatment groups. These results suggest that the depletion of alveolar macrophages lead to a decrease in chemotactic factors, causing the decrease in PMN in infected airspaces. Animals depleted of alveolar macrophages were able, however, to respond normally to instilled chemotactic factor. *Significant at $P < 0.01$; †significant at $P < 0.05$.

To ascertain whether the liposomes containing clodronate had somehow inhibited chemotactic activity by a mechanism independent of alveolar macrophage depletion, we instilled recombinant MIP-2 into rats depleted of alveolar macrophages. The lavage fluids from these rats contained 8 × 10^7 PMN, a response similar to that seen in nondepleted rats given this dose of MIP-2 (9) (Fig. 3). These results suggested that the depletion of alveolar macrophages caused a decrease in factors affecting PMN chemotaxis and that the depleted animals were still able to respond to instilled chemotactic factors. These results led us to assay chemotaxis and some of the products produced by alveolar macrophages that influence PMN, including TNF-α, MIP-2, and CINC/gro.

Chemotactic Factors

The amount of PMN chemotactic factors was evaluated in rats pretreated with either PBS(−), empty liposomes, or clodronate-containing liposomes 3 days before an airspace bacterial challenge for 4 h (Fig. 4). The BALF from rats that had received aerosolized PBS(−) or empty liposomes had similar amounts of chemotactic factors. In contrast, in the lavage fluids obtained from the rats that had received aerosolized clodronate-containing liposomes 3 days before the instillation of the bacteria, only minimal amounts of chemotactic factors were detected (Fig. 4).

TNF-α and CINC/gro Levels

The concentrations of TNF-α as well as CINC/gro were significantly decreased in the lavage fluids obtained from the rats that had received aerosolized clondronate-containing liposomes 3 days before the instillation of airspace bacteria, compared with the concentrations of these factors in the other experimental groups (Figs. 5 and 6). The concentrations of TNF-α in the lavage fluids obtained from the rats that had received aerosolized empty liposomes 3 days before bacterial instillation were insignificantly lower than the concentrations found in the rats treated with PBS(−). Depletion of the alveolar macrophages decreased the TNF-α concentration in the BAL to almost zero.

The concentration of CINC/gro was decreased significantly but less completely by the clodronate-containing liposome treatment. The aerosolization of empty liposomes did not decrease, but in fact insignificantly increased, the concentration of CINC/gro detected (Fig. 6). This result suggests that the empty liposomes did not affect chemotaxis.

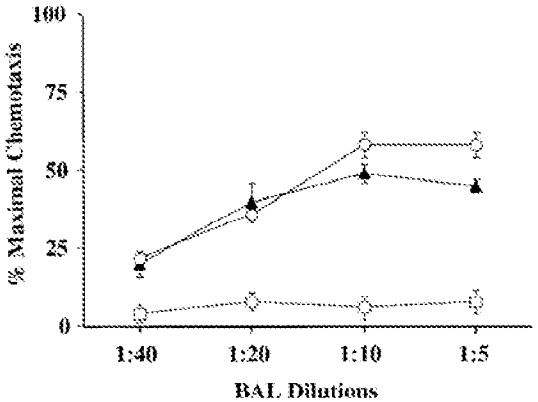

Fig. 4. BALF from macrophage-depleted rats does not cause PMN chemotaxis in vitro. Each experimental group contained 3 rats. The ability of airspace instilled bacteria (5×10^6 CFU) to promote production of PMN chemotactic factors was measured in rats pretreated with clodronate-liposomes (□; i.e., macrophage-depleted, $n = 3$), rats pretreated with empty liposomes (▲; $n = 3$), or rats treated with aerosolized PBS(−) (○; $n = 3$). Presence of NCF in BALF was measured in a modified Boyden chamber at several concentrations. Rats pretreated with either aerosolized PBS(−) or pretreated with aerosolized empty liposomes produced similar amounts of NCF in response to the bacterial airspace challenge; $P > 0.05$ for all dilutions tested. In contrast, macrophage-depleted rats produced significantly less NCF in their airspaces in response to airspace bacterial challenge compared with the 2 other groups; $P < 0.01$ for all dilutions of BAL; means ± SE.

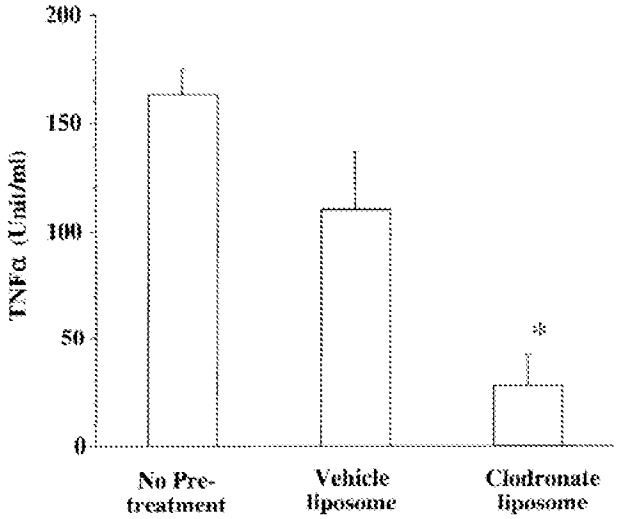

Fig. 5. Concentration of TNF-α in BALF obtained from infected rats depleted of alveolar macrophages is significantly decreased. Three groups of rats (each experimental group, $n = 3$) were pretreated with aerosolized PBS(−), empty vehicle liposomes, or clodronate-containing liposomes 3 days before bacterial instillation. After 4 h, BALF was obtained and TNF-α was assayed, using the WEHI-164 subclone 13 cytotoxicity assay. A log dose-response curve from 1 nmol to 1 mmol of clodronate added to fluids tested for TNF-α did not affect assay results. Infected rats pretreated with aerosolized PBS(−) or with aerosolized empty liposomes had significant amounts (>120 pg/ml) of TNF-α in their lavage fluids. In contrast, BAL obtained from infected rats pretreated with aerosolized clodronate-containing liposomes had <25 pg/ml of TNF-α. *$P < 0.05$ compared with both other treatment groups.

The concentration of CINC/gro was also measured in the experiments where the 10-fold larger inoculum (5×10^7 CFU) was instilled. In these experiments there was no difference between the levels of the CINC/gro be-

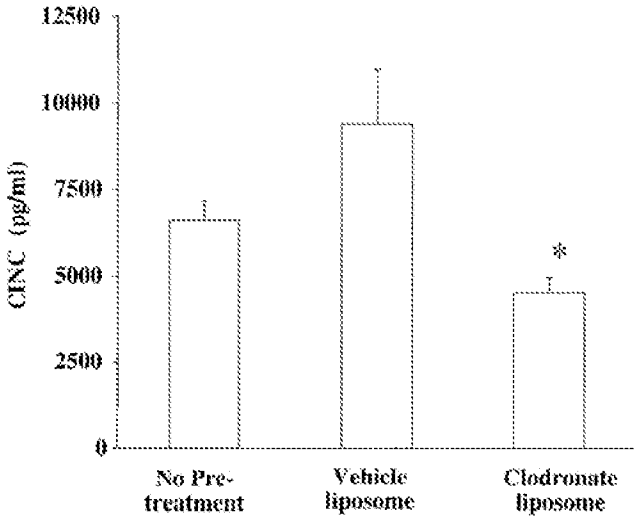

Fig. 6. CINC/gro concentration in BALF obtained from rats depleted of alveolar macrophages and then exposed to airspace bacteria is significantly decreased. Rats were exposed to aerosolized PBS(−) empty liposomes, or clodronate-containing liposomes; 3 days later, after anesthesia, bacteria were instilled into their airspaces ($n = 3$ for each experimental group). BALF was obtained 4 h later and assayed for CINC/gro, using a sandwich enzyme-linked immunosorbent assay. The only significant difference in CINC concentrations was found in infected rats pretreated with clodronate-containing liposomes. *$P < 0.05$ compared with both other treatment groups.

tween the animals that received PBS(−) pretreatment and then the larger bacterial inoculum (5,728 ± 1,361 pg/ml) and the levels measured in the animals that were depleted of alveolar macrophages and then had a larger inoculum instilled (6,450 ± 1,271 pg/ml).

MIP-2 Northern Blots

Figure 7 shows the three groups of rats in these studies. Half the rats received bacteria and half did not. None of the rats that were not given bacteria had expression of mRNA for MIP-2. Note that the rats that received aerosolized PBS(−) and then 3 days later had bacterial instillations had a large amount of mRNA for MIP-2 detected on their autoradiographs (Figs. 7 and 8). Rats that had received aerosolized empty liposomes 3 days before the instillation of the airspace bacteria did have a slight decrease in their detectable mRNA for MIP-2 (Figs. 7 and 8). However, the rats that received aerosolized clodronate-containing liposomes 3 days before the instillation of airspace bacteria had very little mRNA for MIP-2 detected, suggesting a profound effect by alveolar macrophage depletion on the expression of this chemokine (Figs. 7 and 8).

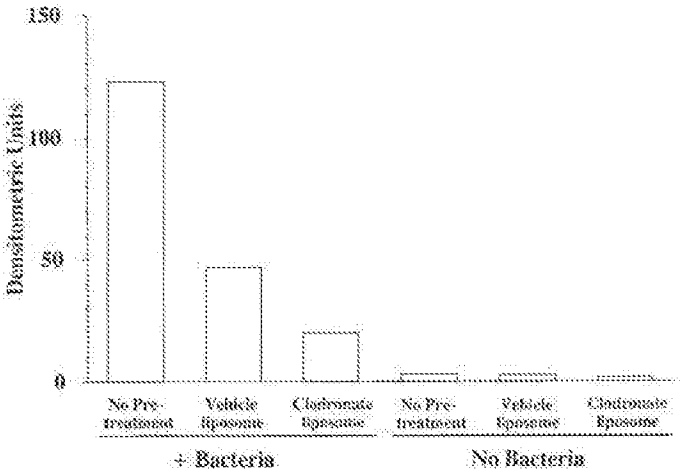

Fig. 8. Values for MIP-2 are expressed as % maximum signal. Graphic representation of scanning densitometry results of MIP-2 mRNA expression found in experiments shown in Fig. 7. Note that mRNA expression in rats exposed to aerosolized clodronate-containing liposomes was significantly decreased. There was no mRNA expression for MIP-2 in rats that were pretreated with aerosolized empty liposomes or clodronate-containing liposomes or that had not received pretreatment and did not receive airspace bacteria. Pretreatment with liposomes or vehicle did not cause expression of MIP-2 mRNA.

DISCUSSION

The alveolar macrophage plays a critical role in host defense against lung bacterial pathogens (11, 20, 21, 24). However, the role of the alveolar macrophage in initiating PMN infiltration into infected airspaces has not been fully explored. We wondered whether depletion of alveolar macrophages would decrease the lung macrophage-derived chemoattractant cytokines and lead to decreased neutrophilia in infected airspaces.

In rats depleted of alveolar macrophages, the instillation of moderate or large inoculums of live *P. aeruginosa* into the rat's lungs failed to cause the expected number of PMN (seen in nondepleted animals) to enter the airspaces, as demonstrated by BAL cell counts and a paucity of PMN on morphological sections. The initial PMN response in the airspaces to the moderate dose of bacteria was examined in great detail for several reasons. At the moderate dose of 5×10^6 CFU, this bacteria causes less alveolar epithelial damage (16), the bacteria does not disseminate, and therefore the PMN response in the airspace may reflect the effect of the alveolar macrophage depletion and perhaps would be less influenced by systemic responses.

The normal bacterial-induced increase of TNF-α and CINC/gro levels was found to be significantly attenuated in the BAL obtained from the animals depleted of alveolar macrophages that received this moderate inoculum. The BALF from these depleted rats had significant decreases in measured chemotactic activity compared with the BALF of PBS(−)-pretreated or empty liposome-pretreated rats that received the same size inoculum of bacteria. The mRNA expression for MIP-2 was found to be decreased in the lungs of the rats depleted of alveolar macrophages that were exposed to the airspace bacteria. Therefore the presence of a normal complement of alveolar macrophages appears essential for the initial entry of the expected number of PMN into infected airspaces.

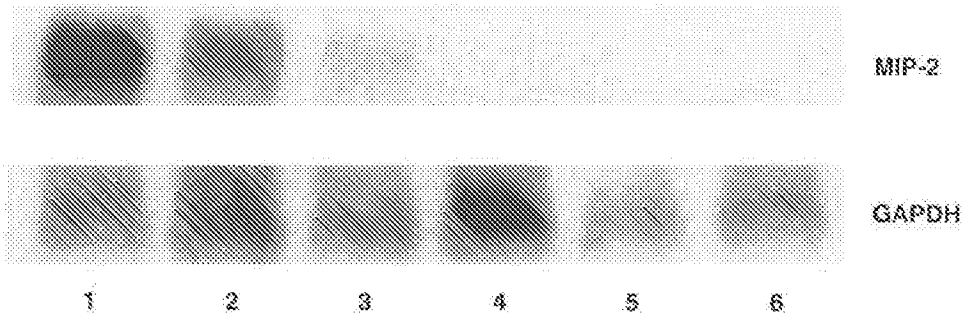

Fig. 7. Macrophage-depleted rats have decreased expression of MIP-2 mRNA after airspace challenge with bacteria. Northern blot analysis of MIP-2 mRNA collected from whole lung homogenates was performed on lungs obtained from rats in 3 pretreatment groups: untreated controls (*lanes 1* and *4*), rats pretreated with empty liposomes (*lanes 2* and *5*), and rats pretreated with clodronate-containing liposomes (*lanes 3* and *6*). After this initial treatment, rats either were exposed to an airspace challenge of bacteria (*lanes 1–3*) or had no bacterial instillation (*lanes 4–6*). Northern blot was probed with ^{32}P-labeled MIP-2, or GAPDH cDNA as an internal standard. Densitometric data were normalized on basis of hybridization to GAPDH mRNA, which corresponded closely with ethidium bromide staining of mRNA.

The number of PMN did increase in the depleted rats exposed to the larger bacterial inoculum, although the number of airspace PMN was still significantly decreased compared with the nondepleted infected rats. However, the results from the animals receiving the larger inoculum are more difficult to interpret, as the bacteria used in these experiments are cytotoxic to the alveolar epithelium at the larger dose utilized (5×10^7 CFU) and disseminate to the bloodstream at this dose. Therefore the PMN influx in the animals depleted of alveolar macrophages in the animals receiving the larger inoculum will reflect complement activation secondary to dissemination as well as other systemic factors. Nonetheless, significantly fewer PMN entered the airspaces in the rats depleted of alveolar macrophages, even after the instillation of the larger inoculum. Therefore, despite airspace injury, bacterial dissemination and systemic factors increasing chemotaxis, the depletion of alveolar macrophages caused a significant decrease in the PMN influx into the infected airspaces.

A number of other factors merit consideration. Not all possible macrophage-derived chemotactic factors were assessed. Also, we could achieve only 95% depletion of the normal number of alveolar macrophages, so there may have been some effect from the remaining macrophages. Nonetheless, depletion of 95% of the alveolar macrophages was associated with significantly decreased numbers of PMN in the airspaces of lungs filled with moderate or large inoculums of live bacteria. The administration of either liposomes or of clodronate was not associated with this finding, suggesting that these drugs did not cause the decrease in the numbers of PMN that entered the infected lungs. Rats depleted of alveolar macrophages using clodronate-containing liposomes were able to respond to the instillation of a chemotactic factor (MIP-2), and the expected numbers of PMN entered their airspaces. Therefore the clodronate and the liposomes did not appear to affect the results; the depletion of the alveolar macrophages led to the decreased PMN infiltration into infected lungs.

Depletion of alveolar macrophages has been achieved in the past with the use of the administration of silica, asbestos, colloidal carbon, trypan blue, carrageenan, and alpha emission. However, these methods were neither specific nor complete and often produced systemic responses after these interventions. We chose to deplete alveolar macrophages with the use of liposomes containing clodronate, because previous investigators using this technique had succeeded in depleting 70% of the alveolar macrophages (3, 28, 29). The exact mechanism of action by clodronate is not known. Van Rooijen (29) postulates that clodronate's strong affinity for calcium ions and its chlorine groups aid in the ability of this chemical to eliminate macrophages.

Modifying the published techniques for the use of clodronate-containing liposomes to deplete alveolar macrophages (3, 28, 29), we were able to more completely rid the airspaces of alveolar macrophages without causing alveolar epithelial injury or an influx of PMN. One of our modifications included the use of oligolamellar liposomes made by the reverse-evaporation method (25). This enabled us to encapsulate more clodronate in these liposomes compared with smaller unilamellar liposomes or multilamellar liposomes. Because the aerosolization of clodronate alone did not eliminate alveolar macrophages as completely, our formulation of liposomes clearly increased macrophage ingestion of the drug.

The use of an aerosol chamber to ensure more uniform distribution of the clodronate-containing liposomes to both lungs was also an important modification of previous techniques. Berg et al. (3) used intratracheal insufflation of clodronate-containing liposomes. They were able to deplete ~70% of the alveolar macrophages found in control animals; however, they also found that ~1 million PMN entered the airspaces 3 days after their tracheal instillation of the clodronate-containing liposomes (3). In contrast, BALF obtained from rats 3 days after aerosolization of the clodronate-containing liposomes revealed few if any PMN. A lack of inflammation or alveolar epithelial damage was further confirmed by the morphology results and the experiments utilizing radioactive protein tracers in the airspaces of the lung and in the vascular compartment. There was no increase in the bi-directional movement of the radioactive tracers after the delivery of the clodronate-containing liposomes. These results suggest that there was no increase in the permeability of the alveolar epithelium (16, 22). Furthermore, alveolar liquid clearance (data not shown) was normal in these experiments, as were LDH levels in the BALF, suggesting that the alveolar epithelium was functioning in a normal fashion (16, 22) and that there was no significant cellular injury. Therefore, these results suggest our modifications have improved the published technique to make alveolar macrophage depletion more efficacious and less toxic to the lung.

Others have found that macrophage depletion is associated with a decrease in TNF-α (2, 3). However, as 95% of the alveolar macrophages were destroyed by our technique, the levels of TNF-α measured in these depleted rats are the lowest reported. The levels of TNF-α measured corroborate the extent of the depletion of alveolar macrophages and the importance of the alveolar macrophage to TNF-α production in the airspaces. Finally, we did not find that concentrations of clodronate well above those that would be expected in BALF after the administration of the small doses of clodronate we administered, affected the assay used for TNF-α.

MIP-2 and CINC/gro were measured, as they have been identified in rats as two significant chemokines that are involved in PMN chemotaxis (9, 10, 13, 14, 30). MIP-2 and CINC/gro are members of the IL-8 or PF-4 cytokine super family (9, 10, 13, 14, 30). MIP-2 mRNA levels have been found to be upregulated in rat models of chronic bronchitis (7) and endotoxin-induced lung injury (10). Furthermore, a recent study found that the intratracheal instillation of MIP-2 caused a significant influx of PMN into the airspaces of the lung and caused PMN activation (9). These results suggest that MIP-2 is important in PMN recruitment during acute inflammation in rat disease models. CINC/gro appears to be similar to rat KC (14, 30). CINC/gro appears to be an

important, but clearly not the exclusive, mediator of PMN activation and recruitment into inflamed rat lungs (14, 30).

In conclusion, we have modified published techniques for depletion of alveolar macrophages and have been able to deplete at least 95% of the alveolar macrophages in the lavage fluid without causing PMN infiltration into the lung. Depletion of 95% of the alveolar macrophages in rats, followed by the instillation of live bacteria into the airspaces of their lungs, resulted in airspaces filled with bacteria and abnormally low numbers of PMN. Measurement of some of the alveolar macrophage products involved with PMN chemotaxis showed these factors to be significantly decreased. These results suggest that the lack of alveolar macrophages can lead to a decrease in the number of PMN in infected lungs, probably secondary to a critical decrease in the macrophage-derived chemotactic factors. One implication of these results is that significant alteration of alveolar macrophage number or perhaps function could affect chemotaxis of PMN into infected lungs.

The authors wish to thank Richard Shanks for his technical help with the experiments and Dr. Norman Staub for his advice regarding the experiments.

This work was supported by National Institutes of Health Grants HL-49810 (J. Wiener-Kronish), GM-52654 (G. Bagby), and HL-19170 (L. Kobzik); by a Cystic Fibrosis Grant (J. Wiener-Kronish); and by a Travel Grant from the Japanese Ministry (S. Hashimoto).

Address for reprint requests: J. Wiener-Kronish, Box 0624, Dept. of Anesthesia/Critical Care, Univ. of California, San Francisco, CA 94143–0624.

Received 12 April 1995; accepted in final form 29 November 1995.

REFERENCES

1. **Barlet, G. R.** Phosphate assay. *J. Biol. Chem.* 234: 466–468, 1959.
2. **Bautista, A. P., N. Skrepnik, M. R. Niesman, and G. J. Bagby.** Elimination of macrophages by liposome-encapsulated dichloromethylene diphosphonate suppresses the endotoxin-induced priming of Kupffer cells. *J. Leukocyte. Biol.* 55: 321–327, 1994.
3. **Berg, J. T., S. T. Lee, T. Thepen, C. Y. Lee, and M. F. Tsan.** Depletion of alveolar macrophages by liposome-encapsulated dichloromethylene diphosphonate. *J. Appl. Physiol.* 74: 2812–2819, 1993.
4. **Cardozo, C., J. Edelman, J. Jagirdar, and M. Lesser.** Lipopolysaccharide-induced pulmonary vascular sequestration of polymorphonuclear leukocytes is complement independent. *Am. Rev. Respir. Dis.* 144: 173–178, 1991.
5. **DeForge, L. E., J. S. Kenney, M. L. Jones, J. S. Warren, and D. G. Remick.** Biphasic production of IL-8 in lipopolysaccharide (LPS)-stimulated human whole blood. Separation of LPS- and cytokine-stimulated components using anti-necrosis factor and anti-IL-1 antibodies. *J. Immunol.* 148: 2133–2141, 1992.
6. **Espevik, T., and M. J. Nissen.** A highly sensitive cell line, WEHI 164 clone 13, for measuring cytotoxic factor/tumor necrosis factor from human monocytes. *J. Immunol. Meth.* 95: 99–105, 1986.
7. **Farone, A., S. Huang, J. D. Paulauskis, and L. Kobzik.** Airway neutrophilia and chemokine mRNA expression in SO_2-induced bronchitis. *Am. J. Respir. Cell Mol. Biol.* 12: 345–350, 1995.
8. **Freeman, G. E., C. A. Dalton, and P. M. Brooks.** A nycodenz gradient method for the purification of neutrophils from peripheral blood of rats. *J. Immunol. Meth.* 139: 241–249, 1991.
9. **Frevert, C. W., A. Farone, H. Danaee, J. D. Paulauslis, and L. Kobzik.** Functional characterization of the rat chemokine macrophage inflammatory protein-2. *Inflammation* 19: 133–142, 1995.
10. **Frevert, C. W., A. Warner, and C. Kobzik.** Defective pulmonary recruitment of neutrophils in a rat model of endotoxemia. *Am. J. Respir. Cell Mol. Biol.* 11: 716–723, 1995.
11. **Goldstein, E., W. Lippert, and D. Warshauer.** Pulmonary alveolar macrophage. Defender against bacterial infection of the lung. *J. Clin. Invest.* 54: 519–528, 1974.
12. **Hansen, M. B., S. E. Nielsen, and K. Berg.** Re-examination and further development of a precise and rapid dye method for measuring cell growth/cell kill. *J. Immunol. Meth.* 119: 203–210, 1989.
13. **Huang, S., J. D. Paulauskis, J. J. Godleski, and L. Kobzik.** Expression of macrophage inflammatory protein-2 and KC mRNA in pulmonary inflammation. *Am. J. Pathol.* 141: 981–988, 1992.
14. **Iida, M., K. Watanabe, M. Tsurufuji, K. Takaishi, Y. Iizuka, and S. Tsurufuji.** Level of neutrophil chemotactic factor CINC/gro, a member of the interleukin-8 family, associated with lipopolysaccharide-induced inflammation in rats. *Infect. Immun.* 60: 1268–1272, 1992.
15. **Kleinbaum, P., L. Kupper, and K. Muller.** *One-Way Analysis of Variance.* Boston, MA: PWS-Kent, 1987, p. 341.
16. **Kudoh, I., J. P. Wiener-Kronish, S. Hashimoto, J. F. Pittet, and D. Frank.** Exoproduct secretions of *Pseudomonas aeruginosa* strains influence severity of alveolar epithelial injury. *Am. J. Physiol.* 267 (*Lung Cell. Mol. Physiol.* 11): L511–L556, 1994.
17. **Kunkel, S. L., T. Standiford, K. Kasahara, and R. M. Strieter.** Interleukin-8 (IL-8): the major neutrophil chemotactic factor in the lung. *Exp. Lung. Res.* 17: 17–23, 1991.
18. **Lovchik, J. A., and M. F. Lipscomb.** Role for C5 and neutrophils in the pulmonary intravascular clearance of circulating *Cryptococcus neoformans*. *Am. J. Respir. Cell Mol. Biol.* 9: 617–627, 1993.
19. **Nicas, T. I., and B. H. Iglewski.** Isolation and characterization of transposon-induced mutants of *Pseudomonas aeruginosa* deficient in production of exoenzyme S. *Infect. Immun.* 45: 470–474, 1984.
20. **Onofrio, J. M., G. B. Toews, M. F. Lipscomb, and A. K. Pierce.** Granulocyte-alveolar-macrophage interaction in the pulmonary clearance of *Staphylococcus aureus*. *Am. Rev. Respir. Dis.* 127: 335–341, 1983.
21. **Ozaki, T., M. Maeda, H. Hayashi, Y. Nakamura, H. Moriguchi, T. Kamei, S. Yasuoka, and T. Ogura.** Role of alveolar macrophages in the neutrophil-dependent defense system against *Pseudomonas aeruginosa* infection in the lower respiratory tract. Amplifying effect of muramyl dipeptide analog. *Am. Rev. Respir. Dis.* 140: 1595–1601, 1989.
22. **Pittet, J. F., M. A. Matthay, G. Pier, M. Grady, and J. P. Wiener-Kronish.** *Pseudomonas aeruginosa*-induced lung and pleural injury in sheep. Differential protective effect of circulating versus alveolar immunoglobulin G antibody. *J. Clin. Invest.* 92: 1221–1228, 1993.
23. **Rehm, S. R., G. N. Gross, and A. K. Pierce.** Early bacterial clearance from murine lungs. Species-dependent phagocyte response. *J. Clin. Invest.* 66: 194–199, 1980.
24. **Sibille, Y., and H. Y. Reynolds.** Macrophages and polymorphonuclear neutrophils in lung defense and injury. *Am. Rev. Respir. Dis.* 141: 471–501, 1990.
25. **Szoka, F. J., and D. Papahadjopoulos.** Procedure for preparation of liposomes with large internal aqueous space and high capture by reverse-phase evaporation. *Proc. Natl. Acad. Sci. USA* 75: 4194–4198, 1978.
26. **Tekamp-Olsen, P., C. Gallegos, D. Bauer, J. McClain, B. Sherry, M. Fabre, S. van Deventer, and A. Cerami.** Cloning and characterization of cDNAs for murine macrophage inflammatory protein 2 and its human homologues. *J. Exp. Med.* 172: 911–919, 1990.
27. **Thepen, T., N. Van Rooijen, and G. Kraal.** Alveolar macrophage elimination in vivo is associated with an increase in pulmonary immune response in mice. *J. Exp. Med.* 170: 499–509, 1989.
28. **Toew, G. B., E. J. Hansen, and R. M. Strieter.** Pulmonary host defenses and oropharyngeal pathogens. *Am. J. Med.* 88 *Suppl.*: 20S–24S, 1990.
29. **Van Rooijen, N.** The liposome-mediated macrophage "suicide" technique. *J. Immunol. Meth.* 124: 1–6, 1989.
30. **Watanabe, K., F. Koizumi, Y. Kurashige, S. Tsurufuji, and H. Nakagawa.** Rat CINC, a member of the interleukin-8 family, is a neutrophil-specific chemoattractant in vivo. *Exp. Mol. Pathol.* 55: 30–37, 1991.

Journal of Controlled Release 136 (2009) 30–37

Contents lists available at ScienceDirect

Journal of Controlled Release

Journal homepage: www.elsevier.com/locate/jconrel

Novel irinotecan-loaded liposome using phytic acid with high therapeutic efficacy for colon tumors

Yoshiyuki Hattori *, Li Shi, Wuxiao Ding, Kimiko Koga, Kumi Kawano, Motoki Hakoshima, Yoshie Maitani

Department of Fine Drug Targeting Research, Institute of Medicinal Chemistry, Hoshi University, Ebara 2-4-41, Shinagawa-ku, Tokyo, 142-8501, Japan

ARTICLE INFO

Article history:
Received 7 October 2008
Accepted 18 January 2009
Available online 24 January 2009

Keywords:
Liposomes
Phytic acid
CPT-11
Irinotecan
Colon tumor

ABSTRACT

Phytic acid (IP-6) is a polyphosphorylated carbohydrate with antitumor activity for many kinds of tumors. In this study, we developed a novel method of loading irinotecan (CPT-11) into liposomes using IP-6, and evaluated its antitumor effect on colon tumors *in vivo*. Liposomal CPT-11 was prepared by loading CPT-11 to distearoylphosphatidylcholine/cholesterol/methoxy-poly(ethyleneglycol)-distearylphosphatidylethanolamine liposomes prepared in IP-6 solution, $CuSO_4$ solution and citrate buffer, respectively (IP6-, Cu- and Cit-L). CPT-11 loading efficiency for IP6-L (90–100%) was higher than that for Cit-L (less than 40%), and similar to Cu-L when CPT-11 to total lipid weight ratio was increased from 0.2 to 0.6. Plasma elimination and biodistribution of liposomal CPT-11 and its metabolite SN-38 were measured after intravenous administration. IP6-L following *i.v.* injection showed 1.3- and 1.7-fold higher plasma area under the curves of CPT-11 and SN-38, respectively, than Cu-L. Finally, therapeutic activity was determined in mouse Colon 26 and human COLO 320DM tumor xenografts in mice. IP6-L significantly exhibited superior anticancer activity to Cu-L and free CPT-11 in Colon 26 tumor. Using IP-6 as a drug-trapping agent in liposome, IP6-L improved CPT-11 pharmacokinetics and increased antitumor activity in colon tumors.

1. Introduction

Irinotecan (CPT-11) is a water-soluble derivative of camptothecin, which is a natural alkaloid originally extracted from the Chinese tree *Camptotheca acuminata*. CPT-11 inhibits the resealing of single-strand DNA breaks mediated by topoisomerase I by stabilizing cleavable complexes [1–3]. CPT-11 has excellent antitumor activity against a variety of human xenografts *via* intravenous, intraperitoneal and oral administration. The clinical introduction of CPT-11 had a significant impact on cancer treatment, particularly colorectal adenocarcinoma [4,5]. CPT-11 is subjected to an enzymatic conversion that yields a number of metabolites, including SN-38 [6,7], which is reported to be up to 1000-fold more active than CPT-11 *in vitro* [8]. Therefore, CPT-11 requires conversion to SN-38 for optimal activity yet must avoid inactivation *via* simple hydrolysis of the requisite lactone configuration to an inactive carboxylate. After intravenous administration of free CPT-11, less than 5% of CPT-11 is converted to SN-38, mainly in the liver. PEGylated liposomal CPT-11 has long circulation in the blood and will therefore improve conversion from CPT-11 to SN-38, and increase antitumor activity. Use of drug delivery technologies, such as a PEGylated carrier system including liposome, have focused on strategies to stabilize the lactone ring of CTP-11.

It has already been established that CPT-11 was encapsulated within liposomes using a remote loading method. CPT-11 can be actively loaded into liposomes *via* a transmembrane pH gradient using citrate [9], ammonium sulfate or ionophore A23187/divalent cation [10–12]. The acidified liposomal interior causes the loading and retention of CPT-11 with ionizable amine groups, however, the acidified liposome can introduce instability by hydrolyzing lipid at acidic pH during long-term storage. Recently, a loading method was developed using copper adjusted to neutral pH with triethanolamine (TEA) without generation of a pH gradient [10,13]; however, there is a possibility that serum copper causes systemic toxicity [14–16]. As an alternative, CPT-11 loading systems have been successful using a polyanionic trapping agent of either polyphosphate or sucrose octasulfate, adjusted to neutral pH with triethylammonium [17].

Phytic acid (inositol hexakisphosphate, IP-6) is also a naturally occurring negatively charged polyphosphorylated carbohydrate, and has been reported to reduce abnormal gene expression and to induce the expression of tumor suppressive gene in tumors [18–20]. In combination with doxorubicin in breast tumor cells, IP-6 synergically inhibited tumor growth [21,22]. We expected that negatively charged IP-6 could electrostatically interact with CPT-11 as a intraliposomal drug-trapping agent like polyphosphate [17] and might increase antitumor activities if it is co-encapsulated with CPT-11 in liposomes. In this report, therefore, we developed a novel CPT-11 loading system using IP-6 as a polyanionic trapping agent, and adjusted to pH 6.5 with TEA. A novel liposomal CPT-11 with IP-6 (IP6-L) was evaluated in terms of plasma elimination and the biodistribution of CPT-11 and its metabolite SN-38 after intravenous administration. Furthermore, the therapeutic activity of IP6-L was evaluated in mouse Colon 26 tumor and human COLO 320DM tumor xenografts in mice.

* Corresponding author. Tel./fax: +81 3 5498 5097.
E-mail address: yhattori@hoshi.ac.jp (Y. Hattori).

0168-3659/$ – see front matter © 2009 Elsevier B.V. All rights reserved.
doi:10.1016/j.jconrel.2009.01.013

2. Materials and methods

2.1. Materials

CPT-11 was a kindly gift from Yakult Co., Ltd. (Tokyo, Japan). Distearoylphosphatidylcholine (DSPC) and methoxy-poly(ethyleneglycol)-distearylphosphatidylethanolamine (PEG-DSPE, PEG mean molecular weight, 2000) were purchased from the NOF Corporation (Tokyo, Japan). SN-38 and cholesterol (Ch) were purchased from Wako Pure Chemical Industries, Ltd. (Osaka, Japan). IP-6 solution was obtained from Nacalai Tesque Inc. (Kyoto, Japan). RPMI-1640 medium and fetal bovine serum (FBS) were obtained from Invitrogen Corp. (Carlsbad, CA, USA). Other reagents were of analytical or HPLC grade.

2.2. Preparation of liposomal CPT-11

Liposomes were prepared by a modified ethanol injection method [23]. Briefly, DSPC, Ch and PEG-DSPE at a molar ratio of 55:45:5 (40 mg/16 mg/12.5 mg) were dissolved in ethanol. Ethanol was removed by rotary evaporation at 70 °C to a smaller volume until one-tenth of the volume of hydration buffers. To prepare liposomal IP-6, liposomal Cu and liposomal Cit, 1.5 mL of 100 mM IP-6 solution adjusted to pH 6.5 using triethanolamine (TEA), 300 mM $CuSO_4$ solution adjusted to pH 3.4 with H_2SO_4, and 500 mM citrate buffer adjusted to pH 3.0 with HCl were used as hydration buffer, respectively. Hydration buffer was added to the lipid-ethanol solution immediately, followed by extensive vortex mixing and sonication at 70 °C. Liposomal IP-6 and Cu were treated with 5 circles of freezing (−80 °C) and thawing (60 °C), and extraliposomal buffer was exchanged for SHE-buffer (300 mM sucrose, 20 mM HEPES and 15 mM EDTA, pH 7.4) by size exclusion chromatography on a Sephadex G-50 column. In liposomal Cit, extraliposomal pH was adjusted to 7.4 with NaOH before CPT-11 loading according to the pH gradient method [9]. The particle size distribution was measured by ELS-Z2 (Otsuka Electronics Co., Ltd., Osaka, Japan) at 25 °C after diluting the dispersion to an appropriate volume with water.

CPT-11 was added to liposomal IP-6, Cu and Cit at a desired CPT-11-to-DSPC weight ratio of 0.2 to 2.0 (equivalent to CPT-11-to-total lipid of 0.12 to 1.2), and incubated at 60 °C for 1 h for drug loading, and then quenched on ice for 5 min. Here, liposomal CPT-11 prepared by the pH gradient method with citrate buffer, and Cu- and IP-6-mediated methods were named as Cit-, Cu- and IP6-L, respectively. Unencapsulated CPT-11 was removed using a Sephadex G-50 column eluted with saline adjusted to pH 7.4. CPT-11 concentration was determined using a fluorometer (Wallac ARVO SX1420 multi-label counter, PerkinElmer Japan, ex: 375 nm, em: 535 nm) in a solubilized sample after the addition of an equal volume of cold acid methanol (5 mM HCl in methanol), and then the loading efficiencies of CPT-11 in the liposomes were calculated. The concentration of phospholipid (DSPC) was measured with the Phospholipids C-test Wako (Wako Pure Chemical Industries, Ltd.). IP-6 concentration in the liposome was determined by inductively coupled plasma (ICP) analysis (SPS7800, SII Nano Technology Inc., Tokyo, Japan). Briefly, the phosphorus concentration of IP-6 in IP6-L was calculated by subtracting the phosphorus concentration of empty liposomes from that of IP6-L.

2.3. Pharmacokinetic analysis

CPT-11 in saline and IP6-, Cu- and Cit-L were used for *in vivo* studies. Female ddY mice (5 weeks old; Sankyo Lab Service Corp., Tokyo, Japan) were injected with a single intravenous bolus *via* the lateral tail vein at a dose of 10 mg/kg. At 1, 6, 24 and 48 h after injection, blood was collected using a heparinized syringe and centrifuged to obtain plasma at 1500 g for 30 min. CPT-11 and SN-38 in plasma were extracted with the addition of an equal volume of cold acidic methanol. The mixture was vortexed for 10 s and incubated at −80 °C for more than 5 h until analysis. After thawing, the samples were centrifuged at 100,000 g for 30 min at 4 °C by ultracentrifugation (CS120 GXL, Hitachi, Japan) to remove aggregated protein. The supernatant was applied to a TSKgel ODS-80Ts QA 5 μm column (4.6 mm I.D.×25 cm, Tosoh, Co., Ltd., Tokyo, Japan) equilibrated in 75 mM ammonium acetate, 35% acetonitrile, pH 4.0, at a flow rate of 1 mL/min. CPT-11 and SN-38 were detected with an HPLC system (Shimadzu Co.) composed of an LC-10AS pump, an SIL-10A autoinjector and an RF-10A_{XL} fluorescence detector using an excitation wavelength of 375 nm and an emission wavelength of 530 nm. Under these conditions, CPT-11 and SN-38 were eluted at 4.7 min and 7.2 min, respectively. The CPT-11 dose%/mL plasma and dose% /g tissue were calculated by dividing the amount of CPT-11 per total plasma volume (mL) and per total tissue weigh (g), respectively, by that of the injected liposomal CPT-11. The total volume of plasma was calculated using the reported volume of mouse plasma, 48.8 mL/kg [24]. Pharmacokinetic parameters were calculated using the bootstrap method [25], including the plasma area under the curve (AUC) from 1 to 48 h, clearance (CL), mean residence time (MRT) and half life period ($T_{1/2}$).

2.4. Drug sensitivity in vitro

Murine colon carcinoma Colon 26 cells were obtained from the Cell Resource Center for Biomedical Research, Tohoku University (Miyagi, Japan). Human colorectal adenocarcinoma COLO 320DM cells were purchased from the American Type Culture Collection (Masassas, VA, USA). The cells were cultured in RPMI-1640 medium with 10% heat-inactivated FBS and 100 μg/mL kanamycin sulfate in a humidified atmosphere containing 5% CO_2 at 37 °C.

Colon 26 cells were seeded separately at a density of 1×10^3 cells per well in 96-well plates and maintained for 24 h before treatment in RPMI-1640 medium supplemented with 10% FBS. To examine cytotoxicity for IP-6, the cells were treated with medium containing from 0.0625 to 1 mM IP-6. For combination therapy, the cells were treated with medium containing various concentrations of CPT-11, ranging from 0.625 to 10 μM, or SN-38, ranging from 0.625 to 10 nM, in the presence or absence of 0.1 mM IP-6. The cells were incubated for 72 h. The cell number was determined with a cell counting kit (Dojindo Laboratories, Kumamoto, Japan). Cell viability was expressed relative to the absorbance at 450 nm of untreated cells.

2.5. CPT-11 biodistribution in Colon 26 tumor

To generate Colon 26 tumor, 1×10^6 cells suspended in 100 μL of RPMI medium were inoculated subcutaneously into the flank of female CDF1 mice (5 weeks of age; Sankyo Labo Service Corporation, Tokyo, Japan). The tumor volume was calculated using the formula: tumor volume $= 0.5\times a\times b^2$, where a and b are the larger and smaller

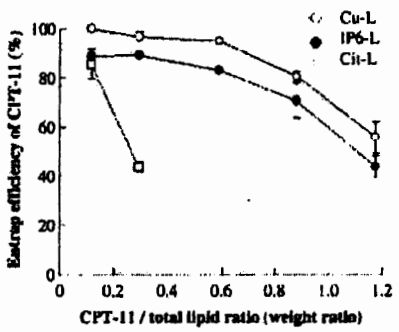

Fig. 1. The effect of the drug-to-lipid weight ratio on CPT-11 loading to liposomal Cit, Cu and IP-6 incubated at 60 °C for 1 h. The extent of CPT-11 encapsulation was determined. Each result represents the mean ± S.D. ($n=3$).

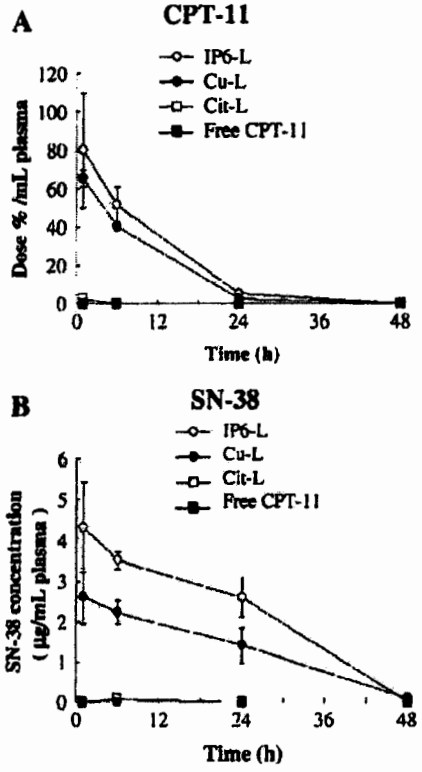

Fig. 2. Plasma CPT-11 dose% (A) and SN-38 concentration (B) in mice following a single intravenous injection dose of liposomal CPT-11 (equivalent to 10 mg CPT-11/kg) in ddY mice. The plasma concentration was determined as a function of a time. Data points represent the mean CPT-11 dose% (A) and SN-38 concentration (B) ± SD ($n = 3$).

diameters, respectively. When the average volume of the tumors reached 100–150 mm^3, CPT-11 solution and IP6-, Cu- and Cit-L were intravenously administered *via* lateral tail veins at a dose of 10 mg CPT-11/kg (24.7 mg lipid/kg). Twenty-four hours after injection, blood was collected with a heparinized syringe and centrifuged to obtain plasma. The tumor, liver, spleen, kidney and lung were excised and homogenized in phosphate-buffered saline (pH 7.4). CPT-11 and SN-38 were extracted with cold acid methanol and analyzed by the HPLC system as described above.

2.6. Therapeutic study

To generate COLO 320DM tumor xenografts, 1×10^7 cells suspended in 100 μl of RPMI-1640 medium were inoculated subcutaneously into the flank of female BALB/c nu/nu mice (5 weeks of age; CLEA Japan, Inc., Tokyo, Japan). Colon 26 tumors were generated as described above. When the average volume of Colon 26 tumor and COLO 320DM tumor xenografts reached 50–100 mm^3 (day 1), CPT-11 solution, and IP6- and Cu-L were injected (10, 20 or 60 mg/kg) into a tail vein at once or in three injections at three-day intervals. IP6-L administered at 20 mg CPT-11/kg resulted in co-administration of IP-6 at 36 mg/kg. IP6-L was concentrated with Amicon Ultra centrifugal filter devices (Millipore, MA, USA) when injected at 60 mg/kg. Tumor volume and body weights were measured for individual animals. Animal experiments were performed with approval from the Institutional Animal Care and Use Committee at Hoshi University.

2.7. Statistical analysis

The statistical significance of differences between mean values was determined using Welch's *t* test. Multiple comparisons were evaluated by analysis of variance (ANOVA) with Tukey's multiple comparison test. *P*-values less than 0.05 were considered significant.

3. Results

3.1. Preparation of liposomal CPT-11

IP-6 was used for the proposed novel loading process of CPT-11 in liposomes as an intraliposomal trapping agent to improve encapsulation efficiency and tumor toxicity. Liposomal IP-6 was prepared using 100 mM IP-6 solution adjusted with TEA to pH 6.5, in which total lipid concentration was 14.6 mg/mL. For comparison with traditional loading methods of CPT-11, we prepared liposomal Cu for the ion chelating method [10], and liposomal Cit for the pH gradient method [9]. In all cases, the average particle diameter of each liposome was approximately 100–150 nm with a narrow, monodisperse distribution (less than 0.2 in polydispersity index). After loading CPT-11 into the liposomes, all liposomal CPT-11 were approximately 150 nm in size (data not shown). IP6- and Cu-L at CPT-11 to total lipid ratios from 0.12 to 0.6 exhibited 90–100% loading efficiency (Fig. 1). In contrast, Cit-L showed only 40% loading efficiency at a CPT-11 to total lipid ratio of 0.3. At least two weeks after preparation, encapsulated CPT-11 in IP6-L was stable and did not release CPT-11 (data not shown). For this reason, in subsequent experiments, we prepared IP6-, Cu- and Cit-L at CPT-11 to total lipid weight ratios of 0.6, 0.6 and 0.12, respectively. The final CPT-11 concentration was 0.5–0.8 mg/mL, and drug-to-IP-6 (mol/mol) in IP6-L was 0.54.

3.2. Plasma CPT-11 and SN-38 levels in mice after intravenous injection of liposomal CPT-11

To investigate the stability of liposome *in vivo*, plasma dose% and concentrations of CPT-11 and SN-38 were shown in Fig. 2 and the pharmacokinetic parameters of IP6- Cit- and Cu-L were calculated (Table 1). After administration of free CPT-11 and Cit-L, CPT-11 was eliminated rapidly from plasma, and SN-38 had almost disappeared from plasma 24 h after injection. In contrast, IP6- and Cu-L maintained higher CPT-11 and SN-38 levels throughout 24 h (Fig. 2A and B). The AUC of CPT-11 in Cu- and IP6-L (1477.16 and 1929.35 μg h mL^{-1}) was 62- and 81-fold higher than that of Cit-L (23.83 μg h mL^{-1}), respectively. These trends were also observed in SN-38. Clearances of CPT-11 in IP6- and Cu-L were greatly reduced, but that of Cit-L was faster than those of IP6- and Cu-L, indicating that CPT-11 in Cit-L leaked rapidly from liposomes. MRT and $T_{1/2}$ for CPT-11 in Cu-L and IP6-L were longer than those in Cit-L. IP6-, Cu- and Cit-L had the

Table 1
The calculated CPT-11 and SN-38 pharmacokinetic parameters following a single i.v. dose of liposomal CPT-11.

Liposome	CPT-11				SN-38	
	$AUC_{0-48\ h}$ (μg h mL^{-1})	CL (L h^{-1} kg^{-1})	MRT (h)	$T_{1/2}$ (h)	$AUC_{0-48\ h}$ (μg h mL^{-1})	MRT (h)
Cit-L	23.83 ± 1.93	0.42 ± 0.04	4.12 ± 0.38	2.9	1.20 ± 0.11	9.79 ± 0.98
Cu-L	1477.16 ± 50.77 *	0.01 ± 0.00	6.20 ± 0.37	4.3	64.63 ± 8.23 *	14.40 ± 1.28
IP6-L	1929.35 ± 241.75 *	0.01 ± 0.00	6.82 ± 0.55	4.8	108.34 ± 9.10 *	14.55 ± 0.85

AUC: area under the curve, CL: clearance, MRT: mean residence time, $T_{1/2}$: half-life period. *$P < 0.05$ ddY mice were given a single i.v. bolus dose equivalent to 10 mg CPT-11/kg.

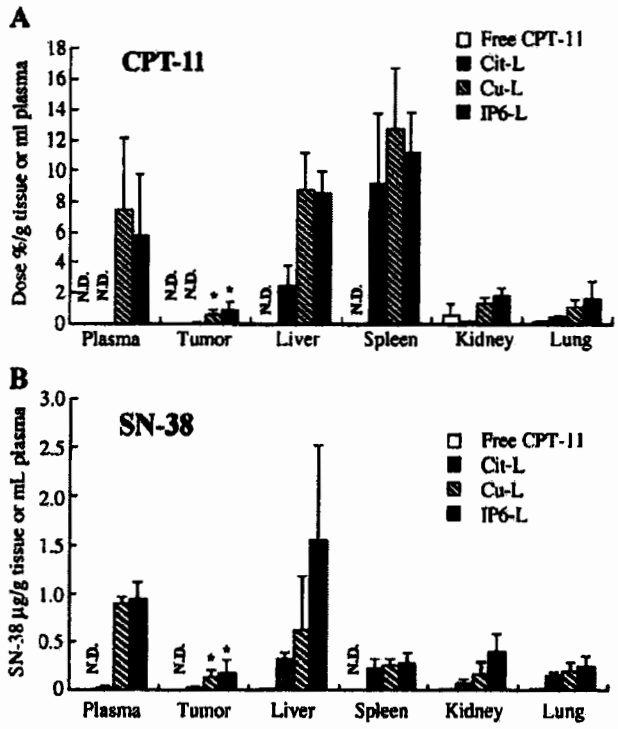

Fig. 3. Biodistribution of liposomal CPT-11 at 24 h after single injection in mice bearing Colon 26 tumor. Tissue and tumor biodistribution of CPT-11 (A) and SN-38 (B) after single intravenous injection doses (equivalent to 10 mg CPT-11/kg) of free CPT-11, Cit-L, Cu-L and IP6-L. Each value represents the mean ± S.D. ($n=3$). *$P<0.05$, compared with free CPT-11. N.D.: not detected.

same lipid formulation, but the pharmacokinetic parameters were completely different. These results indicated that liposomal formulations with intraliposomal drug-trapping agents improved CPT-11 retention in blood following intravenous injection.

3.3. CPT-11 and SN-38 biodistribution in Colon 26 tumor

The biodistribution profiles of liposomal CPT-11 and free CPT-11 were determined 24 h after intravenous injection of 10 mg CPT-11/kg into mice bearing Colon 26 tumor (Fig. 3A and B). After injection of free CPT-11, CPT-11 and SN-38 concentrations in tissues and tumor were very low. In Cit-L, CPT-11 and SN-38 were mainly detected in the liver and spleen. In IP6- and Cu-L, CPT-11 was strongly detected in the plasma, liver and spleen, and SN-38 in the plasma and liver. For the tumor concentration of CPT-11, IP6- and Cu-L showed 183- and 116-fold higher concentrations 24 h after administration than free CPT-11. For tumor concentrations of SN-38, IP6- and Cu-L showed 96- and 77-fold higher concentrations 24 h after administration than free CPT-11.

3.4. In vitro antitumor effect on Colon 26 tumor cells

IP-6 has been reported as an antineoplastic agent and increased the cytotoxic effect in breast tumor cells when combined with doxorubicin or tamoxifen [21]; therefore, we explored the co-treatment of CPT-11 plus IP-6 or SN-38 plus IP-6 to determine whether this treatment results in greater growth suppression or enhancement of cytotoxicity. The IC_{50} of IP-6 alone for Colon 26 cells was 0.27 mM (Fig. 4A), corresponding with the report that IP-6 inhibited cell growth at concentrations ranging from 10 μM to 1 mM in most mammalian tumor cells [26]. CPT-11 and CPT-11 plus 0.1 mM IP-6 did not exhibit cytotoxicity for Colon 26 cells (Fig. 4B). In contrast, SN-38 showed cytotoxicity for the cells ($IC_{50}=9.9$ nM), and SN-38 plus 0.1 mM IP-6 increased the cytotoxicity ($IC_{50}=8.5$ nM) (Fig. 4C). As a result, combination therapy of SN-38 plus IP-6 resulted in a significantly greater suppression of tumor growth than SN-38 alone, but combination therapy of CPT-11 plus IP-6 did not.

3.5. Antitumor effect on Colon 26 and COLO 320DM tumor xenografts

Antitumor activity of liposomal CPT-11 and free CPT-11 was evaluated following one or three intravenous injections into Colon 26 tumor-bearing mice. Protracted dosing schedules would be beneficial for S-phase active drugs like CPT-11. A dose of 60 mg/kg was considered the maximum tolerated dose of free CPT-11, because when free CPT-11 at a dose of 100 mg/kg was administered to mice bearing a Colon 26 tumor, the mice died after a few minutes, but not at 60 mg/kg (data not shown). Three injections of IP6-L at 20 mg/kg showed higher

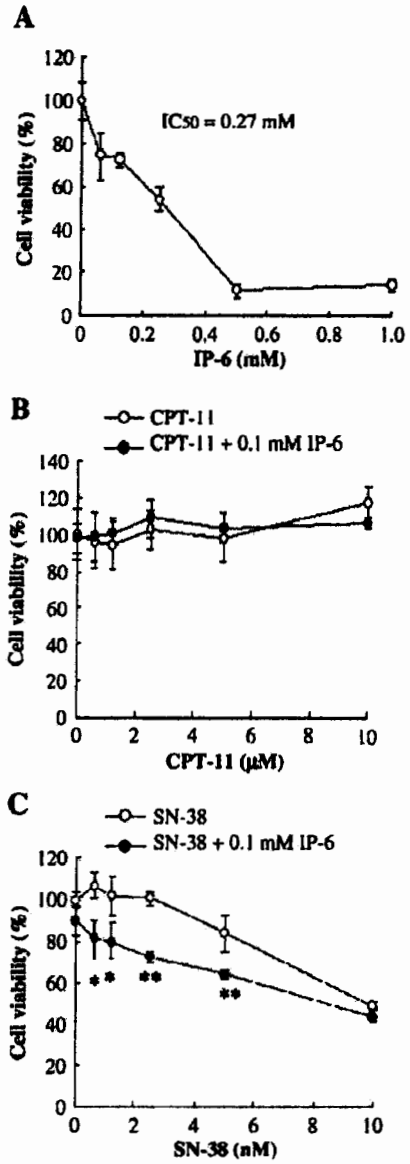

Fig. 4. Cytotoxicity of IP-6 (A) and the combination of CPT-11 (B) or SN-38(C) for Colon 26 cells. Cells were treated with IP-6 at various concentrations and incubated for 72 h (A). In B and C, cells were treated with various concentrations of CPT-11 (B) and SN-38 (C) in the presence of 0.1 mM IP-6. Each result represents the mean ± S.D. ($n=3$). *$P<0.05$, **$P<0.01$, compared with cells treated with SN-38 alone.

antitumor activity than a single injection (Fig. 5A). Antitumor activity by liposomal CPT-11 seemed to depend on the injection frequency fixed at 60 mg/kg; therefore, triple injections of IP6-L were used thereafter.

Next, to examine the dose dependency of the antitumor effect, IP6-L was administered at doses of 10 and 20 mg/kg 3 times at three-day intervals. The tumor suppressive effect by IP6-L seemed to be dose-

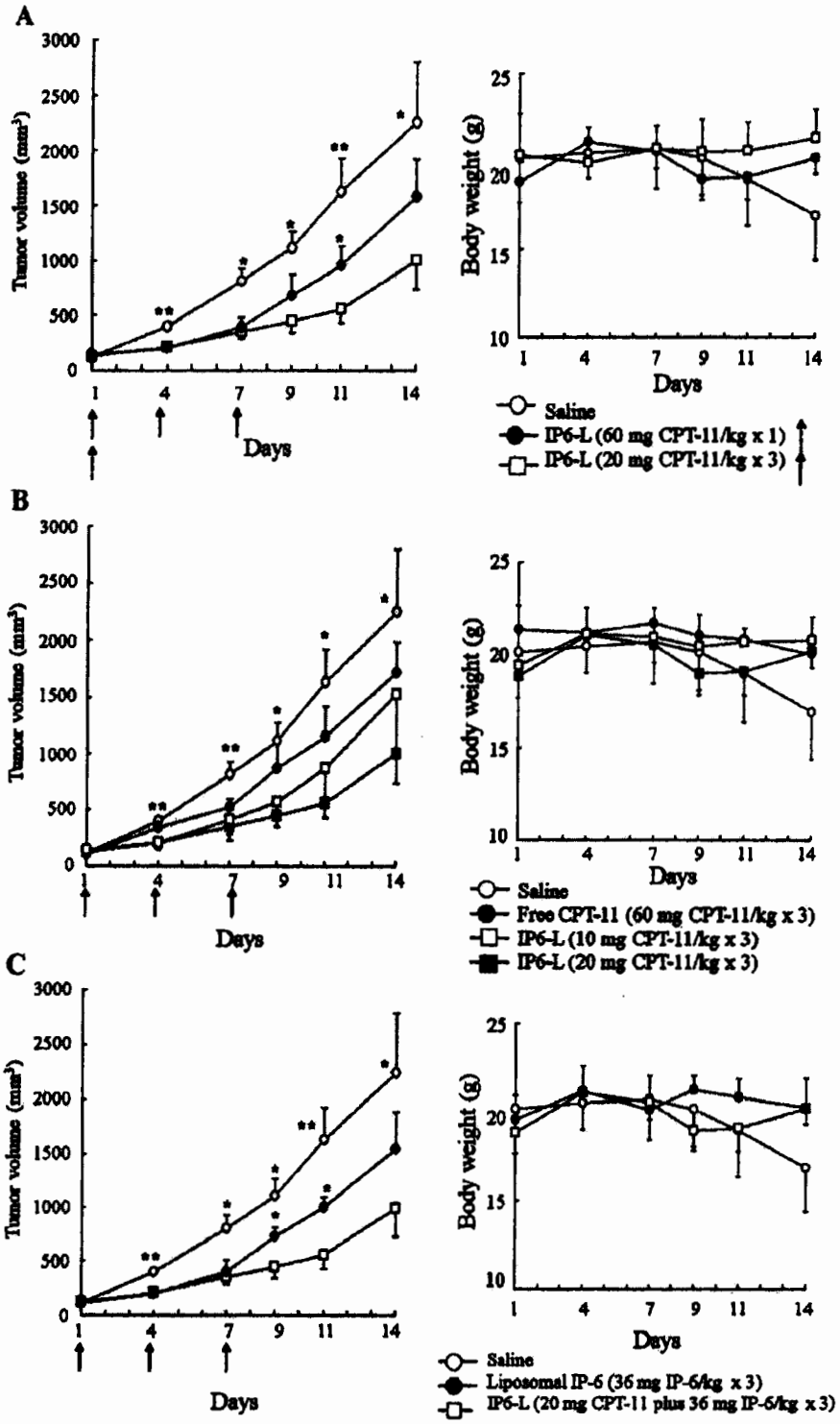

Fig. 5. Antitumor activity of IP6-L as determined in Colon 26 tumor. Antitumor activity and toxicity were assessed by measuring tumor volume and body weight change after intravenous injection of CPT-11. A, Saline (○) was intravenously administered on days 1, 4 and 7. IP6-L was administered by a single injection at 60 mg CPT-11/kg (●) on day 1 or triple injections of 20 mg CPT-11/kg (□) on days 1, 4 and 7. B, Saline (○), free CPT-11 (●) and IP6-L (□: 10 mg CPT-11/kg, ■: 20 mg CPT-11/kg) were administered on days 1, 4 and 7. C, Saline (○), liposomal IP-6 (●) and 20 mg/kg IP6-L (□) were administered on days 1, 4 and 7. Arrows indicate the day of drug injections. Each value represents the mean ± S.D. ($n=4$). $^{*}P<0.05$, $^{**}P<0.01$, compared with mice injected with IP6-L (20 mg CPT-11/kg × 3).

dependent, and IP6-L administered at 20 mg/kg showed the highest tumor growth inhibition (Fig. 5B). Furthermore, IP6-L administered at 10 mg CPT-11/kg was superior in tumor suppression to free CPT-11 at 60 mg/kg. To examine the tumor suppressive effect of IP-6, liposomal IP-6 and IP6-L were injected into the tumors 3 times at 3-day intervals (Fig. 5C). Liposomal IP-6 (36 mg IP-6/kg) showed tumor growth inhibition, and IP6-L (20 mg CPT-11/kg plus 36 mg IP-6/kg) increased its tumor suppressive effect significantly on day 9 and 11. There were no remarkable differences in mice body weight changes after administration of IP6-L.

We investigated whether different loading methods of liposomal CPT-11 improved the therapeutic efficacy of CPT-11.The therapeutic benefits of free and liposomal CPT-11 were assessed in two advanced colon tumor models. We decided to use IP6- and Cu-L as liposomal CPT-11, because Cit-L did not circulate for long in blood and did not accumulate in the tumor (Figs. 2 and 3).

Mice bearing Colon 26 tumors were administered free CPT-11, and Cu- and IP6-L 3 times at a dose of 20 mg CPT-11/kg at 3-day intervals (Fig. 6A). Anticancer efficacy was significantly different for each CPT-11 formulation, and IP6-L-injected mice showed significant tumor growth inhibition compared to Cu-L and free CPT-11. The percentage of tumor growth inhibition (T/C%), which represents the mean difference (%) in tumor size for treated tumors (T) compared with control tumors (C), was calculated from relative tumor volume at day 15 in Colon 26 tumor. The calculated T/C treated with free CPT-11, Cu- and IP6-L in Colon 26 tumor was 75, 64 and 28 on day 15, respectively. We did not observe a significant loss of weight in mice administered Cu- and IP6-L on day 15 in spite of transiently loss of weight immediately after the repeated injections on day 10. This anticancer efficacy of IP6-L indicated that CPT-11 loaded into liposomes was released and co-encapsulated IP-6 increased CPT-11 activity.

Finally, COLO 320DM tumor xenografts were administered with free CPT-11, and Cu- and IP6-L 3 times at a dose of 20 mg/kg at 3-day intervals (Fig. 6B). The tumors in mice treated with IP6- and Cu-L gradually disappeared and were completely gone within 2 weeks after

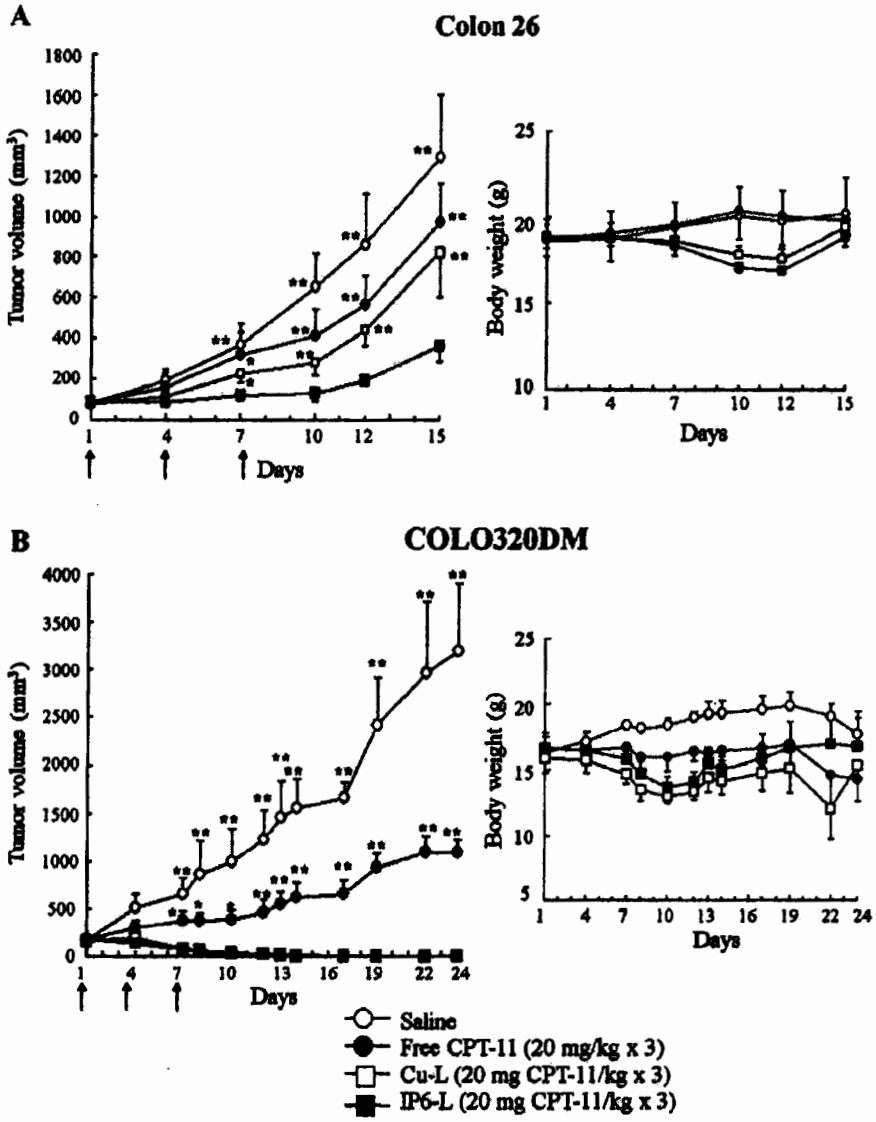

Fig. 6. Antitumor activity of liposomal CPT-11 as determined in Colon 26 tumor (A) and COLO 320DM tumor xenografts (B). Antitumor activity and toxicity were assessed by measuring tumor volume and body weight change after intravenous injection of free and liposomal CPT-11 (equivalent to 20 mg CPT-11/kg). Saline (○), free CPT-11 (●), Cu-L (□) and IP6-L (■) were administered on days 1, 4 and 7. Arrows indicate the day of drug injections. Each value represents the mean ± S.D. ($n = 4$). *$P < 0.05$, **$P < 0.01$, compared with mice injected with IP6-L.

the first administration. Body weight after administration of Cu- and IP6-L temporarily decreased but recovered after 2 weeks, indicating that the dose of liposomal CPT-11 may decrease in nude mice with a tumor to prevent side effects. It has been reported that COLO 320DM cells were sensitive to CPT-11, and even free CPT-11 could suppress tumor growth in COLO 320DM xenografts [27]. In this study, free CPT-11 exhibited significant tumor suppression compared with saline-injected mice, as previously reported [27]. The calculated T/C% values treated with free CPT-11, and Cu- and IP6-L in COLO 320DM xenografts were 40, 0.3 and 0.5 on day 14, respectively.

4. Discussion

In this study, we prepared IP6-L using a non-polymeric negatively charged compound, IP-6, for remote loading of CPT-11 into liposomes, and demonstrated that IP6-L had significantly superior anticancer activity to Cu-L in Colon 26 tumor and human COLO320DM tumor xenografts. As loading methods for CPT-11 into liposomes, the pH gradient method by citrate and the ion-mediated encapsulation method with $CuSO_4$ were reported [9,10]. Therefore, we compared the loading efficiency of CPT-11 in liposomes loaded by IP-6 mediated methods (IP6-L) with those by citrate and $CuSO_4$-mediated methods (Cit-L, Cu-L). IP6- and Cu-L retained high loading efficiencies at a CPT-11 to total lipid ratio of 0.6. It is known that IP-6 is widely used as a chelator for cationic substrate [28] and copper can interact with CPT-11 [29]. The high loading efficiency of CPT-11 in IP6-L supposed that IP-6 may interact with CPT-11 in the liposome interior.

IP6-L prepared with 100–500 mM pH-unadjusted IP-6 solution (pH<2) was aggregated soon after preparation. When the pH of IP-6 solution was adjusted to 6.5 with TEA or NaOH, no aggregations were observed in the IP6-L (data not shown), but IP6-L with TEA showed higher loading efficiency than that with NaOH, indicating that TEA played an important role in remote loading of CPT-11 as it was previously reported that TEA gradient promoted CPT-11 encapsulation into liposomes [13]. As CPT-11 has a pKa of 8.1, it has a different population of both charged and uncharged molecules at pH 7.4 in extraliposomes and at pH 6.5 in intraliposomes; the ratios of charged to uncharged molecules of CPT-11 at pH 7.4 and 6.5 are 5.2 and 41, respectively. When CPT-11 is added to the outside of liposomal IP-6, the uncharged form translocates through the liposome bilayer to the intraliposome, and then changes to the charged form by proton shift from TEA [13]. The positively charged form of CPT-11 may interact with negatively charged phosphate residues of IP-6 and accumulate in liposomes; therefore, IP-6 adjusted with TEA was effective for remote loading of CPT-11.

The most striking observation in this study was the effectiveness of IP6-L in an animal model. The AUC of CPT-11 and SN-38 in IP6-L was significantly higher than that in Cu-L (Table 1), and IP6-L and Cu-L showed similarly high accumulations of CPT-11 and SN-38 in the tumor 24 h after administration (Fig. 3). The amount of SN-38 in the tumor after administration of Cu-L was similar to that in a previous report [30]. As antitumor effects, IP6-L exhibited a significantly higher tumor suppressive effect in Colon 26 tumors compared with Cu-L (Fig. 6A). Three injections of IP6-L at 20 mg CPT-11/kg showed higher antitumor activity than a single injection at 60 mg/kg, suggesting that multiple injections could improve the retention of CPT-11 and SN-38 in blood and induce high antitumor activity. In a COLO320DM tumor model, IP6-L also showed an effective antitumor effect as well as Cu-L (Fig. 6B), and the tumors completely disappeared.

Although the basis of the effect remains incompletely understood, two factors help to explain the result. First, IP6-L with CPT-11 stabilized by IP-6 showed prolonged circulation in the blood compared with free CPT-11 and Cu-L, resulting in high tumor exposure. The sustained release of CPT-11 from liposomes could prevent the saturation of carboxyesterase enzyme in the liver [30], enabling IP6-L to maintain high plasma SN-38 levels over the duration of the experiments. Here, since a relatively low dose (20 mg/kg) was used, the lack of a dose–response effect was observed. Second, IP-6 in IP6-L may exhibit synergic tumor suppression with SN-38 *in vivo* as combination treatment of SN-38 plus IP-6 significantly increased the cytotoxic effect on Colon 26 tumor cells. IP-6 has been found to cause G_1 cell cycle arrest [31], and to stimulate p53 and p21 expression, and to increase the expression of p21 in human colon tumor cell lines [19,20,32]. Exposure of IP-6 in tumor cells and xenografts resulted in a dose-dependent decrease in the expression of vascular endothelial growth factor (VEGF) [33,34]. Furthermore, long circulation in blood leads to increased accumulation of liposomal IP-6 in tumors by enhanced permeability and retention effects. Once IP-6 in IP6-L was accumulated in the tumor, IP-6 could function synergically with SN-38. We are currently investigating whether the activity of CPT-11 is increased *in vivo*, being mediated by a dual-action mechanism encompassing anti-vascular and direct tumor cell cytotoxicity actions of IP-6. Thus, CPT-11 in IP6-L was converted to SN-38 and then suppressed tumor growth in combination with IP-6 *in vivo*. According to our results, we supposed that IP6-L could increase antitumor activity by liposomal CPT-11 and IP-6.

5. Conclusions

We developed a novel loading method of CPT-11 into liposomes, which was mediated by IP-6 and triethanolamine. The loading efficiency of IP6-L was higher than those of Cit-L and similar to Cu-L. IP6-L showed significantly higher AUC than Cit-L and Cu-L, and showed significantly superior anticancer activity than Cu-L in Colon 26 tumors. Liposomal CPT-11 with IP-6 not only could achieve efficient loading at a high drug-to-lipid ratio but also enhanced its antitumor activity against colon tumors.

Acknowledgments

We thank Mr. Takumi Tanaka for his assistance with the experimental work. This study was supported in part by the Japan Health Sciences Foundation, by the Ministry of Education, Culture, Sports, Science and Technology of Japan, and by the Open Research Center Project.

References

[1] Y.H. Hsiang, H.Y. Wu, L.F. Liu, Topoisomerases: novel therapeutic targets in cancer chemotherapy, Biochem. Pharmacol. 37 (1988) 1801–1802.
[2] Y.H. Hsiang, L.F. Liu, Identification of mammalian DNA topoisomerase I as an intracellular target of the anticancer drug camptothecin, Cancer Res. 48 (1988) 1722–1726.
[3] Y.H. Hsiang, M.G. Lihou, L.F. Liu, Arrest of replication forks by drug-stabilized topoisomerase I-DNA cleavable complexes as a mechanism of cell killing by camptothecin, Cancer Res. 49 (1989) 5077–5082.
[4] L.B. Saltz, The role of irinotecan in colorectal cancer, Curr. Oncol. Rep. 1 (1999) 155–160.
[5] L.B. Saltz, J.V. Cox, C. Blanke, L.S. Rosen, L. Fehrenbacher, M.J. Moore, J.A. Maroun, S.P. Ackland, P.K. Locker, N. Pirotta, G.L. Elfring, L.L. Miller, Irinotecan plus fluorouracil and leucovorin for metastatic colorectal cancer. Irinotecan Study Group, N. Engl. J. Med. 343 (2000) 905–914.
[6] Y. Kawato, M. Aonuma, Y. Hirota, H. Kuga, K. Sato, Intracellular roles of SN-38, a metabolite of the camptothecin derivative CPT-11, in the antitumor effect of CPT-11, Cancer Res. 51 (1991) 4187–4191.
[7] Y. Kawato, T. Furuta, M. Aonuma, M. Yasuoka, T. Yokokura, K. Matsumoto, Antitumor activity of a camptothecin derivative, CPT-11, against human tumor xenografts in nude mice, Cancer Chemother. Pharmacol. 28 (1991) 192–198.
[8] F. Lavelle, M.C. Bissery, S. Andre, F. Roquet, J.F. Riou, Preclinical evaluation of CPT-11 and its active metabolite SN-38, Semin. Oncol. 23 (1996) 11–20.
[9] T.H. Chou, S.C. Chen, I.M. Chu, Effect of composition on the stability of liposomal irinotecan prepared by a pH gradient method, J. Biosci. Bioeng. 95 (2003) 405–408.
[10] E. Ramsay, J. Alnajim, M. Anantha, A. Taggar, A. Thomas, K. Edwards, G. Karlsson, M. Webb, M. Bally, Transition metal-mediated liposomal encapsulation of irinotecan (CPT-11) stabilizes the drug in the therapeutically active lactone conformation, Pharm. Res. 23 (2006) 2799–2808.
[11] C.L. Messerer, E.C. Ramsay, D. Waterhouse, R. Ng, E.M. Simms, N. Harasym, P. Tardi, L.D. Mayer, M.B. Bally, Liposomal irinotecan: formulation development and therapeutic assessment in murine xenograft models of colorectal cancer, Clin. Cancer Res. 10 (2004) 6638–6649.

[12] E. Ramsay, J. Alnajim, M. Anantha, J. Zastre, H. Yan, M. Webb, D. Waterhouse, M. Bally, A novel liposomal irinotecan formulation with significant anti-tumour activity: use of the divalent cation ionophore A23187 and copper-containing liposomes to improve drug retention, Eur. J. Pharm. Biopharm. (2007).
[13] A. Dicko, P. Tardi, X. Xie, L. Mayer, Role of copper gluconate/triethanolamine in irinotecan encapsulation inside the liposomes, Int. J. Pharm. 337 (2007) 219–228.
[14] F.M. Walsh, F.J. Crosson, M. Bayley, J. McReynolds, B.J. Pearson, Acute copper intoxication. Pathophysiology and therapy with a case report, Am. J. Dis. Child. 131 (1977) 149–151.
[15] D.G. Barceloux, Copper, J. Toxicol., Clin. Toxicol. 37 (1999) 217–230.
[16] S. Kawanishi, S. Inoue, K. Yamamoto, Hydroxyl radical and singlet oxygen production and DNA damage induced by carcinogenic metal compounds and hydrogen peroxide, Biol. Trace Elem. Res. 21 (1989) 367–372.
[17] D.C. Drummond, C.O. Noble, Z. Guo, K. Hong, J.W. Park, D.B. Kirpotin, Development of a highly active nanoliposomal irinotecan using a novel intraliposomal stabilization strategy, Cancer Res. 66 (2006) 3271–3277.
[18] J.S. Diallo, B. Peant, L. Lessard, N. Delvoye, P.C. Le, A.M. Mes-Masson, F. Saad, An androgen-independent androgen receptor function protects from inositol hexakisphosphate toxicity in the PC3/PC3(AR) prostate cancer cell lines, Prostate 66 (2006) 1245–1256.
[19] L. Weglarz, I. Molin, A. Orchel, B. Parfiniewicz, Z. Dzierzewicz, Quantitative analysis of the level of p53 and p21(WAF1) mRNA in human colon cancer HT-29 cells treated with inositol hexaphosphate, Acta Biochim. Pol. 53 (2006) 349–356.
[20] I.T. Saied, A.M. Shamsuddin, Up-regulation of the tumor suppressor gene p53 and WAF1 gene expression by IP6 in HT-29 human colon carcinoma cell line, Anticancer Res. 18 (1998) 1479–1484.
[21] K. Tantivejkul, I. Vucenik, J. Eiseman, A.M. Shamsuddin, Inositol hexaphosphate (IP6) enhances the anti-proliferative effects of adriamycin and tamoxifen in breast cancer, Breast Cancer Res. Treat. 79 (2003) 301–312.
[22] H.G. Yu, Y.W. Ai, L.L. Yu, X.D. Zhou, J. Liu, J.H. Li, X.M. Xu, S. Liu, J. Chen, F. Liu, Y.L. Qi, Q. Deng, J. Cao, S.Q. Liu, H.S. Luo, J.P. Yu, Phosphoinositide 3-kinase/Akt pathway plays an important role in chemoresistance of gastric cancer cells against etoposide and doxorubicin induced cell death, Int. J. Cancer 122 (2008) 433–443.
[23] Y. Maitani, S. Igarashi, M. Sato, Y. Hattori, Cationic liposome (DC-Chol/DOPE = 1:2) and a modified ethanol injection method to prepare liposomes, increased gene expression, Int. J. Pharm. 342 (2007) 33–39.
[24] Y. Tajima, Biological reference data book on experimental animals, soft science, Tokyo (1989) 96.
[25] S. Takemoto, K. Yamaoka, M. Nishikawa, Y. Takakura, Histogram analysis of pharmacokinetic parameters by bootstrap resampling from one-point sampling data in animal experiments, Drug Metab. Pharmacokinet. 21 (2006) 458–464.
[26] A.M. Shamsuddin, Metabolism and cellular functions of IP6: a review, Anticancer Res. 19 (1999) 3733–3736.
[27] W.J. Jansen, B. Zwart, S.T. Hulscher, G. Giaccone, H.M. Pinedo, E. Boven, CPT-11 in human colon-cancer cell lines and xenografts: characterization of cellular sensitivity determinants, Int. J. Cancer 70 (1997) 335–340.
[28] U.P. Rodrigues-Filho, S. Vaz Jr., M.P. Felicissimo, M. Scarpellini, D.R. Cardoso, R.C. Vinhas, R. Landers, J.F. Schneider, B.R. McGarvey, M.L. Andersen, L.H. Skibsted, Heterometallic manganese/zinc-phytate complex as a model compound for metal storage in wheat grains, J. Inorg. Biochem. 99 (2005) 1973–1982.
[29] A.S. Taggar, J. Alnajim, M. Anantha, A. Thomas, M. Webb, E. Ramsay, M.B. Bally, Copper-topotecan complexation mediates drug accumulation into liposomes, J. Control. Release 114 (2006) 78–88.
[30] E.C. Ramsay, M. Anantha, J. Zastre, M. Meijs, J. Zonderhuis, D. Strutt, M.S. Webb, D. Waterhouse, M.B. Bally, Irinophore C: a liposome formulation of irinotecan with substantially improved therapeutic efficacy against a panel of human xenograft tumors, Clin. Cancer Res. 14 (2008) 1208–1217.
[31] Y.M. El-Sherbiny, M.C. Cox, Z.A. Ismail, A.M. Shamsuddin, I. Vucenik, G0/G1 arrest and S phase inhibition of human cancer cell lines by inositol hexaphosphate (IP6), Anticancer Res. 21 (2001) 2393–2403.
[32] I. Vucenik, A.M. Shamsuddin, Cancer inhibition by inositol hexaphosphate (IP6) and inositol: from laboratory to clinic, J. Nutr. 133 (2003) 3778S–3784S.
[33] R.P. Singh, G. Sharma, G.U. Mallikarjuna, S. Dhanalakshmi, C. Agarwal, R. Agarwal, In vivo suppression of hormone-refractory prostate cancer growth by inositol hexaphosphate: induction of insulin-like growth factor binding protein-3 and inhibition of vascular endothelial growth factor, Clin. Cancer Res. 10 (2004) 244–250.
[34] I. Vucenik, A. Passaniti, M.I. Vitolo, K. Tantivejkul, P. Eggleton, A.M. Shamsuddin, Anti-angiogenic activity of inositol hexaphosphate (IP6), Carcinogenesis 25 (2004) 2115–2123.

Clinical development success rates for investigational drugs

Michael Hay, David W Thomas, John L Craighead, Celia Economides & Jesse Rosenthal

The most comprehensive survey of clinical success rates across the drug industry to date shows productivity may be even lower than previous estimates.

Since the human genome was sequenced ten years ago, the number of compounds in development has increased 62% and total R&D expenditures have doubled[1–3]. And yet, the average number of new drugs approved by the US Food and Drug Administration (FDA) per year has declined since the 1990s. In 2012, 39 novel drugs classified as new molecular entities (NMEs) and biologic license applications (BLAs) were approved by the FDA[4]. Although this represents the highest number of approvals since 1997 and is nearly 50% above the average of 26 approvals per year over the past decade, 25% fewer NME and BLA drugs were approved on average in the past 10 years compared with the 1990s[5]. Several possible explanations for the divergence of R&D spending and new product approvals have been offered by professionals in the industry, such as unbalanced regulatory risk-benefit assessments, higher regulatory efficacy hurdles, commercial and financial decisions driving project termination, and the increased complexity and cost of clinical trials[6,7].

This article aims to measure clinical development success rates across the industry with a view to strengthening benchmarking metrics for drug development. The study is the largest and most recent of its kind, examining success rates of 835 drug developers, including biotech companies as well as specialty and large pharmaceutical firms from 2003 to 2011. Success rates for over 7,300 independent drug development paths are analyzed by clinical phase, molecule type, disease area and lead versus nonlead indication status.

Our results pinpoint weaknesses along the capital-intensive pathway to drug approval. Our hope is that they will prove useful in informing policy makers where to focus changes in regulation and strengthen valuation models used by industry and the investment community.

Michael Hay and Jesse Rosenthal are at BioMedTracker, Sagient Research Systems, San Diego, California, USA; David W. Thomas and Celia Economides are at the Biotechnology Industry Organization (BIO), Washington, DC, USA; and John L. Craighead is at Biotech Strategy & Analytics, Rockville, Maryland, USA. e-mail: mhay@sagientresearch.com

Analyzing success

To measure clinical development success rates for investigational drugs, we analyzed phase transitions from January 1, 2003 to December 31, 2011, in the BioMedTracker database. The BioMedTracker data set contained 4,451 drugs with 7,372 independent clinical development paths from 835 companies and included 5,820 phase transitions. The development paths comprised lead (primary) and nonlead (secondary) indications, with roughly 38% designated as nonlead. A more detailed description of the data collection, composition and analysis methodology is described in **Boxes 1–3** (see also **Tables 1** and **2**).

Unlike many previous studies that reported clinical development success rates for large pharmaceutical companies, this study provides a benchmark for the broader drug development industry by including small public and private biotech companies and specialty pharmaceutical firms. The aim is to incorporate data from a wider range of clinical development organizations, as well as drug modalities and targets. Two landmark publications on the subject, DiMasi *et al.*[6] and Kola *et al.*[8] use 50 and 10 pharmaceutical company pipelines, respectively, to arrive at their conclusions. An important study published by the US Federal Trade Commission Bureau of Economics, Abrantes-Metz *et al.*[9] covered a wide number of drugs over a 14 year period from 1989 to 2002, but did not provide the number or type of companies investigated. Although the impact of company size and experience on R&D productivity has been studied extensively[10–13], success rates established by DiMasi *et al.*[6], Kola *et al.*[8] and Abrantes-Metz *et al.*[9] remain the primary benchmarks for the drug development industry.

We believe it is of great value to report updated success rates that capture the diversity in drug development sponsor types as experience and technology vary widely outside of traditional, large pharmaceutical corporations. Furthermore, the more recent time frame for this study provides insight into the latest industry productivity. A comparison of previously published reports with the current study is summarized in **Table 3** and is discussed below.

One key distinction of the study presented here is our ability to evaluate all of a drug's indications to determine success rates. Danzon *et al.*[12] first considered success rates at the indication level, recognizing that FDA requires clinical trial evidence to establish efficacy for each approved indication. Although these authors included data from 1988 to 2000, an observation period similar to Kola *et al.*[8] and Abrantes-Metz *et al.*[9], their success rates were significantly higher and lacked a characteristic decrease in phase 2 probability reported in previous studies as well as here. Danzon *et al.*[12] concluded that higher clinical development success rates resulted from the analysis of all indications. Even so, evidence presented here strongly suggests that evaluating all indications results in lower probabilities of success across all phases of drug development.

To illustrate the importance of using all indications to determine success rates, consider this scenario. An antibody is developed in four cancer indications, and all four indications transition successfully from phase 1 to phase 3, but three fail in phase 3 and only one succeeds in gaining FDA approval. Many prior studies reported this as 100% success, whereas our study differentiates the results as 25% success for all indications, and 100% success for the lead indication. Considering the cost and time spent on the three failed phase 3 indications, we believe including all 'development paths' more accurately reflects success and R&D productivity in drug development.

Examining individual drug indications allows us to answer the question: "what is the probability that a drug developed for a specific indication will reach approval?" Whereas, using only the lead or most advanced indication seeks to answer the question: "what is the probability that a drug will reach approval for any indication?" This study addresses both questions with emphasis on the findings of the former. In the following sections, we present the results of our analysis as they relate to overall phase success and likelihood of approval (LOA; see **Box 2**), to the type of therapeutic modality, to the disease being treated and to the type of drug application (whether orphan or Special Protocol Assessment (SPA) pathways).

Phase success and likelihood of approval

We found that approximately one in ten (10.4%, $n = 5,820$) of all indication development paths in phase 1 were approved by FDA (**Fig. 1** and **Table 4**). Examining the individual phase components of this compound probability, phase 1 success (the number of phase 1 drugs that successfully transitioned to phase 2 divided by the total transitions in phase 1) was 64.5% ($n = 1,918$). Success in phase 2 (32.4%, $n = 2,268$) was substantially lower than in phase 1, but subsequently increased in phase 3 (60.1%, $n = 975$). The probability of FDA approval after submitting a new drug application (NDA) or biologic license application (BLA) was 83.2% ($n = 659$).

Success rates for lead indication development paths were higher than for all indication development paths in every phase. Lead indications had a LOA from phase 1 of 15.3% ($n = 3,688$).

Success rates by drug classification

Drugs in the BioMedTracker data set were annotated by their FDA classification: new molecular entity (NME), non-NME, biologic and vaccine. However, owing to inconsistency in the FDA classifications, we also used our

Box 1 Data collection and composition

BioMedTracker, a subscription-based product of Sagient Research Systems (San Diego) introduced in 2002, tracks the clinical development and regulatory history of novel investigational drugs in the United States. Analysts with advanced degrees in the life sciences and medicine maintain the database using information from company press releases, analyst conference calls, and presentations at investor and medical meetings. BioMedTracker also uses other sources, including regular communication with companies conducting clinical trials, to ensure the accuracy and timeliness of the data.

Data included in this study were selected using BioMedTracker's Probability of Technical Success (PTS) calculator, which identified 5,820 phase transitions from January 1, 2003, to December 31, 2011. Transitions in all phases of development were recorded in the early years of observation and resulted from clinical studies initiated before 2003. The data set contained 4,451 drugs from 835 companies and 7,372 independent clinical development paths in 417 unique indications.

The composition of these novel drug development sponsors included a wide range of company sizes and types (**Table 1**). Emerging biotech represented 85% (712) of the companies, whereas a small number (33) of large firms (4% of total) were responsible for 48% (3,573) of indications and 47% (2,075) of drugs in development. Similarly, private firms represented 49% (412) of the companies and fewer than 20% of indications and drugs included in the study.

These ownership classifications were recorded at the end of the analysis time period and underestimate the number of drugs and indications developed by biotech companies due to licensing and acquisitions during the study time frame. In addition, ownership was assigned to the licensee controlling and funding the majority of development. In cases where development and economics were shared equally, ownership was generally assigned to the larger organization, further contributing to the conservative estimate of drugs developed by small and private biotech companies. Although generic products were not included, generic manufacturers developing novel investigational drugs were represented.

The study also likely tracked a larger percentage of late-stage studies as these programs are more often in the public domain. Even so, small biotech companies often disclose ongoing phase 1 studies and we would expect their substantial representation in this study to partially offset the under-representation of early-stage discontinuation rates. Only company sponsored development paths designed for FDA approval were considered; investigator sponsored studies and combinations with other investigational drugs were excluded in this analysis.

In addition, this study analyzed development paths organized by disease area, biochemical composition, molecular size, FDA classification and regulatory status (SPA and orphan drug status). Given the increasing complexity of ownership and diversity of invention in the drug development industry, the study did not further classify the database on the discovery origin or licensing status of the drug.

Table 1 Analysis of company size and type

	Companies		Indications		Drugs	
	Number	Percentage	Number	Percentage	Number	Percentage
Company size						
Large pharma/biotech (>$5 billion sales)	33	4%	3,573	48%	2,075	47%
Small to mid-sized pharma/biotech ($0.1 billion–$5 billion sales)	90	11%	1,099	15%	724	16%
Emerging biotech (<$0.1 billion sales)	712	85%	2,700	37%	1,652	37%
Total	835	–	7,372	–	4,451	–
Company type						
Private	412	49%	1,269	17%	841	19%
Public	423	51%	6,103	83%	3,601	81%
Total	835	–	7,372	–	4,451	–

Box 2 Metrics of success: 'Phase Success' and 'Likelihood of Approval'

There are two different types of success rates reported in this study: 'Phase Success' and 'Likelihood of Approval' (LOA). 'Phase Success' is calculated as the number of drugs that moved from one phase to the next phase divided by the sum of the number of drugs that progressed to the next phase and the number of drugs that were suspended. The *n* value associated with the Phase Success represents the number of drugs that have advanced plus the number of drugs that have been suspended, which we label as phase transitions. For example, if there were 100 drugs in phase 2 development and 50 transitioned to phase 3, 20 were suspended and 30 remained in phase 2 development, the phase 2 Phase Success would be 71.4% (50/70; *n* = 70).

Our second metric, LOA, denotes the probability of reaching FDA approval from the current phase, and is also expressed as a percentage. LOA is calculated as the product of each Phase Success probability leading to FDA approval. The *n* value associated with LOA is the sum of the *n* values for each Phase Success included in the LOA calculation. For example, if a drug is currently in phase 2, and the Phase Success for phase 2 is 30% (*n* = 20), phase 3 is 50% (*n* = 10), and FDA approval is 80% (*n* = 5), then the LOA for the phase 2 drug would be 12% (30% × 50% × 80% = 12%, *n* = 35). This calculation is illustrated in **Supplementary Figure 2**.

data to annotate drugs by their biochemical composition (e.g., peptide, nucleic acid, monoclonal antibody (mAb)) and molecular size (i.e., large and small molecules). For example, FDA often designates large-molecule biologics, such as proteins and peptides, as NMEs. Indeed, large molecules, as defined by the BioMedTracker biochemical categories, comprise 13% of the NME data set, making direct FDA NME to biologic classification comparisons somewhat imprecise. FDA's biologic classification comprises a wider group that includes the Center for Drug Evaluation and Research (CDER) regulated products, such as antibodies, cytokines, growth factors and enzymes, as well as the Center for Biologics Evaluation and Research (CBER) regulated products including blood isolates, gene therapies and cell therapy.

FDA's non-NME classification often includes drugs with the same molecular properties as NMEs, but which are frequently reformulations or combinations of approved products. The majority of non-NMEs also use the 505(b)(2) pathway to gain FDA approval. Vaccines were also treated as a separate class in this analysis, and generic and over-the-counter drugs were not included. A comparative analysis of FDA classifications and BioMedTracker categories can be found in **Supplementary Table 1**. The metrics for the different therapeutic modality types is provided in **Table 4**.

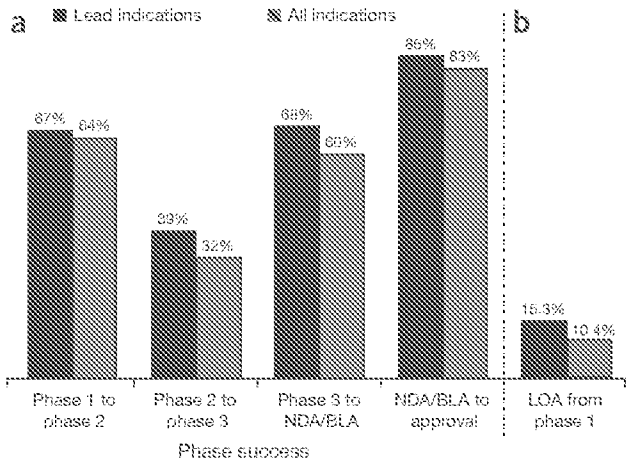

Figure 1 Phase success and LOA rates. (a) Phase success rates for lead and all indications. The rates represent the probability that a drug will successfully advance to the next phase. (b) LOA from phase 1 for lead and all indications. Rates denote the probability of FDA approval for drugs in phase 1 development.

NMEs were found to have the lowest success rates in every phase of development; biologics had nearly twice the LOA from phase 1 (14.6%, *n* = 1,173) as NMEs (7.5%, *n* = 3,496) for all indications (**Table 4**). Similar results are seen when the data are reclassified into large-molecule (excluding low molecular weight chemicals and steroids) and small-molecule NMEs: 13.2% (*n* = 1,834) and 7.6% (*n* = 3,029), respectively. In addition, the LOA from phase 1 for mAbs (14.1%, *n* = 639), a good proxy for CDER-regulated biologics, was also consistent with these broader definitions of biologics.

Non-NMEs had the highest LOA from phase 1 of 20.0% (*n* = 855), with success rates well above those of the NME and biologic classifications in every phase. However, many non-NMEs begin development in phase 2 or phase 3, so the actual approval rate is likely higher (assuming that successful phase 1 outcomes would contribute positively to the LOA from phase 1).

When analyzing lead indications only (i.e., on a per drug basis), we find similar rankings for NME, biologic and non-NME, but at much higher success rates. The LOA from phase 1 for biologics and non-NMEs are near one in four and NMEs approach one in eight (12.6%, *n* = 2,124), almost twice what was found when all indications were considered.

Success rates by disease

We found substantial variation in success rates among disease, as listed in **Table 5** from highest to lowest LOA from phase 1. Oncology drugs had the lowest LOA from phase 1 at 6.7% (*n* = 1,803). Drugs for the 'other' disease group, which combined allergy, gastroenterology, ophthalmology, dermatology, obstetrics-gynecology and urology indications due to small sample size, had the highest LOA from phase 1, at 18.2% (*n* = 720). Drugs for infectious disease and autoimmune-immunology groups had the next two highest LOAs from phase 1, at 16.7% (*n* = 537) and 12.7% (*n* = 549), respectively.

On a lead indication basis, also in **Table 5**, we found that cardiovascular drugs had the lowest LOA from phase 1 at 8.7% (*n* = 318) and the 'other' disease category again had the highest success rate at 24.5% (*n* = 499). The largest difference between lead and all-indication for LOA from phase 1 was observed in oncology: 6.7% (*n* = 1,803) for lead indication and 13.2% (*n* = 796) for all indications. Oncology drugs also had the most nonlead indications (56% of all development paths compared with 28% of non-oncology indications) as a result of the large number of cancers investigated using the same drug. Unfortunately, in oncology, when all indications are considered, only around 1 in 15 drugs entering clinical development in phase 1 achieves FDA approval compared with close to 1 in 8 using the lead indication methodology. As noted above, the result for lead indications represents the most successful development path for a particular compound, thereby addressing LOA on a per drug

Box 3 Methods used in this study

Data used for this study were extracted from BioMedTracker using a probability of technical success (PTS) tool, which identified all 'Advanced' and 'Suspended' drugs by development phase from January 1, 2003, to December 31, 2011. BioMedTracker tracks the clinical development and regulatory history of investigational drugs to assess its Likelihood of Approval (LOA) from phase 1 by the FDA. The database is populated in near real-time with updated information from press releases, corporate earnings calls, investor and medical meetings, and numerous other sources. These data are recorded in BioMedTracker and tagged with a date.

Phase is defined as the stage of clinical development in the United States (**Table 2**). Although it is rare, drugs that were removed from development in the United States, but approved in Europe (e.g., vildagliptin for type II diabetes) were considered 'suspended' for the sake of our analysis. In this time period, 7,372 development paths were analyzed, encompassing 4,451 unique compounds. 5,820 unique phase transitions were used to determine the reported success rates. **Table 4** includes the number of observed transitions by phase (a description of the success rate analysis is described). Phase 2 transitions accounted for the highest percentage of the data set with 39% ($n = 2,268$), compared with 33% in phase 1 ($n = 1,918$), 17% in phase 3 ($n = 975$) and 11% in NDA/BLA ($n = 659$). Nonlead indications comprise 38% ($n = 2,132$) of the 5,820 total transitions and success rates by phase can be found in **Supplementary Table 2**.

Development paths track a specific indication for each drug. For example, Rituxan (rituximab) in non-Hodgkin's lymphoma qualifies as a development path different from Rituxan in multiple sclerosis (MS). BioMedTracker assigns a unique internal identifier that can be used to isolate all development paths. In addition to tracking the phase of development, BioMedTracker assigns 'lead' status to certain development paths. This is used to denote the most advanced indication in clinical development for a specific drug. Drugs can only have one lead development path, except in specific circumstances where two development paths are being developed simultaneously (e.g., type I and type II diabetes). For example, the Avastin (bevacizumab) colorectal cancer development path was marked as a 'lead' indication, and other Avastin development paths were labeled 'nonlead'. Using this metric, Avastin clinical development can more accurately be viewed as a series of successes and failures, as opposed to simply one success and no failures. However, a drug's lead indication may also change if it fails in development in the lead indication. The lead indication success rate will therefore be higher due to selection bias than the nonlead success rate. This bias does not affect the LOA from phase 1 rate for all indication development paths.

BioMedTracker also records a number of other variables including the following:

- FDA classification (e.g., NME, non-NME, biologic or vaccine)
- Biochemical profile (e.g., small molecule, monoclonal antibody, antisense)
- Disease area (e.g., autoimmune, cardiovascular, oncology)
- Indication (e.g., diabetes, acute coronary syndrome)

In contrast with many earlier studies, which included only a limited sample of drugs from large companies, the current study included BioMedTracker data from small biotech companies as well as specialty and large pharmaceutical firms.

Table 2 Definitions of terms used in this study

BioMedTracker term	Description for purposes of this study
I	Drug is currently in phase 1
I/II, II, IIb	Drug is currently in phase 2
II/III, III	Drug is currently in phase 3
NDA/BLA	Application for approval has been submitted to the FDA and is currently under review
Approved, withdrawn from market, approved (Generic competition)	Drug has been approved for marketing in the United States
Suspended	Drug is no longer in development
Approved in Europe, Approved in other than US/EU, Development, Development outside US	The company developing this drug does not plan to market it in the United States

Phase success and LOA rates calculation. A common method of determining drug development success rates detailed in DiMasi *et al.*[6] and Abrantes-Metz *et al.*[9] was used in this study. Phase Success, defined as the probability of a drug moving from phase X to phase X + 1, was used as the basis for all analyses. To arrive at this value, the following questions are used to categorize each drug development path: first, was the drug development path ever in phase X? Second, if so, did it advance to phase X + 1? And third, was it 'Suspended'? After categorizing all drug development paths, Phase Success is calculated by dividing the number of development paths that advanced from phase X to phase X + 1 by the sum of the number of development paths that advanced from phase X to phase X + 1 and the number of development paths that were suspended from phase X – Advanced/(Advanced + Suspended) = Phase Success.

Using this method, we arrived at the probabilities of an 'average' drug advancing from phase 1 to phase 2, from phase 2 to phase 3, from phase 3 to filing the NDA/BLA and from filing the NDA/BLA to FDA approval. We then compounded these probabilities to determine the probability (LOA) that a drug in phase X is approved. For example, the LOA for a drug which has entered phase 2 is the product of the phase success rates from phase 2, phase 3 and NDA/BLA. An example calculation is illustrated in **Supplementary Figure 2**.

For purposes of this analysis, all indications that were advanced or suspended in any phase during our collection time frame were included. In practice, this means a drug that 'entered' the analysis in 2003 in phase 2, and later advanced to phase 3, was included in the study. This method was selected because there are relatively few drugs that entered development in phase 1 in the range of years analyzed and have subsequently progressed through final FDA review, and there is less disclosure of drugs in phase 1 development. Abrantes-Metz *et al.*[9] also used a similar method and stated, "We did it this way because the data set has very few drugs with complete information for all ... phases." Drugs that remained in the same phase were censored, as were those that moved back a phase but were not suspended[9].

Table 3 Comparison of our study with previous drug development success rate studies

	This study (2013) all indications		This study (2013) lead indications		DiMasi *et al.*[5] lead indications		Kola *et al.*[8] lead indications		Abrantes-Metz *et al.*[9] lead indications	
	Phase success	Phase LOA	Phase success	Phase LOA	Phase success	Phase LOA	Phase success	Phase LOA	Phase success	Phase LOA
Phase 1 to phase 2	64.5%	10.4%	66.5%	15.3%	71%	19%	68%	11%	80.7%	NA
Phase 2 to phase 3	32.4%	16.2%	39.5%	23.1%	45%	27%	38%	16%	57.7%	NA
Phase 3 to NDA/BLA	60.1%	50.0%	67.6%	58.4%	64%	60%	55%	42%	56.7%	NA
NDA/BLA to approval	83.2%	83.2%	86.4%	86.4%	93%	93%	77%	77%	NA	NA
LOA from phase 1[a]		10.4%		15.3%		19%		11%	26.4%[c]	NA
Number of drugs in sample advanced or suspended[b]	5,820		4,736		1,316		NA		2,328	
Dates of source data (duration)	2003–2011 (9 years)				1993–2009 (17 years)		1991–2000 (10 years)		1989–2002 (14 years)	
Number of companies	835				50		10		NA	

[a]Probability of FDA approval for drugs in phase 1 development. [b]Total number of transitions used to calculate the success rate (the *n* value noted in the text). [c]Abrantes-Metz, *et al.*[9] reported 26.4% from phase 1 to phase 3. If we were to conservatively apply the 83.2% NDA/BLA success rate found in this study, Abrantes-Metz would yield the highest LOA from phase 1 (21%). NA, data not available.

basis. Using the lead indication methodology to determine success rates, the scope of the challenge in oncology drug development would be dramatically underestimated.

The largest variation in success rates across disease groups was observed in phase 2. In **Table 5** all-indication phase 2 success rates ranged from 26.3% (for cardiovascular) to 45.9% (for infectious disease). In phase 3, all indication success rates ranged from 45.2% (for oncology) to 71.1% (for other). In contrast, phase 1 and NDA/BLA (As only one application, NDA or BLA, will be filed for any single indication, rates are given below for NDA/BLA.) filing success rates were more consistent across disease groups. All indication data from **Table 5** are charted in **Figure 2** to illustrate the large differences in phases 2 and 3 and LOA from phase 1 success rates across disease areas. The development paths with the two lowest rates of phase 3 success were oncology and cardiovascular disease, with 45.2% (n = 221) and 52.8% (n = 89), respectively. **Figure 2** also highlights the large step-up in success rates from phase 2 to phase 3 for autoimmune, endocrine and respiratory diseases, increasing from 34% to 68%, 34% to 67%, and 28% to 63%, respectively. The low LOA from phase 1 in oncology rate results primarily from the lack of such a step-up, with a low phase 2 rate of 28.3% (n = 827), followed by a phase 3 success rate of only 45.2% (n = 221).

Success rates for oncology and non-oncology drugs. As oncology drugs made up the largest portion of the total data set (31.0% of all transitions) and had the lowest LOA from phase 1 (6.7%, n = 1,803), we investigated their contribution to success rates for the entire data set. To accomplish this, we removed all oncology drug development paths and compared these results to the full data set and oncology development paths alone. **Table 6** shows phase success and LOA rates for drugs for all disease groups, oncology and non-oncology development paths. The LOA from phase 1 across non-oncology indications is nearly twice that for oncology alone, 12.1% (n = 4,017) versus 6.7% (n = 1,803), respectively, reducing the probability of FDA approval in the full data set from nearly one in eight to over one in ten. Interestingly, the LOA from phase 1 for small-molecule NMEs was similar for oncology (6.6%, n = 1,163) and non-oncology (7.9% n = 2,333) indications, and biologics and non-NMEs accounted for much of the difference. For example, oncology biologics had a 7.3% (n = 429) LOA from phase 1 compared with 19.4% (n = 744) for non-oncology biologics.

Table 7 shows phase success and LOA rates in subcategories of cancer type for oncology drugs. Although a high number of transitions in all phases were seen for the solid tumor (n = 1,358) and hematological (n = 409) subgroups, further classification of oncology indications results in low numbers of transition from phase 3 to NDA/BLA. As is true of the full data set, drugs in phase 2 for oncology subgroups display more transitions and represent the strongest data for specific-indication success rate analysis. Oncology phase 2 success rates ranged from 50.0% (n = 12) in head and neck cancer to 20.9% (n = 24) in prostate cancer; however, the phase 2 rank order by tumor type was uncorrelated with LOA from phase 1 (linear regression, R^2 = 0.26). On average, phase 2 success rates were higher in hematological tumors (34.6%, n = 179) than in solid tumors (26.3%, n = 636). Only two phase 3 oncology indications had more than 20 transitions: breast cancer (n = 25) and non–small cell lung cancer (n = 23), which together accounted for ~28% of the solid tumor phase 3 transitions (n = 172). Because of even smaller sample sizes, cancer type success rates were not analyzed by lead indication.

Success rates for neurology, autoimmune and endocrine disease drugs. Neurology and autoimmune/immunology disease groups are

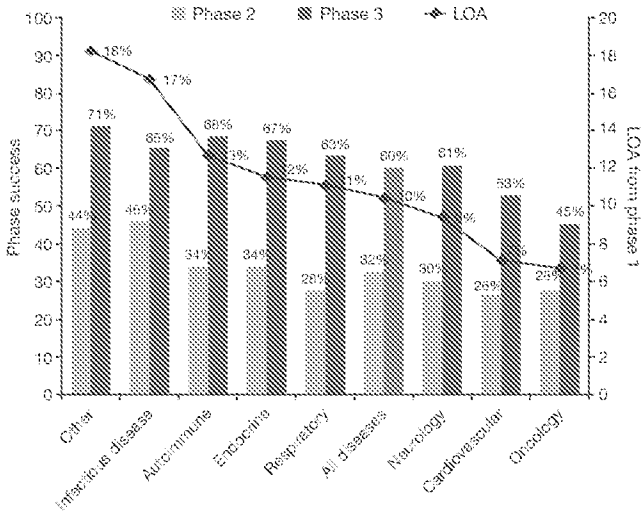

Figure 2 Phase success and LOA from phase 1 by disease for all indications. The bars represent phase 2 and phase 3 success rates and the line represents LOA from phase 1.

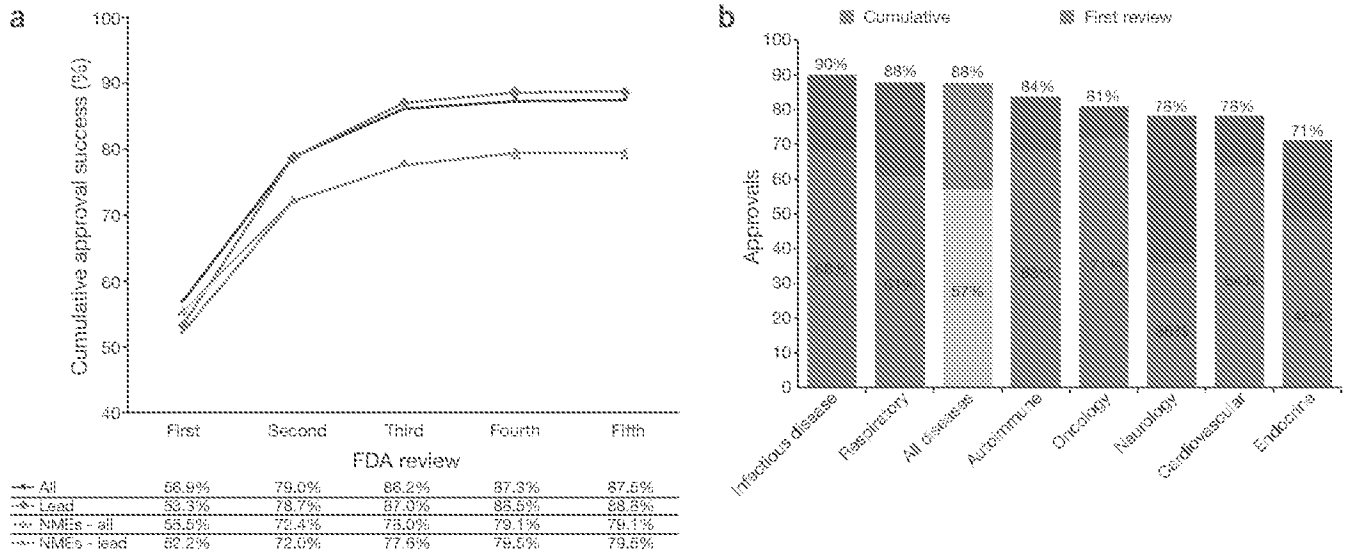

Figure 3 NDA/BLA success rates. (**a**) Cumulative approval rates by FDA review from 2006 to 2011 (914 reviews). (**b**) Cumulative and first FDA approval rates by disease.

well represented, comprising 17% and 9% of the data set, respectively. We subcategorized neurology into pain and psychiatric disorders, the two main therapeutic areas representing 51% of all neurology indications (**Table 8**). Analyzing all development paths, pain indications had a 10.7% ($n = 231$) LOA from phase 1 compared with 7.2% ($n = 294$) for psychiatric disorders. Other neurology indications, mainly representing neurodegenerative diseases, had a 9.8% ($n = 452$) LOA from phase 1.

An autoimmune subset analysis reveals that biologics had more than five times the LOA from phase 1 (22.5%, $n = 288$) than NMEs (5.2%, $n = 202$). **Table 8** also includes success rates for the type II diabetes and rheumatoid arthritis indication subcategories. Although rheumatoid arthritis had a 100% ($n = 5$) NDA/BLA submission success, the LOA from phase 1 was only 10.3% ($n = 130$) due to one of the lowest phase 2 success rates in this study (15.9%, $n = 63$). Diabetes also displayed lower-than-average success rates in all phases, except for NDA/BLA submissions, at 86.4% ($n = 22$).

Regulatory pathway success rates

To investigate the influence of regulation on clinical success we looked at two important pathways for drug oversight: the SPA and orphan drug designation.

SPA success rates. Similar to other analyses, we looked at phase success and LOA rates for drugs with an SPA (**Table 9**). Before

Table 4 Phase success and LOA by drug class

	Phase 1 to phase 2				Phase 2 to phase 3				Phase 3 to NDA/BLA				NDA/BLA to approval			
	Total in phase[b]	Advanced or suspended[b]	Phase success[c]	Phase LOA[d]	Total in phase[b]	Advanced or suspended[b]	Phase success[c]	Phase LOA[d]	Total in phase[b]	Advanced or suspended[b]	Phase success[c]	Phase LOA[d]	Total in phase[b]	Advanced or suspended[b]	Phase success[c]	Phase LOA[d]
FDA classification[a]																
All indications	2,541	1,918	64.5%	10.4%	3,743	2,268	32.4%	16.2%	1,554	975	60.1%	50.0%	908	659	83.3%	83.3%
NMEs	1,585	1,318	64.2%	7.6%	2,375	1,470	28.6%	11.6%	831	515	53.2%	40.7%	426	293	76.5%	76.5%
Biologics	572	411	68.4%	14.6%	819	464	37.9%	21.3%	320	182	63.2%	56.1%	159	116	88.8%	88.8%
Non-NMEs	318	168	68.7%	20.0%	355	226	45.1%	29.9%	321	234	75.5%	66.3%	293	227	87.7%	87.7%
Lead indications	1,770	1,336	66.5%	18.3%	2,070	1,247	39.6%	23.1%	1,009	633	67.6%	58.4%	564	472	86.4%	86.4%
NMEs	1094	848	66.2%	12.0%	1,275	791	38.4%	18.3%	497	300	61.7%	50.3%	283	185	81.6%	81.6%
Biologics	362	257	75.1%	20.8%	403	216	44.0%	27.7%	182	106	71.7%	63.1%	106	75	88.0%	88.0%
Non-NMEs	167	124	66.9%	23.2%	232	153	49.0%	34.6%	254	186	79.0%	70.7%	246	189	89.4%	89.4%
Biomedtracker product category[a]																
Small molecule NMEs	1,335	1,033	65.4%	7.6%	2,053	1,283	29.0%	11.6%	725	449	52.3%	39.8%	369	264	76.1%	76.1%
Large molecules	312	658	66.8%	13.2%	1,379	714	37.7%	20.1%	511	296	60.1%	53.3%	244	166	88.6%	88.6%
mAbs	329	234	70.1%	14.1%	458	268	38.1%	20.1%	147	84	60.7%	52.7%	65	53	86.8%	86.8%
non-mAb proteins	192	161	58.3%	13.1%	280	170	35.3%	22.3%	150	87	69.0%	63.1%	93	59	91.5%	91.5%
Vaccines	121	57	67.1%	14.9%	160	79	44.3%	22.2%	67	34	50.0%	50.0%	23	20	100.0%	100.0%

[a]Number of indications identified. [b]Total number of transitions used to calculate the success rate; the *n* value noted in the text. The difference between 'Total in phase' and 'Advanced or suspended' is the number of indications that remain in development. [c]Probability of successfully advancing to the next phase. [d]Probability of FDA approval for drugs in this phase of development. [e]FDA NME, biologic and non-NME classifications as defined in the results section. Data are presented for all end lead indication development paths. [f]BioMedTracker classification of small molecule NMEs and large molecule drugs. Large molecules are further stratified by biochemical profile.

Table 5 Phase success and LOA by disease[a]

	Phase 1 to phase 2				Phase 2 to phase 3				Phase 3 to NDA/BLA				NDA/BLA to approval			
	Total in phase[b]	Advanced or suspended[c]	Phase success[d]	Phase LOA[e]	Total in phase[b]	Advanced or suspended[c]	Phase success[d]	Phase LOA[e]	Total in phase[b]	Advanced or suspended[c]	Phase success[d]	Phase LOA[e]	Total in phase[b]	Advanced or suspended[c]	Phase success[d]	Phase LOA[e]
All indications																
Other[f]	254	198	78.2%	18.2%	419	281	44.2%	26.3%	252	159	71.1%	57.1%	169	112	80.4%	80.4%
Infectious disease	247	196	65.8%	16.7%	288	187	45.9%	28.4%	159	98	68.3%	55.4%	116	86	84.9%	84.9%
Autoimmune	241	178	68.0%	12.7%	350	315	34.0%	18.7%	149	95	68.4%	55.0%	88	61	80.3%	80.3%
Endocrine	223	180	58.3%	11.6%	293	198	33.8%	19.8%	147	95	67.4%	58.5%	91	61	86.9%	86.9%
Respiratory	110	90	66.7%	11.1%	193	120	27.5%	16.7%	58	30	63.3%	60.8%	33	25	96.0%	96.0%
Neurology	389	298	62.4%	9.4%	520	348	30.2%	15.0%	285	188	60.6%	49.9%	132	102	82.2%	82.2%
Cardiovascular	158	127	60.6%	7.1%	239	152	26.3%	11.7%	121	89	62.8%	44.6%	78	58	84.5%	84.5%
Oncology	319	651	63.9%	6.7%	1,451	827	28.3%	10.5%	383	221	45.2%	37.0%	142	104	81.7%	81.7%
Total	2,541	1,918	64.5%	10.4%	3,743	2,268	32.4%	16.2%	1,554	975	60.1%	50.0%	908	659	83.2%	83.2%
Lead indications																
Other[f]	193	146	75.3%	24.8%	273	157	50.3%	32.5%	174	115	74.8%	64.5%	122	81	86.4%	86.4%
Infectious disease	228	181	66.9%	19.3%	248	136	45.9%	28.6%	127	76	69.7%	62.8%	94	70	90.0%	90.0%
Respiratory	79	66	63.6%	16.3%	120	76	31.6%	38.6%	40	20	85.0%	81.0%	29	21	95.2%	95.2%
Autoimmune	165	127	67.7%	15.4%	178	102	37.3%	22.8%	77	52	80.8%	61.1%	56	37	75.7%	75.7%
Endocrine	188	152	61.2%	14.5%	226	155	38.1%	23.8%	122	78	69.2%	62.4%	78	51	90.2%	90.2%
Oncology	489	334	68.9%	13.2%	527	298	42.3%	19.1%	193	106	54.7%	45.3%	85	58	82.8%	82.8%
Neurology	301	228	62.7%	12.3%	339	218	34.4%	19.6%	191	124	66.9%	56.8%	137	106	84.9%	84.9%
Cardiovascular	127	102	62.7%	8.7%	189	106	27.4%	13.8%	85	62	56.5%	50.6%	63	48	89.6%	89.6%
Total	1,770	1,336	66.5%	15.3%	2,070	1,247	39.8%	23.1%	1,009	633	67.6%	58.4%	664	472	86.4%	86.4%

[a]Categories are listed from highest to lowest LOA from phase 1 for all indications (lead and nonlead). [b]Number of indications qualified. [c]Total number of transitions used to calculate the success rate, the *n* value noted in the text. The difference between 'Total in phase' and 'Advanced or suspended' is the number of indications that remain in development. [d]Probability of successfully advancing to the next phase. [e]Probability of FDA approval for drugs in this phase of development. [f]Includes allergy, gastroenterology, cardiotoxicology, dermatology, obstetrics/gynecology and urology.

initiating a pivotal phase 3 program, companies can submit the protocol to the FDA to obtain the agency's agreement that the trial(s) are adequate to meet its scientific and regulatory requirements. At the same time, these trials are often more complex and investigate treatments for less well understood diseases. This latter point is evident from our analysis. NDA/BLA success rates for SPA-designated drugs are slightly below average at 80.0% ($n = 45$) compared with 83.2% ($n = 659$) for all drugs. On the other hand, phase 3 success rates are nearly identical at 60.0% ($n = 110$) for SPA-designated drug indications compared with 60.1% ($n = 975$) for all drugs.

Orphan drug pathway success rates. A company may request that FDA grant the orphan designation for a drug being studied in a rare disease or condition. This is intended for indications affecting fewer than 200,000 people in the United States. Orphan drug designation was designed to reduce development costs and provide financial incentives (e.g., an extended exclusivity period) to encourage development in these indications. **Table 9** shows that although drugs for orphan indications have high rates of phase 1 and 2 success, phase 3 and NDA/BLA success rates are similar to all indications. Even so, it is important to note that orphan designations can be granted at any point in the clinical development process and are most often received when a drug is in phase 2. Orphan drugs in our data set received orphan status at all stages of development: preclinical (9%), phase 1 (22%), phase 2 (45%), phase 3 (16%) and NDA/BLA (2%). This distribution introduces a positive bias in early development success rates as some trials are not annotated as orphan until later phases. In contrast, by phase 3, 82% of indications that end up with the orphan designation have been annotated. Indeed, orphan indication phase 1 and 2 success rates were well above average at 86.8% ($n = 136$) and 70.0% ($n = 190$), respectively. Orphan phase 3 success rates (66.9%, $n = 148$) also compared favorably with all indications (60.1%, $n = 975$) and orphan NDA/BLA approvals were lower, 81.0% ($n = 84$) compared with 83.2% ($n = 659$), respectively. A subgroup analysis of phase 3 and NDA/BLA stage orphan drugs by indication reveals that oncology success rates were lower than nononcology drugs, a result that is consistent with these categories in the full data set.

NDA/BLA success rates

To complement the NDA/BLA phase success rates gathered above, we examined 910 FDA decisions from 2005 to 2011 and classified each as 'Approved' or 'Not Approved.' In addition, we determined at which FDA review each decision occurred (i.e., the first, second, third, fourth or fifth time the agency reviewed the specific application). **Figure 3a** shows the cumulative success rates for NDA/BLA filings in the all, lead and NME drug classifications. Only 56.9% of all applications were approved on the first NDA/BLA submission, whereas 86.2% were approved by the third submission. After the third submission, there was only a marginal increase in the cumulative approval percentage, as there were few drugs with more than three regulatory reviews. For all NMEs, we found similar first submission success rates, yet fewer than 80% of these drugs were approved by FDA in subsequent submissions.

Analysis of first review approval success rates by disease reveals a variation inconsistent with cumulative approval rates. For example, **Figure 3b** shows that although oncology drugs had a median NDA/BLA success rate (81%), the chances of a first review approval were the highest, at 71%. Neurology drugs, on the other hand, had the lowest first review approval rate at 36%, but the cumulative approval rate reached 78%.

We also examined 304 first review FDA complete response letters and approvable letters issued for approved and suspended drugs. For approved drugs, 46% of the letters to the sponsor cited manufacturing or labeling issues and 47% cited efficacy or safety. In contrast, for suspended drugs, only 2% cited manufacturing or labeling issues and

Table 6 Phase success and LOA for oncology and non-oncology disease groups

	Phase 1 to phase 2				Phase 2 to phase 3				Phase 3 to NDA/BLA				NDA/BLA to approval			
	Total in phase[a]	Advanced or suspended[b]	Phase success[c]	Phase LOA[d]	Total in phase[a]	Advanced or suspended[b]	Phase success[c]	Phase LOA[d]	Total in phase[a]	Advanced or suspended[b]	Phase success[c]	Phase LOA[d]	Total in phase[a]	Advanced or suspended[b]	Phase success[c]	Phase LOA[d]
FDA classification[e]																
All indications	2,541	1,918	64.5%	10.4%	3,743	2,268	32.4%	16.2%	1,554	975	60.1%	50.0%	908	659	83.2%	83.2%
Total oncology	919	651	63.9%	6.7%	1,451	827	28.3%	10.5%	383	221	45.2%	37.0%	142	104	81.7%	81.7%
Oncology NMEs	574	402	65.9%	6.6%	948	534	27.5%	10.0%	246	150	46.0%	36.4%	101	77	79.2%	79.2%
Oncology biologics	244	177	61.6%	7.3%	346	193	30.6%	11.9%	83	41	43.3%	39.0%	24	18	88.9%	88.9%
Oncology non-NMEs	53	39	63.2%	9.4%	76	50	22.0%	13.6%	26	17	70.6%	61.8%	16	8	87.5%	87.5%
Total non-oncology	1622	1267	64.8%	12.1%	2,292	1,441	34.8%	18.7%	1,171	754	64.5%	53.8%	766	555	83.4%	83.4%
Non-oncology NMEs	1011	816	63.4%	7.9%	1,427	936	29.3%	12.4%	566	365	56.2%	42.4%	324	216	75.5%	75.5%
Non-oncology biologics	328	234	73.5%	19.4%	473	271	43.2%	26.4%	237	141	68.8%	61.1%	135	98	88.8%	88.8%
Non-oncology non-NMEs	165	129	65.9%	22.7%	279	176	51.7%	34.5%	295	217	76.0%	66.7%	277	219	87.7%	87.7%
BioMedTracker product category[f]																
All indications	2,541	1,918	64.5%	10.4%	3,743	2,268	32.4%	16.2%	1,554	975	60.1%	50.0%	908	659	83.2%	83.2%
Total oncology	919	651	63.9%	6.7%	1,451	827	28.3%	10.5%	383	221	45.2%	37.0%	142	104	81.7%	81.7%
Oncology small molecule NMEs	492	346	66.5%	7.2%	830	466	26.8%	10.9%	219	136	45.6%	37.8%	93	70	82.9%	82.9%
Oncology mAbs	175	125	68.0%	9.3%	345	140	29.3%	13.7%	56	30	50.0%	46.9%	21	16	93.8%	93.8%
Oncology proteins/peptides	68	50	48.0%	3.4%	108	57	31.6%	7.1%	34	16	37.5%	22.5%	8	5	60.0%	60.0%
Oncology vaccines	41	28	50.0%	1.6%	73	43	39.5%	3.3%	28	12	8.3%	8.3%	1	1	100.0%	100.0%
Total non-oncology	1622	1267	64.8%	12.1%	2,292	1,441	34.8%	18.7%	1,171	754	64.5%	53.8%	766	555	83.4%	83.4%
Non-oncology small molecule NMEs	843	587	64.3%	7.7%	1,223	817	29.1%	11.9%	506	313	55.3%	40.7%	276	194	73.7%	73.7%
Non-oncology mAbs	184	109	72.5%	19.3%	213	128	47.7%	25.6%	92	54	66.7%	55.9%	44	37	83.8%	83.8%
Non-oncology proteins/peptides	228	178	65.7%	18.0%	321	198	42.4%	27.4%	191	118	63.5%	54.7%	125	72	93.1%	93.1%
Non-oncology vaccines	82	57	71.9%	21.8%	87	38	47.4%	30.3%	44	25	64.0%	64.0%	22	19	100.0%	100.0%

[a]Number of indications identified. [b]Total number of transitions used to calculate the success rate, the n value noted in the text. The difference between 'total in phase' and 'advanced or suspended' is the number of indications that remain in development. [c]Probability of successfully advancing to the next phase. [d]Probability of FDA approval for drugs in this phase of development. [e]Oncology and non-oncology disease groups and FDA (NME, biologic, and non-NME) classifications. Data are presented for all indication development paths. [f]Oncology and non-oncology disease groups and BioMedTracker biochemical categories.

83% cited efficacy or safety. Furthermore, we analyzed the time to drug approval after receiving a first complete response letter and found a 15-month average delay across all diseases with a setback of over one year for all diseases except (**Supplementary Fig. 1**) infectious disease (**Supplementary Fig. 2**).

Lead and nonlead indication success rates

Classifying drugs by lead and nonlead indications results in a selection bias favoring lead indication success rates. For lead indications that are suspended, and have a nonlead development path in-progress, the nonlead indication is redefined as the lead indication. The most advanced nonlead indications therefore becomes the lead indications once the initial lead is suspended. The BioMedTracker database is maintained as such for real-time viewing of pipelines, where it is critical to identify a company's lead program for each compound.

This lead indication annotation methodology tracks the most successful development path, and closely resembles the best case scenario for a specific drug. On the other hand, nonlead indication success rates understate the importance of lead indications that were previously designated as nonlead. Nonlead indication success rates are included in **Supplementary Table 2**, and, as expected, have a much lower success rate across all phases. For nonlead indications, the LOA from phase 1 was 4.9% ($n = 2,132$) compared with 15.3% ($n = 3,688$) for lead indications. The most pronounced deviation was found in phase 3, where lead indications had a 67.6% ($n = 633$) success rate, whereas nonlead indications had a 46.2% ($n = 342$) probability of advancing to NDA/BLA. The disparity between lead and nonlead success rates is noteworthy, and the accuracy of nonlead rates must be viewed in the context of the selection methodology.

DISCUSSION

During the time frame of this study, approximately one development path in ten (10.4%) that enters clinical development in phase 1 is expected to advance to FDA approval. We also analyzed lead indication data and found nearly a one-in-six (15.3%) probability a drug will advance from phase 1 to FDA approval. We believe that the lower success rate for all-indication development paths more accurately reflects drug development success rates in industry and is particularly important when considering the cost and time of unsuccessful clinical trials.

One limitation of this study is the direct comparison of these data and methodology on a year-by-year or decade-by-decade basis. For example, a program was designated as

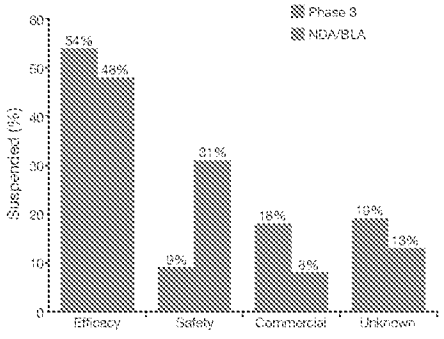

Figure 4 Root-cause analysis for 359 phase 3 and 95 NDA/BLA suspended programs. A program was designated as 'suspended' when conclusive evidence had been gathered regarding a company's plans to discontinue development or communications with regulators were not reinitiated for several years.

'suspended' when conclusive evidence had been gathered regarding a company's plans to discontinue development, or communications with regulators were not reinitiated for several years. Unfortunately, the timing of annotating suspended indications and drugs is not precise enough to analyze yearly changes in success rates. Furthermore, real-time data collection was initiated in 2003; thus, we cannot directly compare prior decades using these data and must rely on results published in the literature.

Many previous studies considered only a drug's most advanced indication to determine drug development success rates. Most published data from the 1960s to present reported success rates ranging from one in five to one in eight[14–19]. For comparison with more recent findings, we summarize in **Table 3** the results from DiMasi *et al.*[6], Kola *et al.*[8] and Abrantes-Metz *et al.*[9]. The most recent publication on the subject, from DiMasi *et al.*[6], reports a nearly one-in-five LOA from phase 1 (19%, $n = 1,316$) from 1993 to 2009. In Kola *et al.*[8], the authors found an LOA from phase 1 of 11%, close to the 10.4% reported here for all indications. However, given the small number of company pipelines (10 versus 835 reported here) and lack of information about the number of drugs advanced or suspended in this study, these results were inconclusive. In addition, the Abrantes-Metz *et al.*[9] data covered a similar period as Kola *et al.*[8], 1989 to 2002 versus 1991 to 2000, respectively, but did not report NDA/BLA success rates. If we were to conservatively apply the 83.2% NDA/BLA success rate found in this study, Abrantes-Metz *et al.*[9] would yield the highest LOA from phase 1 (21%), again near one in five.

Comparing the phase transitions, phase 2 success rates were consistently lower than phase 1, with phase 1 ranging from 65% to 81%, and phase 2 from 32% to 58%. In this study, and in DiMasi *et al.*[6] and Kola *et al.*[8], a step-up in phase 3 success rates from phase 2 rates was observed. Only Abrantes-Metz *et al.*[9] reported a phase 2 success rate (57.7%) in-line with phase 3 (56.7%), a result that was 20 percentage points higher than the phase 2 success rate in Kola *et al.*[8] (38%) for a similar time period (**Table 3**). There are fewer data available to compare NDA/BLA success rates, but our result of 83.2% is similar to that of Kola *et al.*[8] (77%) and 10% lower than that of DiMasi *et al.*[6].

For lead indication success rates, our results are similar to that found by DiMasi *et al.*[6]. Although our LOA from phase 1 for lead indications (15.3%) is below DiMasi *et al.*'s[6] 19% result, it is close to their 16% result for self-originated drugs. We also note that the 16% success rate for self-originated drugs held over multiple time frames (1993–1998 and 1999–2004) in their studies. One possible explanation is that success rates for self-originated drugs at large pharmaceutical companies are less prone to selection bias compared with late-stage, in-licensed drugs.

Factors contributing to lower success rates found in this study include the large number of small biotech companies represented in the data, more recent time frame (2003–2011) and higher regulatory hurdles for new drugs. Small biotech companies tend to develop riskier, less validated drug classes and targets, and are more likely to have less experienced

Table 7 Phase success and LOA for oncology subgroups and cancer types

	Phase 1 to phase 2				Phase 2 to phase 3				Phase 3 to NDA/BLA				NDA/BLA to approval			
	Total in phase[a]	Advanced or suspended[b]	Phase success[c]	Phase LOA[d]	Total in phase[a]	Advanced or suspended[b]	Phase success[c]	Phase LOA[d]	Total in phase[a]	Advanced or suspended[b]	Phase success[c]	Phase LOA[d]	Total in phase[a]	Advanced or suspended[b]	Phase success[c]	Phase LOA[d]
All indications	2,541	1,918	64.5%	10.4%	3743	2268	32.4%	16.2%	1554	975	60.1%	50.0%	908	669	85.2%	83.2%
Total oncology	919	661	63.9%	5.4%	1461	827	28.3%	8.5%	383	147	36.7%	30.0%	142	104	81.7%	81.7%
Total solid tumors	668	483	66.7%	5.7%	1114	636	26.3%	8.6%	299	172	41.3%	32.7%	88	67	79.1%	79.1%
Renal cell cancer (RCC)	20	15	86.7%	18.4%	54	33	30.3%	21.2%	15	10	70.0%	70.0%	7	6	100.0%	100.0%
Head and neck cancer	6	5	100.0%	14.3%	22	12	50.0%	14.3%	14	7	42.9%	28.6%	3	3	66.7%	66.7%
Hepatocellular (liver) cancer (HCC)	18	15	73.3%	6.6%	39	25	36.0%	9.0%	12	4	25.0%	25.0%	1	1	100.0%	100.0%
Breast cancer	54	47	68.1%	5.7%	119	61	21.3%	8.4%	34	25	86.0%	39.2%	14	10	70.0%	70.0%
Non-small cell lung cancer (NSCLC)	63	55	87.3%	5.7%	161	94	29.8%	6.5%	46	23	26.1%	21.7%	11	6	83.3%	83.3%
Prostate cancer	42	8	71.0%	6.6%	103	24	20.9%	7.8%	25	8	56.3%	37.5%	11	3	66.7%	66.7%
Colorectal cancer (CRC)	45	37	62.2%	6.1%	87	56	21.4%	8.2%	18	13	38.5%	38.5%	4	4	100.0%	100.0%
Ovarian cancer	31	25	68.0%	4.6%	72	37	27.0%	6.8%	15	8	25.0%	25.0%	3	1	100.0%	100.0%
Pancreatic cancer	29	24	75.0%	3.3%	66	36	30.6%	3.1%	13	10	20.0%	10.0%	2	2	50.0%	50.0%
Total hematological tumors	216	152	58.6%	9.9%	317	179	34.6%	16.3%	78	45	55.6%	48.8%	48	33	87.9%	87.9%
Multiple myeloma (MM)	43	29	69.0%	3.7%	48	30	23.3%	14.0%	13	5	60.0%	60.0%	5	4	100.0%	100.0%
Non-Hodgkin's lymphoma (NHL)	38	28	57.1%	8.5%	62	35	40.0%	14.8%	19	9	44.4%	37.0%	6	6	83.3%	83.3%
Chronic lymphocytic leukemia (CLL)	17	12	50.0%	7.3%	41	24	29.2%	14.6%	10	8	62.5%	50.0%	7	5	80.0%	80.0%
Myelodysplastic syndrome (MDS)	12	7	71.4%	4.8%	22	9	33.3%	6.7%	6	5	20.0%	20.0%	4	3	100.0%	100.0%

[a]Number of indications identified. [b]Total number of transitions used to calculate the success rate, the *n* value noted in the text. The difference between 'total in phase' and 'advanced or suspended' is the number of indications that remain in development. [c]Probability of successfully advancing to the next phase. [d]Probability of FDA approval for drugs in this phase of development.

Table 8 Phase success and LOA for neurology and autoimmune diseases (broken further into rheumatoid arthritis and type II diabetes)

	Phase 1 to phase 2				Phase 2 to phase 3				Phase 3 to NDA/BLA				NDA/BLA to approval			
	Total in phase[a]	Advanced or suspended[b]	Phase success[c]	Phase LOA[d]	Total in phase[a]	Advanced or suspended[b]	Phase success[c]	Phase LOA[d]	Total in phase[a]	Advanced or suspended[b]	Phase success[c]	Phase LOA[d]	Total in phase[a]	Advanced or suspended[b]	Phase success[c]	Phase LOA[d]
All indications	2,541	1,918	64.5%	10.4%	3,743	2,268	32.4%	16.3%	1,554	975	60.1%	50.0%	908	669	83.2%	83.2%
Total neurology	389	298	62.4%	9.4%	520	348	30.2%	15.0%	285	188	60.6%	49.9%	192	152	82.2%	82.2%
Psychiatric disease	97	80	60.0%	7.2%	148	116	23.3%	12.0%	83	43	63.3%	51.6%	57	49	81.6%	81.6%
Pain	96	73	67.1%	10.7%	113	79	27.8%	15.9%	67	46	67.4%	57.2%	42	33	84.8%	84.8%
Other	136	136	58.8%	9.8%	259	153	38.6%	16.7%	135	93	55.3%	45.5%	93	70	81.4%	81.4%
Total autoimmune disease	241	178	68.0%	12.7%	350	215	34.0%	18.7%	149	95	68.4%	55.0%	88	61	80.3%	80.3%
Total autoimmune disease NMEs	111	88	62.5%	5.2%	181	86	32.1%	8.3%	38	20	50.0%	37.5%	16	8	75.0%	75.0%
Total autoimmune disease biologics	116	80	73.8%	22.5%	171	111	48.0%	30.5%	89	56	75.0%	67.7%	53	41	90.2%	90.2%
Total autoimmune disease non-NMEs	10	8	87.5%	7.9%	22	16	35.0%	9.0%	21	18	72.2%	36.1%	18	12	50.0%	50.0%
Total rheumatoid arthritis	65	54	74.1%	10.3%	102	63	15.9%	13.5%	16	8	87.5%	87.5%	10	5	100.0%	100.0%
Rheumatoid arthritis NMEs	30	29	69.0%	NA	46	29	10.3%	NA	4	1	100.0%	NA	2	0	NA	NA
Rheumatoid arthritis biologics	32	24	79.2%	15.9%	49	29	24.1%	20.1%	13	6	83.3%	83.3%	7	5	100.0%	100.0%
Total type II diabetes	110	89	60.7%	9.3%	128	84	29.8%	15.3%	53	37	59.5%	51.4%	31	22	86.4%	86.4%
Diabetes NMEs	83	68	63.2%	7.5%	100	69	23.0%	11.8%	35	25	56.0%	40.7%	15	11	72.7%	72.7%

[a]Number of indications identified. [b]Number of transitions used to calculate the success rate, the *n* value added at the top. The difference between 'Total in phase' and 'Advanced or suspended' is the number of indications that remain in development. [c]Probability of successfully advancing to the next phase. [d]Probability of FDA approval for drugs in this phase of development. NA, data not available.

development teams and fewer resources than large pharmaceutical corporations. The past nine-year period has been a time of increased clinical trial cost and complexity for all drug development sponsors, and this likely contributes to the lower success rates than previous periods. In addition, an increasing number of diseases have higher scientific and regulatory hurdles as the standard of care has improved over the past decade. More clinical studies are comparative in nature and published data show clinical trials are more complex today than in previous decades[7]. The time frame in this study also coincides with the shift toward greater regulatory uncertainty and stronger emphasis on safety at the FDA since the 2004 Vioxx (rofecoxib) recall. For smaller companies, financing challenges in the past several years have also affected development progression decisions. Phase success rates reported in this study are based on transition rates, not necessarily resulting from safety or efficacy data. Transition rates are negatively affected by early development termination due to commercial and regulatory uncertainty as well as economic and portfolio management decisions.

Lower success rates found when analyzing all indications likely results from including nonlead and/or secondary indications. Nonlead development paths have far lower success rates compared with lead programs. One possible explanation is that many companies first develop drugs in lead indications where the strongest scientific rationale and early efficacy signals are found. Lead indications are also often smaller, better-defined patient populations. After initial success in these populations, companies may decide to investigate nonlead indications, which may not have the same scientific support, homogeneous patient population or development and regulatory path as the lead indication. Nonlead success rates are also important to monitor as many of these indications can be moved directly into late-stage trials, where most clinical development costs occur. Furthermore, our research suggests that these late-stage trials for nonlead indications often enroll a greater number of patients than lead indications.

Phase 3 success rates. In **Figures 1** and **2**, we show that phase 3 success rates are 60% for drugs for all indications, but only around 50% in oncology or cardiology. Such low phase 3 success rates for these diseases are concerning as 35% of all R&D spending is now spent on phase 3 development, and phase 3 trials account for 60% of all clinical trial costs[3]. Some of the low phase 3 rates may be attributed to trial design factors and insufficient communication between sponsors and regulators during their end-of-phase-2 meetings. Both oncology and cardiology, for example, now require outcome studies looking for improved overall survival, but lack well-validated surrogate markers for this outcome. On the other hand, disease areas with validated surrogate markers tend to have higher phase 3 success rates. For example, studies of infectious diseases such as hepatitis C and HIV that use viral load as a primary endpoint as well as glycosylated hemoglobin (HbA1c) in diabetes show higher success rates.

Oncology is a particularly challenging disease area in which to achieve phase 3 success. The FDA requires overall survival as the primary endpoint in most pivotal oncology studies. Crossover designs that allow patients who progress on the comparator arm to cross over and receive the investigational drug, or patients receiving additional approved and experimental salvage therapies, also make it more difficult to design well-controlled phase 3 studies with overall survival as a primary endpoint. Furthermore, current animal models (e.g., xenograft tumor models in mice) can be poor predictors of clinical outcomes in humans. Additionally, recent scientific reports show that certain types of cancer, which were previously thought of as one disease, may actually comprise several subtypes of disease with different etiologies. For example, NSCLC is now considered by many oncologists to be at least ten different mutation-specific diseases, and thus it is not surprising that drugs for NSCLC have one of the lowest LOAs from phase 1 of all oncology indications in **Table 7** (ref. 20).

Table 9 Phase success and LOA for drugs receiving a FDA SPA or orphan drug designation

	Phase 1 to phase 2				Phase 2 to phase 3				Phase 3 to NDA/BLA				NDA/BLA to approval			
	Total in phase[a]	Advanced or suspended[b]	Phase success[c]	Phase LOA[d]	Total in phase[a]	Advanced or suspended[b]	Phase success[c]	Phase LOA[d]	Total in phase[a]	Advanced or suspended[b]	Phase success[c]	Phase LOA[d]	Total in phase[a]	Advanced or suspended[b]	Phase success[c]	Phase LOA[d]
All indications	2,541	1,918	64.5%	10.4%	3,743	2288	32.4%	16.2%	1,554	375	60.1%	50.0%	908	659	83.2%	83.2%
Total SPAs	42	35	97.1%	45.4%	128	116	97.4%	46.7%	171	110	60.0%	48.0%	73	45	80.0%	80.0%
Total orphans	170	136	86.8%	52.2%	328	190	70.0%	37.9%	237	148	66.9%	54.2%	136	84	81.0%	81.0%
Orphan oncology	85	67	85.1%	23.0%	176	105	61.0%	27.1%	102	63	66.7%	44.4%	54	37	75.7%	75.7%
Orphan non-oncology	85	69	88.4%	44.5%	152	85	81.3%	50.4%	135	85	72.9%	62.1%	82	47	85.1%	85.1%

[a]Number of indications identified. [b]Total number of transitions used to calculate the success rate, the p value noted in the text. The difference between 'Total in phase' and 'Advanced or suspended' is the number of indications that remain in development. [c]Probability of successfully advancing to the next phase. [d]Probability of FDA approval for drugs in this phase of development.

Clinical trials targeting heterogeneous patient populations may have lower success rates than trials identifying responders within a population through the use of biomarkers. As predictability of clinical outcomes increases through the use of molecular diagnostics in earlier testing, it is possible that phase 3 trial success rates will rise. Furthermore, the adoption of adaptive trial design may facilitate the identification of targeted subsets of patient populations before study completion. According to the FDA's draft guidance for industry, issued in February 2010, adaptive trial design may make clinical studies more efficient (e.g., shorter duration and fewer patients), more likely to demonstrate an effect of the drug or more informative (e.g., providing broader dose-response information)[21].

Root causes of phase 3 and NDA/BLA development failures. To gain a better understanding of the causes that lead companies to discontinue drug development, we further analyzed publically available information for the 359 phase 3 and 95 NDA/BLA suspensions included in this study. We classified each discontinued development program into four categories based on the primary reason for suspension including: efficacy, safety, commercial and unknown (**Fig. 4**).

Although it was difficult to objectively determine if a phase 3 study did not reach an endpoint due to poor study design or the drug's biological activity, we found that over half of the 359 suspensions were attributable to some measure of efficacy. Indeed, a detailed analysis of the specific inputs, rationale and history for each program would be needed to identify issues related to poor trial design. Furthermore, public information is not available to assess the degree of communication with regulators, adherence to recommendations, changes to prior standards and input from phase 2 data that would inform the design of a phase 3 study.

We found that 18% of the phase 3 suspensions resulted from a company's commercial decision to not file for approval. We do not know the degree to which regulatory uncertainty factored into these decisions, but recognize its important impact on portfolio management, funding and commercial opportunities due to the increased time and costs of drug development.

Safety was the least likely cause for suspension in phase 3 (9%), perhaps due to significant adverse events identified earlier in drug development. Approximately 20% of the suspensions occurred without publicly available information citing the reason for failure.

We also analyzed the 95 suspended NDA/BLA filings in the data set and found that approximately one-third of failures were attributable to safety concerns raised by regulators compared to only 9% in phase 3. Our analysis also revealed that around half involved cases where the FDA requested additional trials. One interpretation of these data is that sponsors file for regulatory approval believing their drug meets safety guidelines, whereas regulators remain concerned about safety, illustrating insufficient communication between regulators and sponsors. During the period of this study, mainly after the 2004 Vioxx recall, many industry observers have discussed how the benefit-to-risk pendulum has swung toward risk, with a greater focus on safety in the regulatory assessment. Some examples of issues brought forward by regulators were the need for longer-term data, inclusion of additional study arms, inclusion of different patient age and at-risk populations, and increases in the number of patients studied.

Further analysis of failures by lead or non-lead indication, disease, modality and company type were not performed because the small sample size has limitations and subjects the results to molecular and therapeutic class-specific issues. Future studies will allow us to identify trends in failed clinical programs as the sample size becomes more reliable.

Conclusions

The data presented in this study suggest industry-wide productivity may have declined from previous estimates. Achieving FDA approval for only one-in-ten drug indications that enter the clinic is a concerning statistic for drug developers, regulators, investors and patients. We believe progress in clinical science and regulatory risk-benefit assessment can improve success rates. Greater flexibility with alternative surrogate endpoints, the utilization of adaptive clinical trial design and improved methodologies for assessing patient benefit-to-risk are some areas where improvements can be made. In addition, improvements in communication between sponsors and regulators could help reduce regulatory applications that lack safety or efficacy data that are later requested by regulators. Simultaneously, improvements in basic science can enable improvements in success rates. For example, more predictive animal models, earlier toxicology evaluation, biomarker identification and new targeted delivery technologies may increase future success in the clinic.

ACKNOWLEDGMENTS

This research was supported by Sagient Research Systems and the Biotechnology Industry Organization (BIO). The authors are indebted to the analysts at BioMedTracker who have collected these data. We would also like to thank our colleagues at BIO and BioMedTracker for their input and advice in the development of this study. The authors are solely responsible for the design, conduct and analysis of the study, and the conclusions that are drawn. The opinions expressed in this article are those of the authors and do not necessarily reflect the views of their employers.

AUTHOR CONTRIBUTIONS

M.H., D.W.T. and J.E.C. all contributed equally to this work.

COMPETING FINANCIAL INTERESTS

The authors declare competing financial interests: details are available in the online version of the paper (doi:10.1038/nbt.2786).

1. Lloyd, I., ed. Citeline Drug Intelligence. *Pharma R&D Annual Review 2011*. http://www.citeline.com/

wp-content/uploads/Citeline-Pharma-R&D-annual-review-2011.pdf (Citeline Drug Intelligence, 2012).
2. EvaluatePharma. *World Preview 2018: Embracing the Patent Cliff*. http://info.evaluatepharma.com/WP2018_ELS_LP.html (2012).
3. Pharmaceutical Research and Manufacturers of America. *Annual Report 2011*. http://www.phrma.org/sites/default/files/159/phrma_2011_annual_report.pdf (2011).
4. Mullard, A. 2012 FDA drug approvals. *Nat. Rev. Drug Discov.* **12**, 87–90 (2013).
5. Cohen, F.J. Macro trends in pharmaceutical innovation. *Nat. Rev. Drug Discov.* **4**, 78–84 (2005).
6. DiMasi, J.A., Feldman, L., Seckler, A. & Wilson, A. Trends in risks associated with new drug development: success rates for investigational drugs. *Clin. Pharmacol. Ther.* **87**, 272–277 (2010).
7. Kaitin, K.I. & DiMasi, J.A. Pharmaceutical innovation in the 21st century: new drug approvals in the first decade, 2000–2009. *Clin. Pharmacol. Ther.* **89**, 183–188 (2011).
8. Kola, I. & Landis, J. Can the pharmaceutical industry reduce attrition rates? *Nat. Rev. Drug Discov.* **3**, 711–715 (2004).
9. Abrantes-Metz, R., Adams, C. & Metz, A. *Pharmaceutical Development Phases: A Duration Analysis*. Working paper no. 274. http://www.ftc.gov/be/workpapers/wp274.pdf (US Federal Trade Commission: Bureau of Economics, 2004).
10. Henderson, R. & Cockburn, I. Scale, scope, and spillovers: the determinants of research productivity in drug discovery. *Rand J. Econ.* **27**, 32–59 (1996).
11. Cockburn, I.M. & Henderson, R.M. Scale and scope in drug development: unpacking the advantages of size in pharmaceutical research. *J. Health Econ.* **20**, 1033–1057 (2001).
12. Danzon, P.M., Nicholson, S. & Pereira, N.S. Productivity in pharmaceutical–biotechnology R&D: the role of experience and alliances. *J. Health Econ.* **24**, 317–339 (2005).
13. Arora, A., Gambardella, A., Magazzini, L. & Pammolli, F. A breath of fresh air? Firm type, scale, scope, and selection effects in drug development. *Manage. Sci.* **55**, 1638–1653 (2009).
14. Sheck, L. *et al.* Success rates in the United States drug development system. *Clin. Pharmacol. Ther.* **36**, 574–583 (1984).
15. Tucker, S.A., Blozan, C. & Coppinger, P. The Outcome of Research on New Molecular Entities Commencing Clinical Research in the Years 1976–79 (OPE Study 77). (Office of Planning and Evaluation, US Food and Drug Administration, Rockville, MD, 1988).
16. DiMasi, J.A. Success rates for new drugs entering clinical testing in the United States. *Clin. Pharmacol. Ther.* **58**, 1–14 (1995).
17. DiMasi, J.A. Risks in new drug development: approval success rates for investigational drugs. *Clin. Pharmacol. Ther.* **69**, 297–307 (2001).
18. DiMasi, J.A., Hansen, R.W. & Grabowski, H.G. The price of innovation: new estimates of drug development costs. *J. Health Econ.* **22**, 151–185 (2003).
19. DiMasi, J.A. & Grabowski, H.G. The cost of biopharmaceutical R&D: is biotech different? *Manag. Decis. Econ.* **28**, 469–479 (2007).
20. Edelman, M.J. in *2010 American Society of Clinical Oncology (ASCO) Annual Meeting* (Chicago, IL, 2010).
21. FDA. *Guidance for Industry: Adaptive Design Clinical Trials for Drugs and Biologics*. http://www.fda.gov/downloads/drugs/guidancecomplianceregulatoryinformation/guidances/ucm201790.pdf (FDA, Center for Drug Evaluation and Research, Center for Biologics Evaluation and Research, 2010).

Gene Therapy (2006) 13, 646–651

www.nature.com/gt

SHORT COMMUNICATION

Genospheres: self-assembling nucleic acid-lipid nanoparticles suitable for targeted gene delivery

ME Hayes[1,2], DC Drummond[1,2], DB Kirpotin[1,2], WW Zheng[1], CO Noble IV[1,3], JW Park[3], JD Marks[4], CC Benz[5] and K Hong[1,2]

[1]*California Pacific Medical Center, San Francisco, CA, USA;* [2]*Hermes Biosciences Inc., South San Francisco, CA, USA;* [3]*Department of Medicine, Division of Hematology-Oncology, Cancer Research Institute, University of California San Francisco, San Francisco, USA;* [4]*Department of Anesthesia, University of California San Francisco, San Francisco, USA and* [5]*The Buck Institute for Age Research, Novato, CA, USA*

We describe the assembly of a cationic lipid-nucleic acid nanoparticle from a liquid monophase containing water and a water miscible organic solvent where both lipid and DNA components are separately soluble prior to their combination. Upon removal of the organic solvent, stable and homogenously sized (70–100 nm) lipid-nucleic acid nanoparticles (Genospheres™) were formed. The low accessibility (< 15%) of the nanoparticle-encapsulated DNA to a DNA intercalating dye indicated well-protected nucleic acids and high DNA incorporation efficiencies. It was demonstrated that Genospheres could be stably stored under a variety of conditions including a lyophilized state where no appreciable increase in particle size or DNA accessibility was observed following reconstitution. Finally, Genospheres were made target-specific by insertion of an antibody-lipopolymer (anti-HER2 scFv (F5)-PEG-DSPE) conjugate into the particle. The target specificity (> 100-fold) in HER2 overexpressing SK-BR-3 breast cancer cells was dependent on the degree of PEGylation, where the incorporation of high amounts of PEG-lipid on the particle surface (up to 5 mol%) had only a minor effect on the transfection activity of the targeted Genospheres. In summary, this work describes a novel, readily scalable method for preparing highly stable immunotargeted nucleic acid delivery vehicles capable of achieving a high degree of specific transfection activity.
Gene Therapy (2006) 13, 646–651. doi:10.1038/sj.gt.3302699; published online 8 December 2005

Keywords: *nonviral gene delivery; plasmid encapsulation; targeted gene delivery; HER2 receptor*

Synthetic nonviral gene delivery vehicles offer the advantages of relatively easy preparation, lower toxicity and less expensive components in comparison with viral-based delivery methods. One common nonviral gene therapy delivery system is lipid mediated, usually assembled from mixtures of cationic liposomes and DNA (lipoplex). This method was first described in 1987 by Felgner *et al.*,[1] and up to July 2005 8.6% of worldwide clinical trials in gene therapy use this protocol or variations of it.[2] The relatively high positive charge, combined with a polymorphic lipid component, helps make these complexes efficient delivery vehicles *in vitro*, where the binding to cells is primarily electrostatic in nature and colloidal stability and target specificity are less of a concern than for delivery *in vivo*.

In contrast, the effectiveness of lipoplexes for targeted gene delivery *in vivo* has been disappointing.[3] It is known that their high cationic charge density aids their rapid clearance from circulation by the reticuloendothelial system and their tendency to form large aggregates enhances accumulation in the microvasculature of 'first pass' organs such as the spleen, liver and particularly the lungs.[4,5]

Newer procedures for encapsulating DNA have been developed, which produce small colloidally stable particles that have shown remarkable improvements in their pharmacokinetic characteristics in comparison to early lipoplexes. These procedures generally rely on assembly of the particles through steps involving precondensing DNA,[6] liquid–liquid phase separations and sonication,[7] extrusion,[8] rehydration of a dried complex previously extracted from an organic solvent,[9] the presence of detergents[10–12] or liposomal entrapment of nucleic acid.[13]

We suggested that formation of DNA-lipid particles could also be facilitated under such conditions where both lipid and DNA were molecularly or micellarly soluble *prior* to their combination. The concentration range of the organic solvent used to prepare these particles was chosen on the basis of the ability of the aqueous/organic solvent monophase to independently solubilize the nucleic acid and the lipid component before combination. For example, it is known that DNA-cationic surfactant complexes become soluble in aqueous/ethanol mixtures above 40% (v/v) ethanol[14] and that DNA precipitates in mixtures containing high concentrations of ethanol. Therefore, it was interesting to us to study the particles formed in intermediate ethanol concentrations where both DNA and lipid

Correspondence: Dr K Hong or Dr M Hayes, Hermes Biosciences Inc., 61 Airport Blvd., Suite D, South San Francisco, CA 94080, USA. E-mail: khong@hermesbio.com or mhayes@hermesbio.com
Received 27 February 2005; revised 13 October 2005; accepted 1 November 2005; published online 8 December 2005

components were soluble prior to combination. Under these conditions, interactions between DNA and cationic lipids would be improved, eliminating the major bilayer structural rearrangements that occur when DNA interacts with cationic liposomes.[15] In the present work, we describe this new method and the resulting nucleic acid-lipid nanoparticles were termed Genospheres™.

A typical composition was a cationic lipid dioctadecyldimethylammonium bromide (DDAB), or 1,2-dioleoyl-3-trimethylammonio)propane (DOTAP), a phosphatidylcholine (e.g. 1-palmitoyl-2-oleoyl phosphatidylcholine-POPC), cholesterol (Chol), and plasmid DNA in a ratio of 6:15:10:1 nmol:nmol:nmol:μg. The average molecular weight of a DNA base is 330 g mol^{-1}, so 1 μg of double-stranded DNA corresponds to approximately 3 nmol phosphate DNA, that is, (1×10^{-6} g DNA/330 g mol^{-1} = 3.03×10^{-9} mol). In the present study, Genospheres were formed with 5–6 nmol cationic lipid per μg DNA giving a $N(CH_3)_3^+/PO_4^-$ ratio from 1.67 to 2. As the majority of the preparations have a $\pm$ ratio of 2, we will only state the charge ratio where it differs from this value.

Genospheres were prepared as follows; cationic and neutral lipids were combined in 100% ethanol (Gold Shield Chemical Co., Hayward, CA, USA) and diluted with an equal volume of 5 mM HEPES, pH 7.4. Plasmid DNA from a stock solution (2 mg/ml in Tris-EDTA buffer, pH 8.0) was placed into a separate tube and the volume adjusted typically to that of the lipid solution volume with 5 mM HEPES, pH 7.4 and ethanol to a final concentration of 50% (v/v). Both tubes were placed in a water bath at 60°C and once thermally equilibrated, the DNA solution was added rapidly to the lipid solution, pipetting gently up and down 4–5 times to ensure complete mixing. The mixture was allowed to attain room temperature, and ethanol was removed by rotary evaporation or dialysis against unbuffered 144 mM NaCl. For ligand directed targeting studies, HER2-targeted Genospheres were prepared by incubation of Genospheres with F5-cys-mal-PEG(2000)-DSPE antibody conjugate in saline overnight at 37°C.[16] Typically, an amount of conjugate equal to 15 μg antibody was added per μmol of POPC in the sample. The antibody conjugate is presented in a solution also containing a proportion of cysteine quenched maleimide-PEG-DSPE[17] and therefore nontargeted control samples were heated in the same manner using an equivalent amount of additional PEG-DSPE. Genosphere samples were stored at 4°C until use.

The volume-weighted size distribution of the resulting particles was measured by dynamic light scattering (DLS), and they displayed an average size of 70–110 nm with a polydispersity in the range of 20–35 nm. Freeze-fracture electron microscopy (FFEM) was also used to characterize the size, shape, and polydispersity of Genosphere particles. The FFEM photographs indicated that the average size of Genospheres after ethanol removal was approximately 100 nm (Figure 1a) and the large number of similarly sized spherical particles observed per FFEM photograph indicates the uniformity of the particles. A FFEM micrograph taken of a Genosphere sample obtained after purification on a sucrose gradient (Figure 1b) shows their uniformity and similar size distribution to that seen before purification. This indicates that the particles formed initially following removal of ethanol from the bulk mixture, corresponded to true cationic lipid/nucleic acid particles and the observed structures are not simply empty lipid vesicles. The smooth fracture plane in the majority of the structures is indicative of the particles having a bilayer structure. In addition, DNA in these particles was well

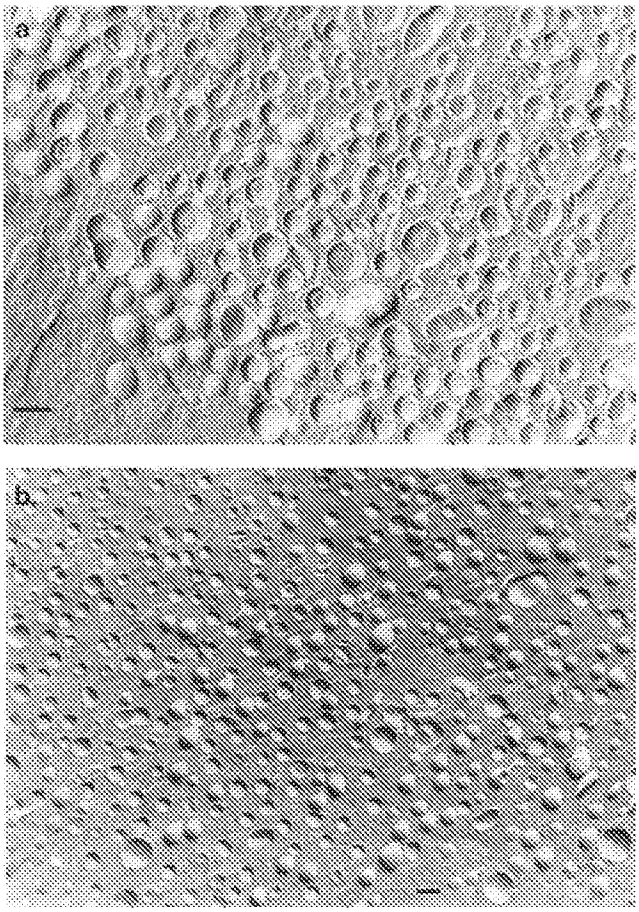

Figure 1 Freeze-fracture electron micrographs (FFEM) of Genospheres. Genosphere samples were analyzed by FFEM before (a) and after (b) purification on a sucrose gradient. Sample aliquots (200 μl) of Genospheres or HBS, pH 6.5 buffer (control) were carefully applied to the top of a 0–15% (w/w) sucrose gradient and the tubes ultra-centrifuged at 192 000 *g* for 10 h at 22°C (Ultracentrifuge L8-70M, Beckman) using an SW50.1 rotor. After centrifugation, aliquots (150 μl) were removed from each tube and in the case of the Genosphere containing tubes, the turbid fraction analyzed by FFEM. The samples were cooled rapidly in liquid propane using the sandwich technique (>10^4 k/sec). The fixed specimens were fractured and shadowed with Pt/C in a Balzers BAF 400D freeze-fracture device at −120°C and 2×10^{-6} Torr and the cleaned replicas subsequently examined by transmission electron microscopy using a Zeiss CEM 902A electron microscope. The particles consisted of DDAB/POPC/Chol/PEG-DSPE (6/6/12/0.12) nmol/nmol/nmol/nmol per μg DNA). Scale bars represent 100 nm in both pictures. All dialkyl lipids were purchased from Avanti Polar lipids (Alabaster, AL, USA) while Chol was purchased from Calbiochem (San Diego, CA, USA). Plasmid DNA (pCMV/luc$^+$) was prepared using an EndoFree Plasmid Giga kit (Qiagen, Chatsworth, CA, USA) from competent *Escherichia coli* amplified in LB medium. Plasmid concentration was determined by absorbance at 260 nm (ε = 6600 l mol^{-1} cm^{-1}) and purity by calculating the ratio $A_{260\,nm}/A_{230\,nm}$ (Shimadzu, UV160U). DNA was considered to be sufficiently protein free with $A_{260\,nm}/A_{230\,nm}$ ratio of at least 1.85. Particle size was also measured by DLS (Nicomp C370 Particle Size Analyzer).

protected from the surrounding medium, as determined from low Picogreen intercalating dye binding (<10%, see Figure 2b), therefore, we assume that DNA resides within the particle core.

The stability of a gene carrier against DNA degradation, particle aggregation and/or dissociation in plasma is an absolute requirement for *in vivo* delivery success. The stability of Genospheres against these processes was characterized *ex vivo* by measuring changes in size, DNA dye accessibility and susceptibility to DNase I digestion following incubation in 50% (v/v) human plasma (Figure 2a–c, respectively). The effect of PEGylation on the plasma stability of Genospheres was investigated by preparing Genospheres with 0.5–5 mol% PEG-DSPE (of cationic lipid and POPC content). The initial sizes of these particles was <100 nm, and the initial dye accessibility was approximately 6%, indicating highly protected DNA. Exposure to 50% (v/v) human plasma resulted in an increase in size over the duration of the study. However, the increase in size was reduced by inclusion of PEG-DSPE. The sample with 0.5 mol% PEG-DSPE exhibited a large increase in size, up to 1 μm. The more highly PEGylated samples (2–5 mol%) also increased in size, to 400 nm, where they remained for up to 24 h. For the Genospheres with a high neutral lipid content (15 nmol of POPC and 10 nmol Chol per μg DNA), the dye accessibility remained below 20% over 24 h. However, the sample with lower neutral lipid content showed higher instability, with approximately 40% dye accessibility over the same period. These results indicate that both PEGylation and the relative neutral lipid content affect Genosphere stability in the presence of plasma. The differences in stability may result from incomplete neutral lipid coverage, or possibly the reduced cationic charge density with higher neutral lipid content reducing protein binding. The resistance of PEGylated Genospheres to extensive aggregation in human plasma is likely to be an important characteristic of these particles with regard to potential *in vivo* utility.

Using an identical formulation, Genospheres and lipoplexes were prepared and tested for their susceptibility to DNase I digestion (Figure 2c). The Genospheres were also incubated with human plasma for 24 h at 37°C

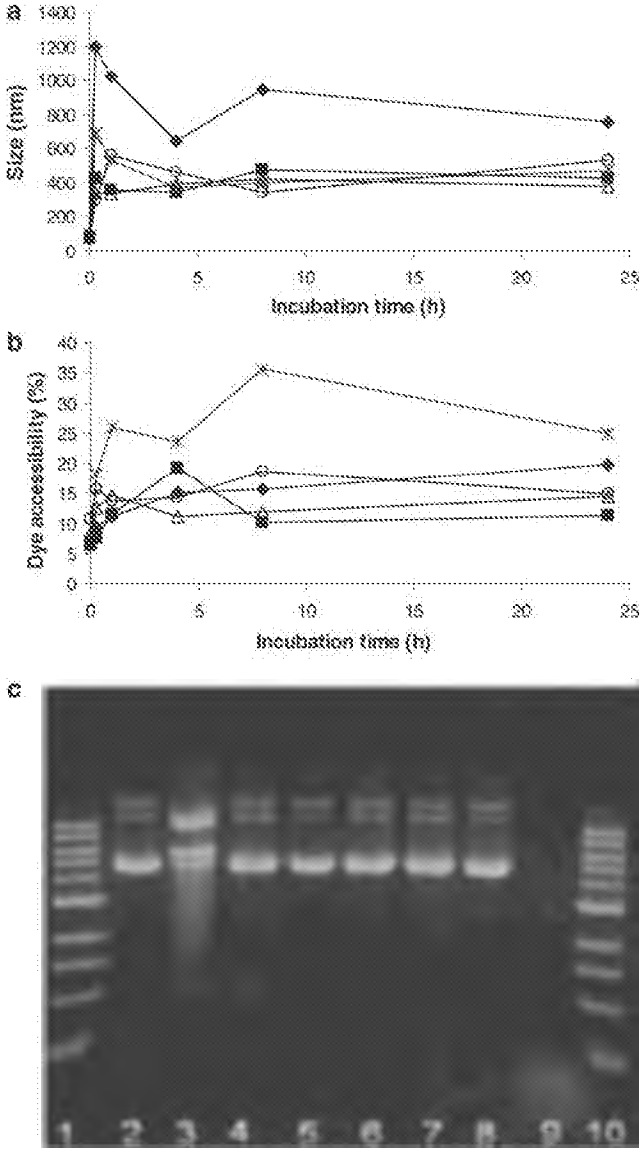

Figure 2 The effect of human plasma on Genosphere particle size (**a**), DNA dye accessibility (**b**) and DNase I digestion sensitivity (**c**). Genosphere particles (320 μg/ml DNA) with varying PEG-DSPE (*N*-(*ω*-methoxy-(poly(oxyethylene)-α-oxycarbonyl))-1,2-distearoyl-3-*sn*-phospatidylcholine) content were incubated with equal volume human plasma at 37°C. The formulations consisted of DOTAP/POPC/Chol (nmol/nmol/nmol) per μg DNA in the ratios (♦) 6/15/10; (■) 6/15/10; (○) 5/15/10 (± = 1.67), (*) 6/12/8 and (Δ) 6/15/10 with 0.5, 2, 4, 4 and 5% PEG-DSPE respectively. At intervals, aliquots (200 μl) were removed and free plasma separated by size exclusion chromatography using Sepharose CL-2B pre-equilibrated with HBS, pH 6.5 and were analyzed for size (DLS) and DNA dye accessibility, by using a fluorescent high affinity DNA binding molecule, Picogreen (Molecular Probes, Eugene, OR, USA). Dye accessibility assays were performed by measuring the fluorescence intensity ratio between nondissociated particle samples and dissociated (solubilized) particles samples. The total amount of DNA was quantified from the fluorescence intensity of the dissociated particle samples using the concurrently run standard curve, performed in quadruplicate using microplate fluorometer (FL-600A, Bio-Tek Instruments Inc., Winooski, VT, USA) equipped with 485/20 nm bandpass excitation filter and 530/25 nm bandpass emission filter. Agarose gel electrophoresis of DNA isolated from Genospheres and lipoplex that had the formulation DOTAP/POPC/Chol/PEG-DSG (6/15/10/0.62 nmol/nmol/nmol/nmol per μg DNA) was performed in similar manner as described previously[12] except that 30 U DNase I (deoxyribonuclease I, type II obtained from Sigma (St Louis, MO, USA)) was incubated with 20 μg DNA at 37°C for 1.5 h and after the phenol/chloroform extraction, no precipitation step was used. Simply the same volume of each DNA solution (approximately containing 250 ng DNA) was mixed with a loading buffer (0.25% (w/w) bromophenol blue, 40% (w/w) sucrose) and subjected to agarose gel electrophoresis. A 0.8% agarose gel was used, and the electrophoretic details and staining procedures described elsewhere.[12] PEG-DSG denotes 1-monomethoxypolyethyleneglycol-2,3-distearoylglycerol (PEG_{2000}). Lanes 1 and 10 contain the 1 kbp DNA ladder (Biolabs, NE, USA), lanes 2 and 3 are DNA isolated from lipoplex in the absence and presence and of DNase I, respectively. Lanes 4 and 5 contain DNA isolated from Genospheres that were incubated with 50% (v/v) human plasma for 24 h at 37°C in the presence and absence of DNase I, respectively, likewise lanes 6 and 7 contain DNA isolated from Genospheres incubated with and without DNase I. Naked plasmid DNA that was incubated in the absence (lane 8) and presence (lane 9) of DNase I were run as controls.

prior to the digestion assay to determine if plasma could alter the integrity of the Genosphere. From an agarose gel electrophoresis study of the isolated DNA, we observed that DNase I causes degradation of naked DNA, giving rise to a DNA smear (lane 9). In contrast, Genospheres treated with DNase I or incubated with plasma and then treated with DNase I give a similar band appearance to untreated plasmid DNA (lane 8). However, it is noticeable that the lipoplex formulation did not protect the DNA very well from digestion with changes in the band migration pattern and the appearance of a smear. The Picogreen dye accessibility measurements of Genospheres, lipoplexes and plasma treated Genospheres were 11 ± 0.2, 73.0 ± 1.7 and 25.0 ± 1.1%, respectively.

The Smoluchowski zeta potential was calculated from electrophoretic measurements made using Beckman-Coulter Delsa 440-SX.[18] Measurements were made in 5 mM HEPES, 5% (w/w) sucrose, pH 7.4. The zeta potential of a typical Genosphere formulation containing DOTAP/POPC/Chol (6/15/10 nmol/nmol/nmol) per μg DNA was found to have a value of +45.6 mV, indicating they are cationic in nature. This fact, along with the low dye accessibility (highly protected DNA) and evidence of a bilayer containing particle (Figure 1) strengthens our assumption that the majority of the particles contain charged neutralized DNA in the core, with the excess cationic lipid and neutral lipid forming one or more bilayers around it.

The stability of Genospheres during storage was determined in terms of changes in mean size and dye accessibility, wherein the degree of increase in particle size or dye accessibility reflected instability and loss of particle integrity. Three storage conditions were studied: (i) Genospheres in low ionic aqueous buffer, with added tonicity agents, refrigerated at 4–6°C or (ii) frozen at −80°C and (iii) Genospheres lyophilized in the presence of a cryoprotectant and a buffer substance, stored lyophilized at 4–6°C and reconstituted in water prior to measurements (Table 1). All three conditions resulted in very small changes in the apparent size of the particles. The degree of dye accessibility following storage under these conditions remained low, close to the value obtained for freshly prepared particles, and suggests that Genospheres can be stably stored under any of these conditions.

Successful *in vivo* gene therapy will require a combination of a stable carrier and an effective selective targeting approach. Examples where ligand-directed targeting provided increases in transfection efficiency are present in the literature.[19–22] We combined Genospheres with a highly internalizable anti-HER2 scFv' fragment (F5)[23] covalently attached to the PEG terminus of an amphiphilic PEG-lipid derivative by a previously described membrane capture method.[24,25] This allows for selective gene targeting to the human breast cancer cell line SK-BR-3, which overexpresses the HER2/neu receptor. The transfection activity of anti-HER2 immunoGenospheres, as well as the original nontargeted Genospheres, in HER2-overexpressing SK-BR3 cells was studied (Figure 3). The Genosphere transfection activity was substantially enhanced by the addition of the targeting antibody. In particular, the specificity of activity increased by a factor of 13–116-fold with increasing PEG-DSPE content. With targeting, the transfection activity was rather independent of the amount of PEGylated lipids present in the formulation, suggesting that ligand-specific targeting overcomes the PEG-related inhibition of the particle-cell association. As controls,

Table 1 The effect of storage for 1 week on the size and dye accessibility of Genospheres

Cryoprotectant % (w/v)	*Storage Condition*	*Size mean ± s.d (nm)*	*% Dye accessibility ± s.d*
5% Dextrose	+4°C	69.7 ± 29.5	10.9 ± 0.7
	−80°C	72.9 ± 30.5	12.8 ± 1.3
	Lyophilized	72.0 ± 30.5	19.7 ± 2.0
5% Sucrose	+4°C	70.5 ± 29.7	9.9 ± 0.9
	−80°C	78.6 ± 30.5	11 ± 1.3
	Lyophilized	75.2 ± 39.6	16.5 ± 1.9
10% Sucrose	+4°C	77.6 ± 30.9	14.2 ± 1.5
	−80°C	74.1 ± 30.5	12.2 ± 1.2
	Lyophilized	78.6 ± 30.5	14.9 ± 3.0

Genosphere of composition DDAB/POPC/Chol/PEG-DSPE (6/15/10/0.21 nmol/nmol/nmol/nmol/μg plasmid DNA) was prepared as described above, with ethanol removal facilitated by dialysis against 5 mM HEPES, pH 7.4. The storage conditions employed were refrigerated at 4°C, frozen at −80°C and lyophilized. After storage for 1 week, samples were brought to room temperature or reconstituted with deionized water, and size and dye accessibility measurements performed as described.

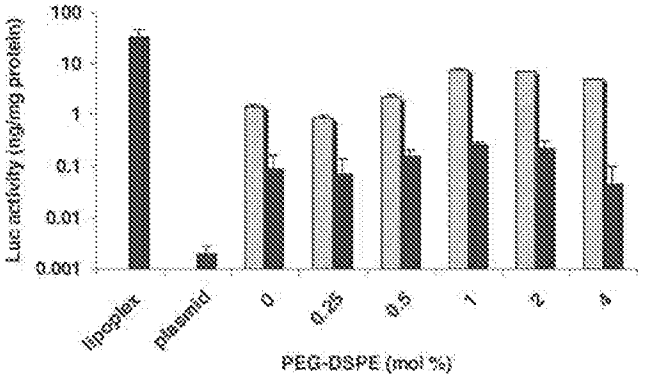

Figure 3 Luciferase expression in SK-BR-3 cells following incubation with Genospheres. The formulation used was DOTAP/POPC/Chol (6/15/10) (nmol lipid per μg DNA) with varying amounts of PEG-DSPE. Targeted and nontargeted Genospheres are represented by hatched and filled bars, respectively. As controls, a lipoplex formulation consisting of DOTAP/DOPE (12/12 nmol/nmol/μg DNA, ± = 4/1) and naked plasmid DNA were included in the study. HER2-overexpressing human breast adenocarcinoma cells SKBR-3 cells (ATT, Rockland, MD, USA) were cultured in McCoy's 5A medium supplemented with 10% (v/v) fetal bovine serum, 100 μg/ml of streptomycin sulfate and 100 U/ml of penicillin G at 37°C, (UCSF Cell Culture Facility, San Francisco) with 5% CO_2. The cells were plated at a density of 250 000 cells per well in a 12-well plate (Corning) and acclimated overnight. The final media volume in each well was 1 ml and each well received 1 μg of pCMV/luc$^+$ in the form of (i) free DNA, (ii) simple plasmid/liposome complexes or (iii) Genosphere preparations. All plasmid preparations were incubated with the cells for 6 h, removed by aspiration following washing with Hank's buffered saline (2 × 1 ml), and the incubation continued for another 18 h following the addition of fresh media (1 ml). The amount of *lux* reporter gene expression was characterized by the amount of luciferase in the cell lysates determined by luminometry (Monolight 3010, Analytical Luminescence Laboratory) and was expressed in ng luciferase per mg of cell lysate protein as described previously.[26]

a highly cationic lipoplex formulation containing DOTAP and the fusogenic lipid DOPE (12/12 nmol/nmol/μg DNA, charge ratio $\pm = 4/1$) had an activity of 33.85 ± 14.7 ng luc/mg protein, while naked DNA had a value of 0.002 ± 0.001 ng luc/mg protein.

Although Genospheres may not be optimal for *in vitro* use, as the absolute transfection efficiency of the targeted Genospheres was lower that the non-PEGylated lipoplex formulation, the optimal design of an *in vivo* formulation, will benefit from inclusion of a certain degree of PEGylation to potentially improve pharmacokinetic properties and reduce nonspecific transfection in non-target organs. PEG-DSPE was shown previously to inhibit transfection of non-targeted lipoplexes in a PEG-DSPE dose dependent manner.[26]

We have previously shown that by conjugation of an anti-HER2 Fab′ to the distal termini of PEG(2000)-DSPE containing liposomes, the inhibitory effect of PEG(2000)-DSPE on cell binding and uptake of liposomes by HER2 overexpressing cells is essentially avoided up to a PEG-DSPE content as high as 5.7 mol% of total lipid.[27] For Genospheres used in these transfection studies, we observed greater anti-HER-2 specificity at higher PEG(2000)-DSPE content. This is essentially due to the decrease in nonspecific binding at higher PEG derivative content. However, quite unexpectedly, the transfection activity at higher PEG-DSPE concentrations of Genospheres was not severely reduced (Figure 3), implying that Genospheres targeted with F5-PEG(2000)-DSPE remain highly internalizable and active at high PEG-lipid content, an important consideration in view of potential *in vivo* applications. This in contrast to the observations made by Song *et al*.[28] who used galactose-PEG-DSPE as a targeting ligand and observed a striking dependence of transfection efficiency on the molecular weight of the PEG moiety, with PEG molecular weights >1450 essentially completely inhibiting transfection activity of the nanoparticles.

Recently, Jeffs *et al*.[15] have developed a procedure that allows for efficient DNA encapsulation, producing small particles that have long circulating properties (plasma half-life of 13 h) and importantly have shown persistent anti-hepatitis B virus activity *in vivo*.[29] They quickly combine an ethanolic lipid solution with an aqueous DNA solution in a T-shaped mixing chamber so that ethanol-destabilized liposomes spontaneously form thereby entrapping the nucleic acid with efficiencies ranging from 60 to 70%. A second mixing step that further reduces the ethanol content increases the encapsulation efficiency to 80–90%.

To our knowledge, the Genosphere methodology is unique in the sense that DNA and lipid are combined in an environment that precludes lipid condensed phases, thereby enhancing the potential for unhindered charge–charge interactions. This is achieved by simply heating the lipid and DNA separately in the same organic/aqueous monophase *above* the lipid solubility temperature and ensures that upon mixing no preformed lipid condensed phases are present and the components are not exposed to local areas of variable solvent concentrations. It is a one-pot process with essentially two well-scalable operations, temperature controlled solution mixing and ethanol removal.

We have described a procedure for making nucleic acid-lipid nanoparticles that are relatively small in size and can be easily stored under a variety of conditions. We have also demonstrated that PEGylation can reduce the levels of aggregation of these cationic Genospheres in human plasma and that they selectively target and transfect HER2 overexpressing cells *in vitro* without loss of activity at higher PEG-lipid content, which may be important for future targeted *in vivo* use.

Acknowledgements

We thank Drs Joel Cohen and Valentina Khorosheva of the University of the Pacific, San Francisco for the zeta potential measurements. We also would like to thank Dr Brigitte Papahadjopoulos-Sternberg for performing the FFEM.

References

1 Felgner PL, Gadek TR, Holm M, Roman R, Chan RW, Wenz M *et al*. Lipofectin: a highly efficient, lipid-mediated DNA-transfection procedure. *Proc Natl Acad Sci USA* 1987; **84**: 7413–7417.
2 Wiley-InterScience. www.wiley.co.uk/genetherapy/clinical.
3 Chesnoy S, Huang L. Structure and function of lipid-DNA complexes for gene delivery. *Annu Rev Biophys Biomol Struct* 2000; **29**: 27–47.
4 Barron LG, Gagne L, Szoka FCJ. Lipoplex-mediated gene delivery to the lung occurs within 60 minutes of intravenous administration. *Hum Gene Ther* 1999; **10**: 1683–1694.
5 Zhang J-S, Liu F, Huang L. Implications of pharmacokinetic behavior of lipoplex for its inflammatory toxicity. *Adv Drug Deliv Rev* 2005; **57**: 689–698.
6 Cui Z, Li S-J, Huang L. Coating of mannan on LDP particles containing HPV E7 peptide significantly enhances immunity against HPV-positive tumor. *Pharm Res* 2004; **21**: 1018–1025.
7 Stuart DD, Allen TM. A new liposomal formulation for antisense oligodeoxynucleotides with small size, high incorporation efficiency and good stability. *Biochim Biophys Acta* 2000; **1463**: 219–229.
8 Smyth Templeton N, Lasic DD, Frederik PM, Strey HH, Roberts DD, Pavlakis GN. Improved DNA: liposome complexes for increased systemic delivery and gene expression. *Nat Biotech* 1997; **15**: 647–652.
9 Boomer JA, Thompson DH, Sullivan SM. Formation of plasmid-based transfection complexes with an acid labile cationic lipid: Characterization of *in vitro* and *in vivo* gene transfer. *Pharm Res* 2002; **19**: 1292–1301.
10 Bally MB, Zhang Y-P, Wong FMP, Kong S, Wasan E, Reimer DL. Lipid/DNA complexes as an intermediate in the preparation of particles for gene transfer: an alternative to cationic liposome/DNA aggregates. *Adv Drug Del Rev* 1997; **24**: 275–290.
11 Wheeler JJ, Palmer L, Ossanlou M, MacLachan I, Graham RW, Zhang YP *et al*. Stabilized plasmid-lipid particles: construction and characterization. *Gene Therapy* 1999; **6**: 271–281.
12 Zheng YP, Reimer DL, Zhang G, Lee PH, Bally MB. Self-assembling DNA-lipid particles for gene transfer. *Pharm Res* 1997; **14**: 190–196.
13 Jeffs LB, Palmer LR, Ambegia EG, Giesbrecht C, Ewanick S, MacLachlan I. A scalable, extrusion free method for efficient liposomal encapsulation of plasmid DNA. *Pharm Res* 2005; **22**: 363–372.
14 Sergeyev VG, Mikhailenko SV, Pyshkina OA, Yamnisky IV, Yoshikawa K. How does alcohol dissolve the complex of DNA with a cationic surfactant? *J Am Chem Soc* 1999; **121**: 1780–1785.
15 Huebner S, Battersby BJ, Grimm R, Cevc G. Lipid–DNA complex formation: reorganization and rupture of lipid vesicles in the

presence of DNA as observed by cryoelectron microscopy. *Biophys J* 1999; **76**: 3158–3166.
16 Park JW, Hong K, Kirpotin DB, Colbern G, Shalaby R, Baselga J *et al*. Anti-HER2 immunoliposomes: Enhanced efficacy attributable to targeted delivery. *Clin Cancer Res* 2002; **8**: 1172–1181.
17 Nielsen UB, Kirpotin DB, Pickering EM, Hong K, Park JW, Refaat Shalaby M *et al*. Therapeutic efficacy of anti-ErbB2 immunoliposomes targeted by a phage antibody selected for cellular endocytosis. *Biochim Biophys Acta* 2002; **1591**: 109–118.
18 Cohen JA. Electrophoretic characterization of liposomes. *Methods Enzymol* 2003; **367**: 148–176.
19 Reddy JA, Abburi C, Hofland H, Howard SJ, Vlahov I, Wils P *et al*. Folate-targeted, cationic liposome-mediated gene transfer into disseminated peritoneal tumors. *Gene Therapy* 2002; **9**: 1542–1550.
20 Xu L, Huang C-C, Huang W, Tang W-H, Rait A, Yin YZ *et al*. Systemic tumor-targeted gene delivery by anti-transferrin receptor scFv-immunoliposomes. *Mol Cancer Ther* 2002; **1**: 337–346.
21 Tan PH, Manunta M, Ardjomand N, Xue SA, Larkin DFP, Haskard DO *et al*. Antibody targeted gene transfer to endothelium. *J Gene Med* 2003; **5**: 311–323.
22 Lee C-H, Hsiao M, Tseng Y-L, Chang P-H. Enhanced gene delivery to HER-2-overexpressing cancer cells by modified immunolipoplexes conjugated with the anti-HER-2 antibody. *J Biomed Sci* 2003; **10**: 337–344.
23 Park JW, Kirpotin DB, Hong K, Shalaby R, Shao Y, Nielsen UB *et al*. Tumor targeting using anti-her2 immunoliposome. *J Control Release* 2001; **74**: 95–113.
24 Nellis DF, Kirpotin DB, Janini GM, Shenoy SR, Marks JD, Tsai R *et al*. Preclinical manufacture of anti-HER2 liposome-inserting, scFv-PEG-lipid conjugate. 2. Conjugate micelle identity, purity, stability, and potency analysis. *Biotechnol Prog* 2005; **21**: 221–232.
25 Nellis DF, Ekstrom DL, Kirpotin DB, Zhu J, Andersson R, Broadt TL *et al*. Preclinical manufacture of an anti-HER2 scFv-PEG-DSPE, liposome-inserting conjugate. 1. Gram-scale production and purification. *Biotechnol Prog* 2005; **21**: 205–220.
26 Hong K, Zheng W, Baker A, Papahadjopoulos D. Stabilization of cationic liposome-plasmid DNA complexes by polyamines and poly(ethylene glycol)-phospholipid conjugates for efficient *in vivo* gene delivery. *FEBS Lett* 1997; **400**: 233–237.
27 Kirpotin DB, Park JW, Hong K, Zalipsky S, Li W-L, Carter P *et al*. Sterically stabilized anti-HER2 immunoliposomes: design and targeting to human breast cancer cells *in vitro*. *Biochemistry* 1997; **36**: 66–75.
28 Song YK, Liu F, Chu S, Liu D. Characterization of cationic liposome-mediated gene transfer *in vivo* by intravenous administration. *Hum Gene Ther* 1997; **8**: 1585–1594.
29 Morrissey DV, Lockridge JA, Shaw L, Blanchard K, Jensen K, Breen W *et al*. Potent and persistent *in vivo* anti-HBV activity of chemically modified siRNAs. *Nat Biotechnol* 2005; **23**: 1002–1007.

articles

molecular pharmaceutics

Increased Target Specificity of Anti-HER2 Genospheres by Modification of Surface Charge and Degree of PEGylation

M. E. Hayes,[†,‡] D. C. Drummond,[†,‡] K. Hong,[†,‡] W. W. Zheng,[†] V. A. Khorosheva,[§] J. A. Cohen,[§] C. O. Noble IV,[†,∥] J. W. Park,[⊥] J. D. Marks,[⊥] C. C. Benz,[#] and D. B. Kirpotin*[,†,‡]

California Pacific Medical Center, San Francisco, California 94115, Hermes Biosciences, Inc., South San Francisco, California 94080, School of Dentistry, University of the Pacific, San Francisco, California 94115, Department of Medicine, Division of Hematology-Oncology, Cancer Research Institute, University of California San Francisco, San Francisco, California 94143, Department of Anesthesia, University of California San Francisco, San Francisco, California 94143, and The Buck Institute for Age Research, Novato, California 95945

Received April 4, 2006

Abstract: Genospheres are cationic lipid−nucleic acid nanoparticles prepared by the assembly of the lipids and nucleic acids from an aqueous/organic liquid monophase that independently dissolves the components, where the resultant particles are homogeneously sized (70−110 nm), with efficiently incorporated and protected DNA. In the present study, we demonstrate pH-dependent modulation of the Genosphere surface charge using pH-titratable lipids. By incorporation of the lipids with titratable anionic or imidazole headgroups, Genospheres with neutral or anionic surface charge at neutral pH were produced and compared for cellular uptake and transfection of a reporter gene (luciferase) in culture of breast cancer cells. The extent of particle−cell association was also studied by fluorescent microscopy and quantified by cytofluorometery. The effects of Genosphere surface modification with poly(ethylene glycol) (molecular weight 2000) at low (0.5 mol %) and high (5 mol %) grafting densities, as well as the effects of HER2-receptor-directed targeting by an internalizable anti-HER2 scFv F5, linked via PEG spacer, were also studied. Inclusion in the Genosphere formulation of pH-titratable lipids CHEMS (cholesteryl hemisuccinate), CHIM (1-(3-(cholesteryloxycarbonylamino)propyl)imidazole), or DSGG (1,2-distearoyl-*sn*-glycero-3-hemiglutarate) rendered the particles surface-charge neutral or slightly anionic at neutral pH, and cationic at mildly acidic pH, as shown by ζ-potential measurements. In HER2-targeted systems, transfection activity and target specificity with HER2-overexpressing SKBR-3 breast cancer cells were dependent on Genosphere surface charge and PEGylation. The highest target specificity correlated with low cationic charge at neutral pH, while incorporation of 5 mol % PEG-lipid had only minor effects on Genosphere-cell association, internalization, and transfection activity. The implications of this work for potential in vivo applications are discussed.

Keywords: Nonviral gene delivery; plasmid encapsulation; targeted gene delivery; HER2 receptor; ζ-potential; surface charge; PEGylation

Introduction

The success of gene therapy relies on delivering nucleic acid efficiently to its cellular target in a functionally intact state. The advantages of using nonviral delivery strategies include lower toxicity, inexpensive components, and the ease

* To whom correspondence should be addressed. Mailing address: Dmitri B. Kirpotin, Ph.D., Hermes Biosciences, Inc., 61 Airport Blvd., Suite D, South San Francisco, CA 94080. Phone: (650) 873-2583, ext. 106. Fax: (650) 873-2501. E-mail: dkirpo@hermesbio.com.

† California Pacific Medical Center.

‡ Hermes Biosciences, Inc.

§ University of the Pacific.

∥ Cancer Research Institute, University of California San Francisco.

⊥ Department of Anesthesia, University of California San Francisco.

The Buck Institute for Age Research.

10.1021/mp060040v CCC: $33.50

of attaching cell surface targeting ligands. Variations of complexes formed from the electrostatic interactions between nucleic acid and cationic liposomes (lipoplex), usually made with an excess of cationic charge, have been used as delivery vehicles in vitro[1] and in vivo.[2]

However, poor pharmacokinetic characteristics with the majority of sample typically accumulating in the first-pass organs (lung, liver, and spleen) shortly after injection,[3] in conjunction with high inflammatory toxicity, serologic toxicity, and hepatotoxicity may limit their utility in vivo.[2] It is known that the increased efficacy of many anticancer liposomal formulations over free drug is in part due to their longer circulation times and natural accumulation in diseased tumor sites, leading to high drug concentrations in close proximity to tumor cells. Recent DNA−lipid complex preparation methods have been devised that attempt to modify the properties of the complexes to enhance the prospects of tumor localization, and therefore produce more suitable candidates for in vivo use.[4−7] To further increase the efficacy of lipid based gene delivery, researchers have often adopted some of the approaches that have been used successfully to enhance liposomal drug delivery, including PEGylation.[8] The reduction of excess cationic surface charge has also been shown to contribute to longer circulation times in a variety of these DNA−lipid particle assemblies.[8,9] Recently a technique involving the selective reduction of thiocholesterol-based cationic lipids on the outer surface of particles has been used to obtain charge-neutral particles.[10]

Targeted delivery of nucleic acids is an important consideration when designing a delivery vehicle. Targeting promotes increased delivery to the cells of interest with decreased nonspecific delivery to other cells. As release and subsequent intracellular delivery is more difficult to control for nucleic acids compared to small molecular weight drugs, molecular targeting provides a promising strategy for specific and efficient intracellular nucleic acid delivery.

Previously, we have shown that DNA−lipid particles (Genospheres) could be formed under conditions where lipid and DNA are each soluble, either in molecular or micellar form, *prior* to their combination.[11,12] Such conditions promote more favorable interactions between DNA and cationic lipids, and eliminate the bilayer structural rearrangements that occur when DNA interacts with preformed cationic liposomes.[13] The Genosphere nanoparticles were small in size (80−110 nm) and afforded excellent protection to the entrapped DNA in the presence of human plasma. In addition, they were capable of being immunotargeted to selectively transfect HER2 overexpressing cells by insertion of an anti-HER2 human single-chain monoclonal antibody (scFv)−PEG conjugate.

In the present work, we describe how altering the surface properties of these particles affects their interactions with cells and the efficiency of gene expression in vitro. Various lipid components were utilized to modulate surface charge, which affected cell binding, internalization, and transfection efficiency. A neutral PEG-diacylglycerol analogue was used to enhance the steric stability of the particles without affecting surface charge. We used an anti-HER2 human single-chain monoclonal antibody (scFv)−PEG conjugate to facilitate intracellular delivery of the Genospheres and selectively enhance gene transfection efficiency. Finally, we discuss the potential of Genospheres for various in vivo applications

Results

Construction and Characterization of Genospheres. The mixing of the nucleic acid solution to the lipid solution in 50% (v/v) aqueous ethanol medium at 55−60 °C, and subsequent removal of the ethanol by vacuum evaporation or dialysis at room temperature, effected the self-assembly of Genospheres.[12] The resulting particles had size distributions with a volume-weighted average of 80−150 nm and a standard deviation of 35−65 nm as determined by dynamic light scattering. The extent of DNA and lipid encapsulation in the particles under these conditions is typically over 90%.[11]

(1) Felgner, P. L.; et al. Lipofectin: a highly efficient, lipid-mediated DNA-transfection procedure. *Proc. Natl. Acad. Sci. U.S.A.* **1987**, *84*, 7413−7417.
(2) Zhang, J.-S.; Liu, F.; Huang, L. Implications of pharmacokinetic behavior of lipoplex for its inflammatory toxicity. *Adv. Drug Delivery Rev.* **2005**, *57*, 689−698.
(3) Barron, L. G.; Gagne, L.; Szoka, F. C. J. Lipoplex-mediated gene delivery to the lung occurs within 60 minutes of intravenous administration. *Hum. Gene Ther.* **1999**, *10*, 1683−1694.
(4) Wheeler, J. J.; et al. Stabilized plasmid-lipid particles: construction and characterization. *Gene Ther.* **1999**, *6*, 271−281.
(5) Pastorino, F.; et al. Targeted liposomal c-*myc* antisense oligonucleotides induce apoptosis and inhibit tumor growth and metastases in human melanoma models. *Clin. Cancer Res.* **2003**, *9*, 4595−4605.
(6) Maurer, N.; et al. Spontaneous entrapment of polynucleotides upon electrostatic interaction with ethanol-destabilized cationic liposomes. *Biophys. J.* **2001**, *80*, 2310−2326.
(7) Jeffs, L. B.; et al. A scalable, extrusion free method for efficient liposomal encapsulation of plasmid DNA. *Pharm. Res.* **2005**, *22*, 363−372.
(8) Semple, S.; et al. Efficient encapsulation of antisense oligonucleotides in lipid vesicles using ionizable aminolipids: formation of novel multilamellar vesicle structures. *Biochim. Biophys. Acta* **2001**, *1510*, 152−166.
(9) Smart, D. D.; Kao, G. Y.; Allen, T. M. A novel, long-circulating, and functional liposomal formulation of antisense oligodeoxynucleotides targeted against MDR1. *Cancer Gene Ther.* **2000**, *7*, 466−475.
(10) Huang, Z.; Li, W.; MacKay, J. A.; Szoka, F. C. Thiocholesterol-based lipids for ordered assembly of bioresponsive gene carriers. *Mol. Ther.* **2005**, *11*, 409−417.
(11) Hayes, M. E.; et al. Assembly of nucleic acid-lipid nanoparticles from aqueous−organic monophase. *Biochim. Biophys. Acta* **2006**, *1758*, 429−442.
(12) Hayes, M. E.; et al. Genospheres: Self-assembling nucleic acid-lipid nanoparticles suitable for targeted gene delivery. *Gene Ther.* **2006**, *13*, 646−651.
(13) Huebner, S.; Battersby, B. J.; Grimm, R.; Cevc, G. Lipid-DNA complex formation: reorganization and rupture of lipid vesicles in the presence of DNA as observed by cryoelectron microscopy. *Biophys. J.* **1999**, *76*, 3158−3166.

Table 1. ζ-Potentials (ζ) of Genospheres at Different pH[a,g]

sample formulation	composition (nmol/μg of DNA)	Genosphere size (nm)	ζ (mV) pH 5.5	ζ (mV) pH 7.0
DOTAP/POPC/Chol	6/15/10 (A)	93.8 ± 41.7	nd[b]	+116.0[c](3)
DOTAP/POPC/Chol/CHEMS/CHIM	6/25/7/6/3.67 (B)	88.9 ± 48.9	+95.1(4)	~0(1)
	6/18/6/5/1	81.1 ± 43.6	+70.9(3)	−6.1(1)
	5/25/7/6/3.67	88.2 ± 51.1	+70.1(3)	−3.9(3)
	5/15/3/5/2	96.8 ± 39.6	+55.3(5)	−6.0(1)
	5/15/5/5/1	82.7 ± 40.9	+55.2(3)	−1.2(1)
	6/25/6/9/1.67	100.5 ± 39.5	+37.6(3)	−30.8(3)
	5/25/6/8/2.67	89.0 ± 45.7	+24.1[c](3)	−24.9[c](3)
	5/25/6/9/1.67	98.6± 47.0	+24.0(3)	−39.3(3)
	6/25/5/10/1.67	115.7 ± 43.1	+16.7(3)	−32.8(3)
DOTAP/POPC/Chol/DSGG	6/25/16.67/5	78.5 ± 45.6	+82.6[c](2)	+46.3[c](4)
	5/25/16.67/6 (C)	149.2 ± 60.6	+23.6[c](3)	−18.1[c](3)
DOTAP/POPC/Chol/DSGG/CHIM	6/25/14.67/4/2	124.4 ± 63.8	+59.2[c](3)	+25.5[c](4)

[a] Genosphere samples were prepared as described in Materials and Methods. Ionizable headgroups: DOTAP, a quaternary amine; CHEMS, a weak acid, $pK_a = 5.1$; CHIM, a weak base, $pK_a = 6.65$; DSGG, a weak acid, $pK_a = 5.1$. The samples were divided into two groups (approximately 50 μg of DNA per sample) and dialyzed against either 5 mM Na-HEPES, 5% (w/w) sucrose, pH 7.0, or 5 mM Na-MES, 5% (w/w) sucrose, pH 5.5. [b] Not determined. [c] Measured in 5 mM Na-HEPES, pH 7.4 with 5% (w/w) sucrose). [d] Solutions contain 5 mM NaCl in addition to the indicated buffers and sucrose. Electrophoretic mobilities were measured with a Beckman-Coulter Delsa 440-SX, and ζ-potentials were calculated as previously described. Uncertainties of the ζ-potentials are 5% or less, and the number of electrophoretic runs for each data point is given in parentheses. [e] In line 1, the ζ-potential reported for Genospheres prepared with DOTAP/POPC/Chol 6/15/10 (nmol of lipid/μg of DNA) at pH 7.0 is an estimate. Due to an uncertainty in ionic strength, the measured mobility was greater than the predicted O'Brien−White maximum value. The actual ζ-potential is estimated to lie between +58 mV (Smoluchowski value) and +116 mV (O'Brien−White value at the mobility maximum).

therefore the lipid and DNA compositon of the particles closely follows the composition of the initial lipid−DNA mixture. The proportion of DNA accessible to the environment as determined by a DNA-binding dye (PicoGreen) accessibility assay[11] of the Genospheres in the present study was ~20%. In contrast, lipoplex particles, prepared by complexation of plasmid DNA with premade cationic liposomes, tend to encapsulate DNA rather incompletely, with higher proportions of the DNA "accessible" to the dye. Previously, we found that lipoplexes of identical lipid and nucleic acid compositon had considerably higher dye accessibility for DNA than the particles produced by the Genosphere method.[11]

Engineering the Charge on Genosphere Particles. The surface ionic charge of Genospheres was characterized by electrophoretic mobility and expressed in terms of ζ-potential (ζ). ζ-Potentials were calculated from the mobilities by the O'Brien−White algorithm,[14] using particle sizes determined by dynamic light scattering and ionic strengths determined by conductometry. The O'Brien−White calculations are necessary when the Debye screening length (κ^{-1}) is non-negligible compared to the particle size, which was the case in our study. In the case of nontitratable cationic lipids, Genosphere constructs were prepared with approximately two ionic equivalents of cationic lipid to one ionic equivalent of DNA. At near-neutral pH (5 mM HEPES, 5% (w/w) sucrose at pH 7.4), these particles had positive ζ (Table 1). However, the positive surface charge is unfavorable for iv targeted gene delivery using lipid-based carriers,[15] while favorable for cytoplasmic delivery of the DNA once in the cell. Therefore, in order to construct Genospheres whose positive surface charge would decrease at neutral pH but increase upon acidification typical for endosomes, pH-titratable lipids (Figure 1) were included in the formulations.

Titratable lipids can be cationic or anionic and their net charge can be altered in a physiologically relevant pH range (4.5−7.5). Cationic titratable lipids increase their positive charge at low pH and diminish it at neutral or slightly basic pH. The lipophilic imidazole derivatives behave as cationic titratable lipids,[16] cholesteryl imidazole (CHIM) being an example. Anionic titratable lipids reduce their negative charge at low pH, and increase it at neutral or slightly basic pH. Examples of anionic titratable lipids are fatty acids, succinyl and glutaric esters of lipids, such as cholesteryl hemisuccinate (CHEMS), dioleoylglyceride hemisuccinate (DOGHEMS), and distearoylglyceride hemiglutarate (DSGG) (see Figure 1A−D). Genospheres with incorporated titratable lipids were prepared, mobilities measured, and ζ-potentials calculated at acidic and neutral pH (Table 1). While the inclusion of titratable lipids did not significantly affect the average particle size (range, 78−146 nm), the particle surface charge changed noticeably between pH 5.5 and pH 7.4. At pH 5.5, typical of endosomes or lysosomes, all the Genosphere constructs had a positive ζ, indicating the presence of

(14) O'Brien, R. W.; White, L. R. *J. Chem. Soc., Faraday Trans. 2* **1978**, *74*, 1607.

(15) Mastrobattista, E.; van der Aa, M. A. E. M.; Hennik, W.; Crommelin, D. Artifical viruses: a nanotechnological approach to gene therapy. *Nat. Rev. Drug Discovery* **2006**, *5*, 115−121.

(16) Solodin, I.; et al. A novel series of amphiphilic imidazolinium compounds for in vitro and in vivo gene delivery. *Biochemistry* **1995**, *34*, 13537−13544.

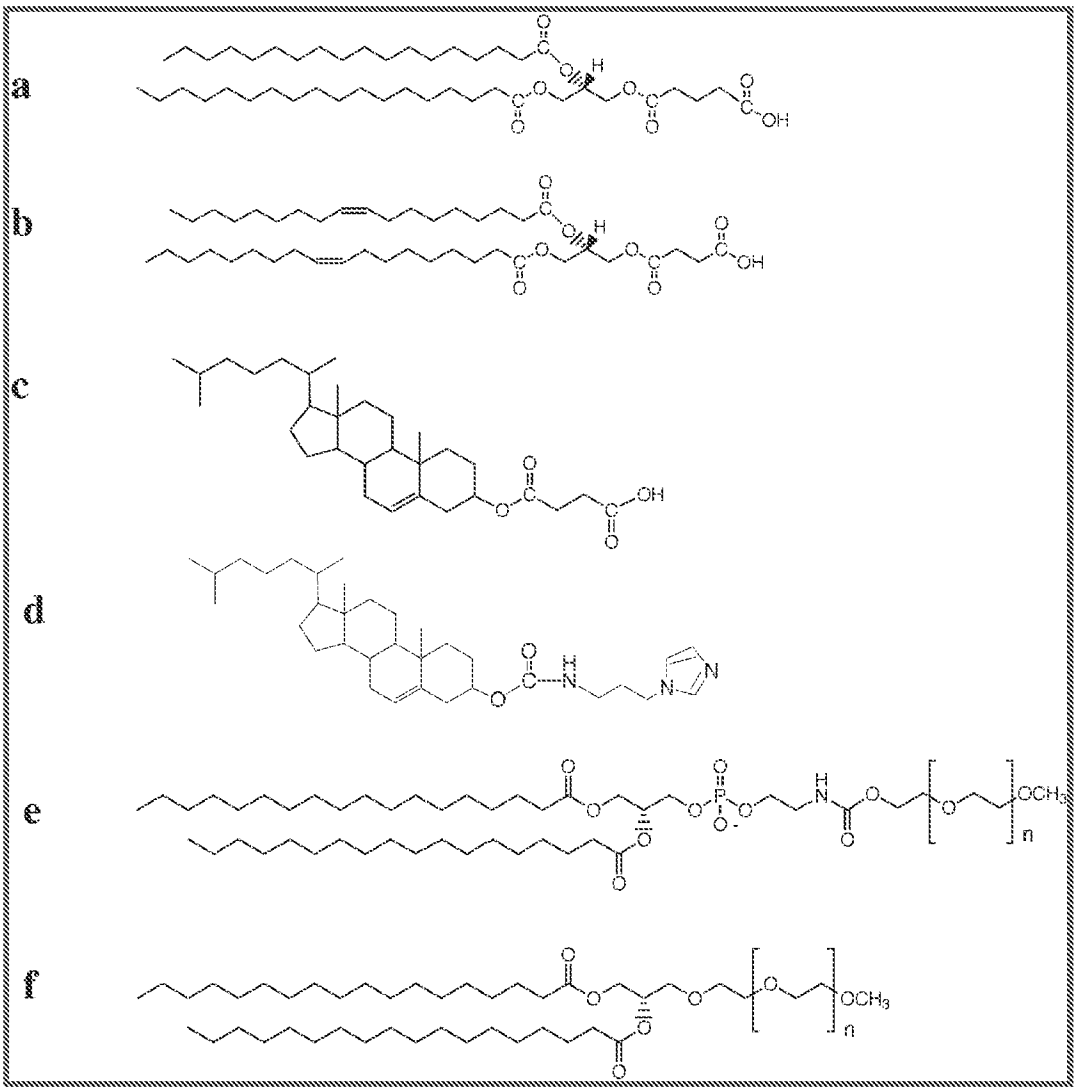

Figure 1. The chemical structures of Genosphere-modifying lipids used in this work: (a) 1,2-distearoyl-*sn*-glycero-3-hemiglutarate (DSGG); (b) 1,2-dioleoyl-*sn*-glycero-3-hemisuccinate (DOGHEMS); (c) cholesteryl hemisuccinate (CHEMS); (d) 1-(3-(cholesteryloxycarbonylamino)propyl)imidazole (CHIM); (e) *N*-[*ω*-methoxy-(poly(oxyethylene)-α-oxycarbonyl)]-DSPE (PEG_{2000}) (PEG-DSPE); (f) 2,3-distearoylglycerol 1-monomethoxypolyethyleneglycol ether (PEG_{2000}) (PEG-DSG).

un-neutralized cationic lipid charges. Addition of the anionic titratable lipid derivatives caused a reduction in ζ, detectable at low pH and much more prominent at neutral pH. In some instances this caused the charge to change sign, indicating a functioning pH-dependent "switch" of surface charge. Five of the formulations studied had ζ values close to 0 (i.e., deviating less than 10 mV) at neutral pH and were, therefore, designated as "neutral". Formulations containing CHEMS and CHIM showed the largest amplitude of surface charge switch, in the range of 50−96 mV.

The Effect of Charge, Degree of PEGylation, and Anti-HER2-Antibody Targeting on Cell Association and Transfection Activity of Genospheres. On the basis of ζ measurements, we selected for further studies three Genosphere formulations, having cationic, neutral, or anionic surface charge at neutral pH (Table 1, formulations A, B, and C, respectively). To effect target-specific internalization of Genospheres into cells, a highly internalizable anti-HER2 scFv′ fragment (F5)[17,18] was attached to the surface of Genospheres by coincubation with the F5−lipopolymer conjugate (F5-scFv−PEG-DSPE).[17−19] Grafting of PEG on the Genosphere surface at various densities (0.5 mol % and 5 mol % of the total lipid) was achieved by inclusion of a charge-neutral PEG-lipid derivative, PEG-DSG, in the lipid mixture prior to complexation of DNA.

The effect of PEGylation, charge, and anti-HER2-antibody targeting on the degree of Genosphere association with HER2-overexpressing cells was characterized qualitatively

(17) Nielsen, U. B.; et al. Therapeutic efficacy of anti-ErbB2 immunoliposomes targeted by a phage antibody selected for cellular endocytosis. *Biochim. Biophys. Acta* **2002**, *1591*, 109−118.

(18) Nellis, D. F.; et al. Preclinical manufacture of an anti-HER2 scFv-PEG-DSPE, liposome-inserting conjugate. 1. Gram-scale production and purification. *Biotechnol. Prog.* **2005**, *21*, 205−220.

(19) Nellis, D. F.; et al. Preclinical manufacture of anti-HER2 liposome-inserting, scFv-PEG-lipid conjugate. 2. Conjugate micelle identity, purity, stability, and potency analysis. *Biotechnol. Prog.* **2005**, *21*, 221−232.

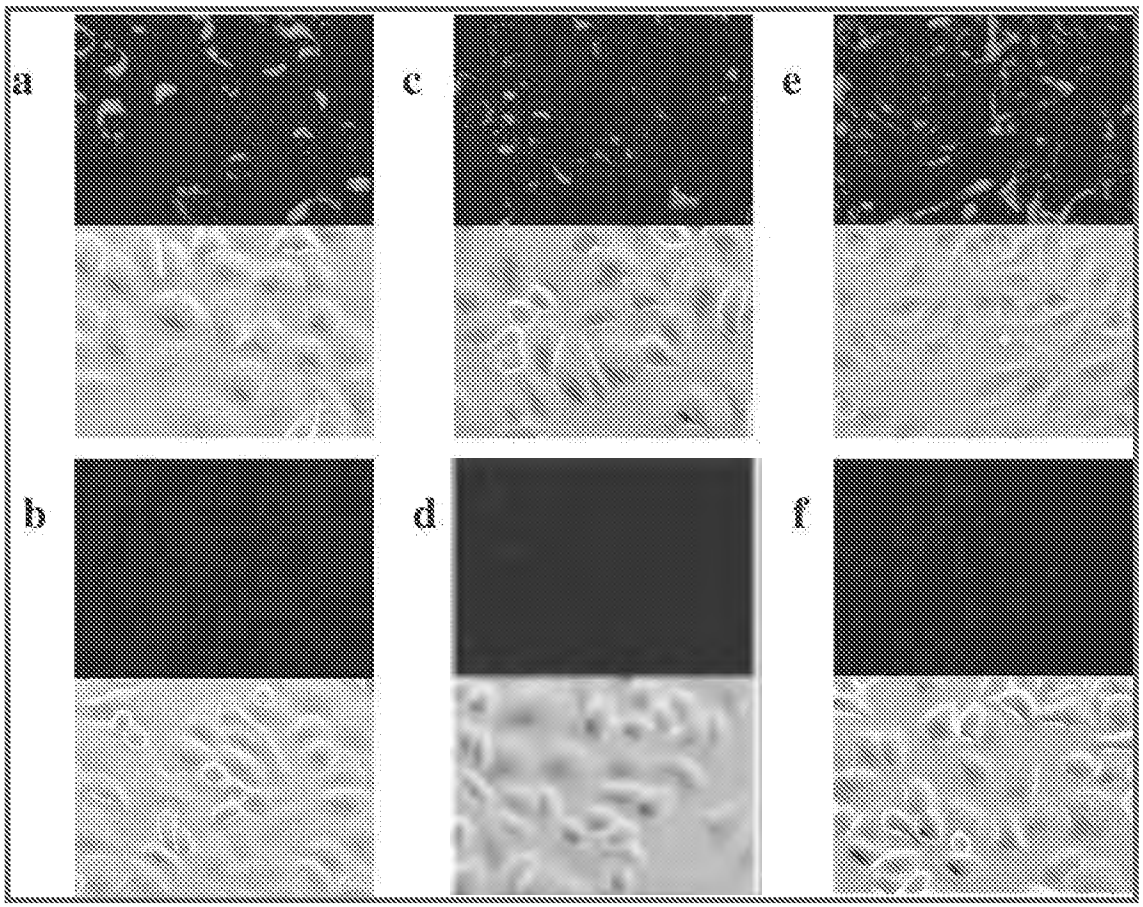

Figure 2. Representative fluorescent microscopy pictures of SKBR-3 cells incubated with Genospheres of various surface charge and PEGylation. Panels: neutral anti-HER2 targeted and nontargeted Genospheres with 0.5% PEG-DSG (panels a and b, respectively); anionic targeted and nontargeted Genospheres 5% PEG-DSG (panels c and d, respectively). The lipoplex formulation with 5% PEG-DSG is shown in panel e, and cells with no treatment are shown in panel f. Fluorescent and phase contrast modes are displayed on the top and bottom respectively for each panel.

by fluorescence microscopy (Figure 2) and quantified by cytofluorometry (Figure 3) using Genospheres and lipoplexes containing a fluorescent lipid label. HER2-directed antibody targeting significantly increased the extent of cell association of the particles in a manner dependent both on particle charge and on degree of PEGylation. Reducing the cationic charge and increasing the PEG-DSG content to 5 mol % significantly increased the specificity of targeting neutral and anionic particles as judged by the magnitude of increase in the average fluorescence intensity. It was apparent that cationic Genospheres and lipoplexes bound to the cells in a relatively nonspecific manner. However, while higher PEGylation attenuated the cellular association of cationic Genospheres, it did not affect lipoplex binding.

In addition to increased association with the receptor-overexpressing cells, targeted preparations rapidly entered the cells forming a characteristic punctate perinuclear pattern, indicative of endosomal/lysosomal localization[20,21] (Figure 2, panels a and c). Nontargeted Genospheres displayed only weak binding and primarily localized at the cell surface (Figure 2, panels b and d), while the lipoplexes appeared to be located both intracellularly and surface bound in a pattern different from that of targeted Genospheres.

The transfection activity of anti-HER2 immunoGenospheres, as well as of nontargeted Genospheres and lipoplexes in HER2-overexpressing SKBR-3 cells, is shown in Figure 4. The activity for targeted Genospheres at low and high PEG-DSG content was comparable to that obtained for the lipoplex formulation with 0.5 mol % PEG-DSG. Lipoplexes with high PEG-DSG content had low transfection activities. Remarkably, the transfection efficiency of the plasmid delivered by the HER2-targeted Genospheres was *less* dependent on the degree of PEGylation. Targeted preparations showed enhanced transfection activities over their nontargeted counterparts, with neutral and anionic Genospheres exhibiting the largest increases in activity (167- and 850-fold, respectively). The lower transfection activities of the nontargeted preparations varied with surface charge and degree of PEGylation. Generally, the cationic particle exhibited higher nonspecific transfection at both PEG-DSG

(20) Kirpotin, D. B., et al. Sterically stabilized anti-HER2 immunoliposomes: Design and targeting to human breast cancer cells in vitro. *Biochemistry* **1997**, *36*, 66−75.

(21) Meyer, O., et al. Cationic liposomes coated with polyethylene glycol as carriers for oligonucleotides. *J. Biol. Chem.* **1998**, *273*, 15621−15627.

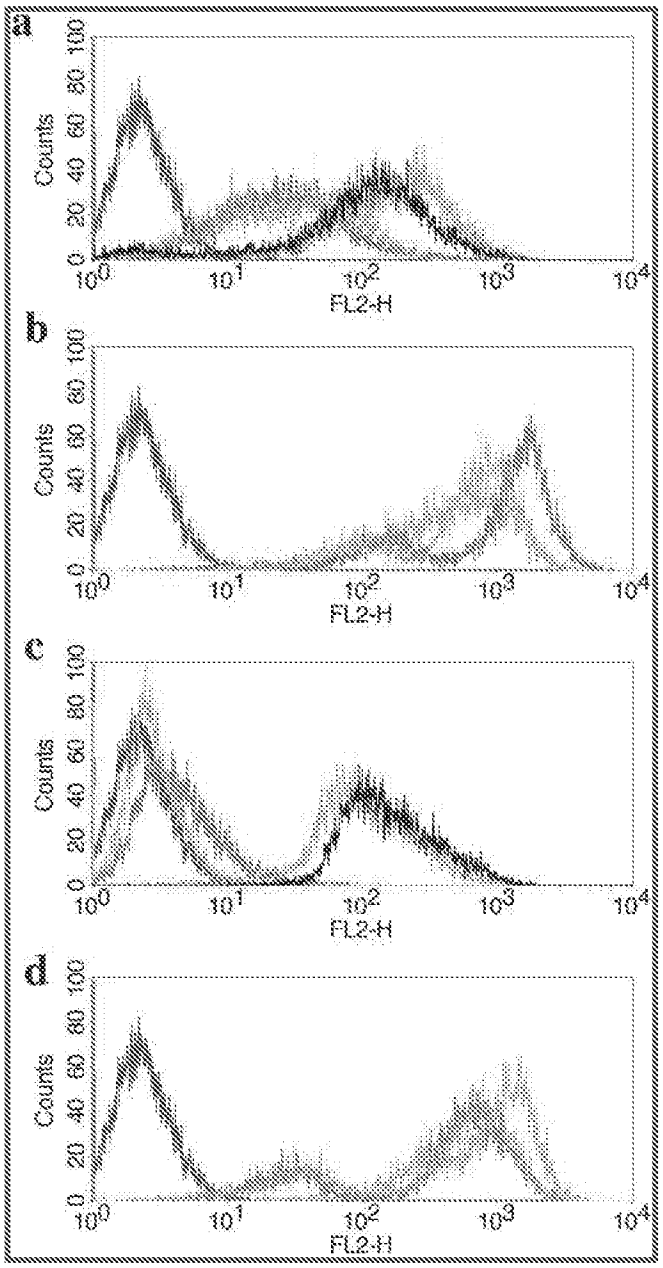

Figure 3. Cytofluorometric analysis of the uptake of fluorescently-labeled Genospheres and lipoplexes by SKBR-3 cells. Signal intensity histograms of cells incubated with fluorescently labeled Genospheres. Nontargeted (panels A, C) or HER2-targeted, scFv-conjugated Genospheres (panels B, D) containing either 0.5 mol % (panels A, B) or 5 mol % (panels C, D) PEG-DSG. Genosphere compositions are in nmol of respective lipids per μg of DNA: cationic (green lines), DOTAP/POPC/DOPE/Chol (6/12/3/10); neutral (red lines), DOTAP/POPC/DOPE/Chol/CHEMS/CHIM (6/20/5/7/6/3.67); anionic (orange lines), DOTAP/POPC/DOPE/Chol/DOGHEMS (5/20/5/16.67/6). DOTAP/DOPE (12/12) lipoplexes with "low-0.5% PEG-DSG" and "high-5% PEG-DSG" (black lines) are displayed alongside the nontargeted particles in panels a and c, respectively. Blue lines are nontreated cells (autofluorescence controls).

concentrations, and is in agreement with the results found previously using folate-targeted liposomal entrapped polylysine-condensed DNA.[22] In contrast, in the absence of a targeting ligand, the levels of transfection activity for both the neutral and anionic particles decreased with additional PEGylation and increasing anionic surface charge.

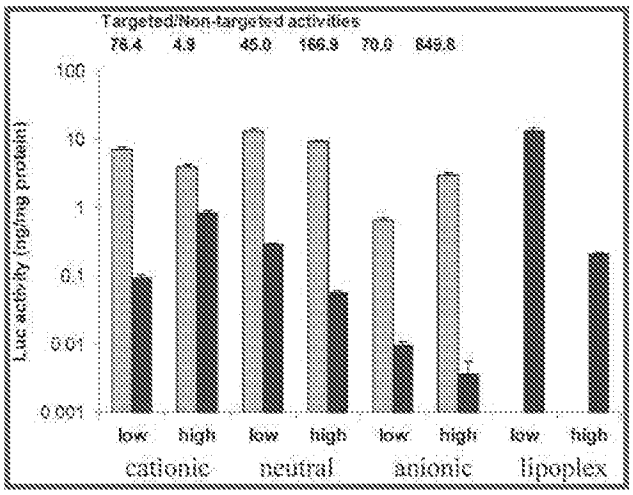

Figure 4. Luciferase expression in SKBR-3 cells following incubation with Genospheres of varying surface charge and degree of PEGylation. The Genosphere compositions are given in the Figure 2 legend. Hatched and filled bars represent targeted and nontargeted particles, respectively (n = 3). Labels "low" and "high" refer to complexes containing 0.5 and 5 mol % PEG-DSG (total lipid), respectively. Numbers above the bars indicate ratios of activities for targeted Genospheres/activities for nontargeted Genospheres.

However, the levels of gene expression of the targeted particles did not always correlate with the levels of cell association. For the targeted cationic and neutral Genospheres with low PEG-DSG content (0.5 mol %), cell association and transfection correlated well, with neutral particles having approximately twice the cell association and transfection levels of the cationic particles. In the case of anionic particles having lower positive charge attainable under endosomal/lysosomal pH levels, gene expression was considerably reduced even in the presence of the targeting ligand, although the target-dependent cell association was of the same magnitude as that of targeted cationic and neutral particles. On the other hand, lipoplexes with low PEGylation had transfection activity equal to that of the targeted neutral particles with 0.5% PEG-DSG, while having 8 times less cell association.

At higher PEG content (5 mol %), the targeted neutral and anionic Genospheres had similar cell association values, but the neutral Genosphere was approximately 3 times more active in the transfection assay. In agreement with our previous findings, higher PEGylated lipid content did not substantially inhibit the activity of the targeted cationic Genospheres, and moreover had very little effect on the activity of the neutrally charged targeted Genospheres. In

(22) Lee, R. J., Huang, L. Folate-targeted, anionic liposome-entrapped polylysine-condensed DNA for tumor cell-specific gene transfer. *J. Biol. Chem.* **1996**, *271*, 8481−8487.

contrast, increased levels of PEG-DSG (5 mol %) rendered lipoplexes substantially less active (65 times lower) than lipoplexes containing 0.5 mol % PEG-DSG, even though the cell association values were similar.

As a control, the transfection activity of the targeted and nontargeted neutral formulation (with 5% PEG-DSG) in a non-HER2 overexpressing cell line (MDAMB468) were similar at 0.03 ± 0.02 and 0.04 ± 0.02 ng luciferase/mg cell protein, respectively. Under identical conditions, a commercial transfection formulation (Lipofectamine 2000) complexed with the same plasmid gave luciferase values approximately 20,000 times higher.

Discussion

Previously, we described a methodology for producing small, stable, target-selective particles (Genospheres) from lipids and nucleic acids micellarly or molecularly dissolved in a mixture of water and infinitely water-miscible organic solvent that can be used for delivery of therapeutic nucleic acids.[11] Initially, Genospheres were constructed with excess cationic lipid. Genospheres formed with 5−6 nmol of a cationic lipid per μg of plasmid DNA, which gives a positive/negative charge ratio of 1.67−2, assuming the average nucleotide weight of 330. This was enough cationic lipid charge to completely neutralize the DNA phosphate charge and ensure stability, as well as highly efficient entrapment of the nucleic acid (plasmid DNA) during formation of the particle. However, the uptake of such particles by tumors may be impaired due the presence of persistent cationic charge that increases the particle clearance and accumulation in vascular sites other than tumors. Reducing the cationic charge on lipid carriers promotes longer circulation times, decreases interactions with opsonins and uptake by macrophages, and reduces nonspecific interactions with cell surfaces.[23,24] To avoid excessive positive surface charge of a DNA−lipid particle while in the bloodstream, and at the same time provide for sufficient cationic charge to effect intracellular transfection, we took a 2-fold approach. First, we partially substituted titratable anionic and/or cationic lipid for a strongly charged cationic lipid species (such as lipids with quaternary-amine headgroups, e.g., DOTAP) in the particle formulation (Table 1). As the entrapment of DNA was carried out at a reduced pH (pH 5.5), the particles containing anionic titratable lipids in an amount enough to bring the particle's surface charge at neutral pH (pH 7.0) to close to neutral, or even anionic, still entrapped the plasmid very effectively. Upon a change of pH from 7.0 to 5.5, the particles containing nontitratable cationic lipid components along with the titratable anionic lipids showed an amplitude of the charge change of about 40 mV. Addition of a titratable cationic lipid (positive-to-neutral), along with the charge-changing anionic lipid (neutral-to-negative), increased the amplitude of the charge change to 50−90 mV (Table 1), producing more effective transfecting particles (Figure 4). The strategy of modulating surface charge in DNA/lipid microparticles, using lipids with titratable amines as the cationic component at low pH, is known; however, the entrapment efficiencies of the nucleic acids in such particles are limited.[6] Supplementing a titratable aminolipid with a strongly cationic lipid component, counterbalanced at neutral pH with a titratable anionic lipid component, seems to improve the entrapment of DNA and particle recharging upon cytophysiologically relevant acidification.

Second, we used a ligand-directed "active targeting" approach to achieve specific uptake of the Genospheres into acidifying intracellular compartments via receptor-mediated endocytosis. While cationic particles have natural and often nonspecific tendency to bind to cell surfaces and become endocytosed,[1] neutral or anionic lipid particles are taken up much less, as we also observed in our cytofluorometric studies (Figure 3a,c). To make Genospheres targetable, they were incubated with the micelles of a lipopolymer (PEG-DSPE) conjugated to a ligand (scFv antibody) to the free terminus of the PEG chain, effecting "insertion" of the DSPE anchor in the outer lipid bilayer of the Genosphere particle and appending the ligand, via PEG spacer, to the particle surface, as we described previously.[12] HER2, a tyrosine kinase receptor of EGFR family, was chosen as a targeting epitope. HER2 is a validated target for anticancer therapeutic strategies, as it is a readily accessible surface antigen, is overexpressed in many cancer cell types such as breast, lung, and ovarian carcinomas,[25,26] and is essential for tumor progression. A single chain Fv antibody ligand, F5, is highly internalizable by HER2-overexpressing cells[27] and effectively internalizes appended lipid nanoparticles, such as liposomes, in vitro[17] and in vivo.[28] Conjugation of F5 scFv with maleimide-terminated PEG-DSPE via C-terminally engineered cysteine residue produced stable, water-soluble, micellar F5−PEG-DSPE conjugate, that, upon incubation with liposomes, self-inserted into the outer monolayer of the liposome membrane, forming anti-HER2 immunoliposomes.[17,18]

This targeting strategy leads to a more than 100-fold increase in luciferase reporter gene expression in HER2-overexpressing cells.[12] In the present report, we observe a

(23) Chonn, A.; Semple, S. C.; Cullis, P. R. Association of blood proteins with large unilamellar liposomes in vivo. *J. Biol. Chem.* **1992**, *267*, 18759−18765.

(24) Semple, S. C.; Chonn, A.; Cullis, P. R. Interactions of liposomes and lipid-based carrier systems with blood proteins: Relation to clearance behavior in vivo. *Adv. Drug Delivery Rev.* **1998**, *32*, 3−17.

(25) Salomon, D. S.; Brandt, R.; Ciardiello, F.; Normanno, N. Epidermal growth factor-related peptides and their receptors in human malignancies. *Crit. Rev. Oncol. Hematol.* **1995**, *19*, 183−232.

(26) Scholl, S.; Beuzeboc, P.; Pouillart, P. Targeting HER2 in other tumor types. *Ann. Oncol.* **2001**, *12*, S81−S87.

(27) Neve, R. M.; et al. Biological effects of anti-ErbB2 single chain antibodies selected for internalizing function. *Biochem. Biophys. Res. Commun.* **2001**, *280*, 274−279.

(28) Kirpotin, D. B.; et al. Antibody targeting of long-circulating lipidic nanoparticles does not increase tumor localization but does increase internalization. *Cancer Res.* **2006**, *66*, 6732−6740.

5- to 850-fold enhancement of luciferase expression with targeted Genospheres compared to nontargeted Genospheres in SKBR-3 cells, while in human breast carcinoma cells with low expression of HER2 (MDA-MB-468), the expression was not increased by attachment of HER2-specific, internalizable scFv ligand. The HER2-directed targeting of Genospheres increased the level of reporter gene expression in absolute terms, and decreased the dependence of transfection efficiency on the particle charge and the density of particle surface coating with sterically stabilizing hydrophilic polymer (PEG) (Figure 4). The charge-changing Genospheres that were neutral at neutral pH and had an increased PEG coating (5 mol %) showed increased selectivity of transfection in the HER2 overexpressing cells compared to our previously described nontitratable cationic Genospheres.

Surface coating with a hydrophilic polymer terminally grafted to lipid residues is a recognized method for improvement of blood stability and longevity of lipidic microcarriers.[29,30] The effect of surface PEGylation on the association and transfection activity of Genospheres was studied using a charge-neutral PEG-lipid derivative, PEG-DSG (Figure 1), to avoid imparting additional negative charge carried by a more conventional PEG-lipid, PEG-DSPE. Reducing the magnitude of cationic surface charge alone diminished nonspecific Genosphere−cell interactions regardless of the PEG-DSG content. We previously observed that addition of PEG-DSPE to nontargeted lipoplexes inhibited transfection in a PEG-DSPE dose-dependent manner.[31] In this study we observed a similar effect, with transfection activity of 5 mol % PEG-DSG lipoplexes having only ~1.5% of the activity of 0.5 mol % PEG-DSG lipoplexes. Increasing surface density of PEG chains further reduced nonspecific, i.e., targeting-independent, association of Genospheres with the cells. However, addition of a targeting ligand restored the transfection activity, leading to increased specificity of transfection. HER2-targeted Genospheres with 5 mol % PEG-DSG transfected HER2-overexpressing cells in vitro 15−45 times more efficiently than DOTAP/DOPE cationic lipoplexes with similar PEG-DSG content, and the neutrally charged, PEGylated, HER2-targeted Genospheres were the most active (Figure 4). Higher PEGylation of Genospheres (2−5 mol % PEG-DSPE compared to 0.5 mol % PEG-DSPE) also improves the particle size stability in the presence of human plasma.[12]

Anti-HER2 immunoliposomes are rapidly taken up by SKBR-3 cells into acidifying compartments (endosomes and lysosomes), consistent with coated pit receptor-mediated endocytosis, forming distinct, punctate perinuclear patterns revealed by epifluorescent microscopy of the liposomal fluorescent label.[20] In this study we observed a similar intracellular pattern of the fluorescently labeled HER2-targeted Genospheres (Figure 2) after incubation with the same cell line, suggesting that HER2-targeted Genospheres were similarly internalized via HER2-mediated endocytosis.

The steps subsequent to the receptor-mediated endocytosis of the targeted Genospheres and the mechanisms that govern the release of DNA with further entry into cytoplasm and to the nucleus are as yet unclear. An interesting observation is that charge-changing Genospheres which contained an imidazole-lipid derivative CHIM were more active than those that did not (formulations B and C, Table 1; Figure 4). This might be related to additional cationic charge from the protonation of an imidazole ring, by the "proton sponge" effect observed with imidazole-containing transfection reagents,[32] or both, leading to the rupture of endosomes and escape of the particles into cytoplasm. It was hypothesized that the anionic lipids normally found on the cytoplasmic facing side of an endosome interact with the cationic lipid and cause a destabilization of the cationic lipid−DNA complex.[33] The observation of lower transfection activity of "anionic" Genospheres that attain less positive surface potential upon contact with acidified endosomal interior (commonly reported pH for endosomal interior is 5.0[34]) seems to support this hypothesis.

Despite 8-times-lower levels of cellular association for lipoplexes, that is, complexes of plasmid DNA with premade, small cationic lipid vesicles, they showed the same transfection activity as targeted, neutral Genospheres. We believe that the combination of increased amounts of the polymorphic lipid DOPE, and the nonspecific mode of cellular uptake by highly cationic lipoplexes, may contribute to the higher transfection activity. However, the loss of specificity, aggregation stability, and DNA protection against degradation[11] are unacceptable tradeoffs in the choice of lipoplexes vs Genospheres for future in vivo systemic applications. Unlike lipoplexes, Genospheres stably entrapped DNA within the lipid matrix of the particle, shielding the DNA from nuclease degradation even in the presence of human plasma, as measured both by an intercalating dye assay and by a DNase enzymatic degradation assay.[11]

Comparing Genospheres with two other well-known methodologies for formulating DNA−lipid particles, we found that Genospheres exhibited the unexpected combination of small size, high degree of lipid and DNA incorporation, and narrow particle density distribution.[11] This indicated

(29) Drummond, D. C.; et al. Optimizing liposomes for delivery of chemotherapeutic agents to solid tumors. *Pharmacol. Rev.* **1999**, *51*, 691−743.

(30) Papahadjopoulos, D.; et al. Sterically stabilized liposomes: improvements in pharmacokinetics and antitumor therapeutic efficacy. *Proc. Natl. Acad. Sci. U.S.A.* **1991**, *88*, 11460−11464.

(31) Hong, K.; Zheng, W.; Baker, A.; Papahadjopoulos, D. Stabilization of cationic liposome-plasmid DNA complexes by polyamines and poly(ethylene glycol)-phospholipid conjugates for efficient in vivo gene delivery. *FEBS Lett.* **1997**, *400*, 233−237.

(32) Veron, L.; et al. New hydrolysable pH responsive cationic polymers for gene delivery: a preliminary study. *Macromol. Biosci.* **2004**, *4*, 431−444.

(33) Xu, Y.; Szoka, F. C. Mechanism of DNA release from cationic liposome/DNA complexes used in cell transfection. *Biochemistry* **1996**, *35*, 5616−5623.

(34) Drummond, D. C.; Zignani, M.; Leroux, J.-C. Current status of pH-sensitive liposomes in drug delivery. *Prog. Lipid Res.* **2000**, *39*, 409−460.

good particle homogeneity and leads us to suggest that the Genosphere methodology may serve as a good tool for producing uniform nucleic acid carrying particles that are stable enough to be used in vivo.

Successful in vivo gene delivery may require not just a stable carrier system but also selective targeting. In the present work we have demonstrated that Genospheres can selectively target and transfect HER2-overexpressing cells in vitro and can be tailored by formulating with a judicious choice of surface modifying lipids for reduced nonspecific cell interactions. The nonreactive nature of the carrier and its ease of combination with a targeting ligand make the use of Genospheres an attractive methodology for efficient nucleic acid delivery. Future studies will concentrate on the evaluation of Genospheres as a targetable gene delivery vehicle in vivo.

Materials and Methods

Materials. 1,2-Dioleoyl-3-(trimethylammonio)propane (DOTAP), 1-palmitoyl-2-oleoyl-3-*sn*-phosphatidylcholine (POPC), 1,2-dioleoyl-3-*sn*-phosphatidylethanolamine (DOPE), and 1,2-dioleoyl-*sn*-glycero-3-hemisuccinate (DOGHEMS) were purchased from Avanti Polar Lipids (Alabaster, AL) and used without further purification. Dioctadecyldimethylammonium bromide (DDAB), cholesteryl hemisuccinate (CHEMS), *N*-(2-hydroxyethyl)piperazine-*N*′-2-ethanesulfonic acid (HEPES), and 2-morpholinoethanesulfonic acid (MES) were obtained from Sigma (St. Louis, MO). 1-Monomethoxypoly(ethylene glycol)-2,3-distearoylglycerol PEG_{2000} (distearoylglycerol-PEG_{2000}, Sunbright DSG-20H, PEG-DSG) was acquired from NOF Corporation (Tokyo). Cholesterol was purchased from Calbiochem (San Diego, CA). Stock solutions of lipids dissolved in ethanol were stored at −40 °C. 1,1′-Dioctadecyl-3,3,3′,3′-tetramethylindocarbocyanine-5,5′-disulfonic acid ($DiIC_{18}$(3)-DS) and the DNA intercalating dye Picogreen were purchased from Molecular Probes (Eugene, OR). A pH-titratable lipid 1-(3-(cholesteryloxycarbonylamino)propyl)imidazole (CHIM) was synthesized as described previously.[16] Donor human plasma was obtained from the local blood bank.

Purified firefly luciferase and D-(−)luciferin were obtained from Roche (Indianapolis, IN). Other reagents of the highest possible grade were purchased and used without further purification. Cell culture media were obtained from the UCSF cell culture facility (UCSF, San Francisco), and cells were obtained from ATCC (Rockland, MD). F5−PEG-DSPE conjugate was prepared from the purified anti-HER2 scFv, F5, by conjugation to the maleimide-activated PEG terminus of the PEG-DSPE lipid anchor through an engineered C-terminal cysteine as described previously.[18,19]

A bacterial plasmid containing firefly luciferase gene under the control of an early cytomegalovirus promoter (pCMV/luc$^+$) and a penicillin resistance gene was constructed, amplified, and purified as described previously.[31] The plasmid concentration was determined by absorbance at 260 nm (ϵ = 6600 L mol^{-1} cm^{-1}), and purity was determined from the ratio A_{260nm}/A_{280nm} (Shimadzu, UV160U). DNA was considered to be sufficiently protein-free, with an A_{260nm}/A_{280nm} ratio of at least 1.85.

Synthesis of 1,2-Distearoyl-*sn*-Glycero-3-Hemiglutarate (DSGG). 1,2-*O*-Dioctadecyl-*sn*-glycerol (0.2 g, 0.335 mmol), glutaric anhydride (76.4 mg, 0.76 mmol), and 4-(dimethylamino)pyridine (81.8 mg, 0.76 mmol) were stirred in anhydrous chloroform under argon at room temperature for 12 h. The solvent was removed by rotary evaporation and the product purified on a silica gel column by isocratic elution with hexane/ethyl acetate (2:1). The product-containing fractions were combined, and the solvent was removed by rotary evaporation, yielding 115 mg (0.162 mmol, 48.4%) of product. The purity and identity were confirmed by TLC and ^{1}H NMR. Analytical data: ^{1}H NMR ($CDCl_3$, 400 MHz) δ 0.866 (t, 3H, CH_2−CH_3), 1. 26 (s, 60H, CH_2), 1.55 (q, 4H, O−CH_2−CH_2−CH_2), 1.95 (q, 2H, CO−CH_2−CH_2−CH_2−CO), 2. 40 (s, 4H, CO−CH_2−CH_2−CH_2−CO), 3.47 (q, 4H, O−CH_2−CH_2), 3.57 (t, 2H, CHO−CH_2−O), 3.64 (q, 1H, O−CH(CH_2)−O), 7.39 (s, 1H, COOH).

Genosphere Preparation. Genospheres were prepared as described previously.[12] Briefly, the plasmid DNA and the mixture of lipids, as indicated in the text, were separately dissolved in 5 mM aqueous HEPES−Na, pH 7.4, containing 50 vol % ethanol, and combined at 60 °C at a DNA concentration of 0.2−0.5 mg/mL. The mixtures were allowed to attain ambient temperature, and dialyzed overnight against unbuffered saline to remove ethanol. The dialyzed samples containing Genosphere-formulated DNA at about 0.1 mg/mL were used without further purification. If titratable lipids were used in the formulation, 5 mM MES, pH 5.5, was used instead of 5 mM HEPES, pH 7.4, in the aqueous-ethanolic solutions and then dialyzed against 5 mM Mes, 144 mM NaCl in order to increase the positively charged lipid species and reduce anionic charges if present, thus maximizing interactions of the lipids with DNA. HER2-targeted Genospheres were prepared by incubation of Genospheres with F5-cys-mal−PEG(2000)-DSPE antibody conjugate in saline overnight at 37 °C.[32] Typically the amount of conjugate equal to 15 μg of antibody was added per μmol of POPC in the sample. The antibody−PEG-DSPE conjugate is presented in a micellar solution containing a proportion of cysteine-quenched maleimide-PEG-DSPE,[17] and therefore, to account for the effects of PEG introduced in the course of antibody conjugation, nontargeted control samples were incubated with an equivalent amount of PEG-DSPE (i.e., 0.22 mol % of the PC content). Genosphere samples were stored at 4 °C until use.

In Vitro Delivery and Gene Expression. HER2-overexpressing human breast adenocarcinoma cells (SKBR-3 cells) were cultured in McCoy's 5A medium supplemented with 10% (v/v) fetal bovine serum, 100 μg/mL streptomycin sulfate, and 100 units/mL penicillin G at 37 °C, 5% CO_2. The cells were plated at a density of 250 000 cells per well in a 12-well plate (Corning) and acclimated overnight. The final medium volume in each well was 1 mL, and each well received 1 μg of pCMV/luc$^+$ in the form of (i) free DNA, (ii) simple plasmid/liposome complexes, or (iii) Genosphere

preparations. Genospheres were sterilized by passing through a 0.2 μm polyethersulfone (PES) filter (Corning) and the DNA concentration was measured as described previously using the Picogreen assay. The control lipoplexes were aseptically prepared by the addition of pCMV/luc$^+$ to a sonicated dispersion of DOTAP/DOPE (1:1) liposomes for a final ratio of 12 nmol of DOTAP/μg of DNA in 5 mM HEPES, pH 7.4. Both plasmid and liposome solutions were filter-sterilized prior to mixing, and the resulting suspension was added to the cells 20 min following complexation.

All plasmid preparations were incubated with the cells for 6 h and removed by aspiration following washing with Hanks buffered saline (2 $\times$ 1 mL), and the incubation continued for another 18 h following the addition of fresh media (1 mL). The cells were washed with PBS (2 $\times$ 1 mL), detached from the plate by incubation with 1 mL of PBS (containing 3 mM EDTA) at 37 °C for 10 min, pelleted by centrifugation at 3500*g* for 3 min, and resuspended in cold PBS. The cells were lysed by two cycles of freezing (−80 °C) and thawing (37 °C). The lysates were centrifuged (7200*g*, 30−40 s) for removal of cellular debris and assayed for luciferase activity as described previously.[12] Luciferase activity was normalized to the protein concentration in the lysates, determined using the Micro-BCA assay (Pierce, Rockford, IL). A HER2-negative human breast adenocarcinoma cell line MDA-MB468 was transfected with the F5-targeted and nontargeted variants of the neutral Genosphere formulation in the same fashion.

Genosphere Size Measurements. Particle size was measured by dynamic light scattering (DLS) using a Nicomp C370 particle size analyzer (Nicomp Particle Sizing Systems, Santa Barbara, CA). For measurements, the samples were diluted in 0.2 μm filtered HBS, pH 6.5, chosen for its biocompatibility, isotonicity, and pH reported to be optimal for preventing phospholipid hydrolysis.[35] The particle-size distribution (mean and standard deviation) were calculated using the volume weighted Gaussian method and either the solid-particle mode (Genospheres) or vesicle mode (liposomes).

ζ-Potential Measurements. Electrophoretic mobility measurements were made using a Coulter Delsa 440-SX (Beckman Coulter, Fullerton, CA). Each value quoted is the average of a number of runs and is indicated in the table. Measurements were made in either 5 mM Na-HEPES, 5% (w/w) sucrose, pH 7.0, or 5 mM Na-MES, 5% (w/w) sucrose, pH 5.5. All buffers were degassed prior to use. The ζ-potentials were calculated from the measured electrophoretic mobilities using the O'Brien−White algorithm[14] as described in the Results section. Electrical conductivities were measured with the Delsa 440-SX and used to calculate the ionic strengths, required for determination of the Debye−Hückel constants (κ) of the electrolytes. The particle sizes of Genospheres measured at pH 5.5 or pH 7.0 were identical regardless of the presence of titratable lipids (data not shown). The particle radii (a) were then used to determine the parameters κa required in the O'Brien−White calculations.

Cell Association and Transfection Activity of Genospheres of Varying Surface Charge. For transfection studies, formulations of Genospheres having at neutral pH cationic (A), neutral (B),or anionic (C) charges were prepared as described above. The lipid compositions A, B, and C of Table 1 were used, where, instead of a saturated fatty acid derivative DSGG, we used an unsaturated, anionically titratable lipid DOGHEMS, so that the acyl chain composition was consistent with the most abundant dialkyl-lipid in the formulation, unsaturated POPC. Also, up to 20 mol % of the POPC content of the Genospheres in these formulations was replaced with the zwitterionic fusogenic lipid DOPE, which is known to improve transfection of lipoplexes in vitro.[36] Each formulation was prepared with a low and a high PEG-DSG content (0.5 and 5 mol % of total lipid, respectively). The fluorescent membrane probe DiIC$_{18}$(3)-DS was added to all samples (0.2 mol % total lipid) to facilitate quantification of cell association by FACS and visualization by fluorescent microscopy. The DOTAP/DOPE/DNA lipoplex samples were prepared as described above, adding either 0.5 or 5 mol % PEG-DSG. Genospheres were sterilized by passing through a 0.2 μm polyethersulfone filter (Nalgene), and lipoplexes were prepared aseptically as described previously.

SKBR-3 cells were plated in a 12-well plate (Corning) as described above, and the following day the cells were washed with Hanks BSS (2 $\times$ 1 mL). Individual samples (1 μg of DNA) were added to each of 6 wells in McCoy's 5A medium supplemented with 10% (v/v) FBS and 1% (v/v) Pen-Strep in a final volume of 1 mL. After 6 h, the wells were washed with Hanks BSS (3 $\times$ 1 mL), and 1 mL of medium was replaced in 3 of the wells and incubated further at 37 °C. The cells in these wells were analyzed for luciferase activity and protein content 24 h post-transfection using the freeze−thaw lysis method outlined above. The remaining cells were photographed through a fluorescence microscope (Eclipse TE 3000, Nikon, Japan) using a constant exposure time for all phase contrast (1/30 s) and for all fluorescence (1/15 s) photographs. The cells were harvested by incubation with 3 mM EDTA in PBS fixed with 2% paraformaldehyde in PBS for 15 min, and collected by centrifugation at 3500*g* for 5 min. The cells were resuspended in 1 mL of cold PBS and analyzed by cytofluorometry (FACSCalibur 2, Becton Dickinson) using the FL2 channel with (λ_{Ex} 488 nm and λ_{Em} 585 nm). The values reported are the mean and standard deviation of three experiments with 1 $\times$ 10^4 events counted per run.

Abbreviations Used

CHEMS, cholesteryl hemisuccinate; CHIM, 1-(3-(cholesteryloxycarbonylamino)propyl)imidazole; Chol, cholesterol;

(35) Grit, M.; Crommelin, D. J. Chemical stability of liposomes: implications for their physical stability. *Chem. Phys. Lipids* **1993**, *93*, 3−18.

(36) Farhood, H.; Serbina, N.; Huang, L. The role of dioleoyiphosphatidylethanolamine in cationic liposome mediated gene transfer. *Biochim. Biophys. Acta* **1995**, *1235*, 289−295.

DDAB, dioctadecyldimethylammonium bromide; $DiIC_{18}(3)$-DS, 1,1′-dioctadecyl-3,3,3′,3′-tetramethylindocarbocyanine-5,5′-disulfonic acid; DOGHEMS, 1, 2-dioleoyl-*sn*-glycero-3-hemisuccinate; DOPE, 1,2-dioleoyl-3-*sn*-phosphatidylethanolamine; DOTAP, 1,2-dioleoyl-3-(trimethylammonio)propane; DSGG, 1,2-distearoyl-*sn*-glycero-3-hemiglutarate; DSPE, 1,2-disteroyl-3-*sn*-phosphatidylethanolamine; HBS, HEPES buffered saline (5 mM HEPES, 144 mM NaCl, pH 6.5); HEPES, 2-(4-(2-hydroxyethyl)piperazino)ethanesulfonic acid; MES, 2(*N*-morpholino)ethanesulfonic acid; PBS, phosphate buffered saline; PEG-DSG, 2,3-distearoylglycerol 1-monomethoxypolyethyleneglycol ether (PEG_{2000}); PEG-DSPE, *N*-[*ω*-methoxy-(poly(oxyethylene)-*α*-oxycarbonyl)]-DSPE (PEG_{2000}); POPC, 1-palmitoyl-2-oleoyl-3-*sn*-phosphatidylcholine.

Acknowledgment. This work was supported by Hermes Biosciences, Inc., and in part by grants from the National Cancer Institute (NIH P50 CA 58207-01, NIH P50 CA CA097257, and NIH U54 CA90788). Genospheres is a trademark of CPMCRI and Hermes Biosciences Inc.

Note Added after ASAP Publication. An explanatory footnote not present in the version published ASAP on September 15, 2006, was added to Table 1 as footnote *e* in the version published ASAP on November 9, 2006.

MP060040V

ANTICANCER RESEARCH 25: 1531-1538 (2005)

Brain Metastases in Breast Cancer – an *In Vitro* Study to Evaluate New Systemic Chemotherapeutic Options

A. HONIG, L. RIEGER, A. SUTTERLIN, M. KAPP, J. DIETL, M.W. SUTTERLIN and U. KÄMMERER

Department of Obstetrics and Gynecology, University of Wuerzburg, Germany

Abstract. *Background: Fifteen-30% of breast cancer patients develop central nervous system (CNS) metastases. The most potent drugs for the treatment of breast cancer like taxanes, anthracyclines and trastuzumab have limited efficacy for brain metastases. No standardized therapy has yet been established for this condition. Drugs with proven efficacy in the CNS and which are commonly used for primary brain tumors were applied.. We evaluated the capacity of these drugs to inhibit breast tumor cell growth in vitro. Materials and Methods: Twelve primary cell cultures of pulmonary/pleural metastases of breast cancer and 3 commercially available cell lines were used for non-radioactive cytotoxicity assays to evaluate the efficacy of 3 different concentrations of Topotecan, Cisplatin, Nimustine, Vincristine, Irinothecan, Caelyx® (pegylated liposomal Doxorubicin) and Etoposide. Results: Topotecan, Cisplatin, Caelyx® and Vincristine showed significantly higher cytostatic activity in vitro than Irinotecan, Etoposide and Nimustine. With regard to the median cytotoxicity, the order of drugs in our assays was Topotecan, Cisplatin, Vincristine, Caelyx®, Irinotecan, Etoposide and Nimustine. Nimustine showed almost no efficacy against breast cancer cells. Conclusion: Topotecan, Cisplatin, Vincristine and Caelyx® seem to be suitable candidates for further clinical evaluation. The data and the "liposomal packaging" suggest that Caelyx® might be effective in the CNS. Since pulmonary metastases are often associated with brain metastases, evaluating primary cell cultures from malignant pleural effusions could be a valuable approach for the testing of new cytostatic drugs for brain metastases.*

Brain metastases (BM) from systemic primary cancers are the most common cause of neoplastic disease of the central nervous system (CNS). They outnumber primary intracranial neoplasms by at least 10 to 1 (13, 36). After lung cancer, breast cancer is the second most common cause of brain metastases. Overall 15-30% of all metastasized breast cancers lead to CNS metastases (14, 44). Breast cancer, which is characterized by early and frequent metastases, is the most frequent cancer in women with approximately 500,000 cases each year worldwide.

Nowadays, systemic treatment of breast cancer is beneficial for survival in the adjuvant and metastatic setting. Both, the 20-year follow-up of the Bonadonna study and a meta-analysis of the early breast cancer triallists' Collaborative Group (1998) demonstrated the benefits of chemotherapy (CT) concerning disease-free and overall survival (6, 42). However, the incidence of diagnosed brain metastases is increasing (7). This is partly due to the use of modern imaging techniques like MRI, PET and SPECT. Moreover, longer survival of patients with metastasized breast cancer leads to an increase of metastases in uncommon locations such as the brain, skin and vagina. The frequency of the different metastatic locations in breast cancer is 20-30% CNS, 55% lung and pleura, 35% liver, 35% chest wall and 77% bone metastases.

The most potent drugs used in modern breast cancer therapy are anthracyclines, taxanes and trastuzumab (24). In many cases, good control of disease spread to lungs, liver, or bones can be achieved. Unfortunately, none of these drugs reach the central nervous system in efficacious concentrations. Hence, there are several reports of patients showing a good response of their visceral metastases who suffer from newly occurring or progressing CNS metastases (16, 11, 24, 25, 34, 17). A recent retrospective review of 122 women with metastatic breast cancer treated with trastuzumab found that one-third developed CNS metastases in a median time of 6 months after starting trastuzumab therapy. Remarkably, at the time brain metastases (BM) were identified, in half of the patients other systemic disease was either stable or responding to therapy (4).

For the management of BM corticosteroids, radiotherapy and surgical therapy have an established place (36). Surgical resection is preferable in cases of single accessible BM and

Correspondence to: Honig A., MD, Josef-Schneider Str.4, D-97080 Wuerzburg, Germany. Tel: +49/931/201 25293, Fax: +49/931/201 25406, e-mail: arnd_hoenig@hotmail.com

Key Words: Chemotherapy, breast cancer, primary cell culture, cytotoxicity assay, brain metastases.

0250-7005/2005 $2.00+.40

no evidence of progressive extracranial disease. Surgery should be followed by radiotherapy (36, 42). All other patients should be offered radiotherapy. Systemic therapy for BM of breast cancer is a palliative approach aiming to control disease and neurologic dysfunction. Therefore, only single substances expected to be less toxic than combinations were tested. Patients with BM that have progressive extracranial metastatic disease or relapse after radiotherapy are candidates for chemotherapy (29). Contraindications are acute danger of cranial herniation, severe neurological dysfunction or poor general condition.

A frequently anticipated obstacle for chemotherapy of metastatic CNS disease is the blood-brain barrier (BBB), which acts as a barrier for most hydrophilic and large lipophilic substances in normal brain, due largely to the tight junctions between brain capillary endothelial cells. Other mechanisms contributing to form the BBB are high electric resistance, organic anion transporters, transmembrane efflux mechanism, *e.g.* P-glycoprotein and multidrug-resistance associated proteins (MRP). Remarkably, the BBB seems to be more permeable in the situation of BM (7, 20, 21, 33). This also seems to be the case in primary brain tumors like glioma, where formation of pathological tumor vessels inhibits the forming of a functioning BBB (38).

The lung is the most frequently involved distant metastatic site associated with breast cancer (39, 9, 44). In a series of patients investigated by Saito and coworkers (39), 27 patients with node-negative breast cancer developed BM, whereas 26 had developed pulmonary or pleural metastases before CNS spread. Based on this observation, we used primary cell cultures from pleural effusions to test drugs with proven efficiency in the treatment of primary CNS tumors.

Currently, there is not enough clinical evidence to recommend a specific drug or drug regimen for BM of breast cancer. In order to offer these patients the most efficacious chemotherapeutic options, we tested drugs with efficacy in the CNS as proven by their established use in the treatment of primary central nervous tumors (18, 27, 37). In the present study, we investigated primary cell cultures of metastasized breast cancer with cytotoxicity assays, aiming to discover the most promising candidates for future clinical testing in patients suffering from BM.

Materials and Methods

Patients. The median age of patients was 50 years (range 34-75 years) at the time of occurrence of malignant pleural effusion. Receptor status and grading of the tumors is shown in Table I. All patients were pretreated with standard adjuvant chemotherapy. In most cases, additional second- and third-line chemotherapy had been necessary in the course of the disease. Hormonal treatment was administered in case of positive hormone receptor status. At the time of this writing, four patients have died. One had developed multiple BM and died from progress of systemic/pulmonary disease.

Table I. *Characteristics of breast cancer patients from which primary cell cultures were gained.*

Patient	Age	Histology	Grading	Receptor
1	35	ductal invasive	III	neg
2	37	ductal invasive	II	neg
3	39	ductal invasive	II	ER+, PR+
4	47	ductal invasive	III	neg
5	47	lobular invasive	III	ER+, PR+
6	48	ductal invasive	II	neg
7	51	ductal invasive	II	ER+, PR+
8	63	ductal invasive	II	ER+, PR+
9	64	ductal invasive	III	ER+, PR+
10	70	lobular invasive	III	ER+, PR+
11	71	ductal invasive	III	ER+, PR+
12	75	ductulolobular	III	ER+, PR-

Chemotherapeutic agents. The following substances were used in the study: Nimustine (ACNU®; Baxter Oncology), Vincristine (Vincritinsulfat®; Hexal), Cisplatin (Platinex®; Bristol Myers Squibb), Topotecan (Hycamtin®; Glaxo Smith Kline Beecham) and Etoposide (Eto-Gry®; Grypharma). Pegylated liposomal Doxorubicin (Caelyx®; Essex Pharma) was also tested.

Three different concentrations of all drugs were used in the experiments. The institutional pharmacy prepared and dissolved the agents for our tissue culture experiments in the same way as they are prepared and transported for patient use. Drugs were compared in their efficacy with respect to the doses administered in humans. The assumed doses for one cycle were: Topotecan 7.5 mg/m^2, Cisplatin 100 mg/m^2, Nimustine 100 mg/m^2, Caelyx® 20 mg/m^2, Etoposide 700 mg/m^2, Irinotecan 300 mg/m^2 and Vincristine 1.4 mg/m^2. These doses were considered for the preparation of the stock solutions for cytotoxicity assays.

Primary tumor cell culture and commercial cell lines. Primary tumor cell lines from 17 patients with metastasizing breast cancer were isolated and cultivated from pleural effusions. In 12 of these patients, we were able to gain a suitable primary cell culture, which enabled us to perform cytotoxicity experiments. Tumor cells were grown in several different media to establish a primary cell line and the culture from the medium in which the cells grew best was selected. Experiments were performed in RPMI1640 medium (Biochrom, Berlin, Germany).

Effusions (20 - 50 ml) were centrifuged, cell pellets washed twice in phosphate-buffered saline (PBS, Biochrom) and then cultivated in HBCA-medium supplemented with 10% fetal bovine serum (FBS, PAA Laboratories, Cölbe, Germany) and gentamycin at 1 x 10^6 cells/ml in a plastic cell culture flask, in a humidified incubator under 5% CO_2 atmosphere. Fibroblasts were deleted by trypsin treatment every other day and the remaining tumor cell monolayer was cultivated until homogeneous morphology of the cells (passage 3-4). If tumor cells had divided adequately, leukocytes and fibroblasts were absent after a few passages.

In order to establish the experimental setting, we used commercially available cell lines (MCF7, MDA-MB, BT20) to test different concentrations and incubation times. These cell lines were

Table II. *Comparison of median cytotoxicities exhibited by the tested chemotherapeutics (Mann-Whitney U-test).*

	Cisplatin	Topotecan	Caelyx®	Vincristine	Irinotecan	Etoposid	Nimustine
Cisplatin	*	n. s.	n. s.	n. s.	$p<0.05$	$p<0.05$	$p<0.01$
Topotecan	n. s.	*	n. s.	n. s.	$p<0.01$	$p<0.01$	$p<0.01$
Caelyx®	n. s.	n. s.	*	n. s.	$p<0.05$	$p<0.05$	$p<0.01$
Vincristine	n. s.	n. s.	n. s.	*	n. s.	$p<0.05$	$p<0.01$
Irinotecan	n. s.	n. s.	$p<0.05$	n. s.	*	n. s.	$p<0.01$
Etoposide	$p<0.05$	$p<0.01$	$p<0.05$	$p<0.05$	n. s.	*	$p<0.01$
Nimustine	$p<0.01$	$p<0.01$	$p<0.01$	$p<0.01$	$p<0.01$	$p<0.01$	*

not significant = n.s.

obtained from Cell Line Services (Heidelberg, Germany) and cultivated in RPMI1640 medium (Biochrom) supplemented with 10% FBS and gentamycin (R10).

Cytotoxicity assay and photometric evaluation. To quantify the cytotoxicity of drugs, viability of cells was measured with a non-radioactive cell counting assay (Cell Counting Kit-8 Alexis® Biochemicals, Grünberg, Germany), which allows a sensitive colorimetric determination of viable cells in cell proliferation and cytotoxicity assays. A tetrazolium salt (WST-8; 2-(2-methoxy-4-nitrophenyl)-3-(4-nitrophenyl)-5-(2,4-disulfophenyl)-2H-tetrazolium, monodium salt) is reduced by dehydrogenases in cells to give a yellow-colored product (formazan), which can be analyzed *via* absorbance at 460 nm in an ELISA plate reader. The amount of formazan dye generated is directly proportional to the number of living cells. We seeded approximately 20,000 cells in a volume of 95 µl R10 medium per well in a 96-well cluster plate. Quintuplicate wells were set for each drug at each concentration.

Drugs in various concentrations were added in a volume of 5 µl. Dilutions of the drugs were done in conventional NaCl 0.9%-solution. For establishing the experimental system, MCF7, MDA-MB and BT20 cells were initially seeded on 4 plates each and identical settings of drugs were added. For each cell line, one of the plates was then analyzed with the cell counting kit after the specified incubation time of 12, 24, 48 and 72 hours, respectively. Best signal/noise ratios were obtained with the plates incubated for 48-hours. Therefore, we decided to perform all the following trials with a 48-hour incubation time. Several dilutions were tested (1:20, 1:100, 1:500). After 48 hours, 10 ml of WST-8 were added, and after one-hour incubation, the plates were evaluated with the plate reader. Controls were run with PBS, media and NaCl.

Statistical evaluation of results. The median numbers of viable cells in percent were determined using the non-parametric Mann-Whitney *U*-test (significance set at $p<0.05$) using Statistica version 6 (Statsoft).

Results

Pre-testing. Testing with the commercially available breast cancer cell lines MCF-7, MDA-MB and BT20 revealed that the results gained with the cell counting assay were reproducible (data not shown). These cell lines have a rather high proliferation activity. Smaller differences in the capacity of drugs to inhibit cell growth were easier to discover with these cells. We tested different incubation times (12, 24, 48 and 72 hours) and dilutions of chemotherapeutics to establish the experimental setting.

Testing. We aimed to imitate the *in vivo* situation in our experimental *in vitro* setting. Therefore, we used primary cell cultures of 12 patients with as few passages (3-5) *in vitro* as possible. We tested seven different chemotherapeutic agents (Table II) at three different concentrations with regard to their ability to inhibit growth of breast cancer cells. The determined differences in the number of viable cells after exposure to the cytostatic compounds was smaller in primary cell lines compared to commercial cell lines. The results are illustrated in Figure 1.

A dilution of 1:500 of the chemotherapeutic agents proved to be too high and did not result in reproducible rates of cytotoxicity. Nimustine, Etoposide and Irinotecan were less efficacious than the other agents tested and did not exhibit sufficient inhibition of cell growth if diluted 1:100 to allow a reliable comparison of the whole group of drugs. Therefore, drugs were compared in terms of their median cytotoxicities after 48 hours at a dilution of 1:20. We administered a dilution of 1:20 resulting in concentrations for Topotecan of 3.75×10^{-3}mg/ml, Cisplatin 0.05mg/ml, Nimustine 0.05mg/ml, Caelyx® 0.01mg/ml, Etoposide 0.35mg/ml, Irinotecan 0.15mg/ml and Vincristine 7×10^{-4}mg/ml. This dilution yielded the most reproducible results in the cytotoxicity assays.

Topotecan proved to be the most potent drug based on the median cytotoxicity evaluated for all drugs in our cell culture assays. It was significantly more potent than Irinotecan, Etoposide and Nimustine. Through all experiments performed, Cisplatin was always among the most potent agents. Cisplatin showed a slightly higher median cytotoxicity than Vincristine and Caelyx®, but was not statistically significantly more efficacious than the other two. The anthracycline Caelyx® also showed a considerable inhibition of tumor cell growth. Vincristine, Topotecan, Cisplatin, and pegylated liposomal Doxorubicin form a group of four drugs that are significantly more toxic to breast cancer cells than the rest of the agents tested. Irinotecan and

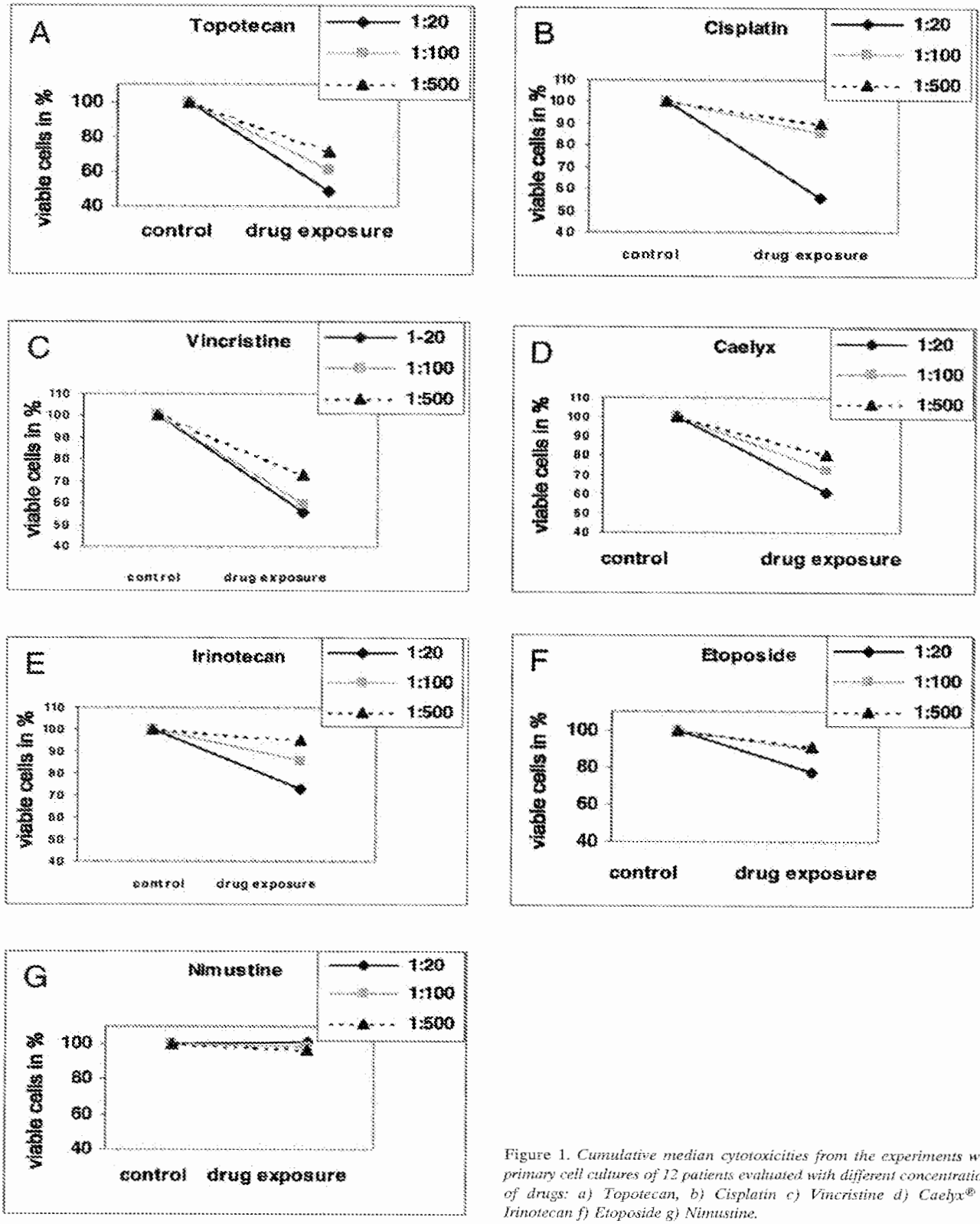

Figure 1. *Cumulative median cytotoxicities from the experiments with primary cell cultures of 12 patients evaluated with different concentrations of drugs: a) Topotecan, b) Cisplatin c) Vincristine d) Caelyx® e) Irinotecan f) Etoposide g) Nimustine.*

Etoposide showed comparable rates of growth inhibition, but were significantly less cytotoxic ($p<0.05$) than the drugs mentioned above. The data are shown in Table II. Nimustine turned out to be significantly weaker than all the other substances tested ($p<0.01$). Surprisingly, in a few primary cell lines cells incubated with Nimustine, tumor cells grew better than the control (Figure 1G).

The variation of the proliferation activity between the different primary cell lines was substantial. When the same drug was tested in different cell lines, consequently the standard deviation of the median cytotoxicity of a specific drug was enlarged.

We also compared the capacities of agents with regard to the age of patients. The median age of all patients was 49 years and was used as a cut off to split the collective into two subgroups. There was a tendency, for tumors from younger patients to be more resistant to cytostatic agents than malignancies of elderly women, but the difference did not prove to be statistically significant. The lack of statistical significance could be attributed to the relatively small numbers of subjects.

Discussion

In the present study, we performed an *in vitro* evaluation of chemotherapeutics in order to search for potent therapeutic options for brain metastases (BM) from breast cancer. Patients that suffer from this condition are, in general, relatively young and have mostly hormone receptor-negative and more aggressive undifferentiated G2 and G3 tumors (10, 40, 44). These young patients are frequently in good general condition and demand valuable treatment. It is noteworthy that patients with BM from breast cancer are a diverse group characterized by a large subset of patients surviving only a few months, but also a remarkable number of patients that survive for more than a year, with an unsatisfying median overall survival of 6 months (28).

Hall *et al.* showed, in an retrospective analysis of patients with brain metastases from different tumors, that among other therapeutic approaches, chemotherapy was a beneficial factor for prolonged survival (23). One of the crucial factors for a successful systemic treatment of BM is that the BBB becomes permeable in the situation of metastatic brain disease. Some authors (16) claim that most substances with good penetration of the BBB have limited activity against breast cancer. In contrast, Landonio *et al.* stated, that chemotherapy has proven efficacy in patients with BM from several different primaries, of which breast cancer is just one. Surprisingly, the observed responses to chemotherapy almost resemble those in other metastatic sites (27). Effective treatment of the extracranial disease is often possible. Consequently, as opposed to patients with BM from other solid tumors who generally die of extensive systemic disease, at least half of the patients with BM from breast cancer die of their neurological disease (14, 22).

In our *in vitro* study, we applied drugs that have proven efficacy in the CNS and are used for primary brain tumors (18, 27, 37). We evaluated the capacity of these drugs to inhibit the growth of breast cancer cells. Topotecan belongs to a class of agents that has shown substantial promise in preclinical studies (37). It is a campothecin derivative which inhibits topoisomerase I. Topotecan is one of the chemotherapeutic agents with the highest cerebrospinal fluid levels after intravenous administration, reaching 30-40% of plasma concentrations (5). In spite of encouraging *in vitro* findings, so far there is no clinical evidence of good response rates *in vivo*. There might be some inhibitory mechanism against, or efflux transport of, Topotecan that only takes effect *in vivo*. In one study performed by Levine *et al.* only 4 out of 53 Topotecan-treated patients showed an objective response (30). In general, clinical evidence regarding the systemic treatment of BM is limited (16). In spite of its superiority in *in vitro* assays, Topotecan might not be the first choice for the situation *in vivo*. Other compounds with satisfying results in *in vitro* assays, like platinum analogs, have clinically shown efficacy against breast cancer in the past. Cisplatin is very active as first-line chemotherapy of metastasized breast cancer, with response rates of 50% (31) Naturally, sensitivity to drugs varies between tumor cells, but Cisplatin showed comparable efficacy to Topotecan and might be a valuable alternative option, especially in cases where Topotecan is not tolerated or leads to progressive disease.

Interest in platinum compounds in the treatment of breast cancer has been reawakened, because preclinical studies indicated a possible synergism between trastuzumab and platinum compounds in human breast cancer cell lines overexpressing Her2/neu (12, 31). In early trials, platinum-taxane-trastuzumab combinations have shown promising clinical activity (12). Our data justify the evaluation of platinum analogs clinically in BM of breast cancer. This adds another oncological disease setting in which the very widely used platinum analogs are applicable.

Caelyx® showed good cytotoxicity in our experiments. It has no established role for the treatment of CNS neoplastic disease yet, but its "lipophilic packaging" suggests that it enters the CNS. It was seen in one clinical study that the accumulation of radiolabelled liposomal Doxorubicin in glioblastoma tissue and BM from breast cancer was 10 times higher than in the surrounding normal brain. Objective responses were seen in all 3 breast cancer patients treated with liposomal Doxorubicin (26). The primary breast cancer cultures we exposed to Caelyx® reflected the expected cytotoxicity of an anthracycline, but more evidence is needed that it reaches the metastatically affected CNS in efficacious concentrations *in vivo*.

Vincristine showed good efficacy in inhibiting growth of breast cancer cells in our *in vitro* model. It has to be mentioned

that Vincristine generally exhibits good cytotoxicity in tissue culture experiments. Nevertheless, our results warrant clinical testing in breast cancer patients. Proteins like P-glycoprotein and multidrug resistance-associated protein (MRP) maintain the BBB by transmembrane efflux mechanisms that are believed to transport vinca alkaloids out of the CNS (3). To some minor extent, these mechanisms could take effect even if the BBB is disrupted by metastases, weakening the effect of Vincristine on metastatic tumor growth *in vivo*.

Etoposide is a topoisomerase II inhibitor used for high-grade gliomas. Our results revealed only a minimal efficacy of Etoposide against breast cancer cells and, even for the treatment of primary brain tumors like gliomas, the data in the literature is ambiguous (43).

Nitrosoureas were among the earliest agents to have demonstrable clinical efficacy in brain tumors (45). They are widely used as compounds of drug regimens. We tested the nitrosourea Nimustine with regard to its ability to inhibit breast cancer cell growth. It did not exhibit considerable cytotoxicity in our *in vitro* assays. Nevertheless, the results have to be interpreted with caution. It could very well be that it has minor efficacy as monotherapy, but is a valuable compound if combined with other substances, as demonstrated for the combination Nimustine and Irinotecan (18). Furthermore, its comparably weak performance in *in vitro* assays has frequently been observed and, therefore, a final judgment on Nimustine is difficult. The conclusion from our results is that there is no *in vitro* basis that would warrant clinical evaluation of the drug as monotherapy for BM from breast cancer.

Irinotecan (CP-11) belongs to the family of topoisomerase I inhibitors similar to Topotecan. As pointed out for Nimustine, as part of a drug regimen it might have considerable value but, considering our results, Irinotecan, Etoposide and Nimustine are not the first choice for a clinical evaluation in breast cancer patients with BM.

Final evaluation of all these drugs was not done in commercially available cell lines. It is characteristic of such cell lines that they divide rather rapidly, but they seem to loose a lot of their *in vivo* properties during several years of *in vitro* culturing and obtain new ones while adapting to culture conditions. Some of those properties lost and/or gained might play an important role for the cell's susceptibility to cancer drugs. Bahr *et al.* showed that culturing of glioma cell lines can lead to a multidrug resistance (MDR)-phenotype that primary glioma tumor cells do not show (2). The authors hereby exemplified a possible pitfall of *in vitro* testing. This illustrates how crucial it is to mimic the situation *in vivo* as far as possible, which we attempted with the use of primary cell lines and only 3-5 passages *in vitro*.

To the best of our knowledge, this is the first report using primary cell lines derived from pleural effusions to test chemotherapeutics which potentially can be used for the therapy of BM in breast cancer patients. The data presented here might help to increase the treatment options. This will enable us to take age, performance status, tumor biology and prior therapy into account when deciding about treatment of metastatic CNS disease.

The approach of testing potential therapies with primary tissue cultures with the non-radioactive cell counting kit appears to be a valid option for preclinical testing of new chemotherapeutics for the treatment of breast cancer. Therefore, this experimental approach could be applied for promising substances, such as Capecitabine (41), Thiotepa and Temozolamide (1), to enlarge the therapeutic spectrum for metastatic CNS disease. Clinical trials with large patient populations are needed to identify the subgroup of patients that would benefit the most from chemotherapy for brain metastases.

Acknowledgements

Mrs. Steigerwald and Mrs. Stäblein from the Department of Pharmacology, Subdivision Oncology for providing chemotherapeutics and valuable advice.

References

1 Abrey LE, Olson JD, Raizer JJ, Mack M, Rodavitch A, Boutros DY and Malkin MG: A phase II trial of temozolomide for patients with recurrent or progressive brain metastases. J Neurooncol *53(3)*: 259-265, 2001.

2 Bahr O, Rieger J, Duffner F, Meyermann R, Weller M and Wick W: P-glycoprotein and multidrug resistance-associated protein mediate specific patterns of multidrug resistance in malignant glioma cell lines, but not in primary glioma cells. Brain Pathol *13(4)*: 482-494, 2003.

3 Bart J, Groen JM, Hendrikse NH, van der Graaf WTA, Vaalburg W and de Vries EGE: The blood-brain barrier and oncology: new insights into function and modulation. Cancer Treat Rev *26*: 449-462, 2000.

4 Bendell JC, Domchek SM, Burstein HJ, Harris L, Younger J, Kuter I, Bunnell C, Rue M, Gelman R and Winer E: Central nervous system metastases in women who receive trastuzumab-based therapy for metastatic breast carcinoma. Cancer *97*: 2972-2977, 2003.

5 Blaney SM; Cole DE, Balis FM, Godwin K and Poplack DG: Plasma and cerebrospinal fluid pharmacokinetic study of topotecan in nonhuman primates. Cancer Res *53*: 725-727, 1993.

6 Bonadonna G, Valagussa P, Moliterni A, Zambetti M and Brambilla C: Adjuvant cyclophosphamide, methotrexate, and fluorouracil in node-positive breast cancer: the results of 20 years of follow-up: N Engl J Med *332(14)*: 901-906, 1995.

7 Boogerd W: Central nervous system metastasis in breast cancer. Radioth Oncol *40*: 5-22, 1996.

8 Brandes AA, Palmisano V and Monfardini S: Medulloblastoma in adults: clinical characteristics and treatment. Cancer Treat Rev *25(1)*: 3-12, 1999.

9 Clamon G and Doebbeling B: Meningeal carcinomatosis from breast cancer: spinal cord *vs.* brain involvement. Breast Cancer Res Treat *9*: 213-217, 1987.

10 Clark GM, Sledge GW Jr, Osborne CK and McGuire WL: Survival from first recurrence: relative importance of prognostic factors in 1,015 breast cancer patients. J Clin Oncol *5(1)*: 55-61, 1987.
11 Crivellari D, Pagani O, Veronesi A, Lombardi D, Nole F, Thurlimann B, Hess D, Corner M, Bauer J, Martinelli G, Graffeo R, Sessa C and Goldhirsch A: High incidence of central nervous system involvement in patients with metastatic or locally advanced breast cancer treated with epirubicin and docetaxel. Ann Oncol *12*: 353-356, 2001.
12 Crown J and Pegram M: Platinum-taxane combinations in metastatic breast cancer: an evolving role in the era of molecularly targeted therapy. Breast Cancer Res Treat *79(Suppl 1)*: 11-18, 2003.
13 DeAngelis LM: Current diagnosis and treatment of leptomeningeal metastasis. J Neurooncol *38*: 245-252, 1998.
14 DiStefano A, Yong Yap Y, Hortobagyi GN and Blumenschein GR: The natural history of breast cancer patients with brain metastases. Cancer *44*: 1913-1918, 1979.
15 Early breast cancer trialists' Collaborative Group: Polychemotherapy for early breast cancer: an overview of the randomized trials. Lancet *352*: 930-942, 1998.
16 Fenner MH and Possinger K: Chemotherapy for breast cancer brain metastases. Onkologie *25*: 474-479, 2002.
17 Freilich RJ, Seidmann AD and DeAngelis LM: Central nervous system progression of metastatic breast cancer in patients treated with paclitaxel. Cancer *76*: 232-236, 1995.
18 Friedman HS, Keir ST and Houghton PJ: The emerging role of irinotecan (CPT-11) in the treatment of malignant glioma in brain tumors. Cancer *97(9 Suppl)*: 2359-2362, 2003.
19 Fuchs IB, Loebbecke M, Buhler H, Stoltenburg-Didinger G, Heine B, Lichtenegger W and Schaller G: HER2 in brain metastases: issues of concordance, survival and treatment. J Clin Oncol *20*: 4130-4133, 2002.
20 Greig NH: Brain tumors and the blood tumor barrier. *In*: Implications of the Blood-Brain Barrier and its Manipulation, Plenum Press, Vol. 2, pp. 77-106, 1989.
21 Greig NH: Optimizing drug delivery to brain tumours. Cancer Treat Rev *14*: 1-28, 1987.
22 Hagemeister FB, Buzdar AU, Luna MA and Blumenschein GR: Causes of death in breast cancer: a clinicopathologic study. Cancer *46*: 162-167, 1980.
23 Hall WA, Djalilian HR, Nussbaum ES and Cho KH: Long-term survival with metastatic cancer to the brain. Med Oncol *17*: 279-286, 2000.
24 Kirsch DG and Hochberg FH: Targeting HER2 in brain metastases from breast cancer Clin Cancer Res *9*: 5435-5436, 2003.
25 Kosmas C, Malamos NA, Tsavaris N and Antonopoulos M: Chemotherapy-induced complete remission of choroidal metastases and subsequent isolated leptomeningeal carcinomatosis in advanced breast cancer: a case report and literature review. J Neurooncol *47*: 161-165, 2000.
26 Koukourakis MI, Koukouraki S, Fezoulidis I, Kelekis N, Kyrias G, Archimandritis S and Karkavitsas N: High intratumoral accumulation of stealth liposomal doxorubicin (Caelyx) in glioblastomas and in metastatic brain tumours. Br J Cancer *83*: 1281-1286, 2000.
27 Landonio G, Sartore-Bianchi A, Gianetta L, Renga M, Riva M and Sienna S: Controversies in the management of brain metastases: the role of chemotherapy. Forum *11(1)*: 59-74, 2001.
28 Lentzsch S, Reichardt P, Weber F, Budach V and Dörken B: Brain metastases in breast cancer: prognostic factors and management. Eur J Cancer *35(4)*: 580-585, 1999.
29 Lesser GJ: Chemotherapy of cerebral metastases from solid tumors. Neurosurg Clin N Am *7(3)*: 527-536, 1996.
30 Levine EG, Cirrincione CT, Szatrowski TP, Canellos G, Norton L and Henderson IC: Phase II trial of topotecan in advanced breast cancer: a Cancer and Leukemia Group B study. Am J Clin Oncol *22(3)*: 218-222, 1999.
31 Martin M: Platinum compounds in the treatment of advanced breast cancer. Clin Breast Cancer *2*: 190-209, 2001.
32 Massot-Punyet R, Almajano J and Camacho JM: Cerebral metastasis. Rev Neurol *31(12)*: 1242-1247, 2000.
33 Morrow CP and Curtin JP: *In*: Synopsis of Gynecologic Oncology 5th edition. Churchill Livingstone pp. 343, 1998
34 Oberhoff C, Kieback DG, Wurstlein R, Deertz H, Schouli J, van Soest C, Hilfrich J, Mesrogli M, von Minckwitz G, Staab HJ and Schindler AE: Topotecan chemotherapy in patients with breast cancer and brain metastases: results of a pilot study. Onkologie *24*: 256-260, 2001.
35 Patchell RA, Tibbs PA, Walsh JW, Dempsey RJ, Maruyama Y, Kryscio RJ, Markesbery WR, Macdonald JS and Young B: A randomized trial of surgery in the treatment of single metastases to the brain. N Engl J Med *322*: 494-500, 1990.
36 Patchell RA: The management of brain metastases. Cancer Treat Rev *29*: 533-540, 2003.
37 Pollack IF, Boyett JM and Finlay JL: Chemotherapy for high-grade gliomas of childhood. Child's Nerv Syst *15*: 529-544, 1999.
38 Rieger J, Roth W, Glaser T, Winter S, Rieger L, Dichgans J and Weller M: Glioblastoma multiforme: mechanisms of resistance to chemotherapy. Neurol Psych Brain Res *7*: 37-46, 1999.
39 Saito M, Yoshimoto M, Akiyama F, Sakamoto G, Kasumi F and Kaminishi M: Characteristics of brain metastases from node negative breast cancer. Breast *12 (Suppl 1)*: 28-29, 2003.
40 Schouten LJ, Rutten J, Huveneers HA and Twijnstra A: Incidence of brain metastases in a cohort of patients with carcinoma of the breast, colon, kidney, and lung and melanoma. Cancer *94(10)*: 2698-2705, 2002.
41 Siegelmann-Danieli N, Stein M and Bar-Ziv J: Complete response of brain metastases originating in breast cancer to capecitabine therapy. Isr Med Assoc J *5(11)*: 833-834, 2003.
42 Singletary SE, Walsh G, Vauthey JN, Curley S, Sawaya R, Weber KL, Meric F and Horobagyi GN: A role for curative surgery in the treatment of selected patients with metastatic breast cancer. Oncologist *8(3)*: 241-251, 2003.
43 Tirelli U, D'Incalci M, Cancetta *et al*: Etoposide (VP-16-213) in malignant brain tumors; a phase II study. J Clin Oncol *2*: 432-437, 1984.
44 Tsukada Y, Fouad A, Pickren JW and Lane WW: Central nervous system metastasis from breast carcinoma. Autopsy study. Cancer *52(12)*: 2349-2354, 1983.
45 Walker MD, Alexander E Jr, Hunt WE, MacCarty CS, Mahaley MS Jr, Mealey J Jr, Norrell HA, Owens G, Ransohoff J, Wilson CB, Gehan EA and Strike TA: Evaluation of BCNU and/or radiotherapy in the treatment of anaplastic gliomas. A cooperative clinical trial. J Neurosurg *49(3)*: 333-343, 1978.

Received August 2, 2004
Accepted February 4, 2005

Biochimica et Biophysica Acta, 720 (1982) 411–419
Elsevier Biomedical Press

BBA 11048

INTERACTIONS OF LIPOSOMES WITH THE RETICULOENDOTHELIAL SYSTEM.

II: NONSPECIFIC AND RECEPTOR-MEDIATED UPTAKE OF LIPOSOMES BY MOUSE PERITONEAL MACROPHAGES

M.J. HSU and R.L. JULIANO

Department of Pharmacology, The University of Texas Medical School at Houston, P.O. Box 20708, Houston, TX 77030 (U.S.A.)

(Received October 6th, 1981)
(Revised manuscript received April 21st, 1982)

Key words: Receptor; Liposome uptake; Reticuloendothelial system; (Macrophage)

Liposomes are taken up as intact vesicles by mouse peritoneal macrophages in a process which is temperature sensitive and is affected by inhibitors of glycolytic metabolism and of microfilament activity. Macrophages take up negatively charged vesicles more readily than positively charged vesicles (2-fold) or neutral vesicles (4-fold). Macrophages take up similar amounts of multilamellar liposomes, reversed phase liposomes and small unilamellar liposomes in terms of lipid, however this corresponds to vastly different numbers of particles and amounts of trapped volume. Coating the liposomes with macromolecular ligands capable of interacting with macrophage surface receptors can markedly promote liposome uptake. Thus, formation of an IgG-antigen complex on the liposome surface results in a 10^2-fold enhancement of liposome uptake, while coating the vesicles with fibronectin results in a 10-fold augmentation of uptake. Uptake via IgG-mediated and fibronectin-mediated processes seem to be independent since excess unlabelled, IgG-coated liposomes will inhibit the uptake of radioactively-labelled IgG-coated liposomes much more effectively than the uptake of radioactively-labelled fibronectin-coated liposomes. Cell-bound liposomes can readily be visualized on and inside of the macrophages using fluorescence microscopy techniques.

Introduction

Liposomes have attracted great interest as a system for the controlled delivery of drugs. Many pharmaceuticals can be encapsulated in lipid vesicles, and such encapsulated drugs have pharmacodynamic and therapeutic properties which are often radically different from the free drug [1–5]. One of the major characteristics of the liposomal drug delivery system is the propensity of these vesicles to be taken up by the mononuclear phagocytes of the reticuloendothelial system [6]. This can be advantageous in terms of directing drugs or immunomodulating agents to macrophages [7], or can be disadvantageous in terms of diverting drug bearing vesicles away from other sites of interaction (e.g., tumor cells). For these reasons it seems important to enhance our understanding of the possible interactions between liposomes and reticuloendothelial cells.

There is an extensive literature on the interaction of liposomes with various tissue culture cells and with lymphoid cells (reviewed by Pagano and Weinstein, Ref. 8), including several reports on the uptake of liposomes by polymorphonuclear leukocytes [9,10]. An interesting feature of the process is the potentiation of uptake caused by coating the liposomes with aggregated IgG which

Abbreviations: IgG, immunoglobulin G.

presumably promotes interaction with cellular Fc receptors [11]. There are also a limited number of reports of liposome interaction with mononuclear phagocytes. Thus Leserman et al. [12] have examined the uptake of antibody-coated small unilamellar vesicles by various tumor cell lines, and have found that P388D_1, a macrophage-like cell type which is Fc positive and capable of phagocytosis, took up such vesicles better than cells which possessed the Fc receptor but were nonphagocytic (P388). Finkelstein et al. [13] studied uptake of liposomes by mixed human leukocyte populations and found that monocytes are more active than neutrophils and lymphocytes. Petty et al. [14] have examined the uptake of vesicles containing a lipid haptene and complexed with antibodies by RAW 264, a macrophage-like cell line. They have found a marked potentiation of uptake via antibody coating, an effect which is probably mediated via the Fc receptor. In addition they noted that uptake of antibody-coated vesicles suppressed the ability of RAW 264 cells to bind antibody-coated sheep erythrocytes via the Fc receptor, but did not suppress their ability to bind IgM- plus complement-coated erythrocytes via the C3b receptor, thus providing additional documentation for the independence of these two receptor types. Much of the most interesting work on liposome-macrophage interactions was done with macrophage-like cells lines, rather than with true macrophages; thus experimental work on the 'classic' macrophage preparation, from mouse peritoneal exudates, has been rather limited, at least in terms of details of liposomes uptake and quantitation [15,16].

In the present study, we investigate basic facets of liposome-macrophage interaction such as the role of vesicle size and surface charge in controlling nonspecific uptake of liposomes. In addition we examine ligand-mediated uptake via the cellular receptors for the Fc domain of IgG and for fibronectin; we also examine possible interactions between the Fc and fibronectin-mediated uptake systems.

Methods

Preparation of liposomes

Reversed phase liposomes. Large unilamellar vesicles were prepared by a modification [17] of the reversed phase method of Szoka and Papahadjopoulos [18]. The vesicles were passed through a 0.6 μm polycarbonate filter and then collected by centrifugation at $2000 \times g$ for 10 min. As described previously [17], such vesicles have a median diameter of approx. 1 μm.

Small unilamellar liposomes. Small unilamellar vesicles were prepared by sonication using a Heat System 375W instrument with microprobe tip at a power setting of 40%. Sonication was carried out under a flow of N_2 for approx. 10 min or until the sample had clarified. Residual large vesicles were removed by centrifugation at 42000 rpm, for 1 h as described [17]; this gives rise to a vesicle preparation with a range of diameters between 0.02 and 0.05 μm.

Multilamellar liposomes. Large multilamellar liposomes were prepared by hand-shaking lipid dispersions in buffer, passing the material through a 0.6 μm filter and then centrifugation at $2000 \times g$ for 10 min.

Liposomes were usually prepared in physiologically isotonic phosphate-buffered saline at pH 7.4. In most cases the liposomes were composed of dipalmitoylphosphatidylcholine and cholesterol in a 1 : 1 molar ratio. In some cases 10 mol% of either (a) phosphatidylserine (an anionic lipid), (b) stearylamine (a cationic lipid) or (c) dinitrophenylcaproylphosphatidyl ethanolamine, a lipid antigen, were included in the liposome preparation. Cholesterol oleate, labelled with ^{14}C, was used as a marker for the lipid phase of the vesicles [17], while [^{3}H]sucrose was used as a marker for the acqueous phase. Usually 50 μCi of [^{14}C]cholesterol oleate per 10 mg phospholipid was used.

Macrophage cultures. Thioglycolate-elicited mouse peritoneal macrophages were prepared essentially according to the procedures of Edelson et al. [19]. Thus, outbred white mice were injected with 0.5 cm^3 thioglycolate medium 4 days before death. After killing by cervical dislocation, exudate cells were harvested from the peritoneal cavity in phosphate-buffered saline plus 100 U/cm^3 heparin. The cells were washed and resuspended in α medium containing 10% calf serum and antibiotics and counted by hemocytometry. Approx. $2-4 \cdot 10^6$ cells per well were plated into Costar tissue culture trays (No. 3506), and the cells were placed at 37°C

in a CO_2 incubator for 2 h. Non-adherent cells were removed by washing with medium and the adherent cells were returned to the incubator overnight. Cultures prepared in this manner contained greater than 95% macrophages as evidenced by ability to take up latex beads, and by positive staining using the nonspecific esterase test [20].

Uptake experiments. Macrophage monolayers established in Costar trays were rinsed with α medium + 1 mg/ml bovine albumin and then re-equilibrated in a CO_2 incubator with this medium. In some cases various inhibitors were included in the medium at this time. At the start of the experiment a small volume of radioactively-labelled liposome suspension was added. At various times thereafter the macrophage monolayers were rinsed three times in phosphate-buffered saline, the cells were removed by scraping, these were then centrifuged and washed twice with phosphate-buffered saline. The final cell pellet was suspended in a known volume of buffer and aliquots were used for radiation counting with duplicates for protein analysis. [21].

Materials

Lipids including dipalmitoylphosphatidylcholine, L-α-phosphatidylserine, stearylamine and cholesterol were from Sigma. Dinitrophenylaminocaproylphosphatidylethanolamine was from Avanti Polar Lipids. Cholesteryl [^{14}C]oleate was from Amersham, while [^{3}H]sucrose [fructose-1-^{3}H(N)] was from New England Nuclear. Tissue culture medium, antibiotics and calf serum were obtained from Gibco. Anti-dinitrophenol serum (rabbit anti-dinitrophenyl albumin) was from Miles-Yeda. Cytochalasin B was purchased from Aldrich Chemicals. Bovine fibronectin was prepared as described [22].

Results

Kinetics

As seen in Fig. 1 the uptake of radioactively-labelled dipalmitoylphosphatidylcholine/cholesterol reversed phase liposomes by mouse peritoneal macrophages displays a brief lag phase, is approx. linear from 60 to 240 min and then begins to plateau. For the first 120 min there is a close correspondence of the calculated values of

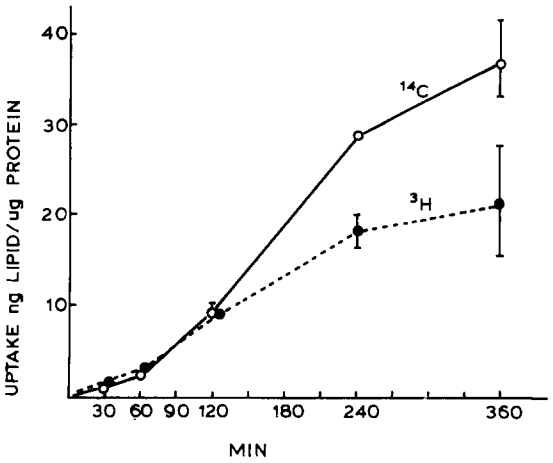

Fig. 1. Kinetics of liposome uptake by macrophages. Reverse phase large unilamellar vesicles were prepared from dipalmitoylphosphatidylcholine and cholesterol 1 : 1 molar ratio. The vesicles were labelled with [^{3}H]sucrose (200 μCi) as a marker for the aqueous phase and [^{14}C]cholesterol oleate (10 μCi) as a marker for the lipid phase. Macrophage monolayers were established, pre-equilibrated in α medium plus 1 mg/cm^3 bovine albumin at 37°C, aliquots of liposomes were added (200 μg) and at various times the cells were harvested, processed, and counted. Points are the mean ±S.E. of triplicate determinations. O------O, uptake of ^{14}C label; ●------●, uptake of ^{3}H label.

liposome uptake using the lipid phase marker ([^{14}C]cholesterol oleate) or the aqueous phase marker ([^{3}H]sucrose), indicating that the uptake process involves intact vesicles. After 120 min the values calculated for the two markers begin to diverge; this might indicate an increased tendency for uptake of the lipid marker via exchange processes, may be a reflection of metabolic degradation and reutilization of liposome components after an extended period of incubation, or may indicate gradual leakage of the [^{3}H]sucrose. During the first 90 min period, when the uptake process seems to involve intact vesicles and where little evidence of separation of markers due to metabolic breakdown is observed, the total accumulation of cell-associated liposomal lipid ranged, in different experiments, from 2–15 ng/μg cell protein, with an average of 7 ng/μg. As we will see, alteration of vesicle charge, or coating the vesicle with various protein ligands can markedly alter the total uptake.

Uptake of dipalmitoylphosphatidylcholine/

cholesterol reversed phase liposomes was linear with cell number over the range of $2-8 \cdot 10^6$ cells plated per dish. Uptake was linear with lipsome doses of 0–300 μg/dish; at greater doses an apparent 'saturation' was observed, however, the precise meaning of this is unclear since macrophages could take up amounts of ligand-coated vesicles (see below) far in excess of the amount of uncoated vesicles which accumulated at apparently 'saturating' doses of such vesicles. The apparent saturation may represent full occupancy of surface sites for nonspecific uptake.

Effects of vesicle charge and size

Data presented in Tables I and II indicates that alteration of vesicle physical parameters such as charge and size can have a substantial impact upon the total amount of lipid and the total volume of liposome-encapsulated material accumulated by the macrophages. As seen in Table I, macrophage uptake of negatively charged vesicles at 37°C is substantially higher than the uptake of positive vesicles which in turn is higher than uptake of neutral vesicles. The amount of liposomal material which becomes cell associated at 4°C is, in all cases, less than 10% of that taken up at 37°C.

TABLE I

EFFECT OF CHARGE ON LIPOSOME UPTAKE BY MACROPHAGES

Reversed phase liposomes were prepared composed of (a) dipalmitoylphosphatidylcholine/cholesterol, 1 : 1 molar ratio (neutral); (b) dipalmitoylphosphatidylcholine/cholesterol/stearylamine, 1 : 1 : 0.2 molar ratio (positive); (c) dipalmitoylphosphatidylcholine/cholesterol/phosphatidylserine, 1 : 1 : 0.1 molar ratio (negative). All vesicles were labelled with 10 μCi [^{14}C]cholesterol oleate. Macrophage monolayers were preincubated in α medium plus 1 mg/cm^3 bovine albumin at 4 or 37°C. Liposomes (120 μg) were added and the cells were washed, harvested and processed for counting after a 90 min incubation. The data represent the mean ±S.E. for triplicate determinations.

	Liposome type	Uptake in ng lipid/μg cell protein	
		37°C	4°C
(a)	Neutral	17.0±7.0	2.0
(b)	Positive	36.1±9.0	3.5
(c)	Negative	63.0±4.0	3.0

Since phagocytosis, but not absorption, is impaired at 4°C, this material probably represents surface bound liposomes; thus surface bound material probably represents only a small fraction of the material accumulated at 37°C.

In Table II a number of interesting items can be noted. First, although roughly similar amounts of lipid were taken up when the macrophages were exposed to multilamellar, unilamellar or reversed phase liposomes, this actually corresponded to vastly different numbers of particles and to greatly different uptakes of liposome-trapped volume. For example, in terms of particle number, uptake of small unilamellar liposomes exceeded uptake of reversed phase liposomes by a factor of about 10^2. However, in terms of uptake of trapped volume, reversed phase liposome uptake exceeded uptake of unilamellar liposomes by a factor of about 10^2 and uptake of multilamellar liposomes by a factor of about 10^1. It is also interesting to note that an apparent saturation of uptake occurs corresponding to the internalization of $3-4 \cdot 10^6$ M^2 of surface area per μg cell protein.

Effects of metabolic and cytoskeletal inhibitors

The effect of various metabolic and cytoskeletal inhibitors on the uptake of dipalmitoylphosphatidylcholine/cholesterol reversed phase liposomes is shown in Table III. Inhibitors of glycolysis (such as iodoacetate) or inhibitors affecting the microfilament system (cytochalasin B) markedly reduce liposome uptake; by contrast uncouplers of oxidative phosphorylation (azide) have little effect on uptake. This pattern of inhibition is typical of 'classic' phagocytosis [23]; these inhibitors would not be expected to affect liposome binding to the cell surface, or liposome-cell fusion. Thus, most of the liposomal material taken up by macrophages seems to enter by an endocytotic process similar to that used by the macrophage to take up other types of particulate material [24].

Receptor-mediated liposome uptake

Effects of IgG. Formation of an antigen-antibody complex on the liposome surface has a dramatic effect on the uptake of these particles by macrophages. As seen in Fig. 2, uptake of dipalmitoylphosphatidylcholine/cholesterol/dinitrophenylphosphatidyl ethanolamine reversed phase

TABLE II

UPTAKE OF VARIOUS TYPES OF LIPOSOMES BY MACROPHAGES

Liposomes composed of dipalmitoylphosphatidylcholine/cholesterol 1 : 1 and labelled with [^{14}C]cholsterol oleate were prepared. Macrophage monolayers in α medium plus 1 mg/ml bovine serum albumin were incubated with various doses of these types of vesicles for 90 min at 37°C. The samples were processed and the uptake calculated as ng phospholipid/μg cell protein. Further calculations were made as described below.

Assumptions: The values in the table were calculated based on the following assumptions. 1. The average diameters for the small unilamellar vesicles was 350 A^0 and for the reversed phase liposomes and multilamellar vesicles 1.0 μm [17]. 2. The bilayer surface area corresponding to 1 μmol phospholipid is 2100 cm^2 [29]. 3. The average molecular weight of the phospholipid used was 750. 4. Small unilamellar vesicles, reverse phase liposomes and multilamellar vesicles were all assumed to be spheres. 5. The trapped volume for multilamellar vesicles is 2 μl/μmol (based on trapping of water soluble markers).

The calculations were made as follows: 1. The amount of μmol lipid taken was converted to surface area taken up using (2) above. 2. The number of vesicles taken up was calculated from the surface area taken up and the surface area of an individual vesicle (πd^2). 3. The trapped volume taken up was calculated from the number of vesicles taken up and the volume of an individual vesicle ($\frac{4}{3}\pi r^3$). 4. Surface area and number of vesicles was not calculated for the case of multilamellar vesicles, since the average number of lammellae was not known. 5. For small unilamellar vesicles it was assumed that the internal and external bilayer halves occupied the same area (this is probably incorrect by a factor of 0.4–0.6). In calculating small unilamellar vesicle volumes the thickness of the bilayer was neglected.

Input dose	Uptake				
	ng/μg protein	mol	Surface area of vesicles	Number of vesicles	Trapped volume
MLV					
100 μg	7.4±0.7	$9.8\cdot10^{-6}$	–	–	$2.0\cdot10^{-14}$ M^3
500 μg	25.9±2.5	$34.5\cdot10^{-6}$	–	–	$7.1\cdot10^{-14}$ M^3
1000 μg	24.5±3.3	$32.6\cdot10^{-6}$	–	–	$6.5\cdot10^{-14}$ M^3
REV					
100 μg	7.9±0.5	$10.6\cdot10^{-6}$	$2.2\cdot10^{-6}$ M^2	$0.7\cdot10^{6}$	$3.6\cdot10^{-13}$ M^3
500 μg	13.3±1.8	$17.7\cdot10^{-6}$	$3.7\cdot10^{-6}$ M^2	$1.2\cdot10^{6}$	$6.2\cdot10^{-13}$ M^3
1000 μg	10.7±1.9	$14.2\cdot10^{-6}$	$3.0\cdot10^{-6}$ M^2	$1.0\cdot10^{6}$	$5.2\cdot10^{-13}$ M^3
SUV					
100 μg	2.2±0.1	$2.9\cdot10^{-6}$	$0.6\cdot10^{-6}$ M^2	$1.5\cdot10^{8}$	$3.4\cdot10^{-15}$ M^3
500 μg	4.2±0.7	$5.6\cdot10^{-6}$	$1.2\cdot10^{-6}$ M^2	$3.0\cdot10^{8}$	$6.8\cdot10^{-15}$ M^3
1000 μg	6.6±0.3	$8.8\cdot10^{-6}$	$1.8\cdot10^{-6}$ M^2	$4.6\cdot10^{8}$	$10.4\cdot10^{-15}$ M^3

liposomes was markedly potentiated by pre-incubation of the vesicles with an anti-dinitrophenol antibody. Maximal levels of antibody-coated vesicle uptake ranged between 500–1000 ng lipid/μg cell protein, 100-fold enhancement of over uptake in the absence of antibody. Since we have observed that a variety of serum proteins, including IgG, can readily bind to liposome surfaces, we tested if simply pre-coating the vesicles with antibody would be as efficacious in promoting uptake as formation of an antibody-antigen complex. As seen in Fig. 2, coating dipalmitoylphosphatidylcholine/cholesterol liposomes (no antigen) with the same antibody does promote vesicle uptake, but is less effective, since approx. 10-fold greater concentration of antibody is required to produce the same degree of uptake. At this point, it is not clear if formation of an antigen-antibody complex results in changes in Fc domain conformation [25] which enhance the binding of the liposomal antigen-antibody complex to the macrophage Fc receptor, or if the presence of antigen in the liposome simply causes the binding of more IgG molecules at any given serum dilution. The cellular uptake of IgG-antigen-liposome complexes was markedly inhibited (> 80%) by 5 mM iodoacetate, indicating that the process involves active phagocytosis rather than just cell surface binding.

Effects of fibronectin. Serum fibronectin (cold

TABLE III

EFFECTS OF METABOLIC AND CYTOSKELETAL INHIBITORS ON THE UPTAKE OF LIPOSOMES BY MACROPHAGES

Dipalmitoylphosphatidylcholine/cholesterol reverse phase liposomes labelled with [^{14}C]cholesterol oleate were prepared. Macrophage monolayers were prepared and preincubated for 15 min at 37°C in α medium + 1 mg/cm^3 bovine albumin plus the indicated metabolic or cytoskeletal inhibitor. Liposomes (260 μg) were added and then incubation carried out for a further 90 min after at 37°C.

Treatment	Uptake in ng lipid/μg cell protein
Control	6.65 ± 1.65
5 mM iodoacetate	0.13 ± 0.02
1 mM sodium azide	5.79 ± 1.04
Iodoacetate + azide	0.10 ± 0.02
5 μg/cm^3 cytochalasin B	0.70 ± 0.14
10 μg/cm^3 cytochalasin B	0.50 ± 0.05

insoluble globulin), is known to play roles as a factor in cell adhesion and as an opsonic factor promoting phagocytosis by macrophages [22,26]. Treatment of gelatin-coated particles with fibronectin markedly increases their uptake by macrophages; heparin serves as a cofactor in this system and enhances the fibronectin effect [27]. As seen in Table IV, fibronectin can also markedly increase the uptake of liposomes by macrophages. As in the case of gelatinized particles, the effect is enhanced by heparin. With positively charged liposomes fibronectin coating produced a 5–10-fold increase in vesicle uptake during 90 min. With neutral and negatively charged vesicles smaller effects were observed; this is probably related to the tendency of fibronectin to bind most strongly to positively charged vesicles [28]. Thus, the uptake of liposomes coated with an appropriate ligand can occur both via the Fc receptor system and via the fibronectin receptor system. We have not tested the possibility of uptake via other macrophage receptor systems such as that for the third component of complement.

Interaction of IgG- and fibronectin-mediated uptake of liposomes

We wished to determine if uptake via the Fc receptor system and via the fibronectin receptor system were coupled in some way or if they could occur independently. To test this we performed experiments somewhat analogous to those of Petty et al. [14] who studied the independence of the Fc and complement receptor systems. Thus, macrophages were preincubated with unlabelled IgG-coated vesicles and subsequently incubated with radioactively-labelled IgG-coated or fibronectin-coated vesicles and the uptake of label was determined. If the Fc and fibronectin cellular bind-

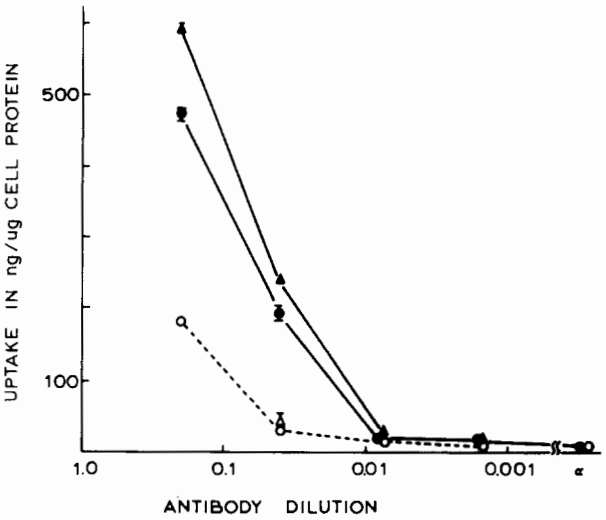

Fig. 2. Effect of IgG on liposome uptake by macrophages. Reverse phase vesicles were prepared composed of dipalmitoylphosphatidylcholine/cholesterol 1 : 1 molar ratio with or without 10 mol% dinitrophenylaminocaproylphosphatidylethanolamine and labelled with [^{14}C]cholesterol oleate. Dilutions of mouse anti-dinitrophenol antibody (IgG fraction) were prepared in phosphate-buffered saline (500 μl total). To this was added liposomes (500 μg) either with or without the lipid antigen. The mixtures were incubated at room temperature for 15 min and then the liposome-antibody complexes were pelleted at 8000 rpm, and washed twice in phosphate-buffered saline. The washed liposome-antibody complexes (150 μg lipid) were added to macrophage monolayers which had been pre-equilibrated in α-medium plus 1 mg/cm^3 bovine albumin and the samples were incubated at 37°C for 90 min. Expt. 1. ●------●, liposomes with dinitrophenylaminocaproylphosphatidylethanolamine. Expt. 1. ○------○, liposomes without dinitrophenylaminocaproylphosphatidylethanolamine. Expt. 2. ▲------▲, liposomes with dinitrophenylaminocaproylphosphatidylethanolamine. Expt. 2. △------△, liposomes without dinitrophenylaminocaproylphosphatidylethanolamine.

ing sites are coupled, then uptake of large quantities of unlabelled vesicles via the Fc-mediated system should suppress uptake of labelled fibronectin-coated vesicles as well as uptake of labelled IgG-coated vesicles; if the two systems function independently, as do the Fc- and complement-mediated uptake systems [14], then the pre-incubation with 'cold' IgG-coated vesicles should block uptake of labelled IgG-coated vesicles, but not uptake of labelled fibronectin-coated vesicles.

As seen in Fig. 3a coating a fixed amount of unlabelled dinitrophenylated liposomes with increasing concentrations of anti-dinitrophenol antibody did not suppress subsequent uptake of radioactively-labelled fibronectin-coated vesicles. In Fig. 3b, it can be seen that increasing the amount of unlabelled dinitrophenol liposomes coated with a fixed concentration of anti-dinitrophenol antibody suppressed the uptake of fibronectin-coated radioactively-labelled liposomes only at levels considerably higher than those required to suppress the uptake of radioactively-labelled IgG-coated liposomes. This evidence suggests that uptake of vesicles via the Fc-mediated receptor system is not strongly coupled to uptake via the fibronectin-mediated system and that the two types of 'receptors' are thus independent. It should also be noted

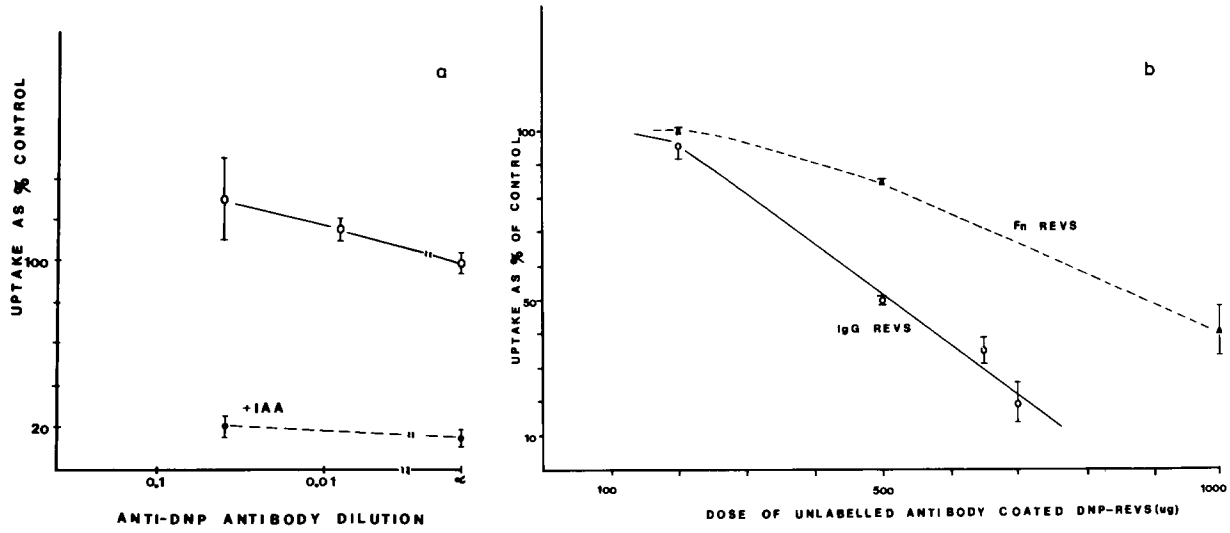

Fig. 3. a. Effects of unlabelled IgG liposomes on uptake of radioactively-labelled fibronectin liposomes. A set of reverse phase liposomes was prepared composed of dipalmitoylphosphatidylcholine/cholesterol/dinitrophenylaminocaproyl phosphatidylethanolamine 1 : 1 : 0.1 molar ratio (DNP-REVs). Another set of liposomes was prepared containing dipalmitoylphosphatidylcholine/cholesterol/stearylamine 1 : 1 : 0.1 molar ratio; this latter set was labelled with 10 μCi [^{14}C]cholesterol oleate. The DNP-REVs were pre-incubated with dilutions of mouse anti-DNP antibody as in Fig. 2. The radioactive vesicles were pre-incubated wtih 500 μg/cm^3 fibronectin as in Table IV (^{14}C-Fn-REVs). The washed IgG-DNP-REV complexes (180 μg lipid) were added to macrophage monolayers in α medium plus 1 mg/cm^3 bovine albumin. After 30 min aliquots of the ^{14}C-Fn-REV mixtures were added (210 μg lipid), as well as 100 U heparin, and the incubation was continued for 90 min at 37°C. In some cases 5 mM iodoacetate was added to the samples. Data points are the means ±S.E. of triplicate determinations. Results are expressed as % of control where the control is infinite antibody dilution (no antibody). O------O, uptake of ^{14}C-Fn-REVs (−iodoacetate): ●------●, uptake of ^{14}C-Fn-REVs (+iodoacetate). b. Effects of unlabelled IgG liposomes on the uptake of radioactively-labelled fibronectin liposomes and IgG liposomes. A set of reverse phase liposomes was prepared composed of dinitrophenyl aminocaproylphosphatidylethanolamine 1 : 1 : 0.1 molar ratio (DNP-REVs). Another set of DNP-REVs was prepared with the inclusion of 10 μCi [^{14}C]cholesterol oleate (^{14}C-DNP-REVs). A set of liposomes containing dipalmitoylphosphatidylcholine/cholesterol/stearylamine 1 : 1 : 0.1 molar ratio plus 10 μCi [^{14}C]cholesterol oleate was also prepared and preincubated with 500 μg/cm^3 fibronectin as described in Table IV (^{14}C-Fn-REVs). Both the DNP-REVs and the ^{14}C-DNP-REVs were pre-incubated with a 1/25 dilution of anti-DNP antibody and washed as described in Fig. 2. Macrophage monolayers in α medium plus 1 mg/cm^3 bovine serum albumin were incubated with various doses (0→1000 μg) IgG-coated DNP-REVs for 90 min at 37°C. Thereafter either IgG-coated ^{14}C-DNP-REVs (80 μg) or ^{14}C-Fn-REVs were added and the incubation continued for 90 min. The monolayers were washed and uptake of radioactive label determined. Results are expressed as % of control where the control monolayers received no DNP-REVs. Results are the means ±S.E. of three determinations.

TABLE IV

EFFECT OF FIBRONECTIN ON LIPOSOME UPTAKE BY MACROPHAGES

Amount of fibronectin used to coat liposomes	Liposome uptake in ng lipid/μg cell protein	
	−heparin	+heparin
0	7.5±2.5	9.0±2.0
100 μg/ml	12.0±5.0	22.0±4.0
500 μg/ml	24.2±8.0	48.0±7.0

Reverse phase liposomes were prepared composed of dipalmitoylphosphatidylcholine/cholesterol/stearylamine 1:1:0.1 molar ratio and labelled with [^{14}C]cholesterol oleate. These vesicles were preincubated for 1 h at room temperature with 2 cm^3 affinity-purified bovine plasma fibronectin at the dicated concentrations. The vesicle-fibronectin mixtures (125 μg lipid) were added to macrophage monolayers in α medium plus 1 mg/cm^3 bovine albumin and these were incubated for 90 min at 37°C. In some cases heparin (100 U) was added to the incubation mixture.

(Fig. 3a) that iodoacetate (5 mM) markedly blocked (>80%) uptake of fibronectin-coated liposomes, indicating that this process is also due to active phagocytosis.

Interestingly in the experiments where dinitrophenylated liposomes plus increasing concentrations of antibody were used to block uptake of radioactively-labelled fibronectin liposomes (Fig. 3a), the presence of antibody-coated liposomes actually seemed to enhance uptake of fibronectin-coated liposomes. In Fig. 3b where a fixed antibody concentration but increasing doses of dinitrophenylated liposomes were used, only a partial inhibitory effect on uptake of radioactively-labelled fibronectin liposomes was seen.

Visualization of liposome uptake by macrophages

As seen in Fig. 4 the uptake of lipid vesicles by mouse macrophages is easily visualized by the incorporation of a fluorescent marker in the vesicles. Uptake is not uniform but varies considerably from cell to cell. Most of the cell-associated fluorescence is seen as punctate accumulations in the perinuclear region. However some diffuse fluorescence, which may be due to the release of carboxyfluorescein from the acidic lysosomal environment, is also seen. Cells incubated at 4°C had little cell-associated fluorescence.

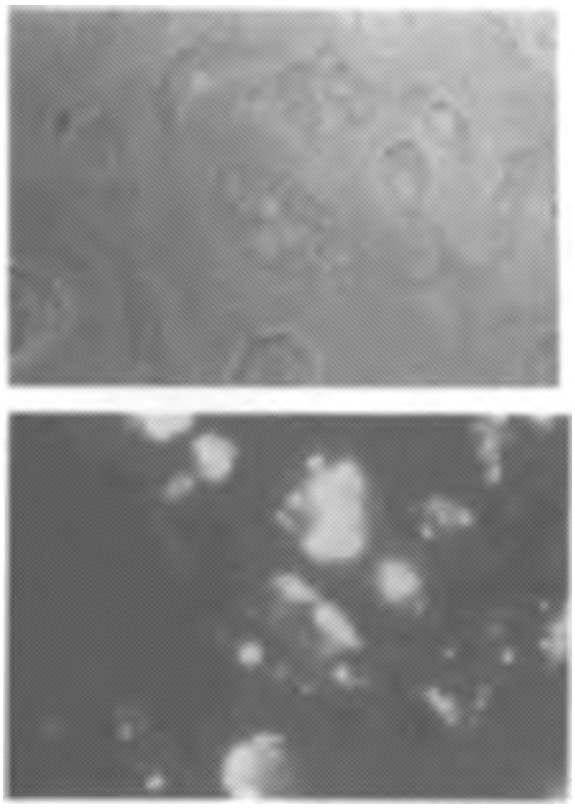

Fig. 4. Visualization of liposome uptake by macrophages. Reverse phase liposomes composed of dipalmitoylphosphatidylcholine/cholesterol/phosphatidylserine 1:1:0.1 molar ratio and containing 100 mM carboxy fluorescein were prepared. The liposomes were incubated with macrophage monolayers on glass cover slips for 90 min at 37°C, the monolayers were then washed and examined by phase and fluorescence microscopy.

Discussion

Our findings suggest that mouse peritoneal macrophages can take up large unilamellar lipid vesicles as intact particles over a period of 120 min; thereafter breakdown of internalized particles may begin to occur. The uptake process is sensitive to temperature and to various metabolic and cytoskeletal inhibitors, suggesting that it represents a 'classic' phagocytic mechanism. Macrophages seem to take up negatively charged liposomes somewhat better than either positive or neutral liposomes.

When macrophages are presented to several

types of vesicles the total amount of lipid taken up is similar in each case within a factor of 5. However when uptake is expressed in terms of the number of particles or in terms of entrapped aqueous volume, very large differences (10^2) are noted between the various vesicle types. In particular, uptake of reversed phase liposomes results in the uptake of large amounts of trapped volume per unit weight of lipid; thus reversed phase liposomes seem best suited as a means for delivery of water-soluble drugs to macrophages.

Macrophage uptake of liposomes is greatly enhanced by coating the surface of the lipid vesicle with ligands capable of interacting with macrophage cell surface receptors. Formation of an IgG-antigen complex on the liposome results in as much as a 10^2 enhancement of uptake, presumably via the macrophage Fc receptor system. Coating the liposomes with fibronectin, an opsonic protein from serum, can also result in a 10–20-fold enhancement of liposome uptake. The Fc receptor-mediated and the fibronectin-mediated uptake systems seem to function independently, as is the case for Fc-mediated uptake and C3b receptor-mediated binding [14]. Since the submission of this report a study similar to ours on the effects of antibody on liposome uptake by peritoneal macrophages has appeared [30]; some of the findings of these two reports are similar, particularly with regard to the enhancement of liposome uptake by coating the particles with ligands capable of interacting with the macrophage cell surface.

These studies serve to expand our knowledge of liposome-reticuloendothelial system interactions. They also demonstrate that liposomes can be a useful investigative tool in study of nonspecific and receptor-mediated endocytotic processes.

References

1 Juliano, R.L. and Layton, D. (1980) in Drug Delivery Systems: Characteristics and Biomedical Applications (Juliano, R.L., ed.), pp. 189–236, Oxford University Press, New York
2 Gregoriadis, G. (1978) Ann. N.Y. Acad. Sci. 308, 333–353
3 Juliano, R.L. and Stamp, D. (1978) Biochem. Pharm. 27, 21–27
4 Kimelberg, H.K. and Atchison, M.L. (1978) Ann. N.Y. Acad. Sci. 308, 395–409
5 Mayhew, E., Papahadjopoulos, D., Rustum, Y.M. and Dave, C. (1978) Ann. N.Y. Acad. Sci. 308, 371–389
6 Scherhof, G., Roerdink, F., Hoekstra, D., Zborowski, J. and Wisse, E. (1980) in Liposomes in Biological Systems (Gregoriadis, G. and Allison, A., eds.), pp. 179–209, J. Wiley and Sons, Chichester
7 Fidler, I.J. (1980) Science 208, 1469–1470
8 Pagano, R. and Weinstein, J.N. (1978) Annu. Rev. Biophys. Bioeng. 7, 435–468
9 Stendahl, O. and Tagesson, C. (1977) Exp. Cell. Res. 108, 167–174
10 Dalhgren, C., Kihlstrom, E., Magnusson, K.E., Stendahl, O. and Tagesson, C. (1977) Exp. Cell. Res. 108, 175–184
11 Weissmann, G., Bloomgarden, D., Kaplan, R., Cohen, C., Hoffstein, S., Collins, T., Gottlieb, A. and Nagle, D. (1975) Proc. Natl. Acad. Sci. U.S.A. 72, 88–92
12 Leserman, L.D., Weinstein, J.N., Blumenthal, R. and Terry, W.D. (1980) Proc. Natl. Acad. Sci. U.S.A. 77, 4089–4093
13 Finkelstein, M.C., Kuhn, S.H., Schieren, H., Weissmann, G. and Hofstein, S. (1981) Biochim. Biophys. Acta 673, 286–302
14 Petty, H.R., Hafeman, D.G. and McConnell, H.M. (1980) J. Immunol. 125, 2391–2396
15 Mattenberger-Kreber, L., Auderset, G., Schneider, M., Louis-Broillet, A., Strolin-Bendeitti, M. and Malnoe, A. (1977) Experimentia 32, 1522–1524
16 Poste, G., Kirsch, R., Folger, W.E. and Fidler, I.J. (1979) Cancer Res. 39, 881–892
17 Kao, Y.J. and Juliano, R.L. (1981) Biochim. Biophys. Acta 677, 453–461
18 Szoka, F. and Papahadjopoulos, D. (1978) Proc. Natl. Acad. Sci. U.S.A. 75, 4194–4208
19 Edelson, P.J., Zweibel, R. and Cohn, Z.A. (1975) J. Exp. Med. 142, 1150–1164
20 Tucker, S.B., Pierre, R.V. and Jordon, R.E. (1977) J. Immunol. Methods 14, 267–269
21 Lowry, O.H., Rosebrough, N.J., Farr, A.L. and Randall, R.J. (1981) J. Biol. Chem. 193, 265–275
22 Harper, P.A. and Juliano, R.L. (1980) J. Cell Biol. 87, 755–763
23 Karnovsky, A. (1975) Adv. Exp. Biol. Med. 73a, 121
24 Silverstein, S.C., Steinman, R.M. and Cohn, Z.A. (1977) Annu. Rev. Biochem. 46, 669–772
25 Caldwell, J.S. (1980) in Basic and Clinical Immunology (Fudenberg, H.H., Sites, D.P., Caldwell, J.S. and Wells, J.V., eds.), pp. 53–63, Lange, Los Altos, CA
26 Yamada, K.M. and Olden, K. (1978) Nature 275, 179–184
27 Van de Water, L., Schroeder, S., Crenshaw, E.B. and Hynes, R.O. (1980) J. Cell Biol. 87, 427–433
28 Juliano, R.L. and Lin, G. (1980) in Liposomes and Immunobiology (Tom, B. and Six, H., eds.), pp. 49–66, Elsevier, New York
29 Szoka, F. and Paphadjopoulos, D. (1980) Annu. Rev. Biophys. Bioeng. 9, 467–508
30 Geiger, B. (1981) Eur. J. Immunol. 11, 710–716

[CANCER RESEARCH 54, 2186–2191, April 15, 1994]

Liposomes and Hyperthermia in Mice: Increased Tumor Uptake and Therapeutic Efficacy of Doxorubicin in Sterically Stabilized Liposomes[1]

Shi Kun Huang,[2] Paul R. Stauffer, Keelung Hong, John W. H. Guo, Theodore L. Phillips, Anthony Huang, and Demetrios Papahadjopoulos

Cancer Research Institute [S. K. H., K. H., J. W. H. G., D. P.], Radiation Oncology [P. R. S., T. L. P.], University of California, San Francisco, 94143, and Liposome Technology, Inc., Menlo Park [A. H.], California 94025

ABSTRACT

We have shown that sterically stabilized (Stealth) liposomes (SL), can accumulate in the extracellular space within tumors, and may improve pharmacokinetics and therapeutic efficacy of encapsulated doxorubicin (SL-DOX). When SL-DOX were incubated *in vitro* at different temperatures with 50% bovine serum, approximately 20% of the encapsulated DOX was released at 42°C within 1 min, compared with less than 1% DOX released at 37°C. *In vivo*, mice were implanted s.c. with C-26 colon carcinoma in both flanks to produce matched tumors 6–10 mm in diameter. Topical hyperthermia treatment consisting of 42°C minimum tumor temperature for 30 min was applied with a microwave device to the tumor on one side only at 1 h after i.v. injection of SL-DOX or free DOX. Tumor DOX concentration in the group which was given injections of SL-DOX and sacrificed 2 h after drug injection was 1.5-fold higher compared with the nonheated tumor in mice given injections of SL-DOX. At 24 h after injection the thermal enhancement ratio for DOX accumulation in tumor remained at 1.5. In addition, there was a 15-fold higher concentration of DOX in tumor from the group given injections of SL-DOX compared to mice given injections of free doxorubicin. To assess therapeutic efficacy, we treated mice with hyperthermia for 15 min either at 1, or at 24 h or at both time points after injection of SL-DOX. We have found that the life span of the group of mice treated with SL-DOX and two 15-min hyperthermia treatments increased 51% compared with control groups receiving the same dosage of SL-DOX but without hyperthermia, and 59% compared to those receiving two hyperthermia treatments but with free DOX. A single hyperthermia treatment either at 1 or 24 h was less effective in increasing life span compared with two treatmeuts, but all groups treated with SL-DOX and single hyperthermia were still superior to the control groups, showing a 27–38% increase in life span.

INTRODUCTION

Several studies have demonstrated that it is feasible to formulate liposomes which will significantly increase circulation time in blood, diminish uptake by the reticuloendothelial system, and enhance uptake by solid tumors (1–3). Liposomes containing a polyethylene glycol-derivatized phospholipid have been reported to circulate in the bloodstream of mice and rats for up to several days following injection (4–7) and have been referred to as "Stealth" liposomes (8). As has been discussed recently (9), the long circulating property of liposomes is derived essentially from steric stabilization by the relevant hydrophilic headgroups and we prefer the term "sterically stabilized" liposomes. Our recent studies have demonstrated that sterically stabilized liposomes which are labeled with colloidal gold accumulate in the extracellular space within implanted tumors at a higher rate than in the surrounding normal tissues, probably due to the leakiness of tumor vasculature (10, 11). A number of more recent investigations have shown that SL liposomes encapsulating DOX,[3] epirubicin, or other drugs, show improved pharmacokinetics and therapeutic efficacy after i.v. injection in animals (2, 12, 13, 14, 15).

For increased therapeutic efficacy and reduced toxicity, the rate of drug released from liposomes locally in tumors should be higher than within normal sensitive tissues. Local hyperthermia has been used to augment the effectiveness of chemotherapy, generally by increasing blood flow, membrane permeability, local metabolism, and drug uptake (16–19). For more than a decade, thermosensitive liposomes have been studied in conjunction with localized hyperthermia (20–23). Experimental data as well as theoretical considerations have shown the feasibility of targeting therapy with localized hyperthermia and temperature-sensitive liposomes encapsulating antitumor drugs. However, the conventional liposome formulations can be of only limited value *in vivo* due to their short half-life in the blood stream and consequent low accumulation in tumors (20, 21). Although conceptually appealing, the temperature-sensitive liposomes can only work well in tumor chemotherapy if they are stable in blood and have long circulation times for achieving substantial accumulation in tumors. New formulations of sterically stabilized liposomes appear to have a very promising combination of both long circulation times (13), and sensitivity to the environment within tumors (24).

In this study, we describe the properties of a formulation of SL-DOX which show both a long circulation time and thermal sensitivity in a clinically acceptable range of temperatures. In order to take advantage of these properties, SL-DOX were injected i.v. into mice bearing C-26 colon carcinoma implanted s.c. and treated by local hyperthermia, 1 and 24 h after injection of liposomes. The results indicate that increased therapeutic efficacy of SL-DOX was obtained by adding local hyperthermia treatment at 42°C.

MATERIALS AND METHODS

Materials. The various chemicals were obtained as follows: HSPC (>98%) from Nattermann Phospholipid GmbH, Koln, Germany; cholesterol (USP) from Croda Inc., Fullerton, CA; DL-α-tocopherol (USP) from Hoffman La Roche, Nutley, NJ; distearoylphosphatidylethanolamine (>98%) from CalBiochem, La Jolla, CA; and Dowex resin 50 × 4–400 from Aldrich, Milwaukee, WI. Distearoylphosphatidylethanolamine derivatized at its amino position with a M_r 1900 segment of polyethylene glycol was synthesized as before (7). Bulk doxorubicin-HCl (USP) was obtained from Farmitalia (Milan, Italy), and was dissolved in 5.4% glucose.

Preparation of Drug-loaded Liposomes. The liposome preparations used in this study (Doxil) were provided by Liposome Technology Inc., and were prepared as before (2). The liposome bilayer consists of polyethylene glycol-distearoylphosphatidylethanolamine/HSPC/cholesterol/DL-α-tocopherol (molar ratios, 5.5:56.1:38.2:0.2). DOX is encapsulated in the internal aqueous phase via an ammonium sulfate gradient, at a drug:lipid ratio of approximately 125 μg DOX:mg lipid. Approximately 95% of the total drug present is in the encapsulated form. The particle size of the preparation is approximately 100 nm as determined by dynamic light scattering. Doxil is formulated at a concentration of 2 mg DOX/ml and stored at −20°C in glass vials.

Received 10/1/93; accepted 2/18/94.

The costs of publication of this article were defrayed in part by the payment of page charges. This article must therefore be hereby marked *advertisement* in accordance with 18 U.S.C. Section 1734 solely to indicate this fact.

[1] This work was supported by grants from Liposome Technology, Inc., and Yen Microlithography.

[2] To whom requests for reprints should be addressed, at Liposome Technology, Inc., 1050 Hamilton Court, Menlo Park, CA 94025.

[3] The abbreviations used are: DOX, doxorubicin; SL, sterically stabilized liposomes; SL-DOX, doxorubicin encapsulated in sterically stabilized liposomes; HSPC, hydrogenated soy phosphatidylcholine; UCSF, University of California, San Francisco.

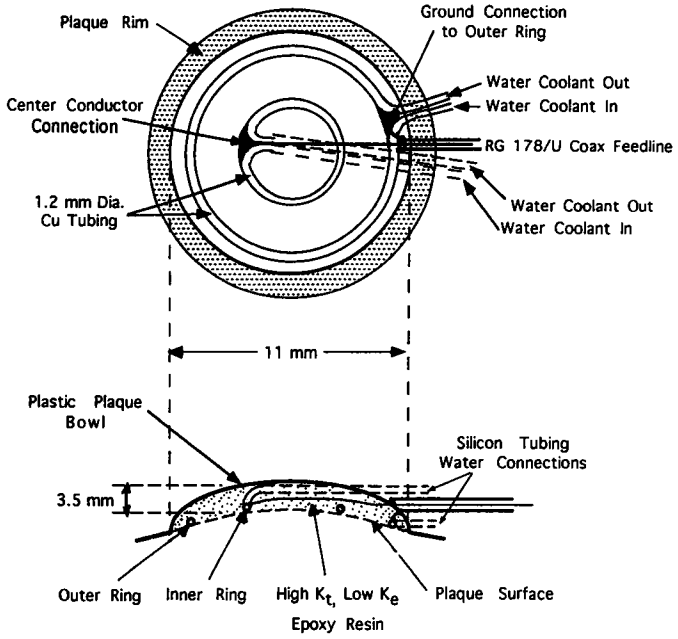

Fig. 1. Hyperthermia microwave antenna. A bowl-shaped plaque of 11-mm diameter size allowed circulation of water inside the plaque to cool the tissue surface and provided deeper heating field penetration for s.c. tumor treatment.

Release of Doxorubicin from Liposomes. The rate of the release of encapsulated DOX was monitored by following the increase in fluorescence intensity of DOX, which was initially encapsulated at self-quenched concentration inside liposomes. Fluorescence was measured in a Spex Fluorolog fluorometer. DOX was excited at 470 nm and the fluorescence at 590 nm was measured. The liposome suspension (0.2 μmol lipid/ml) was stirred continuously. The temperature was either increased at a rate of 1°C/min or kept constant by circulating water around the cuvet and was recorded with a thermocouple. Maximal fluorescence (100%) was determined by releasing the liposome contents with detergent, 0.1% ($C_{12}E_8$) octaethyleneglycol dodecyl ether (Calbiochem). The fluorescence intensity in each experiment was expressed as percentage of the maximum fluorescence (25).

Animal and Tumor Models. Female BALB/c mice in the weight range of 17–20 g (Simonsen Laboratories, Gilroy, CA.) were used. The mice were inoculated s.c. with 1×10^6 single cell suspension isolated from s.c. C-26 mouse colon carcinomas by treatment with collagenase 0.25%, pronase 0.25%, DNase 0.02% (26). Cells were injected by using a volume of 50 μl into both side flanks for the liposome uptake study, or the left flank only for the tumor growth delay study. The C-26 tumor is a relatively undifferentiated carcinoma and shows no significant antitumor sensitivity to free DOX at doses up to 10 mg/kg animal weight when grown s.c. (13, 27).

Local Tumor Hyperthermia. Heating was accomplished with a UCSF-built surface temperature-controlled microwave ring radiator (Fig. 1) embedded in an 11- or 13-mm-diameter, 4-mm-thick contoured epoxy "plaque" base (26). Prior to the therapeutic experiments, thermal dosimetry studies were performed in 8 mice to establish the variability of temperature distributions expected in 8- to 13-mm-diameter tumors extending 6–10 mm deep in the mouse flank, and to determine the optimum temperature of circulating water surface coolant. Tumor temperature distributions possible with this microwave plaque-mounted antenna were characterized by recording temperature at 1-mm increments along no. 22 gauge catheters located along the central tumor axis and at 1–3 different depths in tumor, and correlated with temperatures just underneath the tumor. A multichannel microwave system (Labthermics Microtherm 1000) was used to treat multiple mice simultaneously for the *in vivo* studies.

Hyperthermia Treatment. Prior to hyperthermia, animals were anesthetized with injection of pentobarbital. In the experimental groups receiving local tumor hyperthermia, heating was initiated either 1 h, 24 h, or 1 and 24 h after administration of DOX or SL-DOX. Mice given a single dose of hyperthermia were heated for 30 min at a steady state temperature of 42°C measured centrally just beneath the tumor apex. Mice receiving split dose hyperthermia were given two heat treatments lasting 15 min each at 42°C steady state.

Measurement of Liposomal DOX Uptake by Tumor. Mice bearing two similar size C-26 tumors growing s.c. in both side flanks (at least 5 mice per group) were given injections via the tail vein of 0.2 ml buffer containing 0.4 mg free DOX or SL-DOX. Local tumor hyperthermia was initiated 1 h after administration of drug. After 3–5 min of heating, a steady state temperature of 42°C was reached at the reference point just under the tumor apex and was maintained for 30 min. In order to avoid destruction of tumor vasculature, no temperature probes were placed directly in the tumor for the *in vivo* studies and the minimum tumor temperatures were determined from previous thermal dosimetry experiments to be the temperature of the reference point measured centrally just beneath the tumor mass. The mice were sacrificed either 2 or 24 h after injection of SL-DOX or free DOX. Immediately following sacrifice, the s.c. tumors were perfused with heparinized buffered saline by heart catheterization to eliminate blood remaining in the tissue vessels. The tumors were then removed and cleaned of any superficial non-tumor tissue. DOX was extracted from tissues as before (15) and was measured by fluorometer at 470 nm excitation and 590 nm emission wavelengths.

Tumor Growth Delay Experiments. At day 0, mice were given injections s.c. in the left flank of C-26 tumor cells and then randomized into experimental groups and numbered. Treatment was started at 11 or 12 days after tumor implant when tumors had grown an average size of 0.3 ± 0.1 cm^3. Tumor size was determined by measuring three orthogonal diameters (a, b, c) of each tumor and the volume was calculated as $(a \times b \times c) \times 0.5$ cm^3 (28). Tumor size was measured two or three times weekly starting after hyperthermia treatment. Mice were treated with either free DOX or SL-DOX at 8 mg/kg animal weight, administered by tail vein injection (i.v.). The day of death of each mouse was recorded. Experiments were terminated 45 days after injection of tumor, when all remaining mice were sacrificed. All animal studies were done in accordance with protocols approved by the institutional Animal Care Committees at UCSF and Liposome Technology, Inc.

RESULTS

Thermosensitive Properties *in Vitro*. The liposomes used in this study were composed of phospholipids (HSPC) with high-phase transition temperature (29). However, because of the relatively high cholesterol content, the phase transition temperature of these liposomes was very broad and hard to detect by differential scanning calorimetry (results not shown). The release rates of the drug at different temperatures were monitored by DOX fluorescence which was self-quenched inside the liposomes and increased after being released into the medium. Incubating in the presence of 50% bovine serum, release of DOX from liposomes started slowly at 37°C, then dramatically increased at temperatures above 40°C. At 42°C, liposomes released about 20% of the encapsulated DOX within 1 min, and about 30% within 5 min (Fig. 2). The rate of release reached a plateau within 30 min, when approximately 50% of DOX had been released. In contrast, only approximately 2% of the encapsulated DOX was released within 25 min at 37°C (Fig. 2). Additionally, there was less than 1% DOX released from liposomes when they were incubated in phosphate-buffered saline in the absence of serum at either 37°C or at 42°C.

The role of serum in enhancing the release of DOX from liposomes having different lipid compositions has been examined in detail and the results will be reported separately.[4] The maximal (100%) release of DOX shown on the right-hand side of the curves in Fig. 2 is obtained by the addition of detergent as explained in "Materials and Methods." We have confirmed by gel-filtration columns that the increase in fluorescence observed in Fig. 2 represents actual release of DOX from liposomes.

Thermal Enhancement of Liposome Uptake in Tumor Tissue. DOX uptake in hyperthermia-treated tumors was measured and compared to tumor uptake of DOX in matched size untreated tumors in the

[4] M. Gaber, K. Hong, S. K. Huang, and D. Papahadjopoulos, unpublished observations.

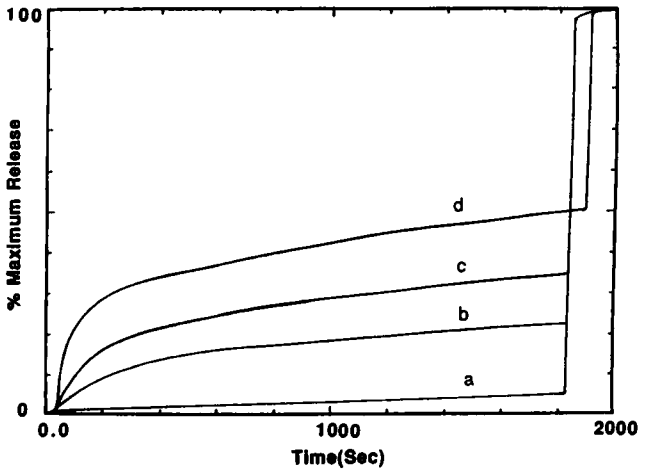

Fig. 2. The kinetics of relative fluorescence intensity due to the release and dequenching of encapsulated DOX from liposomes incubated with 50% bovine serum at different temperatures *in vitro*: *a*, 37°C; *b*, 40°C; *c*, 41°C; *d*, 42°C. Maximum fluorescence (100%) represents the total fluorescence intensity obtained by lysing the liposomes with detergent.

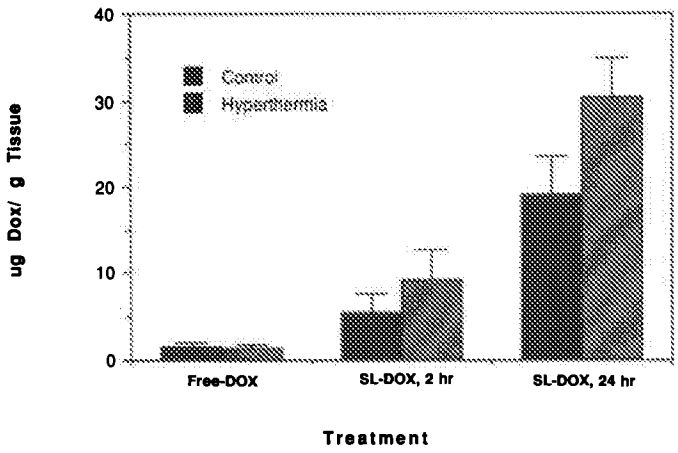

Fig. 3. Comparison of DOX uptake in tumors. Mice were inoculated with C-26 tumor cells s.c. in both flanks, one side with hyperthermia treatment, the other side without hyperthermia treatment as a control. DOX was extracted from the tumor tissue. *Free-DOX*, tumor with hyperthermia treatment at 42°C for 30 min, 1 h after 0.2 mg i.v. injection of free DOX, both heated and unheated tumors were collected at 2 h after injection of drug. *SL-DOX, 2 h* and *SL-DOX, 24 h*, with hyperthermia treatment at 42°C for 30 min, 1 h after i.v. injection 0.2 mg SL-DOX, tumors were collected at 2 h and 24 h after drug injection, respectively. Statistical analysis of the significance of differences (P values) between treatments and controls were as follows: SL-DOX, 2 h (control *versus* hyperthermia), $P < 0.05$. SL-DOX, 24 h (control *versus* hyperthermia), $P < 0.01$. Hyperthermia (Free-DOX *versus* SL-DOX, 2 h), $P < 0.001$. Hyperthermia, Free-DOX *versus* SL-DOX, 24 h, $P < 0.001$.

same mouse. Following heat treatment for 0.5 h starting at 1 h after SL-DOX injection, tumor tissues were collected either at 2 or 24 h after SL-DOX injection. DOX uptake by tumors treated with hyperthermia was 5 μg/g tissue higher than unheated tumors when evaluated 2 h after injection, and 12 μg/g tissue higher than unheated tumors when evaluated 24 h after injection (Fig. 3). Thus, DOX concentration in the tumors treated with hyperthermia was significantly higher than in the unheated tumors in which liposomes accumulated spontaneously. The enhancement of drug uptake in hyperthermia-treated tumors was slightly higher at 24 h (63%) compared with 2 h (50%) after hyperthermia treatment. Thermal enhancement ratios were 1.6 and 1.5, respectively. This indicates that the hyperthermia treatment had a long-lasting effect on the uptake of liposomes by the tumor. This may be due to enhanced extravasation of SL-DOX, rather than strictly increased drug release, as will be discussed later.

There was no significant difference of DOX uptake between hyperthermia-treated and untreated tumors following injection with free DOX. Uptake of DOX by heat-treated and untreated tumors after administration of free DOX was much lower than that obtained after administration of SL-DOX. The concentration of DOX in heat-treated tumors was 15-fold higher in the group given SL-DOX compared to the group given free DOX. The insignificant increase in free DOX extravasation is probably related to the fact that we apply heat 1 h after injection, when most of the injected free DOX has been cleared from blood.

Tumor Growth Delay and Increase in Life Span. To test the therapeutic efficacy of combined treatment with SL-DOX and hyperthermia, we used a DOX dosage of 8 mg/kg animal weight, and selected mice with tumor size of approximately 0.3 cm^3 at 11–12 days after inoculation s.c. in one flank. Administration of SL-DOX without hyperthermia and free DOX with two hyperthermia treatments were used in two groups as controls (Fig. 4). Following administration of SL-DOX alone without hyperthermia, the mean tumor size was 2.5 cm^3 within 29 days after tumor inoculation and 17–18 days after treatment (Fig. 4*A*). A similar pattern of tumor growth was observed in mice given two hyperthermia treatments, of 15 min each, at 1 and 24 h after injection with free DOX (Fig. 4*B*). The best therapeutic efficacy was obtained in the group treated twice with hyperthermia at 42°C, for 15 min each, at 1 and 24 h following 8-mg/kg SL-DOX injection (Fig. 4*C*). The mean tumor size of this group at 29 days was approximately one-third that of the group treated with SL-DOX but without hyperthermia, or the group treated twice with hyperthermia but with free DOX (Fig. 4). Administration of a single 15-min hyperthermia treatment given at 1 h (Fig. 4*D*) or 24 h (Fig. 4*E*) after SL-DOX injection also inhibited tumor growth compared to the controls given SL-DOX without hyperthermia, or two hyperthermia treatments with free DOX. Tumor growth rates in groups receiving single hyperthermia treatment were similar, and approximately twice that of groups receiving two hyperthermia treatments (Fig. 4*F*). For single hyperthermia treatments, given either at 1 or at 24 h after SL-DOX injection, the tumor size was 1.3 cm^3 and 1.5 cm^3, respectively, within 29 days after tumor cells were implanted in animals (Fig. 4*F*).

The results on survival of mice presented in Fig. 5 show clearly that SL-DOX followed by two hyperthermia treatments caused a marked improvement in therapeutic efficacy compared to control groups treated either with SL-DOX without hyperthermia, or with free DOX and two hyperthermia treatments. A substantial (51 and 59%) increase in life span was obtained by the treatment with SL-DOX and two hyperthermia doses, compared to the treatment with the same dosage of SL-DOX but without hyperthermia, and the treatment with two hyperthermia doses and free DOX, respectively (Table 1). Moreover, the split hyperthermia combination with SL-DOX produced 3 of 8 long-term survivors, whereas there were no long-term survivors in either control group. For the groups with SL-DOX, intermediate results were obtained with a single hyperthermia treatment. The mean survival times were 27.9 and 30.3 days for groups treated with SL-DOX and single hyperthermia at 1 and 24 h, respectively, as compared to 22 and 23.8 days for the two controls (Table 1). There was also one animal still surviving in each single hyperthermia treatment group (Table 1).

DISCUSSION

The introduction of sterically stabilized liposomes has expanded the potential for targeting to tumors (1, 2, 30). Recent studies have shown that polyethylene glycol provides a hydrophilic surface coating on the liposomes, resulting in a pronounced increase in blood residence time with a parallel decrease in uptake by liver and spleen (7–13). In

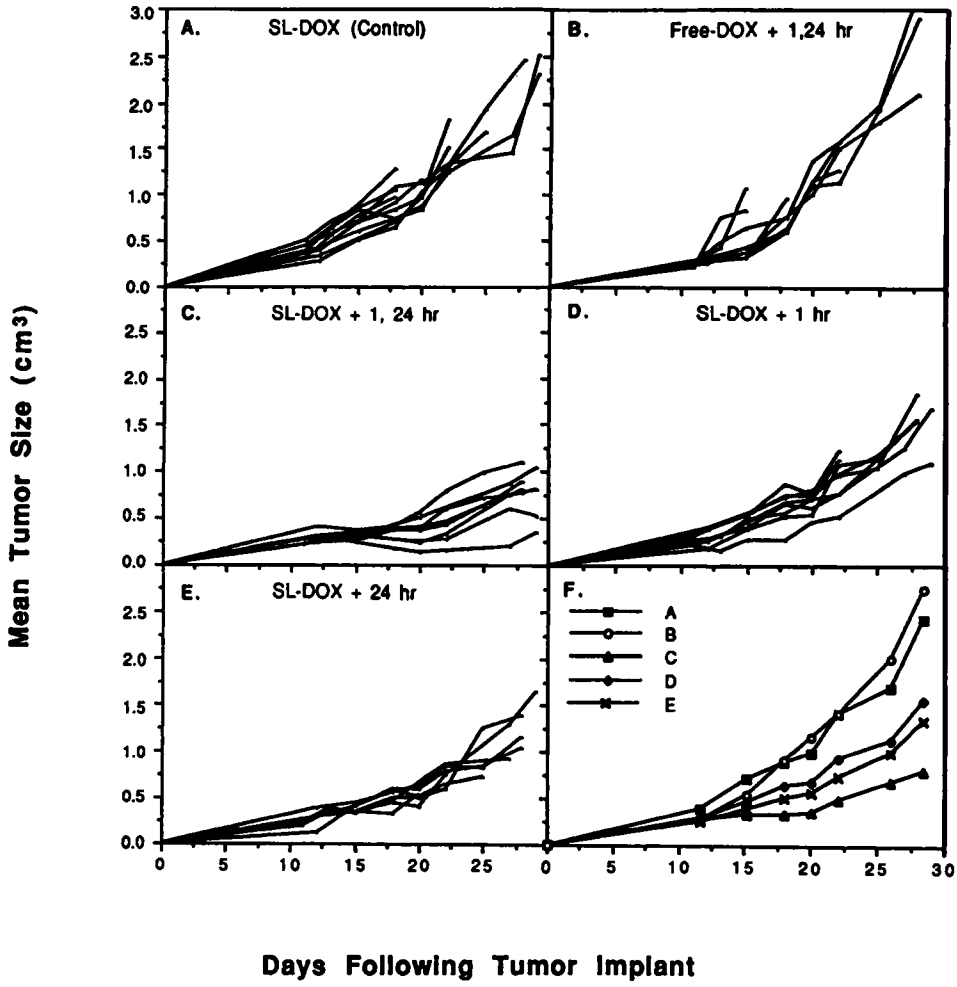

Fig. 4. Comparison of tumor growth following injection of free DOX or SL-DOX and various cotreatments. Hyperthermia was performed on day 12 after the mice were inoculated with C-26 tumor cells. *A (Control):* 8 mg/kg SL-DOX without hyperthermia treatment. *B* (DOX control): 8 mg/kg free DOX with two treatments of hyperthermia at 42°C for 15 min each, 1 h and 24 h after drug injection. *C (SL-DOX + 1, 24 h):* 8 mg/kg SL-DOX with two treatments of hyperthermia at 42°C for 15 min each, 1 h and 24 h after drug injection. *D (SL-DOX + 1 h):* 8 mg/kg SL-DOX with hyperthermia at 42°C for 15 min, 1 h after drug injection. *E (SL-DOX + 24 h):* 8 mg/kg SL-DOX with hyperthermia at 42°C for 15 min, 24 h after drug injection. *F:* Summary of *A* to *E* by using mean average values. Statistical analysis of the significance of differences between treatments and controls, (*P* values) were as follows: *B versus C*, Free DOX *versus* SL-DOX 1, 24 h, $P < 0.005$. *A versus C*, SL-DOX control vs SL-DOX 1, 24 h, $P < 0.05$. *C versus D*, SL-DOX 1, 24 h *versus* 24 h, $P < 0.05$. *B versus E*, Free DOX *versus* SL-DOX 24 h, $P < 0.05$. *A versus D* or *E*, SL-DOX control *versus* 1 or 24 h; *P*, not significant.

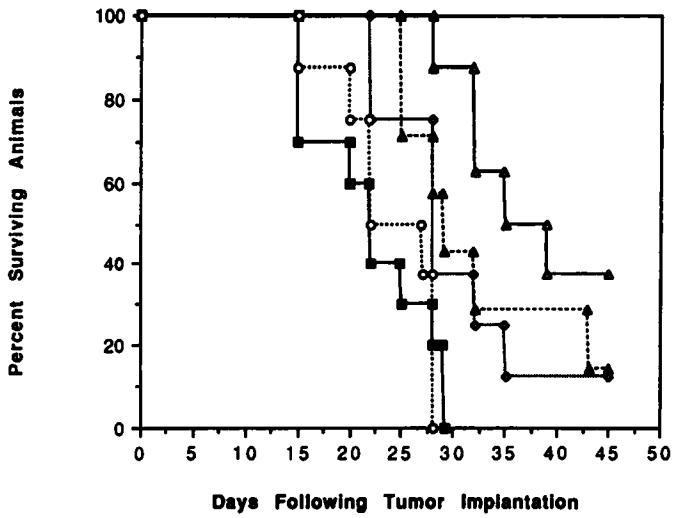

Fig. 5. Effects of free-DOX and SL-DOX injection and cotreatment with hyperthermia on survival of mice inoculated with C-26 tumor cells. Treatment started 12 days after tumor inoculation. ■ (Control), 8-mg/kg SL-DOX injection, without hyperthermia treatment. △ (SL-DOX + 1, 24 h), with two treatments of hyperthermia at 42°C for 15 min each, 1 h and 24 h after 8-mg/kg SL-DOX injection. ◇ (SL-DOX + 1 h), with hyperthermia at 42°C for 15 min, 1 h after 8-mg/kg SL-DOX injection. ▲ (SL-DOX + 24 h), with hyperthermia at 42°C for 15 min, 24 h after 8-mg/kg SL-DOX injection. ○ (free DOX control), with two treatments of hyperthermia at 42°C for 15 min each, 1 h and 24 h after 8-mg/kg free DOX injection. Statistical analysis (*P* values) of differences between treatments and controls, as follows: SL-DOX, control *versus* 1, 24 h, $P < 0.001$. SL-DOX, control *versus* 1 h, $P < 0.05$. SL-DOX, control *versus* 24 h, $P < 0.05$. SL-DOX, 1, 24 h *versus* 1 h, $P < 0.05$. SL-DOX, 1, 24 h *versus* 24 h, *P*, not significant. Free DOX control *versus* SL-DOX 1, 24 h, $P < 0.001$. Free DOX control *versus* SL-DOX 24 h, $P < 0.01$. Free DOX control *versus* SL-DOX, 1 h, $P < 0.05$.

addition, the solid-phase phospholipids and cholesterol (over 50% of total lipids) minimize drug release at body temperature, but allow enhanced release at higher temperatures. These two important properties provided the possibility to combine SL-DOX treatment with hyperthermia. As would be expected from earlier studies (2, 12–14), normal tissues would be relatively protected from drug toxicity following i.v. injection of this drug carrier, while local release of the drug from liposomes would be achieved by applying local hyperthermia at 42°C in the tumors growing s.c. in the mouse flank. Tissue temperatures of 42°C for 1 h or more is a widely accepted hyperthermia dose without tissue toxicity (31, 32). We found that with adjuvant 42°C hyperthermia, the SL-DOX released 50% of DOX within 30 min *in vitro*. The mechanism of the temperature-induced release of encapsulated drug is dependent on many factors, including the interaction between liposomes and serum proteins, as well as the compositional ratio of phospholipid to cholesterol, and the stability of the sulfate-DOX complex inside liposomes (33). Discussion of the relative contributions of these effects on drug release will be presented in a subsequent communication.

The results of the present studies on uptake of SL-DOX by tumor tissue indicate that hyperthermia had a marked effect in promoting extravasation of intact liposomes. The direct comparison of drug uptake by hyperthermia-treated *versus* unheated tumors in the same mouse was possible by heating only one of a matched pair of similar size tumors. The results show that uptake of DOX was always higher in the heat-treated tumors compared to the untreated tumors. Our early studies on pharmacokinetics (2, 13) as well as localization (10, 11) in this type of tumor have shown that long-circulating liposomes can

Table 1 *Therapeutic effects of SL-DOX with and without hyperthermia*

The results shown here were obtained as described in legend to Fig. 5.

Treatment	Dose (mg/kg)	Mean survival time (days ± SD)	Increase in life span (%)[a]	Long-term survivors/ total mice	Significance (P) vs control
Control (SL-DOX)	1 × 8	22.0 ± 5.4	0	0/10	
SL-DOX + 1, 24 h	1 × 8	33.2 ± 3.7	+50.9	3/8	<0.001
SL-DOX + 1 h	1 × 8	27.9 ± 4.4	+26.8	1/8	<0.05
SL-DOX + 24 h	1 × 8	30.3 ± 6.1	+37.7	1/7	<0.05
Free-DOX + 1, 24 h	1 × 8	23.8 ± 4.5	−8.0	0/8	NS[b]

[a] % of increase in life span = mean survival time of treated ÷ mean survival time of controls × 100 − 100.
[b] NS, not significant ($P > 0.05$).

accumulate in tumor sites spontaneously without hyperthermia treatment. The maximal liposome accumulation (20% of injected dose per g of tumor tissue) was around 24 h after liposome injection, while at that time the plasma concentration had been reduced to 20% of injected dose per ml (1, 2). Our present results show that uptake of DOX by untreated tumor was 6 μg/g tissue at 2 h and up to 19 μg/g at 24 h after SL-DOX injection (Fig. 3). At 1 h after liposome injection most liposomes are still present in the blood circulation (1, 2, 13). Therefore, any enhancement of vascular permeability due to hyperthermia (34) at this early period after liposome injection may allow a nearly maximal concentration of liposomes to extravasate from blood circulation into the tumor region. The amount of DOX taken up by tumors following a single 30-min heat treatment given at 1 h after liposome injection was 9 μg/g tissue at 2 h and 31 μg/g tissue at 24 h after liposome injection (Fig. 3). The enhanced uptake seen 24 h later indicates that the liposomes continue to accumulate at a higher rate in heat-treated tumors during the period after hyperthermia. Our interpretation is that hyperthermia may open gaps in the endothelial wall of tumor blood vessels and that these gaps remain open for some time after hyperthermia treatment. Our results also showed that hyperthermia promoted extravasation of DOX only when encapsulated in liposomes, not in its free drug form. Since SL-DOX at 37°C has a half-life in blood circulation of around 12 h in mice (1, 2, 13) and 42 h in patients (35), the majority of liposomes remain in the blood circulation during the period of heat treatment. In contrast, the half-life of free DOX is very short, approximately 12 min in mice (13–15). Thus, hyperthermia has only a very limited effect on extravasation of free DOX (Fig. 4), since only a small amount of free DOX is left in the blood for much of the 30-min heat treatment. Our previous studies have shown that extravasation of liposomes through discontinuous capillaries and the open terminals of blood vessels during angiogenesis in tumors are the main mechanisms for the spontaneous accumulation of liposomes (10). Adjuvant local hyperthermia may open more of the endothelial gaps and/or increase local blood flow, thus allowing more liposomes to extravasate from the blood circulation into the tumor region (23). This appears to be in agreement with studies showing enhanced delivery of antibody fragments into s.c. tumors in mice following hyperthermia (34).

In the therapeutic efficacy study presented here, administration of SL-DOX without hyperthermia was used as a control to obtain a maximal difference of therapeutic efficacy between control and experimental groups. We selected to administer SL-DOX in a single dose of 8 mg/kg animal weight 11 to 12 days after tumor cell inoculation for the following reasons. First, without hyperthermia, the dose of 8 mg/kg is not the optimal cure dosage. The MTD of DOX for mice is 10–15 mg/kg (36, 37). Moreover, multiple doses have superior therapeutic efficacy compared to a single dose (2). Second, administration of SL-DOX at 11 to 12 days after tumor inoculation is not the best timing for optimal cure rate (2). The maximal antitumor activity of a single dose was obtained when there was a delay of 6–9 days between the injection of the tumor cells and liposomes with much diminished activity after 14 days (2). Six days is probably necessary time to develop new vasculature in the tumor mass. Our conclusion is that under these conditions liposomes can extravasate through discontinuous capillaries, and the drug can be released from liposomes that localize within the tumor. After more than 9 days following tumor implantation, the tumor is generally too big to be cured, and tumor growth cannot be controlled despite the liposome treatment. Thus our choice of timing gives tumors that are too big to be treated with drug alone or drug in liposomes, and therefore provide the opportunity to quantitatively determine the effect of heat treatment.

In addition to the enhanced extravasation of intact liposomes discussed above, the present study indicates that another important factor for the increase in therapeutic efficacy achieved by applying local hyperthermia is the increased rate of release of the drug from liposomes accumulated in the tumor. Delay in tumor growth and increase in life span were obtained with single heat treatment, given at either 1 or 24 h after injection of SL-DOX. For a single heat treatment given at 1 h after injection, we can see a time-dependent tumor uptake of DOX: 9 μg/g at 2 h and 31 μg/g at 24 h (Fig. 3). It is probable that most accumulated liposomes were at least initially intact, because systemic drug release in blood during the process of local tumor heating was very low due to the passage of only a small blood volume through the tumor compared with the whole body. If DOX was released from liposomes into the blood as a free molecule, it would be taken up by liver and spleen rather than be accumulated in tumors, in accord with its short half life (13, 14). We expect that the increased therapeutic efficacy is achieved from a combination of increased extravasation of intact liposomes into tumor, followed by an increased rate of release of drug from the liposomes after accumulation in tumor, induced by local heat. For the single heat treatment given 24 h after SL-DOX injection, the therapeutic efficacy achieved was probably not due to increased extravasation, but was primarily due to the heat effects directly on the 19-μg/g liposome-encapsulated DOX already accumulated in the tumor. We conclude this from the uptake of DOX by the control tumor at 24 h after SL-DOX injection, which also showed high DOX accumulation (Fig. 3). Thus, the heat-activated release of DOX from already extravasated liposomes produced a transient increase in the local drug concentration, which enhanced the anti-tumor activity of the same liposome accumulation. A comparison of 1 h with 24 h single hyperthermia treatment after injection of SL-DOX, indicates that the mechanism of these two is probably different: Heat treatment at 1 h enhanced primarily the extravasation of intact liposomes not only during the heat treatment, but also for some time afterward, while heat treatment at 24 h enhanced primarily the simultaneous drug release from liposomes already accumulated in the tumor. Therefore, both of the treatments produced an enhanced therapeutic efficacy compared to the controls.

Maximum therapeutic efficacy was observed with split dose hyperthermia treatments given 1 and 24 h after SL-DOX injection. The results indicate that the two treatments have at least an additive and possibly a synergistic effect due to both increased extravasation of liposomes into the tumor and enhanced release of drug from the

liposomes already accumulated in the tumor region. This study, therefore, demonstrates that local heat adjuvant to thermosensitive SL liposomes can increase their accumulation in tumors and maximize drug-targeting index by promoting local release of drug in tumors. This should provide enhanced potential for antitumor therapy in solid tumors amenable to local hyperthermia by maximizing drug concentration in tumors, reducing normal tissue toxicity, and possibly overcoming drug resistance.

ACKNOWLEDGMENTS

We thank Drs. Frank Martin and Bob Abra (Liposome Technology, Inc.) for helpful discussions and Dave Bozzo (UCSF) for technical assistance.

REFERENCES

1. Gabizon, A., and Papahadjopoulos, D. Liposome formulations with prolonged circulation time in blood and enhanced uptake by tumors. Proc. Natl. Acad. Sci. USA, *85:* 6949–6953, 1988.
2. Huang, S. K., Mayhew, E., Gilani, S., Lasic, D. D., Martin, F. J., and Papahadjopoulos, D. Pharmacokinetics and therapeutics of sterically stabilized liposomes in mice bearing C-26 colon carcinoma. Cancer Res., *52:* 6774–6781, 1992.
3. Allen, T. M., and Conn, A. Large unilamellar liposomes with low uptake into the reticuloendothelial system. FEBS Lett., *223:* 42–46, 1987.
4. Klibanov, A. L., Maruyama, K., and Torchilin, V. P. Amphipathic polyethyleneglycols effectively prolong the circulation time of liposomes. FEBS Lett., *26:* 8235–8237, 1990.
5. Blume, G., and Cevc, G. Liposomes for sustained drug release *in vivo*. Biochim. Biphys. Acta, *10:* 2991–2997, 1990.
6. Woodle, M. C., Neuman, N., Cellius, L. R., Redemann, C., and Martin, F. J. Improved long circulating "Stealth" liposomes using synthetic lipids. Proceedings of the 17th International Symposium Controlled Release Bioactive Material, pp. 77–78. Lincolnshire, Ill: Control Release Society, 1990.
7. Allen, T. M., Hansen, C., Martin, F. J., Redemann, C., and Yau-Young, A. Liposomes containing synthetic lipid derivatives of polyethylene glycol show prolonged circulation half-lives *in vivo*. Biochim. Biophys. Acta, *1066:* 29–36, 1991.
8. Allen, T. M. Stealth liposomes avoiding reticuloendothelial uptake. *In:* G. Lopez-Berestein, I. J. Fidler (eds.), Liposomes in the Therapy of Infectious Diseases and Cancer, pp. 405–415. New York: Alan R. Liss, Inc., 1989.
9. Lasic, D. D., Martin, F. J., Gabizon, A., Huang, S. K., and Papahadjopoulos, D. Sterically stabilized liposomes: a hypothesis on the molecular origin of the extended circulation times. Biochim. Biophys. Acta, *1070:* 187–192, 1991.
10. Huang, S. K., Lee, K-D., Hong, K., Friend, D. S., and Papahadjopoulos, D. Microscopic localization of sterically stabilized liposomes in colon carcinoma-bearing mice. Cancer Res., *52:* 5135–5143, 1992.
11. Huang, S. K., Martin, F. J., Jay, G., Vogel, J., Papahadjopoulos, D., and Friend, D. S. Extravasation and transcytosis of liposomes in Kaposi's sarcoma-like dermal lesions of transgenic mice bearing the HIV tat gene. Am. J. Pathol., *143:* 10–14, 1993.
12. Mayhew, E., Lasic, D. D., Barbar, S., and Martin, F. J. Pharmacokinetics and antitumor activity of epirubicin encapsulated in long-circulating liposomes incorporating a polyethylene glycol-derivatized phospholipid. Int. J. Cancer, *51:* 302–309, 1992.
13. Papahadjopoulos, D., Allen, T. M., Gabizon, A., Mayhew, E., Matthay, K., Huang, S. K., Lee, K-D., Woodle, M. C., Lasic, D. D., Redemann, C., and Martin, F. J. Sterically stabilized liposomes; improvements in pharmacokinetics and anti-tumor therapeutic efficacy. Proc. Natl. Acad. Sci. USA, *88:* 11460–11464, 1991.
14. Gabizon, A. A. Selective tumor localization and improved therapeutic index of anthracyclines encapsulated in long-circulating liposomes. Cancer Res., *52:* 891–896, 1992.
15. Gabizon, A. A., Shiota, R., and Papahadjopoulos, D. Pharmacokinetics and tissue distribution of doxorubicin encapsulated in stable liposomes with long circulation times. J. Natl. Cancer Inst., *81:* 1489–1490, 1989.
16. Dahl, O., and Mella, O. Hyperthermia and chemotherapeutic agents. *In:* S. B. Field and J. W. Hand (eds.), An Introduction to the Practical Aspect of Clinical Hyperthermia. New York: Taylor & Francis, 1990.
17. Hahn, G. M. Potential for therapy of drugs and hyperthermia. Cancer Res., *39:* 2264–2268, 1979.
18. Arcangeli, G., Cicidalli, A., Mauro, F., Nervi, C., and Pavin, G. Enhanced effectiveness of Adriamycin and Bleomycin combined with local hyperthermia in neck node metastases from head and neck cancers. Tumori, *65:* 441–486, 1979.
19. Wallah, D. F. H. Basic mechanisms in tumor thermotherapy. J. Mol. Med., *17:* 381–403, 1977.
20. Weinstein, J. N., Magin, R. L., Yatvin, M. B., and Zaharko, D. S. Liposomes and local hyperthermia: selective delivery of methotrexate to heated tumors. Science (Washington DC), *204:* 188–191, 1979.
21. Khoobehi, B., Peyman, G. A., McTurnan, W. G., Niesman, M. R., and Magin, R. L. Externally triggered release of dye and drugs from liposomes into the eye. An *in vitro* and *in vivo* study. Opthalmology, *95:* 950–955, 1988.
22. Zou, Y. Y., Ueno, M., Yamagishi, M., Horikoshi, I., Yamashita, I., Tazawa, K., and Gu, X. Q. Targeting behavior of hepatic artery injected temperature sensitive liposomal Adriamycin on tumor-bearing rats. Sel. Cancer Ther., *6:* 119–127, 1990.
23. Zou, Y., Yamagishi, M., Horikoshi, I., Ueno, M., Gu, X., and Perez-Soler, R. Enhanced therapeutic effect against liver W256 carcinosarcoma with temperature-sensitive liposomal Adriamycin administered into the hepatic artery. Cancer Res., *53:* 3046–3051, 1993.
24. Liu, D., and Huang, L. pH-sensitive, plasma-stable liposomes with relatively prolonged residence in circulation. Biochim. Biophys. Acta, *1022:* 348–354, 1990.
25. Meers, P., Bentz, J., Alford, D., Nir, S., Papahadjopoulos, D., and Hong, K. Synexin enhances the aggregation rate but not the fusion rate of liposomes. Biochemistry, *27:* 4430–4439, 1988.
26. Swift, P. S., Stauffer, P. R., Fries, P. D., Michaels, S. K., Murray, T., Sneed, P. K., Phillips, T. L., and Char, D. H. Microwave hyperthermia for choroidal melanoma in rabbits. Invest. Ophthalmol. Visual Sci., *31:* 1754–1760, 1990.
27. Corbett, T. H., Griswold, D. P., Roberts, B. J., Peckham, J., and Schabel, F. M. A mouse colon-tumor model for experimental therapy. Cancer Chemother. Rep., *5:* 169–186, 1975.
28. Begg, A. C. Principles and practices of the tumor growth delay assay. *In:* R. F. Kallman (ed.), Rodent Tumor Models in Experimental Cancer Therapy, pp. 114–121. New York: Pergamon Press, 1987.
29. Lang, J., Vigo-Pelfrey, C., and Martin, F. J. Liposomes composed of partially hydrogenated egg phosphatidylcholines: fatty acid composition, thermal phase behavior and oxidative stability. Chem. Phys. Lipids, *53:* 91–101, 1990.
30. Papahadjopoulos, D. Optimal liposomal drug action: from serendipity to targeting. *In:* G. Gregoriadis (ed.), Liposome Technology, Ed. 2, Vol. 3, pp. 1–14, Boca Raton, FL: CRC Press, 1992.
31. Oleson, J. R., Samulski, T. V., Leopold, K. A., Clegg, S. T., Dewhirst, M. W., Dodge, R. K., and George, S. L. Sensitivity of hyperthermia trial outcomes to temperature and time: implications for thermal goals of treatment. Int. J. Radiat. Oncol. Biol. Phys., *25:* 289–297, 1993.
32. Sapareto, S. A., and Dewey, W. C. Thermal dose determination in cancer therapy. Int. J. Radiat. Oncol. Biol. Phys., *10:* 787–800, 1984.
33. Lasic, D. D., Frederik, P. M., Stuart, M. C. A., Barenholz, Y., and MacIntosh, T. J. Gelation of liposome interior: a novel method of drug encapsulation. FEBS Lett., *312:* 255–258, 1992.
34. Cope, D. A., Dewhirst, M. W., Friedman, H. S., Bigner, D. D., and Zalutsky, M. R. Enhanced delivery of a monoclonal antibody fragment to subcutaneous human glioma xenografts using local hyperthermia. Cancer Res., *50:* 803–1809, 1990.
35. Gabizon, A. A., Catane, R., Uziely, B., Kaufman, G., Safra, T., Barenholz, Y., and Huang, A. A pilot study of doxorubicin encapsulated in long-circulating (Stealth) liposomes (S-DOX) in cancer patients. Proc. Am. Soc. Clin. Oncol., *11:* 124 (Abstract), 1992.
36. Wasserman, T. H., Comis, R. L., Goldsmith, M., Handelsman, H., Penta, J. S., Slavik, M., Soper, W. T., and Carter, S. K. Tabular analysis of the clinical chemotherapy of solid tumors. Cancer Chemother. Rep., *6:* 399–419, 1975.
37. Mayhew, E., Goldrosen, M., Vaage, J., and Rustum, Y. Effects of liposome-entrapped Doxorubicin on liver metastases of mouse colon tumors C-38 and C-26. J. Natl. Cancer Inst., *78:* 707–713, 1987.

Liposomes and Hyperthermia in Mice: Increased Tumor Uptake and Therapeutic Efficacy of Doxorubicin in Sterically Stabilized Liposomes

Shi Kun Huang, Paul R. Stauffer, Keelung Hong, et al.

Cancer Res 1994;54:2186-2191.

Biochimica et Biophysica Acta, 1069 (1991) 117–121

ADONIS 000527369100372C

BBAMEM 70689

BBA Report

Light microscopic localization of silver-enhanced liposome-entrapped colloidal gold in mouse tissues

S.K. Huang [1], K. Hong [1], K.-D. Lee [1], D. Papahadjopoulos [1] and D.S. Friend [2]

[1] *Cancer Research Institute, University of California, San Francisco, CA (U.S.A.) and* [2] *Department of Pathology, University of California, San Francisco, CA (U.S.A.)*

(Received 14 February 1991)
(Revised manuscript received 23 July 1991)

Key words: Colloidal gold; Liposome; Silver enhancement; Light microscopy; (Mouse)

Silver-enhanced liposome-entrapped colloidal gold was developed for light microscopic localization of liposomes. Preparation of colloidal gold entrapped in liposomes was achieved by a modified method of Hong, et al. (1983) Biochim. Biophys. Acta 732, 320–323). In this report, a gold chloride / citrate solution of low pH (3.4) was used to inhibit the formation of gold granules during the liposome preparation. The diameter of most liposomes ranged from 80 to 100 nm. Following liposome preparation, the pH was adjusted to 6, and the temperature increased to 55°C. The majority of the liposomes contained one to three gold particles. Liposomes were injected into mice via tail vein; 24 h later, tissues were collected. Sections were processed for silver enhancement of the gold particles and examined by light microscopy. Silver-enhanced gold particles were clearly observed in both liver and implanted tumor. Localization was confirmed by electron and fluorescence microscopy. Thus, we have shown that silver enhancement of colloidal gold liposomes is a direct and sensitive method for tracing the fate of liposomes in vivo, providing minimal background interference and a good definition of various cell types.

As a modality for drug delivery, liposomes have been shown to increase drug retention, reduce toxicity, and enhance therapeutic efficacy compared with unencapsulated compounds [1,2]. To better understand the mechanism of liposome uptake by various tissues, and to improve therapeutic efficacy, it would be advantageous to know the pathway and the final localization of liposomes in tissues. A variety of markers such as proteins (ferritin) [3], enzymes (horseradish peroxidase) [4], and fluorescent molecules (pyranine and carboxyfluorescein) [5,6] have been encapsulated in liposomes and used to monitor their interaction with cultured cells in vitro; however, it is difficult to use these methods in vivo because of interference of the natural occurrence of these markers or problems of resolution of tissue morphology. At the ultrastructural level, chemicals (5-Br,4-Cl,3-indolylphosphate) [7], paired enzymes (glucose oxidase, horseradish peroxidase) [8], and colloidal gold [9] have been used in vivo as liposome-encapsulated cytochemical or histological markers. Of these methods, colloidal gold entrapped in liposomes can provide an unambiguous image with high electron density, and uniform size and shape. The endocytosis of liposomes by Kupffer cells in the reticuloendothelial system (RES) rich tissue of the liver has been demonstrated by this method [10]. It is still difficult, however, to detect the small gold particles in thin sections of non-RES tissues such as tumor, where liposome distribution is relatively low [11]. Recent pharmacokinetic studies revealed that small liposomes (< 100 nm in diameter) can achieve prolonged circulation time in blood, thus increasing accumulation in tumor of radioactive ^{67}Ga as a liposome marker [11,12].

It has also been established that silver enhancement of immunogold-labeled tissue makes it possible to detect certain molecules by light microscopy [13], probably because the tissue sections used for light microscopy are about 30 times thicker and 30 times larger than those used for electron microscopy. In this report,

Abbreviations: RES, reticuloendothelial system; PC, egg phosphatidylcholine; C, cholesterol; G_{M1}, monosialoganglioside G_{M1}; Hepes, *N*-2-hydroxyethylpiperazine-*N'*-2-ethanesulfonic acid; RITC-Dex, Rhodamine B isothiocyanate-dextran.

Correspondence: S.K. Huang, Cancer Research Institute, Box-0128, University of California, San Francisco, CA 94143, U.S.A.

we present a new application of silver enhancement on colloidal gold entrapped in small liposomes, that enables us to localize liposomes in tissues by light microscopy.

For best results, gold chloride/citrate solution was made immediately before the preparation of liposomes. Fresh citric acid (120 mM)/K_2CO_3 (30 mM) solution was mixed with $HAuCl_4$ (12.72 mM) in a ratio of 1 : 1, and the final pH of the solution was adjusted to 3.4. Low pH aqueous phase is necessary to prevent gold granules from forming and precipitating during liposome preparation.

Liposomes with a desired lipid composition of $PC/C/G_{M1}$ (mol ratio 2 : 1 : 0.2), were prepared by the method of reverse-phase evaporation with gold chloride/citrate in aqueous phase [9,14]. A thin lipid film (10 μmol phospholipid) was dissolved in 1 ml of diethyl ether, and mixed with 0.5 ml gold chloride/citrate solution. The mixture was emulsified by sonication for 3 min, and diethyl ether was removed at room temperature. The liposomes formed by the above method [14] underwent three cycles of freezing (−56°C) and thawing (55°C), and then were extruded through Nuclepore membranes (Pleasanton, CA), twice with pore-size 0.1 μm and five times with pore-size 0.05 μm [15,16]. Immediately after final extrusion, the pH of the liposome suspension was raised to 6 by adding NaOH. Formation of gold particles was initiated by incubating the suspension at 55°C for 30 min. The color of liposome suspension turned pink-purple, which indicated an appropriate size of gold particles. Unencapsulated free gold and excess citrate were removed by passing the liposome suspension through a column (1 × 15 cm) of Sephacryl S-500 (Pharmacia, Piscataway, NJ). Liposome size and clearance of free colloidal gold were examined by electron microscopy of negatively stained (2% ammonium molybdate) preparations.

Colloidal gold-containing liposomes (0.25 ml, 2 μmol phospholipid) were injected into mice (female BALB/c) via the tail vein. The mice were sacrificed 24 h after liposome injection. Tissues were collected following perfusion with heparinized PBS and fixative (1.5% glutaraldehyde, 0.1 M sodium cacodylate, 1% sucrose, pH 7.4). All procedures involving tissue handling were performed at 4°C. Dehydration, infiltration and embedding procedures were done under vacuum (15–20 mmHg). The specimens were fixed for 2–4 h with occasional agitation. After fixation, the specimens were rinsed with PBS and then allowed to set in PBS for from 1 h to overnight. The specimens were dehydrated with 50%, 95% acetone/water and 100% acetone at 30 min sequences. For infiltration, the specimens were incubated in 50% acetone/50% glycol methacrylate monomer for 30 min and then transferred to 100% glycol methacrylate monomer for 4–8 h. The specimens were embedded in a mixture of glycol methacrylate monomer (20 ml), benzol peroxide (0.09 gm), and glycol polyethylene glycol 400 with 0.5 ml *N,N*-dimethylaniline (JB-4, Polysciences, Inc., Warrington, PA) for 12 h [17]. Sections were cut from embedded specimens with a Sorvall JB-4 microtome at a thickness of 2.5 μm.

Reagents A (enhancer) and B (initiator) for silver enhancement were purchased from Amersham (Arlington Heights, IL). Reagent A and B were mixed immediately before using. The sample area on the slide was covered with silver-enhancement mixture for 15 min at 22°C. To avoid the self-nucleation of the silver-enhancement solution, the duration of treatment was controlled 5 min below the safety margin of an acceptable background. The slide was washed thoroughly in distilled water. The thin sections were stained with hematoxylin for 1 min, Eosin Y (1%) for 15 min and Azure II (0.1%) for 30 s, and washed after each interval.

For electron microscopy, colloidal gold liposome injection and tissue collection were performed as described for light microscopy. The specimens were embedded in Epox 812 resin (Ernest F. Fullam, Inc., Latham, NY), and specimens (70 nm thickness) examined with a JEOL 100CX transmission electron microscope operating at 80 kV.

For fluorescence microscopy, $PC/C/G_{M1}$ liposomes were prepared by reverse-phase evaporation method described above, but with aqueous contents of 100 mg/ml Rhodamine B isothiocyanate-dextran (RITC-Dex) (M_r 9000, with excitation and emission wavelengths of 546 nm and 590 nm, respectively) in 10 mM Hepes buffer. The final solution was adjusted to 300 mosmol/kg with NaCl (pH 7.4). Unencapsulated RITC-Dex was removed by the combination of G-150 Sephadex gel filtration and Amicon concentration unit (Amicon, Beverly, MA) with 30000 mol. wt. cut off filter membrane. RITC-Dex encapsulated liposomes (0.25 ml, 2 μmol phospholipid) were injected into the tail vein of mice. The mice were killed after 24 h. Tissues were collected following perfusion with heparinized PBS, and fixed with 4% paraformaldehyde. Frozen-sections (5 μm thickness) of the specimens were examined by fluorescence microscopy.

Negatively stained colloidal gold-containing liposomes are shown in Fig. 1. Most of the liposomes are between 80 and 100 nm in diameter. More than 80% of the liposomes contained one to three gold particles. There are very few free gold grains present. The negative staining process has probably distorted some images of gold localization inside the liposome. Several clear pictures of gold-liposomes in thin section electron microscopy were published in our earlier studies [9,10,18].

The stability of colloidal gold liposomes was investigated both *in vitro* and *in vivo*. During 2 weeks of

storage under argon at 4°C, there was no appearance of precipitation of liposomes or aggregated gold particles separated from liposomes. Moreover, no gold particles were separated from liposomes after 1 min vortexing at room temperature and maximum scale. We have also determined the extent to which gold particles were separated from liposomes during blood circulation. Blood was collected from retroorbital sinuses at 1 h and 24 h after injection, and the plasma was examined by negative staining electron microscopy. By scoring more than 50 liposomes in the size range from 80 to 150 nm, we found that the relative ratios of gold-containing liposomes to the plain ones were almost the same as the ratio before injection in blood. The ratios varied within 5%.

The localization of colloidal gold-containing liposomes in normal liver was examined by light microscopy after silver enhancement. Heavy silver enhancement of colloidal gold was clearly observed almost exclusively within the cytoplasm of Kupffer cells with a clean background of hepatocytes (Fig. 2). Furthermore, silver enhancement of colloidal gold was also found in regions of tumor produced by S.C. implanted colon carcinoma [19] (Fig. 3). Similar silver treatments did not produce any enhanced particles in the sections of either liver or tumor tissues from the mice without colloidal gold liposome injection. The fine resolution of electron micrograph of liver section (Fig. 4) showed gold particles in the intracellular vesicles of Kupffer cells but not in hepatocytes. This confirmed our interpretation that silver-enhancement image was derived from the gold particles either free or still liposome-encapsulated.

The fate of liposome-free gold in circulation was examined by obtaining a similar number of gold particles, which were separated from gold liposomes by high speed centrifugation ($10000 \times g$ for 5 min), into mice. The silver-enhanced gold was seen exclusively in the Kupffer cells, rarely in the tumor region 24 h after injection. This suggests that if any gold particles were separated from liposomes in the circulation, they would probably be removed by Kupffer cells before reaching the tumor. Thus, we consider the silver particles in the tumor region are most likely due to accumulation of gold-liposomes which have reached that region intact.

As an additional control to ensure that the silver enhancement image represents the true liposome localization, we have used a second liposome marker, fluorescent RITC-Dextran, in frozen section fluorescence microscopy. The fluorescence patterns show a striking similarity to the silver enhancement image in the liver (Fig. 5) and the tumor region. No fluorescence could be observed in the liver and tumor region of control mice injected with 10 mg of free RITC-Dex. This indicates that even if the aqueous contents marker (RITC-Dex) leaks out of the liposomes, it does not remain in the tissues, so the fluorescence signal from frozen-sections of the tissues with liposomal RITC-Dex

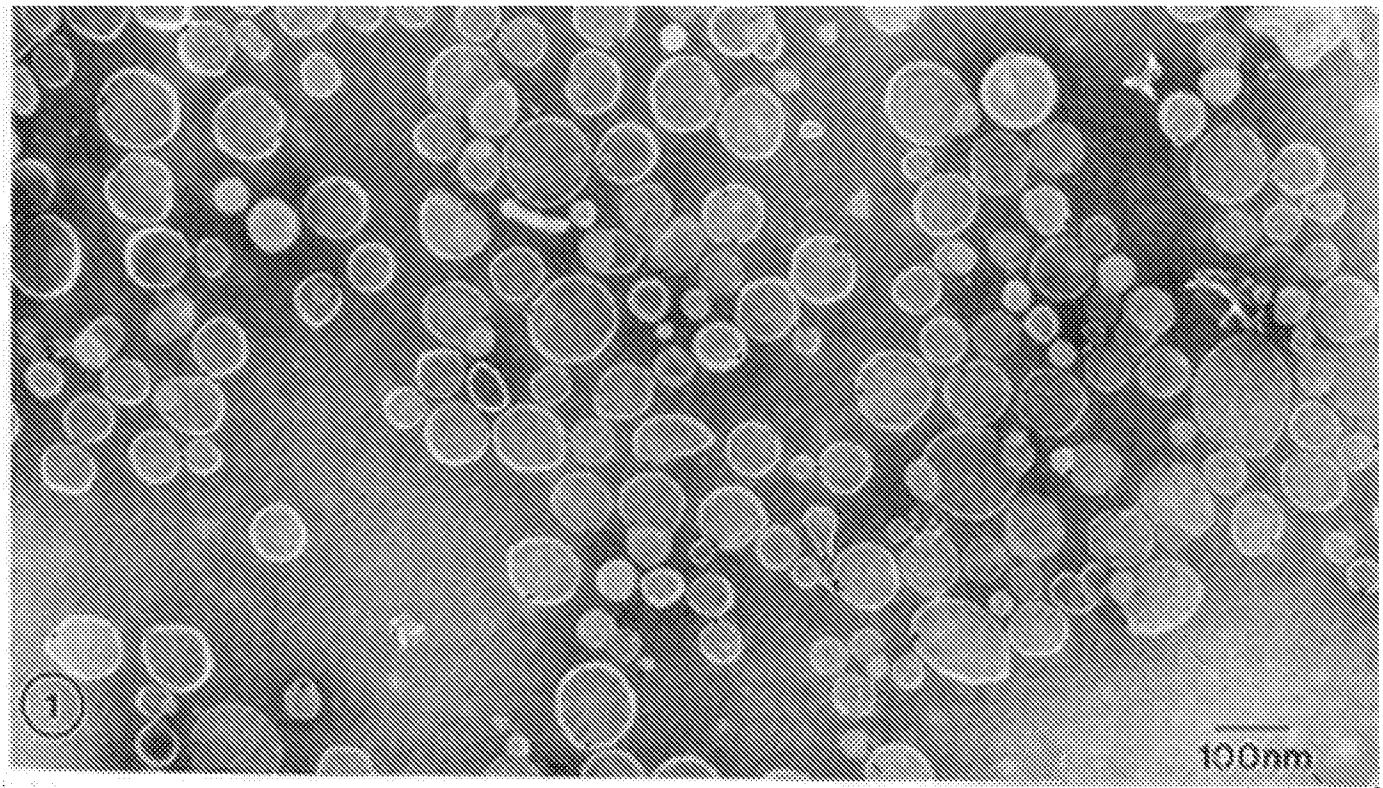

Fig. 1. Negative-stain electron micrograph showing that the size of most colloidal gold-containing liposomes, PC/C/G_{M1} (2:1:0.2), is between 80 and 100 nm in diameter. The majority of them contain one to three gold particles.

is truly reporting the localization of the intact liposomes.

The method presented here indicates that it is possible to localize the presence of liposome contents within tissues such as tumors, where liposomes do not accumulate in large amounts. The ability to detect colloidal gold-containing liposomes by silver enhancement light microscopy is much easier and more sensitive than by electron microscopy. It is also obvious from the results that the resolution of silver enhancement light microscopy is much better than fluorescence microscopy because it allows morphological staining in the same tissue section for positive identification of various cells. However, fluorescence microscopy provides additional control for the presence of intact liposomes irrespective of colloidal gold particles, and might also be useful for quantitation purposes in specific regions of different tissues.

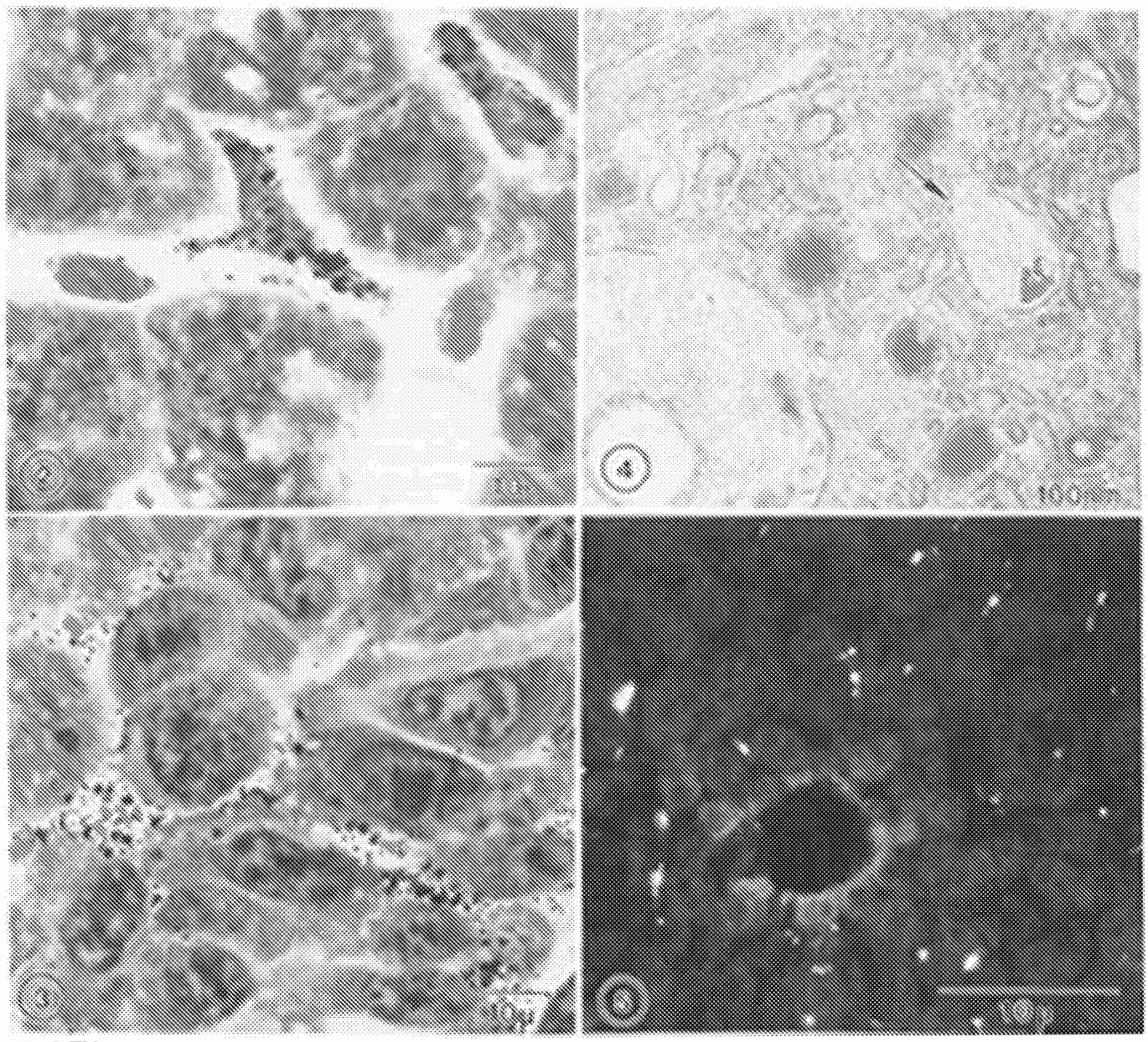

Fig. 2. Thick section of mouse liver. Silver-enhanced gold particles heavily label Kupffer cells, but very few particles can be seen in hepatocytes.

Fig. 3. Thick section of C-26 colon carcinoma implanted S.C. tumor. The silver-enhanced gold particles are seen in the extracellular space between the poorly differentiated tumor cells.

Fig. 4. Electron micrograph of mouse liver. Colloidal gold particles are observed in an intracellular vesicles of Kupffer cell.

Fig. 5. Fluorescence micrograph of a frozen section of mouse liver. Fluorescence of Rhodamine Dextran (encapsulated in liposomes) can be clearly seen in the small and elongated Kupffer cells residing along the sinusoids.

We thank Mrs. Ivy Hsieh for technical assistance. Supported by NIH grant (CA 25526-07A3) and LTI grant EXM 38-90 to D.S.F.

References

1 Forssen, E.A. and Tokes, Z.A. (1979) Biochem. Biophys. Res. Commun. 91, 1295–1301.
2 Mayhew, E., Rustum, Y. and Vail, W.J. (1983) Cancer Drug Deliv. 1, 43–58.
3 Magee, W.E., Goff, C.W., Schoknecht, J., Smith, M.D. and Cherian, K. (1974) J. Cell Biol. 63, 492–504.
4 Wu, P., Tin, G.W. and Baldeschwieler, J.D. (1981) Proc. Natl. Acad. Sci. USA 78, 2033–2037.
5 Straubinger, R.M., Hong, K. and Papahadjopoulos, D. (1990) J. Biochem. 29, 4929–4939.
6 Weinstein, J.N., Yoshikami, S., Henkart, P., Blumenthal, R. and Hagins, W.A. (1977) Science, 196, 489.
7 Ho, S.-C. and Huang, L. (1983) J Histochem. Cytochem. 31, 404–410.
8 Bugelski, P.J., Gennaro, D.E., Poste, G. and Hoffstein, S.T. (1989) J. Histochem. Cytochem. 37, 843–851.
9 Hong, K., Friend, D.S., Glabe, C.G. and Papahadjopoulos, D. (1983) Biochim. Biophys. Acta 732, 320–323.
10 Straubinger, R.M., Hong, K., Friend, D.S., Düzgüneş, N. and Papahadjopoulos, D. (1985) in Receptor-mediated Targeting of Drugs (Gregoriadis, G., Poste, G., Senior, J. and Trouet, A., eds.), pp. 297–315, Plenum Press, New York.
11 Gabizon, A. and Papahadjopoulos, D. (1988) Proc. Natl. Acad. Sci. USA 85, 6949–6953.
12 Allen, T.M. (1981). Biochim. Biophys. Acta 640, 385–397.
13 Waele, D. (1986) J. Histochem. Cytochem. 34, 1257–1267.
14 Szoka, F. Jr. and Papahadjopoulos, D. (1978) Proc. Natl. Acad. Sci. USA 75, 145–1497..
15 Olson, F., Hunt, C. Szoka, F., Vail, W. and Papahadjopoulos, D. (1979) Biochim. Biophys. Acta 557, 9–23.
16 Szoka, F., Olson, F., Heath, T., Vail, W., Mayhew, E. and Papahadjopoulos, D. (1980) Biochim. Biophys. Acta 601, 559–571.
17 Beckstead, J.H. Stenberg, P.E., McEver, R.P., Shuman, M.A. and Bainton, D.F. (1986) Blood, 67, 285–293.
18 Straubinger, R.M., Hong, K., Friend, D.S. and Papahadjopoulos, D. (1983) Cell 32, 1069–1079.
19 Mayhew, E., Goldrosen, M., Vaage, J. and Rustum, Y. (1987) J. Natl. Cancer Inst. 78, 707–713.

[CANCER RESEARCH 52, 5135–5143, October 1, 1992]

Microscopic Localization of Sterically Stabilized Liposomes in Colon Carcinoma-bearing Mice[1]

S. K. Huang[2], K-D. Lee, K. Hong, D. S. Friend, and D. Papahadjopoulos

Cancer Research Institute [S. K. H., K-D. L., K. H., D. P.] and Department of Pathology [D. S. F.], University of California, San Francisco, California 94143

ABSTRACT

Using light and electron microscopy, we investigated the *in vivo* distribution of liposomes sterically stabilized by specific lipids which prolong their circulation in blood. Tissue distribution of sterically stabilized liposomes composed of distearoyl phosphatidylcholine: cholesterol:monosialoganglioside G_{M1} (10:5:1)-encapsulated ^{67}Ga-Desferal indicates that more than 30% of liposomes still remain in the blood at 24 h after tail vein injection. Moreover, such liposomes accumulated in tumors (C-26 colon carcinoma cells implanted s.c.), reaching almost the same level of uptake as liver (~20% injected dose/g tissue). The microscopic localization of liposomes labeled with encapsulated colloidal gold or rhodamine-labeled dextran coincided well with the tissue distribution. To evaluate circulation parameters, two sizes of gold-containing egg phosphatidylcholine:cholesterol:distearoyl phosphatidylethanolamine (derivatized at its amino position with a 1900 molecular weight segment of polyethylene glycol) (10:5:0.8) liposomes were injected. The plasma was examined by electron microscopy of negative-stained preparations at 0.5, 4, and 24 h after liposome injection. It was found that the ratio of small (<100 nm diameter) to large (>100 nm) liposomes increased with time, indicating a much faster clearance of the larger liposomes. To detect the localization of liposomes in various tissues, appropriate samples were fixed 24 h after the injection of gold-containing liposomes (between 80 and 100 nm in diameter) composed of egg phosphatidylcholine:cholesterol:monosialoganglioside G_{M1} (10:5:1) or egg phosphatidylcholine:cholesterol:derivatized distearoyl phosphatidylethanolamine. The tissues examined for this study included normal liver, bone marrow, and implanted neoplasms. Silver-enhanced colloidal gold was found predominantly within Kupffer cells in the normal liver and within macrophages in the bone marrow. Rarely were any silver-enhanced gold particles detected in hepatocytes. In all preparations, electron microscopy revealed the presence of gold in endosomes and lysosomes of fixed sinusoidal lining macrophages in the liver and bone marrow. Peripheral to the implanted tumors, silver enhancement revealed gold in small blood vessels and focally beyond the vessel boundaries in extracellular spaces around tumor cells. Gold particles were not observed within the tumor cell cytoplasm. At the tumor border, nonenhanced gold was occasionally seen by electron microscopy in cells of the mononuclear phagocyte system. We obtained the same localization pattern as with silver enhancement by using an alternative aqueous content marker, rhodamine B isothiocyanate-dextran. We conclude that liposomes of specific composition, which have the ability to remain in circulation with a half-life of 12–24 h, are also able to traverse the endothelium of small blood vessels, including those in tumors, and extravasate into extracellular spaces. The persistence of such liposomes in the circulation and their ability to reach tumor cells within a solid carcinoma make them highly attractive vehicles for chemotherapeutic agents.

INTRODUCTION

Recent pharmacokinetic and therapeutic studies with tumor-bearing mice revealed that sterically stabilized liposomes have considerable potential as drug carriers (1). Liposomes composed of phosphatidylcholine and cholesterol mixed with a small amount of either PEG-DSPE[3] or G_{M1} have a prolonged circulation time in blood and reduced uptake by liver and spleen (1–3). Most importantly, increased accumulation has been demonstrated in solid tumors (2, 4). Results from recent studies on the administration of liposome-encapsulated doxorubicin as a chemotherapeutic agent have demonstrated increased therapeutic efficacy and reduced toxicity compared to the administration of the free drug (1).

Despite extensive studies on tissue distribution (1, 3, 5), and with the exception of the liver, it is still not known where liposomes are localized at the cellular level in various tissues following i.v. injection. The localization of liposomes in the liver has been examined by various markers, including 5-Br, 4Cl,3-indolylphosphate (6), single or paired enzymes such as glucose oxidase and horseradish peroxidase (7), and colloidal gold (8). All of these studies have shown that in the liver, liposomes were internalized by Kupffer cells of the mononuclear phagocyte system, more commonly referred to as the reticuloendothelial system (6, 9–11). Other tissues where liposomes have been localized are spleen (12); bone marrow for small liposomes (13); lungs for large liposomes (14); and implanted tumors for sterically stabilized liposomes (2). However, there are several important long-standing key questions in the liposome field that need to be answered: By what cells are liposomes taken up into other tissues, including tumors? Are there any tissues or pathologic conditions where the liposomes can cross blood vessel endothelium and basal lamina? Are intact liposomes present in extravascular spaces?

To understand better the mechanism of liposome uptake in various tissues, we have developed a liposome preparation with encapsulated colloidal gold particles and applied silver enhancement of the colloidal gold to monitor the *in vivo* fate of liposomes by optical and electron microscopy (15). We chose sterically stabilized liposomes of well-defined particle size, which had been shown by earlier studies to give superior accumulation in implanted tumors (1, 2).

MATERIALS AND METHODS

Materials. Egg PC and DSPC were purchased from Avanti Polar Lipids, Inc. (Pelham, AL). PEG-DSPE synthesized as described earlier (16) was from Liposome Technology, Inc. (Menlo Park, CA). Cholesterol (highly purified) was from Calbiochem (La Jolla, CA). Monosialoganglioside G_{M1}, morpholino-ethane-sulfonic acid, 4-morpholinepropanesulfonic acid, 8-hydroxyquinoline sulfate (oxine), and RITC-Dex (M_r 9000) were from Sigma Chemical Co. (St. Louis, MO). ^{67}Ga citrate was from New England Nuclear (Boston, MA); Desferal was from CIBA-Geigy (Summit, NJ); Dowex resin 50x4-400 was from Aldrich (Milwaukee, WI); and the acetate form of AG 1X2 resin was

Received 9/24/91; accepted 7/23/92.

The costs of publication of this article were defrayed in part by the payment of page charges. This article must therefore be hereby marked *advertisement* in accordance with 18 U.S.C. Section 1734 solely to indicate this fact.

[1] Supported by NIH Grant CA25526 to D. P. and LTI Grant EXM 38-90 to D. S. F.

[2] To whom requests for reprints should be addressed, at Cancer Research Institute, Box 0128, University of California, San Francisco, CA 94143.

[3] The abbreviations used are: PEG-DSPE, distearoyl phosphatidylethanolamine derivatized at its amino position with a 1900 molecular weight segment of polyethylene glycol; PC, egg phosphatidylcholine; DSPC, distearoyl phosphatidylcholine; G_{M1}, monosialoganglioside G_{M1}; RITC-Dex, rhodamine B isothiocyanate-dextran; Desferal, deferoxamine mesylate.

from Bio-Rad (Richmond, CA). All organic solvents used were reagent grade or high-pressure liquid chromatography grade. All other materials were as previously described (1).

Preparation of ^{67}Ga-labeled Liposomes. Liposomes composed of DSPC:cholesterol:G_{M1} (molar ratio, 10:5:1) or PC:cholesterol:PEG-DSPE (molar ratio, 10:5:0.8) were prepared by shaking thin lipid films with an isotonic solution of morpholino-ethane-sulfonic acid (0.05 mM) and 4-morpholinepropanesulfonic acid (0.05 mM) containing deferoxamine mesylate at 55°C for 30 min. After four cycles of freezing (−56°C) and thawing (55°C), the liposomes were extruded under pressure (300 psi) (18) through a stack of two Nucleopore membranes (Pleasanton, CA) (0.2-μm pore size two times; 0.1-μm pore size two times; and 0.05-μm pore size seven times). The extruder device was preheated to 55°C, due to the high-phase-transition phospholipids used. To obtain homogeneous size, liposomes were spun in a microcentrifuge at 10,000 × *g* for 5 min. The precipitate containing any large liposomes was discarded. The average diameter of liposomes was ~90 nm, as measured with a Malvern dynamic laser scattering machine (Malvern Instruments, Ltd., Malvern, England) and based on mass distribution. Unencapsulated Desferal was removed by passage twice through Dowex dry columns at 3000 × *g* for 15 min. The labeling procedure used was as before (2). One hundred μCi of ^{67}Ga citrate was incubated with 1 mg oxine sulfate in 1 ml 0.9% saline for 1 h at 50°C. Liposome suspensions were incubated overnight at 4°C with 2 μCi of ^{67}Ga-labeled oxine/μmol of phospholipid. ^{67}Ga-labeled Desferal was entrapped in the aqueous interior of liposomes. Unencapsulated ^{67}Ga-labeled oxine and excess oxine sulfate were removed by passing the liposome suspension through an anion-exchange resin (AG1X2, acetate form, 200–400 mesh) and a Dowex dry column.

Preparation of Colloidal Gold-Liposomes. A solution of citric acid (120 mM) and K_2CO_3 (30 mM) was freshly prepared and mixed with gold tetrachloride $HAuCl_4$ (12.72 mM) in a ratio of 1:1 (pH 3.4). Liposomes composed of either PC:cholesterol:G_{M1} (molar ratio, 10:5:1) or PC:cholesterol:PEG-DSPE (molar ratio, 10:5:0.8) were prepared by reverse-phase evaporation (17) with gold chloride:citrate in the aqueous phase (15). A thin lipid film (10 μmol phospholipid) was dissolved in 1 ml of diethyl ether and mixed with 0.5 ml gold chloride:citrate. The mixture was emulsified for 3 min in a bath sonicator, and diethyl ether was removed under vacuum at room temperature. The liposomes underwent three cycles of freezing (−56°C) and thawing (55°C) and then were extruded under pressure (18) through Nucleopore membranes, twice through pore size 0.1 μm and five times through 0.05 μm. Immediately after final extrusion, the pH of the liposome suspension was raised to 6 by adding NaOH. It was then incubated at 55°C for 30 min. The color of liposome suspension turned pink-purple, which indicated an appropriate particle size. After gold particles had formed, unencapsulated free gold and excess citrate were removed by passing the liposome suspension through a column (1 x 15 cm) of Sephacryl S-500 (Pharmacia, Piscataway, NJ). The average diameter of the liposomes was 80–100 nm, as determined by electron microscopy. The percentage of liposomes containing gold as determined by negative-stain electron microscopy (15) was between 60 and 90%, varying among preparations. Most of them contained more than one gold particle. The gold-liposomes were stable during 2 weeks of storage under argon at 4°C. *In vivo*, gold-containing liposomes remain intact in the bloodstream; the relative ratio of gold-containing to plain liposomes recovered in plasma at 24 h after i.v. injection in mice was almost the same as before injection (15).

Animals and Tumor Models. Female BALB/c mice, 4–5 weeks old (West Seneca Laboratory, West Seneca, NY), were inoculated with a single-cell suspension of C-26 mouse colon carcinoma (10^5 cells) directly into the liver or subcutaneous tissue (19). Mice were tested 2 weeks after tumor cell seeding. Tumor diameters were from 5 to 10 mm.

Determination of Liposome Tissue Uptake. Mice (5/group) were injected via the tail vein, with 1 μmol phospholipid and 0.25 μCi ^{67}Ga/0.25 ml liposome suspension. The mice were sacrificed, and tissues were excised at 1, 16, 24, and 48 h after liposome injection. The tissues were counted for radio label in a Beckman 8000 gamma counter. Tissues were sampled, including plasma, skeletal muscle, liver, and tumor. Blood volumes and correction factors for the blood content of various tissues were determined by examining the tissue distribution of ^{111}In-oxine-labeled erythrocytes 10–15 min after i.v. injection (20).

Determination of Liposomes in Plasma. Populations of liposomes of different sizes were prepared as described previously, except that the larger liposomes were extruded once only through only 0.1-μm pore Nucleopore membranes. Liposome diameter ranged from 50 to 500 nm, with 100 nm set arbitrarily as the line of demarcation between small and large liposomes. Liposomes were injected into the tail vein, and blood was collected from the retroorbital sinuses under anesthesia after 0.5, 4, and 24 h. The heparinized blood was diluted with 1 volume of phosphate-buffered saline and left at 4°C for 4 h without centrifuging. The liposomes in plasma were stained with 2% ammonium molybdate for electron microscopy. The relative ratio of small to large colloidal gold-liposomes was determined by a random count of 100 liposomes in a random electron microscopic field.

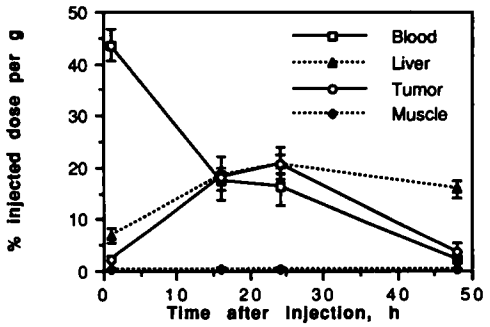

Fig. 1. Tissue distribution of liposome-encapsulated ^{67}Ga-Desferal as an aqueous content marker. The liposome-encapsulated ^{67}Ga remaining in blood (□), uptake by skeletal muscle (♦), liver (▲), and s.c. implanted tumor (○) were determined at 1, 16, 24, and 48 h after i.v. injection. Mean ± SD, $n = 5$.

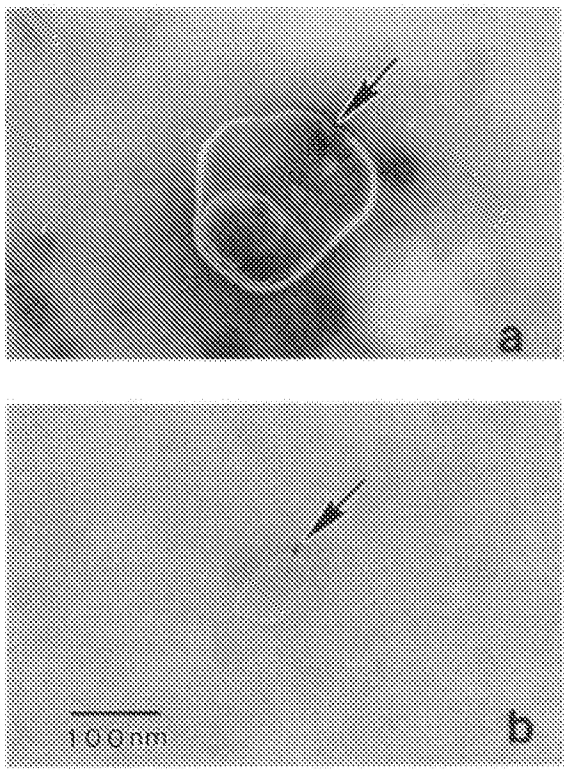

Fig. 2. Negative-stain electron micrographs of colloidal gold-containing liposomes in plasma. The liposomes were composed of PEG-DSPE:PC:cholesterol (0.8:10:5). *a* and *b*, typical large and small liposomes, respectively, in plasma 4 h after injection. Both contain more than one gold particle (*arrows*).

Tissue Collection and Fixation for Microscopy. Colloidal gold-containing liposomes (0.25 ml, 2 μmol phospholipid) were injected into mice via the tail vein. The mice were sacrificed 24 h after liposome injection. Tissues were collected following perfusion with heparinized phosphate-buffered saline and fixative (1.5% glutaraldehyde, 0.1 M sodium cacodylate, 1% sucrose, pH 7.4).

Light Microscopy following Silver Enhancement of Colloidal Gold. The tissue specimens were embedded in water-soluble JB-4 resin (21) from Polysciences, Inc. (Warrington, PA). All procedures involving tissue handling were performed at 4°C. Sections were cut from embedded specimens with a Sorvall JB-4 microtome at a thickness of 2.5 μm.

Reagents A (enhancer) and B (initiator) for silver enhancement were purchased from Amersham (Arlington Heights, IL). The sample area on the slide was covered with mixture (A and B) for 15 min at 22°C. Then, the tissue sections were stained with hematoxylin for 1 min and Eosin Y (1%) for 15 min.

Electron Microscopy. Injection and tissue collection of colloidal gold-liposomes were performed as described for light microscopy. The specimens were further fixed, dehydrated in graded series of alcohols, and embedded in Epox 812 resin (Ernest F. Fullam, Inc., Latham, NY), and thin sections were examined with a JEOL 100CX transmission electron microscope operating at 80 kV.

Fluorescence Microscopy. Liposomes composed of PC:cholesterol:G_{M1} were prepared according to the method described above, but with aqueous contents of 100 mg/ml RITC-Dex in 10 mM *N*-2-hydroxyethylpiperazine-*N*-2-ethanesulfonic acid buffer. This fluorescent liposome marker has a molecular weight of 9000, with excitation and emission wavelengths of 546 and 590 nm, respectively. The final solution was adjusted to 300 mOsm with NaCl (pH 7.4). Unencapsulated RITC-Dex was removed by G150 Sephadex gel filtration and by passage through an Amicon concentration unit (Amicon, Beverly, MA) with a 30,000 molecular weight cutoff filter membrane. Liposomes with encapsulated RITC-Dex (0.25 ml, 2 μmol phospholipid) were injected into the tail vein, and mice were sacrificed 24 h later. Tissues were collected following perfusion with heparinized phosphate-buffered saline and fixed with 4% paraformaldehyde. Frozen sections (5 μm thickness) of the specimens were examined by fluorescence microscopy.

RESULTS

Tissue Distribution of Liposome-encapsulated ^{67}Ga-Desferal. ^{67}Ga-Desferal complex as a marker for aqueous contents was encapsulated in liposomes composed of DSPC:cholesterol:G_{M1} (molar ratio, 10:5:1). ^{67}Ga-labeled liposomes were injected into the tail vein of mice bearing C-26 colon carcinoma implanted s.c. The level of liposomes remaining in blood and their uptake by liver, muscle, and tumor at different times are shown in Fig. 1. G_{M1}-liposomes showed their sterically stabilized property in the blood circulation, where 66% of the injected dose was present in 1 ml (approximately 1 g) blood 1 h after

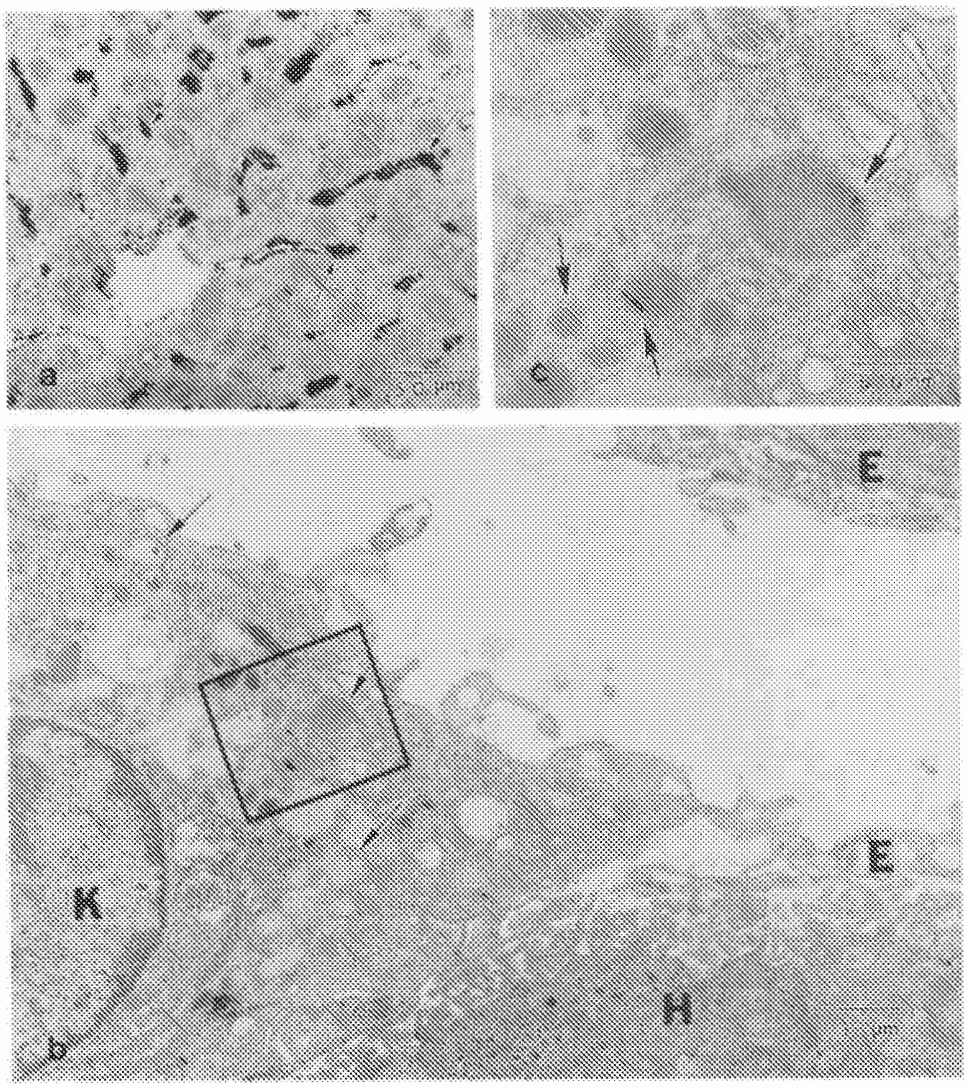

Fig. 3. Localization of liposomes in liver. Liver tissue was collected 24 h after colloidal gold liposome injection. a, light micrograph of overall view of liposome localization. Silver-enhanced gold particles (*arrows*) heavily label Kupffer cells. Rare particles may be seen in hepatocytes. *b*, electron micrograph of a Kupffer cell directly exposed in a sinusoid of mouse liver. Colloidal gold particles (*arrows*) are observed in the Kupffer cell only. In *c*, the portion of Kupffer cell (*inset*) at higher magnification (*b*) shows accumulated colloidal gold particles in secondary lysosomes. *K*, Kupffer cell; *H*, hepatocyte; *E*, endothelial cell.

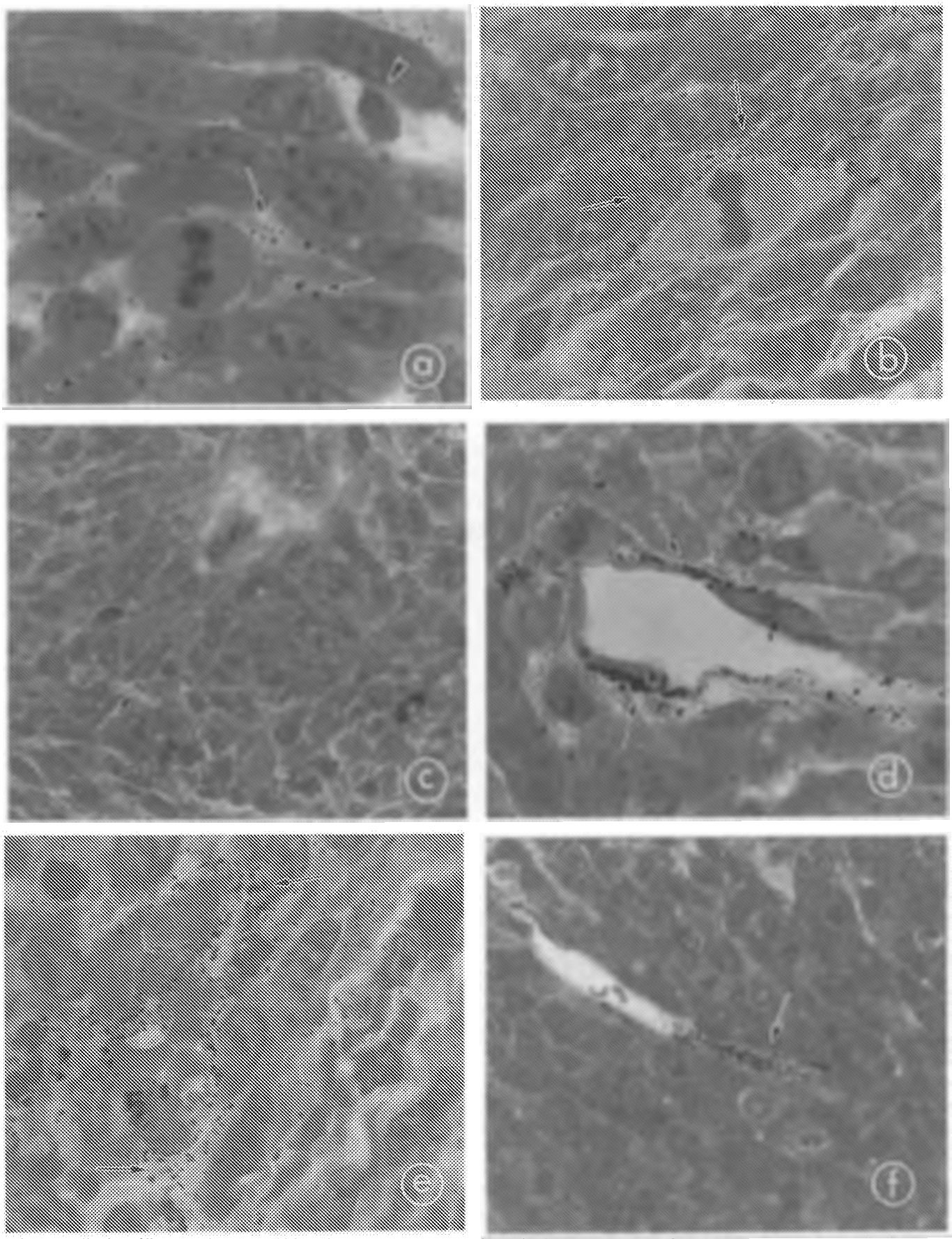

Fig. 4. Localization of liposomes in tumor. Thick sections show C-26 colon carcinoma implanted s.c. (*a, c, d, e, f*), *and directly in the liver (b).* A mast cell shows *red* due to metachromatic staining (*a, arrowhead*). Silver-enhanced gold particles (*arrows*) infiltrate into the extracellular space of the poorly differentiated tumor cells. *c* and *d*, various sizes of penetrating blood vessels show dense accumulations of silver-enhanced colloidal gold markers surrounding blood vessels. *d*, silver-enhanced

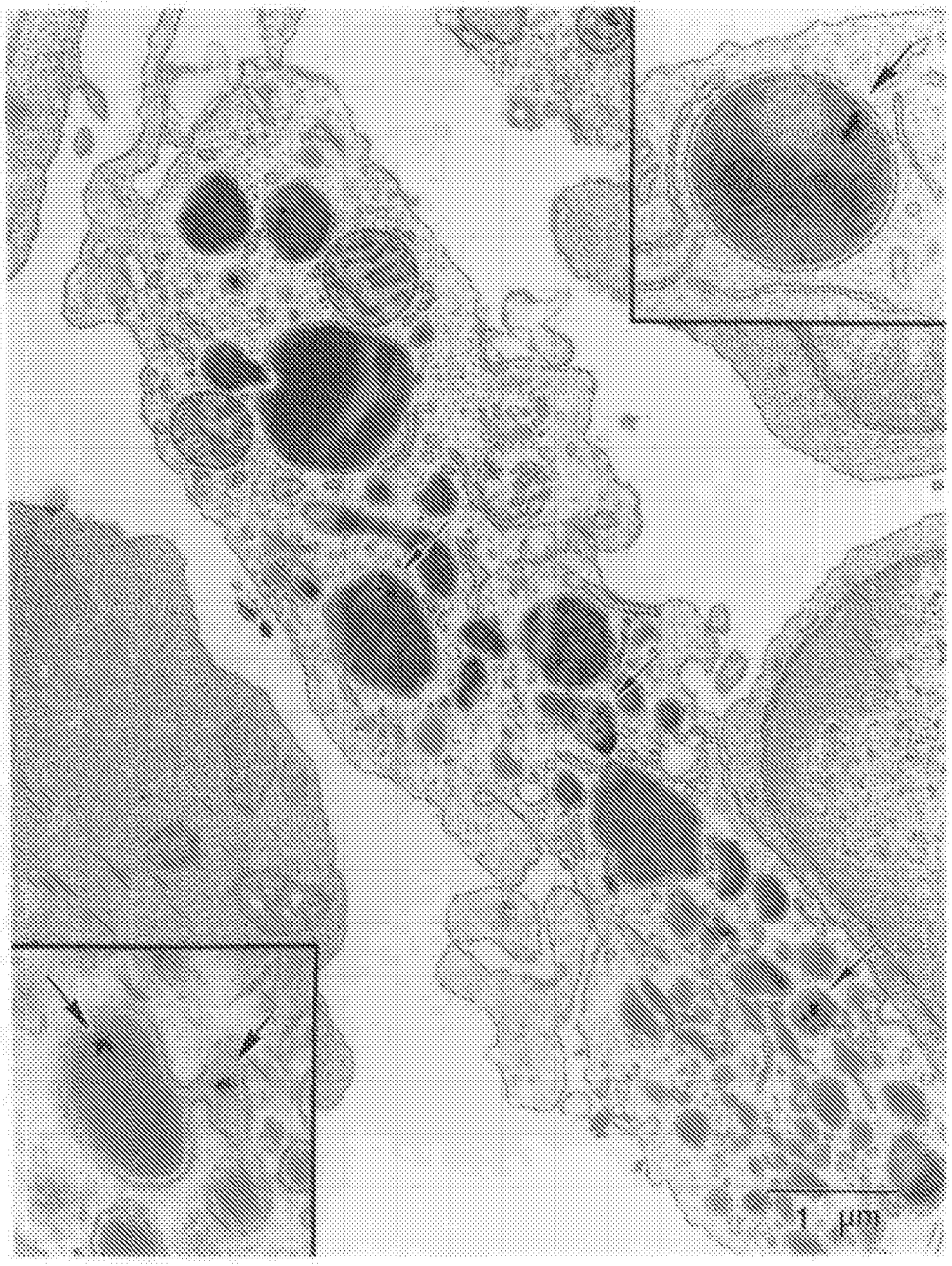

Fig. 5. Electron micrographs showing colloidal gold (*arrows*) in the intracellular vesicles of a typical mononuclear phagocyte. The colloidal gold often can be found within the endosomes (*lower inset*) and secondary lysosomes (*upper inset*) of macrophages at the border of the liver-implanted tumor.

injection. Approximately one-third of injected liposomes remained in circulation at 24 h after injection. For tissue distribution within 1 h following injection, liposome uptake by tumor was lower compared with the uptake by liver. However, liposomes appeared to accumulate rapidly at increased concentrations in the tumor, reaching almost the same level as in the liver (more than 20% of injected dose/g) at 24 h after injection. In contrast, the liposome uptake level of normal tissue (skeletal muscle) was still lower than 0.5% of injected dose/g 24 h after injection. These results confirm earlier observations obtained with other tumors (2, 4) that sterically stabilized liposomes not only have a prolonged circulation time but also exhibit a favorable tumor uptake:liver uptake ratio.

Selective Clearance of Liposomes in Blood Circulation. A mixture of two size populations of gold-labeled liposomes composed of PC:cholesterol:PEG-DSPE was examined by electron microscopy before injection. Most of them had diameters between 50 and 500 nm. Liposomes greater than 100 nm [182 ± 58 (SD) nm] were termed large liposomes, and those under 100 nm [80 ± 12 (SD) nm], small liposomes. Forty-four % of liposomes were greater than 100 nm, and 56% were less than 100 nm, in a random count of 100. The mixture was injected into the tail veins of mice. Micrographs of large and small liposomes in plasma are shown in Fig. 2, *a* and *b*, respectively. Half an hour after injection, fewer large liposomes remained in the bloodstream, and the ratio of small to large

gold on the parenchymal side of the endothelial cells. *e*, region in the tumor scattered with erythrocytes and colloidal gold particles, possibly in a region of angiogenesis. *f*, in many areas of tumors, colloidal gold particles are trapped in the blood vessels without any penetration into the surrounding tissue. H & E. *a, b, d,* and *e*, × 1500; *c* and *f*, × 600.

liposomes changed to 73:27. This ratio continued to change over time, becoming 90:10 at 4 h and 98:2 at 24 h after injection. Thus, the relative number of large liposomes in plasma decreased rapidly, with a rate represented by an exponential decay. In addition to the disappearance of large liposomes from the blood, a decrease in the number of small liposomes was noted as well, but the large liposomes disappeared much more rapidly. For all the localization studies described below, we have used exclusively the preparation of small (80–100 nm) liposomes, composed of PC:cholesterol:G_{M1} and PC:cholesterol:PEG-DSPE. The results obtained with these two preparations were identical.

Localization of Liposome-encapsulated Markers in Normal Liver. Localization of colloidal gold-containing liposomes in liver was studied by light microscopy of silver-enhanced thick sections. The cytoplasm of Kupffer cells was heavily labeled (Fig. 3*a*). Some erythrocytes could still be seen in sinusoids due to imperfect perfusion. It is difficult to see endothelial cells lining sinusoids by light microscopy; however, Kupffer cells containing silver-enhanced colloidal gold could be easily distinguished (Fig. 3*a*). Very rare and weak labeling could also be seen in hepatocytes. Alternatively, Kupffer and endothelial cells lining a sinusoid can be seen by electron microscopy in Fig. 3*b*, with colloidal gold particles localized in lysosomes within Kupffer cells (Fig. 3*c*). In previous experiments (15), we used RITC-Dex as an alternative marker for aqueous contents, and results showed that RITC-Dex-containing liposomes were also localized in Kupffer cells, in agreement with the silver enhancement observations. The above observations correspond to those of previous studies demonstrating that liposomes are internalized by endocytosis in liver Kupffer cells (6, 9–11).

Localization of Liposome-encapsulated Markers in Tumors. We investigated the localization of liposomes in mouse colon carcinoma (C-26) implanted s.c. and in the liver (19). Tumors implanted s.c. formed ovoid nodules and could be easily separated from surrounding tissues. The tumor implanted directly into the liver formed a solitary solid tumor without satellite nodules or metastases. Although the interface between normal liver and tumor slightly interdigitated, it was possible to separate the tumor (white) from liver (red) tissue. Poorly differentiated tumor cells can be seen in the thick sections of tumors implanted s.c. (Fig. 4*a*) and in the liver (Fig. 4*b*). The cell morphology and architecture of the tumor in these two locations are the same. Mitoses are abnormally frequent. In some regions, silver-enhanced colloidal gold particles are seen to be predominantly scattered in the extracellular space between tumor cells (Fig. 4, *a* and *b*). Silver was rarely found in tumor cell cytoplasm. It is interesting to note that metachromatic staining mast cells, an important source of vasoactive amines, were also present among the tumor cells (Fig. 4*a*).

Blood vessels penetrated into the tumor mass of the C-26 colon carcinomas. The tumor exhibited numerous vessels of various diameters (Fig. 4, *c* and *d*). Dense, silver-enhanced colloidal gold often surrounded blood vessels. In these areas, the silver particles often could be seen in streams connected to blood vessels (Fig. 4*c*). In some areas close to small blood vessels, silver-enhanced gold was clearly localized on the parenchymal side of the endothelial cells (Fig. 4*d*). In addition, silver-enhanced gold particles could be observed to cross the blood vessel endothelium, extensively penetrating into the extravascular, interstitial space between tumor cells (Fig. 4*d*). In other areas, silver-enhanced colloidal gold was scattered around non-endothelial-bound streams of erythrocytes, possibly in a region of angiogenesis (Fig. 4*e*). However, not all of the observed silver-enhanced colloidal gold particles observed traversed blood vessels (Fig. 4*f*).

By electron microscopy, gold particles were seen to be ingested by macrophages and found in their endosomes and secondary lysosomes (Fig. 5), including mononuclear phagocytes at the border of the tumor implanted in the liver (Fig. 5, *upper inset*). Gold particles could also be seen, but less frequently in the extracellular space and occasionally within endothelial cells. Quite likely, it is much more difficult to observe single particles in the extracellular space, because of the limited width of the thin sections used for electron microscopy, compared to the much thicker sections used for optical microscopy (15).

Liposome localization monitored by a second marker, RITC-Dex, revealed a pattern of localization similar to that resulting from silver enhancement of colloidal gold. Fig. 6 shows a phase-contrast view of a 5-μm frozen section of subcutaneous tumor (*a*) and its corresponding fluorescence image (*b*). The fluorescence signals inside the tumor mass are focal, mostly surrounding the vasculature, with a gradual decrease away from them. Injection of free-RITC-Dex under similar conditions did not show any fluorescence in the tumor region. These results indicate that the fluorescence signals were derived from RITC-Dex encapsulated in liposomes.

Localization of Liposome-encapsulated Marker in Bone Marrow. Silver-enhanced gold particles were seen exclusively in the resident macrophages of bone marrow (Fig. 7), although we cannot discount the possibility of some particles being present in the extracellular space. All hematopoietic cells, megakaryocytes, and developing myeloid and erythroid cells were unlabeled. As in other tissues, electron micrographs revealed colloidal gold in dense bodies within macrophages (Fig. 5).

DISCUSSION

In this study, we used liposomes partially composed of PEG-derivatized phospholipid or G_{M1} glycolipid. Both types of liposomes evade the rapid uptake by the reticuloendothelial system and thereby remain longer in circulation (1–3). This increase in circulation time is probably due to their bulky hydrophilic head groups and has been termed "steric stabilization" (1, 22). Our comparative pharmacokinetic studies indicate that at 24 h after

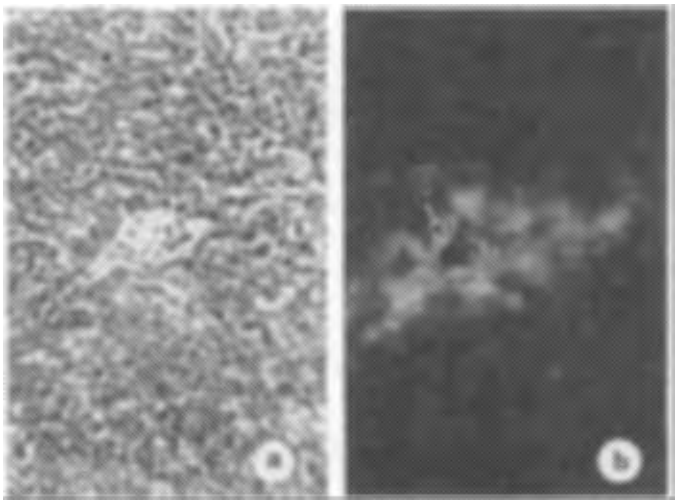

Fig. 6. *a* and *b*, phase and fluorescence micrographs, respectively, obtained with liposome-encapsulated RITC-Dex in the same s.c. tumor region. The fluorescence is visible well beyond the endothelial layer of a blood vessel (*arrow*), which is dark in *b*.

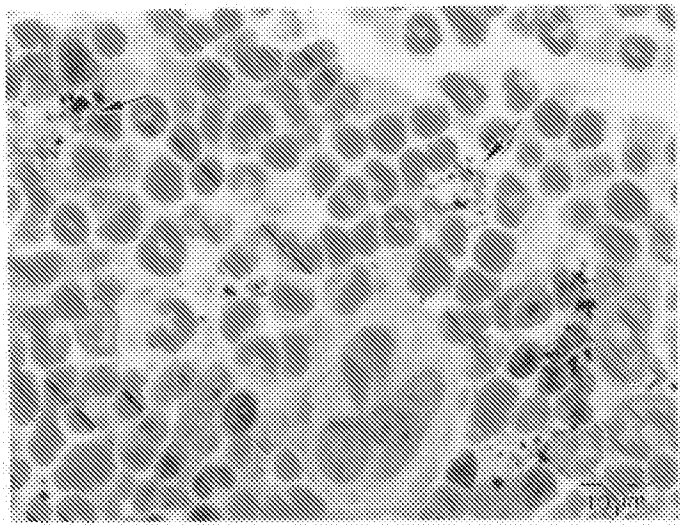

Fig. 7. Localization of liposomes in bone marrow. The gold label (*arrows*), presumably in liposomes, is found predominantly in macrophages.

liposome injection, G_{M1}-containing liposomes (80–100 nm diameter) have a 4-fold higher plasma concentration, one-fourth less uptake in the liver, and a 4-fold increase within a C-26 subcutaneous tumor compared to commonly used liposomes composed of DSPC and cholesterol without any glycolipid.[4] PEG-containing liposomes also showed effects similar to those of G_{M1}-containing liposomes when compared with conventional DSPC:cholesterol liposomes (1). These ratios are even much higher when liposomes sterically stabilized with G_{M1} or PEG-DSPE are compared with conventional liposomes composed of phosphatidylglycerol:PC:cholesterol (2–4). Most of the experiments referred to above were carried out by using encapsulated ^{67}Ga-Desferal. ^{67}Ga labeling has been applied as a quantitative method to measure liposome distribution in various tissues. The results shown in Fig. 1 indicate liposome retention as intact liposomes because the free ^{67}Ga-Desferal complex remains in the circulation only for a very short time (1, 2). However, the pharmacokinetic studies provide no definitive information on the cellular or intracellular localization of liposomes. In this investigation, in addition to Ga-Desferal liposomes we used liposomes of similar composition and size containing colloidal gold and a fluorescent marker in order to clarify their localization at the cellular and subcellular level, in C-26 colon carcinoma and other tissues.

Many studies have shown that the size of liposomes is one of the most important determinants of their longevity in the bloodstream (23, 24). Small unilamellar liposomes (<100 nm diameter) remain significantly longer in the circulation than large liposomes (25, 26). Our observations that large liposomes (>100 nm) disappear from plasma much faster than small ones (<100 nm) confirm this finding. Furthermore, it has been shown in our previous investigations (15) that the ratio of colloidal gold-liposomes and plain liposomes in plasma was almost unchanged for 24 h after injection. These results indicate that gold-labeled liposomes stay intact in the blood without losing their contents.

Much early work, including our pharmacokinetic studies, has shown that liposome uptake by liver is increased sharply within 1-4 hours after injection. Hepatic sinusoids connect the arterial and venous circulation. It is widely accepted that the liver sinusoidal lining is composed of interdigitating cells. One cell type is the typical endothelial cell, the other is the fixed macrophage called the Kupffer cell (27). Kupffer cells are directly exposed to the sinusoid (Fig. 3*b*), giving them the opportunity to ingest circulating particles such as liposomes. That the large liposomes were cleared faster than small liposomes may be due to two reasons. First, large liposomes may be more easily entrapped in sinusoids. Second, their larger surface may promote faster endocytosis. In most other tissues, whether the blood vessels and capillaries are continuous or fenestrated, circulating liposomes must cross the endothelial barrier to reach the extravascular space.

Many types of tumors are well vascularized, increasing the opportunity for liposome delivery. In general, vessels within tumors have been reported to have wide endothelial junctions, a large number of fenestrae, transendothelial channels formed by vesicles, and discontinuous or absent basement membranes (28). The C-26 carcinoma when implanted s.c. or in the liver is well vascularized, growing rapidly, but without obvious metastases. In the thick sections through the tumor, numerous penetrating vessels and branches of varying size could be seen. In order to penetrate into the tumor region, liposomes in the bloodstream must traverse the thin endothelial barrier. Our studies of liposome pharmacokinetics and uptake by tumors revealed that this process is not as fast as the uptake by Kupffer cells, which are directly exposed in the sinusoids of the liver. The maximum concentration of liposome-encapsulated Ga-Desferal in the subcutaneous tumor was observed 24 h after i.v. injection (Fig. 1). Since the ^{67}Ga-Desferal complex itself does not accumulate in tumors (2), its presence in tumor indicates intact liposomes. In order to ascertain whether the presence of gold particles in the tumor mass unequivocally signifies the presence of intact liposomes, we used one alternative liposome marker, RITC-Dex. The results indicate a similar pattern of distribution. Moreover, in a previous study (15), when we injected i.v. free gold particles, which were retrieved from gold-labeled liposomes after they were disrupted by centrifugation, the silver-enhanced marker was found exclusively within Kupffer cells 24 h after injection, rather than in the tumor region. This demonstrated that the particles in the tumor region were most likely derived from the accumulation of gold-containing liposomes that penetrated the tumor, albeit slowly.

Initial studies with a fluorescent marker indicated liposome infiltration into the interstitial space between tumor cells (1). The data presented here provide definitive evidence for this in some instances, as well as clues to the possible mechanism by which liposomes escaped from blood vessels and extravasated into the tumor. We have considered the following three possibilities.

First, the liposomes may have escaped from discontinuous capillaries reported to be present in tumors of poorly differentiated mammary (29) and human renal carcinomas (30). Vessels supplying tumors may be lined by inherently leaky, fenestrated endothelium (31, 32). In our study, the dense silver-enhanced particles and fluorescence pattern always surrounded and localized to the penetrating vessels (Figs. 4, *c* and *d*; Fig. 5), consistent with the previous suggestion that macromolecular particles may cross gaps between endothelial cells (29–32). Mast cells, found among the poorly differentiated tumor cells in some regions (Fig. 4*a*), synthesize histamine and other vasoactive

[4] S. K. Huang, E. Mayhew, S. Gilani, D. D. Lasic, F. J. Martin, and D. Papahadjopoulos. Pharmacokinetics and therapeutics of sterically stabilized liposomes in mice bearing C-26 colon carcinoma, Cancer Res., in press.

amines. Defects in tight junctions between venular endothelial cells could form in response to vasoactive mediators (27), permitting liposomes to flow into the interstitial space.

Second, the silver-enhanced gold was not only scattered throughout the vessels in tumors, it was also heavily deposited in the endothelial basement membrane away from junctional clefts, most likely due to transendothelial vesicular transport (Fig. 4*d*). The occasional observation of gold particles within the endothelial cells indicates that vesicular transport may well be one of the pathways that transfer liposomes from blood vessels to the interstitial space. This was observed more frequently in some transgenic mice.[5] Earlier studies reported vesicular transport of macromolecules (33) and even colloidal carbon particles 50 nm in diameter (34) in tumors. Our observations support this mechanism.

Third, tumor angiogenesis includes the formation of capillary sprouts (35). The sprouts are highly permeable because of gaps between adjacent endothelial cells and openings at the vessel termini, allowing virtually unlimited passage of materials, including erythrocytes, into the surrounding tissue (34). Scattered silver-enhanced gold can be seen in thick sections, along with erythrocytes in tumor areas that we interpret to be capillary sprouts (Fig. 4*e*). It is important to note that although liposomes could escape from tumor blood vessels by the above pathways in some areas, silver-enhanced gold was absent in many other areas of the tumor region, even where dense accumulation of silver-enhanced gold was found entrapped in small vessels (Fig. 4*f*).

Bone marrow was also considered as one of the major sites of interest for liposome localization because of possible drug toxicity and attendant leukopenia after i.v. injection. We observed the silver-enhanced gold exclusively in the resident macrophages. This may be advantageous in reducing the toxic effect of liposome-encapsulated drugs on the hematopoietic cells in the bone marrow, including megakaryocytes and developing myeloid and erythroid cells.

Sterically stabilized small liposomes containing PEG-DSPE or G_{M1} ganglioside can remain in the circulation for a relatively long period of time. The present study provides definitive evidence that they are also able to traverse the endothelium of small blood vessels in tumors and extravasate into interstitial spaces. In liver and bone marrow they are endocytosed primarily by cells of the mononuclear phagocyte system. The persistence of such liposomes in the circulation and their ability to reach sites of a solid carcinoma make them highly attractive vehicles for chemotherapeutic agents. The evidence presented here provides a possible mechanism for the increased therapeutic efficacy of anthracyclines encapsulated in sterically stabilized liposomes against mouse colon carcinoma and lymphoma (1). It is quite likely that the encapsulated drug, being much more diffusible through the tumor mass than the macromolecular carrier itself, can reach distant tumor cells within the same area where liposomes have extravasated and exert its cytotoxic effect. In this respect, sterically stabilized liposomes provide a unique opportunity for increasing the therapeutic index of a variety of therapeutic agents against tumors that allow their extravasation beyond the endothelial barrier.

[5] S. K. Huang, F. J. Martin, G. Jory, J. Vogel, D. Papahadjopoulos, and D. S. Friend, Extravasation and transcytosis of liposomes in Kaposis sorcoma-like dermal lesions of transgenic mice bearing the HIV Tqt gene, submitted for publication.

ACKNOWLEDGMENTS

We thank Ivy Hsieh for her technical assistance.

REFERENCES

1. Papahadjopoulos, D., Allen, T., Gabizon, A., Mayhew, E., Matthay, K., Huang, S. K., Lee, K-D., Woddle, M. C., Lasic, D. D., Redemann, C., and Martin, F. J. Sterically stabilized liposomes: improvements in pharmacokinetics and anti-tumor efficacy. Proc. Natl. Acad. Sci. USA, *88:* 11460–11464, 1991.
2. Gabizon, A., and Papahadjopoulos, D. Liposome formulations with prolonged circulation time in blood and enhanced uptake by tumors. Proc. Natl. Acad. Sci. USA, *85:* 6949–6953, 1988.
3. Allen, T. M., and Chonn, A. Large unilamellar liposomes with low uptake into the reticuloendothelial system. FEBS Lett., *223:* 42–46, 1987.
4. Gabizon, A., Price, D. C., Huberty, J., Bresalier, R. S., and Papahadjopoulos, D. Effect of liposome composition and other factors on the targeting of liposomes to experimental tumors: biodistribution and imaging studies. Cancer Res., *50:* 6371–6378, 1990.
5. Hwang, K. J., and Beaumier, P. L. Disposition of liposomes *in vivo*. *In:* G. Gregoriadis (ed.), Liposomes as Drug Carriers, pp. 19–35. New York: John Wiley and Sons, 1988.
6. Ho, S-C., and Huang, L. A novel cytochemical marker for liposome decomposition in lysosomes. J. Histochem. Cytochem., *31:* 404–410, 1983.
7. Bugelski, P. J., Gennaro, D. E., Poste, G., and Hoffstein, S. T. A new cytochemical method for ultrastructural detection of liposomes in tissues *in vivo*. J. Histochem. Cytochem., *37:* 843–851, 1989.
8. Hong, K., Friend, D. S., Glabe, C. G., and Papahadjopoulos, D. Liposomes containing colloidal gold are a useful probe of liposome-cell interactions. Biochim. Biophys. Acta, *732:* 320–323, 1983.
9. Segal, A. W., Willis, E. J., Richmond, J. E., Slavin, G., Black, C. D. V., and Gregoriadis, G. Morphological observations on the cellular and subcellular destination of intravenously administered liposomes. Br. J. Exp. Pathol., *55:* 320–327, 1974.
10. Scherphof, G., Roerdink, F., Dukstra, J., Ellens, H., de Zanger, R., and Wisse, E. Uptake of liposomes by rat and mouse hepatocytes and Kupffer cells. Biol. Cell, *47:* 47–58, 1983.
11. Straubinger, R. M., Hong, K., Friend, D. S., Duzgunes, N., and Papahadjopoulos, D. Endocytosis of liposomes and intracellular fate of encapsulated molecules: strategies for enhanced cytoplasmic delivery. *In:* G. Gregoriadis, G. Poste, J. Senior, and A. Trouet (eds.), Receptor-mediated Targeting of Drugs, pp. 297–315. New York: Plenum Publishing, 1985.
12. Senior, J. H. Fate and behavior of liposomes *in vivo*: a review of controlling factors. CRC Crit. Rev. Ther. Drug Carrier Syst., *3:* 123–193, 1988.
13. Senior, J., Crawley, J. C. W., and Gregoriadis, G. Tissue distribution of liposomes exhibiting long half-lives in the circulation after intravenous injection. Biochim. Biophys. Acta, *839:* 1–8, 1985.
14. Hunt, C. A., Rustum, Y. M., Mayhew, E., and Papahadjopoulos, D. Retention of cytosine arabinoside in mouse lung following intravenous administration in liposomes of different size. Drug Metab. Dispos., *7:* 124–128, 1979.
15. Huang, S. K., Hong, K., Lee, K-D., Papahadjopoulos, D., and Friend, D. S. Light microscopic localization of silver enhanced liposome entrapped colloidal gold in mouse tissues. Biochim. Biophys. Acta, *1069:* 117–121, 1991.
16. Allen, T. M., Hansen, C., Martin, F., Redemann, C., and Yau-Young, A. Liposomes containing synthetic lipid derivatives of polyethylene glycol show prolonged circulation half-lives *in vivo*. Biochim. Biophys. Acta, *1066:* 29–36, 1991.
17. Szoka, F., Jr., and Papahadjopoulos, D. Procedure for preparation of liposomes with large internal aqueous space and high capture by reverse-phase evaporation. Proc. Nal. Acad. Sci. USA, *75:* 145–1497, 1978.
18. Olson, F., Mayhew, E., Maslow, D., Rustum, Y., and Szoka, F. Characterization, toxicity and therapeutic efficacy of Adriamycin encapsulated in liposomes. Eur. J. Cancer, *18:* 167–176, 1982.
19. Mayhew, E. G., Goldrosen, M. H., Vagge, J., and Rustum, Y. M. Effects of liposome-entrapped doxorubicin on liver metastases of mouse colon carcinomas 26 and 38. J. Natl. Cancer Inst., *78:* 707–713, 1987.
20. Corbett, T. H., Griswold, D. P., Robeots, B. J., Peckham, J., and Schabel, F. M. A mouse colon-tumor model for experimental therapy. Cancer Chemother. Rep., *5:* 169–186, 1975.
21. Beckstead, J. H., Stenberg, P. E., McEver, R. P., Shuman, M. A., and Bainton, D. F. Immunohistochemical localization of membrane and granule proteins in human megakaryocytes: application to plastic-embedded bone marrow biopsyspecimens. Blood, *67:* 285–293, 1986.
22. Lasic, D. D., Martin, F. J., Gabizon, A., Huang, S. K., and Papahadjopoulos, D. Sterically stabilized liposomes: a hypothesis on the molecular origins of the extended circulation times. Biochim. Biophys. Acta, *1070:* 187–192, 1991.
23. Proffitt, R. T., Williams, L. E., Presant, C. A., Tin, G. W., Uliana, J. A., Gamble, R. C., and Baldeschwieler, J. D. Liposomal blockage of the reticuloendothelial system: improved tumor imaging with small unilamellar vesicles. Science (Washington DC), *200:* 502–505, 1983.
24. Abra, R. M., and Hunt, C. A. Liposome disposition *in vivo*. III. Dose and vesicle size effects. Biochim. Biophys. Acta, *666:* 493–503, 1981.

25. Allen, T. M., and Everst, J. M. Effect of liposome size and drug release properties on pharmacokinetics of encapsulated drug in rats. J. Pharmacol. Exp. Ther., *266:* 539–554, 1983.
26. Juliano, R., and Stamp, D. The effect of particle size and charge on the clearance rates of liposomes and liposome encapsulated drugs. Biochem. Biophys. Res. Commun., *63:* 651–658, 1979.
27. Weiss, L., and Greep, W. Histology. New York: McGraw-Hill Book Company, 1979.
28. Jain, R. K. Transport of molecules across tumor vasculature. Cancer Metastasis Rev., *6:* 559–593, 1987.
29. Vogel, A. W. Intratumoral vascular changes with increased size of a mammary adenocarcinoma: new methods and results. J. Natl. Cancer Inst., *34:* 571–578, 1965.
30. Warren, B. A., and Chauvin, W. J. Transmission and scanning electron microscopy of renal adenocarcinoma. Ann. R. Coll. Physicians Surg. Can., *10:* 74–80, 1977.
31. Papadimitriou, J. M., and Woods, A. E. Structural and functional characteristics of the microcirculation in neoplasms. J. Pathol., *116:* 65–72, 1975.
32. Granger, D. N., and Perry, M. A. Permeability characteristics of the microcirculation. Physiol. Pharmacol. Microcirc., *1:* 157–208, 1983.
33. Taylor, A. E., and Granger, D. N. Exchange of macromolecular across the microcirculation. *In:* E. M. Renkin and L. Micher (eds.), Handbook of Physiology—The Cardiovascular System, Vol. 4, pp. 309–374. Bethesda: American Physiology Society, 1984.
34. Dvorak, H. F., Nagy, J. A., Dvorak, J. T., and Dvorak, A. M. Identification and characterization of the blood vessels of solid tumors that are leaky to circulating macromolecules. Am. J. Pathol., *133:* 95–109, 1988.
35. Folkman, J., and Haudenschild, C. Induction of capillary growth *in vitro. In:* J. T. Dingle and J. L. Gordon (eds.), Cellular Interactions, pp. 119–136. Amsterdam: Elsevier, 1981.

Microscopic Localization of Sterically Stabilized Liposomes in Colon Carcinoma-bearing Mice

S. K. Huang, K-D. Lee, K. Hong, et al.

Cancer Res 1992;52:5135-5143.

[CANCER RESEARCH 52, 6774–6781, December 15, 1992]

Pharmacokinetics and Therapeutics of Sterically Stabilized Liposomes in Mice Bearing C-26 Colon Carcinoma[1]

Shi Kun Huang,[2] Eric Mayhew, Syed Gilani, Danilo D. Lasic, Frank J. Martin, and Demetrios Papahadjopoulos

Cancer Research Institute [S. K. H., D. P.] and Department of Pharmacology [D. P.], University of California, San Francisco, California 94143-0128; Departments of Experimental Pathology and Experimental Therapeutics [E. M.] and Department of Nuclear Medicine [S. G.], Roswell Park Cancer Institute, Buffalo, New York 14263; and Liposome Technology Inc., Menlo Park, California 94025 [D. D. L., F. J. M.]

ABSTRACT

Three different liposome types were compared for blood clearance and tissue uptake in mice bearing C-26 colon carcinoma growing either s.c. or in liver. Therapeutic experiments were performed with the liposome preparation showing the highest tumor uptake. Liposomes were composed of solid-phase phosphatidylcholine, either distearoyl phosphatidylcholine or hydrogenated soy phosphatidylcholine, and cholesterol at a 2:1 molar ratio. These liposomes were compared with similar but sterically stabilized liposomes (SL) which, in addition, contained either G_{M1} ganglioside or phosphatidylethanolamine derivatized with poly(ethylene glycol). Pharmacokinetic analysis of drug disposition was based on the areas under the curve for liposome-entrapped ^{67}Ga uptake per gram of tissue up to 96 h following i.v. injection. The highest tissue area under the curve values with both liposome types were obtained in spleen, liver, and tumor. However, the sterically stabilized liposomes gave an area under the curve value 2–3-fold higher in the s.c. tumor and about 2-fold lower in liver and spleen. The therapeutic efficacy of doxorubicin (DOX) and epirubicin (EPI) encapsulated in poly(ethylene glycol)-derivatized phosphatidylethanolamine-containing liposomes was compared with that of free drug at two doses, 6 and 9 (or 10) mg/kg animal weight. Liposomes containing drug were injected either as a single dose, at different times following tumor implantation, or as three weekly doses starting 10 days after implantation. When injected as a single dose, liposome-encapsulated DOX had the maximal effect on tumor growth when injected 6 to 9 days after tumor implantation. When injected as three weekly doses, with treatment starting with a delay of 10 days, tumors which had grown to a size of ~0.05–0.1 cm^3 regressed in groups of animals treated with either liposome-encapsulated drug (SL-DOX or SL-EPI) but continued to grow unabated in untreated mice and in mice receiving either of the free drugs. Survival of tumor-bearing animals treated with either SL-EPI or SL-DOX was significantly prolonged. Animals receiving saline, EPI, or DOX survived a mean of 50, 62, and 49 days, respectively, following tumor implantation. Eight of nine and nine of 10 animals receiving 6 and 9 mg/kg SL-EPI, respectively, survived to 120 days. Ten of 10 animals in both groups receiving 6 and 9 mg/kg SL-DOX survived to 120 days. None of the surviving animals in the SL-EPI and SL-DOX group showed any histological evidence of tumor at the conclusion of the experiment (120 days). These data show that EPI and DOX encapsulated in sterically stabilized liposomes are significantly more active against C-26 colon carcinoma than is free drug. These two drugs appear to have similar potency under the experimental conditions used in this study.

INTRODUCTION

Studies using cancer chemotherapeutic agents such as doxorubicin encapsulated in liposomes have generally shown reduced toxicity (1–3) and in some cases (4) enhanced therapeutic efficacy, compared to administration of free drug, in some animal tumor models. Studies on the tissue distribution of liposome uptake after i.v. administration have indicated that liposome size, membrane rigidity, and surface charge are among the major factors that determine the clearance of circulating liposomes from the bloodstream (5). Liposome uptake by liver and spleen after i.v. injection is positively correlated with increasing liposome size (5). Small unilamellar liposomes have reduced rates of uptake into the liver and spleen, which result in significantly prolonged circulation time (6–9). Small unilamellar liposomes composed of cholesterol and a solid-phase (at 37°C) phospholipid such as DSPC[3] or sphingomyelin have been shown to be cleared slowly from the circulation, compared to liposomes composed of fluid phospholipids (10, 11). In addition, rigid solid-phase liposomes have greatly reduced rates of leakage of aqueous-phase contents (12), which may be advantageous in therapeutic applications.

Studies by Allen and Chonn (13) and earlier work from this laboratory (14) showed that administration of liposomes composed of G_{M1} in combination with solid-phase phospholipid and cholesterol resulted in a pronounced increase in blood residence time with a parallel decrease in uptake by RES. The term "stealth" has been proposed (15) for such long-circulating liposomes.[4] More recently, liposomes containing a poly(ethylene glycol)-derivatized phospholipid have been reported to circulate in the bloodstream of mice and rats for up to several days following injection (16–19). We consider that such liposomes are sterically stabilized by the relevant hydrophilic headgroups on their surface (20).

We have previously reported significantly improved antitumor activity of SL-DOX against mouse colon carcinoma C-26 (21). Although anthracyclines are cytotoxic to this tumor *in vitro* (22), they lack significant activity *in vivo* (23) and thus this model mimics the relative insensitivity of human colon carcinomas to these agents (24). Therefore, studies were undertaken to compare the antitumor effects of SL-DOX with those of SL-EPI in the same C-26 model.

In this study, we have investigated the correlation between tissue and tumor uptake, pharmacokinetics, and therapeutic efficacy using both conventional and sterically stabilized liposomes. Both types were of relatively small particle size (≤100-nm diameter), composed of solid-phase phosphatidylcholine and Chol in the same molar ratio (2:1), but one liposome type included G_{M1} or PEG-PE whereas the other did not. The studies were carried out using the C-26 mouse colon carcinoma implanted s.c. and were undertaken to compare the antitumor effects of SL-DOX with those of SL-EPI in the same

Received 3/30/92; accepted 10/5/92.

The costs of publication of this article were defrayed in part by the payment of page charges. This article must therefore be hereby marked *advertisement* in accordance with 18 U.S.C. Section 1734 solely to indicate this fact.

[1] This work was supported by NIH Grant CA 25526-07A3 and American Cancer Society Grant RD264.

[2] To whom requests for reprints should be addressed, at Cancer Research Institute, Box 128, University of California, San Francisco, CA 94143.

[3] The abbreviations used are: DSPC, distearoyl phosphatidylcholine; AUC, area under the curve; RES, reticuloendothelial system; Chol, cholesterol; CL_p, total clearance of liposomes from plasma; DOX, doxorubicin in solution; EPI, epirubicin in solution; G_{M1}, monosialoganglioside G_{M1}; PEG-DSPE, poly(ethylene glycol) conjugated to distearoylphosphatidylethanolamine; SL-DOX, doxorubicin encapsulated in sterically stabilized liposomes; SL-EPI, epirubicin encapsulated in sterically stabilized liposomes.

[4] Stealth refers to liposomes containing specific glycolipids or polymer-derivatized phospholipids which partially evade rapid recognition and uptake by cells of the reticuloendothelial system. The term has been registered as a trademark by Liposome Technology Inc.

C-26 model. We have also studied the optimal timing for a single liposome injection and compared the therapeutic effects of one *versus* three injections. The results indicate that sterically stabilized liposomes have a pronounced effect in increasing the therapeutic efficacy of both drugs, while also producing a small decrease in acute toxicity.

MATERIALS AND METHODS

Materials. The various chemicals were obtained as follows: DSPC from Avanti Polar Lipids, Inc. (Pelham, AL); G_{M1}, 2-(*N*-morpholino)-ethanesulfonic acid, 3-(*N*-morpholino)propanesulfonic acid, and 8-hydroxyquinoline (oxime) from Sigma Chemical Co. (St. Louis, MO); hydrogenated soy phosphatidylcholine (>98%) from Nattermann Phospholipid GmbH (Koln, Germany); cholesterol (USP) from Croda Inc. (Fullerton, CA); DL-α-tocopherol (USP) from Hoffman LaRoche (Nutley, NJ); and distearoylphosphatidylethanolamine (>98%) from CalBiochem (La Jolla, CA). Distearoylphosphatidylethanolamine derivatized at its amino position with a M_r 1900 segment of poly(ethylene glycol) was synthesized as before (19). Gallium-67 citrate was from New England Nuclear (Boston, MA); deferoxamine mesylate (Desferal) from CIBA-Geigy (Summit, NJ); Dowex resin 50Wx4–400 from Aldrich (Milwaukee, WI); and the acetate form of AG 1X2 resin and Econo-Pac 10 DG desalting columns (polyacrylamide gel) from Bio-Rad (Richmond, CA). All organic solvents used were reagent or high pressure liquid chromatography grade. Commercial epirubicin HCl for injection, distributed by Farmitalia (Milan, Italy), was obtained from a hospital pharmacy and reconstituted according to label instructions. Bulk doxorubicin HCl (USP) also obtained from Farmitalia and was dissolved in 5.4% glucose.

Preparation of ^{67}Ga-labeled Liposomes. Liposomes composed of either DSPC, Chol, and G_{M1} (molar ratio, 2:1:0.2) or DSPC and Chol (molar ratio, 2:1) were prepared by shaking thin lipid films with an isotonic NaCl solution of the components, buffered to pH 7.4 with 2-(*N*-morpholino)ethanesulfonic acid (0.05 mM) and 3-(*N*-morpholino) propanesulfonic acid (0.05 mM), containing 20 mM deferoxamine mesylate at 55°C for 30 min under N_2. After four freezing (−56°C) and thawing (55°C) cycles, the liposomes were extruded (25) through a stack of two Nucleopore membranes, 0.2 μm pore size twice, 0.1 μm pore size twice, and 0.05 μm pore size 7 times. The extruder device was preheated to 55°C, because a high-phase transition phospholipid was used. To obtain high liposome recovery (above 95%) without dilution, unencapsulated deferoxamine was removed by Dowex dry column filtration, followed by centrifugation for 15 min at 3000 × *g*; this was repeated once.

The labeling procedure used was similar to that described by Gabizon and Papahadjopoulos (14). Gallium-67 citrate (100 μCi) was incubated with 1 mg oxine sulfate in 1 ml 0.9% saline for 1 h at 50°C. Liposome suspensions were incubated overnight at 4°C with 2 μCi of ^{67}Ga-labeled oxime/μmol of phospholipid. ^{67}Ga-labeled deferoxamine complex was entrapped in the aqueous interior of liposomes. Unencapsulated ^{67}Ga-labeled oxine and excess oxine sulfate were removed by passing the liposome suspension through an anion exchange resin (AG 1X2, acetate form, 200–400 mesh) and a Dowex column.

The morphology and size of the two types of liposomes used, DSPC/Chol/G_{M1} and DSPC/Chol, were determined by electron microscopy of negatively stained preparations (2% ammonium molybdate staining after hydrophilic treatment of grids with bacitracin). The diameters ranged between 80 and 100 nm. Aggregation was not observed with DSPC/Chol/G_{M1} liposomes, but neutral DSPC/Chol liposomes were aggregated to some extent.

Preparation of Drug-loaded Liposomes. A drug-free liposome intermediate was first prepared by dissolving an appropriate amount of lipid in a 4/1 (v/v) ethanol/dimethoxyethane mixture at 60–65°C. The lipid composition used was PEG-DSPE/hydrogenated soy phosphatidylcholine/Chol/DL-α-tocopherol (molar ratio, 5.5:56.1:38.2:0.2). The lipid solution was injected into a 155 mM ammonium sulfate solution, also at 60–65°C. The hydrated lipid was incubated for 1 h at 60°C. The dispersion was downsized at 60–65°C by sequential extrusion through polycarbonate membranes with the following pore sizes: 0.4, 0.2, 0.1, 0.08, and 0.05 μm. The solvent was removed by diafiltration against ammonium sulfate solution (4 times volume exchange). The nonliposomal encapsulated ammonium sulfate was removed by diafiltration against 10 volume exchanges of 10% sucrose solution containing 200 μM deferoxamine mesylate.

EPI and DOX were encapsulated (to prepare SL-EPI and SL-DOX, respectively) by mixing these ammonium sulfate-containing liposomes with an appropriate amount of epirubicin HCl or doxorubicin HCl dissolved in 10% sucrose containing 200 μM deferoxamine mesylate, pH 7.0. Approximately 50 mM liposomes were incubated with an equal volume of 7 mg/ml drug solution. The incubation took place in a water bath at 60°C with mild agitation. The unencapsulated drug was removed by passing suspensions of liposomes through a Dowex cation exchange resin (50Wx4, 200–400 mesh; 1 g of wet resin/ml of solution; flow rate, 5 ml/min). The drug and lipid concentrations were measured and the product was diluted to the proper final concentration with 10% sucrose, 200 μM desferal mesylate, pH 5.5.

Lipid phosphorus was measured by the calorimetric method of Bartlett (26) following acid digestion. EPI and DOX were quantified by a standard absorbance method (molar extinction coefficient, 13,042 cm^{-1} mol^{-1} at 480 nm). As a quality control, drug encapsulation was measured following separation of unencapsulated drug from liposomes by passage through a Bio-Gel column (A15M, 30 cm x 1.0 cm); liposome-encapsulated and free drug fractions were measured by absorbance as described above. Drug encapsulation was >94% for both SL-EPI and SL-DOX preparations. Liposome suspensions were terminally sterile filtered (0.45-μm sterile Gelman Acrodisc syringe filters) and transferred to sterile, pyrogen-free, 15-ml glass vials that were stoppered and sealed under aseptic conditions. The following specifications were set for drug-loaded preparations: 20 μmol/ml (±20%) total lipid phosphorous; 2 mg/ml (±20%) epirubicin HCl or doxorubicin HCl concentration; and 100 μg/mol (±20%) drug/lipid ratio.

The size of SL-EPI and SL-DOX following preparation ranged between 86 and 88 nm as determined by dynamic light scattering. In the case of SL-EPI the final epirubicin HCl and lipid phosphorus concentrations were 2.02 mg/ml and 21.63 μmol/ml, respectively; the comparable values for SL-DOX were 1.98 mg/ml and 21.04 μmol/ml, respectively.

Animals and Tumor Models. Female BALB/c mice (in the weight range of 17–20 g) from West Seneca Laboratories (West Seneca, NY) were used. Single tumor cells were isolated with 0.25% collagenase, 0.25% Pronase, 0.02% DNase (27), from s.c. C-26 colon carcinomas. The viability of these cells was >85% by trypan blue exclusion. The mice were inoculated under anesthesia with the tumor cells directly into the liver left lobe (2.5×10^5 cells) using a volume of 20 μl or s.c. into the left flank (4×10^5 to 1×10^6 cells) using a volume of 50 μl. C-26 is a relatively undifferentiated carcinoma and normally does not respond to free DOX at doses up to 10 mg/kg animal weight (27), when grown s.c. or in the liver.

Tissue Uptake and Pharmacokinetics. Mice (5/group) were given injections into a tail vein of 0.25 ml liposome-encapsulated ^{67}Ga, containing 0.25 μCi. At selected times after injection, *i.e.*, 0.5, 1, 2, 4, 8, 16, 24, 48, and 96 h, the mice were sacrificed and tissues were excised and counted for ^{67}Ga using a Beckman 8000 gamma counter. Tissues sampled included liver, spleen, kidney, lung, muscle, heart, brain, and tumor. Subcutaneous tumors could be removed and cleaned of any superficial nontumor tissue. In liver, tumors grew in a distinctive nodular form and could be removed easily but it was not possible to remove all nontumor tissue because the tumor can have "pockets" of normal tissue within it. Tumor-bearing mice were used 2–3 weeks after tumor implantation, when the tumor weight were between 0.5 and 2 g. Plasma was prepared from supernatants of heparinized blood removed by heart puncture, under anesthesia, before sacrifice. Blood volumes and correction factors for the blood content of various tissues were determined by examining the tissue distribution 10–15 min after i.v. injection of indium-111 oxine-labeled RBC (28). A Lagrange computer program was applied for pharmacokinetic analysis, to calculate AUC from percentage dose per gram tissue *versus* time after injection and CL_p (29).

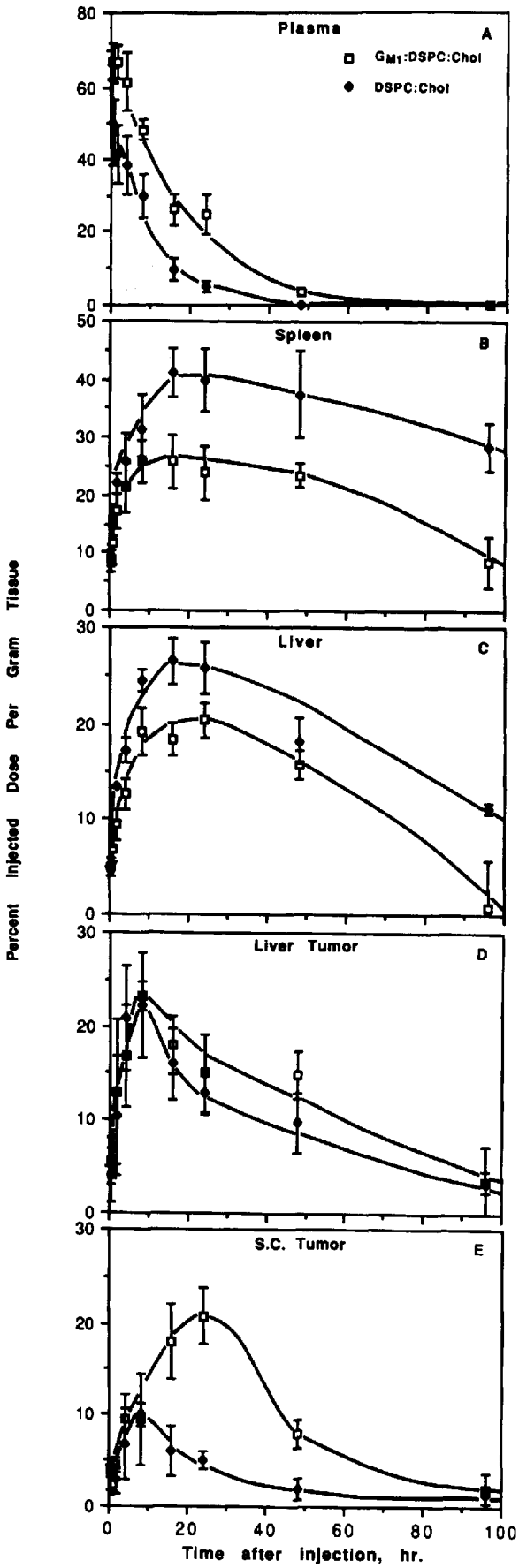

Fig. 1. Plasma pharmacokinetics of ^{67}Ga encapsulated in DSPC/Chol/G_{M1} (2:1:0.2) (□), and DSPC/Chol (2:1) (♦) liposomes. *A*, plasma; *B*, spleen; *C*, liver; *D*, tumor in liver; *E*, s.c. tumor. Samples were taken from 5 mice at each time point (0.5, 1, 2, 4, 8, 16, 24, 48, and 96 h after i.v. injection). The same batch of liposomes was injected on the same day. All data are corrected for blood volume.

Therapeutic Experiments. At day 0, mice were given s.c. injections of C-26 tumor cells in the left flank and were then randomized to groups and numbered. Treatment was started at 1 to 14 days after tumor implantation and consisted of tail vein injection (i.v.) of drug in a volume of 0.2 ml or less per animal. Mice were treated with a saline control, EPI or DOX at 6 mg/kg, or SL-EPI or SL-DOX at 6 or 9 mg/kg. Treatment was repeated weekly to a maximum of three injections. Mice were weighed once or twice weekly. Tumor size was determined by measuring three orthogonal diameters (*a*, *b*, and *c*) of each tumor and the volume was calculated as $(a \times b \times c) \times 0.5$ cm^3 (30). Tumor size was measured twice weekly after tumor injection starting after tumors had reached about 2 x 2 x 2 mm in size. If tumors were not palpable they were counted as 0 volume (no visible tumor). Tumor size was not determined after tumors had diameters greater than about 2 cm (volume of approximately 4 cm^3). The day of death of each mouse was recorded. Experiments were terminated 120 days after injection of tumor, when all remaining mice were sacrificed. All animal studies were done in accordance with protocols approved by the Institute Animal Care Committees at Roswell Park Cancer Institute and University of California, San Francisco. Survival data were analyzed for statistical significance by analysis of variance using NESS statistical software (Keysville, UT).

RESULTS

Tissue Distribution of Labeled Liposomes. The comparative kinetics of ^{67}Ga-labeled DSPC/Chol/G_{M1} and DSPC/Chol liposomes remaining in plasma and uptake by spleen, liver, and tumor tissues are shown in Fig. 1, and the calculated pharmacokinetic parameters are presented in Table 1. The kinetics of liposomes remaining in plasma showed an exponential decay with time. Fig. 1*A* shows that the amount of DSPC/Chol/G_{M1} liposomes remaining in plasma 24 h after injection was 5 times higher than for DSPC/Chol liposomes. By 48 h after injection there were no detectable DSPC/Chol liposomes remaining in plasma, whereas 3.3% of the DSPC/Chol/G_{M1} liposomes were present per ml plasma. The CL_p of both liposomes is compared in Table 1. The CL_p of DSPC/Chol liposomes was almost 2.5 times higher than the CL_p of DSPC/Chol/G_{M1} liposomes.

The uptake in liver and spleen, which are tissues rich in cells of the RES, was higher for DSPC/Chol liposomes, compared to DSPC/Chol/G_{M1} liposomes (Fig. 1, *B* and *C*). At 96 h after injection, there was 29% and 11% of the injected dose per gram in spleen and liver, respectively, for DSPC/Chol liposomes, compared to 8.6% and 0.8% for DSPC/Chol/G_{M1} liposomes (Fig. 1, *B* and *C*), suggesting much greater long term retention of DSPC/Chol liposomes in these tissues. The calculated AUCs of DSPC/Chol liposome uptake were 1.7-fold greater in spleen and 1.4-fold greater in liver, compared to the AUCs of DSPC/Chol/G_{M1} liposomes (Table 1).

The liposome uptake by other normal tissues was much lower than uptake by RES-rich tissues for both DSPC/Chol/G_{M1} and DSPC/Chol liposomes. But, in contrast to liposome uptake by RES, the AUCs of DSPC/Chol/G_{M1} liposomes for other normal tissues (except brain) were much higher than AUCs of DSPC/Chol liposomes (Table 1). The sequence of decreasing liposome uptake levels was spleen, liver, kidney, lung, heart, muscle, and brain and was similar for the two types of liposomes.

Liposome uptake by C-26 tumors implanted s.c. or in the liver (Fig. 1, *D* and *E*) was also investigated. The AUCs of

Values are mean ± SD (n = 5). BALB/c, 6–8-week-old, female mice were implanted with C-26 mouse colon carcinoma directly in liver or s.c., 2 weeks before sacrifice. Tumor weight was 0.5–1.5 g.

Table 1 *Pharmacokinetic analysis of the uptake of DSPC/Chol/G_{M1} and DSPC/Chol liposomes by various tissues*

Liposome composition	Plasma CL_p[a]	AUC[b]								
		Spleen	Liver	Kidney	Lung	Heart	Muscle	Brain	Liver tumor	s.c. Tumor
DSPC/Chol/G_{M1}	0.0837	1974	1299	241.8	141.5	83.25	38.04	2.179	1272	662.2
DSPC/Chol	0.2013	3348	1757	40.48	28.30	31.98	3.945	2.079	983.2	256.2

[a] Total clearance of liposomes from plasma (CL_p = dose/AUC).
[b] Percentage dose (100) per g of tissue *versus* time (h) after injection.

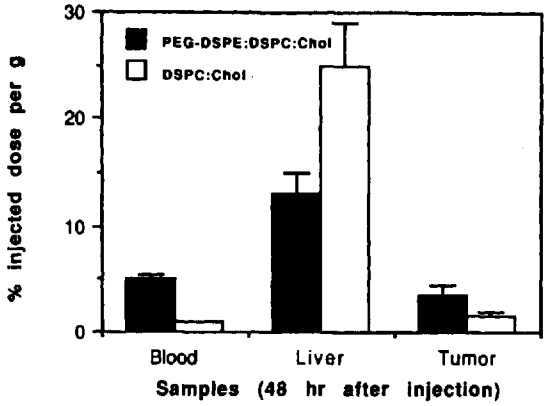

Fig. 2. Comparison of tissue distribution of ^{67}Ga encapsulated in DSPC/Chol/PEG-DSPE (2:1:0.2) and DSPC/Chol (2:1) liposomes in blood, liver, and s.c. implanted C-26 colon carcinoma. Values are mean ± SD (n = 3).

liposome uptake by tumors were markedly higher than the AUCs for normal tissues, except for liver and spleen, the RES-rich tissues (Table 1). The AUC of DSPC/Chol/G_{M1} liposome uptake by tumor was almost 2.5 times higher than that for DSPC/Chol liposome uptake by s.c. tumor (Fig. 1*E* and Table 1) and 1.3 times higher than that for DSPC/Chol liposome uptake by liver tumor (Table 1). The AUC of either DSPC/Chol/G_{M1} or DSPC/Chol liposome uptake by liver tumor was higher than the AUC for s.c. tumors (1.9 and 3.8 times higher for DSPC/Chol/G_{M1} and DSPC/Chol liposomes, respectively).

In separate experiments, shown in Fig. 2, we have studied the tissue distribution of another liposome composition with prolonged circulation time, containing the newly synthesized derivative of poly(ethylene glycol) (19). Although this study included only a few time points, the data show clearly that the DSPC/Chol/PEG-DSPE liposomes behave very similarly to the DSPC/Chol/G_{M1} liposomes. A comparison with the control DSPC/Chol liposomes shows that the DSPC/Chol/PEG-DSPE liposomes accumulated at 48 h in s.c. tumors with a ratio of 2.5 compared with control DSPC/Chol, while they were present in liver at lower amounts than control liposomes, with a ratio of only 0.4 for DSPC/Chol/PEG-DSPE compared with DSPC/Chol (Fig. 2).

Antitumor Activity with One Liposome Injection. Initial studies revealed that treatment of liver tumors, 1 day after tumor inoculation, with DOX at 10 mg/kg entrapped in DSPC/Chol/G_{M1} liposomes resulted in a significant increase in mean survival time of 28% ($P < 0.005$) (Table 2, experiment I). At 10 mg/kg, free DOX treatment produced no significant change in survival time (−2.8%), compared to controls. Treatments with lower doses (3 mg/kg) of either free or liposome-encapsulated DOX resulted in slight 13.1% ($P > 0.05$) or 16.7% ($P < 0.05$) increases in survival time, respectively, compared to control. Plain liposomes and plain liposomes mixed with free DOX did not have any therapeutic effects; the mean survival times were the same as controls. We conclude that treatment with liposome-entrapped DOX at 10 mg/kg was therapeutically superior to the treatment with free doxorubicin (statistical significance, $P < 0.005$).

The effects of DOX entrapped in liposomes composed of DSPC/Chol were also investigated (Table 2, experiment II). Treatment at the lower dose (3 mg/kg) with either free DOX or doxorubicin encapsulated in conventional liposomes did not result in any changes in survival time compared to controls. At 10 mg/kg free DOX treatment resulted in a slightly decreased survival time (−4.2%, $P > 0.05$) compared to control. The same higher dose of DOX encapsulated in DSPC/Chol liposomes resulted in a slight but not statistically significant increase in survival time compared to control (5.1%, $P > 0.05$) (Table 2, experiment II).

In summary, comparison of the two liposome formulations, both encapsulating DOX, revealed that the increase in life span of mice bearing liver tumors after a single treatment with

Table 2 *Comparative therapeutic efficacy of doxorubicin encapsulated in liposomes against C-26 liver tumor in mice*

Treatment	No. of mice/group	Doxorubicin (mg/kg)	Mean survival time (days)	Increase in life span (%)[a]	Significance (P) *versus* controls
Expt. 1: single dose, day 1, liposome composed of DSPC/Chol/G_{M1}					
Untreated (controls)	10	None	25.1 ± 3.9[b]		
Free doxorubicin	8	3	28.4 ± 5.3	+13.1	NS[c]
Free doxorubicin	10	10	24.4 ± 4.6	−2.8	NS
Doxorubicin entrapped in liposomes	9	3	29.3 ± 2.9	+16.7	<0.05
Doxorubicin entrapped in liposomes	10	10	32.3 ± 5.7	+28.7	<0.005
Free doxorubicin and plain liposomes	6	10	24.3 ± 6.2	−3.1	NS
Plain liposomes	6	0[d]	25.3 ± 4.3	−0.8	NS
Expt. II: single dose, day 1, liposome composed of DSPC/Chol					
Untreated (controls)	10	None	31.2 ± 8.3		
Free doxorubicin	8	3	31.3 ± 6.5	+0.3	NS
Free doxorubicin	10	10	29.9 ± 7.4	−4.2	NS
Doxorubicin entrapped in liposomes	9	3	31.6 ± 8.3	+1.3	NS
Doxorubicin entrapped in liposomes	9	10	32.8 ± 7.5	+5.1	NS

[a] % increase in life span = (mean survival time of treated/mean survival time of controls × 100) − 100.
[b] Mean ± SD.
[c] NS, not significant ($P > 0.05$).
[d] Dose of lipid, 100 μmol phospholipid/kg animal weight.

DSPC/Chol/G_{M1} liposomes was significantly higher at both 3 mg/kg and 10 mg/kg, compared to the treatment with DSPC/Chol liposomes or free DOX, showing that sterically stabilized liposomes were more effective therapeutically.

Following these initial experiments, we investigated the optimal timing of a single liposome injection, using DOX encapsulated in liposomes sterically stabilized with PEG-DSPE. In this experiment, we injected i.v. a single dose (10 mg/kg) at day 1, 3, 6, 9, or 14 following the s.c. tumor inoculation. The results are shown in Fig. 3 in terms of mean tumor size (cm^3) for both free DOX (Fig. 3*A*) and SL-DOX (Fig. 3*B*). It is clear from the data shown that the maximal tumor growth inhibition was obtained when liposomes were injected 6 to 9 days after tumor inoculation. The smallest effect was observed when liposomes were injected either 1 day (as in the initial experiments described above) or 14 days after tumor. At all times of injection SL-DOX was superior to free DOX. These results indicate that therapy with SL-DOX is schedule dependent; they were confirmed by survival data obtained from the same experiment. These data are presented in Table 3 and show maximal effect when treatment was between 3 and 9 days after tumor inoculation.

Antitumor Activity with Three Liposome Injections. In order to maximize the antitumor effects observed above, we also performed a series of experiments with PEG-DSPE liposomes encapsulating either DOX or EPI, injected 10, 17, and 24 days after tumor inoculation. The results, presented in Fig. 4, *A* and *B*, compare the mean tumor sizes when treatment was initiated on day 10 after s.c. tumor implantation for seven different treatment groups: saline control, free EPI and DOX at 6 mg/kg, encapsulated EPI at 6 and 9 mg/kg, and encapsulated DOX at 6 and 9 mg/kg. By day 10 tumor volume was approximately 0.05 cm^3. The results show that free DOX (Fig. 4*A*) and free EPI (Fig. 4*B*) only slightly delayed tumor growth compared with the saline control, whereas in mice receiving either encapsulated drug at doses of 6 mg/kg or 9 mg/kg tumors regressed to nonmeasurable sizes (Fig. 4*C*).

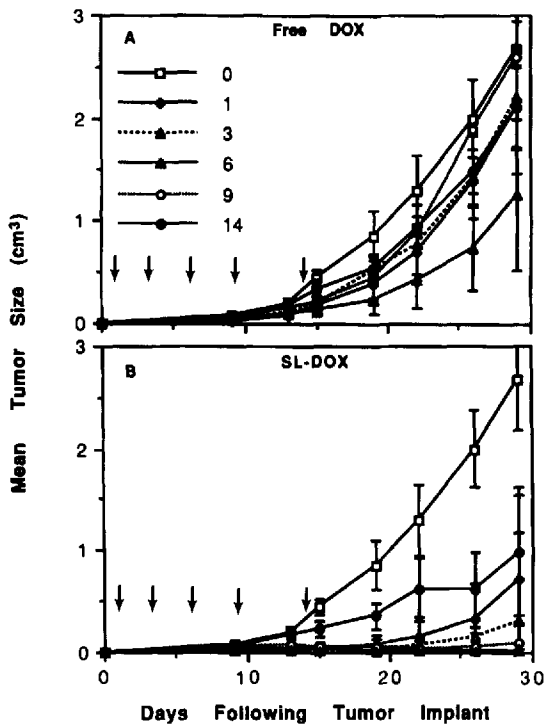

Fig. 3. Relationship between tumor growth kinetics and day of free DOX (*A*) and SL-DOX (*B*) injection. Mice were treated i.v. with a single dose (10 mg/kg) of free DOX (*A*) or SL-DOX (*B*) on various days after C-26 tumor cells were inoculated s.c. Days after inoculation for each treatment group are indicated in the figure. *Arrows* represent the times of injection.

Table 3 *Therapeutic efficacy of single SL-DOX injection following tumor inoculation*

Day of injection following tumor inoculation	Survival time (days)[a]		
	Untreated (controls)	Free-DOX (10 mg/kg)	SL-DOX (10 mg/kg)
0	41.2 ± 10.2 (0/10)		
1		33.0 ± 0.0 (0/10)	61.1 ± 11.5[b] (3/10)[c]
3		50.4 ± 3.9 (0/10)	68.3 ± 13.0[b] (6/10)
6		60.8 ± 7.7 (0/10)	66.0 ± 6.7[b] (5/10)
9		43.4 ± 13.4 (0/10)	65.3 ± 16.3[b] (6/10)
14		43.4 ± 3.1 (0/10)	48.9 ± 7.3 (0/10)

[a] Values are mean ± SD.
[b] Survival time results include only mice dead before day 120.
[c] Numbers in parentheses: number of surviving mice over total number.

Survival data plotted in Fig. 5 indicate that treatment with either DOX or EPI encapsulated in PEG-DSPE liposomes extended mouse survival relative to saline, as did free EPI and DOX treatment. Tumor-bearing animals survived a mean of 50, 62, and 49 days for the saline, free EPI, and free DOX groups, respectively. Eight of nine and nine of 10 animals survived 120 days in the 6 and 9 mg/kg encapsulated EPI groups, respectively. All animals (10 of 10) survived 120 days in both the 6 and 9 mg/kg encapsulated DOX groups. Free EPI or free DOX treatment at a dose of 6 mg/kg did not significantly alter the mean survival time, compared to saline administration ($P < 0.05$). It is therefore clear that both EPI and DOX encapsulated in PEG-DSPE liposomes are highly superior to their corresponding free drug counterparts at equal doses ($P < 0.05$). Treatment with either drug in the encapsulated form at all dose levels tested was quite effective in prolonging survival time.

DISCUSSION

The results of the present studies indicate that liposomes which contained either G_{M1} or PEG-DSPE had a markedly prolonged circulation time in blood, compared to DSPC/Chol liposomes lacking these ingredients. All liposomes were prepared to be of similar homogeneous small size. The CL_p of DSPC/Chol/G_{M1} liposomes was decreased 2.4-fold compared to the CL_p of DSPC/Chol liposomes. It should be noted that the clearance rate of the nonencapsulated liposome label (^{67}Ga-Desferal) is many orders of magnitude faster, with <1% remaining in blood 5 h after injection (14, 21). The same is true for free (unencapsulated) DOX, compared to DOX encapsulated in sterically stabilized liposomes (21, 36). The AUCs of DSPC/Chol/G_{M1} liposome uptake by liver and spleen were considerably less than the AUCs of DSPC/Chol liposomes. The results indicate that liposomes containing the G_{M1} glycolipid achieved prolonged circulating time and slow clearance from blood, presumably because of the reduced rate and extent of uptake by the RES-rich tissues, and this resulted in a significant increase in retention of liposome contents by various other tissues, including tumor (13, 14, 21). While the AUC was 2.5 times higher in s.c. tumor for DSPC/Chol/G_{M1} compared to DSPC/Chol liposomes, the difference comparing SL-DOX with free DOX could be much higher, as indicated by recent studies (21, 42).

The implanted tumors weighed around 100 mg by 1 week and around 1 g by 2 weeks after implantation. For practical reasons, tumors were used in the pharmacokinetic experiments 2 weeks after implantation. Tumors of this size could be easily separated

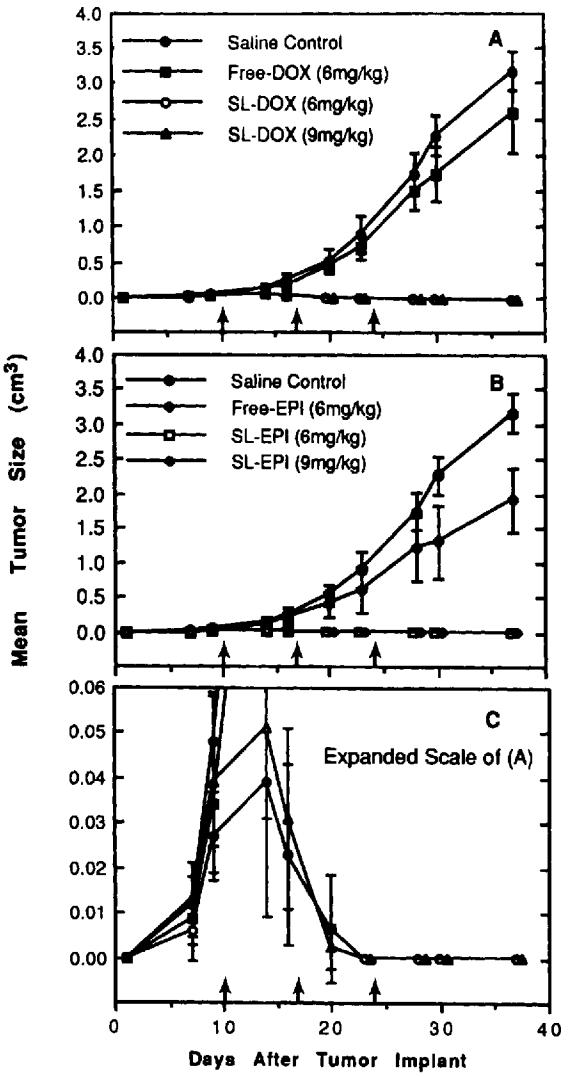

Fig. 4. Effect of DOX (*A* and *C*) and EPI (*B*) formulations on growth of C-26 colon tumor. Mice were given s.c. injections of 1×10^6 C-26 cells day 0. Treatment (bolus i.v. injection) commenced 10 days later and was repeated at 17 and 24 days (*arrows*). The mean tumor size, calculated from data for each mouse in the group, is plotted against time following tumor implantation. Note that tumor size scale in *C* is expanded 50-fold compared to *A* and *B*. Treatment groups are indicated in *A* and *B*. The expanded scale (*C*) represents results obtained with DOX (*A*). The results with EPI were very similar. *Arrows* represent the times of injection.

from most superficial normal tissue. In many types of tumors, the tumor bed is well vascularized and may be better vascularized than some normal tissues (31), increasing the opportunities for liposome delivery to tumor regions with efficient blood circulation. Furthermore, liposomes may escape to the extravascular space surrounding tumor cells, due to defects in the tumor vasculature and discontinuous or absent basement membrane (31). This may be the reason why the AUCs for the liver tumor or s.c. tumor were higher than those for normal tissues. Similar results have been reported by Gabizon and Papahadjopoulos (14). In addition, our results show that the AUC values were >2 times higher for both DSPC/Chol/G_{M1} and DSPC/Chol liposomes in liver tumors compared to s.c. tumors. This may be due to a more direct access of liposomes to tumor regions in liver and also due to "leakage" of DOX from normal liver cells to tumor cells (32, 33).

Initial therapeutic studies, with single dose treatment at day 1, indicated that G_{M1}-containing liposomes entrapping DOX were effective in inhibiting C-26 liver tumor growth (28% prolongation of survival time, $P < 0.005$), whereas liposomes lacking G_{M1} were ineffective. The results also show that the antitumor effects were due to encapsulation of DOX in liposomes, since plain liposomes or plain liposomes mixed with DOX were without therapeutic effects. Free DOX was without therapeutic effect at 10 mg/kg, possibly because of nonspecific toxicity. These results are in accordance with earlier observations that DOX liposomes are less toxic than free DOX (1, 2, 5, 11, 14, 34).

All our subsequent studies were conducted with PEG-DSPE liposomes encapsulating either DOX or EPI because of their superior pharmacokinetic properties and the availability of this lipid in relatively large quantities and at lower cost, compared to G_{M1} ganglioside. Experiments investigating the optimal timing for a single dose (Fig. 3) indicated that the maximal antitumor activity was obtained when there was a delay of 6–9 days between the injections of the tumor cells and liposomes. We interpret this result to indicate that the liposome-derived antitumor effect is not due to the systemic release of the drug but is due to its release from liposomes that localize within the growing tumor mass. The delay is probably due to the necessary development of new vasculature around the tumor mass, which allows for increased localization of liposomes (35).

The next series of experiments involved three different injections of liposomes timed to span the optimal timing observed and discussed above. The antitumor activity of SL-DOX was found to be similar to that of SL-EPI against the mouse colon

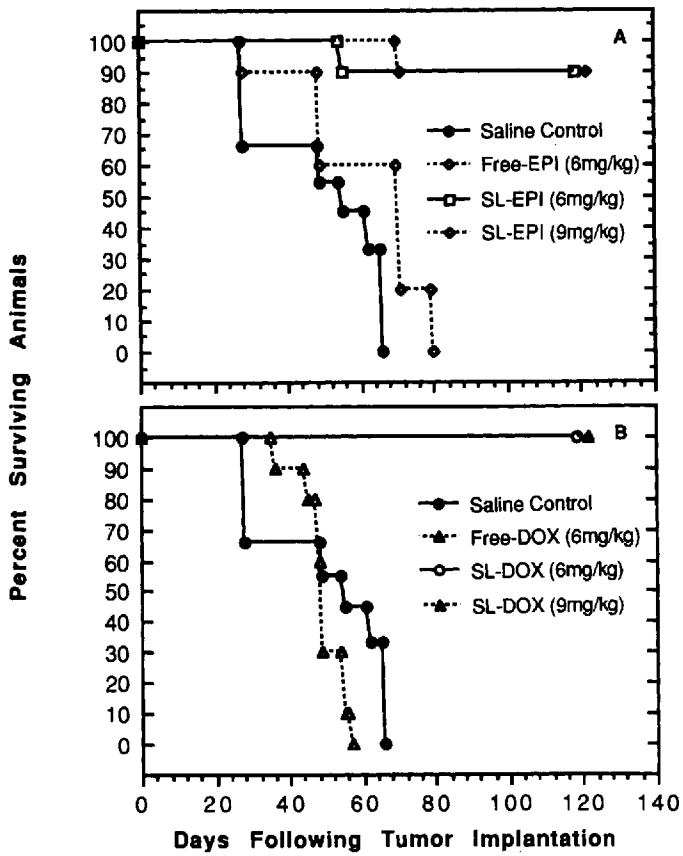

Fig. 5. Effects of EPI (*A*) and DOX (*B*) formulations on survival of mice inoculated with C-26 colon carcinoma. Mice were implanted s.c. with 1×10^6 C-26 tumor cells on day 0. Treatment began 10 days later and was repeated twice for a total of three injections at weekly intervals. The day of death of each mouse was determined and the percentage of surviving mice in each experimental group was plotted against time up to 120 days. Treatment groups are indicated in the figure.

carcinoma C-26 at comparable doses. Both drugs caused regression of tumors which had reached about 0.05–0.1 cm^3 in size, and both increased mouse survival. All animals in the two groups receiving free drug died by day 80. Survival data for animals receiving 6 or 9 mg/kg doses of either SL-DOX or SL-EPI confirm that both are very active against the C-26 tumors. Significantly, the vast majority of animals in the SL-EPI group and all animals receiving SL-DOX were cured of their tumor at the termination of the study.

C-26 tumor is not significantly sensitive *in vivo* to free DOX (34) and therefore can be considered to be a useful model of human disease, since human metastatic colon carcinomas are usually not considered to be sensitive to DOX. It is therefore of interest that, under conditions where free DOX has only slight therapeutic effects, SL-DOX shows enhanced activity. C-26 cells *in vitro* are somewhat sensitive to DOX (50% inhibitory dose, 2×10^{-7} M) (34). Thus, it is reasonable to propose that increased antitumor efficacy could result from increased delivery directly to the tumor cells, local release of DOX from liposomes in the extravascular space within the tumors, local release of DOX from liposomes bound to/in nontumor cells present in the tumor, or release from neighboring normal liver cells.

Previous studies with DOX in liposomes containing phosphatidylglycerol showed that such liposomes were able to inhibit C-26 liver metastases but did not show any antitumor effect on s.c. tumors (34) and showed comparatively little accumulation in implanted tumors (14). Recent studies with sterically stabilized liposomes (containing either phosphatidylinositol, G_{M1}, or PEG-PE) exhibiting long circulation times have shown a >300-fold increase in plasma levels of DOX compared to conventional phosphatidylglycerol liposomes (36) and >10-fold increased uptake by tumors (14, 37). Most significantly, sterically stabilized liposomes have also been shown recently to increase antitumor effects of DOX against s.c. tumors (21, 38), mouse lymphoma (42), and mouse mammary carcinomas (43) and of 1-β-D-arabinofuranosylcytosine against mouse leukemia (40).

A recent study comparing antitumor effects of DOX encapsulated in egg phosphatidylglycerol/egg phosphatidylcholine/Chol, egg phosphatidylcholine/Chol, or DSPC/Chol liposomes in a mouse leukemia system (39) showed higher therapeutic efficacy for DSPC/Chol. In the present work, we have chosen to emphasize the additional stabilizing effect of G_{M1} or PEG-PE over DSPC/Chol, with the latter being the most promising composition known before the report of the new data on steric stabilization (13, 14, 16, 17, 19, 21).

All the earlier studies on liposome-encapsulated DOX except those based on liver metastasis models (1, 2, 5, 11, 14, 20) had shown that a decrease in toxicity was the basis for the observed increase in therapeutic index. The development of sterically stabilized liposomes with long circulation times (13, 14), showing increased localization in implanted tumors (14, 37), enhanced the likelihood of an increased therapeutic effect in addition to the decrease in toxicity. The present study, demonstrating both increased localization and increased antitumor efficacy, is a step in this direction. Furthermore, we have shown that with appropriate dose optimization we can obtain long term survival for most animals. Parallel toxicity studies have shown that the PEG-DSPE-containing liposomes show reduced toxicity for the encapsulated drug (38). These results taken together indicate a substantial increase in the therapeutic index of anthracyclines in rodents. Recent pharmacokinetic results with sterically stabilized liposomes in cancer patients indicate a much prolonged plasma half-life for DOX (41) and increased accumulation of the drug in biopsy samples from these patients' cancers.[5] It is therefore reasonable to predict a substantially increased therapeutic index of these drugs in cancer patients.

REFERENCES

1. Forssen, E. A., and Tokes, Z. A. *In vitro* and *in vivo* studies with Adriamycin liposomes. Biochem. Biophys. Res. Commun., *91:* 1295–1301, 1979.
2. Mayhew, E., Rustum, Y., and Vail, W. J. Inhibition of liver metastases of M5076 tumor by liposome-entrapped Adriamycin. Cancer Drug Delivery, *1:* 43–58, 1983.
3. Rahman, A., Fumagalli, A., Barbieri, B., Schein, P., and Casazza, M. Antitumor and toxicity evaluation of free doxorubicin entrapped in cardiolipin liposomes. Cancer Chemother. Pharmarcol., *16:* 22–27, 1986.
4. Gabizon, A., Goren, D., Fuks, Z., Meshorer, A., and Barenholz, Y. Superior therapeutic activity of liposome-associated Adriamycin in a murine metastatic tumor model. Br. J. Cancer, *51:* 681–689, 1985.
5. Senior, J. H. Fate and behavior of liposomes *in vivo*: a review of controlling factors. Crit. Rev. Ther. Drug Carrier Syst., *3:* 123–193, 1987.
6. Proffitt, R. T., Williams, L. E., Presant, C. A., Tin, G. W., Uliana, J. A., Gamble, R. C., and Baldeschwieler, J. D. Liposomal blockage of the reticuloendothelial system: improved tumor imaging with small unilamellar vesicles. Science (Washington DC), *220:* 502–505, 1983.
7. Abra, R. M., and Hunt, C. A. Liposome disposition *in vivo*. III. Dose and vesicle size effects. Biochim. Biophys. Acta, *666:* 493–503, 1981.
8. Allen, T. M., and Everst, J. M. Effect of liposome size and drug release properties on pharmacokinetics of encapsulated drug in rats. J. Pharmacol. Exp. Ther., *226:* 539–544, 1983.
9. Juliano, R., and Stamp, D. The effect of particle size and charge on the clearance rates of liposomes and liposome encapsulated drugs. Biochem. Biophys. Research Commun., *63:* 651–658, 1975.
10. Allen, T. M., Hansen, C., and Rutledge, J. Liposomes with prolonged circulation times: factors affecting uptake by reticuloendothelial and other tissues. Biochim. Biophys. Acta, *981:* 27–35, 1989.
11. Hwang, K. J., Luk, K. K., and Beaumier, P. L. Hepatic uptake and degradation of unilamellar sphingomyelin/cholesterol liposomes: a kinetic study. Proc. Natl. Acad. Sci. USA, *77:* 4030–4034, 1980.
12. Senior, J., and Gregoriadis, G. Stability of small unilamellar liposomes in serum and clearance from the circulation: the effect of the phospholipid and cholesterol components. Life Sci., *30:* 2123–2136, 1982.
13. Allen, T. M., and Chonn, A. Large unilamellar liposomes with low uptake into the reticuloendothelial system. FEBS Lett., *223:* 42–46, 1987.
14. Gabizon, A., and Papahadjopoulos, D. Liposome formulations with prolonged circulation time in blood and enhanced uptake by tumors. Proc. Natl. Acad. Sci. USA, *85:* 6949–6953, 1988.
15. Allen, T. M. Stealth liposomes avoiding reticuloendothelial uptake. *In:* G. Lopez-Berestein and I. J. Fidler (eds.), Liposomes in the Therapy of Infectious Diseases and Cancer, pp. 405–415. New York: Alan R. Liss, Inc., 1989,
16. Klibanov, A. L., Maruyama, K., and Torchilin, V. P. Amphipathic polyethyleneglycols effectively prolong the circulation time of liposomes. FEBS Lett., *268:* 235–237, 1990.
17. Blume, G., and Cevc, G. Liposomes for sustained drug release *in vivo*. Biochim. Biophys. Acta, *1029:* 91–97, 1990.
18. Woodle, M. C., Newman, M., Collins, L. R., Redemann, C., and Martin, F. J. Improved long circulating (Stealth®) liposomes using synthetic lipids. *In:* V. H. L. Lee (ed.), Proceedings of the 17th International Symposium on Controlled Release Bioactive Material, pp. 77–78. Lincolnshire, IL: Control Release Society, 1990.
19. Allen, T. M., Hansen, C., Martin, F., Redemann, C., and Yan-Young, A. Liposomes containing synthetic lipid derivatives of polyethylene glycol show prolonged circulation half-lives *in vivo*. Biochim. Biophys. Acta, *1066:* 29–36, 1991.
20. Lasic, D. D., Martin, F. J., Gabizon, A., Huang, K. S., and Papahadjopoulos, D. Sterically stabilized liposomes: a hypothesis on the molecular origin of the extended circulation times. Biochim. Biophys. Acta, *1070:* 187–192, 1991.
21. Papahadjopoulos, D., Allen, T. M., Gabizon, A., Mayhew, E., Matthay, K., Huang, S. K., Lee, K-D., Woodle, M. C., Lasic, D. D., Redemann, C., and Martin, F. J. Sterically stabilized liposomes: improvements in pharmacokinetics and anti-tumor therapeutic efficacy. Proc. Natl. Acad. Sci. USA, *88:* 11460–11464, 1991.
22. Mayhew, E., Goldrosen, R., and Vaage, J. Effects of liposome-entrapped doxorubicin on liver metastases of mouse colon tumors 26 and 38. J. Natl. Cancer Inst., *78:* 707–713, 1987.
23. Corbett, T. H., Griswold, D. P., Roberts, B. J., *et al.* A mouse colon tumor model for experimental therapy. Cancer Chemother. Rep., *5:* 169–186, 1975.
24. Wasserman, T. H., Comis, R. L., Goldsmith, M., *et al.* Tabular analysis of the clinical chemotherapy of solid tumors. Cancer Chemother. Rep., *6:* 399–419, 1975.

[5] A. Gabizon, personal communication.

25. Olson, F., Mayhew, E., Maslow, D., Rustum, Y., and Szoka, F. Characterization, toxicity and therapeutic efficacy of Adriamycin encapsulated in liposomes. Eur. J. Cancer, *18:* 167–176, 1982.
26. Bartlett, G. R. Phosphorus assay in column chromatography. J. Biol. Chem., *234:* 466–468, 1959.
27. Corbett, T. H., Griswold, D. P., Robeots, B. J., Peckham, J., and Schabel, F. M. A mouse colon-tumor model for experimental therapy. Cancer Chemother. Rep., *5:* 169–186, 1975.
28. Heaton, W. A., Davis, H. H., Welch, M. J., Mathias, C. J., Joist, H. H., Sherman, L. A., and Siegel, B. A. Indium-111: a new radionuclide label for studying human platelet kinetics. Br. J. Haematol., *42:* 613–622, 1979.
29. Rocci, M. L., Jr., and Jusko, W. J. LAGRAN program for area and moments in pharmacokinetic analysis. Comput. Programs Biomed., *16:* 203–216, 1983.
30. Begg, A. C. Principles and practices of the tumor growth delay assay. *In:* R. F. Kallman (ed.), Rodent Tumor Models in Experimental Cancer Therapy, pp. 114–121. New York: Pergammon Press, 1987.
31. Jain, R. K. Transport of molecules across tumor vasculature. Cancer Metastasis Rev., *6:* 559–593, 1987.
32. Strom, G., Van Gessel, H. J., Steerenberg, P. A., Speth, P. A., Roerdink, F. K., Regts, J., Van Veen, M., and De Jong, W. H. Investigation of the role of mononuclear phagocytes in the transportation of doxorubicin-containing liposomes into a solid tumor. Cancer Drug Delivery, *4:* 89–104, 1987.
33. Liu, D., Mori, A., and Huang, L. Large liposomes containing ganglioside G_{M1} accumulate effectively in spleen. Biochim. Biophys. Acta, *1066:* 159–165, 1991.
34. Mayhew, E., Goldrosen, M., Vaage, J., and Rustum, Y. Effects of liposome-entrapped doxorubicin on liver metastases of mouse colon tumors C-38 and C-26. J. Natl. Cancer Inst., *8:* 707–713, 1987.
35. Hori, K., Suzuki, M., Tanda, S., and Sito, S. *In vivo* analysis of tumor vascularization in the rat. Jpn. J. Cancer Res. Clin. Oncol., *81:* 279–288, 1990.
36. Gabizon, A., Shiota, R., and Papahadjopoulos, D. Pharmacokinetics and tissue distribution of doxorubicin encapsulated in stable liposomes with long circulation times. J. Natl. Cancer Inst., *81:* 1485–1488, 1989.
37. Gabizon, A., Price, D. C., Huberty, J., Bresalier, R. S., and Papahadjopoulos, D. Effect of liposome composition and other factors on the targeting of liposomes to experimental tumors: biodistribution and imaging studies. Cancer Res., *50:* 6371–6378, 1990.
38. Mayhew, E., Lasic, D. D., Babbar, S., and Martin, F. J. Pharmacokinetics and antitumor activity of epirubicin encapsulated in long-circulating liposomes incorporating a polyethylene glycol-derivatized phospholipid. Int. J. Cancer, *51:* 302–309, 1992.
39. Mayer, L. D., Tai, L. C. L., Ko, D. S. C., Masin, D., Ginsberg, R. S., Cullis, P. R., and Bally, M. B. Influence of vesicle size, lipid composition, and drug-to-lipid ratio on the biological activity of liposomal doxorubicin in mice. Cancer Res., *49:* 5922–5930, 1989.
40. Allen, T. M., and Hansen, C. Stealth liposomes: an improved delivery system for 1-β-D-arabinofuranosylcytosine. Proc. Am. Assoc. Cancer Res., *33:* 444, 1992.
41. Gabizon, A., Catane, R., Uziely, B., Kaufman, G., Safra, T., Barenhloz, Y., and Huang, A. A pilot study of doxorubicin encapsulated in long-circulating (Stealth®) liposomes (S-DOX) in cancer patients. Proc. Am. Soc. Clin. Oncol., *11:* 124, 1992.
42. Gabizon, A. Selective tumor localization and improved therapeutic index of anthracyclines encapsulated in long-circulating liposomes. Cancer Res., *52:* 891–896, 1992.
43. Vaage, J., Mayhew, E., Lasic, D. D., and Martin, F. Therapy of primary and metastatic mouse mammary carcinomas with doxorubicin encapsulated in long circulating liposomes. Int. J. Cancer, *51:* 942–948, 1992.

Pharmacokinetics and Therapeutics of Sterically Stabilized Liposomes in Mice Bearing C-26 Colon Carcinoma

Shi Kun Huang, Eric Mayhew, Syed Gilani, et al.

Cancer Res 1992;52:6774-6781.

Clinical Study

Oncology

Oncology 2006;71:159–163
DOI: 10.1159/000106064

Received: September 7, 2006
Accepted after revision: January 13, 2007
Published online: July 17, 2007

A Multicenter Phase II Study of Docetaxel in Combination with Gefitinib in Gemcitabine-Pretreated Patients with Advanced/Metastatic Pancreatic Cancer

Michail Ignatiadis[a] Aris Polyzos[b] George P. Stathopoulos[c]
Evangelos Tselepatiotis[d] Charalambos Christophylakis[e] Kostas Kalbakis[a]
Lambros Vamvakas[a] Athanasios Kotsakis[a] Anna Potamianou[f]
Vassilis Georgoulias[a]

[a]Department of Medical Oncology, University General Hospital of Heraklion, Heraklion, [b]Medical Oncology Unit, Medical Propaedeutic Department, Medical School, University of Athens, 'Laikon' General Hospital, [c]Second Department of Medical Oncology, 'Errikos Dynan' General Hospital, [d]Department of Internal Medicine, 'Patision' General Hospital, and [e]Department of Medical Oncology, 'Iaso General' Hospital, Athens, and [f]First Department of Medical Oncology, 'Metaxa' Anticancer Hospital of Piraeus, Piraeus, Greece

Key Words
Pancreatic cancer · Docetaxel · Gefitinib · Second-line treatment

Abstract
Purpose: To evaluate the efficacy and tolerance of the docetaxel/gefitinib combination as second-line treatment in patients with advanced pancreatic cancer. ***Patients and Methods:*** Twenty-six patients pretreated with gemcitabine-based chemotherapy were enrolled in the study. Docetaxel (75 mg/m^2, i.v.) was administered every 3 weeks for a maximum of 6 cycles and gefitinib (250 mg/day, p.o.) was given continuously. ***Results:*** Five (19.2%) patients achieved stable disease. The median duration of disease control was 4.8 months (range 1–13.2), the median time to disease progression 2.1 months (range 1–7.3) and the median survival time 2.9 months (range 1–13.9). Grade 3/4 neutropenia was recorded in 9 (34.6%) patients, although only 1 (3.8%) developed grade 2 febrile neutropenia. One (3.8%) patient experienced grade 3 fatigue and 2 (7.7%) grade 3 diarrhea. Grade 1/2 rash was observed in 13 (50%) patients. There were no treatment-related deaths. ***Conclusion:*** The docetaxel/gefitinib combination, although safe, has no activity as salvage treatment for advanced pancreatic cancer after failure of gemcitabine-based chemotherapy.

Introduction

Patients with locally advanced or metastatic adenocarcinoma of the pancreas have a poor prognosis, since less than 5% of them survive 5 years after diagnosis despite treatment with single-agent gemcitabine [1, 2]. There is no established salvage regimen for advanced pancreatic cancer in patients failing front-line gemcitabine-based chemotherapy.

Docetaxel (Taxotere) has been evaluated either as a single agent or in combination with other chemothera-

KARGER
Fax +41 61 306 12 34
E-Mail karger@karger.ch
www.karger.com

0030–2414/06/0714–0159$23.50/0

Accessible online at:
www.karger.com/ocl

Vassilis Georgoulias, MD, PhD
Department of Medical Oncology, University General Hospital of Heraklion
PO Box 1352
GR–71110 Heraklion, Crete (Greece)
Tel. +30 2810 392 823, Fax +30 2810 392 802, E-Mail georgoul@med.uoc.gr

peutic agents for the management of advanced pancreatic cancer [3, 4]. Objective responses ranging from 0 to 15% with a median survival of 4–9 months have been reported with single-agent docetaxel [4–6]. Promising results were also observed when docetaxel was combined with other cytotoxic agents [4].

The epidermal growth factor receptor (EGFR) autocrine regulatory pathway has been shown to have a critical role in pancreatic carcinogenesis [7]. EGFR was immunohistochemically detected in 95% of pancreatic adenocarcinomas [8]. Coexpression of EGFR and its ligands in pancreatic tumors has been associated with decreased survival [9]. Therapeutic strategies for pancreatic cancer integrating either tyrosine kinase inhibitors (TKIs) or monoclonal antibodies against EGFR have been evaluated in vitro [10, 11]. Gefitinib (Iressa), an EGFR-TKI, has been shown to enhance the activity of various cytotoxic agents, including taxanes, in preclinical studies [12, 13].

Based on the above data, a multicenter phase II study was conducted by the Gastrointestinal Working Group of the Hellenic Oncology Research Group (HORG) in order to evaluate the feasibility and efficacy of the docetaxel/gefitinib combination in gemcitabine-pretreated patients with unresectable pancreatic cancer.

Patients and Methods

Eligibility Criteria

Patients aged ≥18 years, with histologically confirmed unresectable pancreatic adenocarcinoma and bidimensionally measurable diseases, were enrolled. Other eligibility criteria were: WHO performance status 0–2; adequate bone marrow function (absolute granulocyte count >1,500/μl, platelet count >100 × 10^3/μl) as well as adequate renal (serum creatinine level <1.5 mg/dl) and hepatic (serum bilirubin level <1.5 mg/dl, transaminases <twice the upper limit of normal) function; absence of active infection, history of cardiac disease, or malnutrition (loss of >20% of body weight); no other medical problems severe enough to affect the patient's compliance with the protocol. Previous radiotherapy was allowed provided that the measurable lesions were outside the radiation fields and the dose delivered was limited to <20% of the bone marrow-containing bones; previously irradiated and neurologically stable brain metastases were also allowed. Patients with a second primary tumor other than nonmelanoma skin cancer or in situ cervical carcinoma were excluded from the study. Patients were required to have received a palliative gemcitabine-based chemotherapy regimen as first-line treatment. A treatment-free interval of at least 4 weeks from prior chemotherapy or radiotherapy was required. Biliary obstruction had to be resolved in all patients before inclusion in the study. The study protocol was approved by the Ethics and Scientific Committees of the participating hospitals, and all patients gave written informed consent.

Treatment Protocol and Dose Modifications

Docetaxel (Taxotere; Sanofi-Aventis, Collegeville, Pa., USA) was given intravenously at the dose of 75 mg/m^2, as a 60-min infusion every 3 weeks. All patients received standard premedication with oral dexamethasone and antiemetic treatment with ondansentron. Gefitinib (ZD1839, Iressa; AstraZeneca, Wilmington, Del., USA) was continuously administered orally at the dose of 250 mg once a day. Treatment was continued for a maximum of 6 cycles in patients without disease progression or unacceptable toxicity.

The docetaxel dose was reduced by 20% in cases of febrile neutropenia, grade 4 neutropenia or grade 4 thrombocytopenia and/or if any other severe (WHO grade ≥3) organ toxicity occurred. Docetaxel could be delayed for up to 2 weeks until adverse events resolved or improved to grade 1. In case of recurrent toxicity despite the dose reduction or more than 2 weeks delay for recovery of adverse reactions, the patient was removed from the study.

Gefitinib was interrupted for a maximum of 14 days in case of any severe (WHO grade ≥3) toxicity and was readministered if adverse effects resolved or improved to grade 1 (with the exception of skin toxicity where gefitinib could be administered in the event of toxicity grade ≤2). Dose reduction was not allowed for gefitinib. In case of persistent toxicity for more than 14 days despite gefitinib interruption, the drug was permanently stopped.

Response and Toxicity Assessments

Pretreatment evaluation included a complete medical history and physical examination, a complete blood cell count, a standard biochemical profile, an electrocardiogram and a chest radiograph as well as computed tomography scans of the chest and upper and lower abdomen. Before each treatment cycle, a medical history was taken and a physical examination was performed. A neurologic evaluation was performed every 3 weeks to assess docetaxel neurotoxicity. During treatment, a complete blood cell count was performed weekly and in cases of grade 3/4 neutropenia or thrombocytopenia or febrile neutropenia it was performed daily until hematologic recovery. Biochemical tests were done every 3 weeks. All patients were assessed for response by computed tomography scans every 3 cycles of chemotherapy. Imaging studies were reviewed by an external panel of radiologists. All patients who received at least 1 cycle of treatment were evaluable for toxicity and response. Standard WHO toxicity and response criteria were used [14].

Statistical Methods

The primary endpoint was objective response rate and secondary endpoints were disease control rate [complete remission, partial response or stable disease (SD)], time to tumor progression (TTP) and overall survival (OS).

Sample size was calculated based on Simon's two-stage optimal design [15]. With a 5% α and a 10% β error, a p0 response probability of 4% (which, if true, would mean the study is discontinued at the first stage) and a clinically relevant response probability of 15%, the first-stage sample size was calculated to be 27 patients and maximum sample size 68 patients. All clinical data were centrally collected and analyzed (Clinical Trial Office, Department of Medical Oncology, University Hospital of Heraklion, Crete, Greece), using the SPSS version 10.0 statistical software. Analysis was performed on an intent-to-treat basis. The

duration of response was measured from the day of the first documentation of response to chemotherapy until disease progression. The TTP was measured from study entry until the day of the first evidence of disease progression and the OS from study entry to death or last contact. The probability of survival was estimated by the method of Kaplan and Meier [16] and tested for differences by using the log-rank test. All tests were two-sided and considered significant when the resulting p value was ≤ 0.05.

Results

Patient Characteristics

According to the initial statistical design, the study was terminated after the first 26 patients had been enrolled, due to the absence of objective responses. The characteristics of the 26 patients enrolled in this study are presented in table 1.

Efficacy

In an intent-to-treat analysis, 5 (19.2%) patients had SD. Seventeen (65.3%) patients developed progressive disease and 4 (15.5%) were nonevaluable (2 patients were lost to follow-up and 2 voluntarily withdrew from the study). In the intent-to-treat analysis, the nonevaluable patients were considered as having progressive disease. Among the 5 patients with SD, 3 had a performance status of 0 and 2 a performance status of 1; moreover, 1 achieved a partial response, 1 reached SD and 3 progressed on previous gemcitabine-based treatment.

The median duration of the disease control (SD) was 4.8 months (range 1–13.2), the median time to disease progression 2.1 months (range 1–7.3) and the median OS 2.9 months (range 1–13.9).

Treatment Compliance

A total of 88 cycles were delivered, with a median of 3 cycles/patient (range 1–6). The median interval between treatment cycles was 21 days (range 21–24). Five (19.2%) patients completed 6 cycles of treatment as per protocol. Reasons for treatment discontinuation were mainly disease progression (17 patients), consent withdrawal (2 pa-

Table 1. Patient characteristics

Patients enrolled	26
Age	
Median, years	65
Range, years	31–77
Sex	
Male	17 (65.4%)
Female	9 (34.6%)
Performance status (WHO)	
0	10 (38.5%)
1	14 (53.8%)
2	2 (7.7%)
Organs involved	
Liver	16 (61.5%)
Lung	7 (26.9%)
Retroperitoneal nodes	7 (26.9%)
Peritoneal implants	3 (11.5%)
Bones	2 (7.7%)
Line of treatment	
Second	24 (92.3%)
Third	2 (7.7%)
Response to first-line treatment	
Complete remission	1 (3.8%)
Partial response	4 (15.4%)
Stable disease	10 (38.5%)
Progressive disease	11 (42.3%)

Table 2. Toxicity profile of the docetaxel/gefitinib combination in patients with advanced pancreatic cancer

	Toxicity			
	Grade 1	Grade 2	Grade 3	Grade 4
Anemia	19 (73.1%)	3 (11.5%)		
Neutropenia	3 (11.5%)	3 (11.5%)	5 (19.2%)	4 (15.4%)
Febrile neutropenia	–	1 (3.8%)	–	–
Thrombocytopenia	8 (30.8%)	–	–	–
Nausea/vomiting	2 (7.7%)	1 (3.8%)	–	–
Diarrhea	1 (3.8%)	2 (7.7%)	2 (7.7%)	–
Rash	10 (38.5%)	3 (11.5%)	–	–
Neurotoxicity	1 (3.8%)	–	–	–
Constipation	2 (7.7%)	–	–	–
Fatigue	6 (23.1%)	5 (19.2%)	1 (3.8%)	–

tients) and loss to follow-up (2 patients). Dose reductions were required in 7 (7.9%) cycles because of hematologic (4 cycles) and nonhematologic (3 cycles) toxicity.

Safety

All patients were assessable for toxicity (table 2). Grade 3/4 neutropenia occurred in 9 (34.6%) patients. There was no grade 4 nonhematologic toxicity. Ten (38.5%) patients developed grade 1 and 3 (11.5%) grade 2 rash. There were no treatment-related deaths.

Discussion

Pancreatic adenocarcinoma remains a chemoresistant tumor. Combinations of gemcitabine with other chemotherapeutic or targeted agents have failed to produce superior results over single-agent gemcitabine [2]. Only a recently reported trial in previously untreated patients, which tested the addition of erlotinib, an EGFR-TKI to gemcitabine, demonstrated a marginal though statistically significant increase in median survival of 0.5 months at the expense of increased toxicity, mainly mild rash and diarrhea [17].

The present study evaluated the docetaxel/gefitinib combination in patients with locally advanced/metastatic pancreatic cancer failing 1 or 2 prior chemotherapy regimens. Treatment, which was well tolerated, resulted in a disease control rate of 19.2%, a median TTP of 2.1 months and OS of 2.9 months. In 2 studies in patients with pretreated disease, the combination of celecoxib with infusional 5-fluorouracil and raltitrexed with irinotecan produced a disease control rate of 25% and 48%, respectively, a median TTP of 2 and 4 months, respectively, and a median OS of 3.75 and 6.5 months, respectively [18, 19]. Monotherapy with weekly paclitaxel [20], oxaliplatin [21] and irinotecan [22] did not produce encouraging results in this setting.

To our knowledge, this is the first study that evaluates the activity of docetaxel in combination with gefitinib in the second-line setting in patients with pancreatic cancer. The absence of objective responses to the combination could be related to different factors such as prior chemotherapy, the concomitant administration of the chemotherapeutic agent and gefitinib as well as the dosage of docetaxel. Indeed, front-line docetaxel monotherapy in patients with pancreatic cancer resulted in objective responses at the dose of 100 mg/m^2 but not at the dose of 60 mg/m^2 [4]. For gefitinib, both the dose and the schedule of continuous administration used may not be optimal. Recent preclinical data suggest that a more effective way to combine chemotherapy with EGFR-targeted agents is the sequential administration of a cytotoxic treatment followed by a short-term and intermittent exposure to the EGFR agent [23].

Despite the absence of objective responses in our study, we cannot exclude that there might be a role for the docetaxel/gefitinib combination in a selected group of patients with pancreatic cancer. In non-small cell lung cancer, both EGFR mutations and gene amplification were associated with increased response to gefitinib alone [24]. In pancreatic adenocarcinoma no such EGFR mutations have been reported. Better knowledge of the role of EGFR signaling and EGFR molecular abnormalities in pancreatic carcinogenesis may allow selection of patients that could benefit from gefitinib. Recent studies suggest a role for EGFR-targeted agents in this disease [8, 17]. Thus, a more in-depth understanding of the molecular events leading to pancreatic cancer and better patient selection, based on validated predictive markers, may lead to more substantial improvements in the treatment of this disease.

Acknowledgment

This work was partly supported by the Cretan Association for Biomedical Research (CABR).

References

1 American Cancer Society. Cancer Facts and Figures 2005. http://www.cancer.org.

2 Burris HA 3rd: Recent updates on the role of chemotherapy in pancreatic cancer. Semin Oncol 2005;32(suppl 6):S1–S3.

3 Lutz MP, Van Cutsem E, Wagener T, Van Laethem JL, Vanhoefer U, Wils JA, et al: Docetaxel plus gemcitabine or docetaxel plus cisplatin in advanced pancreatic carcinoma: randomized phase II study 40984 of the European Organisation for Research and Treatment of Cancer Gastrointestinal Group. J Clin Oncol 2005;23:9250–9256.

4 Lopes G, Rocha Lima CM: Docetaxel in the management of advanced pancreatic cancer. Semin Oncol 2005;32(suppl 4):S10–S23.

5 Androulakis N, Kourousis C, Dimopoulos MA, Samelis G, Kakolyris S, Tsavaris N, et al: Treatment of pancreatic cancer with docetaxel and granulocyte colony-stimulating factor: a multicenter phase II study. J Clin Oncol 1999;17:1779–1785.

6 Okada S, Sakata Y, Matsuno S, Kurihara M, Sasaki Y, Ohashi Y, et al: Phase II study of docetaxel in patients with metastatic pancreatic cancer: a Japanese cooperative study. Cooperative Group of Docetaxel for Pancreatic Cancer in Japan. Br J Cancer 1999;80:438–443.

7 Xiong HQ, Abbruzzese JL: Epidermal growth factor receptor-targeted therapy for pancreatic cancer. Semin Oncol 2002;29(suppl 14):31–37.

8 Xiong HQ, Rosenberg A, LoBuglio A, Schmidt W, Wolff RA, Deutsch J, et al: Cetuximab, a monoclonal antibody targeting the epidermal growth factor receptor, in combination with gemcitabine for advanced pancreatic cancer: a multicenter phase II trial. J Clin Oncol 2004;22:2610–2616.

9 Yamanaka Y, Friess H, Kobrin MS, Buchler M, Beger HG, Korc M: Coexpression of epidermal growth factor receptor and ligands in human pancreatic cancer is associated with enhanced tumor aggressiveness. Anticancer Res 1993;13:565–569.

10 Bruns CJ, Solorzano CC, Harbison MT, Ozawa S, Tsan R, Fan D, et al: Blockade of the epidermal growth factor receptor signaling by a novel tyrosine kinase inhibitor leads to apoptosis of endothelial cells and therapy of human pancreatic carcinoma. Cancer Res 2000;60:2926–2935.

11 Bruns CJ, Harbison MT, Davis DW, Portera CA, Tsan R, McConkey DJ, et al: Epidermal growth factor receptor blockade with C225 plus gemcitabine results in regression of human pancreatic carcinoma growing orthotopically in nude mice by antiangiogenic mechanisms. Clin Cancer Res 2000;6:1936–1948.

12 Sirotnak FM, Zakowski MF, Miller VA, Scher HI, Kris MG: Efficacy of cytotoxic agents against human tumor xenografts is markedly enhanced by coadministration of ZD1839 (Iressa), an inhibitor of EGFR tyrosine kinase. Clin Cancer Res 2000;6:4885–4892.

13 Ciardiello F, Caputo R, Bianco R, Damiano V, Pomatico G, De Placido S, et al: Antitumor effect and potentiation of cytotoxic drugs activity in human cancer cells by ZD-1839 (Iressa), an epidermal growth factor receptor-selective tyrosine kinase inhibitor. Clin Cancer Res 2000;6:2053–2063.

14 Miller AB, Hoogstraten B, Staquet M, Winkler A: Reporting results of cancer treatment. Cancer 1981;47:207–214.

15 Simon R. Optimal two-stage designs for phase II clinical trials. Control Clin Trials 1989;10:1–10.

16 Kaplan E, Meier P. Nonparametric estimation from incomplete observations. J Am Stat Assoc 1958;53:457–481.

17 Moore MJ, Goldstein D, Hamm J, Figer A, Hecht J, Gallinger S, et al: Erlotinib plus gemcitabine compared to gemcitabine alone in patients with advanced pancreatic cancer: a phase III trial of the National Cancer Institute of Canada Clinical Trials Group (NCIC-CTG). Proc Am Soc Clin Oncol 2005;23:1.

18 Milella M, Gelibter A, Di CS, Bria E, Ruggeri EM, Carlini P, et al: Pilot study of celecoxib and infusional 5-fluorouracil as second-line treatment for advanced pancreatic carcinoma. Cancer 2004;101:133–138.

19 Ulrich-Pur H, Raderer M, Verena KG, Schull B, Schmid K, Haider K, et al: Irinotecan plus raltitrexed vs raltitrexed alone in patients with gemcitabine-pretreated advanced pancreatic adenocarcinoma. Br J Cancer 2003;88:1180–1184.

20 Oettle H, Arnold D, Esser M, Huhn D, Riess H: Paclitaxel as weekly second-line therapy in patients with advanced pancreatic carcinoma. Anticancer Drugs 2000;11:635–638.

21 Androulakis N, Syrigos K, Polyzos A, Aravantinos G, Stathopoulos GP, Ziras N, et al: Oxaliplatin for pretreated patients with advanced or metastatic pancreatic cancer: a multicenter phase II study. Cancer Invest 2005;23:9–12.

22 Klapdor R, Fenner C: Irinotecan (Campto R): efficacy as third/forth line therapy in advanced pancreatic cancer. Anticancer Res 2000;20:5209–5212.

23 Morelli MP, Cascone T, Troiani T, De VF, Orditura M, Laus G, et al: Sequence-dependent antiproliferative effects of cytotoxic drugs and epidermal growth factor receptor inhibitors. Ann Oncol 2005;16(suppl 4):iv61–iv68.

24 Bell DW, Lynch TJ, Haserlat SM, Harris PL, Okimoto RA, Brannigan BW, et al: Epidermal growth factor receptor mutations and gene amplification in non-small-cell lung cancer: molecular analysis of the IDEAL/INTACT gefitinib trials. J Clin Oncol 2005;23:8081–8092.

Stealth liposomes: review of the basic science, rationale, and clinical applications, existing and potential

Maria Laura Immordino
Franco Dosio
Luigi Cattel

Dipartimento di Scienza e Tecnologia del Farmaco, University of Turin, Turin, Italy

Abstract: Among several promising new drug-delivery systems, liposomes represent an advanced technology to deliver active molecules to the site of action, and at present several formulations are in clinical use. Research on liposome technology has progressed from conventional vesicles ("first-generation liposomes") to "second-generation liposomes", in which long-circulating liposomes are obtained by modulating the lipid composition, size, and charge of the vesicle. Liposomes with modified surfaces have also been developed using several molecules, such as glycolipids or sialic acid. A significant step in the development of long-circulating liposomes came with inclusion of the synthetic polymer poly-(ethylene glycol) (PEG) in liposome composition. The presence of PEG on the surface of the liposomal carrier has been shown to extend blood-circulation time while reducing mononuclear phagocyte system uptake (stealth liposomes). This technology has resulted in a large number of liposome formulations encapsulating active molecules, with high target efficiency and activity. Further, by synthetic modification of the terminal PEG molecule, stealth liposomes can be actively targeted with monoclonal antibodies or ligands. This review focuses on stealth technology and summarizes pre-clinical and clinical data relating to the principal liposome formulations; it also discusses emerging trends of this promising technology.

Keywords: liposomes, stealth liposomes, targeted liposomes, immunoliposomes

Introduction

Clinical medicine possesses an extremely broad range of drug molecules currently in use, and new drugs are added to the list every year. One of the main goals of any treatment employing xenobiotics is to increase the therapeutic index of the drug while minimizing its side-effects. The clinical utility of most conventional chemotherapeutics is limited either by the inability to deliver therapeutic drug concentrations to the target tissues or by severe and harmful toxic effects on normal organs and tissues. Different approaches have been attempted to overcome these problems by providing "selective" delivery to the affected area; the ideal solution would be to target the drug only to those organs, tissues, or cells affected by the disease. Selected carriers, such as molecular conjugates and colloidal particulates, can be suitable for this purpose. Colloidal particulates result from physical incorporation of the drug into a particulate colloidal system such as liposomes, niosomes, micro- and nano-spheres, erythrocytes, and polymeric and reverse micelles. Among these carriers, liposomes have been most studied. Their attraction lies in their composition, which makes them biocompatible and biodegradable. They consist of an aqueous core entrapped by one or more bilayers composed of natural or synthetic lipids. Liposomes composed of natural phospholipids are biologically inert and weakly immunogenic, and they possess low intrinsic toxicity. Further, drugs with different lipophilicities can be encapsulated into liposomes: strongly lipophilic drugs are entrapped almost completely in the lipid

Correspondence:
Maria Laura Immordino
Via Pietro Giuria 9, 10125,
Torino, Italy
Tel +39 011 6707697
Fax +39 011 2367697
Email
marialaura.immordino@unito.it

bilayer, strongly hydrophilic drugs are located exclusively in the aqueous compartment, and drugs with intermediate logP easily partition between the lipid and aqueous phases, both in the bilayer and in the aqueous core (Gulati et al 1998).

Liposomes can be classified according to their lamellarity (uni-, oligo-, and multi-lamellar vesicles), size (small, intermediate, or large) and preparation method (such as reverse phase evaporation vesicles, VETs). Unilamellar vesicles comprise one lipid bilayer and generally have diameters of 50–250 nm. They contain a large aqueous core and are preferentially used to encapsulate water-soluble drugs. Multilamellar vesicles comprise several concentric lipid bilayers in an onion-skin arrangement and have diameters of 1–5 μm. The high lipid content allows these multilamellar vesicles to passively entrap lipid-soluble drugs.

Since liposomes were first developed (around 1980) the related technology has made considerable progress, and several important formulations for the treatment of different diseases are now available commercially or in advanced clinical trials. As shown in Figure 1, the interest in liposome technology and clinical applications remains high, and almost 800 papers and 50 reviews were published in 2005 alone.

The present review will briefly outline the characteristics of liposomes and look at the related problems and solutions proposed, with a focus on advanced liposome formulations. In particular, we revisit the literature relating to high-stability, long-circulating liposomes (stealth liposomes), their field of application, and future trends concerning novel stealth formulations.

Conventional liposomes

Liposomal formulations of several active molecules are currently in pre-clinical and clinical trials in different fields, with promising results. Two of the key problems in drug therapy (biodistribution throughout the body and targeting to specific receptors) can be overcome by using liposomal formulations: liposomes protect encapsulated molecules from degradation and can passively target tissues or organs that have a discontinuous endothelium, such as the liver, spleen, and bone marrow. On intravenous administration, liposomes are rapidly captured by the mononuclear phagocyte system (MPS) and removed from the blood circulation (Scherphof 1985). This behavior has been exploited for efficient delivery of antiparasitic and antimicrobial drugs to treat infections localized in the mononuclear phagocytic system (eg, antimonial drugs against leishmaniasis) (Alving 1978; Agrawal and Gupta 2000; Basu and Lala 2004), or in order to encapsulate immunomodulators in activated macrophages in cancer models, to produce tumoricidal agents.

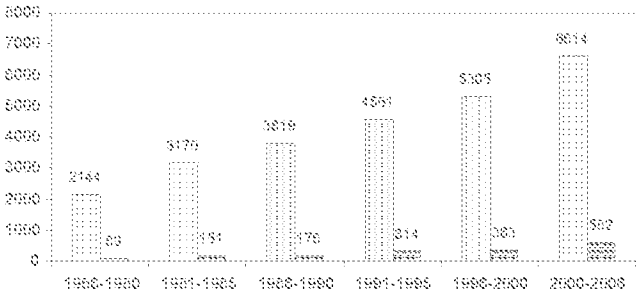

Figure 1 Increase in scientific research on liposomes: papers (vertical line) and reviews (horizontal line) published (total numbers on vertical axis). Data obtained from Ovid-Medline search keyword "liposomes".

However, when the target site is beyond the MPS, efficient liposome uptake by the macrophages, and their consequent removal from circulation, is one of the main disadvantages for possible use of liposomes as drug delivery systems.

Binding of selected serum proteins (opsonins) is the first signal for removal of liposomes: the MPS does not recognize the liposomes themselves but, rather, recognizes opsonins, which are bound to the surface of the liposomes. A limited number of possible opsonizing proteins that affect the fate of liposomes have been identified, eg, immunoglobulins (Patel 1992), fibronectin (Faloone 1986; Patel 1992), beta 2-glycoprotein (Chonn et al 1995), C-reactive protein (CRP) (Volanakis and Narkates 1981), and beta 2-macroglobulin (Murai et al 1995).

Complement components (Patel 1992; Devine et al 1994; Harashima et al 1994) comprise another important system able to recognize liposomes, which evolved as an immediate host defense against invading pathogens. This system acts through initiating membrane lysis and enhancing uptake by the MPS cells (neutrophils, monocytes, macrophages). In particular, the assembly of C5b-9 complexes (membrane attack complex: MAC) of the complement system is able to produces lytic pores, which induce cell lysis or, in the case of liposomes, the release of their contents. The complement-dependent release of liposomal contents appears to be one of the dominant factors in determining the biological fate of liposomes. However, serum components that inhibit the phagocytosis of pathogens or particles, referred to as dysopsonins, have also been identified. Human serum albumin and IgA possess dysopsonic properties and their presence on particle surfaces has been shown to reduce recognition and phagocytosis. A balance between blood opsonic proteins and suppressive proteins has been found to regulate the rate of liposome clearance (Ishida et al 2002).

The instability of liposomes in plasma due to their

interaction with high (HDL) and low density (LDL) lipoproteins is another limitation, since this interaction results in the rapid release of the encapsulated drug into the plasma.

The physicochemical properties of liposomes, such as net surface charge, hydrophobicity, size, fluidity, and packing of the lipid bilayers, influence their stability and the type of proteins that bind to them (Chonn et al 1992; Oja et al 1996). One of the first attempts to overcome these problems was focused on manipulation of lipid membrane components in order to modify bilayer fluidity. Damen et al (2005) demonstrated that incorporation of cholesterol (CHOL), by causing increased packing of phospholipids in the lipid bilayer, reduces transfer of phospholipids to HDL; Senior (1982) demonstrated that liposomes obtained from phosphatidylcholine (PC) with saturated fatty acyl chains (with a high liquid crystalline transition temperature) or from sphingomyelin (SM) are more stable in the blood than liposomes prepared from PC with unsaturated fatty acyl chains.

Several approaches have also involved modulating liposome size and charge, so as to reduce MPS uptake. In general, larger liposomes are eliminated from the blood circulation more rapidly than smaller ones (Senior 1982). Small unilamellar vesicles (SUVs) have a half-life longer than that of multilamellar liposomes (MLVs) (500–5000 nm). This suggests that phagocytes can distinguish between the sizes of foreign particles.

Based on these observations, it is evident that the binding of opsonins to liposomes depends on the size of the liposomes, and that in consequence the enhanced MPS uptake of liposomes by the liver is likewise size-dependent (Harashima et al 1994).

Negatively charged liposomes have a shorter half-life in the blood than do neutral liposomes, although the contrary has also been found (Nishikawa 1990; Funato 1992); positively charged liposomes are toxic and thus quickly removed from circulation (Senior 1987).

The complement system has been reported to be activated by both negatively charged and positively charged liposomes in man (Chonn et al 1991; Marjan et al 1994; Bradley et al 1998; Price et al 2001). Chonn et al (1991) report that, for both human and guinea-pig serum, surface charge is a key determinant in complement-system activation by liposomes: negatively charged liposomes activate the complement system via the classical pathway, while positively charged liposomes activate it via the alternative pathway.

Clinical applications of conventional liposomes

Based on these studies, "conventional" liposomes composed of neutral and/or negatively charged lipids plus CHOL have been prepared; some of these formulations have reached the market (Table 1) or are now entering clinical trials. Ambisome® (Gilead Sciences, Foster City, CA, USA) in which the encapsulated drug is the antifungal amphotericin B (Veerareddy and Vobalaboina 2004), Myocet® (Elan Pharmaceuticals Inc., Princeton, NJ, USA) encapsulating the anticancer agent doxorubicin (Alberts et al 2004), and Daunoxome® (Gilead Sciences), in which the drug incorporated is daunorubicin (Allen and Martin 2004), are the principal examples of such formulations. To obtain stable formulations incorporating a constant amount of drug, various mechanisms are exploited. Ambisome is lyophilized; Myocet is supplied in three separate vials, one containing doxorubicin as dry powder, one a solution of empty liposomes in citric buffer, and the third a solution of sodium carbonate. In this case drug entrapment must be achieved immediately prior to administration. Daunoxome is at present the only pure-lipid MPS-avoiding liposomal formulation; it is available as a stable ready-to-inject liposomal formulation.

By addition of sphingomyelin and saturated fatty acid chain lipids to the lipidic formulation, two commercial liposome formulations have been produced. A novel liposomal formulation of vincristine (Marqibo®, formerly Onco TCS; Inex Pharmaceuticals Co., Vancouver, BC, Canada and Enzon Pharmaceuticals Inc., Bridgewater, NJ, USA), based on sphingomyelin–cholesterol uni-lamellar vesicles, has recently been shown to be efficacious in the treatment of relapsed non-Hodgkin's lymphoma (Anonymous 2004). Inex Pharmaceuticals Co. has in development two further candidate formulations: INX-0125™ (liposomal vinorelbine) (Semple et al 2005) and INX-0076™ (liposomal topotecan) (Tardi et al 2000), also based on the use of sphingomyelin–CHOL mixture.

Another liposomal formulation composed of hydrogenated soy phosphatidylcholine (HSPC) and CHOL and containing lurtotecan has been developed and named OSI-211™ (OSI Pharmaceuticals, Inc., Melville, NY, USA). Clinical results have shown that incorporation of OSI-211 in the acid aqueous core of the vesicle, in addition to providing the known therapeutic advantages of a liposomal carrier, can also favor maintenance of lactone ring closure of lurtotecan (the active form), which increases stability of the active compound, consequently improving its tumor toxicity (Seiden et al 2004; Dark et al 2005).

Table 1 Approved and emerging liposome formulations

Active agent (product name)	Composition	Stealth	Company, year of product marketing	Application	Trial phase
DaunoXome® (daunorubicin)	DSPC/CHOL	no	Nexstar Pharmaceuticals, 1995	Kaposi's sarcoma	Approved
DOXIL®/Caelyx® (doxorubicin)	SoyHPC/CHOL/DSPE-PEG	yes	Sequus Pharmaceuticals, 1997	Kaposi's sarcoma	Approved
Myocet®/Evacet® (doxorubicin)	EPC/CHOL	no	Elan Pharma, 2000	Metastatic breast cancer	Approved
SPI-077 (cisplatin)	SoyHPC/CHOL/DSPE-PEG	yes	Sequus Pharmaceuticals	Head and neck cancer, Lung cancer	Phase I/II
Lipoplatin™ (cisplatin)	SoyPC/DPPG/CHOL	yes	Regulon Inc.	Several cancer type	Phase II/III
S-CKD602 (camptothecin analog)	---	yes	Alza Co	Several cancer type	Phase I
Aroplatin (oxaliplatin analog)	DMPC/DMPG	no	Antigenics Inc	Colorectal cancer	Phase II
Depocyt	DOPC/DPPG/CHOL/triolein	no	SkyePharma 1999	Lymphomatous meningitis	Approved
LEP-ETU (paclitaxel)	DOPE/CHOL/cardiolipin	no	NeoPharm Inc	ovarian, breast, and lung cancer	Phase I
LEM-ETU (mitoxantrone)	DOPE/CHOL/cardiolipin	no	NeoPharm Inc	leukemia, breast, stomach, liver, ovarian cancers	Phase I
LE-SN38 (irinotecan)	DOPE/CHOL/cardiolipin	no	NeoPharm Inc	advanced cancer	Phase I
MBT-0206 (paclitaxel)	DOPE/DO-trimethylammoniumpropane	no	MediGene AG	Anti-angiogenic properties Breast cancer	Phase I
OSI-211 (lurtotecan)	SoyHPC/CHOL	no	Enzon Co	Ovarian cancer Head and neck cancer	Phase II
Marqibo® (vincristine)	DSPPC/CHOL/sphingosine	no	Inex Pharm	Non-Hodgkin's lymphoma	Phase II/III
Atragen® (t-retinoic acid)	DMPC, and soybean oil	no	Aronex Pharm	advanced renal cell ca, acute pro-myelocytic leucemia	Phase I/II
INX-0125 (vinorelbine)	DSPPC/CHOL/sphingosine	no	Inex Pharm	breast, colon and lung cancer	Preclinical Phase I
INX-0076 (topotecan)	DSPPC/CHOL/sphingosine	no	Inex Pharm	advanced cancer	Preclinical
Liposomal-Annamycin®	DSPC/DSPG/Tween	no	MD Anderson CC	breast cancer	Phase II
Ambisome® (amphotericin)	SoyHPC/DSPPC/CHOL	no	Fujisawa USA Inc. and Nexstar Pharm 1997	Fungal infections in immuno-compromised patients	Approved
Nyotran® (nistatin)	DMPC/DMPG/CHOL	no	Aronex Pharm	Fungal infections in immuno-compromised patients	Phase II/III

Two other liposome formulations employing saturated phospholipids have been launched for clinical development: Nyotran® (Aronex Pharmaceuticals, The Woodlands, TX, USA) and Aroplatin® (Antigenics Inc., Lexington, MA, USA). These are multilamellar liposomal formulations consisting of dimyristoyl phosphatidylcholine (DMPC) and dimyristoyl phosphatidylglycerol (DMPG). Nyotran contains nystatin A1, a membrane-active polyene antifungal antibiotic that is structurally related to amphotericin B (Anonymous 1999; Arikan and Rex 2001). Aroplatin is a multilamellar liposomal formulation of cis-bis-neodecanoato-trans-R,R-1,2-diaminocyclohexane platinum (II), a hydrophobic structural analog of oxaliplatin. Aroplatin is in clinical trials for a wide range of tumors and more recently for

advanced solid tumors and B-cell lymphoma (Hau et al 1993; Verschraegen et al 2003; Lu et al 2005).

Aronex Pharmaceuticals has also developed a liposomal-all/trans/retinoic acid formulation (Atragen®) containing tretinoin, dimyristoyl phosphatidylcholine (DMPC), and soybean oil. The formulation has shown efficacy in the treatment of acute promyelocytic leukemia and other retinoid-responsive cancers (Ozpolat et al 2003).

Several interesting liposome preparations have been developed by NeoPharm (NeoPharm Inc., Waukegan, IL, USA including LEM-ETU™, LEP-ETU™, and LE-SN38™). In LEM-ETU, mitoxantrone (Ugwu et al 2005) is encapsulated in multilamellar liposomes (composed of dioleoyphosphatidyl choline [DOPC] and CHOL) after charge interaction with cardiolipin. LEP-ETU (Zhang et al 2005), a liposome-entrapped "easy to use" paclitaxel formulation, recently demonstrated bio-equivalence with Taxol® (Bristol-Myers Squibb, New York, NY, USA) and interesting activity in Phase I trials. This formulation, composed of DOPC, CHOL, and cardiolipin, is capable of carrying paclitaxel in the liposome bilayer at a maximum mole percent of about 3.5%. This is a higher loading capacity than those obtained in our previous studies with paclitaxel (Crosasso et al 2000) and docetaxel (Immordino et al 2003). In LE-SN38™, the active metabolite of irinotecan (7-ethyl-10-hydroxycamptothecin) is encapsulated in PC, CHOL, and cardiolipin liposomes (Zhang et al 2004a). LE-SN38 was in Phase I trials in 2004 (Kraut et al 2004).

Paclitaxel has also been encapsulated in other modern formulations of cationic lipid complexes (MBT-0206) that have been shown to be bounded and internalized selectively by angiogenic tumoral endothelial cells after intravenous injection. A Phase II clinical trial is in progress for candidate drug EndoTAG™-1 (MediGene A.G., Martinsried, Germany) in the treatment of advanced pancreatic cancer (Eichhorn et al 2006).

Cytarabine is an anti-metabolite, anti-neoplastic agent used in clinical applications for acute lymphoid leukemia, myeloid leukemia and meningeal leukemia. DepoCyt® (SkyePharma PLC, London, UK) is a slow-release formulation of cytarabine designed for intrathecal administration in the treatment of neoplastic meningitis due to breast cancer (Jaeckle et al 2001; Bomgaars et al 2004). In DepoCyt, cytarabine is encapsulated in the aqueous compartment of a spherical 20-μm matrix comprised of lipids biochemically similar to normal human cell membranes (phospholipids, triglycerides and CHOL) (also called DepoFoam™) (Mantripragada 2002).

Annamycin (3'-deamino-4'-epi-3'-hydroxy-2'-iodo-4-demethoxy doxorubicin) is a "second-generation" highly lipophilic anthracycline developed by the M.D. Anderson Cancer Center. Its molecular design will be able to avoid the multi-drug-resistance mechanism of tumor cells, and its lipophilicity produces increased encapsulation in liposomes (Priebe and Perez-Soler 1993). Liposomal annamycin (composed of DMPC, DMPG, and Tween) (Andreff and Estey 2004) was in Phase II trials in late 2005 in patients with refractory or relapsed acute lymphocytic leukemia.

Long-circulating liposomes

The use of saturated phospholipids and cholesterol in the formulation of liposome delivery systems cannot fully overcome their binding with serum components, and the consequently decreased MPS uptake of the vesicles: saturation of the MPS with a previous administration of "empty" liposomes may be necessary. Moreover, SUVs possess the disadvantage of low aqueous entrapment volume, and the use of charged liposomes can be toxic. Several different strategies have been developed to overcome these difficulties by coating the surface of the liposomes with inert molecules to form a spatial barrier.

The first strategy studied was the preparation of liposomes mimicking the erythrocyte membrane; in this case the liposome surface was modified with gangliosides and sialic acid derivatives, such as monosialoganglioside (GM1) (Gabizon and Papahadjopoulos 1988; Allen et al 1989). The subsequent step was to increase the hydrophilicity of the liposomal surface by using hydrophilic polymers.

The mechanism whereby steric stabilization of liposomes increases their longevity in circulation has been extensively discussed (Drummond et al 1999). The basic concept is that a hydrophilic polymer or a glycolipid, such as PEG or GM1, possessing a flexible chain that occupies the space immediately adjacent to the liposome surface ("periliposomal layer"), tends to exclude other macromolecules from this space. Consequently, access and binding of blood plasma opsonins to the liposome surface are hindered, and thus interactions of MPS macrophages with such liposomes are inhibited.

By reducing MPS uptake, long-circulating liposomes can passively accumulate inside other tissues or organs. This phenomenon, called passive targeting, is especially evident in solid tumors undergoing angiogenesis: the presence of a discontinuous endothelial lining in the tumor vasculature during angiogenesis facilitates extravasation of liposomal formulations into the interstitial space, where they

accumulate due to the lack of efficient lymphatic drainage of the tumor, and function as a sustained drug-release system. This causes the preferential accumulation of liposomes in the tumor area (a process known as enhanced permeation and retention effect or EPR) (Maeda et al 2001). Liposome formulations do not extravasate from the bloodstream into normal tissues that have tight junctions between capillary endothelial cells. These mechanisms appear to be responsible for the improved therapeutic effects of liposomal anticancer drugs versus free drugs. However, the processes involved in delivery of these carriers and release of active agent, the variability of such processes, and the degree to which the active agent is released into the tumor's extracellular fluid or into tumor cells, are still unknown.

GM1 and glucoronide liposomes

Several glycolipids have been tested in studies of MPS uptake of liposomes after iv injection: the glycolipid GM1 (a brain-tissue-derived monosialoganglioside) significantly decreased MPS uptake when incorporated on the liposome surface, and the formulation remained in blood circulation for several hours. GM1 grafted liposomes with a diameter in the 90–200 nm range have longer blood retention, with consequent accumulation in tumor tissues, than those out of this size range (Liu et al 1992). Large liposomes with a diameter of >300 nm preferentially accumulate in the spleen, whereas those with a diameter of <40 nm probably penetrate the interstitial spaces of the liver.

Unfortunately, the effect of GM1 liposomes in prolonging half-life in bloodstream has been observed only in mouse models. Among different gangliosides, only GM3-grafted liposomes showed increased circulation time in rats, whereas sialic-acid-modified liposomes exhibit prolonged blood retention in both mice and rats.

The degree of macrophage uptake depends on the concentration of GM1 in PC liposomes: a concentration of 10 mol% decreased MPS uptake by 90%. This MPS-avoiding effect was reversed by the removal of the sialic acid moiety, demonstrating the important role played by this molecule in MPS-trapping avoidance (Yamauchi et al 1994).

On the basis of the studies reported above, two possibilities have been proposed to explain the mechanism of MPS avoidance by ganglioside liposomes. (1) Specific moieties (ie, GM1, but not other gangliosides in mice) grafted to the liposome surface reduce opsonization. (2) These moieties bind dysopsonins, reducing recognition by the MPS. It has also been suggested that the topology of carboxyl groups on the liposome surface plays an important role in liposome circulation time. One problem for the extensive use of sialic acid is its cost, a fact which stimulated the investigation of other derivatives, including glucuronic acid (Park et al 1992). Oku and Namba (2005) recently summarized their research on glucuronate-modified long circulating liposomes. Utilizing palmityl-D-glucuronide, they obtained reduced MPS recognition in vitro, reduced hepatic accumulation in vivo, and consequently increased tumor accumulation and thus therapeutic efficacy of adriamicin encapsulated in long circulating liposomes.

Other recent interesting applications of GM-coated liposomes involve their use for oral administration and delivery to the brain. In particular, Taira et al (2004) suggest that among liposomal formulations used as oral drug carriers, those containing GM1 and GM type III have better possibilities of surviving through the gastrointestinal tract. Mora et al (2002) observed higher brain-tracer uptake for GM1 liposomes than for control liposomes in the cortex, basal ganglia, and mesencephalon of both hemispheres; conversely, no significant changes were observed in liver uptake or blood concentration of the tracer.

PEG-coated liposomes (stealth liposomes)

Among the different polymers investigated in the attempt to improve the blood circulation time of liposomes, poly-(ethylene glycol) (PEG) has been widely used as polymeric steric stabilizer. It can be incorporated on the liposomal surface in different ways, but the most widely used method at present is to anchor the polymer in the liposomal membrane via a cross-linked lipid (ie, PEG-distearoylphosphatidylethanolamine [DSPE] as schematized in Figure 2) (Allen et al 1991, 2002).

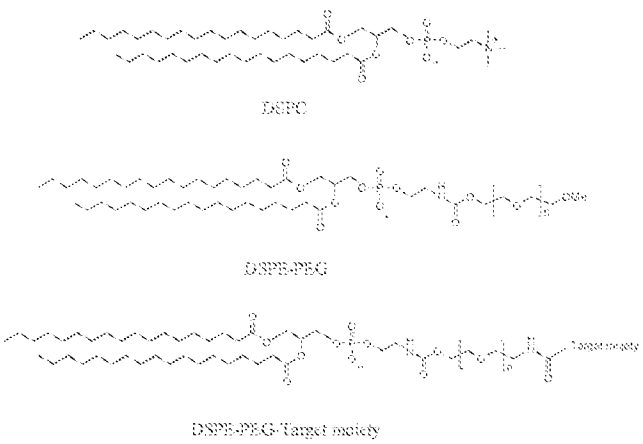

Figure 2 Chemical structures of distearoylphosphatidylcholine (DSPC), distearoylphosphatidylethanolamine after conjugation with poly-(ethylene glycol) (PEG) (DSPE-PEG) and DSPE-PEG linked with a targeting moiety.

PEG (CAS number 25322-68-3) is a linear polyether diol with many useful properties, such as biocompatibility (Powell 1980), solubility in aqueous and organic media (Powell 1980), lack of toxicity, very low immunogenicity and antigenicity (Dreborg and Akerblom 1990), and good excretion kinetics (Yamaoka et al 1994). These properties allow its use in a variety of applications (Harris 1992), including the biomedical field.

Moreover, unlike GM1, molecular weight and structure of PEG molecules can be freely modulated for specific purposes, and it is easier and cheaper to conjugate the polymer with the lipid.

Poly-ethylene glycols have been used to derivatize therapeutic proteins and peptides, increasing drug stability and solubility, lowering toxicity, increasing half-life (Caliceti and Veronese 2003), decreasing clearance and immunogenicity. These benefits have been particularly observed using branched PEG in the derivatization (Monfardini and Veronese 1998). For the most part, reaction with PEG derivatives does not alter the mechanism of action of a therapeutic protein; rather it enhances its therapeutic effect by altering its pharmacokinetics. PEG-adenosine (utilized to treat immunodeficiency), PEG-visomant (human growth hormone), PEG-aspargase (for leukemias), PEG-interferon-alpha (for chronic hepatitis C), PEG-aldesleukin (PEG-IL-2) (an anticancer agent), and PEG-filgrastim (for chemotherapy-induced transferase neutropenia) are the principal PEGylated proteins in clinical use (Mahmood and Green 2005).

Surface modification of liposomes with PEG can be achieved in several ways: by physically adsorbing the polymer onto the surface of the vesicles, by incorporating the PEG-lipid conjugate during liposome preparation, or by covalently attaching reactive groups onto the surface of preformed liposomes.

Grafting PEG onto liposomes has demonstrated several biological and technological advantages. The most significant properties of PEGylated vesicles are their strongly reduced MPS uptake and their prolonged blood circulation and thus improved distribution in perfused tissues. Moreover, the PEG chains on the liposome surface avoid the vesicle aggregation, improving stability of formulations.

Needham et al (1992) demonstrated that the presence of PEG on the liposome surface provides a strong interbilayer repulsion that can overcome the attractive Van der Waals forces, thus stabilizing liposome preparations by avoiding aggregation. In particular, from X-ray analysis of bilayers incorporating PEG1900-lipid, their research showed that the grafted polymer moiety extends about 50Å from the lipid surface and gives rise to strong inter-membrane repulsive forces.

Regarding MPS uptake, Blume et al have found that the increased blood circulation time is due to a reduced interaction with plasma proteins and cell-surface proteins (Blume 1993; Vert and Domurado 2000), although other studies have found no direct evidence of this reduced interaction with plasma components (Johnstone et al 2001). One possible explanation for the reduced interaction is the steric hindrance effect, which is generated by the surface-grafted methoxy-PEG molecules. Complement fixation on PEG-bearing liposomes thus appears to occur in a cryptic location inaccessible to ligation to complement receptors. Another possible contributor to the stealth behavior of such vesicles is competition for CR3 between surface-bound and free-complement proteins iC3b. Furthermore, degradation of surface-bound C3b to fragments inhibiting recognition by phagocytic complement receptors might also explain the anti-phagocytic effect. Studies with freshly isolated macrophages have also indicated the presence of unidentified serum factors (called dysopsonins) that act synergistically with the steric barrier of long circulating particles, thereby further suppressing particle recognition by phagocytic cells (Moghimi et al 1993; Johnstone et al 2001).

A number of reports have indicated that PEG does not completely avoid cumulative uptake by cells of the MPS, and an interesting review updates progress in this area. Moghimi and Szebeni (2003) critically examine the supposed mechanisms that contribute to prolonged circulation times of sterically protected liposomes. They point out that PEGylated liposomes are not completely biologically inert and that there is some evidence the polymer can still induce activation of complement systems: a PEGylated liposomal doxorubicin (PLD) (DOXIL® in the US, Caelyx® in Europe, Schering-Plough, Kenilworth, NJ, USA) (Gabizon and Muggia 1996), is a strong activator of the human complement system, with activation taking place within minutes.

The behavior of PEGylated liposomes depends on the characteristics and properties of the specific PEG linked to the surface. Figure 3 represents the regimens proposed by deGennes, when polymers are attached to the liposome surface, depending on the graft density of the polymer (de Gennes 1980). The molecular mass of the polymer, as well as the graft density, determine the degree of surface coverage and the distance between graft sites.

The most evident characteristic of PEG-grafted liposomes (PEGylated-liposomes) is their circulation longevity,

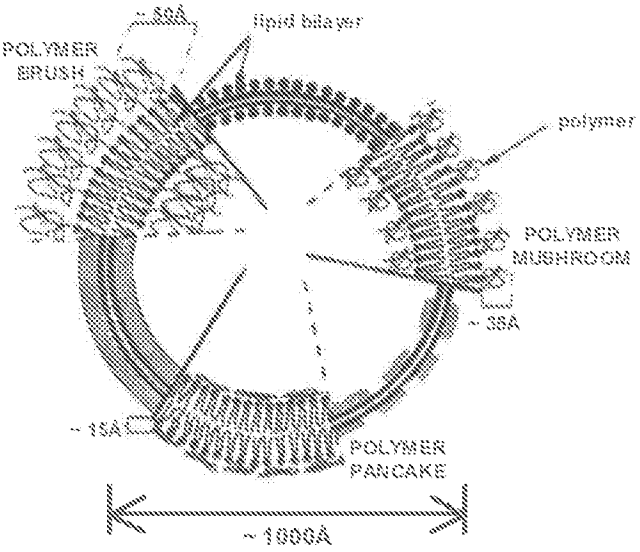

Figure 3 Schematic diagrams of poly-(ethylene glycol) (PEG) configurations regimes (mushroom, brush and pancake) for polymer grafted to the surface of liposome bilayer.

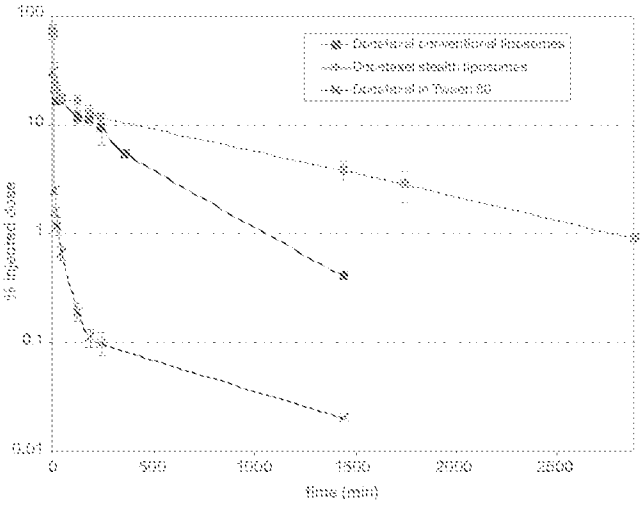

Figure 4 Plasma values obtained from mice iv injected determined by ^{14}C radioactivity associated to docetaxel in Tween 80 (crosses), docetaxel in conventional (black squares), and in PEGylated (gray squares) liposomes.

regardless of surface charge or the inclusion of stabilizing agent such as cholesterol. Figure 4 represents the degree of longevity as determined by a pharmacokinetic evaluation of PEGylated liposomes containing docetaxel (Immordino et al 2003).

The ability of the hydrophilic shell of PEG to avoid aggregation between liposomal particles and to decrease the extent of particle–protein interaction in biological fluids is due not only to the molecular mass of the bound polymer and its uniformity ("molecular cloud") but also to its considerable conformational flexibility (Torchilin et al 1994a). A more rigid polymer, like dextran, grafted to liposomes and used in comparable quantities, does not cause an analogous decrease in liposome-protein interactions.

In liposomes composed of phospholipids and cholesterol, the ability of PEG to increase the circulation lifetime of the vehicles has been found to depend on both the amount of grafted PEG and the length or molecular weight of the polymer (Allen et al 1991). In most cases, the longer-chain PEGs have produced the greatest improvements in blood residence time. For example, Allen et al (1991) reported that blood levels were higher for SM/PC/CHOL/DSPE-PEG liposomes with longer molecular weight PEG (ie, PEG 1900 and PEG 5000) than for liposomes containing PEG-lipid with a shorter chain PEG (ie, PEG 750 and PEG 120). The presence of PEG 2000 doubled the amount of lipid remaining in the plasma compared to formulations containing PEG 350 to 750.

The area of protection of PEG molecules of different molecular weights may be calculated: the calculation is based on a simple approach that was developed by Torchilin and Papisov (Torchilin and Papisov 1994).

A conclusive link has not yet been established between chemical and physical properties of PEG and its ability to extend circulation lifetime. Although the accepted opinion is that PEG increases circulation longevity of drug carriers by reducing or preventing protein binding and/or by inhibiting cell binding/uptake, there is sufficient conflicting data to warrant a reassessment of the mechanism(s) by which surface grafted PEGs improve liposome properties (Allen et al 2002).

Subcutaneous administration of PEGylated liposomes also appears interesting; this administration route could become very important, especially for targeting to the lymph nodes and to achieve sustained drug release in vivo. Targeting liposomes to the lymph nodes for administration of antitumor, antibacterial, and antiviral drugs is of particular interest, and the pharmacokinetics and biodistribution of PEG-DSPE liposomes have been examined after subcutaneous administration (Allen et al 1993). Furthermore, the use of subcutaneously administered liposomes in the field of vaccination and rheumatism, with the aim of prolonging release of antigens or forming a local drug depot, is also in the focus of interest (Babai et al 1999; Corvo et al 1999). PEG-coating on liposomal surface may have a negative effect on lymph node uptake (reduced adsorption by phagocytosis). However, as hypothesized above, lymphatic absorption from the s.c. injection site may increase as a results of the steric stabilization effect and, therefore, the net amount of

liposomes taken up by the lymph nodes may be slightly higher despite the stealth effect. Indeed Oussoren and Storm (1997) compared liposome formulations composed of ePC/CHOL and DPPC/CHOL with or without PEG 2000 or 5000 (5 mol%) with diameter 70 or 150 nm. After s.c. administration, the highest blood peak was in all cases that of the PEGylated liposomes; the authors concluded that "the results did not indicate that steric stabilization of liposome has profound effects on lymphatic uptake".

Although these favorable characteristics have extended clinical applications of PEGylated liposomes, the evidence suggests some caution is needed, and that investigation of some aspects in greater depth, such as multiple dose administration or biodistribution in tumor tissues, is indicated.

Ishida et al (2005) and Laverman et al (2001) recently reported that intravenous injection in rats of PEG-grafted liposomes may significantly alter the pharmacokinetic behavior of a second dose when this second dose is administered after an interval of several days. This phenomenon, called "accelerated blood clearance" (ABC), appears to be inversely related to the PEG content of liposomes. By the same token, an inverse relationship has been observed between dose and magnitude of the ABC effect.

Stealth liposomes are important in cancer treatment for their passive targeting effect, which may lead to preferential accumulation in tumor tissue, but this phenomenon is not fully understood: Stealth liposomes are able to lodge in the interstitial spaces among tumor cells but, once in the tumor area, they locate in the extracellular fluid surrounding the tumor cell without entering it. Thus, to deliver the active form of an anticancer agent, such as doxorubicin or cisplatin, the drug must be released from the liposomes into the tumor extracellular fluid and then diffuse into the cell (Harrington et al 2000a, 2000b). As a result, the ability of liposomes to carry the anticancer agent to the tumor (which depends on their stability) and to release it into the tumor extracellular fluid (depending on membrane composition and fluidity) are equally important factors in determining the anti-tumor effect of liposome-encapsulated anticancer agents. Unfortunately, little is known of the kinetics of drug release from liposomes into the interstitial space: only the free drug can penetrate into the solid tumor, and it is difficult to determinate the ratio between free/liposome-encapsulated drug in the tumor extracellular fluid (Zamboni et al 2004).

Current research on PEG liposomes has concentrated on attaching PEG to the liposome surface in a removable fashion, in order to facilitate subsequent liposome capture by the cells. After PEG liposomes accumulate at the target site through the EPR effect, the PEG coating is detached under the action of local pathological conditions (decreased pH in tumors). New, detachable PEG conjugates have been described (Zalipsky et al. 1999) in which the PEG release process is based on mild thiolysis of the dithiobenzylurethane linkage between PEG and an amino-containing substrate (such as PE).

Clinical applications of stealth liposomes

PEGylated liposomal doxorubicin (PLD) (DOXIL/ Caelyx) was the first and is still the only stealth liposome formulation to be approved in both the USA and Europe for treatment of Kaposi's sarcoma (Krown et al 2004) and recurrent ovarian cancer (Rose 2005). DOXIL/Caelyx is now undergoing trials for treatment of other malignancies such as multiple myeloma (Hussein and Anderson 2004), breast cancer (Robert et al 2004), and recurrent high-grade glioma (Hau et al. 2004). Several studies are under way to investigate the anticancer activities of PLD in combination with other therapeutics, including the taxanes (paclitaxel or docetaxel) (Briasoulis et al 2004; Vorobiof et al 2004), temozolomide (Temodal® Schering-Plough, Kenilworth, NJ, USA) (Awada et al 2004), and vinorelbine (Katsaros et al 2005).

The rigid bilayer of PLD is composed of HSPC, CHOL, and mPEG-DSPE (molecular weight 2000) at a molar ratio of 55:40:5. Liposomes with a mean diameter of 85 nm are able to incorporate doxorubicin at a concentration of 2 mg/mL. The pharmacokinetics is very slow: plasma elimination follows a biexponential curve, with half-lives of 1.5 and 45 hours (median values); in comparison, plasma half-lives are 0.2 hours for free drug, 2–3 hours for Myocet and 5 hours for Daunoxome. Nearly 100% of the drug detected in the plasma after PLD injection was in liposome-encapsulated form; plasma clearance is clearly slow (0.1 L/hour) and the distribution volume small (4 L).

Due to its pharmacokinetic behavior, cardiotoxicity, myelosuppression, alopecia and nausea are significantly decreased with PLD compared with an equi-effective dose of conventional doxorubicin. These bio-distribution characteristics also make skin treatment of localized cancers such as Kaposi's sarcoma possible; on the other hand, due to its reduced clearance, the palmar-plantar skin reaction and stomatitis/mucositis are the chief dose-related toxicities of PLD (Lyass et al 2000).

Another stealth liposome formulation is SPI-077™ (Aiza Corporation, Mountain View, CA, USA), in which cisplatin

is encapsulated in the aqueous core of sterically stabilized liposomes (fully hydrogenated soy HSPC, CHOL, and DSPE-PEG). The stealth behavior of these compounds is evident from their apparent half-life of approximately 60–100 hours. Phase I/II clinical trials have been run to treat head and neck cancer and lung cancer (Kim et al 2001). Although the toxicity profile was promising, the therapeutic efficacy requires improvement (Harrington et al 2001). To obtain the desired balance between encapsulation and release of cisplatin from liposomes, another formulation was evaluated by Alza Corporation (SPI-077 B103); they chose B103, in which HSPC is replaced by unsaturated phospholipids, because of its greater theoretical propensity to release cisplatin (Alza Corporation, data on file). However, Zamboni et al (2004) were not able to detect released cisplatin in in vitro systems, plasma, or tumor extracellular fluid after administration of either stealth formulation of liposomal cisplatin.

Recently, S-CKD602 (Alza Corporation), a PEGylated stealth liposomal formulation of CKD-602, which is a semi-synthetic analog of camptothecin, was submitted for a Phase I trial. After administration of S-CKD602 at doses of 0.5 mg/m^2, the plasma AUC was 50-fold that of non-liposomal CKD-602; S-CKD602 showed minimal toxicity and interesting activity (Zamboni et al 2005).

Lipoplatin™ (Regulon Inc. Mountain View, CA, USA) is another liposomal cisplatin formulation composed of dipalmitoyl phosphatidyl glycerol (DPPG), soy PC, CHOL, and mPEG2000-DSPE. Its reported half-life is 60–117 hours, depending on the dose (Boulikas et al 2005; Stathopoulos et al 2005). The study found that Lipoplatin has no nephrotoxicity up to a dose of 125 mg/m^2 every 14 days without the serious side effects of cisplatin.

Mitoxantrone (Novantrone®, Wyeth Lederle, Madison, NJ, USA) is a drug used for the treatment of acute myeloid leukemia, multiple sclerosis, and prostate cancer. Despite the promising early results of a PEGylated mitoxantrone formulation (Gabizon-Hutcheon et al 1999) the only currently existing formulations with lipids and cardiolipine are in clinical trials (as described above).

PEG alternatives

Despite the well-developed chemistry of PEG coupled to pharmaceuticals, the search for alternative polymers is ongoing; this might be explained both by the patent limitations on PEG and its derivatives, and by the hope of achieving even better control over the properties of modified drugs and drug carriers. Suggested theoretical models for modified protein behavior, and the experimental data available, enable some general requirements for polymers to confer steric protection to drug carriers to be formulated. These polymers should be soluble, hydrophilic, have highly flexible main chain, and high biocompatibility. Synthetic polymers, such as poly(vinyl pyrrolidone) (PVP) and poly(acryl amide) (PAA), are the most prominent examples of other potentially protective polymers (Torchilin et al 1994b, 1994c, 1995). Liposomes containing DSPE covalently linked to poly(2-methyl-2-oxazoline) or to poly(2-ethyl-2-oxazoline) also exhibit extended blood circulation time and decreased uptake by the liver and spleen (Woodle et al 1994). Similar observations have been reported for phosphatidyl polyglycerols (Maruyama et al 1994).

More recent papers describe long circulating liposomes prepared using poly[*N*-(2-hydroxypropyl) methacrylamide] (Whiteman et al 2001), amphiphilic poly-*N*-vinylpyrrolidones (Torchilin et al 2001), L-amino-acid-based biodegradable polymer–lipid conjugates (Metselaar et al 2003), and polyvinyl alcohol (Takeuchi et al 2001). All groups of polymer-coated liposomes reported have been found to extend blood circulation time, while liver capture was diminished. These results are comparable with those for PEG-liposomes; the efficacy of the steric effect quite naturally depends on the quantity of incorporated polymer. The prolonged circulation time of polyvinyl alcohol-(molecular weight: 20000) coated liposomes (1.3 mol% coating) was comparable with that of a stealth liposome prepared with 8 mol% of DSPE–PEG2000.

Also, L-amino-acid-based polymers also showed prolonged circulation time and reduced uptake by the MPS, to the same extent as DSPE–PEG2000. Furthermore, these polymers appear to be attractive alternatives for designing long-circulation liposomes, because they have the advantage of being biodegradable.

Targeted liposomes

To increase liposomal drug accumulation in the desired tissues, producing higher and more selective therapeutic activity, the use of targeted liposomes has been suggested. This involves the coupling of targeting moieties capable of recognizing target cells, binding to them, and inducing the internalization of liposomes or encapsulated drugs. Targeting moieties include monoclonal antibodies (MAb) or fragments, peptides, growth factors, glycoproteins, carbohydrates, or receptor ligands (Lopes De Menezes et al 1999; Sapra and Allen 2003; Medina et al 2004). Targeted liposomes offer various advantages over individual drugs targeted by means of polymers or antibodies. One of the most compelling

advantages is the dramatic increase in drug amount that can be delivered to the target. Furthermore, the number of ligand molecules exposed on the liposome surface can be increased, improving ligand avidity and degree of uptake. Immunoliposomes also provide a "bystander killing" effect, because the drug molecules can diffuse into adjoining tumor cells.

In order to behave in this fashion, immunoliposomes are built so as to be long-circulating and non-immunogenic, using the stealth technique. Briefly, a PEG (MW 3400) derivative of PE or DSPE containing a maleimide group at the end of the PEG chain is mixed into the liposome formulation (Figure 2). After liposome preparation, reduced thiol groups of Fab or scFv fragments are joined via surface linkage to the maleimide group of the aforementioned PEG-liposome, obtaining a stable thioether bond. This method for preparing immunoliposomes starting from preformed liposomes is the most widely used. Alternatively, commercially available doxorubicin-loaded long-circulating liposomes (DOXIL) have been modified by post-insertion of a monoclonal antibody, MAb, modified with DSPE–PEG conjugate, in which the free PEG terminus is activated with the p-nitrophenylcarbonyl group, has been inserted into preformed liposomes (Lukyanov et al 2004). Therapeutic targets and immunoliposomal compositions are reported in Table 2.

At present, the only immunoliposome formulation undergoing clinical trials is the PEGylated liposome DXR targeted with the F(ab')2 fragment of the human MAb GAH, which is able to recognize gastric, colon, and breast cancer cells (Matsumura et al 2004). Another important target antigen is the p185 HER2/*neu* glycoprotein (HER2), a member of the epidermal growth factor receptor family. This antigen is suitable for targeting because, although HER2 is expressed in healthy tissue, overexpression is unique to tumors, specifically some human breast cancers (25%–30% of cases), gastric, colon, ovarian, and non-small-cell lung carcinoma (Baselga and Mendelsohn 2000).

The monoclonal antibody anti-HER2 trastuzumab (Herceptin®, Genentech Inc., Vacaville, CA, USA) was the first humanized Mab approved by the FDA and in the EU as monotherapy for metastatic breast cancer. This antibody is widely used in breast cancer, both alone and in combination with chemotherapy agents, and two recent papers describe the GMP- compliant process for producing the F5 single-chain Fv antibody fragment-PEG-lipid conjugate; therapeutic assemblies are made by post-insertion into preformed doxorubicin-encapsulating liposomes (Nellis et al 2005a, 2005b).

In the last few years, antibody-based therapeutics have emerged as important components of therapies for an increasing number of human malignancies (Adams and Weiner 2005) and it is expected that several immunoliposomes will be in trials in the near future.

The main therapeutic area for immunoliposome application is against cancer, but interesting papers describe other applications, such as reducing hemorrhagic transformation after thrombolytic therapy with tissue plasminogen activator in cerebral ischemia (Asahi et al 2003).

Other ligands have been used to specifically target stealth liposomes to receptors over-expressed in cancer cells. Folic acid, which has been used for liposome-specific targeting of DXR, daunorubicin, cisplatin, and other drugs, is one of the most extensively studied (for a recent review (Stephenson et al 2004)) and it has been proposed for boron neutron capture therapy (Stephenson et al 2003). Transferrin is a popular ligand for specific delivery of anticancer drugs, proteins and

Table 2 Targeted liposomes in advanced phase of trial

Targeted with	Encapsulated drug	Disease	References
Anti-HER2 (trastuzumab)	DOXIL®	breast, ovarian cancer	(Park et al 2002)
Anti-EGF	doxorubicin, vinorelbine, methotrexate, DNA	solid tumors	(Mamot et al 2003)
Anti CD19	vincristine	lymphoma	(Theng et al 1999)
Anti CD22	doxorubicin	anti-B-cell lymphoma	(Lundberg et al 2000)
Anti CD19	imatinib	ALL	(Harasa et al 2004)
Anti-beta1 integrin	doxorubicin	several cancers	(Sugano et al 2000)
Anti GD2	doxorubicin	neuroblastoma	(Pastorino et al 2003)
GAH MAb	doxorubicin	gastric, colon and breast cancer	(Hamaguchi et al 2004)
Anti-EGF receptor	RNA	brain cancer	(Zhang et al 2004b)

genes to malignant cells (Ishida et al 2001) as well as for boron neutron capture therapy (Maruyama et al 2004).

Sigma receptors (subtype of opioid receptor) have recently been proposed as an interesting target for different malignancies (breast, melanoma, prostate). An ansamide-derivatized stealth liposomal formulation (DXR) showed high specific toxicity and superior therapeutic effect versus untargeted liposomes (Banerjee et al 2004) and recently haloperidol-associated stealth liposomes can efficiently target genes to sigma receptor overexpressing breast cancer cells (Mukherjee et al 2005).

Further, peptides involved in cell-to-cell interactions have been used as targeting agents for liposomes (now in preclinical trials). Targeting with L-peptide increased liposomal DXR toxicity on nasopharyngeal cells (Lee et al 2004), while vasoactive intestinal peptide 28-mer conjugated with (^{99m}Tc) loaded liposome increased the imaging of breast cancer cells (Dagar et al 2003). In addition, stealth liposomes (DXR or 5-FU) have been targeted through RGD-sequence peptides to the integrin of tumor vasculature, demonstrating interesting activity on neuroblastoma, melanoma, and colon in vivo models. Stealth liposomes conjugated with sequences of an angiogenic homing peptide (for instance GPLPLR, APRPG) were able to suppress tumor neovasculature in colon, melanoma and sarcoma cells growing in mice (Kondo et al 2004; Asai and Oku 2005).

Liposome applications

Cationic liposomes for gene delivery

Among various synthetic carriers currently in use in gene therapy, cationic liposomes are the most suitable transfecting vectors. Gene encapsulation in liposomal vesicles allows condensation of DNA plasmid into a highly organized structure, and protects DNA against degradation during storage and in the systemic circulation of the gene encoding a therapeutic protein. Moreover, structural organization of the gene-delivery system must bypass the cell membrane and facilitate endosomal escape, avoiding DNA degradation in the lysosomal compartment (Figure 5).

Numerous cationic lipids have been tested in the formulation of liposomes for gene delivery (the structural formulas of some of them are presented in Figure 6). Transfection efficiency is strongly affected by the presence of three components in the structure of these lipids: a positively charged head-group that interacts with negatively charged DNA, a linker group (which determines the lipid's chemical stability and biodegradability), and a hydrophobic region to anchor the cationic lipid into the bilayer. Among these, the most often used are N-[1-dioleyloxy)propyl]-N,N,N-trimethylammonium (DOTMA) and dioleoylphophatidylethanolamine (DOPE) in a 1:1 phospholipid mixture (Lipofectin®, Invitrogen Corporation, Carlsbad, CA, USA). Other commercially-available lipids are 2,3-dioleyloxy-N-[2(sperminecarboxamido)ethyl]-N,N-dimethyl-1-propanammonium trifluoroacetate (DOSPA or LipofectAMINE®), 1,2-bis(oleoyloxy)-3-(trimethylammonio)propane (DOTAP), 1,2-dimystyloxypropyl-3-dimethylhydroxyethyl ammonium bromide (DMRE), 3β[N-(N',N'-dimethylaminoethane)-carbomoyl] cholesterol (DC-CHOL), and dioctadecylamino-glycyl-spermine (DOGS or Transfectam®) (Mahato 2005).

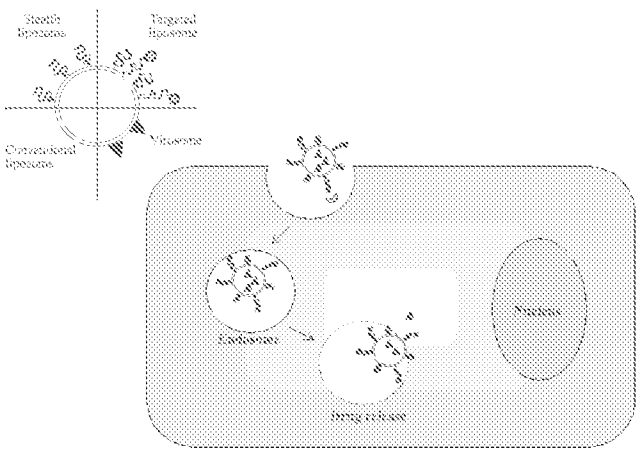

Figure 5 Schematic representation of conventional, stealth, targeted liposomes, and virosomes. Among different mechanism of intracellular uptake of liposomes, endocytosis of targeted liposomes is exemplified.

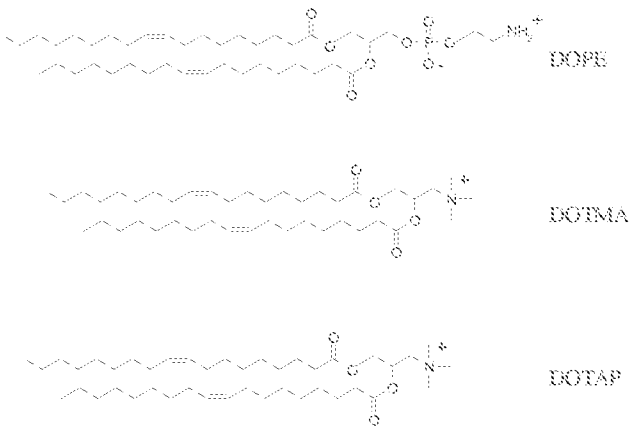

Figure 6 Chemical structures of the cationic lipids: dioleoylphosphatidylethanolamine (DOPE), N-(1- dioleyloxy)propyl]-N,N,N-trimethylammonium (DOTMA) and 1,2-bis(oleoyloxy)-3-(trimethylammonio)propane (DOTAP).

Nevertheless, the clinical use of cationic liposomes is limited by their instability, rapid clearance, large particle size, toxicity at repeated administration, and induction of immunostimulation and complement activation. Water-soluble lipopolymers, obtained by conjugating different fatty acid chains to branched polethylenimine (PEI) of 25 kDa or above, have been shown to be effective for gene delivery; they can be delivered into the cytoplasm after endosomal disruption. Similarly, phosphatidyl ethylene glycol (PhosEG) has been linked to the amino group of branched PEI (Mahato 2005).

On the other hand, PEGylation of cationic liposomal vesicles is a promising alternative way to overcome these problems, prolonging circulation time in vivo and increasing accumulation at the disease site, even if the transfecting efficiency might be significantly reduced.

In liposomes composed of a cationic lipid (DOTAP, DOGS, dimethyldioctadecylammonium bromide-DDAB), a neutral lipid (DOPE) and a phospolipid derivative of PEG (PEG-PE), complexing 18-mer phosphothioate as a model for active oligodexyribonucleotide (ODN), surface modification with a relatively large amount of PEG (5.7 mol%) has been showed to improve ODN loading without losing structural activity or stability of the resulting complexes, retaining size without vesicle aggregation. Moreover, the hydrophilic shell of PEG enhances the in vitro stability by evading mononuclear phagocyte clearance, and retains a high level of the originally loaded ODN in the complex after plasma incubation. Only after modification of PEG cationic liposomes with targeting agents can cytoplasmatic delivery of DNA material be observed. The PEG-modified complex conjugated anti-HER2 F(ab') dramatically enhanced cell uptake, increasing diffuse cytoplasmatic and nuclear localization of ODN in SK-BR-3 cells (Meyer et al 1998).

In liposomes composed of DODAC/DOPE, the inclusion of 5 mol% of PEG lipid conjugate did not inhibit uptake by the cell membrane of lipid/DNA complex, but substantially modified the ability of the cationic liposomal carrier to disrupt the endosomal membrane. Endosomal escape into the cytoplasm depended on the acyl chain of the lipid complex and on the molecular weight of the PEG. Optimizing the desorbtion rate of PEG-lipids may be one approach to overcoming the inhibitory effect on intracellular delivery of plasmid (Song et al 2002).

To contrast the low transfection efficiency of PEG-modified cationic liposomes due to the absence of a net positive charge on the vesicle surface, a series of cationic PEG-lipids with one or more positive charges have been synthesized and designed for post-insertion in preformed stabilized plasmid-lipid particles (Figure 7). Incorporation of cationic-poly(ethylene glycol)-lipid conjugates (CPL4) in DOPE/DODAC/PEG-CerC20 liposomes resulted in both improved uptake into BHK cells and dramatically enhanced transfection potency in the presence of Ca^{2+}, which assists in destabilizing the endosomal membrane following uptake. However, in this type of liposomal preparation, aggregation of vesicles was observed, probably due to formation of H-bonding between the amino and carbonyl groups present in the distal head-group at the end of the PEG chain (Palmer et al 2003). In order to optimize CLP-liposomes for systemic delivery, the length of PEG linker in the CPL can be modulated. When the PEG3400 linker extended beyond the PEG-CerC20 "cloud" was employed for liposomal insertion, charged liposomal systems were produced that rapidly cleared from circulation; it was suggested that a shorter PEG linker might be used, such as PEG1000, allowing the PEG-CerC20 to shield the positive charge of CPL. Moreover, PEG-CerC20 can be designed to slowly dissociate at the disease site, achieving exposure of the CPL at the target area with retention of long-circulation properties and interaction between liposomes and targeting cell (Chen et al. 2004).

Overall, the most suitable use of PEG is as a tether for a specific ligand on the surface of these systems, in order to obtain a target-specific gene delivery facilitating internalization in cells and endosomal escape. Cell-penetrating peptides (CPP), such as Trans-activating transcriptional activator (TAT), homeodomain of antennapedia (Antp), herpex simplex virus type I protein VP22 and transportan, have been reported to guarantee direct cytosolic delivery when coupled with several carriers, including liposomes. Multiple TATp molecules can be attached on the surface of liposomes via the spacer group of p-nitrophenylcarbonyl-PEG-phosphatidylethanolamine.

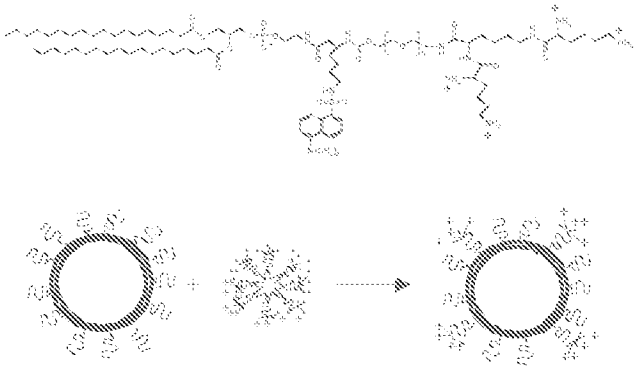

Figure 7 Structure of dansylated cationic poly(ethylene glycol)-lipid (CPL_4) and schematic representation of the post-insertion method for the production of CPL_4 lipocomes (redrawn from Palmer et al 2003).

TATp-liposomes-DNA complexes were found to be capable of transfection of both normal and cancer cells in vitro and in vivo with lower cytotoxicity that the commonly used lipid-based gene delivery systems (Gupta et al 2005).

Liposomes for diagnostic imaging

Actively or passively targeted liposomes can be used as carriers for contrast agents to increase the signal difference between areas of interest and background, and to specifically localize the contrast moieties in the target tissues or organs. The versatility of liposomal vesicles to carry different types of compound in the bilayer or in the aqueous compartment makes them suitable for all contrast procedures, including gamma-scintigraphy, magnetic resonance imaging (MRI), computed tomography imaging (CT), and sonography. Using liposomes in diagnostic imaging leads to several advantages, owing to their capability to incorporate multiple contrast moieties, to specifically deliver the agent to the target area, and to enhance the contrasting signal.

In order to incorporate diagnostic agents (^{111}In, ^{99}Tc, Mn, Gd, etc) in liposomes, metals can be complexed with a soluble chelating agent (such as DTPA) that will be encapsulated in the aqueous core of the vesicles. Alternatively, the chelating compound complexing with the metal can be derivatized with a hydrophobic group for insertion in the lipid bilayer. Gd-DTPA complexes were the first to be incorporated in the aqueous core. Among the various lipophilic DTPA--conjugates that have been synthesized, DTPA-sterylamine (DTPA-SE) and DTPA-phosphatidyl ethanolamine (DTPA-PE) show reduced leakage and toxicity of potentially toxic metals. (DTPA-polylysil)glutaryl phosphatidyl ethanolamine (DTPA-PLL-NGPE) is a poly-chelating amphiphilic polymer suitable for liposome incorporation that drastically increases the number of metal ions attached to a single lipid conjugate. In these cases, metals are situated on the liposomal surface, directly exposed to the aqueous environment, thus enhancing the contrast proprieties.

To increase the stability and half-life of vesicles in the body after administration, liposomes for use as contrast agent can be modified with PEG. DTPA-PLL-NGPE liposomes with PEG5000 containing Gd improved visualization in the lymph nodes: PEG moieties increase the amount of water directly in contact with the Gd on the liposomal surface, and contrast phagocytic cell uptake at the injection site.

Long-circulating Gd liposomes have been successfully used for blood pool imaging, prolonging the presence of the contrast agent in the body. After systemic administration of Gd-DTPA-PLL-NGPE/PEG-liposomes, the signal was immediately clear and lasted for up to 4 hours (Torchilin 2000).

Incorporation of large amount of Gd-containing lipids in sterically stabilized PEGylated DSPC- or DOPC-based liposomes showed increased relaxivity compared with traditional Gd-DTPA; because of the higher accessibility of water, liposomes containing unsaturated phospholipids also showed increased relaxivity in comparison with liposomes composed of saturated phospholipids. These liposomes are therefore highly potent contrast agents for application in MR imaging (Strijkers et al 2005).

Liquid-filled liposomes have been demonstrated to be echogenic. The liquid-like composition of the vesicles makes them more resistant to pressure and mechanical stress than encapsulated gas microbubbles. Moreover, their long circulation characteristics and their small size are favorable in echography. Definity® (Bristol-Myers Squibb Medical Imaging, Inc. New York, NY, USA) is a contrast agent containing perfluoropropane with a phospholipid shell approved in the US for use in cardiology.

After lyophilization, liposomes can encapsulated small amounts of air, being echogenic upon rehydration. Is it possible to modulate the liposomal composition by changing the ratio between PC, PE, PG, and CHOL to produce agents that are echogenic in vitro and in vivo (Dayton and Ferrara 2002). Echogenic liposomes have also been utilized for intravascular ultrasound imaging, targeting the vesicles to the vascular signature associated with arteroma development (Morawski et al 2005).

A pH liposomal MRI contrast agent has recently been introduced as a potential marker of low pH in tumor interstitium. DPPE/DSPG/GdDTPA-BMA liposomes displayed increased relaxivity in the blood when the pH was below the physiological level, due to aggregation and leakage of GdDTPA-BMA. To optimize these liposomal formulations it is necessary that they retain pH sensitivity in the blood and accumulate in the tumor. Blood circulation time was prolonged by incorporating 1.5mol% in DPPE/DSPG liposomal GdDTPA-BMA, but the pH-response was reduced. A compromise would be necessary between long blood retention and pH-sensitivity (Lokling et al 2004).

Liposomes for vaccines

Genetic vaccination-encoding antigens from bacteria, virus, and cancer has shown promise in protecting humoral and cellular immunity. The success of liposomes-based vaccines has been demonstrated in clinical trials and further human trials are also in progress. Liposomes are of interest as

carriers of antigens, especially because they act as effective adjuvants for the immune system response, without causing granulomas at the injection site and producing no hypersensitivity reactions (Chen and Huang 2005). Liposome formulations would also protect their DNA content from deoxyribonuclease attack. Moreover, their transfection efficiency could be improved by modulating surface charge, size, and lipid composition of the vesicle and entrapping additional adjuvant or immunostimulator compounds in the antigen formulation. Several strategies have been followed to target liposomes to cell receptors, such as antibodies (or Fc-γ) or branched chain mannose moieties. Cationic or pH-sensitive liposomes that are able to release their contents into the cytoplasm following endocytosis have also been developed.

Two commercial vaccines based on virosome technology are currently on the market. Epaxal® (Berna Biotech Ltd, Bern, Switzerland), a hepatitis A vaccine, has inactivated hepatitis A virus particles adsorbed on the surface of the immunopotentiating reconstituted influenza virosomes (IRIV). In Inflexal® V (Berna Biotech Ltd) the virosome components themselves are the vaccine protective antigens (Copland et al 2005). Virosomes are liposomal formulations that have viral envelope proteins anchored to their lipid membrane. The lipid bilayer is composed of PC intercalated with the virus-derived proteins hemagglutinin and neuraminidase. These virus-like particles have proven to be effective immunogens with unique adjuvant properties (Felnerova et al 2004).

Liposome-encapsulated malaria vaccine contains monophosphoryl lipid A as adjuvant in the bilayer and the formulation is adsorbed on aluminum hydroxide. In a Phase I dose-escalating study, the formulation showed induction of higher level of anti-malaria antibody in human volunteers (Chen and Huang 2005). Some liposomal formulations are under investigation in preclinical studies against Yersina pestis, ricin toxin and Ebola Zaire virus. Liposomes against ricin or pestis, composed of PC/CHOL/DDA containing KWC vaccine, were administered intranasally to C57BL/6 mice; liposome formulations gave higher protection from infection than KWC in buffer. Liposomes composed of PC and CHOL containing ricin toxoid and ricin A-chain (rA) increased antibody responses to the rA chain. Liposomes composed of DMPC/DMPG/CHOL with or without lipid A containing Ebola Zaire virus have been tested in mice and cynomolgus monkeys (Brarnwell et al 2005).

Liposome vaccination also has the potential to be a powerful weapon in cancer treatment. Chen et al (Chen and Huang 2005) developed a novel liposome-based system for the delivery of plasmid DNA. Lipid-polycation-DNA particles are formed by combining cationic liposomes and polycation-condensed DNA organized in a virus-like structure able to release its content in the cytoplasm. Cationic liposomes promote a much higher humoral and cytotoxic T lymphocyte immune response against the antigen encoded by the entrapped DNA vaccine. Liposome-stabilized prostate cancer vaccine is under investigation in a series of Phase I trials in patient with advanced prostate cancer. The new liposome-lipid A-prostate-specific antigen formulation showed greater safety and higher immunological potency than other formulations and has been transitioned to Phase II trials (Chen and Huang 2005).

Other pharmaceutical uses of stealth liposomes

Active research is in progress in the area of liposomes for use as vesicular containers, in particular for hemoglobin as blood substitute. Liposome-encapsulated hemoglobin (LEH) is being developed as an oxygen therapeutic. The spatial isolation of hemoglobin by a lipid bilayer potentially minimizes the cardiovascular/hemodynamic effects associated with other modified forms of hemoglobin; moreover, it is possible to co-encapsulate reductants, antioxidative enzyme systems, and oxygen-affinity modifiers with hemoglobin so as to artificially recreate the red blood cell environment. The circulation half-life is 65 hours for this PEG-LEH formulation; the results demonstrate that LEH circulates for a prolonged time after administration and that the animals tolerate at least 25% of blood exchange without any distress (Phillips et al 1999; Arifin and Palmer 2005).

Conclusions

The development of liposomes as carriers for therapeutic molecules is an ever-growing research area. The possibility of modulating the technological characteristics of the vesicles makes them highly versatile both as carriers of several types of drug (from conventional chemotherapeutics to proteins and peptides) and in therapeutic applications (from cancer therapy to vaccination). In recent years, several important formulations for the treatment of different diseases have been developed. Among these, PEG-coated liposomes are becoming increasingly important, giving technological and biological stability to liposomal systems. At present, few PEGylated liposomal formulations have been approved or are in advanced trials (DOXIL, SPI077, Lipoplatin, S-CKD-

602), but stealth technology for different applications is destined to continue developing. PEG-derivatized liposomes with increased stability can easily be modified using a wide array of targeting moieties (MAb, ligands) to deliver the drug specifically to the target tissues with increasing accuracy. Moreover, PEG grafted onto the liposome surface can guide the liposome to a specific intracellular target, using for example cell-penetrating proteins and peptides as targeting agents. The development of liposome delivery to particular subcellular compartments is a field of great interest in different fields, such as gene therapy and vaccination. The interaction of stealth liposomes with cell membranes, and release of the drug in the neighborhood of target tissues are still under investigation, but some recent studies indicate that the use of detachable PEG may facilitate cell penetration and/or intracellular delivery of vesicles.

Taking into account these considerations and the great advantages of PEGylated liposomes in decreasing aspecific drug toxicity and in passively targeting the incorporated molecules to the site of action, new and "improved" stealth liposomal formulations designed for different therapeutic and diagnostic areas may soon be expected to arrive on the market.

References

Adams GP, Weiner LM. 2005. Monoclonal antibody therapy of cancer. *Nat Biotechnol*, 23:1147–57.

Adlakha-Hutcheon G, Bally MB, Shew CR, et al. 1999. Controlled destabilization of a liposomal drug delivery system enhances mitoxantrone antitumor activity. *Nat Biotechnol*, 17:775–9.

Agrawal AK, Gupta CM. 2000. Tuftsin-bearing liposomes in treatment of macrophage-based infections. *Adv Drug Deliv Rev*, 41:135–46.

Alberts DS, Muggia FM, Carmichael J, et al. 2004. Efficacy and safety of liposomal anthracyclines in phase I/II clinical trials. *Semin Oncol*, 31(Suppl 13):53–90.

Allen C, Dos SN, Gallagher R, et al. 2002 Controlling the physical behavior and biological performance of liposome formulations through use of surface grafted poly(ethylene glycol). *Biosc Rep*, 22:225–50.

Allen TM, Hansen C, Martin F, et al. 1991. Liposomes containing synthetic lipid derivatives of poly(ethylene glycol) show prolonged circulation half-lives in vivo. *Biochim Biophys Acta*, 1066:29–36.

Allen TM, Hansen C, Rutledge J. 1989. Liposomes with prolonged circulation times: factors affecting uptake by reticuloendothelial and other tissues. *Biochim Biophys Acta*, 981:27–35.

Allen TM, Hansen CB, Guo LSS. 1993. Subcutaneous administration of liposomes: a comparison with the intravenous and intraperitoneal routes of injection. *Biochim Biophys Acta*, 1150.9–16.

Allen TM, Martin FJ. 2004, Advantages of liposomal delivery systems for anthracyclines. *Semin Oncol*, 31(Suppl 13):5–15.

Alving CR. 1978. Therapy of leishmaniasis: superior efficacies of liposome-encapsulated drugs. *Proc Natl Acad Sci U S A*, 75:2959–63.

Andreff M, Estey EH. 2004. Method of cancer treatment [patent]. US20040577989.

Anonymous. 1999. Nystatin-liposomal. AR 121, Nyotran. *Drugs R D*, 1:181–3.

Anonymous. 2004. Vincristine liposomal--UNEX: lipid-encapsulated vincristine, onco TCS, transmembrane carrier system--vincristine, vincasome, vincristine sulfate liposomes for injection, VSLI. *Drugs R D*, 5:119–23.

Arifin DR, Palmer AF. 2005. Physical properties and stability mechanisms of poly(ethylene glycol) conjugated liposome encapsulated hemoglobin dispersions. *Artif Cells Blood Substit Immobil Biotechnol*, 33:137–62.

Arikan S, Rex JH. 2001. Nystatin LF (Aronex/Abbott). *Curr Opin Investig Drugs*, 2:488–495.

Asahi M, Famnohan R, Sumii T, et al. 2003. Antiactin-targeted immunoliposomes ameliorate tissue plasminogen activator-induced hemorrhage after focal embolic stroke. *J Cereb Blood Flow Met*, 23:895–9.

Asai T, Oku N. 2005. Liposomalized oligopeptides in cancer therapy. *Methods Enzymol*, 391:163–76.

Awada A, Gil T, Saleo F, et al. 2004. Prolonged schedule of temozolomide (Temodal) plus liposomal doxorubicin (Caelyx) in advanced solid cancers. *Anticancer Drugs*, 15:499–502.

Babai I, Samira S, Barenholz Y, et al. 1999. A novel influenza subunit vaccine composed of liposome-encapsulated haemagglutinin/neuraminidase and IL-2 or GM-CSF. I. Vaccine characterization and efficacy studies in mice. *Vaccine*, 17:1223–38.

Banerjee R, Tyagi P, Li S, et al. 2004. Anisamide-targeted stealth liposomes: a potent carrier for targeting doxorubicin to human prostate cancer cells. *Int J Cancer*, 112:693–700.

Baselga J, Mendelsohn JM. 2000. Monoclonal antibodies: Clinical applications: Monoclonal antibodies directed against growth factor receptors. in Rosenburg SA (ed). Principles and practice of biological therapy of cancer. Philadelphia: Lippincott Williams, Wilkins: p 475–89.

Basu MK, Lala S. 2004. Macrophage specific drug delivery in experimental leishmaniasis. *Curr Mol Med*, 4:681–9.

Blume GaCG. 1993. Molecular mechanism of the lipid vesicle longevity in vivo. *Biochim Biophys Acta*, 1146:157–68.

Bomgaars L, Geyer JR, Franklin J, et al. 2004 Phase I trial of intrathecal liposomal cytarabine in children with neoplastic meningitis. *J Clin Oncol*, 22:3916–21.

Boulikas T, Stathopoulos GP, Volakakis N, et al. 2005. Systemic Lipoplatin infusion results in preferential tumor uptake in human studies. *Anticancer Res*, 25:3031–9.

Bradley AJ, Devine DV, Ansell SM, et al. 1998. Inhibition of liposome-induced complement activation by incorporated poly(ethylene glycol)-lipids. *Arch Biochem Biophys*, 357:185–94.

Brunwell VW, Eyles JE, Oya, AH. 2005. Particulate delivery systems for biodefense subunit vaccines. *Adv Drug Del Rev*, 57:1247–65.

Briasoulis E, Karavasilis V, Tzamakou E, et al. 2004. Interaction pharmacokinetics of pegylated liposomal doxorubicin (Caelyx) on coadministration with paclitaxel or docetaxel. *Cancer Chemother Pharmacol*, 53:452–7.

Caliceti P, Veronese FM. 2003. Pharmacokinetic and biodistribution properties of poly(ethylene glycol)-protein conjugates. *Adv Drug Del Rev*, 55:1261–77.

Chen T, Palmer LR, Fenske DB, et al. 2004. Distal cationic poly(ethylene glycol) lipid conjugates in large unilamellar vesicles prepared by extrusion enhance liposomal cellular uptake. *J Liposome Res*, 14:155–73.

Chen WC, Huang L. 2005. Non-viral vector as vaccine carrier. *Adv Genet*, 54:315–37.

Chonn A, Cullis PR, Devine DV. 1991. The role of surface charge in the activation of the classical and alternative pathways of complement by liposomes. *J Immunol*, 146:4234–41.

Chonn A, Semple SC, Cullis PR. 1992 Association of blood proteins with large unilamellar liposomes *in vivo*. Relation to circulation lifetimes. *J Biol Chem*, 267:18759–765.

Chonn A, Semple SC, Cullis PR. 1995. Beta 2-glycoprotein I is a major protein associated with very rapidly cleared liposomes *in vivo*, suggesting a significant role in the immune clearance of "non-self" particles. *J Biol Chem*, 270:25845–9.

Copland MJ, Rades T, Davies NM, et al. 2005. Lipid based particulate formulations for the delivery of antigen. *Immunol Cell Biol*, 83:97–105.

Corvo ML, Boerman OC, Oyen WJ, et al. 1999. Intravenous administration of superoxide dismutase entrapped in long circulating liposomes. II. In vivo fate in a rat model of adjuvant arthritis. *Biochim Biophys Acta*, 1419:325–34.

Crosasso P, Ceruti M, Brusa P, et al. 2000. Preparation, characterization and properties of sterically stabilized paclitaxel-containing liposomes. *J Control Release*, 63:19–30.

Dagar S, Krishnadas A, Rubinstein I, et al. 2003. VIP grafted sterically stabilized liposomes for targeted imaging of breast cancer: in vivo studies. *J Control Release*, 91:123–33.

Damen J. 2005. Transfer and exchange of phospholipid between small unilamellar liposomes and rat plasma high-density lipoproteins: dependence on cholesterol and phospholipid composition. *Biochim Biophys Acta*, 665:538–45.

Dark GG, Calvert AH, Grimshaw R, et al. 2005. Randomized trial of two intravenous schedules of the topoisomerase I inhibitor liposomal lurtotecan in women with relapsed epithelial ovarian cancer: a trial of the national cancer institute of Canada clinical trials group [see comment]. *J Clin Oncol*, 23:1859–66.

Dayton PA, Ferrara KW. 2002. Targeted imaging using ultrasound. *J Magn Reson Imaging*, 16:362–77.

de Gennes PG. 1980. Conformations of polymers attached to an interface. *Macromolecules*, 13:1069–75.

Devine DV, Wong K, Serrano K, et al. 1994. Liposome-complement interactions in rat serum: implications for liposome survival studies. *Biochim Biophys Acta*, 1191:43–51.

Dreborg S, Akerblom EB. 1990. Immunotherapy with monomethoxy-polyethylene glycol modified allergenes. *Crit Rev Ther Drug Carrier Syst*:315–65.

Drummond DC, Meyer O, Hong K, et al. 1999. Optimizing liposomes for delivery of chemotherapeutic agents to solid tumors. *Pharmacol Rev*, 51:691–743.

Eichhorn ME, Becker S, Strieth S, et al. 2006. Paclitaxel encapsulated in cationic lipid complexes (MBT-0206) impairs functional tumor vascular properties as detected by dynamic contrast enhanced magnetic resonance imaging. *Cancer Biol Ther*, 5. In press.

Falcone DJ. 1986. Fluorescein opsonization assay: binding of plasma fibronectin to fibrin-derivatized fluorescent particles does not change their uptake by macrophages. *J Leukoc Biol*, 39:1–12.

Felnerova D, Viret JF, Gluck R, et al. 2004. Liposomes and virosomes as delivery systems for antigens, nucleic acids and drugs. *Curr Opin Biotechnol*, 15:518–29.

Funato KYRKH. 1992. Contribution of complement system on destabilization of liposomes composed of hydrogenated egg phosphatidylcholine in rat fresh plasma. *Biochim Biophys Acta*, 1103:204.

Gabizon A, Papahadjopoulos D. 1988. Liposome formulations with prolonged circulation time in blood and enhanced uptake by tumors. *Proc Natl Acad Sci U S A*, 85:6949–53.

Gabizon AA, Muggia FM. 1998. Long circulating liposomes: old drugs, new therapeutics. Springer-Verlag and Landes Bioscience.

Gulati M, Grover M, Singh S, et al. 1998. Lipophilic drug derivatives in liposomes. *Int J Pharm*, 165:129–68.

Gupta B, Levchenko TS, Torchilin VP. 2005. Intracellular delivery of large molecules and small particles by cell-penetrating proteins and peptides. *Adv Drug Deliv Rev*, 57:637–51.

Hamaguchi T, Matsumura Y, Nakamura Y, et al. 2004. Antitumor effect of MCC-465, pegylated liposomal doxorubicin tagged with newly developed monoclonal antibody GAH, in colorectal cancer xenografts. *Cancer Sci*, 95:608–13.

Han B,Ling YH, al-Baker S, et al. 1993. Cellular pharmacology of liposomal cis-bis-neodecanoato-trans-R,R-1,2-diaminocyclohexaneplatinum(II) in A2780/S and A2780/PDD cells. *Cancer Res*, 53:4913–19.

Harashima R, Sakata E, Funato K, et al. 1994. Enhanced hepatic uptake of liposomes through complement activation depending on the size of liposomes. *Pharm Res*, 11:402–6.

Harata M, Soda Y, Tani K, et al. 2004. CD19-targeting liposomes containing imatinib efficiently kill Philadelphia chromosome-positive acute lymphoblastic leukemia cells. *Blood*, 104:1442–9.

Harrington KJ, Lewanski CR, Northcote AD, et al. 2001. Phase I-II study of pegylated liposomal cisplatin (SPI-077) in patients with inoperable head and neck cancer. *Ann Oncol*, 12:493–6.

Harrington KJ, Rowlinson-Busza G, Syrigos KN, et al. 2000a. Influence of tumour size on uptake of(111)In-DTPA-labelled pegylated liposomes in a human tumour xenograft model. *Br J Cancer*, 83:684–8.

Harrington KJ, Rowlinson-Busza G, Syrigos KN, et al. 2000b. Biodistribution and pharmacokinetics of 111In-DTPA-labelled pegylated liposomes in a human tumour xenograft model: implications for novel targeting strategies. *Br J Cancer*, 83:232–8.

Harris JM. 1992. Poly(ethylene glycol) chemistry: biotechnical and biomedical applications. Plenum Press.

Hau P, Fabel K, Baumgart U, et al. 2004. Pegylated liposomal doxorubicin-efficacy in patients with recurrent high-grade glioma. *Cancer*, 100:1199–207.

Hussein MA, Anderson KC. 2004. Role of liposomal anthracyclines in the treatment of multiple myeloma. *Semin Oncol*, 31(Suppl 13):147–60.

Immordino ML, Brusa P, Arpicco S, et al. 2003. Preparation, characterization, cytotoxicity and pharmacokinetics of liposomes containing docetaxel. *J Control Release*, 91:417–29.

Ishida, O, Maruyama, K, Tanahashi, H, et al. 2001. Liposomes bearing polyethyleneglycol-coupled transferrin with intracellular targeting property to the solid tumors in vivo. *Pharm Res*, 18:1042–8.

Ishida T, Harada M, Wang XY, et al. 2005. Accelerated blood clearance of PEGylated liposomes following preceding liposome injection: effects of lipid dose and PEG surface-density and chain length of the first-dose liposomes. *J Control Release*, 105:305–17.

Ishida T, Harashima H, Kiwada H. 2002. Liposome clearance. *Biosci Rep*, 22:197–224.

Jaeckle KA, Phuphanich S, Bent MJ, et al. 2001. Intrathecal treatment of neoplastic meningitis due to breast cancer with a slow-release formulation of cytarabine. *Br J Cancer*, 84:157–63.

Johnstone SA, Masin D, Mayer L, et al. 2001. Surface-associated serum proteins inhibit the uptake of phosphatidylserine and poly(ethylene glycol) liposomes by mouse macrophages. *Biochim Biophys Acta*, 1513:25–37.

Kavanos D, Oletti MV, Rigault de la Longrais A, et al. 2005. Clinical and pharmacokinetic phase II study of pegylated liposomal doxorubicin and vinorelbine in heavily pretreated recurrent ovarian carcinoma. *Ann Oncol*, 16:360–6.

Kim ES, Lu C, Khuri FR, et al. 2001. A phase II study of STEALTH cisplatin (SPI-77) in patients with advanced non-small cell lung cancer. *Lung Cancer*, 34:427–32.

Kondo M, Asai T, Katanasaka Y, et al. 2004. Anti-neovascular therapy by liposomal drug targeted to membrane type-1 matrix metalloproteinase. *Int J Cancer*, 108:301–6.

Kraut EH, Fishman MN, Lorusso PM, et al. 2004. Pharmacogenomic and pharmacokinetic assessment of liposome encapsulated SN-38 (LE-SN38) in advanced cancer patients. *J Clin Oncol (Meeting Abstracts)*, 22:2501.

Krown SE, Northfelt DW, Osoba D, et al. 2004. Use of liposomal anthracyclines in Kaposi's sarcoma. *Semin Oncol*, 31(Suppl 13):36–52.

Laverman P, Carstens MG, Boerman OC, et al. 2001. Factors affecting the accelerated blood clearance of polyethylene glycol liposomes upon repeated injection. *J Pharmacol Exp Ther*, 298:607–12.

Lee TY, Wu HC, Tseng YL, et al. 2004. A novel peptide specifically binding to nasopharyngeal carcinoma for targeted drug delivery. *Cancer Res*, 64:3002–8.

Liu D, Mori A, Huang L. 1992. Role of liposome size and RES blockade in controlling biodistribution and tumor uptake of GM1-containing liposomes. *Biochim Biophys Acta*, 1104:95–101.

Lobling KE, Fossheim SL, Klaveness J, et al. 2004. Biodistribution of pH-responsive liposomes for MRI and a novel approach to improve the pH-responsiveness. *J Control Release*, 98:87–95.

Lopes De Menezes DE, Kirchmeier MJ, Gagne J-F, et al. 1999. Cellular trafficking and cytotoxicity of anti-CD19-targeted liposomal doxorubicin in B lymphoma cells. *J Liposome Res*, 9:199–228.

Lu C, Perez-Soler R, Piperdi B, et al. 2005. Phase II study of a liposome-entrapped cisplatin analog (L-NDDP) administered intrapleurally and pathologic response rates in patients with malignant pleural mesothelioma. *J Clin Oncol*, 23:3495–501.

Lukyanov AN, Elbayoumi TA, Chakilam AR, et al. 2004. Tumor-targeted liposomes: doxorubicin-loaded long-circulating liposomes modified with anti-cancer antibody. *J Control Release*, 100:135–44.

Lundberg BB, Griffiths G, Hansen HJ. 2000. Specific binding of sterically stabilized anti-B-cell immunoliposomes and cytotoxicity of entrapped doxorubicin. *Int J Pharm*, 205:101–8.

Lyass O, Uziely B, Ben-Yosef R, et al. 2000. Correlation of toxicity with pharmacokinetics of pegylated liposomal doxorubicin (DOXIL) in metastatic breast carcinoma. *Cancer*, 89:1037–47.

Maeda H, Sawa T, Konno T. 2001. Mechanism of tumor targeted delivery of macromolecular drugs, including the EPR effect in solid tumor and clinical overview of the prototype polymeric drug SMANCS. *J Control Release*, 74:47–61.

Mahato RI. 2005. Water insoluble and soluble lipids for gene delivery. *Adv Drug Deliv Rev*, 57:699–712.

Mahmood I, Green MD. 2005. Pharmacokinetic and pharmacodynamic considerations in the development of therapeutic proteins. *Clin Pharmacokinet*, 44:331–47.

Mamot C, Drummond DC, Greiner O, et al. 2003. Epidermal growth factor receptor (EGFR)-targeted immunoliposomes mediate specific and efficient drug delivery to EGFR- and EGFRvIII-overexpressing tumor cells. *Cancer Res*, 63:3154–61.

Mantripragada S. 2002. A lipid based depot (DepoFoam technology) for sustained release drug delivery. *Prog Lipid Res*, 41:392–406.

Marjan J, Xie Z, Devine D. 1994. Liposome-induced activation of the classical complement pathway does not require immunoglobulin. *Biochim Biophys Acta*, 1192:35–44.

Maruyama K, Ishida O, Kasaoka S, et al. 2004. Intracellular targeting of sodium mercaptoundecahydrododecaborate (BSH) to solid tumors by transferrin-PEG liposomes, for boron neutron-capture therapy (BNCT). *J Control Release*, 98:195–207.

Maruyama K, Okuizumi S, Ishida O, et al. 1994. Phosphatidyl polyglycerols prolong liposome circulation in vivo. *Int J Pharm*, 111:103–7.

Matsumura Y, Gotoh M, Muro K, et al. 2004. Phase I and pharmacokinetic study of MCC-465, a doxorubicin (DXR) encapsulated in PEG immunoliposome, in patients with metastatic stomach cancer. *Ann Oncol*, 15:517–25.

Medina OP, Zhu Y, Kairemo K. 2004. Targeted liposomal drug delivery in cancer. *Curr Pharm Des*, 10:2981–9.

Metselaar JM, Bruin P, de Boer LW, et al. 2003. A novel family of L-amino acid-based biodegradable polymer-lipid conjugates for the development of long-circulating liposomes with effective drug-targeting capacity. *Bioconjug Chem*, 14:1156–64.

Meyer O, Kirpotin D, Hong K, et al. 1998. Cationic liposomes coated with polyethylene glycol as carriers for oligonucleotides. *J Biol Chem*, 273:15621–7.

Moghimi SM, Muir IS, Illum L, et al. 1993. Coating particles with a block copolymer (Poloxamine 908) suppresses opsonization but permits the activity of dysopsonins in the serum. *Biochim Biophys Acta*, 1179:157–65.

Moghimi SM, Szebeni J. 2003. Stealth liposomes and long circulating nanoparticles: critical issues in pharmacokinetics, opsonization and protein-binding properties. *Prog Lipid Res*, 42:463–72.

Monfardini C, Veronese FM. 1998. Stabilization of substances in circulation. *Bioconj Chem*, 9:418–50.

Mora M, Sagrista ML, Trombetta D, et al. 2002. Design and characterization of liposomes containing long-chain *N*-acylPEs for brain delivery: penetration of liposomes incorporating GM1 into the rat brain. *Pharm Res*, 19:1430–8.

Morawski AM, Lanza GA, Wickline SA. 2005. Targeted contrast agents for magnetic resonance imaging and ultrasound. *Curr Opin Biotechnol*, 16:89–92.

Mukherjee A, Prasad TK, Rao NM, et al. 2005. Haloperidol-associated stealth liposomes: a potent carrier for delivering genes to human breast cancer cells. *J Biol Chem*, 280:15619–27.

Murai M, Aramki Y, Tsuchiya S. 1995. Identification of the serum factor required for liposome primed activation of mouse peritoneal macrophages: modified 2-macroglobulin enhances Fc gamma receptor mediated phagocytosis of opsonized sheep red blood cells. *Immunology*, 86:64–70.

Needham D, McIntosh TJ, Lasic DD. 1992. Repulsive interactions and mechanical stability of polymer-grafted lipid membranes. *Biochim Biophys Acta*, 1108:40–8.

Nellis DF, Ekstrom DL, Kirpotin DB, et al. 2005a. Preclinical manufacture of an anti-HER2 scFv-PEG-DSPE, liposome-inserting conjugate. 1. Gram-scale production and purification. *Biotechnol Prog*, 21:205–20.

Nellis DF, Giardina SL, Janini GM, et al. 2005b. Preclinical manufacture of anti-HER2 liposome-inserting, scFv-PEG-lipid conjugate. 2. Conjugate micelle identity, purity, stability, and potency analysis. *Biotechnol Prog*, 21:221–32.

Nishikawa KAHK. 1990. Scavanger receptor-mediated uptake and metabolism of lipid vesicles containing acidic phospholipids by mouse peritoneal macrophages. *J Biol Chem*, 265:5226–31.

Oja CDM, Semple SC, Chonn A, et al. 1996. Influence of dose on liposome clearance: critical role of blood proteins. *Biochim Biophys Acta*, 1281:31–7.

Oku N, Namba Y. 2005. Glucuronate-modified, long-circulating liposomes for the delivery of anticancer agents. *Methods Enzymol*, 391:145–62.

Oussoren C, Storm G. 1997. Lymphatic uptake and biodistribution of liposomes after subcutaneous injection: III. Influence of surface modification with poly(ethyleneglycol). *Pharm Res*, 14:1479–84.

Ozpolat B, Lopez-Berestein G, Adamson P, et al. 2003. Pharmacokinetics of intravenously administered liposomal all-trans-retinoic acid (ATRA) and orally administered ATRA in healthy volunteers. *J Pharm Pharm Sc*, 6:292–301.

Palmer LR, Chen T, Lam AM, et al. 2003. Transfection properties of stabilized plasmid-lipid particles containing cationic PEG lipids. *Biochim Biophys Acta*, 1611:204–16.

Park JW, Hong K, Kirpotin DB, et al. 2002. Anti-HER2 immunoliposomes: enhanced efficacy attributable to targeted delivery. *Clin Cancer Res*, 8:1172–81.

Park YS, Maruyama K, Huang L. 1992. Some negatively charged phospholipid derivatives prolong the liposome circulation *in vivo*. *Biochim Biophys Acta*, 1108:257–60.

Pastorino F, Brignole C, Marimpietri D, et al. 2003. Doxorubicin-loaded Fab' fragments of anti-disialoganglioside immunoliposomes selectively inhibit the growth and dissemination of human neuroblastoma in nude mice. *Cancer Res*, 63:86–92.

Patel HM. 1992. Serum opsonins and liposomes: their interaction and opsonophagocytosis. *Crit Rev Ther Drug Carrier Syst*, 9:39–90.

Phillips WT, Klipper RW, Awasthi VD, et al. 1999. Polyethylene glycol-modified liposome-encapsulated hemoglobin: a long circulating red cell substitute. *J Pharmacol Exp Ther*, 288:665–70.

Powell GM. 1980. Polyethylene glycol. In Davidson RL (ed). Handbook of water soluble gums and resins. McGraw-Hill. p 18–31.

Price ME, Cornelius RM, Brash JL. 2001. Protein adsorption to polyethylene glycol modified liposomes from fibrinogen solution and from plasma. *Biochim Biophys Acta*, 1512:191–205.

Priebe W, Perez-Soler R. 1993. Design and tumor targeting of anthracyclines able to overcome multidrug resistance: a double-advantage approach. *Pharmacol Ther*, 60:215–34.

Robert NJ, Vogel CL, Henderson IC, et al. 2004. The role of the liposomal anthracyclines and other systemic therapies in the management of advanced breast cancer. *Semin Oncol*, 31(Suppl 13):106–46.

Rose PG. 2005. Pegylated liposomal doxorubicin: optimizing the dosing schedule in ovarian cancer. *Oncologist*, 10:205–14.

Sapra P, Allen TM. 2003. Ligand-targeted liposomal anticancer drugs. *Prog Lipid Res*, 42:439–62.

Scherphof GL. 1985. Uptake and intracellular processing of targeted and nontargeted liposomes by rat Kupffer cells in vivo and in vitro. *Ann N Y Acad Sci*, 446:368–84.

Selden MV, Muggia F, Astrow A, et al. 2004. A phase II study of liposomal lurtotecan (OSI-211) in patients with topotecan resistant ovarian cancer. *Gynecol Oncol*, 93:229–32.

Semple SC, Leone R, Wang J, et al. 2005. Optimization and characterization of a sphingomyelin/cholesterol liposome formulation of vinorelbine with promising antitumor activity. *J Pharm Sci*, 94:1024–38.

Senior J. 1982. Is half-life of circulating liposomes determined by changes in their permeability? *FEBS Lett*, 145:109–14.

Senior JH. 1987. Fate and behavior of liposomes *in vivo*: a review of controlling factors. *Crit Rev Ther Drug Carrier Syst*, 3:123–93.

Song LY, Ahkong QF, Rong Q, et al. 2002. Characterization of the inhibitory effect of PEG-lipid conjugates on the intracellular delivery of plasmid and antisense DNA mediated by cationic lipid liposomes. *Biochim Biophys Acta*, 1558:1–13.

Stathopoulos GP, Boulikas T, Vougiouka M, et al. 2005. Pharmacokinetics and adverse reactions of a new liposomal cisplatin (Lipoplatin): phase I study. *Oncol Rep*, 13:589–95.

Stephenson SM, Low PS, Lee RJ. 2004. Folate receptor-mediated targeting of liposomal drugs to cancer cells. *Methods Enzymol*, 387:33–50.

Stephenson SM, Yang W, Stevens PJ, et al. 2003. Folate receptor-targeted liposomes as possible delivery vehicles for boron neutron capture therapy. *Anticancer Res*, 23:3341–45.

Strijkers GJ, Mulder WJM, van Heeswijk RB, et al. 2005. Relaxivity of liposomal paramagnetic MRI contrast agents. *MAGMA*, 18:186–92.

Sugano M, Egilmez NK, Yokota SJ, et al. 2000. Antibody targeting of doxorubicin-loaded liposomes suppresses the growth and metastatic spread of established human lung tumor xenografts in severe combined immunodeficient mice. *Cancer Res*, 60:6942–9.

Taira MC, Chiaramoni NS, Pecuch KM, et al. 2004. Stability of liposomal formulations in physiological conditions for oral drug delivery. *Drug Deliv*, 11:123–8.

Takeuchi H, Kojima H, Yamamoto H, et al. 2001. Evaluation of circulation profiles of liposomes coated with hydrophilic polymers having different molecular weights in rats. *J Control Release*, 75:83–91.

Tardi P, Choice E, Masin D, et al. 2000. Liposomal encapsulation of topotecan enhances anticancer efficacy in murine and human xenograft models. *Cancer Res*, 60:3389–93.

Torchilin VP. 2000. Polymeric contrast agents for medical imaging. *Curr Pharm Biotechnol*, 1:183–215.

Torchilin VP, Levchenko TS, Whiteman KR, et al. 2001. Amphiphilic poly-N-vinylpyrrolidones: synthesis, properties and liposome surface modification. *Biomaterials*, 22:3035–44.

Torchilin VP, Omelyanenko VG, Papisov MI, et al. 1994a. Poly(ethylene glycol) on the liposome surface: on the mechanism of polymer-coated liposome longevity. *Biochim Biophys Acta*, 1195:11–20.

Torchilin VP, Papisov MI. 1994. Why do polyethylene glycol-coated liposomes circulate so long? *J Liposome Res*, 4:725–39.

Torchilin V, Shtilman M, Trubetskoy V, et al. 1994c. Amphiphilic vinyl polymers selectively prolong liposome circulation time in vivo. *Biochim Biophys Acta*, 1195:181–4.

Torchilin V, Trubetskoy V, Whiteman K, et al. 1995. New synthetic amphiphilic polymers for steric protection of liposomes in vivo. *J Pharm Sci*, 84:1049–53.

Tseng YL, Hong RL, Tao MH, et al. 1999. Sterically stabilized anti-idiotype immunoliposomes improve the therapeutic efficacy of doxorubicin in a murine B-cell lymphoma model. *Int J Cancer*, 80:723–30.

Ugwu S, Zhang A, Parmar M, et al. 2005. Preparation, characterization, and stability of liposome-based formulations of mitoxantrone. *Drug Dev Ind Pharm*, 31:223–9.

Veerareddy PR, Vobalaboina V. 2004. Lipid-based formulations of amphotericin B. *Drugs Today*, 40:133–45.

Verschraegen CF, Kumagai S, Davidson B, et al. 2003. Phase I clinical and pharmacological study of intraperitoneal cis-bis-neodecanoato (trans-R, R-1, 2-diaminocyclohexane)-platinum II entrapped in multilamellar liposome vesicles. *J Cancer Res Clin Oncol*, 129:549–55.

Vert M, Domurado D. 2000. Poly(ethylene glycol): protein-repulsive or albumin-compatible? *J Biomater Sci Polym Ed*, 11:1307–17.

Volanakis JE, Narkates AJ. 1981. Interaction of C-reactive protein with artificial phosphatidylcholine bilayers and complement. *J Immunol*, 126:1820–5.

Vorobiof DA, Rapoport BL, Chasen MR, et al. 2004. First line therapy with paclitaxel (Taxol) and pegylated liposomal doxorubicin (Caelyx) in patients with metastatic breast cancer: a multicentre phase II study. *Breast*, 13:219–26.

Whiteman KR, Subr V, Ulbrich K, et al. 2001. Poly(HPMA)-coated liposomes demonstrate prolonged circulation in mice. *J Liposome Res*, 11:153–64.

Woodle M, Engbers C, Zalipsky S. 1994. New amphipatic polymer-lipid conjugates forming long-circulating reticuloendothelial system-evading liposomes. *Bioconjug Chem*, 5:493–6.

Yamaoka T, Tabata Y, Ikada Y. 1994. Distribution and tissue uptake of poly(ethylene glycol) with different molecular weights after intravenous administration in mice. *J Pharm Sci*, 83:601–6.

Yamauchi H, Yano T, Kato T, et al. 1994. Effects of sialic acid derivative on long circulating time and tumor concentration of liposomes. *Int J Pharmacol*, 113:141–8.

Zalipsky S, Qazen M, Walker JA, et al. 1999. New detachable polyethylene glycol) conjugates: cysteine-cleavable lipopolymers regenerating natural phospholipid, diacyl phosphatidylethanolamine. *Bioconjug Chem*, 10:703–7.

Zamboni WC, Gervais AC, Egorin MJ, et al. 2004. Systemic and tumor disposition of platinum after administration of cisplatin or STEALTH liposomal-cisplatin formulations (SPI-077 and SPI-077 B103) in a preclinical tumor model of melanoma. *Cancer Chemother Pharmacol*, 53:329–36.

Zamboni WC, Ramalingam S, Friedland DM, et al. 2005. Phase I and pharmacokinetic (PK) study of STEALTH liposomal CKD-602 (S-CKD602) in patients with advanced solid tumors. *J Clin Oncol (Meeting Abstracts)*, 23:2069.

Zhang JA, Anyarambhatla G, Ma L, et al. 2005. Development and characterization of a novel Cremophor EL free liposome-based paclitaxel (LEP-ETU) formulation. *Eur J Pharm Biopharm*, 59:177–87.

Zhang JA, Xuan T, Parmar M, et al. 2004a. Development and characterization of a novel liposome-based formulation of SN-38. *Int J Pharm*, 278:93–107.

Journal of Clinical Oncology®
An American Society of Clinical Oncology Journal

DEVELOPMENTAL THERAPEUTICS: CYTOTOXIC CHEMOTHERAPY

Phase I and pharmacokinetic (PK) study of IHL-305 (pegylated liposomal irinotecan) in patients with advanced solid tumors

S. F. Jones , W. C. Zamboni , H. A. Burris III , E. Chan , J. R. Infante , V. Keedy...

Show More

Abstract

2547

Background: Irinotecan (CPT-11) is a prodrug of SN-38 that has antitumor activity in a wide range of solid tumors. IHL- 305 is a PEGylated-liposomal formulation of irinotecan designed to increase the therapeutic index by prolonging the duration

COMPANION ARTICLES

No companion articles

ARTICLE CITATION

DOI: 10.1200/jco.2009.27.15_suppl.2
Journal of Clinical Oncology 27, no. 15_suppl (May 20, 2009) 2547-2547.

Published online May 20, 2009.

PMID: 27961859

of exposure in both plasma and tumors. IHL-305 demonstrates superior anti-tumor activity in preclinical models. **Methods:** Eligible patients (pts) had advanced solid tumors, ECOG ≤2, adequate organ function and no prior exposure to CPT-11. In a standard 3+3 escalation, IHL-305 was infused over 60 minutes q 28 days. UGT1A1*28 genotyping was performed with the homozygous (*28/*28) variants treated at 50% of current dose (subsequent escalation allowed). The area under the plasma concentration- time curve (AUC) of sum total (encapsulated + released) CPT-11, released CPT-11, SN-38, and SN-38 glucuronide (SN-38G) was calculated. The % CPT-11 released was calculated as the ratio of released CPT-11 AUC to sum total CPT-11 AUC x 100. The primary objectives were to determine the dose limiting toxicities (DLTs), phase II recommended dose (P2RD), and clinical pharmacology of IHL- 305. **Results:** 42 pts treated; homozygous wild-type (*wt/wt*; n=23), heterozygous (*wt*/*28; n=13) and homozygous variants (*28/*28; n= 6). 10 dose levels explored; 7, 14, 28, 37, 50, 67, 88, 120, 160 and 210 mg/m^2. DLTs included: 1 Gr 3 acute nausea/vomiting at 67 mg/ m^2 (subsequent pts received premedication), 1 Gr 3 delayed-onset diarrhea at 160 mg/m^2, and 1 Gr 3 delayed nausea/vomiting and one Gr 3 febrile neutropenia at 210mg/m^2. Pts received repeated courses of IHL-305 with no delays for myelosuppression or diarrhea. 7 pts had stable disease ≥ 6 cycles. The mean ± SD PK parameters are summarized in the table below. **Conclusions:** The MTD and P2RD of IHL-305 is 160 mg/m2 IV q 28 days. IHL-305 shows a high and prolonged exposure of sum total and released CPT-11 and SN-38.

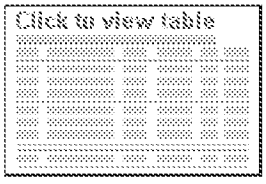

Table

Author Disclosure

Employment or Leadership	Consultant or Advisory Role	Stock Ownership	Honoraria	Research Funding	Expert Testimony	Other Remuneration
Yakult Honsha Co., Ltd.	Yakult Honsha Co., Ltd.			Yakult Honsha Co., Ltd.		

American Society of Clinical Oncology

QUICK LINKS

Content
Newest Articles
Archive
Meeting Abstracts

Journal Information
About
Editorial Board
Contact Us
Permissions

Resources
Authors
Reviewers
Subscribers
Institutions
Advertisers

Submit Your Manuscript

Subscribe to this journal

ASCO FAMILY OF SITES

Journals
Journal of Clinical Oncology
JCO Oncology Practice
JCO Global Oncology
JCO Clinical Cancer Informatics
JCO Precision Oncology

Publications
ASCO Educational Book
ASCO Daily News
ASCO Connection
The ASCO Post
JCO OP DAIS

Education
ASCO eLearning
ASCO Meetings
Cancer.Net

Other Sites
ASCO.org
ASCO Author Services
ASCO Career Center
CancerLinQ
Conquer Cancer Foundation
TAPUR Study

Journal of Clinical Oncology®

Table 1 of 1

Dose (mg/m^2)	Sum Total CPT-11 AUC (ug/mL•h)	Released CPT-11 AUC (ug/mL•h)	SN-38 AUC (ug/mL•h)	SN-38G AUC (ug/mL•h)	% CPT-11 Released
67	1,158 ± 235	4.6 ± 1.2	0.21 ± 0.10	2.8 ± 2.3	0.40 ± 0.08
88	1,388 ± 396	4.0 ± 1.8	0.10 ± 0.05	1.2 ± 0.2	0.30 ± 0.10
120	1,744 ± 738	11.9 ± 9.7	0.17 ± 0.23	3.4 ± 2.0	1.0 ± 1.2
160	2,541 ± 1,128	10.9 ± 1.5	0.36 ± 0.27	4.5 ± 0.9	0.53 ± 0.32

with advanced solid tumors

S. F. Jones, W. C. Zamboni, N. A. Burris III, E. Chan, J. R. Infante, V. Keedy...

Show More

Abstract

2547

Background: Irinotecan (CPT-11) is a prodrug of SN-38 that has antitumor activity in a wide range of solid tumors. IHL- 305 is a PEGylated-liposomal formulation of irinotecan designed to increase the therapeutic index by prolonging the duration

COMPANION ARTICLES

No companion articles

ARTICLE CITATION

DOI: 10.1200/jco.2009.27.15_suppl.2
Journal of Clinical Oncology 27, no. 15_suppl (May 20, 2009) 2547-2547.

Published online May 20, 2009.

PMID: 22961858

of exposure in both plasma and tumors. IHL-305 demonstrates superior anti-tumor activity in preclinical models. **Methods:** Eligible patients (pts) had advanced solid tumors, ECOG ≤2, adequate organ function and no prior exposure to CPT-11. In a standard 3+3 escalation, IHL-305 was infused over 60 minutes q 28 days. UGT1A1*28 genotyping was performed with the homozygous (*28/*28) variants treated at 50% of current dose (subsequent escalation allowed). The area under the plasma concentration- time curve (AUC) of sum total (encapsulated +

Table 1 of 1

Dose (mg/m^2)	Sum Total CPT-11 AUC (ug/mL•h)	Released CPT-11 AUC (ug/mL•h)	SN-38 AUC (ug/mL•h)	SN-38G AUC (ug/mL•h)	% CPT-11 Released
67	1,158 ± 235	4.6 ± 1.2	0.21 ± 0.10	2.8 ± 2.3	0.40 ± 0.08
88	1,388 ± 396	4.0 ± 1.8	0.10 ± 0.05	1.2 ± 0.2	0.30 ± 0.10
120	1,744 ± 738	11.9 ± 9.7	0.17 ± 0.23	3.4 ± 2.0	1.0 ± 1.2
160	2,541 ± 1,128	10.9 ± 1.5	0.36 ± 0.27	4.5 ± 0.9	0.53 ± 0.32

repeated courses of IHL-305 with no delays for myelosuppression or diarrhea. 7 pts had stable disease ≥ 6 cycles. The mean ± SD PK parameters are summarized in the table below. **Conclusions:** The MTD and P2RD of IHL-305 is 160 mg/m2 IV q 28 days. IHL-305 shows a high and prolonged exposure of sum total and released CPT-11 and SN-38.

Click to view table

Table

Author Disclosure

Employment or Leadership	Consultant or Advisory Role	Stock Ownership	Honoraria	Research Funding	Expert Testimony	Other Remuneration
Yakult Honsha Co., Ltd.	Yakult Honsha Co., Ltd.			Yakult Honsha Co., Ltd.		

American Society of Clinical Oncology

QUICK LINKS

ASCO FAMILY OF SITES

Table 1 of 1

Dose (mg/m^2)	Sum Total CPT-11 AUC (ug/mL•h)	Released CPT-11 AUC (ug/mL•h)	SN-38 AUC (ug/mL•h)	SN-38G AUC (ug/mL•h)	% CPT-11 Released
67	1,158 ± 235	4.6 ± 1.2	0.21 ± 0.10	2.8 ± 2.3	0.40 ± 0.08
88	1,388 ± 396	4.0 ± 1.8	0.10 ± 0.05	1.2 ± 0.2	0.30 ± 0.10
120	1,744 ± 738	11.9 ± 9.7	0.17 ± 0.23	3.4 ± 2.0	1.0 ± 1.2
160	2,541 ± 1,128	10.9 ± 1.5	0.36 ± 0.27	4.5 ± 0.9	0.53 ± 0.32

Submit Your Manuscript

Subscribe to this Journal

ASCO Meetings
Cancer.Net

Other Sites
ASCO.org
ASCO Author Services
ASCO Career Center
CancerLinQ
Conquer Cancer Foundation
TAPUR Study